Autonomous wireless sensor networks for the implementation of communicating materials. Application to civil engineering industry

Gael Loubet

THÈSE

En vue de l'obtention du

DOCTORAT DE L'UNIVERSITÉ DE TOULOUSE

Délivré par l'Institut National des Sciences Appliquées de Toulouse

---

Présentée et soutenue par

Gaël LOUBET

Le 24 septembre 2021

Réseaux de capteurs sans fil autonomes pour la fabrication de matériaux communicants. Application au domaine du génie civil.

Ecole doctorale : **GEETS - Génie Electrique, Electronique, Télécommunications et Santé : du système au nanosystème**

Spécialité : **MicroNano Systèmes**

Unité de recherche :
LAAS - Laboratoire d'Analyse et d'Architecture des Systèmes

Thèse dirigée par
Prof. Daniela DRAGOMIRESCU et Dr. Alexandru TAKACS

Jury

Prof. Ke WU, Président, Professeur, Ecole Polytechnique de Montréal, Canada (IEEE Fellow)
Prof. Nuno BORGES DE CARVALHO, Rapporteur, Professeur, Université d'Aveiro, Portugal (IEEE Fellow)
Prof. Alessandra COSTANZO, Rapporteure, Professeure, Université de Bologne, Italie
M. Vincent LE CAM, Examinateur, Directeur du laboratoire SII de l'IFFSTAR, Université Gustave Eiffel, France
Prof. Florin UDREA, Examinateur, Professeur, Université de Cambridge, Royaume-Uni
Prof. Jean-Paul BALAYSSAC, Invité, Professeur, Université Toulouse III - Paul Sabatier, LMDC, France
Dr. William DERIGENT, Invité, Maître de Conférence, HDR, Université de Lorraine, CRAN, France
Prof. Daniela DRAGOMIRESCU, Directrice de thèse, Professeure, INSA Toulouse, LAAS-CNRS, France
Dr. Alexandru TAKACS, Directeur de thèse, Maître de Conférence, HDR, Université Toulouse III - Paul Sabatier, LAAS-CNRS, France

Réseaux de capteurs sans fil autonomes pour la fabrication de matériaux communicants. Application au domaine du génie civil.

Résumé : Les "matières communicantes" sont des matériaux intrinsèquement capables de générer, traiter, stocker et échanger de l'information. Elles ont la capacité de quantifier leur environnement et leur propre état à travers la mesure de divers paramètres physiques. Ce concept a été appliqué au domaine de la construction avec un prototype basé sur un ensemble d'étiquettes RFID enfouies dans du béton. Cependant, ces étiquettes sont limitées en termes de mesure, de traitement, de mémoire et de communication sans fil (communications de courte portée et sur demande d'un lecteur). Parallèlement, les données et modèles issus du BIM (*Building Information Modelling*) sont très souvent cloisonnés dans la phase de conception et ne sont ni réutilisés, ni accessibles pour les acteurs en aval. La proposition du projet ANR McBIM (Matière Communicante au service du BIM) consiste en concevoir un "béton communicant" fait de béton armé, équipé avec un réseau de capteurs sans fil enfouis capables de mesurer les paramètres de la structure et de transmettre les données vers des plateformes BIM. Ces données peuvent être mesurées et utilisées durant tout le cycle de vie des composants, notamment à des fins de suivi de l'état de santé des structures.

Cette thèse de doctorat, inscrite dans le cadre du projet ANR McBIM, a comme objectif la conception d'un réseau de capteurs sans fil enfoui dans du béton permettant de rendre cette structure communicante durant toute sa vie. Afin de mener à bien ce projet, une cartographie de l'existant a été menée qui concerne :
- les bétons dits "intelligents" ;
- les paramètres pertinents dans le suivi de l'état de santé des bétons armés, ainsi que leurs méthodes de mesure ;
- les technologies de communications sans fil entre machines dans des milieux électromagnétiquement contraints ;
- et les techniques permettant l'autonomie d'énergie des réseaux de capteurs sans fil.

Une architecture à deux niveaux a été proposée pour la conception du réseau de capteurs sans fil : un réseau maillé de nœuds communicants, accessibles de l'extérieur et alimentés, permettant de récupérer, stocker et transmettre les données issues de la caractérisation du béton vers une base de données *via* Internet afin notamment de permettre la conception de jumeaux numériques de la construction ; et des réseaux en étoile de nœuds de mesure sans fil enfouis dans le béton armé, qui ont pour objectif de mesurer et transmettre à chaque nœud communicant environnant des données concernant l'environnement et les propriétés du béton armé. Devenant inaccessibles une fois enfouis, ces nœuds de mesure sans fil se doivent d'être autonomes en énergie durant toute leur durée de vie. Pour permettre cela, un système de transfert d'énergie électromagnétique radiative sans fil a été conçu afin d'alimenter les nœuds de mesure depuis les nœuds communicants. La conception d'un réseau de nœuds communicants et de nœuds de mesure tels que décrits, sans fil et autonomes, et utilisant la technologie LoRa a été conçu comme preuve de concept et a permis de réaliser des mesures de température, d'humidité, de contrainte et de résistivité au sein d'une poutre de béton armé. Des travaux complémentaires utilisant la technologie Bluetooth Low Energy ont également été menés afin de fournir une solution multi-technologies, à la fois en termes de capteurs que de communication sans fil. De même, les aspects concernant la sécurité matérielle ont été étudiés. Ainsi, un réseau maillé de nœuds communicant récupérant, agrégeant, prétraitant, stockant et échangeant entre eux et sur Internet les données issues des nœuds de mesure sans fil enfouis dans une poutre de béton armé, mais également télé-alimentant ces mêmes nœuds de mesure par du transfert d'énergie électromagnétique radiatif sans fil, a été développé, testé et caractérisé. Enfin, le contrôle de la périodicité de mesure et d'émission des nœuds de mesure est réalisé matériellement par la commande du système de transfert d'énergie sans fils.

Mots-clefs : Matériaux communicants ; Réseaux de capteurs sans fil ; Récupération d'énergie ambiante ; Transfert d'énergie sans fil ; Communications sans fil ; McBIM - Matière Communicante au service du BIM (*Building Information Modelling*).

Autonomous wireless sensor networks for the implementation of communicating materials. Application to civil engineering industry.

Abstract: "Communicating materials" are materials that are intrinsically able to measure, process, store and exchange information. These have the ability to quantify their environment and their own state through the measurement of various physical parameters. This concept has been applied to the civil engineering field with a prototype based on a set of RFID tags embedded in concrete. However, these tags are limited in terms of measurement, processing, memory and wireless communication (short-range communications and on demand from a reader). At the same time, data and models from BIM (Building Information Modelling) are used in the design phase but neither reused nor accessible to downstream actors. The proposal of the ANR McBIM (Communicating Material within the BIM) project consists in designing a "communicating concrete" made of reinforced concrete, equipped with a network of buried wireless sensors capable of generating and exchanging data with BIM platforms, and which can be used throughout the entire life of the components, in particular for monitoring the health of the structures.

The objective of this doctoral thesis, which is part of the ANR McBIM project, is to design a wireless sensor network embedded in reinforced concrete, to make communicating this reinforced concrete during its entire lifetime. In order to carry out this project, the state of art has been carried out, concerning:

- "smart" concretes;
- the relevant parameters for the health monitoring of reinforced concretes, as well as their measurement methods;
- the wireless communication technologies between machines in electromagnetically constrained environments;
- and the techniques allowing the energy autonomy of wireless sensor networks.

A two-level architecture was proposed for the design of the wireless sensor network:

- a mesh network of externally accessible and powered communicating nodes to retrieve, store and transmit data from the concrete characterization to a database *via* the Internet to enable, in particular, the design of a digital twin of the construction;
- a star network of wireless sensing nodes buried in the reinforced concrete, which aims to measure and transmit to each surrounding communicating node data concerning the environment and properties of the reinforced concrete. As these wireless sensing nodes become inaccessible once embedded, these must be energy self-sufficient during all their life. To enable this, a wireless radiative electromagnetic power transfer system was designed to power the sensing nodes from the communicating nodes. The design of a network of communicating nodes and sensing nodes as described, wireless and autonomous, and using LoRa technology was designed as a proof-of-concept and enabled temperature, humidity, stress and resistivity measurements within a reinforced concrete beam. Additional work using Bluetooth Low Energy technology was also carried out to provide a multi-technology solution, both in terms of sensors and wireless communication. The physical security aspects were also investigated. A mesh network of communicating nodes retrieving, aggregating, pre-processing, storing and exchanging among themselves and over the Internet the data from wireless sensing nodes embedded in a reinforced concrete beam, but also remotely powering these same sensing nodes by wireless radiative electromagnetic power transfer, has been developed, tested and characterized. The control of the measurement and transmission periodicity of the sensing nodes is achieved entirely materially by the control of the wireless power transfer system.

Keywords: Communicating materials; Wireless sensor networks (WSN); Ambient energy harvesting; Wireless Power Transfer (WPT); Wireless communications; McBIM - Material Communicating with the BIM (Building Information Modelling).

Résumé de la thèse en français

Ce résumé en français concerne la thèse de doctorat intitulée "Réseaux de capteurs sans fil autonomes pour la fabrication de matériaux communicants. Application au domaine du génie civil." (ou "*Autonomous wireless sensor networks for the implementation of communicating materials. Application to civil engineering industry.*") présentée dans le présent manuscrit rédigé entièrement en anglais. Ce résumé tentera d'introduire chacun de ses chapitres et d'en expliciter succinctement le contenu. De plus, une traduction des introduction et conclusion générales est proposée.

I. Introduction

Le projet McBIM (Matière communicante au service du *BIM (Building Information Modelling*)) a pour principal objectif de proposer une mise en œuvre du concept de matière communicante dans le domaine du génie civil. Une matière communicante est un matériau intrinsèquement capable de mesurer ses propres propriétés internes, et de traiter, stocker et partager des données, tant avec le monde physique que le monde numérique. Il s'agit donc d'un système cyber-physique. Étant les matériaux de construction les plus utilisés dans le monde, les bétons, et plus particulièrement les bétons armés, sont les candidats parfaits pour cette mise en œuvre. Ces derniers ont une durée de vie d'au moins plusieurs dizaines d'années et doivent être surveillés tout au long de celle-ci afin d'éviter leurs défaillances qui peuvent entraîner des catastrophes aussi bien matérielles que humaines. C'est donc un béton armé communicant, capable de s'auto-surveiller et interfacé avec le monde numérique (notamment avec un BIM) qui est visé par ce projet.

Dans le cadre du projet McBIM, les travaux menés durant cette thèse de doctorat se devaient de fournir une solution matérielle pour concevoir et mettre en œuvre un béton armé communicant. La solution proposée -et présentée dans ce manuscrit- est basée sur un réseau de capteurs sans fil à deux couches, composé de deux types de nœuds : les nœuds de mesure et les nœuds communicants. Les nœuds de mesure sont entièrement enterrés dans le béton armé -donc inaccessibles- et sont destinés à mesurer les propriétés du béton armé. La transmission des données collectées est réalisée par une communication sans fil. De plus, leur autonomie énergétique est assurée grâce à une architecture sans batterie et la possibilité de récolter l'énergie électromagnétique rayonnée. Les nœuds communicants -moins contraints car accessibles- assurent le traitement, le stockage et le partage des données collectées et transmises par les nœuds de mesure, tant avec le monde physique (à travers un réseau maillé de nœuds communicants) qu'avec le monde numérique (*via* Internet). De plus, ces derniers alimentent sans fil et à distance les nœuds de mesure, et contrôlent -toujours sans fil et à distance- leur périodicité de mesure et de communication, grâce à l'utilisation d'un système de transmission d'énergie sans fil basé sur la génération d'ondes électromagnétiques rayonnantes.

Le deuxième chapitre rassemble l'état de l'art des cinq domaines considérés dans cette thèse de doctorat :

* les bétons armés, que l'on veut rendre communicants, et dont les propriétés physiques (notamment électromagnétiques) contraignent à la fois la conception et la mise en œuvre des solutions proposées ;
* les méthodes d'évaluation des bétons armés, que nous voulons mettre en œuvre de manière innovante, sans fil, et autonome en énergie, pour des applications de surveillance à long terme de l'état de santé des structures ;
* les technologies de communication sans fil, que nous voulons utiliser pour transmettre et partager diverses données à travers du béton armé, un milieu de propagation inhabituel ;
* les solutions de récupération d'énergie ambiante et de transmission d'énergie sans fil, que nous voulons utiliser pour assurer l'autonomie énergétique et une longue durée de vie à notre système ;
* et les matériaux communicants, qui sont le lien entre les quatre domaines précédents.

Le troisième chapitre contextualise cette thèse de doctorat en détaillant le projet McBIM - et son consortium de recherche- dans lequel elle s'inscrit, et décrit les architectures matérielles de la solution proposée pour rendre communicant les bétons armés. Certains choix technologiques seront présentés dans les chapitres suivants, lorsqu'ils seront rencontrés.

Le quatrième chapitre traite de la conception et de l'implémentation des nœuds communicants basés sur la technologie de communication sans fil LoRaWAN, dont le rôle est d'agréger, de traiter et de stocker les données de mesure envoyées par les nœuds de mesure et d'alimenter ces derniers à distance et sans fil.

Le cinquième chapitre présente la conception et la mise en œuvre des nœuds de mesure basés sur la technologie de communication sans fil LoRaWAN. Ces nœuds sont au cœur de la solution proposée et constituent le plus grand défi : ils doivent être enterrés dans le béton armé (donc inaccessibles) ; ils doivent mesurer les paramètres pertinents afin d'assurer la surveillance de la santé structurelle du béton armé ; ils doivent transmettre sans fil des données depuis et à travers du béton armé, et enfin, être autonomes en énergie pendant toute la durée de vie du béton armé. Ce dernier aspect sera traité par l'utilisation de la transmission d'énergie sans fil sur plusieurs mètres ; et une architecture aussi fiable que possible.

Le sixième chapitre traite des premiers travaux réalisés pour concevoir et mettre en œuvre des nœuds communicants basés sur la technologie de communication sans fil Bluetooth Low Energy, tandis que le septième chapitre présente les premiers travaux réalisés pour concevoir et mettre en œuvre des nœuds de mesure basés sur la technologie de communication sans fil Bluetooth Low Energy.

Le huitième chapitre conclut en comparant les deux solutions proposées et implémentées, et en les positionnant dans l'état de l'art des solutions à la fois pour la surveillance de la santé structurelle des bétons armés, et pour les réseaux de capteurs sans fil alimentés sans fil et à distance en énergie. Enfin, une étude des aspects de sécurité de bas niveau propose un nouveau point de comparaison entre les technologies de communication sans fil LoRaWAN et Bluetooth Low Energy.

Même si l'application ultime ciblée par ces travaux est la mise en œuvre d'un béton armé communicant pour assurer le suivi de son état de santé structurelle et sa traçabilité tout au long de sa vie, les solutions conçues et implémentées peuvent également être adaptées à d'autres applications, avec divers capteurs et/ou actionneurs, dans différents domaines industriels, de consommation et d'ingénierie. Ainsi, plusieurs cas d'études peuvent être imaginés : assurer la traçabilité de produits et matériaux divers ; suivre et localiser des biens ; surveiller des machines industrielles, des infrastructures industrielles ou des environnements industriels (difficiles ou dangereux), des structures du génie civil, des véhicules, les performances d'individus (par exemple faisant du vélo, etc.), des niveaux de fluides, des environnements naturels, etc. ; alimenter sans fil, ou recharger partiellement ou totalement des objets (tels que des stations météos, des détecteurs d'intrusions et des alarmes sonore, des montres, des réveils, des périphériques (claviers, souris, écouteurs, manettes, etc.), des cartes, des téléphones intelligents, des veilleuses, de petites pompes, etc.) ; etc. Les principales limitations concernent les distances d'utilisation et les puissances en jeu qui sont limitées à la fois par les réglementations en vigueur et par l'efficacité énergétique des certains composants utilisés.

II. Etats de l'Art

Etant à la croisée de plusieurs domaines, ces travaux de thèse de doctorat doivent être considérés dans chacun d'entre eux. C'est pourquoi le deuxième chapitre de ce manuscrit traite de cinq états de l'art.

Le premier concerne les matériaux visés : les bétons armés. Ceux-ci sont très largement utilisés à travers le monde et leurs propriétés physiques imposent des contraintes dont il faut tenir compte dans le choix et la mise en œuvre des solutions proposées.

Ainsi, une première partie introduit ce qu'est un béton et un béton armé, puis quelles sont leurs recettes, leurs utilisations, leurs propriétés -mécaniques et électromagnétiques-, et leurs principaux défauts qui peuvent conduire à des défaillances structurelles.

Une deuxième partie présente les bétons dits "intelligents" dans le domaine du génie civil. Il s'agit de béton qui sont intrinsèquement capable de s'auto-mesurer, s'auto-réparer, s'auto-ajuster (selon différents paramètres), etc., ou qui ont des caractéristiques particulières (par exemple : peu affectés par les contraintes environnementales, capables de se déformer, électriquement conducteurs, translucides ou générateurs de lumière, photo-catalyseurs, hydrophobiques, perméables, etc.).

Une troisième partie traite des bétons instrumentés et connectés. Ceux sont des bétons considérés comme extrinsèquement intelligents.

Cet état de l'art se conclue par le positionnement du projet McBIM au sein de ces bétons dits "intelligents".

Le deuxième concerne la principale application visée : la surveillance de l'état de santé structurelle des bétons armés. Celle-ci repose sur différentes méthodes de test.

De fait, une première partie détaille les paramètres les plus pertinents à suivre en fonction de l'étape du cycle de vie des bétons armés.

Une deuxième partie liste les différentes méthodes de test dites destructives. Celles-ci se composent des trois grandes familles de tests : les tests physiques, les tests chimiques et les tests biologiques ; qui peuvent être réalisés soit sur site, soit en laboratoire.

Une troisième partie énumère les différentes méthodes de test dites non-destructives. Elles comprennent entre autres les méthodes : optiques ou visuelles, acoustiques ou ultrasonores, électromagnétiques, radiologiques, sclérométriques, thermographiques, etc.

Une quatrième partie traite de l'utilisation, aussi bien académique qu'industrielle, des réseaux de capteurs sans fil pour le suivie de l'état de santé structurelle des bétons armés, ou des structures faites en ces matériaux.

Cet état de l'art se conclue une nouvelle fois par le positionnement du projet McBIM au sein de méthodes de test des bétons armés, et par la justification partielle des choix de capteurs implémentés par la suite.

Le troisième concerne les technologies de communication des données visées : les communications sans fil. Celles-ci doivent permettre de répondre aux exigences induites par le milieu de propagation que sont les bétons armés ainsi qu'aux besoins de l'application visée.

Ainsi, une première partie présente les technologies de communications sans fil basées sur la propagation d'ondes électromagnétiques, à la fois en champ proche et en champ lointain. Dans la première catégorie, on retrouve les technologies NFC et RuBee, tandis que dans la seconde on retrouve une grande partie des technologies basées sur les standards 802 de l'IEEE (dont le Wi-Fi (IEEE 802.11), le Bluetooth et le Bluetooth Low Energy (IEEE 802.15.1), l'ultra-wide band (IEEE 802.15.3), le ZigBee et ses alternative (IEEE 802.15.4), le WiMAX (IEEE 802.16), ou le iBurst (IEEE 802.20)), mais également les technologies de LPWAN (dont DASH7, LoRaWAN, ou SigFox), les technologies cellulaires et leurs versions dédiées à l'IoT, les technologies satellitaires, ainsi que les solutions académiques basées sur la rétrodiffusion opportuniste. Les technologies RFID, quant à elles, peuvent à la fois être utilisées en champ proche et en champ lointain.

Une deuxième partie introduit les technologies de communication sans fil basées sur la propagation d'ondes lumineuses, dont le Li-Fi (IEEE 802.15.7).

Une troisième partie présente les technologies de communication sans fil basées sur la propagation d'ondes mécaniques, sonores ou ultrasonores.

Une quatrième partie liste les technologies utilisées par les industrielles et les académiques pour transmettre des données au travers du béton ou pour des applications de suivi de l'état de santé structurelle des bétons armés ou de structures faites de béton armé, ainsi que les axes de recherches connexes.

A nouveau, cet état de l'art se conclue par une justification partielle des technologies considérées dans le projet McBIM.

Le quatrième concerne les technologies de gestion de l'énergie pour le réseau de capteurs sans fil, en particulier l'alimentation en énergie des nœuds de mesure enfouis dans le béton armé. Celle-ci doit permettre d'assurer son autonomie durant toute sa période d'utilisation (*i.e.* des décennies), tout en répondant aux exigences induites par le milieu qu'est le béton armé, ainsi qu'aux besoins de l'application visée.

De fait, une première partie explique les différentes méthodes de récupération de l'énergie ambiante. Il est donc question de récupération de l'énergie : lumineuse *via* l'effet photovoltaïque ; mécanique (ou cinétique) *via* la combinaison des effets électrostatique et triboélectrique, l'effet électromagnétique inductif ou l'effet piézoélectrique ; thermique *via* l'effet pyroélectrique ou l'effet thermoélectrique ; et électromagnétique *via* les effets capacitif et inductif en champ proche ou les ondes rayonnées en champ lointain. Des méthodes hybrides sont également présentées.

Dans une deuxième partie, ceux sont les méthodes de transmission d'énergie sans fil qui sont explicitées. Il est donc question des transferts d'énergie par les ondes lumineuses, les ondes mécaniques et les ondes électromagnétiques à la fois en champ proche (par les méthodes capacitives, inductives non-résonantes et inductives résonantes) et en champ lointain (par les méthodes de rayonnement). Les propositions académiques et industrielles sont également présentées. De plus, le paradigme de la transmission simultanée d'informations et d'énergie sans fil est introduit, de même que ses implémentations. Enfin, les principales méthodes d'optimisation et d'amélioration sont spécifiées.

Une troisième partie traite des méthodes et technologies de gestion, d'utilisation et de stockage de l'énergie.

Enfin, une quatrième partie énumère l'ensemble des travaux concernant la récupération de l'énergie ambiante ou le transfert d'énergie sans fil dans le cadre des bétons armés, *i.e.* soit pour le suivi de leur état de santé structurelles, soit à travers ceux-ci.

Cet état de l'art se conclue par la justification partielle de la stratégie de gestion de l'énergie et des technologies employées dans le cadre du projet McBIM.

Le cinquième et dernier concerne le lien entre les quatre précédents : le concept de matière communicante. Celle-ci doit être mise en œuvre dans le cadre du projet McBIM.

Ainsi, une première partie introduit le concept de matière communicante, ainsi que ses premières implémentations partielles.

Une seconde partie présente les travaux pouvant être considérés comme répondant à une partie de la conception et/ou de la mise en œuvre du béton armé communicant, ou comme en étant des alternatives.

Cet ultime état de l'art se conclue par la définition générique du béton armé communicant.

Ce chapitre se conclue par la définition du béton armé communicant visé par le projet McBIM en fonction de l'ensemble des concepts présentés dans les différents états de l'art. La justification des premiers choix réalisés est également rappelée.

III. Le projet de recherche McBIM et son architecture réseau

Dans ce chapitre, le projet McBIM est détaillé, de même que les architectures du réseau, des nœuds communicants et des nœuds de mesure, afin de bien contextualiser les travaux présentés dans les chapitres suivants.

La première partie concerne le projet McBIM. Celui-ci est financé par l'Agence Nationale de la Recherche (ANR).

Une première sous-partie introduit le contexte dans lequel se déroule le projet et propose notamment un certain nombre de mots clefs en lien direct, tels que : Internet des objets, communication inter-machines, réseau de capteurs sans fil, système cyber-physique, jumeau numérique, *Building Information Modelling*, suivi de l'état de santé structurelle, ou encore ville intelligente. Ensuite, les objectifs du projet sont détaillés. Le principal concerne la conception et la mise en œuvre d'un béton communicant, intrinsèquement capable de générer, stocker (aussi bien localement qu'à distance), traiter et échanger des données concernant son propre état de santé structurelle et/ou concernant son environnement. Les échanges de données doivent être réalisées localement avec d'autres nœuds communicants, à distance à travers Internet avec le monde numérique et notamment un jumeau numérique de type BIM,

mais également localement et/ou à distance avec les différentes parties prenantes. Les capacités de mesure, de stockage, de traitement et d'échange de ce béton armé communicant se veulent être utilisables et utiles à chaque étape de son cycle de vie et durant toute sa vie. Ce béton armé communicant doit pouvoir être fonctionnel quel que soit le type de construction ciblée, indépendamment de son environnement et de son application, et être suffisamment générique pour pouvoir être utilisé avec différentes recettes et sous divers formats. De plus, il doit être reconfigurable en termes de périodicité et type de mesure pour répondre aux besoins propres au suivi de son état de santé structurelle à chaque étape de son cycle de vie. Les principales contraintes scientifiques à cette conception et cette mise en œuvre sont explicitées et concernent : la technologie de communication sans fil entre les nœuds de mesure et les nœuds communicants qui doit être robuste, fiable et résiliente sur le long terme et dans un environnement particulièrement contraint (notamment électromagnétiquement) que sont les bétons armés ; la technologie d'alimentation des nœuds de mesure qui sont inaccessibles et qui doivent fonctionner durant des décennies ; la technologie de gestion du partage et du stockage des données, localement et à distance, dans les différents réseaux ; et la technologie d'interconnexion entre le monde physique et le monde numérique, en particulier le jumeau numérique de type BIM, respectant les standards actuels. Les différents impacts (économique, sociétal, écologique, etc.) de ce projet sont également présentés.

Une deuxième sous-partie présente les différents membres du consortium, ainsi que les tâches qui leur sont dévolues. Ainsi, il y a : le LAAS-CNRS (Laboratoire d'Analyse et d'Architecture des Systèmes du Centre National de la Recherche Scientifique, Toulouse, FRANCE) qui doit traiter les deux premières contraintes scientifiques afin de fournir la partie matérielle nécessaire à la mise en œuvre du béton armé communicant ; le CRAN (Centre de Recherche en Automatique de Nancy, Nancy, FRANCE) qui doit traiter la troisième contrainte scientifique pour fournir les stratégies d'échange et de dissémination des données avec une contrainte de coût énergétique ; le LIB (Laboratoire d'Informatique de Bourgogne, Dijon, FRANCE) qui doit traiter la quatrième contrainte scientifique afin d'interfacer le monde physique avec son jumeau numérique de type BIM selon les normes actuelles ; et enfin, FINAO SAS / 360SmartConnect (Trans-en-Provence, France) qui doit assurer le lien avec l'industrie, proposer des cas d'utilisation réels, et fournir des composants en béton armé pour les expérimentations des partenaires académiques.

Une troisième et dernière sous-partie traite des objectifs et des contraintes propres à ces travaux de thèse de doctorat, mais également des hypothèses et simplifications posées. Il est notamment question : de la mise en œuvre du réseau de capteur sans fil dans le béton armé avec des nœuds vus comme des agrégats ; des limites des expérimentation réalisées dans une poutre de béton armé ; des besoins en termes de communications sans fil ; des besoins énergétiques ; ainsi que des principales fonctions ciblées.

La seconde partie introduit les architectures avancées pour répondre aux contraintes du projet.

Une première sous-partie présente l'architecture réseau (Fig. III.4.). Ce réseau se compose de deux types de nœuds : les nœuds communicants et les nœuds de mesure ; organisés sur deux niveaux. Chaque élément fait de béton armé communicant embarque au moins un nœud communicant et plusieurs nœuds de mesure, mais leurs quantités respectives sont fonction de la taille de l'élément et des besoins en termes de mesure. Les nœuds communicants forment un réseau maillé *ad-hoc* au sein d'une même structure ou d'un ensemble de structures, avec pour but d'agréger, de partager et de stocker les données fournies à la fois par les nœuds de mesures mais également par le(s) jumeau(x) numérique(s) dont le BIM. Une technologie de communication sans fil bidirectionnelle ayant une portée d'au moins une dizaine de mètres

dans l'air et/ou le béton armé est requise. De même, au moins un nœud communicant par réseau maillé doit servir d'interface avec Internet. Chaque nœud communicant est également le point central d'un réseau en étoile de nœuds de mesure. Les nœuds de mesure sont dédiés à la mesure des paramètres du béton armé et/ou de son environnement et à leur transmission au(x) nœud(s) communicant(s) associé(s). Les nœuds communicants doivent donc à la fois récupérer les données transmises par les nœuds de mesure, mais également alimenter ces derniers, s'ils sont localisés dans son voisinage, sans fil et à distance, par la transmission d'énergie électromagnétique rayonnée. En contrôlant leur source d'énergie, les nœuds communicants peuvent également contrôler la périodicité de fonctionnement (*i.e.* de mesure et de transmission sans fil) des nœuds de mesures dans leur voisinage. Des technologies de communication sans fil et de transmission d'énergie sans fil directionnelles et ayant une portée d'au moins plusieurs mètres, essentiellement dans le béton armé, sont requises.

Une deuxième sous-partie introduit l'architecture des nœuds communicants (Fig. III.5.). Ceux-ci doivent, comme annoncé, collecter les données envoyées par les nœuds de mesure, agréger, traiter, stocker et partager toutes les données (des nœuds de mesure et du(es) jumeau(x) numérique(s)) au sein du réseau maillé de nœuds communicants et avec le monde numérique à travers Internet, mais également alimenter sans fil et à distance les nœuds de mesure localisés dans son voisinage par un système de transmission d'énergie sans fil. Ainsi, leur architecture se compose de trois blocs : le premier est dédié à la génération et à la transmission de l'énergie électromagnétique rayonnée ; le second concerne la gestion des données ; et le troisième gère l'alimentation en énergie des deux précédents. Ces trois blocs sont définissables par les différentes interfaces qu'ils emploient. Leurs implémentations sont détaillées dans les chapitres IV et VI.

Une troisième et dernière sous-partie explicite l'architecture des nœuds de mesure (Fig. III.6.). Ceux-ci doivent, comme annoncé, réaliser des mesures et transmettre les données collectées au(x) nœud(s) communicant(s) associé(s). Ils sont également inaccessibles une fois déployés car enfouis dans le béton armé, et se doivent donc d'être utilisables, fiables, résilients, sans batterie et autonomes en énergie durant toute la vie du béton armé. De fait, ils sont conçus aussi simplement que possible et se composent de deux blocs : un dédié à la gestion des données (mesure, pré-traitement, transmission), l'autre à la gestion de l'énergie (récupération, stockage, utilisation). Leurs implémentations sont détaillées dans les chapitres V et VII.

Ce chapitre se conclue par un court résumé de son contenu.

IV. Implémentation des nœuds communicants basés sur la technologie de communication sans fil LoRaWAN

Dans ce chapitre, la conception, l'implémentation et le test de nœuds communicants basés sur la technologie de communication sans fil LoRaWAN sont proposés. Les nœuds communicants sont considérés comme étant alimentés par une source d'énergie illimitée.

La première partie traite de la conception et de l'implémentation de la source d'énergie électromagnétique rayonnée dédiée à l'alimentation sans fil et à distance des nœuds de mesure.

Dans une première sous-partie, le choix de la transmission sans fil d'énergie électromagnétique en champ lointain est justifié. Il s'agit notamment de proposer une solution générique, utilisable dans toutes les implémentations (indépendamment de l'environnement et

de l'application) et à long terme. Ainsi, les solutions filaires (longues et chères à mettre en œuvre), celles basées sur l'utilisation de piles, de batteries, ou de piles à combustibles (à la durée de vie limitée), ainsi que celles basées sur la récupération d'énergie ambiante (fortement dépendantes de l'environnement et de l'application) sont tour à tour écartées, aux regards des différentes contraintes. Enfin, parmi les solutions de transfert d'énergie sans fils, celle basée sur la transmission d'ondes électromagnétiques rayonnées est choisie, toujours aux regards des besoins (contraintes de propagation et distance d'utilisation).

Dans une deuxième sous-partie, la conception et l'implémentation de cette source d'énergie électromagnétique rayonnée sont présentées, notamment en tenant compte des contraintes réglementaires. Celle-ci fonctionne dans la bande de fréquence ISM des 868 MHz (mais également des 915 MHz), fournit une puissance EIRP de +33 dBm (ou 2 W), génère une onde continue, et se compose de composants sur étagère.

Dans une troisième sous-partie, le contrôle de la périodicité de fonctionnement des nœuds de mesure par les nœuds communicants est rapidement introduit.

Dans une quatrième sous-partie, les travaux en cours sont présentés. Il s'agit notamment du test de différentes formes d'onde, générées par l'utilisation d'outil de radio logicielle.

Une cinquième et dernière sous-partie traite des alternatives et perspectives. Les alternatives se basent sur l'utilisation de générateurs de signaux micro-ondes et des sources d'énergie électromagnétique rayonnée disponibles dans le commerce. Néanmoins, aucune de ces solutions n'est satisfaisante pour le projet (soit en termes de puissance maximale à transmettre, soit en termes de bande de fréquence d'utilisation, soit en termes de reconfigurabilité, soit en termes de coût). Les perspectives sont centrées sur l'utilisation de différentes formes de signaux, de l'implémentation d'une source reconfigurable et de la mise en œuvre de techniques de *beamforming*.

La deuxième partie concerne la conception et l'implémentation du bloc de gestion des données, destiné à collecter, traiter, stocker et échanger (avec différents systèmes) les données provenant des nœuds de mesure et du monde numérique.

Dans une première sous-partie, les contraintes de conception sont rappelées. Il s'agit dans un premier temps d'assurer la réception des données issues des nœuds de mesure, puis de mettre en œuvre les autres fonctions et interfaces de communication.

Dans une deuxième sous-partie, la conception et l'implémentation de ce sous-système sont détaillées. Il est question de chacune des interfaces de communication sans fil : pour la récupération des données transmises par les nœuds de mesure ; pour le partage des données au sein du réseau maillé de nœuds communicants ; pour la connexion avec le monde numérique *via* Internet ; ainsi que pour l'accès local et à distance des différents utilisateurs. S'en suit les solutions de traitement et de stockage des données, ainsi que la mesure de la consommation d'énergie.

Dans une troisième et dernière sous-partie, les alternatives et perspectives en termes de communication sans fil à travers les différentes interfaces sont présentées.

La troisième partie introduit succinctement le sous-système dédié à l'alimentation électrique des deux précédents.

Dans une première sous-partie, les choix technologiques sont présentés.

Dans une deuxième sous-partie, la conception et l'implémentation de ce sous-système sont proposées par des renvois aux parties précédentes détaillant plus ces aspects.

Dans une troisième et dernière sous-partie, les alternatives et leurs limites (utilisation de batteries), ainsi que quelques perspectives (optimisation de cette partie et récupération de l'énergie ambiante) sont présentées.

La quatrième partie concerne la reconfigurabilité, aussi bien matérielle que logicielle, des nœuds communicants, ainsi que quelques axes d'amélioration. Cela concerne à la fois la source d'énergie électromagnétique rayonnée que les sous-systèmes de gestion des données et de gestion de l'énergie.

La cinquième et dernière partie traite de l'implémentation complète et du test des nœuds communicants basés sur la technologie de communication sans fil LoRaWAN. Ceux-ci permettent d'accomplir l'ensemble des tâches qui leur sont confiées : alimenter sans fil et à distance tous les nœuds de mesure localisés dans leur voisinage ; collecter les données transmises par les nœuds de mesure ; traiter, stocker et échanger des données au sein d'un réseau maillé de nœuds communicants, avec le monde numérique à travers Internet et avec les différents utilisateurs aussi bien localement qu'à distance. Des tests ont été menés à la fois dans l'air et depuis une poutre en béton armé. Afin, des axes d'amélioration pour chacun de ces sous-systèmes et pour l'implémentation complète sont proposés. Il est notamment question de réaliser un unique système regroupant l'ensemble des sous-fonctions.

Ce chapitre se conclue par un court résumé de son contenu.

V. Implémentation des nœuds de mesure basés sur la technologie de communication sans fil LoRaWAN

Dans ce chapitre, la conception, l'implémentation et le test de nœuds de mesure basés sur la technologie de communication sans fil LoRaWAN sont proposés.

La première partie concerne la conception et l'implémentation de la partie des nœuds de mesure dédiée à la collecte, au pré-traitement et à la communication sans fil des données mises à disposition par les capteurs.

Dans une première sous-partie, le choix de la technologie de communication sans fil LoRaWAN est justifiée. Celui-ci repose sur de premiers tests de fonctionnement en environnement intérieur et sur les performances recherchées (portée d'au moins plusieurs dizaines de mètres, ne nécessitant pas de voie descendante, débit faible, consommation énergétique limitée, disponible, documentée, etc.), en comparaison aux autres technologies étudiées dans l'état de l'art.

Dans une deuxième sous-partie, la conception et l'implémentation de ce sous-système sont détaillées. Il repose sur l'utilisation d'un module LoRaWAN tout-en-un. Il est à la fois question de la conception matérielle et de la conception logicielle, mais également des performances (débit, portée, etc.) et de la consommation d'énergie en fonction de divers paramètres (dont la puissance d'émission et le débit).

Dans une troisième et dernière sous-partie, les alternatives et les perspectives sont explicitées, aussi bien du point de vue matériel que logiciel. Il est notamment question des stratégies à adopter pour réduire autant que possible la consommation énergétique tout en conservant des performances suffisantes pour assurer la communication sans fil dans les

bétons armés sur des portée utiles suffisamment élevées et avec un taux de bonne réception aussi élevé que possible.

La deuxième partie traite du choix et de l'implémentation de différents capteurs dédiés au suivi de l'état de santé structurelle des bétons armés.

Dans une première sous-partie, le choix des types de capteurs utilisés est justifié. Ce choix repose sur les possibilités d'interconnexion avec la partie précédente, des contraintes en termes de consommation d'énergie, ainsi que des paramètres utiles à suivre dans le cas du suivi de l'état de santé structurelle des bétons armés. Néanmoins, l'objectif est également de proposer la plus large gamme de capteurs possible traitant des différentes propriétés des bétons armés (physique, mécanique et chimique) à chaque étape de son cycle de vie.

Dans une seconde sous-partie, l'implémentation de chaque capteur est expliquée. Sont alors présentées la justification de leur choix, l'explication de leur mise en œuvre matérielle et logicielle, et leur utilisation matérielle et logicielle. Ainsi, des capteurs de paramètre physiques, au travers de deux capteurs de température et d'humidité relative du commerce, ainsi que de deux capteurs de température seule, sont présentés. Parmi les capteurs de température, l'un est basé sur l'utilisation de thermodiodes à la pointe de l'état de l'art en termes de performances (notamment de plage d'excursion, de linéarité et de précision) mais également en termes de taille et d'intégration. Cette solution, à l'état de recherche, a été mise à disposition par l'université de Cambridge (Cambridge, ROYAUME-UNI) et a pu être implémentée dans un système embarqué. Un capteur de paramètre chimique a également été implémenté. Il s'agit d'un capteur de résistivité électrique du béton armé qui permet d'estimer l'état de corrosion de celui-ci. Celui-ci, également à la pointe de l'état de l'art, a été mis à disposition par le LMDC (Laboratoire Matériaux et Durabilité des Constructions, Toulouse, FRANCE) et a pu être implémentée dans un système embarqué. Un capteur de paramètre mécanique a également été implémenté. Il s'agit d'une jauge de contrainte du commerce qui permet de quantifier localement les déformations mécaniques. Le test et la caractérisation (en termes de précision, de plage d'utilisation, de consommation d'énergie, etc.) de chaque capteur ont également été réalisés. De même, la présentation des alternatives et l'explicitation des perspectives ont été proposées pour chacun d'eux.

La troisième partie présente la partie des nœuds de mesure destinée à la gestion de l'énergie, *i.e.* à sa récupération, à son stockage et à son utilisation par les composants actifs des nœuds de mesures.

Dans une première sous-partie, le choix de l'architecture de cette partie est justifié, de même que le choix de la bande de fréquence ISM des 868 MHz pour la transmission de l'énergie sans fil en champ lointain.

Dans une deuxième sous-partie, l'implémentation de chaque composant est détaillée. Sont alors présentées la justification de leur choix, l'explication de leur mise en œuvre matérielle et leur utilisation. Il s'agit notamment de la PMU (unité de gestion de l'énergie) et de l'éventuel convertisseur associé, de la supercapacité en tant que composant de stockage de l'énergie, et de la rectenna, aussi bien du point de vue du redresseur que de l'antenne. Le test et la caractérisation de chaque composant sont également présentés. De même, la présentation des alternatives et l'explicitation des perspectives sont proposées pour chacun d'eux. Enfin, un modèle théorique pour estimer la portée maximale atteignable pour le système de transmission d'énergie sans fil est proposé.

Dans une troisième et dernière sous-partie les alternatives et perspectives de chaque composant sont rappelées et celles propres à l'implémentation complète sont proposées. Il est

notamment question des axes d'amélioration pour augmenter la portée d'utilisation du système de transmission de l'énergie sans fil (qui passe à la fois par la réduction de la puissance consommée par chaque composant de ce sous-système (dont celle requise par la PMU pour fonctionner et celle perdue par la supercapacité), et par l'optimisation de leur efficacité (en particulier celle de la rectenna)) et pour diminuer les temps de charge et de recharge (qui passe par la réduction de l'énergie nécessaire aux composants actifs du nœud de mesure dont le module LoRaWAN et les capteurs).

La quatrième partie traite de l'implémentation complète et du test des nœuds de mesure basés sur la technologie de communication sans fil LoRaWAN. Ceux-ci permettent d'accomplir l'ensemble des tâches qui leur sont confiées : quantifier les propriétés internes du béton armé, transmettre sans fil les données collectées au(x) nœud(s) communicant(s), et être sans batterie et autonome en énergie sur le long terme. Des tests ont été menés à la fois dans l'air et depuis une poutre en béton armé.

Dans une première sous-partie, l'ensemble des prototypes implémentés et testés est présenté. Ceux-ci varient en termes de composants employés, de performances, de capteurs utilisables, d'intégration et de taille. Il est en outre question de l'utilisation d'un circulateur radiofréquence permettant d'utiliser une unique antenne à la fois pour la communication sans fil des données et la récupération de l'énergie électromagnétique rayonnée destinée à l'alimentation du nœud de mesure.

Dans une deuxième sous-partie, la consommation d'énergie de l'ensemble des nœuds de mesures est présentée en fonction de divers paramètres, dont la génération du prototype, la puissance d'émission et le capteur employé.

Dans une troisième sous-partie, le contrôle de la périodicité de fonctionnement (*i.e.* de mesure et de transmission sans fil) des nœuds de mesure par les nœuds communicants, ainsi que l'efficacité énergétique de l'implémentation des nœuds de mesure sont détaillés. Il est entre autres question de : la reconfigurabilité des nœuds de mesures uniquement possible en termes de périodicité de fonctionnement et par l'utilisation du système de transmission d'énergie sans fil (étant inaccessible, aucune modification matérielle n'est envisageable, et n'ayant pas de voie descendante pour les données, aucune modification logicielle n'est envisageable) ; la caractérisation des temps de première charge et de recharge en fonction de l'énergie disponible en entrée du redresseur ; une courte analyse de reproductibilité permettant d'estimer la variabilité des mesures temporelles ; la corrélation entre la caractérisation des temps de première charge et de recharge en fonction de l'énergie disponible en entrée du redresseur dans une configuration d'énergie électromagnétique conduite et dans une configuration d'énergie électromagnétique rayonnée ; l'efficacité énergétique des nœuds de mesure ; et l'impact de l'utilisation d'une antenne unique et d'un circulateur radiofréquence sur l'ensemble des performances du nœud de mesure. Evidemment, des limites, des axes d'améliorations et des perspectives sont proposés pour chaque étude.

Dans une quatrième sous-partie, les tests qualitatifs et les résultats obtenus sont présentés. Des tests ont été menés dans diverses configurations. L'ensemble de ces tests a permis de proposer une preuve de concept complète du réseau de capteurs sans fil destiné à être embarqué sur et dans du béton armé pour assurer le suivi de son état de santé structurelle tout au long de sa vie, et composé de nœuds de mesure sans batterie et alimentés à distance, à travers le béton armé, par transmission d'énergie électromagnétique rayonnée en champ lointain sur plusieurs mètres (une distance de 7 mètres a été obtenue dans l'air mais des distances supérieures sont envisagées).

Une cinquième et dernière sous-partie présente les travaux en cours et les principales perspectives. Il s'agit notamment des axes d'optimisation matérielle et logicielle de chacun des sous-systèmes mais également des limites de l'implémentation actuelle. Il peut être noter en particulier la nécessité future de considérer l'encapsulation du nœud de mesure pour ne pas être altéré et abîmé par le béton armé humide, et le besoin d'amélioration en termes de portée d'utilisation de la transmission d'énergie sans fil, d'efficacité énergétique et de compacité.

Ce chapitre se conclue par un court résumé de son contenu mais également par l'explicitation des résultats obtenus dans la conception et la mise en œuvre du réseau de capteurs sans fil basé sur la technologie de communication sans fil LoRaWAN et destiné à rendre communicant le béton armé.

VI. Premiers travaux sur l'implémentation des nœuds communicants basés sur la technologie de communication sans fil Bluetooth Low Energy

Dans ce court chapitre, la conception, l'implémentation et le test de nœuds communicants basés sur la technologie de communication sans fil Bluetooth Low Energy sont proposés. Etant fortement similaires aux nœuds communicants introduits dans le chapitre IV, seules les différences sont présentées ici.

La première partie traite de la conception et de l'implémentation de la source d'énergie électromagnétique rayonnée dédiée à l'alimentation sans fil et à distance des nœuds de mesure. Celle-ci est strictement identique à celle présentée dans le cas des nœuds communicants basés sur la technologie de communication sans fil LoRaWAN.

La deuxième partie concerne la conception et l'implémentation du bloc de gestion des données, destiné à collecter, traiter, stocker et échanger (avec différents systèmes) les données provenant des nœuds de mesure et du monde numérique.

Dans une première sous-partie, la conception et l'implémentation de ce sous-système sont détaillées. Il est essentiellement question de l'interface de communication sans fil destinée à la récupération des données transmises par les nœuds de mesure. En effet, le partage des données au sein du réseau maillé de nœuds communicants ; la connexion avec le monde numérique *via* Internet ; ainsi que pour l'accès local et à distance des différents utilisateurs n'ont à ce jour pas été implémentés. La réception des trames de donnée est réalisée en mode *observer* sans appairage, ni acquittement.

Dans une deuxième sous-partie, les solutions de traitement et de stockage des données sont très succinctement introduites.

Dans une troisième et dernière sous-partie, les alternatives et perspectives en termes de communication sans fil à travers les différentes interfaces, ainsi que concernant le traitement et le stockage des données, sont présentées.

La troisième partie introduit succinctement le sous-système dédié à l'alimentation électrique des deux précédents.

La quatrième et dernière partie traite de l'implémentation complète et du test des nœuds communicants basés sur la technologie de communication sans fil Bluetooth Low Energy. Ceux-ci permettent d'accomplir une partie des tâches qui leur sont confiées : alimenter sans

fil et à distance tous les nœuds de mesure localisés dans leur voisinage ; collecter les données transmises par les nœuds de mesure ; et traiter (légèrement) et stocker les données reçues. Des tests ont été menés à la fois dans l'air et depuis une poutre en béton armé. Afin, des axes d'améliorations pour chacun de ces sous-systèmes et pour l'implémentation complète sont proposés. Il est notamment question de réaliser un unique système regroupant l'ensemble des sous-fonctions.

Ce court chapitre se conclue par un court résumé de son contenu.

VII. Premiers travaux sur l'implémentation des nœuds de mesure basés sur la technologie de communication sans fil Bluetooth Low Energy

Dans ce chapitre, la conception, l'implémentation et le test de nœuds de mesure basés sur la technologie de communication sans fil Bluetooth Low Energy sont proposés. Etant fortement similaires aux nœuds communicants introduits dans le chapitre V, seules les différences sont présentées ici.

La première partie concerne la conception et l'implémentation de la partie des nœuds de mesure dédié à la collecte, au pré-traitement et à la communication sans fil des données mises à disposition par les capteurs.

Dans une première sous-partie, le choix de la technologie de communication sans fil Bluetooth Low Energy est justifié, aux vues des arguments déjà présentés dans la partie V.A.1. Ce choix repose sur de premiers tests de communication sans fil depuis l'intérieur d'une poutre en béton armé et sur les performances recherchées (portée similaire à celle du système de transmission d'énergie sans fil (au moins une dizaine de mètres), ne nécessitant pas de voie descendante, débit faible, consommation énergétique limitée, disponible, documentée, etc.).

Dans une deuxième sous-partie, la conception et l'implémentation de ce sous-système sont détaillées. Il repose sur l'utilisation d'un module Bluetooth Low Energy tout-en-un. Il est à la fois question de la conception matérielle et de la conception logicielle, mais également des performances et de la consommation d'énergie en fonction de divers paramètres (dont la puissance d'émission). La transmission sans fil fonctionne en mode *broadcaster* et réalise l'envoi des données dans des trames de type *advertising* répétées quatre fois, sur trois canaux différents. Les communications se font sans appairage, ni acquittement. De fait, la voie descendante pour les données n'est pas utilisée et permet de réduire la consommation d'énergie.

Dans une troisième et dernière sous-partie, les alternatives et les perspectives sont explicitées, aussi bien du point de vue matériel que logiciel. Il est notamment question des stratégies à adopter pour réduire autant que possible la consommation énergétique tout en conservant des performances suffisantes pour assurer la communication sans fil dans le béton armé sur des portées utiles suffisamment élevées et avec un taux de bonne réception aussi élevé que possible.

La deuxième partie traite du choix et de l'implémentation de différents capteurs dédiés au suivi de l'état de santé structurelle des bétons armés. Il s'agit d'une partie des capteurs utilisés dans l'implémentation des nœuds de mesure basés sur la technologie de communication sans

fil LoRaWAN et plus particulièrement de capteurs de température et d'humidité relative du commerce.

La troisième partie présente la partie des nœuds de mesure destinée à la gestion de l'énergie, *i.e.* à sa récupération, à son stockage et à son utilisation par les composants actifs des nœuds de mesure.

Dans une première sous-partie, le choix, l'implémentation et l'utilisation d'une PMU différente de la précédente sont présentés, de même que ses alternatives et perspectives.

Dans une deuxième sous-partie, le choix, l'implémentation et l'utilisation d'un composant de stockage de l'énergie différent du précédent sont présentés, de même que ses alternatives et perspectives. Il s'agit d'une capacité et non plus d'une supercapacité, du fait de besoins énergétiques bien plus limités pour ces derniers nœuds de mesure que pour les précédents.

Dans une troisième sous-partie, le choix, l'implémentation et l'utilisation de la rectenna sont présentés, de même que ses alternatives et perspectives. Il s'agit de la même rectenna que pour les précédentes implémentations.

Dans une quatrième et dernière sous-partie, il est question des axes d'amélioration pour augmenter la portée d'utilisation du système de transmission de l'énergie sans fil (qui passe à la fois par la réduction de la puissance consommée par chaque composant de ce sous-système (dont celle requise par la PMU pour fonctionner et celle perdue par la capacité), et par l'optimisation de leur efficacité (en particulier celle de la rectenna)) et pour diminuer les temps de charge et de recharge (qui passe par la réduction de l'énergie nécessaire aux composants actifs du nœud de mesure dont le module Bluetooth Low Energy et les capteurs).

La quatrième partie traite de l'implémentation complète et du test des nœuds de mesure basés sur la technologie de communication sans fil Bluetooth Low Energy. Ceux-ci permettent d'accomplir l'ensemble des tâches qui leur sont confiées : quantifier quelques propriétés internes des bétons armés, transmettre sans fil les données collectées au(x) nœud(s) communicant(s), et être sans batterie et autonomes en énergie sur le long terme. Des tests ont été menés à la fois dans l'air et depuis une poutre en béton armé, et leurs premières caractérisations sont explicitées.

La cinquième partie concerne les travaux en cours et les perspectives. Il s'agit notamment des axes d'optimisation matérielle et logicielle de chacun des sous-systèmes mais également des limites de l'implémentation actuelle. Il peut être noter en particulier le besoin d'amélioration en termes de fiabilité des communications sans fil, de portée d'utilisation de la transmission d'énergie sans fil et des communications sans fil, d'efficacité énergétique et de compacité, mais également l'implémentation d'autres types de capteurs dont ceux de résistivité électrique et de quantification locale de la déformation mécanique.

Ce chapitre se conclue par un court résumé de son contenu mais également par l'explicitation des résultats obtenus dans la conception et la mise en œuvre du réseau de capteurs sans fil basé sur la technologie de communication sans fil Bluetooth Low Energy et destiné à rendre communicant le béton armé.

VIII. Positionnement et aspects concernant la sécurité de bas niveau

Dans ce chapitre, les deux implémentations des réseaux de capteurs sans fil destinés à rendre communicant les bétons armés sont comparées, puis positionnées dans l'état de l'art à la fois des solutions de suivi de l'état de santé structurelle des éléments et/ou constructions en béton armé, et des réseaux de capteurs sans fil alimentés par la transmission d'énergie électromagnétique en champ lointain et donc sans fil. Enfin, une étude de la sécurité bas niveau des deux implémentations est proposée et présente notamment quelques pistes d'amélioration de la sécurité du réseau de capteurs sans fil.

La première partie traite de la comparaison des deux implémentations du réseau de capteurs sans fil destiné à rendre communicant le béton armé et basées respectivement sur les technologies de communication sans fil LoRaWAN et Bluetooth Low Energy.

Ces deux implémentations se basent sur les mêmes architectures, aussi bien pour le réseau que pour les nœuds communicants et les nœuds de mesure. Quelle que soit la mise en œuvre considérée, les nœuds de mesure sont capables de réaliser la mesure de diverses propriétés internes du béton armé et/ou de son environnement, de réaliser le pré-traitement et la transmission sans fil des données collectées vers les nœuds communicants. La voie de données descendante n'est implémentée dans aucune des solutions proposées et comme ils sont enfouis dans le béton armé, aucune modification ni matérielle, ni logicielle n'est possible. De plus, ces nœuds de mesure sont sans batterie, capable de démarrés à froid même avec un composant de stockage de l'énergie complétement vide (donc insensible à la décharge totale) et alimentés à distance par les nœuds communicants à travers l'utilisation d'un système de transmission d'énergie électromagnétique rayonnée sans fil. Comme la puissance disponible est très largement inférieure à la puissance requise pour un fonctionnement en continu, ils récupèrent et stockent l'énergie jusqu'à ce qu'ils en aient assez pour achever un *process* complet (mesure, pré-traitement, transmission sans fil), puis ne sont plus alimentés jusqu'à la prochaine occurrence. Ils peuvent donc être "oubliés" pendant un certain temps, tout en restant fonctionnels. Ainsi, les deux répondent au paradigme de transmission simultanée d'informations et d'énergie sans fil, en utilisant une unique bande de fréquence et une unique antenne dans le cas de LoRaWAN, et deux bandes indépendantes et du multiplexage spatial dans le cas de Bluetooth Low Energy ; donc sans multiplexage temporel, ni partage de puissance sur la voie descendante (ici uniquement dédiée à la puissance). Enfin, il est possible de contrôler leur périodicité de fonctionnement en contrôlant l'énergie générée pour les alimenter à distance et sans fil.

Concernant leurs performances, la solution basée sur LoRaWAN permet des communications sans fil plus fiables, sur de plus longues distances, et moins sensibles à l'effet du béton armé, au prix d'une consommation d'énergie bien plus élevée que pour la solution basée sur Bluetooth Low Energy. Et plus le besoin en énergie est faible, plus rapides sont les temps de charge et de recharge. Ainsi, un compromis doit être trouvé entre qualité des communications et besoin en énergie. Quoi qu'il en soit, les deux implémentations peuvent être améliorées. Pour la solution LoRaWAN, le principal effort doit concerner la réduction du besoin en énergie, tandis que pour la solution Bluetooth Low Energy, c'est l'amélioration de la communication sans fil (portée, fiabilités, etc.) qui doit être privilégiée.

Concernant les parties gérant l'énergie, celles-ci sont relativement proches, car usant de composants identiques (rectenna), de la même famille (PMU) ou ayant des performances semblables (composants de stockage de l'énergie). Elles permettent donc des performances semblables notamment en ce qui concerne la portée d'utilisation. Pour les améliorer deux

points sont à considérer : le besoin en énergie minimal pour fonctionner et l'efficacité énergétique globale et de chaque composant.

Concernant les parties gérant les mesures, celles-ci sont une nouvelle fois semblables car basées sur des capteurs du même type. Les axes d'amélioration concernent à la fois les types de capteurs utilisables, la précision, la plage d'utilisation, ainsi que la consommation énergétique.

Concernant les parties gérant les données, celles-ci sont relativement proches car fonctionnant sur le même principe. Seules leurs consommations énergétiques différent.

Concernant l'implémentation global, celles-ci doivent être optimisées pour être plus compactes, plus efficaces énergétiquement, plus performantes, et devenir insensible aux altérations induites par le béton (notamment humide).

Enfin, les nœuds communicants n'ont pas le même degré de maturité. Les deux implémentations permettent de récupérer, traiter et stocker les données envoyées par les nœuds de mesure et d'alimenter à distance ces derniers par un système de transmission d'énergie sans fil, mais seule l'implémentation en LoRaWAN propose la mise en réseau des nœuds communicants, ainsi qu'un interfaçage avec le monde numérique *via* Internet et avec les utilisateurs, localement et à distance, formant ainsi un système cyber-physique complet.

La deuxième partie concerne le positionnement de la solution proposée dans l'état de l'art des solutions de suivi de l'état de santé structurelle des éléments et/ou constructions en béton armé.

La solution présentée tend à concevoir et implémenter un béton armé communicant. Il s'agit donc d'un béton armé non-intrinsèquement auto-mesurant (par des techniques non-destructives) et stockant de la donnée (dans la matière), basé sur l'emploi d'un réseau de capteurs sans fil embarqué (et en grande partie enfoui) et dédié au suivi de l'état de santé structurelle du béton armé durant toute sa vie (plusieurs décennies) et pour chaque étape de son cycle de vie (fabrication, (stockage,) (transport,) construction, exploitation, démolition, recyclage). Ce réseau de capteurs sans fil a des besoins énergétiques limités et utilise des nœuds de mesure sans batterie, et alimentés sans fil et à distance par transmission d'énergie électromagnétique rayonnée. Chaque cellule du réseau (un nœud communicant et plusieurs nœuds de mesure) suffit à couvrir un volume de plusieurs mètres de rayon, à la fois pour les communications sans fil et pour la transmission d'énergie sans fil. Enfin, son utilisation ne requiert ni intervention humaine, ni équipement extérieur, et est indépendante de l'environnement et de l'application visée.

Aujourd'hui les bétons intrinsèquement et non-intrinsèquement auto-mesurant n'en sont qu'au stade d'études en laboratoire et ne sont capables ni de collecter, ni de stocker, ni de transmettre des données sans l'utilisation d'équipements externes complexes, coûteux financièrement et en énergie, et nécessitant l'intervention d'opérateur(s).

Concernant les quelques solutions passives, celles-ci sont également au rang d'études en laboratoire et ne sont capables ni de collecter, ni de transmettre des données (sur de courte distances) sans l'utilisation d'un lecteur externe usité par un opérateur qui doit connaitre leur localisation. De même, elles ne permettent pas de stocker de grandes quantités de données.

Pour ce qui est des solutions basées sur les réseaux de capteurs sans fil, la majeure partie se base sur l'utilisation d'un *datalogger* sans fil, positionné en surface de l'élément en béton armé, et parfois enfouis à une profondeur de quelques centimètres, et sur lequel sont connectés en filaire un ou des capteurs (enfouis ou positionnés en surface). Ces solutions nécessitent d'être installées manuellement (ce qui est long et onéreux), usent généralement de batteries qui ont une durée de vie limitée, et ne sont dédiées qu'à une unique étape du cycle de

vie (généralement la fabrication ou une courte période de l'exploitation). Peu de ces solutions investigue la récupération de l'énergie ambiante (et généralement seulement l'énergie lumineuse et que très rarement l'énergie mécanique (ou vibratoire)), et uniquement à l'extérieur du béton armé et aux regards de l'environnement et de l'application visés. Une seule propose de recharger sa batterie (enfouie dans le béton) par transmission d'énergie inductive en champ proche (ce qui limite la distance de recharge et impose de connaitre le positionnement du nœud pour le recharger).

La troisième partie présente le positionnement de la solution proposée dans l'état de l'art des solutions de réseaux de capteurs sans fil alimentés par la transmission d'énergie électromagnétique en champ lointain et donc sans fil.

Concernant les rares solutions disponibles dans le commerce, celles-ci sont limitées en termes de distance d'utilisation et d'efficacité, et sont plutôt destinées à augmenter le temps de décharge des batteries employées plutôt que de recharger celles-ci ou d'alimenter le système en continu sur des distances de plusieurs mètres. De plus, pour une recharge efficace, des distances de quelques dizaines de centimètres sont recommandées.

Concernant les solutions académiques, il existe quelques implémentations de nœuds sans fil sans batterie, alimentés par la transmission d'énergie électromagnétique en champ lointain et communicants avec des technologies de LPWAN ou de WPAN. Ces implémentations répondent au paradigme de transmission simultanée d'informations et d'énergie sans fil, par du multiplexage fréquentiel et/ou spatial. Certaines de ces solutions visent des applications de suivi de l'état de santé structurelle des infrastructures civiles, mais sont uniquement déployées en surface de structures préexistantes et peuvent nécessiter l'utilisation de véhicules (voiture ou drone) pour assurer la transmission de l'énergie et la récupération des données sur des distances réduites.

Certains travaux traitent également, théoriquement et expérimentalement, de la transmission d'énergie à travers les bétons armés, à la fois en champ proche et en champ lointain, mais ne considèrent pas de charges réelles, tels que des nœuds sans fil.

Ainsi, la solution proposée, uniquement basée sur des composants sur étagère, permet contrairement aux autres implémentations : l'utilisation d'une unique antenne pour les communication et la transmission d'énergie sans fil qui ont lieu dans la même bande de fréquences, grâce à l'utilisation d'un circulateur radiofréquence ; le déploiement d'un système cyber-physique complet composé de plusieurs nœuds communicants et de mesure, et spécifiquement conçu pour répondre aux besoins du suivi de l'état de santé structurelle des bétons armés durant toute leur vie ; le déploiement et l'utilisation de nœuds de mesure embarqués (car pas encore enfouis) à l'intérieur d'une poutre en béton armé ; et le contrôle de la périodicité de fonctionnement des nœuds de mesure n'est pas réalisé logiciellement (comme la très grande majorité) mais uniquement par le contrôle de l'énergie transmise par les nœuds communicants.

Aux regards des distances d'utilisation, limitée par la distance de transmission d'énergie sans fil (elle-même limitée par les réglementations plus que par les contraintes technologiques), celle proposée est parmi les plus élevées et se chiffre en plusieurs mètres. Les rares solutions proposant des distances supérieures se basent sur l'utilisation d'une PMU non-disponible dans le commerce et conçue pour répondre spécifiquement et efficacement à des besoins précis. Quoiqu'il en soit, en optimisant la solution proposée (en particulier en utilisant des composants nécessitant moins d'énergie pour fonctionner (en particulier la PMU) et ayant moins de pertes (en particulier l'élément de stockage de l'énergie), mais également étant plus efficaces (en particulier la rectenna)), des portées plus élevées semblent

atteignables. De même, en réduisant l'énergie requises par les composants actifs, il est possible de réduit les temps de première charge et de recharge.

La quatrième et ultime partie traite des aspects de sécurité bas niveau pour les solutions de communication sans fil LoRaWAN et Bluetooth Low Energy. Cela concerne l'étude des éléments de sécurité prévus par les standards, des principales vulnérabilités et attaques connues, des solutions de défense envisageables, mais également l'analyse de la sécurité dans le cadre du projet McBIM.

Dans une première sous-partie, la technologie de communication sans fil LoRaWAN est étudiée aux vues des éléments de sécurité prévus par son standard, des principales vulnérabilités connues, et des attaques les plus communes en son encontre, ainsi que leurs impacts.

Dans une deuxième sous-partie, la technologie de communication sans fil Bluetooth Low Energy est étudiée aux vues des éléments de sécurité que prévoit son standard, des principales vulnérabilités connues, et des attaques les plus communes en son encontre, ainsi que leurs impacts.

Dans une troisième et dernière sous-partie, ce sont les aspects de sécurité bas niveau propre au projet McBIM qui sont traités. Il est notamment question : des objectifs malicieux les plus probables (l'altération de la propriété des données, l'altération de la disponibilité du service et des données, l'interruption totale du service et de l'accès aux données) ; des modèles de menaces les plus probables (en termes de localisation et de moyens employés) ; de la définition et de la quantification des risques associés aux attaques (concernent l'altération de la propriété des données, l'altération de la disponibilité du service et des données, et l'interruption totale du service et de l'accès aux données) ; des solutions techniques envisageables (la cryptographie, l'emploi d'un élément de sécurité, l'utilisation de système de détection des intrusions) ; et de l'impact de l'utilisation des éléments de sécurité que prévoit les standards sur les risques associées aux principales attaques.

IX. Conclusion

Au cours de cette thèse de doctorat, plusieurs travaux ont été réalisés afin d'apporter une solution matérielle à la mise en œuvre d'un béton armé communicant. La solution proposée est basée sur un réseau de capteurs sans fil à deux couches, destiné à être embarqué dans du béton armé. Ce réseau est composé de deux types de nœuds : les nœuds communicants et les nœuds de mesure.

Les nœuds communicants, considérés comme accessibles et alimentés par une source d'énergie illimitée, sont dédiés à la collecte, au traitement et au stockage des données reçues des nœuds de mesure, ainsi qu'au partage de ces données au sein d'un réseau maillé de nœuds communicants, avec le monde numérique *via* Internet, et localement et/ou à distance avec les différents utilisateurs. De plus, les nœuds communicants doivent être capables (en utilisant une source d'énergie électromagnétique rayonnante dédiée) d'alimenter sans fil les nœuds de mesure situés autour d'eux et dans un volume de plusieurs mètres de rayon.

Deux implémentations des nœuds communicants ont été fournies, avec différentes technologies de communication sans fil utilisées entre les nœuds de mesure et les nœuds communicants, respectivement LoRaWAN et Bluetooth Low Energy. Dans leur mise en œuvre la plus avancée, les nœuds communicants sont capables de recevoir toutes les données envoyées par les nœuds de mesure, de les traiter localement, de les stocker localement et à distance, et de les partager : dans un réseau réduit de nœuds communicants ; avec le monde

numérique *via* Internet ; et localement et à distance avec les parties prenantes. De plus, grâce à l'utilisation d'une source d'énergie électromagnétique rayonnante, les nœuds communicants peuvent alimenter sans fil tous les nœuds de mesure qui se situent dans leur voisinage et à plusieurs mètres, même si ceux-ci sont placés dans une poutre en béton armé ou positionnés à la surface d'un mur lui-même en béton armé.

Les nœuds de mesure, considérés comme inaccessibles une fois déployés car entièrement enfouis dans le béton armé, sont dédiés à la mesure des propriétés du béton armé et/ou de son environnement. Ils doivent être sans batterie, autonomes en énergie et fonctionnels pendant toute la durée de vie du béton armé, c'est-à-dire pendant des décennies.

Deux implémentations des nœuds de mesure ont été fournies, avec différentes technologies de communication sans fil utilisées pour transmettre les données collectées aux nœuds communicants, respectivement LoRaWAN et Bluetooth Low Energy. Dans les deux implémentations, les nœuds de mesure sont capables de mesurer plusieurs paramètres de l'état interne du béton armé : tels que sa température, son humidité relative, sa résistivité électrique, ou sa déformation mécanique en un point donné. Ces données sont utiles pour estimer la santé structurelle du béton armé considéré, en particulier grâce à l'estimation de son taux de corrosion. Les données collectées sont ensuite prétraitées et transmises sans fil aux nœuds communicants. De plus, les nœuds de mesure sont sans batterie, peuvent démarrer à froid et sont capables de récolter l'énergie électromagnétique rayonnée générée par les nœuds communicants sur plusieurs mètres -même s'ils sont encastrés dans une poutre en béton armé- jusqu'à en avoir assez pour réaliser un traitement complet, et ce même à partir d'un dispositif de stockage d'énergie complètement vide. Afin de réduire la consommation d'énergie des nœuds de mesure, seule la voie montante (c'est-à-dire des nœuds de mesure vers les nœuds communicants) est mise en œuvre pour la transmission de données. La voie descendante (des nœuds communicants aux nœuds de mesure) est uniquement utilisée pour la transmission d'énergie sans fil. En outre, en contrôlant la source d'énergie électromagnétique rayonnante, les nœuds communicants peuvent -à distance- contrôler grossièrement la périodicité de fonctionnement des nœuds de mesure. Parce qu'ils sont essentiellement hors tension, sans batterie, alimentés sans fil et conçus aussi simplement que possible, les nœuds de mesure devraient pouvoir fonctionner de manière fiable sur le long terme. La défaillance d'un composant électronique liée à l'âge semble être la cause la plus probable d'une défaillance complète des nœuds de mesure. Enfin, les nœuds de mesure ont été conçus pour être suffisamment compacts pour pouvoir être enfouis dans le béton armé sans que ses propriétés mécaniques n'en soient fortement altérées. Dans la mesure du possible, les nœuds de mesure utilisent une antenne unique à la fois pour la communication sans fil et pour la collecte de l'énergie électromagnétique.

Les tests des différentes implémentations ont permis le déploiement d'une preuve de concept du réseau de capteurs sans fil imaginé et ciblé. Celui-ci est composé de deux nœuds communicants et de quatre nœuds de mesure situés dans une poutre en béton armé ou dans une grande pièce, mesurant certains paramètres (par exemple la température, l'humidité relative, la résistivité électrique, ou la déformation mécanique) dans ou autour du béton armé, et les transmettant aux nœuds communicants. Les nœuds communicants collectent, traitent, stockent et partagent entre eux, avec des serveurs distants (*via* Internet) et/ou avec les utilisateurs, les données envoyées par les nœuds de mesure. Les communications sans fil sont réalisées sur plusieurs mètres, mais peuvent être étendues à des dizaines ou centaines de mètres (même en intérieur) grâce à la technologie LoRaWAN, tandis que la transmission d'énergie sans fil est actuellement limitée à quelques mètres. La portée maximale testée avec

succès pour la transmission d'énergie sans fil est de 7 mètres dans l'air, mais des portées plus élevées sont attendues.

Bien que des résultats encourageants aient été obtenus, plusieurs axes de progression ont été définis tout au long du manuscrit. Ainsi, et entre autres, la portée d'utilisation et l'efficacité énergétique de nœuds de mesure pourraient être augmentées en utilisant des composants moins gourmands en énergie et des rectennas plus performantes ; les temps de première charge et de recharge des nœuds de mesure pourraient être réduits en limitant le besoin énergétique global ; les nœuds de mesure et de communication pourraient être améliorés pour être plus compacts, consommer moins d'énergie et fournir toutes les fonctionnalités requises par l'application visée ; etc.

En ce qui concerne la surveillance du béton armé, une solution innovante et à faible coût a été proposée. Celle-ci est sans fil, entièrement intégrée et enfouie dans le béton armé, déployable à long terme, alimentée sans fil, et basée principalement sur l'utilisation de capteurs appropriés aux applications ciblées. À notre connaissance, il s'agit du premier nœud de mesure sans batterie et alimenté sans fil par des ondes électromagnétiques rayonnées (*i.e.* en champ lointain) conçu pour être enfoui dans du béton (armé) afin de surveiller la santé structurelle de ce dernier durant toute sa vie.

Finalement, les solutions proposées peuvent être adaptées à d'autres applications et cas d'étude, avec divers capteurs et/ou actionneurs, et dans différents domaines.

En ce qui concerne la transmission d'énergie sans fil, la solution proposée se situe dans l'état de l'art en termes de performances, en particulier en ce qui concerne sa portée d'utilisation ; elle met à disposition une nouvelle technologie de communication sans fil ; elle permet la mise en œuvre d'un système cyber-physique complet basé sur un réseau de capteurs sans fil à deux couches ; et elle répond aux exigences du paradigme de la transmission simultanée d'informations et d'énergie sans fil.

Pour aller plus loin, plusieurs technologies innovantes et à la pointe du progrès pourraient être utilisées pour améliorer la solution actuelle, telles que : l'utilisation de techniques de *beamforming* à la fois pour la communication sans fil et la transmission d'énergie sans fil ; l'utilisation de substrats flexibles et/ou d'impression 3-D et/ou de techniques additives pour la fabrication des nœuds de mesure et de communication ; ou encore, la conception d'un circuit intégré spécifique à l'application (ASIC) performant, dédié à la communication sans fil, à la transmission d'énergie sans fil et aux systèmes de mesure, et si possible compatible avec des capteurs intégrés sur puce.

Acknowledgements

First of all, I would like to sincerely thank my doctoral thesis supervisors Prof. Daniela DRAGOMIRESCU and Assoc. Prof. Alexandru TAKACS for having trusted me and given me the opportunity to successfully complete my doctoral thesis, but also for their valuable support and help, and for all the time they gave me.

All my gratitude must be expressed to all the members of my jury for accepting to examine and evaluate my doctoral work, especially to Prof. Ke WU (Ecole Polytechnique de Montréal, Canada) for chairing my thesis defence, to Prof. Nuno BORGES DE CARVALHO (University of Aveiro, Portugal) and Prof. Alessandra COSTANZO (University of Bologna, Italy) for their report on the manuscript, and to Mr. Vincent LE CAM for his participation and feedbacks.

I would also like to express my deepest thanks to Prof. Florin UDREA, Dr. Andrea DE LUCA and Ethan GARDNER, for their valuable help in the work on the thermodiodes; as well as all the members of the High Voltage Microelectronics & Sensors (HVMS) group that I met, for their welcome at the Centre for Advanced Photonics and Electronics (CAPE) of the University of Cambridge (United-Kingdom).

A huge thanks must be given to Prof. Jean-Paul BALAYSSAC from the Laboratory for Materials and Durability of Constructions (LMDC, Toulouse, France) for its valuable help in the work on the measurement of the resistivity of concrete, and for the loan of a GPR (ground penetrating radar).

I would also like to thank all the partners of the McBIM project, especially Assoc. Prof. William DERIGENT, Prof. André THOMAS, Assoc. Prof. Michael DAVID, Prof. Hind BRIL EL HAOUZI, and Dr. Hang WAN from the Research Centre for Automatic Control in Nancy (CRAN, Nancy, France); Assoc. Prof. Ana-Maria ROXIN, Prof. Dominique GINHAC, and Assoc. Prof. Wahabou ABDOU from the Computer Science Laboratory of Burgundy (LIB, Dijon, France); and Mr. Rolland MELET, Mr. Laurent MONTEGUT and Mr. Jorge-Luis ACOSTA from FINAO SAS/360SmartConnect (Trans-en-Provence, France).

I thank all the members of the MINC (MIcrosystems and Nanosystems for wireless Communications) team in LAAS-CNRS (Laboratory for Analysis and Architecture of Systems of the French National Centre for Scientific Research, Toulouse, France), including its scientific managers: Prof. Hervé Aubert, Assoc. Prof. Marjorie Grzeskowiak, and Prof. Patrick Pons; and its doctors, PhD students, post-doctoral fellows and engineers, but also friends (alphabetic order): Mohammad Abokasem, Bilel Achour, Bilal Benamrouche, Guilherme Buchmeier, Mathieu Chalnot (and Lucile), Maria Valéria De Paoli, Alexandre 'Poussin' Dore, Ahmad El Sayed Ahmad, Dominique 'Dodi' Henri (and Sandrine), Mathilde Lacombrade, Timothée 'Tim' Marchal, Alexandre Monti, Abderrahim Okba, Julien 'Papy' Philippe (and Germercy), Jérôme 'Capitaine' Riondet (and Clothilde), Antoine Roturier, Benoît Rougier, Kevin Sanchez Basse, and Alassane Sidibé.

I would also like to thank all those not yet mentioned but who helped me, as researcher: especially Assoc. Prof. Eric Alata and Assoc. Prof. Christophe Escriba; as engineer: particularly Mr. Alexandre Rumeau; but also, as student (chronological order): Alexandre Regnère, Philippe Hérail, Raktawan Poolsuwan, Clarisse Erpeldinger, Youssouf Souley Iro, Juliette Ikina and Clément Auter.

I thank also all those from the LAAS-CNRS and from the National Institute for Applied Sciences (INSA, Toulouse, France) for their time, help and/or support, in particular the teaching team, the different support and administrative teams, Marie Estruga, Anaïs Moulis and the rugby team of the LAAS-CNRS (Baptiste, Denis, Paul, Raphaël, and all the others).

My warmest thanks must be given to my family (Papa, Maman, Ronan (and Naia), but also grandparents, uncles, aunts and cousins, as well as Patrick, Françoise and Léa) and friends (Marie, Thomas, David, Maxime and Etienne) for their never faulting encouragement and support.

Last but not least: Lyne, thank you for everything!

Thank you all!

Table of contents

Table of figures

Table of tables

Table of codes

Glossary

16-QAM	16-states quadrature amplitude modulation
64-QAM	64-states quadrature amplitude modulation
3D	three-dimension(al)
3GPP	third-Generation Partnership Project
8DPSK	8 states differential phase-shift keying
8-OPSK	8 states orthogonal phase-shift keying
8-PSK	8 states phase-shift keying
ABP	activation by personalisation
AC	alternative current
ADC	analogue-to-digital converter
ADS	Advanced Design System
AES	advanced encryption standard
AET	acoustic energy transmission
AM	air mass
ANR	French National Research Agency
API	application programming interface
ARCEP	*Autorité de régulation des communications électroniques, des postes et de la distribution de la presse*
ASIC	application-specific integrated circuit
ASK	amplitude-shift keying
B	bytes
BAN	body area network
BIM	building information modelling
BLE	Bluetooth Low Energy
bps	bits per second
BPSK	binary phase-shift keying
CDPI	ceramic dual inline package
CdTe	Cadmium-Telluride
CIGS	Copper-Indium-Gallium-di-Selenide
CMOS	complementary metal oxide semi-conductor
CN	communicating node
COM	communication
CPS	cyber-physical system
CRAN	Research Centre for Automatic Control in Nancy
CRC	cyclic redundancy check
cron(tab)	chrono table
CSK	colour shift keying
CSMA/CA	carrier sense multiple access with collision avoidance
CSS	chirp spread spectrum
DAC	digital-to-analogue converter
DBPSK	differential binary phase-shift keying
DC	direct current
DOS	denial of service
DQPSK	differential quadrature phase-shift keying
DSSS	direct-sequence spread spectrum

DS-UWB	direct sequence
e.g.	*exempli gratia*
EC	European Commission
ECC	Electronic Communications Committee
EDLC	electric double layer capacitors
EHF	extremely high frequency
EIRP	effective isotropic radiated power
ERC	European Research Council
ERP	effective radiated power
etc.	*et cetera*
ETSI	European Telecommunications Standards Institute
FAQ	frequently asked questions
FDMA	frequency division multiple access
FFD	full-function device
FHSS	frequency-hopping spread spectrum
FM	frequency modulation
FR4	flame resistant 4
FSK	frequency-shift keying
G	generation
GaAs	Gallium-Arsenide
GaN	Gallium Nitrite
GAP	generic access profile
GATT	generic attribute
GFSK	gaussian frequency-shift keying
GMSK	gaussian minimum-shift keying
GPIO	general purpose input/output
GPR	ground penetrating radar
GPS	global positioning system
GPSK	gaussian phase-shift keying
HF	high frequency
HFSS	High-Frequency Structure Simulator
HRWLAN	high rate wireless personal area networks
i.d.	*id est*
I²C	inter-integrate circuit
I²S	inter-IC sound
IDE	integrated development environment
IDS	intrusion detection system
IEC	International Electrotechnical Commission
IEEE	Institute of Electrical and Electronics Engineers
IFC	Industry Foundation Classes
INSA	National Institute for Applied Sciences
IoT	Internet of things
IR-UWB	impulse radio ultra-wide band
ISM	industrial, scientific and medical
ISO	International Organization for Standardization
ITU	International Telecommunication Union
JSON	JavaScript object notation
JTAG	joint test action group

LAAS-CNRS	Laboratory for Analysis and Architecture of Systems of the French National Centre for Scientific Research
LDO	low dropout
LED	light-emitting diode
LF	low frequency
LIB	Computer Science Laboratory of Burgundy
LMDC	Laboratory for Materials and Durability of Constructions
LoRa	long range
LoRaWAN	long range wide area networks
LPT	laser power transmission
LPWAN	low-power wide area networks
LRWPAN	low rate wireless personal area network
M2M	machine-to-machine
MAC	medium access control
MB-UWB	multi-band ultra-wide band
MBWA	mobile broadband wireless access
McBIM	Material communicating with the Building Information Modelling
MCU	microcontroller unit
MEMS	microelectromechanical systems
MIC	message integrity code
MIFA	meandered inverted-f antenna
MPPT	maximum power point tracking
MQTT	message queuing telemetry transport
NFC	near-field communication
NREL	National Renewable Energy Laboratory
OFDM	orthogonal frequency-division multiplexing
OFDMA	orthogonal frequency-division multiple access
OOK	on/off-keying
O-PSK	orthogonal phase-shift keying
O-QPSK	orthogonal quadrature phase-shift keying
OS	operating system
OSI	open systems interconnection
OTAA	over-the-air activation
PC	personal computer
PCB	printed circuit board
PER	packet error rate
PET	Polyethylene Terephthalate
pH	potential of Hydrogen
PIFA	planar inverted-F antenna
PIN	personal identification number
PMIC	power management integrated circuit
PMU	power management unit
PPM	pulse-position modulation
PSSS	parallel sequence spread spectrum
PVDF	Polyvinylidene Fluoride
PZT	Lead-Zirconate-Titanate
QAM	quadrature amplitude modulation
QPSK	quadrature phase-shift keying

RF	radiofrequency
RFD	reduced-function device
RFID	radiofrequency identification
RSSI	received signal strength indication
SC-FDMA	single-carrier frequency division multiple access
SD	secure digital
SDR	software defined radio
SE	secure element
SHF	super high frequency
SHM	structural health monitoring
SiO2	Silicon Dioxide
SMA	subminiature version A
SN	sensing node
SoC	system-on-chip
SOFDM	spread orthogonal frequency-division multiplexing
SOI	Silicon-on-insulator
SPI	serial peripheral interface
SSH	secure shell
SWD	serial wire debug
SWIPT	simultaneous wireless information and power transmission
TCL	tool command language
TDMA	time-division multiple access
TEG	thermoelectric generator
TH-UWB	time hopping ultra-wide band
U.S. DoD	United States of America Department of Defence
UART	universal asynchronous receiver transmitter
UAV	unmanned aerial vehicle
UDP	user datagram protocol
UHF	ultra-high frequency
URL	uniform resource locator
USB	universal serial bus
USRP	universal software radio peripheral
UWB	ultra-wide band
VCO	voltage control oscillator
VHF	very high frequency
VNA	vector network analyser
VPN	virtual private network
VVA	voltage variable attenuator
Wi-Fi	wireless fidelity
WLAN	wireless local area network
WMAN	wireless metropolitan area network
WPAN	wireless personal area network
WPT	wireless power transfer (or transmission)
WRAN	wireless regional area network
WSN	wireless sensor network
π/4-DQPSK	π/4 offset differential quadrature phase-shift keying

I. Introduction

The McBIM project (Communicating Material within the Building Information Modelling) has for main purpose to propose an implementation of the concept of communicating materials in the civil engineering industry. A communicating material is a material intrinsically able to sense its own internal properties, and to process, store and share data, both with the physical and digital worlds. Being the most used building materials around the world, the concretes, and more specifically the reinforced concretes, are the perfect candidates to this implementation. Moreover, these have a lifespan of several decades and must be monitored during all along it to avoid failures, which can lead to material and human disasters. Thus, a communicating reinforced concrete able to monitor itself and interfaced with the digital world, especially with a Building Information Modelling, is targeted.

Within the McBIM project, this doctoral thesis has to provide a hardware solution to design and implement this communicating reinforced concrete. The proposed and presented solution is based on a two-layer wireless sensor network, composed of two kinds of nodes: the sensing nodes and the communicating nodes. The sensing nodes are fully buried in the reinforced concrete, thus inaccessible, and deal with the measurements of the properties of the reinforced concrete. The transmission of the collected data is achieved by a wireless communication and their energy autonomy is possible thanks to a battery-free architecture and the possibility of harvested the radiative electromagnetic power. The communicating nodes, less constrained because accessible, deal with the processing, the storage and the sharing of the collected data transmitted by the sensing nodes, with both the physical world (through a meshed network of communicating nodes) and the digital worlds (through the Internet). More, these power wirelessly the sensing nodes and wirelessly control their periodicity of measurement and communication, thanks to the use of a wireless power transfer system, based on the generation of radiative electromagnetic waves.

The second chapter compiles the state-of-the-art of the five domains considered in this doctoral thesis:

* the reinforced concretes, that we want to make communicating, and whose the physical (especially the electromagnetic) properties constraint both the design and the implementation of the proposed solutions;
* the methods to evaluate the reinforced concretes, that we want to implement through an innovative wireless and energy autonomous way, especially for long-term structural health monitoring applications;
* the wireless communication technologies, that we want to use to transmit and share various data through the reinforced concretes, which are unusual mediums of propagation;
* the energy harvesting and the wireless power transfer solutions, that we want to use to assure the energy autonomy and a long lifespan to our system;
* and the communicating materials, which are the link between the four other domains.

The third chapter contextualises this doctoral thesis by introducing the McBIM project (and its research consortium) in which it takes place, and describes the hardware architectures of the proposed solution to make communicating the reinforced concretes. Some technology choices will be presented in the next chapters, when met.

The fourth chapter deals with the design and the implementation of the communicating nodes based on the LoRaWAN wireless communication technology, whose the role is to aggregate, process and store the measured data sent by the sensing nodes, and to remotely and wirelessly power these last.

The fifth chapter presents the design and the implementation of the sensing nodes based on the LoRaWAN wireless communication technology. These are the core of the proposed solution and the more challenging: these must be buried into the reinforced concrete (thus, inaccessible); must measure relevant parameters in order to achieve the structural health monitoring of the reinforced concrete; must wirelessly transmit data from and through the reinforced concrete, and also, be energy autonomous for the entire lifetime of the reinforced concrete. This last aspect will be treated by the use of the wireless power transfer over several metres, and with an architecture as reliable as possible.

The sixth chapter deals with the first works carried out to design and implement communicating nodes based on the Bluetooth Low Energy wireless communication technology; whilst the seventh chapter presents the first works performed to design and implement sensing nodes based on the Bluetooth Low Energy wireless communication technology.

The eighth chapter concludes by comparing the two proposed and implemented solutions, and by positioning these in the state-of-the-art solutions for both the structural health monitoring of the reinforced concretes, and the wireless sensor networks wirelessly powered. Ultimately, a study of the low-level security aspects proposes a new point of comparison between the LoRaWAN and the Bluetooth Low Energy wireless communication technologies.

Even though the ultimate targeted application of these works is the implementation a communicating reinforced concrete to ensure its structural health monitoring and traceability throughout its life, the designed and implemented solutions can also be moved to other applications, with various sensors and/or actuators, in different industrial, consumer and engineering areas. Thus, several case studies can be imagined: ensuring the traceability of various products or materials; tracking assets; monitoring industrial machines, industrial infrastructures or industrial (harsh or hazardous) environments, civil engineering structures, vehicles, human performances (e.g. cycling, etc.), fluid levels, natural environments, etc.; wirelessly powering, or fully or partially recharging devices (such as weather stations, intrusion detectors and sound alarms, watches, alarm clocks, peripheral devices (keyboards, mice, earphones, controllers, etc.), cards, smartphones, night lights, tiny pumps, etc.); etc. The main current limitations concern the ranges of use and the powers involved, which are restricted both by the current regulations and by the energy efficiency of some components employed.

II. States of The Art

At the crossroads of several domains, our works within the framework of the McBIM project must be considered through several criteria.

First, the targeted material: the reinforced concretes; widely used around the world and whose the physical properties impose some constraints that must be considered in the choice and implementation of solutions.

Next, the main targeted application: the structural health monitoring (SHM); which rests on different methods for testing.

Then, the targeted technology: the wireless communication; whose the properties must meet the requirements induced by the media of propagation (the reinforced concretes) and the needs of the applications (especially for the structural health monitoring).

Lastly, a further constraint: the energy autonomy; that would allow to use our solution for the entire lifetime of the structure under surveillance, that says for decades.

A. Concrete materials

1. An introduction: uses, recipes and physical properties

Concretes are composite materials essentially used in the construction domain (e.g. for buildings, bridges, engineering structures, water tanks, foundations, roads, etc.) which find their origin in "primitive" lime mortars widely used for thousands of years [1-5].

They are composed of aggregates bonded with a binder. These aggregates come in various sizes and shapes (from fine to coarse and from rolled to crushed) and are mainly mineral (from sands to stones, through gravels), but can be in particular cases vegetable (wood, sawdust, vegetal, etc.) or synthetic (polystyrene, etc.). A mixture of cement and water is usually used as binder, but other binders (lime, asphalt, polymers, etc.) can be used for special purposes. For the usual case, this mixture of cement and water will chemically interact in an exothermal reaction and by hardening -during a phase named curing- will form a solid stone-like material. By adding more water than needed for the reaction, it is possible to obtain a fluid material which can be poured and moulded to form specific elements with more or less complex geometry (beams, walls, stairs, bridge deck, etc.). Some admixtures (plasticizers, air-entraining agents, silica fumes, fly ashes, etc.) can be added in the mixture in order to modify some physical properties of the fresh and/or cured concrete.

It exists hundreds of different concrete recipes that differ in the proportions of their components (very approximately: 70% of aggregates, 20% of water and 10% of cement), in the properties of their components (for the aggregates: their size, their weight, their disparity, their repartition, their material, etc.; for the binder: its nature, its kind, etc.; for the admixtures: their kind, their quantity, their proportion, etc.) and in the environmental conditions of the curing process (especially in terms of temperature and humidity). All that allows to obtain a wide range of materials with various properties which meet various specified requirements [1-5]. A generic composition of the main concretes is shown in Figure II.1. Thus, there is a large number of standards dedicated to the manufacture of concrete elements [6-9]. To certify these standards, extensive controls must be achieved during all the manufacture (respect of the

recipe, mixing conditions, moulding conditions, etc.) and curing (duration, temperature, humidity, etc.) processes, but even during all the life of the elements. In order to design and choose the appropriate recipe for an element, its actual strength must be estimated by considering the mechanical constraints in the nominal case and in hypothetical overload stages significantly above the previous one [1-5]. This design method that considers an overestimation of the constraints that will be applied to the structure to provide significant margins and avoid failure and distresses during all the lifecycle of the structure -even in the worst cases- is called "strength design".

Concrete materials are the most frequently used materials in the construction domain with almost ten billion of cube-meters produced each year worldwide [10]. This plebiscite can be explained by several elements [1-5]. First, it is an economic material, whose the main components (aggregates and water) are in general worldwide locally available at low-costs. Then, concretes are highly resistant to fire and harsh weathers. Moreover, even if their workability decreases during their curing, their compressive strength increases during all the hardening process which can take several years, and so, can reach higher values than the designed one. Conversely, their tensile strength is relatively low. In order to improve the properties in tension of the concretes, their strain resistance and their durability, reinforcing materials (metallic rebars, metallic matrixes, etc.) are embedded to generate more complex composite materials called reinforced concretes. Another solution to increase the tensile strength, the ductility, the resistance, the durability, but even reduce long-term wears, micro-cracks and abrasion of the concretes is to embed fibres (metallic, organic or mineral) to yield fibered concretes. Finally, it is possible to prestress the concretes to produce prestressed (eventually, reinforced or fibered) concretes. A compressive force is applied to the concretes by embedded metallic cables to create an offset in compression which will limit the effects of tensile stresses. This also reduces deflections and tensile cracks at ordinary loads. In spite of the wide use of concrete materials, researches on their environmental impact (in particular with regard to their energy and resources consumption, and their carbon dioxide emissions), on alternatives and on methods for improving their recycling are conducted [10-16].

Structures made of concretes may be defective from various causes and generate real human and material catastrophes [17]. It could be a design defect: e.g. underestimation of the nominal load, and thus, of the actual strength, non-compliance with the strength design procedure and/or standards, failure to consider specific constraints as seismic, etc.; either a defect during the implementation: non-compliance with the recipe, poor distribution of the aggregates and/or high presence of air bubbles, poor curing due to non-controlled environmental parameters (especially temperature and humidity), etc.; or finally a monitoring or warning defect during the service phase of the structure. Indeed, during their ageing, concrete materials evolve and may present defaults. The main defaults are cracks and delamination which weaken the materials and limit their strength. Different sources, generally related, induces these defects. These can be chemical: carbonation, alkali-, sulphate- and alkali-silica- reactions, corrosion of the embedded metallic elements, etc.; environmental: immersion in water or high humidity level, frost or thermal shocks, earthquakes, etc.; or mechanicals: vibrations, shocks, etc.

All materials can be characterized in terms of electromagnetic properties, which include the dielectric permittivity -ability to oppose an electric field- (whose the real part in called "dielectric constant" and the imaginary part "dielectric loss", expressed as "loss tangent"), the

electrical conductivity or resistivity -ability to conduct, respectively to stop, an electric current- and the magnetic permeability -ability to create a magnetic field in response to an applied magnetic field-. In the case of the propagation of electromagnetic waves (e.g. for wireless communication or wireless power transfer), only the dielectric properties can be considered. For concrete materials, the dielectric permittivity is strongly related to the water concentration, to the free-ions concentration for some frequencies, to the frequency of the electromagnetic waves, but even their composition and particularly their water to cement ratio in correlation with the relative humidity of the environment. [18-35]. For instance, the more water there is, the higher the dielectric constant and loss are. Thus, more the concretes are cured, the less concentrated the water is, and lower the dielectric properties are. The fact that the dielectric properties are function of the frequency is named "dispersion" and concrete materials are qualified as dispersive. This characteristic is also linked to the water and free-ions concentrations: the more concentrated the water and free-ions, the more dispersive the concrete. More, the dielectric permittivity of concrete materials, as heterogenous material, is linked to their composition, to the nature and the dielectric properties of each of their components. If the wavelength of the electromagnetic waves is comparable to the size of the aggregates or metallic elements embedded in the binder, electromagnetic reflections, diffusions, diffractions, refractions, multipaths and interferences could appear. These effects can be negligible and the concrete materials considered as quasi-homogenous if the largest aggregate is well below the wavelength. In the same way, if the element made of concrete material is much smaller than the wavelength, this one can be invisible for the electromagnetic waves. Thus, lower the frequency, higher the wavelength, less the concrete impacts electromagnetic waves. Because of the wide variety of concrete materials, with wide variation in composition and hydration, so, there is no generic values for the dielectric properties. Nevertheless, in the published experimental results, the dielectric constant is on average between 4 and 20 and the loss tangent between 0.1 and 0.3, but extensively related to the water and free-ions concentrations and the frequency of test. Thus, the concrete materials are harsh and inhomogeneous propagation media for a large part of the electromagnetic waves.

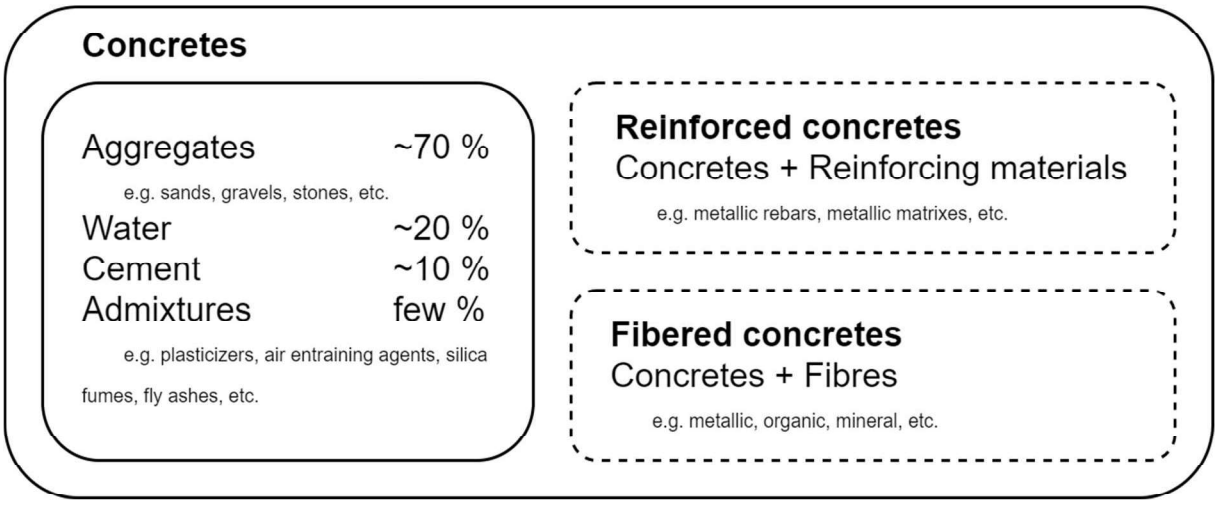

Figure II.1: Generic composition of the concrete materials.

2. Smart concretes

In order to improve, at low cost, the performances, the workability, the serviceability, the safety, the reliability, and/or the sustainability, enhanced concretes are designed by altering their composition. These have particular properties as the ability to react at defined stimuli, in order to meet specific requirements. Thus, these are considered as intelligent, and thus, called "smart concretes". There are several kinds of these smart concretes [36-39].

First, there are intrinsic self-sensing (or self-monitoring, or even self-diagnosing) concretes which can be used as sensors to monitor themselves [37-44]. Thus, the concretes become transducers. It is possible through conductivity/resistivity measurements to quantify elastic and inelastic deformations (or strain), stress, cracks or damages, temperature, humidity, smoke, corrosion, etc. To get these properties, carbon fibres, carbon black, carbon nano-tubes, steel fibres, nickel powder, etc. can be added in the concretes according to the targeted behaviour. By this way, the safety, the reliability and the sustainability can be increased.

Then, the self-healing (or self-repairing) concretes have the properties to repair cracks in a variable amount of time in order to limit damages and recover strength [37-39, 45-48]. There are two types: autogenous and autonomous. For the autogenous, only small cracks can be healed and water is needed. The carbonation, the sealing by water impurities and small concrete losses, the expansion of the hydrated concrete and the hydration of minerals that have not yet reacted are the main mechanisms for autogenous self-healing, that does not need specific admixtures. For the autonomous, admixtures or treatments are required but not always water, and larger cracks can be repaired. The micro-encapsulate agents based, vascular, electrodeposition, microbial, induction energy and embedding shape memory alloys methods are the mains. Again, the safety, the reliability and the sustainability can be increased.

Wear-resisting concretes are designing to resist to the abrasion, the erosion and the cavitation by including (mineral) admixture, latex, microfiber, nanomaterials, etc. [39]. They ensure higher performances and increase the safety, the reliability and the sustainability.

Self-adjusting concretes are able to adapt to loading and environmental changes even in worst cases (e.g. accidental overloads, meteorological disasters (as fires, windstorms, waves, earthquakes, etc.), etc.) [37-39]. It concerns between others self-damping [37-39, 49], temperature self-adjusting [37-39, 50, 51], anti-spalling self-adjusting [37-39, 52] and humidity self-controlling [37-39, 51] concretes. For self-damping concretes, macromolecular admixtures (e.g. polymer latex, silica fumes, methylcellulose, fibres, graphite sheets, etc.) can be used; for temperature self-adjusting, phase change materials; for anti-spalling self-adjusting -especially during fire- organic or polypropylene fibres, air entraining agents or mineral admixtures; and the humidity self-adjusting, zeolite or attapulgite. Additionally, bendable concretes based on engineered cementitious composites have a great ductility (or flexibility) [46, 47, 52-54]. Thus, the performances, the serviceability, the safety, the reliability and the sustainability can be improved.

Vehicles (in particular aircrafts) arresting concretes are designed in order to absorb the kinetic energy of vehicles to slow down and stop them [37-39, 55]. These are manufactured by incorporating foaming agents to generated a lot of spherical, isolated and disorderly

arranged cavities, which will distort without rebounds to convert kinetic energy into deformations. It must be noted that these concretes are essentially single-use.

Electrically conductive concretes are obtained from the addition of electrically conductive fillers [37-39, 56, 57], and are the base for electrothermal (or self-heating) concretes [37-39, 58-61] and electromagnetic waves shielding or absorbing concretes [37-39, 62-64]. Self-heating concretes integrate carbon fibres, steel fibres, steel shaving, nickel powders, graphite, etc. to reduce the resistivity to allow electrical resistance heating based on the Joule effect. Electromagnetic waves shielding concretes use electrically conductive fillers to reflect the waves, whilst the electromagnetic waves absorbing concretes use magnetic loss, dielectric loss and resistive loss fillers to convert and dissipate the electromagnetic energy. The two lasts are used to limit in a wide band the electromagnetic pollution and interferences, and to protect electronics located in the structure.

In a similar way, the radiation shielding concretes are intended to protect from radiations as alpha-, beta-, gamma- and X-rays as well as neutrons due to a high density and a large amount of crystal water [39, 65-68].

There are also light-transmitting and light-emitting concretes [37-39, 69, 70]. Light-transmitting concretes use optical elements, especially optical fibres, to conduct the external light, particularly from the sun, through the element and, to a lesser extent, to conduct heat. Light-emitting concretes use fluorescent powders to collect solar or artificial energy in the light and give off soft visible light in the darkness.

Photocatalytic concretes also use luminous energy but here with a photocatalyst (e.g. titanium dioxide, etc.) added in the recipe in order to realize air depollution, self-cleaning, and self-disinfecting [37-39, 72, 73]. In an alternative way, new approaches to reduce carbon dioxide production during the manufacture of concretes are proposed especially by capturing and trapping it into cements [10, 12, 13, 15, 16, 77-79].

Hydrophobic and superhydrophobic concretes use hydrophobic or respectively superhydrophobic coatings on hardened concretes, or hydrophobic or respectively superhydrophobic admixtures into fresh concretes, in order to be able to repel water [37, 39, 80-83]. Thus, the safety, the reliability and the sustainability can be improved by reducing the water-induced ills as corrosion.

By combining hydrophobic, or superhydrophobic, and photocatalytic properties, it is possible to design self-cleaning concretes [37-39, 84].

At the opposite, permeable concretes contain interconnected voids to allow air and water to evacuate [37-39, 85]. These improve the serviceability, the safety, the reliability and the sustainability.

To go further, non-dispersible underwater concretes are designed by integrating anti-washout admixtures, a kind of water-soluble polymers with long-chain structures and strong absorption capacity [39]. These are self-levelling, self-compacting, low water polluting and easily usable underwater. The performances, the workability, the serviceability, the safety, the reliability and the sustainability are particularly improved for underwater construction.

Next, self-compacting (or self-consolidating) [39, 86, 87], self-expanding (or expansive) [39, 88], self-curing [39, 89] and self-shaping (or printable) [39, 90-92] concretes allow to increase the workability during the manufacturing phase, respectively, by being highly flowable and non-segregating, and spreading into any place by means of its own weight; by volumetrically enlarging during hydration and curing, which can prevent cracks and chemically prestress the element; by optimizing the curing from inside to outside and limiting the self-dehydration; and by being three-dimensional printable even for complex geometries.

Finally, energy-harvesting concretes have the ability to store for reuse ambient energy or even convert ambient energy to electricity [37-39]. The store for reuse strategy is especially used by temperature self-adjusting and light-emitting concretes. The energy converting concretes which provide electricity can used mechanical, thermal or luminous sources, by being respectively based on piezoelectric, pyroelectric or thermoelectric, or photovoltaic effects [54, 93, 94].

3. Instrumented and connected concretes

Another way to make intelligent concretes is to embedded transducers and/or sensors, or even instrument them for more or less long periods.

Non-intrinsic self-sensing concretes are obtained by directly embedding transducers [38]. These transducers can be electrical resistance strain gauges [95-97], fibre optics [96-100], piezoelectric materials [101-103], shape memory alloys [104], self-diagnosing polymer composites [105], resistors mesh [106, 107], etc. and can monitor and evaluate various parameters as: strain, stress, strength, displacement, moisture (or humidity), hydration process, temperature, pH, corrosion, etc., but even detect and localize damages as impacts (or shocks), cracks, delamination, etc. especially for structural health monitoring applications.

If the concrete is not made intelligent during its manufacture, it is possible *a posteriori* to added an external intelligence, for instance by adding sensors, at its surface or inside, for short- or long-term measurements [108]. Today, industrial solutions to instrument and monitor concrete structures are provided by various companies as [109-120].

These solutions are increasingly using wireless communication from each sensor or from dataloggers, in order to remotely and digitally store and process the collected data. By removing the wires, the networks become more easily scalable, need less deployment time, and thus, are less expensive. Using wireless sensor networks is therefore a mean to connect concrete. Another mean to indirectly connected concretes is to use embedded wireless tags (e.g. RFID, NFC, etc.) which provide limited information as an identifier and/or an Internet Uniform Resource Locator (URL) to wirelessly access from a device to data related to the interrogate element [119-122]. This solution is used in particular to traceability during manufacture, maintenance, etc.

4. Conclusion

In this section, a short introduction to concrete materials has been proposed. Especially, the huge variety of recipes, uses and standards have been described, as well as mechanical and dielectric properties, limits and alternatives. Then, smart, instrumented and connected concretes have been presented, and their types are summarized in Figure II.2. In the next section, concrete testing methods will be detailed as well as the use of intrinsic and non-intrinsic self-sensing concretes.

Regarding the McBIM project only under the spectrum of the concrete materials, the objective is to develop an intrinsic self-sensing concrete by embedding a fully wireless sensor network using various kinds of transducers to measure various parameters (e.g. temperature, humidity, resistivity, strain, etc.) during the entire life of the element. Opposite to instrumented concretes, the sensing nodes will not be manually placed to a specific location in the concrete element but must be considered as wide aggregates planned in the recipe, randomly located and physically inaccessible even for maintenance or additional energy supply. This targeted new concrete will be based in a first time on a reinforced concrete, but ideally scalable to other reinforced concretes and to fibred concretes.

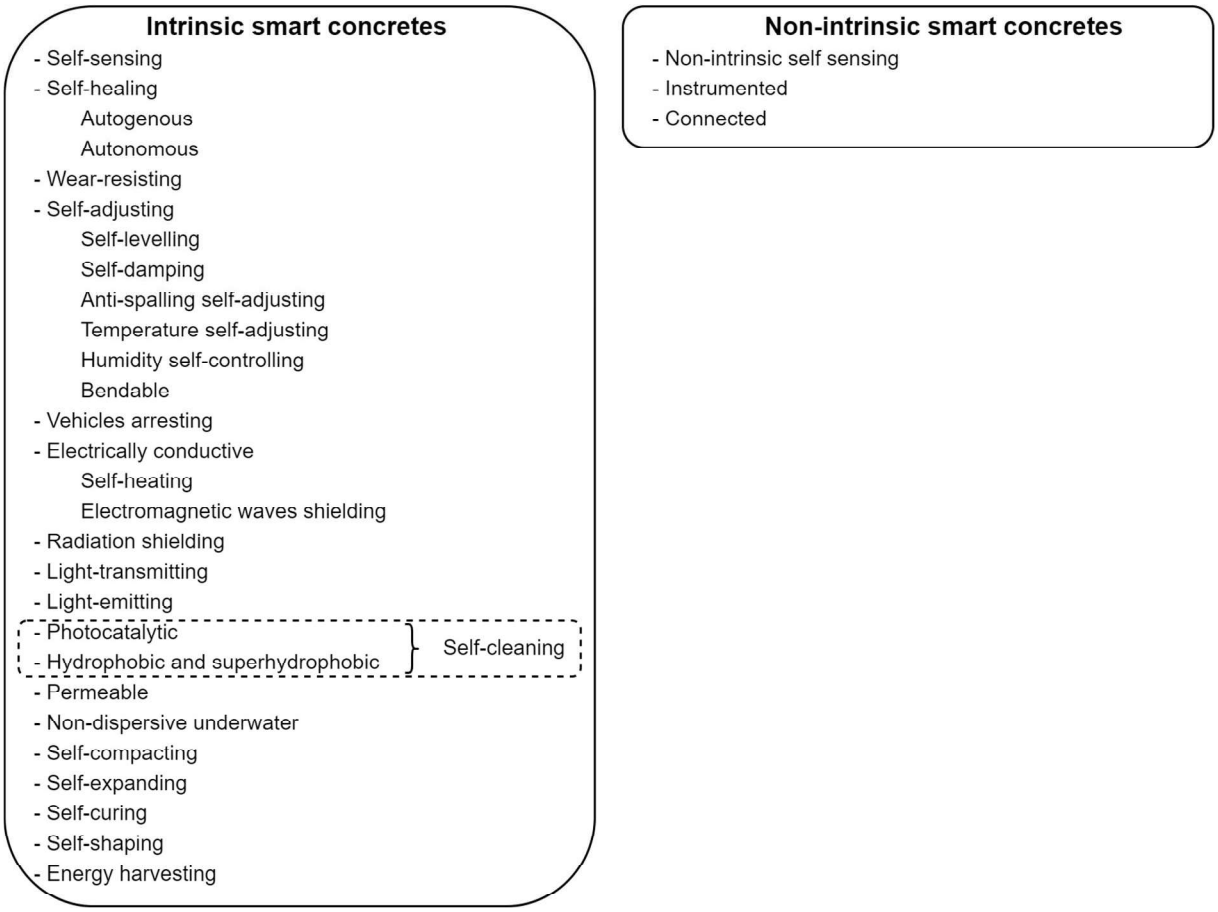

Figure II.2: List of the various kinds of smart concretes.

B. Evaluation of concrete materials

In order to certify standards and mechanical or physical properties of concrete elements, these must be monitored on several parameters during their entire lifecycle: from their manufacture and the construction, to their demolition and recycling, through their curing and their exploitation. There are two main method families for testing concretes: the destructive (or semi-destructive) and non-destructive methods.

1. Parameters to monitor

According to the step in the lifecycle, different parameters of concrete elements may be relevant to monitor in order to warranty the structural safety.

During the manufacture, the quantity and quality (e.g. mineral composition, size, gradation, moisture, organic impurities, etc.) of each component can be checked [4]. The mixing and casting processes can be monitored too (e.g. consistency, density, temperature, composition (in air, in water, in aggregate, in cement, in chloride, etc.), strength, etc.) [4, 123]. More broadly, the traceability of ingredients, assets, equipment and workers can be required [124, 125].

During the curing, which is an exothermic reaction, the concrete will harden until obtaining its maximal strength after at least twenty-eight days. To monitor this process, temperature, humidity and strain parameters can be controlled [126-129]. In some cases, the environmental parameters are constrained and specific techniques can be employed to accelerate this step, for instance through the addition of admixtures, the use of steam, infrared radiations, electromagnetic waves or electric current, etc. [4].

In the cases of precast concrete elements and ready mixed concretes, these must be transported to the construction place, and afterwards, must be installed in a previously defined location. Thus, the tracking must be assured [130] and eventual damages must be controlled [131].

During the exploitation phase of a structure made of concrete elements, its mechanical (e.g. strain, stress, strength, displacement, etc.), physical (e.g. temperature, humidity, etc.) and chemical (e.g. pH, corrosion, etc.) properties as well as its damages (e.g. shocks, cracks, delamination, etc.) can be monitored to warranty a safe use, to check for a proper aging of the material and the structure, and if necessary perform maintenance, or even predictive maintenance [108, 132].

If the concretes become unsafe or the structures useless, these can be dismantled and the concretes recycled, for instance to generate coarse aggregate for new concretes. Once again, the traceability of ingredients and equipment can be required as well as the properties of recycled concrete aggregates [133, 134].

According to [108], the main parameters to monitor into concretes are the temperature, the humidity, the pH, the corrosion and the strain or stress, as well as the cracks detection and location. In all cases, the monitoring can be achieved through destructive or non-destructive testing methods.

2. Destructive methods

Destructive (or semi-destructive or partially destructive) methods consist in physical, chemical or biological tests carry out in field (or *in situ*) or in laboratory and requiring to alter locally the monitored structures or even destroy samples [4, 108, 132, 135].

For field tests, the alteration can be in the core (e.g. a perforation to place an anchor, a drilled core, etc.) or on the surface (e.g. the deposition of a chemical reagent, the pulling out of the coating concrete, etc.) of the concretes.

The main physical tests are dedicated to (1) the strength evaluation: for the compressive strength evaluation, pull-out and torque tests can be used, as well as pull-off or break-off tests for the adhesion; (2) the resistance to the penetration of ionic solutions and water: through penetration and water resistance tests; and (3) the corrosion evaluation: with techniques based on the linear polarization of the reinforcement metal. For instance, the Windsor probe hammer is used as a hardness tester, which quickly and easily provides a way to check the relative strength during penetration tests.

The main chemical tests are used to determine the durability indicators in relation with the corrosion of reinforcements, especially to evaluate the carbonated depth and the chloride content of concretes, with their degree, their surface extent, their penetration depth and their in-depth distribution. This evaluation is based on pH tests, chloride tests and rainbows tests (based on the simultaneous use of several coloured indicators which will progressively colour the different areas of the concretes according to the degree of evolution of the targeted propriety). These tests are qualitative (e.g. reading the colour on the test sample, etc.) or quantitative (e.g. measure the value returned by an embedded probe (or electrode), etc.).

Biological tests are intended to evaluate the nature and quantity of the organisms living on the concretes (e.g. plants, fungi, bacteria, etc.), and are based on macroscopy and microscopy.

For laboratory tests, samples can be produced during the manufacture by collecting freshly mixed concretes and forming test samples, or after curing by drilling cores. In any case, once collected the samples become unusable for the initial structures. These tests use difficult to move, precise, reliable and expensive laboratory equipment.

The main physical tests are dedicated to the strength (compressive, tensile, flexural), the elastic characteristics, the water absorbability, the porosity, the freeze or frost resistance and the abrasion resistance, the sulphate resistance, the alkali-silica reactivity, the alkali-carbonate reactivity, the corrosion resistance evaluation, as well as the computer microtomography based on X-ray.

The main chemical tests are used to determine the constitution of concretes, to evaluate the chloride permeability, the air content, the cement content, the chloride content, the density, the moisture, the carbonation, the pH, etc. These are based on electroanalytic, spectral and chromatographic techniques.

Biological tests are based on advanced microscopy and *in vitro* cultures, and are intended to identify organisms living on the concretes and to determine how these can affect the structure.

All these in field and in laboratory tests allow to quantify some mechanical parameters, the chemical constitution, the water and gases permeability, and indirectly the macrostructure, the microstructure and the discontinuity of the evaluated concretes; and thus, establish the causes for defaults and estimate the remaining service life while planning the maintenance steps.

3. Non-destructive methods

Non-destructive methods consist in tests carried out on site and which do not alter the structures under test [4, 108, 128, 135-138]. These can require to instrument the structures or to use particular equipment.

First, there are optical (or visual) methods which consist in the observation of the concretes in order to get information regarding the geometry of the structures, and the macrostructures, the microstructures, the mechanical parameters and the discontinuity of the surfaces of the concretes (e.g. detection of: delamination, extensive defects, surface inhomogeneities, etc.) [4, 128, 135-138]. These observations can be achieved visually by a human or through specific equipment as microscope, endoscope, borescope, videoscope, geodesic tool, camera, three-dimensional scanner, etc., and thus, be processed by a human or by a computer. It is possible to obtain a three-dimensional image of the structures (photogrammetry), the macrostructures or the microstructures of the surfaces. These observations can be driven on an entire element or on a specific area. Recently, solutions embedding digital image processing resources on unmanned aerial vehicle provide low-cost, less time-consuming, safe and less human-dependent way to inspect large structures [139, 140].

Next, acoustic and ultrasonic methods are based on the propagation of the mechanical waves into the concretes and the digital signal processing of the collected data, especially the velocity [4, 108, 132, 135-138, 141]. These methods allow to obtain volumetric information regarding the geometry of the structures, and the macrostructures, the microstructures, the mechanical parameters and the discontinuity of the concretes (e.g. determination of: the thickness of coating concrete, the location of rebars or of defects as cracks, the density, etc.; and detection of: delamination, air voids, foreign inclusions (as water or material whose physical properties differ from those of the concretes), extensive defects, inhomogeneities, etc.). The main methods are: the impulse-response, the impact echo, the parallel seismic, the ultrasonic pulse velocity, the ultrasonic tomography, the acoustic emission, the resonant frequency test, etc.

In a similar way to the acoustic and ultrasonic methods, the electromagnetic methods are based on the propagation of the electromagnetic waves into the concretes and the digital signal processing of the collected data [4, 108, 132, 135-138, 142-144]. These methods allow to get volumetric information regarding the geometry of the structures, and the macrostructures, the microstructures and the discontinuity of the concretes (e.g. determination of: the thickness of coating concrete, the location of rebars, the degree of corrosion, the moisture content, etc.; and detection of: delamination, large air voids, extensive defects, etc.). The electromagnetic induction, the ground penetrating radar and the electrochemical (e.g. resistivity measurement by a Wenner probe, conductivity measurement, impedance measurement, etc.) are the main techniques.

Radiographic methods are based on the difference in the attenuation of the penetrating of X or gamma radiations into the concretes [4, 132, 135-138, 145, 146]. These methods allow to get volumetric information regarding the geometry of the structures, and the macrostructures, the microstructures and the discontinuity of the concretes (e.g. determination of: the density, location of rebars, etc.; and detection of: defects, etc.), for instance through tomography.

Static and dynamic laser methods generate three-dimensional image of the structures in order to analyse their geometry and their evolution over time, through an analysis of the displacements and of the deformations of themselves or their parts [132, 135-138, 147, 148].

Static and dynamic sclerometric methods allow to determine the hardness and the homogeneity of the structures, as well as to monitor the compressive strength of concretes over time [4, 108, 132, 135-138]. It is a matter of the macrostructures, the microstructures and the mechanical properties of the concretes. For instance, the Schmidt rebound hammer is used as a surface-hardness tester which quickly and easily provides a way to check the uniformity, the compressive strength and the stiffness.

Passive and active thermographic methods, based on infrared waves and using thermal camera, are used in order to obtain information related to the macrostructures, the microstructures and the discontinuity of the concretes (e.g. determination of: location of damages; and detection of: damp areas, etc.) as well as to check the quality of the thermal insulation of the structures [4, 108, 132, 135-138, 149].

The maturity method is only used for the curing and consists in the monitoring of the temperature as a function of time, allowing to estimate the strength [4, 108, 132, 136, 137, 150]. The temperature can come from sensors, as thermocouples or thermistors, embedded into the concretes or on their surface, or from thermograms.

Static and dynamic proof load methods allow to check the mechanical parameters and the discontinuity of the concretes, and consist in testing the response of the structures to different static and periodic loads [4, 132, 135-138, 151]. Strain gauges and fibre optics can be used to achieve the measurements.

Passive radio frequency identification (RFID) tags can be designed in order to be intrinsically able to sense some physical, chemical and mechanical parameters as: temperature, humidity (or moisture), presence of gas, corrosion, strain, cracks, displacement, etc.; by altering its radiofrequency backscattering parameters as: its resonant frequency, its received signal strength indication (RSSI), its frequency signature, etc. [152]. This type of sensors can be embedded in the concretes or located on these, and is wirelessly interrogated by an RFID reader.

All these methods do not allow to have a continuous and automatic monitoring of the concretes. Opposite the use of intrinsic and non-intrinsic sensing concretes as well as instrumented concretes for measurement makes possible to continuously, automatically and eventually remotely monitor the concretes through non-destructive methods. Moreover, embedded or in surface fibre optics can be employed to monitor a lot of concrete parameters, as moisture, temperature, pH, corrosion, strain, load, displacement, etc. but for monitoring the curing too and even for detecting and locating cracks [96-100, 108, 124, 132, 136, 138, 153]. Finally, the use of wireless sensor networks to instrument concretes allows to remotely monitor the concretes according various parameters [108-120, 138]. As said, and according to [108], the main parameters to monitor into concretes are the temperature, the humidity, the pH, the corrosion and the strain or stress, as well as the cracks detection and location.

4. Experimentations on structural health monitoring of concretes and concrete structures with wireless sensor networks

Since the end of the 1990s, academic research is conducted regarding the use of wireless sensor networks dedicated to structural health monitoring, in particular for the civil infrastructures and concrete structures [154]. These early works deal mainly with the frequency analysis of mechanical waves experienced by the structures and measured by various kinds of accelerometers in order to detect structural defects. These measurements can be achieved during high intensity events as earthquakes, or periodically for long-term monitoring. Generally, the collected temporal data are wirelessly transmitted to a more performant datalogger which processes these in order to obtain exploitable frequency data. Temperature and strain are also parameters which are monitored by the early age wireless sensor networks designed for structural health monitoring applications.

Next, research has focused on other aspects of the structural health monitoring of the concretes. For instance, the monitoring of the curing process and of the long-term strength and deterioration were investigated respectively through temperature and humidity, and electromechanical impedance measurements, wirelessly transmitted over meters and during nearly one month [155].

The deployment of a wireless sensor network in the Torre Aquila is a relevant full-scale and well-documented experimentation for long-term structural health monitoring of a civil infrastructure [156]. Indeed, several different wireless sensors were installed everywhere in the four-floor tower to monitor its structural health during months. Three types of wireless sensors were used respectively dedicated to collect data from the deformation (by using fibre optics and temperature sensor), the environment (by using temperature, relative humidity (available but not used) and luminosity (available but not used) sensors), and the acceleration (by using MEMS accelerometers). All the collected data were wirelessly transmitted over tens of meters to a sink to be stored and processed.

Since, more experimentations were conducted; new various sensors and wireless protocols were tested; the energy efficiency, the network topology, the sensors placement, the scalability, the time synchronization, the distribution of the processing, the performance improvement, the software optimization, the fault tolerance, the defects prediction, etc. were studied as well as the possibility to power the sensors by ambient energy harvesting [157-159]. By relocating the storage and processing through the Internet, the initial wireless sensor networks become cyber-physical systems dedicated to the structural health monitoring.

In parallel to the academic research and as previously introduced, it exists since a few years some commercially available solutions to wirelessly monitor concrete structures. All these, sense at least temperature using various kinds of sensors (e.g. thermocouple, thermistor, etc.) [109-120]. A majority can monitor the maturity during the curing through temperature, humidity (or moisture) and strength (e.g. strain, stress, etc.) measurements [109-112, 114-120]. Other mechanical parameters can be monitored as elastic and inelastic deformations (e.g. deflection, extension, dilatation, compression, etc.; and cracks, etc.) [109-112], inclination [109-112], load or pressure [109-112], displacement [110], defects and shocks (e.g. through vibration analysis (e.g. with data obtained by accelerometers, etc.), etc.) [109, 110, 112], etc. Moreover, electrochemical parameters as corrosion can be available for

instance through resistivity measurements [111, 114]. Finally, [109] proposes weather parameters monitoring as well as the possibility to add on demand almost any type of sensor. These industrial solutions provide sensors which can be embedded into concretes [110-116] or located at their surface [109-114, 117-120]. Some are based on autonomous fully wireless sensors [109, 114, 115, 117-120] and others on wired sensors connected to wireless datalogger locally accessible [113], through the Internet [110-112], or both [116]. In function of the wireless strategy, the useful range is between some meters and hundreds of meters. The autonomy of these solutions which used essentially batteries is around a few months, only [110] proposes to connect a solar panel as an energy harvesting source.

5. Conclusion

In this section, the monitoring of concretes and concrete structures has been quickly introduced. In particular, the relevant parameters to monitor in function of the step in the lifecycle has been defined. Then, the main destructive or semi-destructive testing methods were presented, as well as the non-destructive testing methods. These are summarized in Figure II.3. Also, the use of wireless sensor networks dedicated to the structural health monitoring of concretes and concrete structures in the academic and industrial fields has been exposed. In the next section, the candidate wireless communication technologies for the design of a wireless sensor network embedded in concretes to provide communicating concretes will be detailed.

In the framework of the McBIM project and only regarding the monitoring of concretes, the main target is to design a fully wireless sensor network able to sense various relevant parameters during all the lifespan of the monitored concrete elements; and then connect these through the Internet to virtual models, especially building information modelling (BIM), to conserve a detailed historic of their health. It is therefore a question of a non-destructive testing method. Thus, the curing process could be monitored thanks to the maturity method (through temperature, humidity and strain measurements), and its exploitation phase thanks to temperature, humidity, strain and resistivity (e.g. to quantify the corrosion) measurements. By adding a unique identifier and the storage in the material of some data, both wirelessly accessible, the traceability could be covered. The targeted wireless sensor should be a generic platform where all kinds of sensors or transducers could be connected. In a first time and in order to limit the needs in terms of energy and computing capacity, only direct and temporally punctual measurements would be considered, so, methods requiring signal processing and/or energy-consuming equipment (as optic, acoustic and ultrasonic, thermographic, electromagnetic (based on waves propagation), radiographic, sclerometric, proof load, etc.) would be discarded.

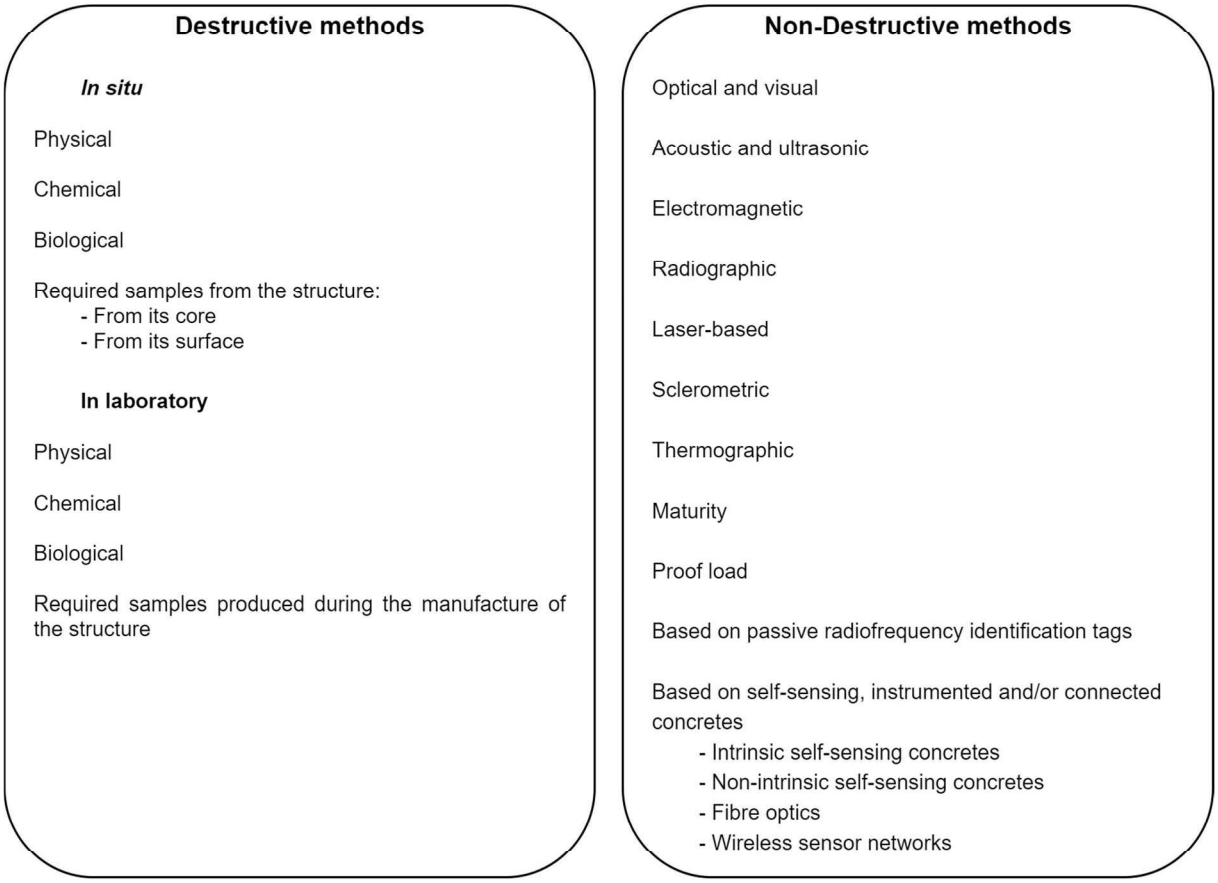

Figure II.3: List of the various kinds of destructive and non-destructive methods use to the structural health monitoring of the concretes.

C. Wireless machine-to-machine communication technologies

With the great rise of the Internet of Things (IoT), the needs in wireless machine-to-machine communication technologies are exploding and solutions answering broad and diverse specification requirements are now available [160-162]. These specifications concern the range, the energy consumption, the frequency band and its bandwidth, the data-rate, the allowed payload, the transmitted power, the modulation scheme, the network topology, the directionality, the media access strategy, the security, etc. Thus, in recent years, several standards have emerged and the mains will be introduced.

1. Wireless electromagnetic communications

To date, electromagnetic communications are the most widespread among wireless communications because these are particularly suitable for communications in the air and are easily adaptable to meet diverse requirements. Two types exist: the near-field (or reactive) based on the inductive coupling; and the far-field (or radiative) based on the electromagnetic radiations. The distinction can be done according to the distance to the source and the wavelength in the propagation medium λ: the near-field is for distances inferior at $\lambda/(2.\pi)$; and the far-field for distances much higher than $\lambda/(2.\pi)$.

i. Near-field wireless electromagnetic communication standards

a. Near-Field Communication (NFC)

Near-Field Communication (NFC) is the main standardized technology using near-field wireless electromagnetic communications [160-164]. It is based on ISO/IEC 14443 types A and B [165], ISO/IEC 18092 [166] and ISO/IEC 21481 [167] standards which specify all the communication protocols, especially for the physical layer. By being compatible with the ISO/IEC 18000-3 standard [168], it can be considered as a subcategory of the radio-frequency identification (RFID) technologies. There are three modes: card emulator (active or passive devices that only respond on request by transmitting or modifying the stored data), reader (active devices that request card emulator to transmit or modify data) and peer-to-peer (active devices that can alternatively take the role of card emulator and reader). This is a master-slave bidirectional communication between only two devices. While passive devices used backscattering to respond to a request, active ones generate their own electromagnetic waves. The maximum communication range is estimated at nearly 20 centimetres in the air but is usually 4 centimetres on average for the conventional implementations. This standard used the industrial, scientific and medical (ISM) 13.56 MHz high frequency (HF) band. There are three main device categories: NFC-A (based on the on/off-keying (OOK) modulation and offering a data-rate of 106 kbps), NFC-B (based on an amplitude-shift keying (ASK) modulation and offering data-rates of 106, 212 or 424 kbps) and NFC-F (based on an amplitude-shift keying (ASK) modulation and offering data-rates of 212 or 424 kbps). The tiniest frame counts 4 bytes with only one for the data and the largest 4 GB. NFC standards consider the data security issues by recommending the use of a secure element and the encryption of the frames. Complete industrial solutions and off-the-shelf components are available now.

b. RuBee

RuBee is a near-field wireless electromagnetic communication technology based on the IEEE 1902.1 standard which specifies all the communication protocols, especially for the physical layer, and that uses the magnetic field [169-172]. The network is based on a star topology with one or more controllers and several responders, and where bidirectional communications with responders are initiated by controllers. Punctual control frames are sent in order to keep the network alive. The maximum communication range is estimated up to 30 metres (with a 10 μW maximum transmission power) even in harsh and highly constrained environments. Indeed, it is designed to be immune to interferences, metals and water. This standard used the low frequency (LF) band between 30 and 450 kHz, especially around the 131 kHz frequency. It also uses amplitude-shift keying (ASK) or binary phase-shift keying (BPSK) modulations, allowing data-rates between 300 bps and 9.6 kbps. The tiniest frame counts 5 bytes with only one for the data. RuBee is a very low energy consumption technology. More, it is considered safe and approved by the United States of America Department of Defence (U.S. DoD). At least, the standard provides a frequency sub-band around 65.536 kHz dedicated to the wireless power transfer (WPT) by a controller to remotely supply responder(s). No industrial solutions and off-the-shelf components are available now.

ii. Near-field or far-field wireless electromagnetic communication standards

a. Radio-frequency identification (RFID)

The designation radio-frequency identification (RFID) covers a wide range of technologies essentially based on the backscattering, both in the near-field and the far-field, and initially designed for identification purpose only [160-162, 173]. These, initiated in the 1950s and widely deployed since the begin of the 21st century, are based on several standards not necessarily interoperable. The ISO/IEC 18000 standard, composed by six sections (one global and one for each frequency band) is the most common and specifies all the communication protocols, especially for the physical layer [168]. There are two kinds of devices: readers and tags; which interact in star or peer-to-peer master-slave bidirectional communications, with only one reader/master, which is able to achieve multiple simultaneous readings of several tags/slaves, and which is generally connected to a database. The reader is also able to modify by writing the data stored in the tags. The tags can be passive (these cannot store energy, thus operate by recovering part of the energy supplied by the reader to power the integrated systems, and backscatter and re-modulate part of the incident electromagnetic wave to communicate), semi-active (these store energy to power the integrated systems, and backscatter and re-modulate part of the incident electromagnetic wave to communicate) or active (these store energy to power the integrated systems, and to generate their own modulated electromagnetic waves to communicate, that allows to increase the maximum communication range up to hundred metres). Solutions using the 125 kHz, the 135 kHz low frequency (LF) or the industrial, scientific and medical (ISM) 13.56 MHz high frequency (HF) bands are based on inductive coupling, thus are near-field solutions, whose the maximum range is from centimetres to a few tens of centimetres. NFC is a subcategory of RFID using this last frequency band. Opposite, these using the industrial, scientific and medical (ISM) 433 MHz very high frequency (VHF), the 860 to 960 MHZ or the 2.45 GHz ultra-high frequency (UHF) bands are based on radiations, thus are far-field solutions, whose the maximum range is from metres to a few tens of metres. Highest the frequency, tiniest the antenna (thus the tag), and the more sensitive to environmental constraints. The frame length

(initially only an identifier) are not standardized, thus a frame could count 4, 8, 16 or 32 bytes as well as 2 kB. Even if RFID are very low energy consumption technologies, these are not yet consider as safe wireless communication technologies. A lot of complete industrial solutions and off-the-shelf components are available now. As previously introduced, passive radio frequency identification tags can be designed in order to be intrinsically able to sense some physical, chemical and mechanical parameters by altering their radiofrequency backscattering parameters [152].

iii. Far-field wireless electromagnetic communication standards

Most of the wireless communication technologies available today belong to the family of far-field communications. Data are exchanged over large distances by electromagnetic radiations.

a. Standards provided by the IEEE 802 committee

The 802 committee of the Institute of Electrical and Electronics Engineers (IEEE) is the main provider of standards for far-field wireless electromagnetic communications [174]. All its standards presented below define at least the physical and data link layers of the open systems interconnection (OSI) model.

* Wi-Fi is the implementation of the IEEE 802.11 standard for wireless local area networks (WLAN) and is well established [161, 162, 174-177]. Today, it is in its sixth version. The star topology is often privileged and the carrier sense multiple access with collision avoidance (CSMA/CA) strategy is used for the access and share of the propagation medium. Communications are bidirectional and a lot of frames are sent for control purpose. This standard is used as basis for IP protocols. As there are several sub-standards (802.11-1997, 802.11a, 802.11ac, 802.11ad, 802.11ah, 802.11aj, 802.11ax, 802.11ay, 802.11az, 802.11b, 802.11g, 802.11n, etc.) the maximum communication range varies between 10 and 250 metres, but Wi-Fi is considered as a low range wireless communication technology. For the same raison, several industrial, scientific and medical (ISM) frequency bands are used, in particular around 900 MHz ultra-high frequency (UHF), 2.45 GHz ultra-high frequency (UHF), 5 GHz super high frequency (SHF), 45 GHz or 60 GHz V bands, with a various number of channels (between 1 and 8), various bandwidths (between 1 MHz to 8 GHz) and various modulation schemes: binary phase-shift keying (BPSK), differential binary phase-shift keying (DBPSK), quadrature phase-shift keying (QPSK), differential quadrature phase-shift keying (DQPSK), 16 or 64 quadrature amplitude modulation (QAM), etc. and eventually some spread spectrum and/or multiplexing techniques (frequency-hopping spread spectrum (FHSS), direct-sequence spread spectrum (DSSS), orthogonal frequency-division multiplexing (OFDM), etc.). Thus, the maximum data-rate varies between 600 kbps to 10.53 Gbps, and next up to 100 Gbps, that is considered as high data-rate. The tiniest frame counts 33 bytes with only one for the data and the maximum payload is 2304 bytes. Wi-Fi is a high energy consumption technology and even if some security mechanisms are provided, these are regularly reconsidered following the discovery of flaws. Complete industrial solutions and off-the-shelf components are widely available now.

* The IEEE 802.15 standards family normalizes the wireless personal area networks (WPAN).

\+ Bluetooth and Bluetooth Low Energy (BLE) technologies are based on the IEEE 802.15.1 standard and are also widely established [160-162, 174, 178-181]. Nevertheless, these are not now interoperable.

The Bluetooth technology is now at its fifth version. The star topology with one master: the central; and up to 7 active or 255 inactive slaves: the peripherals; forms a piconet for which the role of each device is not fixed and can change over time. It is even possible to create a meshed network of piconets, if the rule of a unique master for 7 slaves is checked for each piconet at any time. Communications are bidirectional once the devices that want to communicate are well paired, and a lot of frames are sent for control purpose. There are three classes of device: 1, 2 and 3; according to the maximum transmitted power and which respectively have a maximum communication range of 100, 10 and 1 metres. It is also a short-range technology. The industrial, scientific and medical (ISM) 2.45 GHz ultra-high frequency (UHF) band is used as well as the frequency-hopping spread spectrum (FHSS) technique on 79 adjacent 1 MHz wide channels and the frame can be modulated in gaussian frequency-shift keying (GFSK), differential quadrature phase-shift keying (DQPSK), π/4 offset differential quadrature phase-shift keying (π/4-DQPSK) or 8 states differential phase-shift keying (8DPSK). That allows data-rates of 1, 2 or 3 Mbps. The tiniest frame counts 17 bytes with only one for the data and the maximum payload is 343 bytes. The Bluetooth is a high energy consumption technology due to the frequent control frames and the need of pairing the devices. Even if some security mechanisms are provided by the standard, these are regularly reconsidered following the discovery of flaws.

The Bluetooth Low Energy (BLE) technology is an evolution of the fifth version of the Bluetooth technology which tends to limit the energy consumption for similar performances. Thus, two strategies were adopted. The first conserves and simplifies the same functioning than for the Bluetooth technology with the difference that the slaves can be in sleep mode for longer and more frequently thanks to the use of the time-division multiple access (TDMA) strategy controlled by the master, which can impose a sleeping time to the slaves up to 32 seconds. Thus, the piconet have no more a limitation in the number of slaves imposed by the standard, only the practical limitation is effective. The creation of a meshed network of piconets is no more supported. The second is based on bidirectional communications between broadcasters and observers that no longer need to be paired and for which there are no longer any control frames. There is no more piconet because the broadcasters send their frames on the fly and the observers, like sinks, listen continuously and process the received frames. The role can change over time. The maximum communication range in increase beyond 100 metres. The industrial, scientific and medical (ISM) 2.45 GHz ultra-high frequency (UHF) band is used as well as the frequency-hopping spread spectrum (FHSS) technique on 40 adjacent 2 MHz wide channels and the frame is modulated in gaussian frequency-shift keying (GFSK). That allows data-rates of 125 kbps, 1 Mbps or 2 Mbps. The tiniest frame counts 17 bytes with only one for the data and the maximum payload was 31 bytes until the fifth version which increases it up to 255 bytes. The Bluetooth Low Energy is also a low energy consumption technology. Complete industrial solutions and off-the-shelf components are available now both for Bluetooth and Bluetooth Low Energy.

+ The ultra-wideband (UWB) is a technology based on the IEEE 802.15.3 standard for high rate wireless personal area networks (HRWLAN) and particularly suitable for multimedia streams [174, 182-185]. Is called ultra-wideband a communication technology which uses at least a bandwidth of 500 MHz or 20 % of the central frequency that allows to spread to transmitted power over the entire frequency band, and thus, communications take place at an average power below the noise floor, and are therefore robust to interference and do not interfere with narrower band technologies. There are two types of ultra-wideband technologies: with and without carrier. The without carrier solution does not require synchronization process, is easily implementable both for emitter and receiver, and consumes less energy than the with carrier solution.

Without carrier ultra-wideband communications are based on the impulse radio technique (IR-UWB) in which a series of very short and low-energy pulses are transmitted. These pulses sequences can be modulated by on-off keying (OOK), pulse-position modulation (PPM), binary phase-shift keying (BPSK), quadrature phase-shift keying (QPSK), etc. There are two main ways to communicate through impulse radio ultra-wideband: the direct sequence ultra-wideband (DS-UWB), which consists of sending a sequence of pulses at the highest possible rate; and the time hopping ultra-wideband (TH-UWB), which consists of sending a sequence of pulses at pseudo-randomly defined times. Multiplexing is possible in particular through the direct-sequence spread spectrum (DSSS) technique.

With carrier ultra-wideband communications are based on the multi-band ultra-wideband (MB-UWB) technique and orthogonal frequency division multiplexing (OFDM) on 14 adjacent 528 MHz wide channels in the 3.1 to 10.6 GHz band.

The star topology is expected and the communications are bidirectional. The maximum communication range is estimated from metres to tens of metres. The industrial, scientific and medical (ISM) 3.1 to 10.6 GHz super high frequency (SHF) and 57 to 66 GHz extremely high frequency (EHF) bands can be used. The data-rate is between hundreds of Mbps to a few Gbps. The frame format is not yet well defined, thus, the minimal frame length as the maximum payload cannot be given. These technologies have one of the lowest energy consumption per transmitted bit. Today, no industrial solutions and off-the-shelf components for wireless communication are available. Nevertheless, the ultra-wideband technology is used for indoor location.

+ ZigBee is one the possible implementations of the IEEE 802.15.4 standard for low rate wireless personal area networks (LRWPAN) [160-162, 174, 186-189]. Some technologies are based on the physical and data link layers of the 802.15.4 standard and define their own upper layers of the open systems interconnection (OSI) model, as ZigBee, Thread, 6LoWPAN, MiWi, WirelessHART or ISA100.11a. Moreover, there are several sub-standards with various performances, some of which are based on the direct sequence ultra-wideband (DS-UWB) and chirp spread spectrum (CSS) techniques.

For the sub-standards based on the direct sequence ultra-wideband (DS-UWB) technique, the industrial, scientific and medical (ISM) 249,6 to 749,6 MHz ultra-high frequency (UHF) and the 3.1 to 4.8 GHz and 6.0 to 10.6 GHz super high frequency (SHF) bands can be used with 16 channels, a modulation combining the pulse position modulation (PPM) and the binary phase-shift keying (BPSK) schemes, with a medium access through the ALOHA technique, all this allowing data-rates between 110 kbps and 27.24 Mbps.

For the sub-standard based on the chirp spread spectrum (CSS) technique, the industrial, scientific and medical (ISM) 2.45 GHz ultra-high frequency (UHF) band is used with 14 channels, a modulation combining the differential quadrature phase-shift keying (DQPSK)

and the 8 states orthogonal phase-shift keying (8-OPSK) schemes, with a medium access through the carrier sense multiple access with collision avoidance (CSMA/CA), and data-rates between 250 kbps and 1 Mbps are possible.

For other sub-standards, and in particular for ZigBee technology, the star, the multi-hop meshed and the tree cluster topologies are possible and can host up to 65634 systems. There are two types of ZigBee devices: full-function device (FFD) (comprising the full implementation of the standard) and reduced-function device (RFD) (comprising a light and partial implementation of the standard in order to reduce its complexity and its energy consumption).

As well, it exists three roles: coordinator (necessarily a single one per network and of full-function device type, which manages its whole network, especially for the device registration, the routing policy and the security policy, and which can be a gateway to other network, as an access point to the Internet), router (necessarily of full-function device type, which extends the range of the network by repeating the signals received and allowing to increase the number of devices in the network by reducing the load on the coordinator), and end-device (a full-function device or a reduced-function device, which becomes a sensor or an actuator once registered with the concentrator). The carrier sense multiple access with collision avoidance (CSMA/CA) strategy is used for the access and share of the propagation medium. Communications are bidirectional and a lot of frames are sent for control purpose. The maximum communication range varies between 10 and 100 metres. The industrial, scientific and medical (ISM) 868 MHz, 915 MHz and 2.45 GHz ultra-high frequency (UHF) bands can be used; with 1, 10 or 16 channels; with amplitude-shift keying (ASK), binary phase-shift keying (BPSK) or orthogonal quadrature phase-shift keying (O-QPSK) modulation schemes; and with direct-sequence spread spectrum (DSSS) or parallel sequence spread spectrum (PSSS) techniques. That allows data-rates between 20 and 250 kbps. The tiniest frame counts 16 bytes with only one for the data and the maximum payload is 104 bytes. ZigBee is considered as a low energy consumption but not as a safe technology. Complete industrial solutions and off-the-shelf components are available now.

\+ Although not directly within the scope of this work, the IEEE 802.15.6 standard for body area network (BAN) covers some important and shared constraints: because these are used in, on or around living beings, these must substantially meet to the requirements acceptability, security, safety, energy efficiency, robustness to interferences, network load, quality of service and interoperability, while being short or medium range and low energy consumption [190-193]. Also, it must be noted that NFC, RuBee, RFID, Bluetooth, Bluetooth Low Energy, ultra-wideband and ZigBee technologies could meet the requirements of this standard.

* WiMAX is the main implementation of the IEEE 802.16 standard for wireless metropolitan area networks (WMAN) [194-197]. The star topology is widely privileged with an access point and several end devices which must subscribe to the network to communicate. There are two sub-standards respectively dedicated to fixed end devices and mobile end devices, with various constraints and performances. Communications are bidirectional with control frames and require subscriptions. The maximum communication range is below 50 kilometres. The 2 to 66 GHz frequency band is used with between 128 to 2048 sub-channels of width between 1.25 and 20 MHz. The frames can be modulated with the binary phase-shift keying (BPSK), quadrature phase-shift keying (QPSK), 16 or 64 quadrature amplitude modulation (QAM) scheme to provide data-rates between 30 Mbps and 1 Gbps. Time-

division multiple access (TDMA), orthogonal frequency-division multiplexing (OFDM) and spread orthogonal frequency-division multiplexing (SOFDM) techniques can be used for spread spectrum and/or multiplexing purposes. WiMAX is a high energy consumption technology. Complete industrial solutions and off-the-shelf components are available now.

* iBurst is one implementation of the IEEE 802.20 standard for mobile broadband wireless access (MBWA) [198-200]. This standard can be used by mobile devices with a speed up to 250 km/h. A meshed network topology with access points and end devices is required. Communications are bidirectional with frames sent for control purpose. The technology based on this standard can be interconnected to IP networks and to the Internet. The theoretical maximum communication range is around kilometres. The 3.5 GHz super high frequency (SHF) bands is used with the orthogonal frequency-division multiplexing (OFDM) technique on 5, 10 or 20 MHz wide channels. The quadrature phase-shift keying (QPSK), the 8 states phase-shift keying (8-PSK), and the 16 or 64 quadrature amplitude modulation (QAM) modulations can be used. The data-rate can be up to 1 Mbps. iBurst is a high energy consumption technology. Complete industrial solutions and off-the-shelf components are not available today.

* The IEEE 802.22 standard is dedicated to wireless regional area network (WRAN) that opportunistically uses unused television bands [201, 202]. The standard defines a meshed network topology with access points and end devices. The theoretical maximum communication range is of a few tens of kilometres. The 54 to 862 MHz very high and ultra-high frequency (VHF and UHF) bands initially dedicated to television broadcasting are used with the orthogonal frequency-division multiple access (OFDMA) technique. The expected data-rate is a few Mbps. To date, there are no complete industrial solutions and off-the-shelf components available for this standard.

b. Low-power wide area networks (LPWAN)

The low-power wide area networks (LPWAN) designation refers to the technologies that allow long distance, low power and low-cost wireless communication networks, usually at the price of a low data-rate and a high latency [160-162, 203-206].

* DASH7 is one implementation of the ISO 18000-7 standard which defines all the layers provided by the open systems interconnection (OSI) model [162, 168, 203-207]. The tree and star topologies are supported for bidirectional communications. The theoretical maximum communication range is below 5 kilometres. The industrial, scientific and medical (ISM) 433 MHz, 868 MHz and 915 MHz ultra-high frequency (UHF) bands are used with a medium access through the carrier sense multiple access with collision avoidance (CSMA/CA) technique and with 16, 8 or 7 respectively 13, 55, or 200 kHz wide channels. The gaussian phase-shift keying (GPSK) allows to modulated the frames. Thus, the data-rate can be up to 167 kbps. The tiniest frame counts 6 bytes with only one for the data and without considering the physical layer overload, and the maximum payload is 251 bytes. No complete industrial solutions and off-the-shelf components are available today. This technology is introduced as not very sensitive to the presence of concrete and water.

* LoRaWAN is an open-source protocol standard provided by the LoRa Alliance and using the LoRa radio modulation technology (property of Semtech) [161, 162, 203-207, 208-214]. The star topology with gateways and devices is proposed and the interconnection with the Internet is usual. The communications are weakly bidirectional and the downlink is based on three class for the end devices: class A (after a transmission the device waits for a short time for a possible message from the network through the gateway before going back to sleep), class B (similar to class A but with predefined periods during which the network through the gateway can transmit data to the device) and class C (the device is continuously listening for eventual data from the network through the gateway). The maximum communication range is up to 5 kilometres in urban areas and up to 15 kilometres in rural areas. The industrial, scientific and medical (ISM) 433 MHz, 868 MHz and 915 MHz ultra-high frequency (UHF) bands are used with a medium access through the ALOHA technique and with 8 125, 250 or 500 kHz wide channels. The LoRa modulation is based on the chirp spread spectrum (CSS) technique and allows a lower average transmission power than noise which hardly limits the eventual interferences with other wireless communication technologies sharing the same frequency bands. The data-rate is between 300 bps to 50 kbps. The tiniest frame counts 14 bytes with only one for the data and the maximum payload is 250 bytes. LoRaWAN is considered as a low energy consumption technology, but not as safe even if some security mechanisms are provided. Several complete industrial solutions and off-the-shelf components are available today and it is easily to deploy its own LoRaWAN network.

* SigFox is a proprietary technology of wireless communication for Internet of Things purposes and provided by the SigFox company [160-162, 203, 205, 206, 215, 216]. The star topology with gateways and devices is chosen and the gateways allow an interconnection with the Internet. The communications are initially directional but updates allow limited downlink. The theoretical maximum communication range is up to 10 kilometres in urban areas, up to 50 kilometres in rural areas and estimated up to 1000 kilometres in direct line of sight. The industrial, scientific and medical (ISM) 868 MHz and 915 MHz ultra-high frequency (UHF) bands are used with a medium access through the ALOHA technique and with 360 100 Hz ultra-narrow wide channels. The SigFox modulation is based on a combination of temporal and frequency multiplexing and the differential binary phase-shift keying (DBPSK) modulation. Each frame is sent three times, on three different and pseudo-randomly drawn frequencies, and in ultra-narrow band way, *id est* that all the transmitted power is concentrated around one frequency. As each frame could be received by several gateways and thanks to the redundancy induced by the protocol, the probability of good reception is high. Nevertheless, the data-rate is limited at 100 bps. The tiniest frame counts 13 bytes with only one for the data and the maximum payload is 12 bytes. By respecting the regulations governing access to the medium, only 140 frames with 8 bytes of payload can be emitted per day. SigFox is considered as a low energy consumption technology and as moderately safe, because even if some security mechanisms are provided these are at the expense of the end user. Several complete industrial solutions and off-the-shelf components are available today, but a subscription to a network access provider is required.

c. Cellular networks

Cellular networks were initially dedicated to human usages and specifically to voice calls. Nevertheless, through evolutions these networks have allowed to transmit data with high data-rates and to connect to the Internet [160-162, 217-221]. Whatever the generation (from 0G to 5G) as specified by the third-generation partnership project (3GPP), the topology is based on

a meshed network of base stations interconnected with the Internet where the mobile end devices connect and stay connected. At least a unique base station or more commonly a group of three base stations provides a cell which uses a different set of frequencies from neighbouring cells in order to avoid interferences and to warrant service quality within each cell. Nevertheless, the mobile end devices can change their connection cells over time without stop in their support (e.g. non-stopped voice call, etc.). Each cell covers an area between tens of metres and a few kilometres. The communications are bidirectional and subscriptions are required. Table II.1 provides a brief overview of the different generations of the cellular network technologies.

Since a few years, sub-standards were provided in order to propose solutions for machine-to-machine communications in low-power wide area networks (LPWAN) [203-206, 220, 221]. EC-GSM is based on the 2G technology and NB-IoT and LTE-M on the 4G, and thus, are based on the same specifications than for the associated human-oriented technologies. These respectively provide up to 2 Mbps, 159 kbps and 7 Mbps data-rates, thanks to respectively the use of the gaussian minimum-shift keying (GMSK) or the 8 states phase-shift keying (8-PSK) modulations and the time division (TDMA), the frequency division (FDMA) or the orthogonal frequency division medium access (OFDMA) techniques; the orthogonal frequency division medium access (OFDMA) technique; and the 16-quadrature amplitude modulation (QAM) and the orthogonal frequency division medium access (OFDMA) (downlink) or single-carrier frequency division multiple access (SC-FDMA) (uplink) techniques. These three technologies are considered as high energy consumption technologies in comparison with other machine-to-machine low-power wide area network (LPWAN) technologies but as low energy consumption on comparison with conventional

Table II.1: Comparison of the different generations of cellular networks.

Name	Release decade	Standard	Main goal	Type of modulation	Frequency bands	Medium access technique	Maximum data-rate
1G	1980	AMTS	Voice	Analog	800 MHz	FDMA	2.4 kbps
2G	1990	GSM	Media except video	Digital	850/900/ 1800/1900 MHz	TDMA	64 kbps
2.5G	1990	GPRS	Media except video	Digital	850/900/ 1800/1900 MHz	TDMA/CDMA	144 kbps
2.75G	1990	EDGE	Media except video	Digital	850/900/ 1800/1900 MHz	TDMA/CDMA	180 kbps
3G	2000	UMTS/ CDMA2000	Video and games	Digital	850/900/ 1800/1900/ 2100 MHz	CDMA	2 Mbps
3.5G/3G+	2000	HSPA	Video and games	Digital	850/900/ 1800/1900/ 2100 MHz	CDMA	30 Mbps
4G	2010	LTE/LTEA	High data-rate	Digital	1.8/2.3/ 2.6/3.5 GHz	CDMA	100 Mbps
5G	2020	NR	Very high data-rate	Digital	2.4/3.6/5/26 GHz	OFDM/BDMA	1.8 Gbps

cellular network technologies. Moreover, these are considered as safe. Several complete industrial solutions and off-the-shelf components are available today, but a subscription to a network access provider is required. Today, the fifth generation (5G) of cellular network emerges and tends to provide a global network both for humans and objects, objective also pursued by the sixth generation in the process of specification (6G) [222].

d. Satellite networks

Satellite networks -originally designed for voice communications, television broadcasting and the Internet- can be now used by objects for Internet of Things (IoT) purposes [223-227]. Currently, two kinds of technologies for satellite networks are in operation: the low earth orbit satellite constellations (with an altitude between 700 and 1,500 kilometres) such as the late Irridium, as well as Irridium Next or Globalstar; and the geostationary orbit satellite constellations (with an altitude of 36,000 kilometres) such as Inmarsat or Thuraya. The topology is based on a meshed network of satellites interconnected with other terrestrial networks as the Internet and where the mobile end devices connect and stay connected. The mobile end devices can change their connection satellite over time without stop in their support (e.g. non-stopped voice call, etc.). Each satellite constellations covers almost the entire globe (only the poles are not covered by certain satellite constellations). The communications are bidirectional, the data-rates range from 10 kbps to 1 Tbps and subscriptions are required. These are considered as high energy consumption technologies and as relatively safe. A few complete industrial solutions and off-the-shelf components are available today, and a subscription to a network access provider is required (e.g. Eutelsat, Orbcomm, Vodafone, etc.).

e. Proprietary technologies

Other proprietary technologies are available for machine-to-machine wireless communications and their performances are diverse. These will be not presented in this manuscript where only the main and more relevant are considered.

f. Backscattering

By using opportunistic backscattering of ambient electromagnetic waves, it is possible to design systems which communicate together without the need of generating their own electromagnetic waves [228-233]. Today, there are no standards or industrial applications for this kind of opportunistic and low energy consumption technology. In a similar way to radio-frequency identification (RFID) technology, the systems recover a part of the ambient electromagnetic energy to power the integrated systems, and backscatter and re-modulate part of this same incident electromagnetic wave to communicate. The targeted carrier electromagnetic waves are usually those with the most constant power over time, such as from radio or television broadcastings. Nevertheless, electromagnetic waves from cellular networks or even LoRa networks can be used even if these are less predictable. In all cases, these systems are completely transparent to communicating systems unintentionally providing a carrier electromagnetic wave, unless the opportunistic system is very close to the final recipient of the initial communication. There is great diversity in the performances obtained: with ranges from a few tens of centimetres to a few tens of metres, with data-rates from a few bits per second to a few tens of thousands of bits per second, etc.

2. Wireless communications based on the light

i. Li-Fi

The IEEE 802.15.7 standard deals with the physical and link control layers of the open systems interconnection (OSI) model for wireless communications whose information is transmitted by the light [234-237]. Li-Fi is one of the possible implementations. Three types of physical layers are specified: PHY I, PHY II and PHY III. PHY I and PHY II send frames modulated with on-off keying (OOK) or pulse-position modulation (PPM) schemes and use a monochromatic light source. These are respectively dedicated to outdoor and indoor communications and provide data-rates between 11 and 266 kbps and between 1 and 96 Mbps. PHY III send frames modulated with colour shift keying (CSK) scheme and uses a polychromatic light source. It is dedicated to indoor communications and provides data-rates between 16 and 96 Mbps. The star, the peer-to-peer and the broadcasting topologies are available. Communications are bidirectional and there are control frames to network control purposes. The visible spectrum is used, *ie est* the frequency band between 460 and 670 THz. As the light is not altered by ambient electromagnetic fields, the only constraint in terms of range is the need of a direct line of sight between the transceivers. The tiniest frame counts 26 bytes with only one for the data. Li-Fi is considered as a high energy consumption and safe technology. A few complete industrial solutions and off-the-shelf components are available now.

ii. Other technologies

In parallel to Li-Fi, some common technologies are based on light or infrared radiations, such as for remote controllers [238]. Finally, communications based on laser emissions are in development, especially for spatial applications such as the communications between satellites [239, 240].

3. Wireless mechanical communications

Because of their excellent propagation in concretes, the mechanical waves -such as acoustic or ultrasonic waves- are already used to indirect measurements of properties of the concretes (e.g. detection and localization of cracks, monitoring of the curing process, etc.). It is therefore possible to use these mechanical waves to communicate [241-244]. Thus, some prototypes using ultrasonic waves with frequencies between 1 and 10 kHz were tested and allow data-rates up to 10 kbps over metres. These use a star topology and the differential quadrature phase-shift keying (DQPSK), the 8 states differential phase-shift keying (8-PSK) or the 16-states quadrature amplitude modulation (16-QAM) schemes for the modulation.

Since 1999, four main patents have been filed concerning ultrasonic communications notably through reinforced concrete walls [245-248]. These inventions allow data-rates from 280 bps to 50 kbps, with a 1 MHz carrier frequency. These also consider the transfer of mechanical energy, as well as the possibility of backscattering. Nevertheless, energy consumption data is not yet available and there exist no standards, no complete industrial solutions or no off-the-shelf components yet.

4. Wireless communications into concretes

Regarding the wireless sensor networks dedicated to the monitoring of concretes and/or concrete structures and introduced in the previous sections, these use different wireless communication technologies. Both industrial and academic propositions are relatively discrete about the wireless communication technologies used.

Nevertheless, industrial solutions favour cellular technologies [109, 110, 112-115, 119, 120] but also use NFC [118, 119, 120], RFID [109, 113, 118], Wi-Fi [114], Bluetooth or Bluetooth Low Energy [112-114, 116, 119, 120], low power wide area network (LPWAN) [111, 112, 116-118] as LoRaWAN [111, 112] or SigFox [112, 117, 118]. Only [112] specifies providing NB-IoT and LTE-M technologies. Finally, it seems that [109, 112] provide on-demand other or homemade wireless communication solutions.

Academic research uses a wide variety of wireless communication technologies, often without being precise about their choice or designing their own protocol (thus, only the transceiver reference is provided). NFC, RFID, Wi-Fi, ZigBee, Bluetooth, low power wide area network (LPWAN) whose LoRaWAN and SigFox, cellular and satellite technologies can be drawn from [154-159] and their own references.

Another area of research is the study, the design, the manufacturing and the test of antenna buried into concrete. Indeed, the dielectric properties of the medium (e.g. concretes, etc.), which are changing during time, have a large impact on the performance of antennas. Thus, in order to meet the target requirements (e.g. frequency, bandwidth, gain, radiation pattern, polarization, etc.), the antennas dedicated to be buried directly into concretes must be designed by considerating this complex and moving medium. There are relevant examples for the design and the test of antennas embedded into various concretes (e.g. from wet to dry, etc.), using the industrial, scientific and medical (ISM) 868 or 915 MHz and 2.45GHz ultra-high frequency (UHF) bands [249-255]; and based on different topology: microstrip patch [249, 250, 252-255], dipole [251, 252], planar inverted-F antenna (PIFA) [251, 252] or loop [252]; and for various applications: communication for structural health monitoring (SHM) [249-252, 254, 255] or radio-frequency identification (RFID) [251-253] or even wireless power transfer (WPT) [251, 254, 255].

5. Conclusion

In this section, the main wireless machine-to-machine communication technologies have been presented. A large part has concerned the wireless electromagnetic communications, both in near-field and far-field. For the near-field, NFC (Near Field Communication) and RuBee (IEEE 1902.1) have been described. RFID (radio-frequency identification) technologies which can be in near-field or in far-field have next been explained. For the far-field, first have been introduced IEEE 802 standards with Wi-Fi (IEEE 802.11), Bluetooth and Bluetooth Low Energy (BLE) (IEEE 802.15.1), ultra-wide band (UWB) (IEEE 802.15.3), ZigBee (IEEE 802.15.4), WiMAX (IEEE 802.16), iBurst (IEEE 802.20) and opportunistic wireless regional wireless area networks (IEEE 802.22); then the low-power wide area networks such as DASH7, LoRaWAN and SigFox; the cellular networks with especially the 5G and EC-GSM, LTE-M and NB-IoT; next the satellite networks with low-orbit and geostationary constellations; and finally opportunistic backscattering solutions. After these

usual solutions, both the wireless communication technologies based on the light and on the mechanical waves have been presented. In a final subsection, the wireless machine-to-machine communication technologies employed by industrial and academic solutions were specified as well as the area of research that deals with antennas embedded into concretes. Finally, some strategies are investigated in order to decrease a much as possible the energy needed for the transmission of information within a wireless sensor network [256]. In the next section, the energy management in the case of wireless sensor networks will be detailed, especially regarding the ambient energy harvesting and the wireless power transfer, as well as the storage and use of this energy.

In the framework of the McBIM project and focusing only on the wireless communication part, the main goal is to design a wireless sensor network embedded into reinforced concretes able to transmit the collected data from inside the reinforced concretes to the Internet. This wireless sensor network could employ several wireless communication technologies in function of the targeted parameters: range, coverage, data-rate, energy consumption, availability of infrastructure, etc. Thus, some technologies could be good candidates for this project and other could already be discarded. It is the case for wireless communication technologies based on the light because concretes are not intrinsic propagation media for the light. Whatever, the technological choices made during the project will be discussed further in this manuscript (Section V.A.1.).

Table II.2: Characteristics of the wireless communication technologies presented.

Name	NFC	RuBee	RFID
Standard(s)	ISO/IEC 14443 types A and B, ISO/IEC 18092, ISO/IEC 21481, ISO/IEC 18000-3	IEEE 1902.1	ISO/IEC 18000
Type of communication	Near-field electromagnetic	Near-field electromagnetic	Near-field or far-field electromagnetic
Frequency band(s) (Hz)	13.56 M (ISM)	131 k	125 k, 135 k, 13.56 M (ISM), 433 M (ISM), 868/915 M (ISM), 2.45 G (ISM)
Maximum range of use (m)	0.04 (theoretically up to 0.20)	30	Tens of cm Tens of metres
Maximum theoretical data-rate (bps)	424 k	9.6 k	N/A
Network topology	Master-slave, peer-to-peer	Master-slaves, star	Master-slaves, star
Directionality	Bidirectional	Bidirectional	Bidirectional
Maximum payload (byte)	4 G	N/A	N/A
Minimum frame length with a payload of 1 byte (byte)	4	5	N/A
Modulation scheme(s)	OOK, ASK	ASK, BPSK	N/A
Medium access protocol	ALOAH, On request of the master	ALOAH, On request of the master	ALOAH, On request of the master
Multiplexing	N/A	N/A	N/A
Spread spectrum	N/A	N/A	N/A
Estimation of the power consumption	Very low (backscattering)	Very low (wireless power transfer defined in the standard)	Very low (backscattering) to low (active tag)
Estimation of the security	Secure	High secure	Unsecure

Wi-Fi	Bluetooth and Bluetooth Low Energy (BLE)	Ultra-Wide Band (UWB)	ZigBee	WiMAX
IEEE 802.11	IEEE 802.15.1	IEEE 802.15.3	IEEE 802.15.4	IEEE 802.16
Far-field electromagnetic	Far-field electromagnetic	Far-field electromagnetic	Far-field electromagnetic	Far-field electromagnetic
868/915 M (ISM), 2.45 G (ISM), 5.8 G (ISM), 45 G (ISM), 60 G (ISM)	2.45 G (ISM)	3.1 G to 10.6 G, 57 G to 66 G	868/915 M (ISM), 2.45 G (ISM)	2 G to 66 G
Tens (up to few hundreds)	100	Tens	100	Tens of km
10.53 G	3 M (2 M for the BLE)	Few G	250 k	1 G
Star	Master-slaves, star or meshed; broadcaster/observer, star	Star	Star, Tree, Meshed	Star
Bidirectional	Bidirectional or unidirectional	Bidirectional	Bidirectional	Bidirectional
2304	343 (255 for the BLE)	N/A	104	N/A
33	17	N/A	16	N/A
BPSK, DBPSK, QPSK, DQPSK, 16-QAM, 64-QAM, etc	GFSK, DQPSK, π/4-DQPSK, 8-DPSK	OOK, PPM, BPSK, DBPSK, QPSK, DQPSK	ASK, BPSK, O-PSK	BPSK, QPSK, 16-QAM, 64-QAM
CSMA/CA	ALOAH, On request of the master or the slave; or ALOHA	N/A	CSMA/CA	N/A
OFDM	TDMA	OFDM	N/A	TDMA, OFDM, SOFDM
FHSS, DSSS	FHSS	DSSS	DSSS, PSSS	N/A
Very high	Moderate to very low (BLE, with broadcaster/observer)	Low	Low	High
Moderate	Moderately low	N/A	Unsecure	N/A

iBurst	DASH7	LoRaWAN	SigFox
IEEE 802.20	ISO 18000-7	LoRaWAN	SigFox
Far-field electromagnetic	Far-field electromagnetic	Far-field electromagnetic	Far-field electromagnetic
3.5 G	433 M (ISM), 868/915 M (ISM)	433 M (ISM), 868/915 M (ISM)	866/915 M (ISM)
Few km	Few km	Tens of km	Tens of km
1 M	167 k	50 k	100
Meshed	Star, tree	Star	Star
Bidirectional	Bidirectional	Bidirectional or unidirectional	Bidirectional or unidirectional
N/A	251	250	12
N/A	6	14	13
QPSK, 8-PSK, 16-QAM, 64-QAM	GPSK	LoRa	DBPSK
N/A	CSMA/CA	ALOHA	ALOHA
OFMD	N/A	N/A	N/A
N/A	N/A	CSS	N/A
High	Low	Moderately low	Moderately low
N/A	Moderate	Moderate (to the user’s discretion)	Moderate (to the user’s discretion)

Cellular networks	Satellite networks	Li-Fi	Sonic/Ultrasonic
AMTS, GSM, GPRS, EDGE, UMTS, HSPA, LTE/LTE-A, EC-GSM, NB-IoT, LTE-M	N/A	IEEE 802.15.7	N/A
Far-field electromagnetic	Far-field electromagnetic	Light	Mechanical
450 M, 800 M to 900 M, 1.8 G to 1.9 G, 2.1 G, 2.3 G, 2.6 G, 3.5 G, 5 G, 26 G	N/A	460 T to 670 T	1 k to 10 k
Few km	Hundreds of km	Tens	Several
1.8 G	1 T	96 M	50 k
Meshed	Meshed	Master-slaves, star or peer-to-peer	Master-slaves, star
Bidirectional	Bidirectional	Bidirectional	N/A
N/A	N/A	N/A	N/A
N/A	N/A	26	N/A
GMSK, 8-PSK, QAM	N/A	OOK, PPM, CSK	8-DPSK, DQPSK, 16-QAM
N/A	N/A	N/A	ALOHA
TDMA, FDMA, OFDMA	N/A	N/A	N/A
N/A	N/A	N/A	N/A
High	High	High	N/A
High secure	High Secure	Moderate	N/A

D. Energy management for wireless sensor networks

Always with the great rise of the Internet of Things (IoT), the needs in energy for the wireless sensor networks are exploding. In order to make these fully wireless, the use of wired power supply in unfeasible. Actually, the more common solution is to use batteries that require some maintenance and regular recharge or replacement. All that imposes a direct access and has a non-negligible cost. Thus, and in order to increase the lifespan and the autonomy of the wireless sensor networks, alternatives to supply these are researched [257-267]. The ambient energy harvesting as well as the wireless power transfer (WPT) are two relevant and encouraging solutions, which also allow the deployment of difficult to access or even inaccessible wireless sensor networks. As well, once scavenged, the energy must be efficiently stored before used.

1. Ambient energy harvesting

The principle of the energy harvesting is to collect as much as possible the environmental energy which is usually only loss, and convert and/or store it in another form of energy. This is therefore a renewable energy production system. Here, only the ambient energy harvesting directly providing electrical energy will be presented. There are four main types of ambient energies that can be scavenged and converted into electricity: the light, the mechanical, the thermal and the electromagnetics energies, but hybrid approaches are also studied [257-277].

i. Ambient light energy harvesting

Because of their high presence, the solar and artificial lights are the most abundant ambient energy sources. As a consequence, the ambient light energy harvesting is the most common and used technique for supply wireless sensor networks [257-281]. Thanks to the photovoltaic effect, it is possible to convert both solar and artificial lights into direct-current electricity. In fact, when a semiconducting material is illuminated by light and when a photon has an energy higher than the band gap of the illuminated semiconductor, this one can be absorbed by an electron from the valence band. This last is then excited in a higher energy state and can jump to the conduction band by forming an electron-hole pair, which increases the conductivity of the semiconductor, and finally, an electric current is generated. This current may exist until a recombination of an electron-hole pair occurs, which is a fast phenomenon. By adding ohmic contacts to a semiconductor, a photoconductor is created. In order to maintain and also be able to use the generated current, a separation of the carriers can be imposed which induces a voltage. In this way, photodiodes are privileged to simple photoconductors. There are four types: the p-n (p-type (positively charged extrinsic or doped) semiconductor - n-type (negatively charged extrinsic or doped) semiconductor) diodes, the p-i-n (p-type (positively charged extrinsic or doped) semiconductor - intrinsic or undoped semiconductor - n-type (negatively charged extrinsic or doped) semiconductor) diodes, the heterojunction diodes, and the metal-semiconductor or Schottky diodes; which are also called photovoltaic cells when these are large enough. According to the properties of the used semiconductor (e.g. physical structure, chemical impurities, doping, etc.) and of the radiating light (e.g. spectral composition, irradiance, etc.), the electrical properties (e.g. open-circuit voltage, short-circuit current, etc.) vary as well as the efficiency (defined as the ratio between the generated electrical power and the incident light power).

The more common semiconductor used for photodiodes and photovoltaic applications is Silicon. This can be monocrystalline, multi-crystalline or amorphous, which respectively provide an efficiency under the AM1.5G (air mass of 1.5 for a global terrestrial solar irradiance distribution, that corresponds to the solar irradiance at the surface of the Earth from a solar zenith angle of 48.18°, that is 1 $kW \cdot m^{-2}$) standard at 25 °C of 26.7 %, 22.3 % and 14.0 %. It must be noted that these values are the maximum measured ones and even if the amorphous Silicon is less efficient, it is low cost and particularly adapted to artificial lights. Today, the highest efficiency according to the AM1.5G standard for single cell is achieved by the Gallium-Arsenide (GaAs) thin film solution and is 29.1 %. Nevertheless, various other technologies are under research such as Copper-Indium-Gallium-di-Selenide (CIGS), Cadmium-Telluride (CdTe), Perovskite, dye sensitive, organic, quantum-dots, etc. Today, the objective is to design low cost, high efficiency and eco-friendly photovoltaic cells.

It must be noted that there are maximum theoretical values for the efficiency of photovoltaic cell. The ultimate solar cell efficiency is estimated only by considering the energy band gap of the semiconductor and the light temperature. In the case of the Silicon, the ultimate solar cell efficiency is around 44 %. In parallel, the detailed balance limit of maximum efficiency considers all the contributions to the generation and recombination of electron-hole pairs and is assumed to be more precise. Always in the same case of the Silicon, the detailed balance limit of maximum efficiency is around 29.5 %.

In order to increase the overall efficiency per unit area, two techniques can be used: the use of a light concentrator and the multijunction or tandem topology. The first consists in concentrating the light as much as possible on the photovoltaic cell. As more photons are directed to the cell, it is possible to convert more of them on a same area. The second consists in stacking several cells. As each photodiode absorbs almost all photons with energy above its band gap and is transparent for other photons, by stacking cells optimized for specific energy range or specific frequency range within the light spectrum -that says by progressively reducing the band gap-, it is possible to convert more efficiently a larger quantity of photons. If there was only the cell with the highest band gap, only a part on the photons would be converted. Opposite, if there was only the cell with the lowest band gap, more photons would be converted but all the energy above the band gap would be lost. In the same way, it is possible to discriminate photons according to their frequency and stack cells in order to optimize the conversion of the targeted light spectrum. The photodiodes in a tandem topology can be connected in serial (that induces an alignment on the smallest instantaneous current) or be independent. For instance, the highest measured efficiency according to the AM1.5G standard for multijunction cell is achieved by a six-junction cell and is reached 39.2 %. By adding a concentrator, this value increases up to 47.1 %. For the three-junction cells, the maximum measured efficiency is 37.9 % without concentrator and 44.4 % with a concentrator. Finally, for the two-junction cells, the maximum measured efficiency is 32.9 % without concentrator and 35.5 % with a concentrator, and the ultimate solar cell efficiency is estimated at 42.3 % for independent cells and 41.7 % for the serial topology.

Figure II.4 summarizes the maximum efficiencies of the photovoltaic cells in function of their technology and over time.

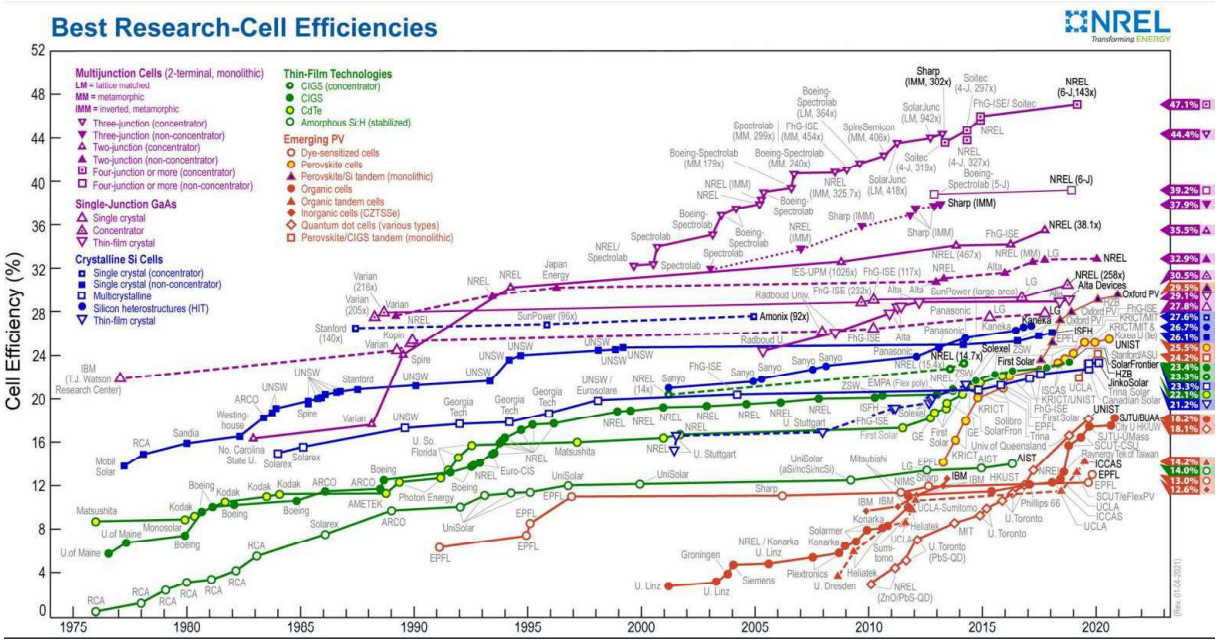

Figure II.4: Best research-cell efficiencies by the National Renewable Energy Laboratory (NREL) of the United States Department of Energy (available online: https://www.nrel.gov/pv/assets/pdfs/best-research-cell-efficiencies.20200104.pdf)

Finally, it exists lots of available academic and industrial photovoltaic cells which can be used to implement ambient light energy harvesters dedicated to wireless sensor networks. For instance [281-297] present low power wide area network (LPWAN) wireless sensors powered by the light energy harvesting. Thus, there are at least nine different LoRa nodes [281-290] and two LoRa gateways [291, 292] which are powered by this way, but some SigFox [293-295], cellular [296] or DASH7 [297] based sensors are also related. These are used in various applications and can be dedicated to the detection of cracks [281], the monitoring of sea water [282, 293], air pollution [283, 284] or environment [285-287, 290, 294], the monitoring of earthquakes [288], the tracking of vehicles [289], the management of heat distribution [297], etc. Then, [298] is an example of a Bluetooth Low Energy (BLE) wireless sensors powered by ambient light energy harvesting able to sense and transmit various environmental parameters such as temperature, humidity, luminosity and pressure. In a different way, [299] reviews some Bluetooth Low Energy (BLE) beacons powered by ambient light energy harvesting and dedicated to the indoor localization, the proximity detection, the notification, the environment interaction, etc. Finally, a procedure to design wireless sensors powered by ambient light energy harvesting is proposed in [300].

ii. Ambient mechanical or kinetic energy harvesting

Mechanical or kinetic energies are due to the movement of material particles and can reveal more forms, such as vibrations, displacements, fluid flows and pressures (or forces). These can be provided by several sources, whose human activities and natural, structure or machine vibrations. And in function of the nature of the mechanical energy sources, the more adapted transducer must be employed. There are three main families: the electrostatic, the electromagnetic and the piezoelectric transducers [257-277, 301-303]. For instance, and in the case of vibrations, the transducer must be tuned in order to increase the coupling coefficient and the transmission coefficient, and thus, convert most efficiently the mechanical energy into

electricity. For this purpose, a cantilever with a well-tuned mass can be employed to amplify vibrations in a particular direction, if the resonance frequency of the system matches with the targeted frequency. Moreover, ambient mechanical harvesters are highly application dependent. To override the limitation induced by the need of a high coupling between the frequency of the harvester and of the source, mechanical or electrical tuning, adaptative tuning or self-tuning of the resonant frequency capabilities can be used, as well as multiband or wideband array of harvesters. In terms of efficiency, this one is maximized when the mass of the system is maximized too, and the resonant frequency is as low as possible, always by achieving the highest coupling.

a. Electrostatic and triboelectric transducer

There are three types of electrostatic transducers [257-277, 302-305]. The two first are based on the capacitive effect. The first consists in harvesting energy from the variation of the charge stored in a variable capacitor charged with a constant voltage. The second consists in harvesting energy from the variation of the voltage in a variable capacitor charged with a constant charge. It is the relative displacement between the capacitor plates which generates the energy. It must be noted that for the two transducers an initial charge must be applied, and there are not linear and the coupling coefficient is also function of the amplitude of the source. Next, the first transducer allows to generate more energy than the second at the price of a more complex implementation and the need to applied a constant voltage. The third combines the electrostatic induction effect with the triboelectric effect, which consists in a contact electrification. These kinds of transducers can be implemented as compact microelectromechanical systems (MEMS).

b. Electromagnetic or inductive transducer

The electromagnetic or inductive transducers are based on Faraday's law of induction and consist in the generation of a voltage (or electromotive force) when a conductor, generally a coil and sometimes a disk or a conductive fluid (e.g. an ionized gas or plasma, etc.), is moving inside a magnetic field [257-265, 267-277, 301-303, 306, 307]. The movement can be linear or circular and usually the magnetic field is generated by permanent magnets. The transducer can provide a direct current such as for the dynamos, or an alternative current such as for the alternators. The electromagnetic transducers are the most widespread in the large-scale energy production. These can be found in the turbine used in hydroelectric dams, in wind mills or in thermal power plants, and even in nuclear power plants. For smaller energy scale, these transducers can be employed to supply a wrist watch or tiny objects in a cantilever topology.

c. Piezoelectric transducer

The piezoelectric transducers are based on the piezoelectric effect: piezoelectric materials generate an electric field when under mechanical stress; and inversely, change their mechanical structure when under electric field [257-263, 265, 267-277, 301-303, 308-311]. This effect is mainly due to the presence of electric dipole moments within the material, that will align on the microscopic scale when under mechanical stress, that which will induce polarization and a voltage along the material at the macroscopic scale. It must be noted that piezoelectric materials are anisotropic, thus, the direction of the mechanical stress and of the electric field have an influence on its behaviour in response. Ferroelectric Perovskites, such as Lead-Zirconate-Titanate (PZT), and piezoelectric polymer materials, such as Polyvinylidene

Fluoride (PVDF), are the most commonly used. These harvesters can be employed (for instance in a cantilever topology) to supply small objects as RFID tags.

d. Hybrid transducer

There are some hybrid transducers based on triboelectric and electromagnetic effects [312-314], on triboelectric and piezoelectric effects [315, 316] and on electromagnetic and piezoelectric effects [303, 317-320], and even on the three previous effects [321].

It exists some of available academic and industrial ambient mechanical energy harvesters based on the different types of transducers. For instance, [322-324] present wireless sensors powered by the mechanical energy harvesting. Thus, there are some which communicate in LoRa [322, 323], Bluetooth [323] or SigFox [324]. These are able to harvest mechanical energy from bridge vibrations [322], from industrial machinery vibrations [323] and even from the movements of oceanic waves [324], respectively to monitor the structural health of the bridge or of the industrial machineries and the water quality.

iii. Ambient thermal energy harvesting

There are two effects that can be used in order to convert thermal energy into electricity: the pyroelectric effect and the thermoelectric effect [257-259, 261-265, 267-277, 325, 326].

a. Pyroelectric transducer

The pyroelectric materials (e.g. some crystals such as Tourmaline, etc., and semiconductors such as Gallium Nitrite (GaN), etc.) are naturally electrically polarized and generate a temporary voltage across themselves when their temperature varies [262-264, 271, 273, 276, 325-329]. Because of leakage current, this effect is not permanent if the temperature stabilises. By subjecting the pyroelectric materials to heating and cooling (or thermodynamic) cycles, it becomes possible to generate low alternative current, and thus, harvests energy.

b. Thermoelectric transducer

There are three thermoelectric effects: the Seebeck effect, the Peltier effect and the Thomson effect. The Seebeck effect says that if there is a temperature gradient between two different metals or semiconductors in contact, then a voltage between these two elements is induced. The Peltier effect is its opposite, if a voltage is applied to two different metals or semiconductors in contact, then a current flow through the junction and a temperature gradient is generated between the two elements. Thus, one element generates thermal energy and the other absorbs thermal energy. The Thomson effect concerns a unique metal or semiconductor: if there is a temperature gradient into the element, then a voltage occurs which generates a current. These three effects are related through the Kelvin relationships.

The thermoelectric generators (TEG) use the Seebeck effect and are generally composed of a matrix of pairs of p-type (positively charged extrinsic or doped) and n-type (negatively charged extrinsic or doped) semiconductors electrically connected in series and thermally in parallel [257-259, 261-265, 267-277, 325, 326, 330-332]. This matrix is generally placed between two thermally conductive terminals where is applied the temperature gradient. The good thermoelectric materials have both high electrical conductivity and low thermal conductivity, and are characterized by their Seebeck coefficient. Their efficiency is relatively low and is highly function of the temperature gradient.

Today, there are a very few academic and no industrial ambient thermal energy harvesters based on the pyroelectric effect, and only a few based on the thermoelectric effect. Again, some LoRa wireless sensors powered by the ambient thermal energy harvesting based on the Seebeck effect are introduced in [333-335] as well as one DASH7 wireless sensor [297]. The temperature gradient is exploited from various sources such as heat pipes [333], tree [334], industrial machineries [335] or domestic radiators [297], for monitoring environment parameters [333, 334], the air pollution [333], industrial processes [335] or the management of heat distribution [297]. More, [336] presents a wireless weather station supplied through a thermoelectric generator and transmitting pressure, humidity and temperature data thanks to Bluetooth Low Energy beacon technology. Finally, [337] introduces a wireless sensor powered by a thermoelectric generator, communicating through ZigBee and dedicated to the monitoring of vibrating industrial machinery, and was specifically tested on a band saw.

iv. Ambient electromagnetic energy harvesting

As well as for wireless electromagnetic communications, the ambient electromagnetic energy can be both harvested in near-field and far-field [257, 258, 260-267, 270-277]. For the near-field, both the electric and magnetic fields can be exploited, respectively by capacitive and inductive coupling. For the far-field, these are the radiated electromagnetic waves which are harvested.

a. Ambient capacitive and inductive, or near-field electromagnetic energy harvesting

Ambient electromagnetic energy sources which can be used by near-field harvesters are commonly issued from alternative current power transmission lines, and more globally from current-carrying materials and structures [261, 271, 273, 338]. Thus, these kinds of energy harvesters are essentially deployed to monitor the smart grids which carry alternative currents. By being alternative, these currents generate varying electromagnetic fields, for which both the electric and magnetic fields fluctuate.

* Capacitive transducers are able to generate electric energy from the electric field by capacitive coupling [261, 271, 273, 338, 339]. In the case of an electrostatic field, as for the continuous component a quasi-static electric field, by locating two electrodes in and along the direction of this field, a potential difference -that says a voltage- appears between the electrodes. By connecting a load between them, a direct current will flow due to the voltage, and thus, the electric field energy is harvested. If the electric field varies, by using the capacitive voltage-division principle, an alternative current will be saw by the load between the two electrodes. It is common to consider one electrode at the potential of the source and the other at the potential of the ground. There are three topologies for using these related to the connection mode and the load position in the created capacitor: the direct mode, the low potential and the high potential. In the direct mode, the load is directly connected between the two electrodes (almost between the almost source potential and the ground); in the low potential and in the high potential, an intermediate electrode is used; if the load is between the intermediate electrode and the ground, it is the low potential topology; and if the load is between the almost source potential and the intermediate electrode, it is the high potential topology. Nevertheless, this kind of harvesters is widely dependent of a high electric field, and thus, required high voltages.

* Inductive transducers are able to generate electric energy from the magnetic field by inductive coupling [261, 271, 273, 338, 340]. In the case of an alternative magnetic field, by locating a coil -with or without a ferromagnetic core- collinearly and in this field, an alternative voltage (with a value depending on the source voltage and the coil geometry) with the same frequency appears inside. By connecting a load at the ports of the coil, an alternative current will flow due to the voltage, and thus, the magnetic field energy is harvested. This is the same principle used for electrical transformers with galvanic isolation. If the magnetic field is constant, this harvester does not work. There are two topologies for using these related to the relative position to the ambient energy source: the low potential or stand-alone; and the high potential. In the low potential or stand-alone topology, the coil is located in the direct neighbourhood of the current-carrying element; and in the high potential, it is directly clamped around of the current-carrying element. Each topology requires specifically designed coils. For the first topology, the coils can be small and produced as compact microelectromechanical systems (MEMS). More, this topology allows more flexibility in terms of deployment because it does not require a direct access to the current-carrier element. The second topology allows a higher efficiency and the possibility to harvest a greater quantity of ambient energy, at the price of a definitive and highly constrained implementation. Nevertheless, this kind of harvesters is widely dependent of a high magnetic field, and thus, required high alternative currents.

Currently, there are several academic and no industrial ambient near-field electromagnetic energy harvesters based on the capacitive and inductive inductions. For instance, [341] provides a sensor powered by the electric field harvesting thanks to a capacitive harvester. In parallel, [342] and [343] propose respectively a LoRaWAN and Bluetooth Low Energy sensors powered by the magnetic field harvesting thanks to inductive harvesters. [343] is used as weather station, able to measure and transmit temperature, humidity and pressure data, whilst [342] allows indirect monitoring of the current consumption in a building. For its part [341] was tested in the two previous use cases.

b. Ambient radiative or far-field electromagnetic energy harvesting

Ambient far-field electromagnetic energy harvesting consists in recovering the electromagnetic waves radiated by various natural and artificial sources and converts these in direct current electricity [257, 258, 260-267, 270, 272, 273, 275-277, 344, 345]. Usually, the electromagnetic radiations with highest power densities and of sufficiently high frequencies, such as radiofrequencies, are preferred, as these obviously provide the largest potential amounts of energy and are easily usable. These electromagnetic radiations are generally issued from human activities and more specifically from wireless communications and broadcastings. In a similar way to wireless communications, an antenna is used to collect the electromagnetic waves in a specific frequency band and to convert these to radiofrequency electric signals. However, it is not the carried information which is sought but the energy. Thus, the radiofrequency signals are then converted into direct current electricity thanks to a radiofrequency rectifier (or RF-to-DC converter) tuned to be properly used in the targeted frequency band. The combination of an antenna and a radiofrequency rectifier is called rectenna (or rectifying antenna). In order to optimise the energy transfer between the antenna and the rectifier, either the rectenna is designed as a single unit (through the complex conjugate impedance matching), or an impedance matching network can be used (with localised (e.g. capacitor, inductor, etc.) or distributed (e.g. line, stub, etc.) components, or even with a hybrid circuit). In semi-active radio identification (RFID) tag, a rectenna is

commonly used to harvest enough energy to power the active components whilst a part of the incident wave is backscattered and re-modulated to transmit data.

Today, rectenna are widely used in academic and industrial semi-active radio identification (RFID) tags, but there are some academic and few industrial ambient far-field electromagnetic energy harvesters dedicated to other applications. For instance [346] harvests the radiative energy lost by a microwave oven to supply various sensors or actuators whose the power consumption is comparable to that of sensors deployed in wireless networks. More, [347] and [348] provide computing nodes fully powered by the radiative energy harvesting from analogue and digital television broadcastings. [349] goes further by powering a wireless sensor able to measure temperature and storage element voltage and to transmit the collected data through the proprietary SimpliciTI wireless technology, thanks to the ambient energy harvesting issued from analogue and digital television broadcastings. As well, [350] provide a sensor able to wirelessly transmit, through the proprietary SimpliciTI technology, the measured luminosity and temperature data and which scavenges the ambient radiofrequency energy produced by the analogue and digital television broadcasters, but even by the cellular networks. More recently, [351] proposes a Bluetooth wireless temperature and self-orientation sensor powered by the harvesting of the ambient radiative energy from frequency modulated (FM) radio broadcasting stations. Finally, [352] explores the feasibility of powering LoRaWAN wireless sensor thanks to the ambient far-field electromagnetic energy harvesting.

v. Hybrid energy harvesters

Because a unique type of ambient energy source may not be sufficient to power a wireless sensor, several "macro" hybrid energy harvesters were proposed in the literature [261-265, 267, 273, 274, 276, 277, 353].

Several hybrid light and mechanical (or kinetic) energy harvesters are presented in [354-357]: [354] proposes a hybrid harvester based on the combination of a piezoelectric microelectromechanical systems (MEMS) and an amorphous Silicon photovoltaic cell which are separated but use a unique power management circuit, intended to be used to power indoor wireless sensor networks; [355] provides a hybrid harvester based on the combination of a piezoelectric cantilever and an poly-crystallin Silicon photovoltaic cell which are separated but use a unique power management circuit, tested as an indoor power supply for a wireless Bluetooth sensor; [356] proposes the design of a hybrid harvester based on a vibration harvester (using a piezoelectric, an electrostatic and an electromagnetic transducers) and a mono-crystallin Silicon photovoltaic cell; and [357] provides a monobloc hybrid harvester using a piezoelectric cantilever transducer where the tip masses are flexible thin film photovoltaic cells, which are intended to power small electronic devices.

Several hybrid light and thermal energy harvesters are presented in [358-360]: [358] proposes the design of a hybrid harvester based on the combination of a thermoelectric generator and a flexible hydrogenate amorphous Silicon photovoltaic cell, used as a substrate for a textile antenna dedicated to the deployment of a wireless body area network; [359] and [360] provide two wireless LoRaWAN sensors using both thermoelectric and photovoltaic transducers and respectively dedicated to the monitoring of the environment (through the use of microelectromechanical systems (MEMS) light, humidity, temperature and pressure sensors and a inertial measurement unit) and the monitoring of water quality (thanks to a floating device which collects and transmits temperature, humidity and pH data).

There are more hybrid light and electromagnetic energy harvesters [231, 361-372]. For instance, [361] provides a combination of a standalone rectenna and a standalone photovoltaic cell connected on a common energy management circuit. In another way [362] reviews the rectenna on which a solar cell is positioned to provide a hybrid energy harvester. Among these solutions, some use flexible substrate and photovoltaic cell [363, 364], others conventional substrate as FR4 [365, 366] or Rogers RO4003 [367] or three-dimensional printing techniques [368]. More, some semi-active radiofrequency identification (RFID) tags use a hybrid light and electromagnetic energy harvester to power their sensors such as [369] or [370], which respectively used a combination of a standalone harvesters and a monobloc harvester. Differently, [371] presents a wireless Bluetooth Low Energy beacon which is powered by a rectenna whose the rectifier is biased by a photovoltaic cell to increase its efficiency. This is, thus, another way to implement a hybrid light and electromagnetic energy harvester. Finally, [231] introduces a wireless ambient LoRaWAN backscatter sensor which harvests ambient radiative electromagnetic waves and ambient light to power its active components; and [372] proposes a wireless LoRaWAN sensor powered by a hybrid light and electromagnetic energy harvester and dedicated to the monitoring of the environment through the measurement and transmission of luminosity, loudness, air-quality, temperature, humidity and pressure data.

To date, only one hybrid mechanical (or kinetic) and thermal energy harvester has been found. Presented in [373], it uses two piezoelectric cantilevers located on a flexible substrate which contains several thermoelectric generators.

Few hybrid mechanical (or kinetic) and electromagnetic energy harvesters are present in the literature. For instances, [374] proposes one based on the combination of a rectenna and an electromagnetic transducer to harvest both radiated electromagnetic waves and mechanical vibrations; and [375] proposes another based on a dipole rectenna whose each pole is used as a cantilever for a piezoelectric transducer in order to collect again both radiated electromagnetic waves and mechanical vibrations.

Very few hybrid thermal and electromagnetic energy harvesters can be found in the literature. Nevertheless, [376] and [377] propose through the addition of a thermoelectric generator on the radiative area of a patch rectenna, an integrated implementation of this kind of hybrid harvester. In another way, [378] presents a standalone rectenna whose the rectifier is biased by a standalone thermoelectric generator to increase its efficiency. This is, thus, another way to implement a hybrid thermal and electromagnetic energy harvester.

There are also hybrid harvesters able to collect energy from three ambient sources. This is the case for the solutions presented in [379-382]. Thus, [379] and [380] provide two hybrid ambient light, mechanical and thermal energy harvesters, whose the latter is intended to power a wireless LoRaWAN sensor. More, [381] introduces an ambient light, mechanical and electromagnetic energy harvester, whilst [382] a monobloc ambient light, thermal and electromagnetic energy harvester. Only solutions for "macro" hybrid ambient mechanical, thermal and electromagnetic, and hybrid ambient light, mechanical, thermal and electromagnetic energy harvesters were not found in the current literature.

In addition to these "macro" harvesters, there are hybrid nanogenerators which are still under study and [383] introduces some of these. Moreover, [384] describes a monobloc

hybrid mechanical and thermal nanogenerator based on the triboelectric, the piezoelectric and the pyroelectric effects, whilst [385] uses the piezoelectric and the pyroelectric effects for a monobloc hybrid mechanical and thermal nanogenerator able to harvest infrared radiations. Finally, [386] presents a monobloc hybrid light, mechanical and thermal nanogenerator based on the photoelectric, the triboelectric, the piezoelectric and the pyroelectric effects.

Two additional examples, [271] and [387], are relevant to present as these respectively convert an ambient electromagnetic field into a mechanical vibration and ambient light into a radiofrequency signal, which are then turned into electricity. Thus, the conversion requires two steps against one for the listed other harvesters.

The ambient energy sources are by nature fluctuating, uncontrollable and unpredictable. Thus, these are widely dependent of various parameters, as the location, the time of day, the time of year, the weather, the human activities, etc. For instance, the indoors and the outdoors ambient lights are not the same. More, the outdoors ambient light, essentially due to the Sun, is not the same at midday and at midnight, during the winter and during the summer, at the equator and at the poles, in a sunny day, in a cloudy day and in a raining day, etc. It is similar for the indoors ambient light which differs in a veranda and in a basement, with the type (e.g. LED versus halogen, etc.) and the density of artificial lightings, etc. As another example, in the case of mechanical or kinetic sources, the natural vibrations of the Earth, of a home, of an office building and of a transportation bridge are largely different, as well as the fluid flows (e.g. the wind, etc.) are not equally distributed in the space and time, etc. In a similar way, the temperature variations do not have the same speed and intensity for an outdoor wall of a house and for an intermittent industrial heater, as well as the temperature gradient between the human skin and its direct environment cannot be compared with the one between the turbine of an aircraft in flight and its direct environment. Finally, the same reasoning can be applied to the ambient electromagnetic waves which depend of the density of wireless equipment, such as television and radio broadcasters, cellular towers, wi-fi gateways, smartphones, connected objects, etc., as well as the distance and the proprieties of the propagation media between the source and the observer, and the properties of the harvesters (e.g. frequency, bandwidth, gain, radiation pattern, etc.). Nevertheless, various values for the power density of each kind of ambient energy source can be read in the literature [257, 258, 260, 261, 264, 265, 270, 272, 274-277, 300]. Thus, the outdoors ambient light power density can be estimated between 150 $nW \cdot cm^{-3}$ and 10 $mW \cdot cm^{-3}$, the indoors ambient light power density between 3 and 400 $\mu W \cdot cm^{-3}$, the ambient mechanical power density between 1 and 800 $\mu W \cdot cm^{-3}$, the ambient temperature variations power density around 10 $\mu W \cdot cm^{-3}$ and the ambient temperature gradient power density between 10 $\mu W \cdot cm^{-3}$ and 10 $mW \cdot cm^{-3}$, and the ambient electromagnetic power density between 80 $pW \cdot cm^{-3}$ and 100 $nW \cdot cm^{-3}$. However, this is only an idea of the orders of magnitude of the power densities which vary largely with various parameters. Thus, only measurements can provide relevant information for the availability of an ambient energy source in a given space and time. That is what is proposed in [273] and [388], respectively by measuring the light, mechanical, thermal and electromagnetically power densities in 2013 in European commercial (POLAND) and residential (UNITED-KINGDOM and SPAIN) buildings, and by measuring the electromagnetically power density in 2021 in Montréal, CANADA.

2. Wireless power transfer

A way to be independent of ambient fluctuating, uncontrollable and unpredictable energy sources is to use specifically dedicated sources to wirelessly transfer power [257, 262, 266, 267, 277, 345, 389]. It is the concept of the wireless power transfer or transmission (WPT). In this case, the energy harvesters used stay the same as those used with ambient sources, but a specifically designed source is then used.

i. Light wireless power transfer

Light or optical wireless power transfer concerns the systems which generate a light beam wirelessly transmitted with the goal to remotely power another system [262, 389]. Commonly, a laser is used as a source, as well as a photovoltaic cell as a harvester. This implementation can be called laser power transmission (LPT). In [390], an overview of the state-of-the-art components (laser diodes and photovoltaic cells) and techniques to design and optimize the laser power transmission systems is proposed. Also, [391] discusses on the first implementations of laser power transmission systems and lists some experimentations and applications, both terrestrial and spatial. Then, [392] and [393] present two terrestrial applications of the laser power transmission systems, the first is an implementation which allows to wirelessly power a smartphone while insuring that the system is safe for human, and the second is an implementation to remotely control a power relay to limit the current loses of domestic appliances when on standby mode. In all cases, even if these systems are efficient, their main weakness is that a direct line of sight is required between the source and the harvester. Thus, these are promising for spatial applications, but less for terrestrial ones.

ii. Mechanical wireless power transfer

Mechanical wireless power transfer concerns the systems which generally generate mechanical vibrations with the goal to remotely power another system [257, 262]. Commonly, acoustic and ultrasonic waves are used as sources, as well as piezoelectric transducers as harvesters. In [394-396], periodic reviews of advances in acoustic energy transmission (AET) are provided. In [397], an experimental ultrasonic power transmission system is presented as a proof-of-concept, tested both in air and underwater and over some centimetres. Lastly, the patents [245-248] relate the possibility to wirelessly power embedded sensors and actuators through the transmission of dedicated and energetic ultrasonic waves.

iii. Electromagnetic wireless power transfer

Electromagnetic wireless power transfer concerns the systems which generate electromagnetic fields with the goal to remotely power another system. This concept was yet imagined and studied by Nikola Tesla at the end of the XIXth century and at the begin of the XXth century. As well as for ambient electromagnetic energy harvesting, the electromagnetic wireless power transfer can be both used in near-field and far-field [257, 262, 266, 267, 277, 389, 398-402]. For the near-field, both the electric and magnetic fields can be exploited, respectively by capacitive and inductive coupling. This latter can be non-resonant or resonant. For the far-field, these are the radiated electromagnetic waves which are transmitted.

a. Capacitive and inductive, or near-field electromagnetic wireless power transfer

Near-field, both capacitive and inductive, electromagnetic wireless power transfer allows short range energy transfer thanks to the use of electromagnetic field [257, 262, 266, 267, 277, 345, 389, 399-402].

* Capacitive wireless power transfer uses only the electric field through capacitive coupling to transfer energy between two systems [399, 401-403]. The capacitive couplers are usually composed of four (sometimes two or six) metal plates, the first half in the transmitter and the second in the receiver, that form capacitors. This technique allows power transmission over millimetres; requires high voltages; is insensitive to the presence of metal, and thus, works properly for the transfers through metal, especially thanks to the negligible eddy-current losses which are induced by the magnetic field; has low electromagnetic interferences because the electric field can be easily contained between the capacitive plates; is not very sensitive to the misalignment between the source and the harvester; and presents an efficiency higher than 90 %. Nevertheless, it is commonly used with moderate power densities and the strong electric field may pose security problems.

* Non-resonant inductive coupling wireless power transfer uses only the magnetic field through coupled inductors, commonly coils, to transfer energy between two systems [257, 262, 266, 267, 277, 345, 389, 398-402]. This technique allows power transmission over centimetres; is highly sensitive to the presence of metal, and thus, does not work for the transfers through metal, especially due to the eddy-current losses which are induced by the magnetic field; requires a high coupling coefficient between the source and the harvester; is dependent of the size and geometry of the coils; is highly sensitive to the misalignment; and presents an efficiency higher than 90 %. Moreover, it is commonly used with high power densities.

* Resonant inductive or magnetic resonant coupling wireless power transfer is an improvement of the non-resonant inductive coupling one and allows to increase the use distance and the efficiency [257, 262, 266, 267, 277, 345, 389, 398-402, 404]. In these systems, the inductor is made to resonate with a capacitor at the same frequency (or pulsation) in the source and in the harvester. This technique allows power transmission from centimetres to meters; is always highly sensitive to the presence of metal, and thus, does not work for the transfers through metal, especially due to the eddy-current losses which are induced by the magnetic field; requires a high coupling coefficient between the resonators in the source and in the harvester; is dependent of the size and geometry of the coils; is highly sensitive to the misalignment; and presents an efficiency higher than 90 %. Moreover, it is commonly used with high power densities.

Today, two consortiums provide standard for resonant inductive coupling wireless power transfer for charging devices: the Wireless Power Consortium [405], which carries Qi; and the Airfuel Alliance [406].

The short-range radio identification (RFID) technologies use generally the resonant inductive coupling to supply the semi-active tags through near-field electromagnetic wireless power transfer. A theoretical study on the feasibility to power LoRaWAN devices by magnetic resonant coupling wireless power transfer over metres is made in [407].

b. Radiative or far-field electromagnetic wireless power transfer

Far-field electromagnetic wireless power transfer allows medium range energy transfer thanks to the use of electromagnetic field [257, 262, 266, 267, 277, 345, 389, 408-410]. This technique allows power transmission over metres, or even tens of metres; the rectenna must be designed in function of the parameters of the source of the radiated electromagnetic waves,

especially in terms of frequency; and presents an efficiency between low and high, highly correlated to the used power densities, which can be low to high.

At their early age, the far-field electromagnetic wireless power transfer systems were mainly designed and optimized for high power supply of a single system by a dedicated source and thus, high efficiencies were successfully reached [277, 398, 399, 408]. However, today, the radiative electromagnetic wireless power transfer systems are oriented towards ubiquitous applications with very low power densities, such as wireless sensor networks, partly because of, on the one hand, the desire to reduce the global energy consumption, and on the other, to ensure the safety of living beings. Thus, these systems are subject to regulations, still in progress, which will be similar to those used for wireless communications. For Europe, the decisions of the European Commission (EC) [411], the recommendations of the Electronic Communications Committee (ECC) of the European Research Council (ERC) [412], and the guidelines of the European Telecommunications Standards Institute (ETSI) [413], as well as, for France, the decision "*Autorité de régulation des communications électroniques, des postes et de la distribution de la presse*" (ARCEP) [414], and their eventual evolving, must be considered.

Today, far-field electromagnetic wireless power transfer is used both by academics and industrials, particularly for wireless sensor networks and the remote charging. The medium-range radio identification (RFID) technologies use generally far-field electromagnetic wireless power transfer to supply the semi-active tags. In another way, [415] proposes an experimental study of a radiative electromagnetic wireless power transfer system to supply an emulator of wireless sensor made of variable loads. This work uses a source generating electromagnetic waves in the industrial, scientific and medical (ISM) 868 MHz frequency band with an effective isotropic radiated power (EIRP) or effective radiated power (ERP) of 3 W (or +34.8 dBm). In this configuration, the emulated wireless sensor can be supply up to 9 metres. Some works related the implementation of wireless sensors dedicated to low-power wide area network (LPWAN). [416] proposes a Bluetooth Low Energy wireless temperature and angular velocity sensor that is continuously and remotely powered up to 1 metre (but possibly further) by an electromagnetic wave source in the 868 MHz industrial, scientific and medical (ISM) frequency band with an effective isotropic radiated power (EIRP) of up to 3.2 W (or +35 dBm), and is dedicated to the monitoring of rotating machines. In parallel, [417] introduces an experimental study on the feasibility to continuously power a LoRaWAN wireless sensor thanks to a radiative electromagnetic wireless power transfer system in the industrial, scientific and medical (ISM) 868 MHz frequency band. It concludes that a 3.2 metres range of use can be reached. As well, [418] presents a LoRa wireless temperature and acceleration sensor that is continuously and remotely powered up to 54 centimetres by two electromagnetic wave sources in the 2.45 MHz industrial, scientific and medical (ISM) frequency band with an effective isotropic radiated power (EIRP) of 500 mW (or +27 dBm), and is dedicated to the monitoring of engine parts, so in harsh metallic environment. Also, a DASH7 wireless temperature and humidity sensor wirelessly powered by radiative electromagnetic wireless power transfer working in the industrial, scientific and medical (ISM) 868 MHz frequency band is introduced in [419] and can respectively be powered up to 17 metres and 8.4 metres from a source with an effective radiated power of 2 W (or +33 dBm) and of 500 mW (+27dBm). Wireless personal area network (WPAN) technologies are also used to designed wireless sensors powered remotely by radiative electromagnetic wireless power transfer. For instance, [420] presents a Bluetooth wireless acceleration, temperature

and pressure sensor that is continuously and remotely powered up to 1.8 metres by an electromagnetic wave source in the 868 MHz industrial, scientific and medical (ISM) frequency band with an effective isotropic radiated power (EIRP) of 500 mW (or +27 dBm). In the same project as for [416], [421] proposes a Bluetooth Low Energy (BLE) wireless temperature and angular velocity sensor that is continuously and remotely powered up to 1.6 metres (but possibly further) by an electromagnetic wave source in the 868 MHz industrial, scientific and medical (ISM) frequency band with an effective isotropic radiated power (EIRP) of up to 2.9 W (or +34.6 dBm), and is dedicated to the monitoring of rotating machines. Finally, [422] describes a ZigBee wireless impedance sensor remotely powered between 1 and 2 metres thanks to a radiative electromagnetic wireless power transfer system in the industrial, scientific and medical (ISM) 2.45 GHz frequency band radiating an effective radiated power (ERP) of 1 W (or +30 dBm). On the industry side, Powercast sells wireless charging systems and wireless continuous supply systems, still based on far-field electromagnetic wireless power transfer for various domestic applications, such as temperature sensors, fully wireless controller, etc. as well as development tools [423]. Its system uses a source of radiated electromagnetic waves in the 915 MHz industrial, scientific and medical (ISM) frequency band and with effective isotropic radiated powers (EIRP) of 1W (or +30 dBm) or 3 W (+34.8 dBm). Ossia provides the Cota solution that allows wireless charging systems and wireless continuous supply systems, both based on far-field electromagnetic wireless power transfer, once again for domestic applications [424]. GreenWake proposes a wireless multi-sensor platform dedicated to deploy wireless sensor networks for structural health monitoring of civil structures, machines, etc., where the wireless sensors are remotely powered thanks to a radiative electromagnetic wireless power transfer system in the industrial, scientific and medical (ISM) 2.45 GHz frequency band radiating an effective radiated power (ERP) between 500 mW (or +27 dBm) and 4 W (or +36 dBm) [425]. Finally, the Airfuel alliance proposes its own standard for wireless power transfer system based on far-field electromagnetic wireless power transfer [406].

To finish with the electromagnetic wireless power transfer, there are a few sources of electromagnetic fields that are energy autonomous. This is the case in [426] and [427] where sources of far-field electromagnetic power are implemented thanks to the ambient light energy harvesting which is directly converted into radiated electromagnetic waves through class-E oscillators connected to an antenna. These systems use low cost flexible substrates, as Polyethylene Terephthalate (PET) and paper. As well, [428] proposes to convert the harvested mechanical energy from rotational movements into an electromagnetic field used to wirelessly power a remoted device through near-field inductive coupling. These autonomous power sources can be easily deployed as additional power sources in a wireless sensor network in which the wireless sensors scavenge the electromagnetic fields.

iv. Simultaneous wireless information and power transmission

The problem of sharing the propagation medium for the simultaneous wireless transmission of the information and of the energy emerged in the last 2000s as a formal optimisation problem [429-432], was primarily intended for the use in wireless electromagnetic communications and in wireless electromagnetic power transfer, and led to the definition of the simultaneous wireless information and power transmission (SWIPT) paradigm [399, 433-437]. The main techniques to share the shared medium between the two functions are based on: the temporal multiplexing (each function has a dedicated time period to be achieved); the frequential multiplexing (the last arrival; each function has its own

specific sub-part of the medium); the power splitting (only a part of the input is used to get the information and all the rest is used to obtain energy); and the spatial multiplexing (either each function has its own receiver, or in the case of an array of receivers, a part of its array is dynamically allocated to one of the function and the rest to the other). More, in the case of star network topology the two functions can be carried out by the same device or be separated, with power sources and information access points. Moreover, the implementation of the simultaneous wireless information and power transmission has been investigated in the case of the deployment of the fifth generation(5G) of cellular networks [438], as well as in the eventual case of the implementation of a first generation (1G) of power network especially dedicated to power supply wireless sensor networks (WSN) for Internet of Things (IoT) applications [439], and even in the automation and transportation domains [440].

Finally, there are lot of practical implementations of the simultaneous wireless information and power transmission (SWIPT) paradigm. Once again, the radio identification (RFID) technologies are the leading candidates. Nevertheless, other solutions were proposed in the literature, such as in [441] where a simultaneous wireless information and power transmission (SWIPT) system is combined with backscatter techniques which allows to transmit information and to power a node that then responds by backscattering; but particularly some of the earlier presented implementations of wireless sensors using the far-field electromagnetic wireless power transfer technique. Thus, [418], [422] and [425] provide implementations of the simultaneous wireless information and power transmission (SWIPT) paradigm by being based on a spatial multiplexing (the same frequency band is used, but with two separated antennas for the two functions), whilst [416], [419], [420] and [421] mix spatial and frequency multiplexing (separated frequency bands and two separated antennas are used for the two functions), and at last [441] uses temporal multiplexing (the same frequency band and the same antenna is used for the two functions, but the communication takes place after an interrogation). One more time, the patents related to the wireless mechanical communication and power transmission seem to implement the simultaneous wireless information and power transmission (SWIPT) paradigm apart from the use of electromagnetic waves as information and power carriers [245-248].

v. Optimization of the energy collection

For all the harvesters previously introduced, some techniques can be used to optimize their efficiency, both in the cases of ambient energy harvesting and wireless power transfer.

For the light energy harvesting [257-300, 389-393], the used materials are designed, especially doped, in order to scavenge as much energy as possible within the available light spectrum; the light concentrators allow the energy to converge in the active area; some photodiodes can be placed in arrays, in series, in parallel or both, to form a photovoltaic cell providing respectively higher voltage and current, or both; or even be stacked to form a multijunction structure and scavenge larger part of the available light spectrum. More, techniques for predicting luminosity as a function of time can be used to optimize the used of light harvesters and to propose a relevant energy management strategy especially with storage [258, 264, 285, 286, 300]. Finally, in the case of light wireless power transfer, the light beams are designed to be as narrow as possible and are precisely targeted at the harvesters to waste as little energy as possible.

For the mechanical energy harvesting [245-248, 257-277, 301-324, 394-397], the harvesters are tuned to deform with the greatest amplitude and periodicity, especially in the case of vibrations, these are designed so that their own frequency matches that of the targeted; cantilevers, rotating systems or other vibrating and rotating elements can be used to transform the random mechanical movements into those best suited to the harvesters; some harvesters, with the same frequency or different ones, can be placed in arrays, particularly in parallel, to scavenge larger part of the available mechanical energy and so, form multiband or wideband array of harvesters. More mechanical or electrical tuning, adaptative tuning or self-tuning of the resonant frequency techniques can be employed. Finally, in several cases, alternative current to direct current (AC-DC) converters must be employed in order to provide a direct current to the load and these rectifiers must also be optimized in terms of frequency, topology, components, etc.

For the thermal energy harvesting [257-259, 261-265, 267-277, 325-337], the pyroelectric harvesters are generally designed in order to follow periodic thermodynamic cycles (e.g. Carnot, Ericson, Olsen, etc.) including passively moving them towards and away from a heat source, whilst the thermoelectric harvesters use matched materials designed in order to be efficiency even with small temperature gradients; heatsinks are commonly used with the thermoelectric harvesters to amplify the heat flux and have the coldest possible temperature to amplify the temperature gradient; and some harvesters with the same properties can be placed in arrays, particularly in series, to scavenge larger part of the available thermal energy and providing a higher voltage. Finally, in the case of pyroelectric harvesters, alternative current to direct current (AC-DC) converters must be employed in order to provide a direct current to the load and these rectifiers must once again be optimized in terms of frequency, topology, components, etc.

For the electromagnetic energy harvesting [257, 258, 260-267, 270-277, 338-352, 389, 398-428], the harvesters, especially coils for inductive coupling and rectenna for radiative cases, are tuned to be the most effective on the targeted frequencies and power densities; more, these can be designed to be multiband or wideband to scavenge a larger part of the available electromagnetic spectrum; magnetic cores can be used with coils to direct the magnetic flux and increase the efficiency; and harvesters can be placed in arrays to scavenge larger part of the available electromagnetic energy. Finally, in the case of electromagnetic wireless power transfer, the electromagnetic beams can be formed to be as narrow as possible and are precisely targeted at the harvesters to waste as little energy as possible.

Finally, the used of hybrid harvesters is another technique used to optimize the efficiency and scavenge a larger part of the ambient energy [261-265, 267, 273, 274, 276, 277 353-387].

To return to the case of radiative electromagnetic energy harvesting, both from ambient sources and in the case of wireless power transfer, and as said, the rectenna must be designed to meet several constraints. This design concerns both the antenna and the rectifier, but also the impedance matching network between these. These impedance matching networks also concern all the harvesters which required an alternative current to direct current (AC-DC) converter. The relevant parameters of an antenna dedicated to become a rectenna are: the type (e.g. patch, dipole, etc.); the frequency band(s) where it is suitable (it can be single band or multiband, whose dual-band); the bandwidth associated to the frequency band(s) (narrow-band or wideband); the polarization (linear, circular or elliptic); the gain in each frequency

band(s) and more generally the radiation pattern; etc. [277, 344-351, 362-368, 370, 374-378, 381, 382, 387, 398-400, 402, 408, 410, 418, 419, 422, 423, 438-440, 443-446, 448, 449, 451-471, 477]. Also, an array of antennas can be used in a rectenna with a unique rectifier [400, 402, 438, 446, 449, 451, 452, 458]. The relevant parameters of a rectifier dedicated to be used in a rectenna are: the topology (e.g. shunt, in series, doubler, Dickson charge pump, etc.); the kind of non-linear rectifying element (e.g. diode, Schottky diode, tunnel diode, metal-insulator-metal diode, spin-diode, complementary metal oxide semi-conductor (CMOS) transistor, etc.); the frequency band(s) where it is suitable (it can be single band or multiband, whose dual-band); the bandwidth associated to the frequency band(s) (narrow-band or wideband); etc. [277, 344-351, 361-365, 367, 368, 370,371, 374, 375, 377, 378, 381, 398, 399, 400, 402, 408-410, 415-419, 421-423, 436, 438-441, 442-447, 451-456, 458, 468, 472-578]. Regarding the frequency band(s) and the bandwidth(s) of a rectenna, these are imposed by the smallest overlap between those of the antenna and those of the rectifier. A rectenna can be designed as a single unit especially through the complex conjugate impedance matching between the antenna and the rectifier, or an impedance matching network can be used (with localised (e.g. capacitor, inductor, etc.) or distributed (e.g. line, stub, etc.) components, or even with a hybrid circuit, between the antenna and the rectifier [277, 344, 345, 347-351, 362-365, 367, 368, 370, 371, 374, 375, 377, 378, 381, 399, 400, 402, 408, 410, 415-419, 421, 439, 440, 442, 443, 445-447, 451-456, 458, 468, 473-478]. The rectenna can be characterized regarding: the frequency band(s); the bandwidth(s); the minimal power density required; the efficiency (as the ratio between the available input power and the provided output power); the output voltage and current; the optimal load; the size (especially relative to the wavelength); the weight; etc. Also, an array of rectenna (similar or different) can be used as a harvester to scavenge a larger part of the available electromagnetic energy (in a unique frequency band or in some frequency bands) [398-400, 402, 408, 410, 422, 438, 443, 451-455, 458, 468]. Thus, the antennas, the rectifiers and the impedance matching circuits are the result of their own research, as is also the rectenna. Concerning these components, these can used new technologies as three-dimensional (3D) or inkjet printing [277, 336, 344, 347, 368, 370, 453, 457, 460-463, 465, 468, 470, 471] or additive techniques [362-365, 367-370, 375-377, 387, 442, 446, 457, 460-463, 465, 470] and can used various substrates (e.g. Polyethylene Terephthalate (PET), paper, textile, etc.), whose some are flexible [277, 344, 362-365, 370, 375, 400, 402, 423, 444, 446, 453, 455, 457, 458, 463, 464, 466-468, 477]. In the case of the radiative electromagnetic wireless power transfer, research is being carried out on the beamforming techniques for the power transmission and quasi-isotropic coverage for the harvester [277, 389, 390, 397, 399, 400, 402, 410, 431, 434-436, 438, 439, 445, 448, 449, 451, 455, 458, 459, 469], on the must efficiency waveforms [277, 345, 400, 402, 442, 446, 447], on the use of relays for increasing the range of the wireless power transfer [437, 445, 450], etc. Finally, there is also solutions used to recover the energy due to the harmonics lost during wireless data transmission [478].

3. Energy use and storage

Once scavenged and released as a direct current power, the energy must be efficiently managed to be used or stored with the aim of supplying a load such as a wireless sensor node.

i. Management and use

There are three main strategies to manage the harvested energy for a wireless sensor node: the "direct consumption" strategy (the load is directly or indirectly connected to the harvester that supplies it, that requires the availability of the source and a sufficiently high input power, and the excess power is wasted); the "store then use" strategy (all the harvested energy is stored and once enough energy is available or when the load needs to be powered, the stored energy is used); and the "simultaneous use and store" strategy (the load is continuously powered by the harvester and the spared energy is stored in order to compensate the variations of the input power over time). In all cases, the minimization of the energy needed to operate the system is sought, as well as the management of the power supply. These can be achieved both on the software and the hardware side. For the software, this one can be optimized; combines various consumption modes such as process, idle, sleep and deep sleep ones; and relevantly controls the power supply of other components in the system: usually, the time in sleep or deep sleep modes is used to accumulate energy, whilst this energy is consumed during the active modes. For the hardware, low power and optimized circuits can be used especially microcontroller unit (MCU), transceivers (as a reminder, the choice of the wireless communication technology, of the communication strategy, of the network topology and of the targeted performances has a great impact on the consumption of each wireless sensor node in the network [257, 258, 260-262, 264, 265, 267, 291, 292, 296, 300, 301, 342-345, 352, 359, 399, 402, 425, 434-439, 479]), sensors, application-specific integrated circuits (ASIC), or power management units (PMU) also called power management integrated circuits (PMIC). These lasts are commonly used when an energy storage function is required because allowing to store all or a portion of the harvested energy in an energy storage element and to consume the stored energy through various terms: these can be controlled by a microcontroller or through threshold voltages from the energy storage element. Today, several commercial power management units dedicated to energy harvesting applications are available such as Texas Instruments BQ24210 [480], BQ25504 [481], BQ25505 [482] and BQ25570 [483], Analog Devices' devices (whose Linear Technology's ones) (ADP5090, LTC3105, LTC3107, LTC3108, etc.) [484], ST Microelectronics' devices (SPV1040 and SPV1050) [485], Maxim Integrated MAX17710 [486] and MAX20361 [487], E-PEAS' ambient energy managers (AEM10941, AEM20940, AEM30940 and AEM40940) [488], Powercast's modules (PCC110, PCC114, P1110B and P2110B) [489], NOWI NH2D0245 [490], Trameto's HarvestAll solution [491], etc. and even academics propose their own circuits [348, 349, 492-499]. Most of these provide a software or hardware maximum power point tracking (MPPT) system in order to optimise the energy transfer from the source to the load or to the energy storage element; as well as a cold-start circuit to operate even with an empty energy storage device. More, and in order to smooth out the current draw and to provide a constant voltage to the load, various direct current to direct current (DC-to-DC) converters can be used: low dropout (LDO), buck, boost, buck-boost, etc.; directly after the harvester for the "direct consumption" strategy or after a power management unit, if not already included in it, for other strategies. Also, in the cases of hybrid harvesters or arrays of harvesters, combining circuits must be employed to efficiently collect the energy provided by each harvester [353-356, 358-362, 365-372, 374, 375, 377-381, 383, 387, 500-502]. More, in cases requiring to recharge wireless sensor nodes or collected locally their data, various strategies can be employed, some of which are based on the use of mobile chargers or readers, sometimes embedded on vehicle, such as drones [264, 265, 292, 399, 402, 422, 434, 435, 437, 503]. Finally, commercial integrated circuits provided by Atmosic in its M3 series which combine in a same chip a power management unit, a low power microcontroller unit and a Bluetooth Low Energy transceiver must be noted [504].

ii. Storage

In order to store the harvested energy, there are several solutions which can be plotted in a Ragone plot expressing the specific energy density (ability to store a large amount of energy) versus the specific power density (ability to redeliver the stored energy quickly) for each energy storage device. Thus, fuel cells provide the highest energy density and the lowest power density (can store a lot of energy but slowly redeliver it) [505-510], whilst capacitors (electrochemical or electrolytic, ceramic, aluminium, polymer, tantalum, thin film, etc.) provide the highest power density and the lowest energy density (can store very little energy but quickly redeliver it) [511-514] and the batteries (both primary and secondary; lead-acid, Nickel-Cadmium, Nickel-metal-hydride, Lithium-ions, Lithium-polymer, etc.) [515-521], the supercapacitors [522-526] occupy the centre of the plot with respectively relatively high energy density and medium power density, and medium energy density and relatively high power density. There are also hybrid structures half battery, half capacitor [527, 528].

Thus, in function of the amount of energy available, the energy required by the system, the time needed the harvest enough energy, etc., the choice of the energy storage device will differ: both the energy and power densities must be considered, as well as the capacity of the energy storage element, its available voltages, its restrictions (e.g. batteries must not be fully discharged nor overcharged, etc.), its lifetime (e.g. expressed in terms of number of charge and discharge cycles), its losses and self-discharge, etc. [257-262, 264, 265, 277, 300, 301]. For instance, fuel cells and batteries are commonly used when a huge quantity of energy is required by the supplied system, when the amount of harvestable energy is insufficient, when periodic recharges or changes are possible, when the energy sources have a periodic availability cycle (e.g. solar light which can easily supply wireless sensor node and recharge an energy storage device during sunny day, but which is unavailable during cloudy night, etc.); whilst conventional capacitors are usually used in the "direct consumption" strategy in order to smooth out the power draws and the inconsistent input powers. Lastly, bank of conventional capacitors and supercapacitors are preferred for the "store then use" strategy respectively with low and medium power consuming wireless sensor nodes and low to high amount of available energy. The bank of conventional capacitors provided low capacities, low available voltages but relatively low current losses. When moderate capacities and available voltages are required, the supercapacitors are favoured but have generally highest current losses.

4. Ambient energy harvesting and wireless power transfer into concretes

To date, no ambient energy harvesting systems embedded in concretes were reported. Moreover, there are few ambient energy harvesting systems powering wireless sensor nodes dedicated to the structural health monitoring of civil infrastructure: [281] and [288] propose respectively a crackmeter and an earthquake monitoring system, both supplied by a battery recharged by the solar energy harvesting, through the photovoltaic effect; and [322] presents a road monitoring system dedicated to circulation bridges and supplied by a mechanical vibrations energy harvesting, through the electromagnetic effect.

Regarding the wireless power transfer, some works theoretically and experimentally study both the inductive [529-532, 537] and radiative [533-537] electromagnetic wireless power transfers into concretes, and especially the impact of the reinforcements. Nevertheless, no load such as wireless sensor node is used during experimentations. Moreover, there are few wireless power transfer systems powering wireless sensor nodes dedicated to the structural

health monitoring of civil infrastructure: [422] presents a network of wireless impedance sensor nodes, experimentally deployed in the case of the structural health monitoring of a concrete circulation bridge and supplied by far-field electromagnetic wireless power transfer from a mobile vehicle; and [425] provides a commercial solution of wireless sensor networks dedicated to the structural health monitoring of civil infrastructure whose sensor nodes are supplied by far-field electromagnetic wireless power transfer.

5. Conclusion

In this section, the main ambient energy harvesting and wireless power transfer technologies, as well as the different strategies to use and/or store the scavenged energy and the main electronic circuits, have been presented. The Figure III.5 summarizes the energy harvesting technologies, the wireless power transfer technologies and the energy storage devices. First, the light, the mechanical (electrostatic and triboelectric, electromagnetic, and piezoelectric), the thermal (pyroelectric, and thermoelectric) and the electromagnetic (capacitive, inductive, and radiative), as well as the hybrid energy harvesters were introduced. Then the light, the mechanical and the electromagnetic (non-resonant and resonant inductive, and radiative) wireless power transfer, as well as the simultaneous wireless information and power transmission paradigm and the optimisation of energy harvesting and/or wireless power transfer systems were explained. After, the different strategies to use and to optimize the use of the scavenged energy were developed, as well as the different energy storage devices (cell fuels, batteries, supercapacitors and capacitors). Last, the applications in the civil engineering of the ambient energy harvesting and of the wireless power transfer were achieved.

In the framework of the McBIM project and focusing only on the energy management part, the choice is to use a far-field wireless power transfer system in order to be independent of fluctuating ambient energy sources (e.g. light is not available into concretes; vibrations can be harvested on a circulation bridge but not necessary in small buildings; local thermal variations and temperature gradients seem not be available into concretes; electromagnetic fields are weak and highly dependent of human activities; etc.), to have a sufficient range of use (e.g. capacitive and inductive are limited from millimetres to tens of centimetres; etc.), and to be scalable in all civil engineering use cases (e.g. bridges, buildings, etc.), especially for structural health monitoring applications. In all cases, the simultaneous wireless information and power transmission paradigm must be met. Regardless of the chosen wireless communication and sensing technologies, the "store then used" strategy with a supercapacitor or a bank of capacitors as energy buffer seems the more relevant. Indeed, a moderate capacity is commonly required to supply low power wireless sensor nodes; low power losses are sought both for electromagnetic ambient energy harvesting and wireless power transfer systems; long lifetime with a lot of charge and discharge cycles and full discharge ability are needed for long term monitoring. Thanks to the use of power management unit, it is possible to manage the power harvesting and the energy use only in a hardware way; and the wireless sensor node can be kept functional for a long time even if not used and supplied during a long period of time. Thus, it is the electronic hardware which will be restrictive in the implementation and deployment of the McBIM solution.

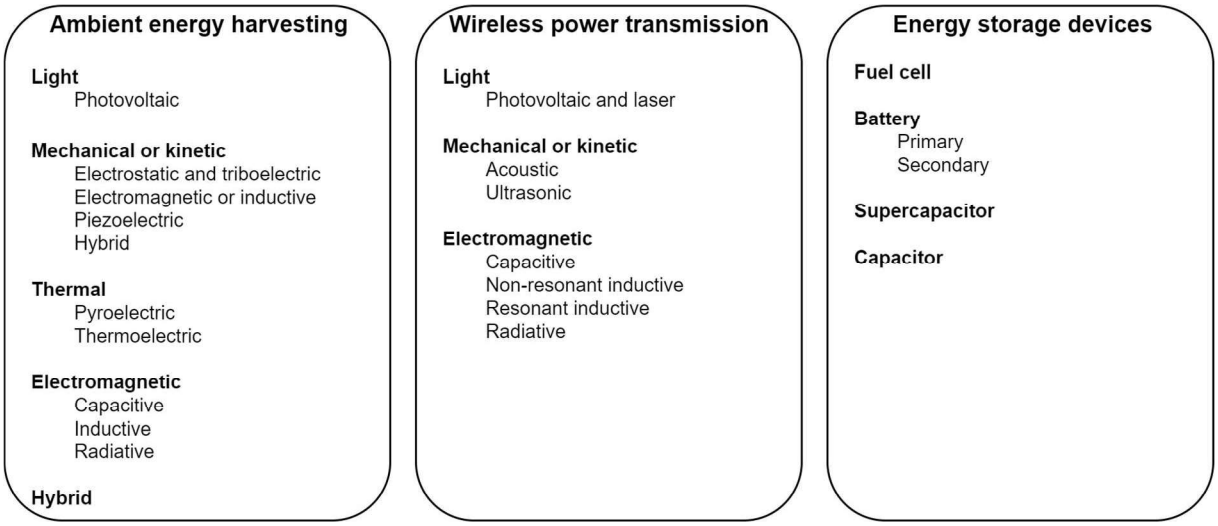

Figure II.5: List of the energy harvesting technologies, of the wireless power transfer technologies and of the energy storage devices.

E. Communicating materials

1. Definition and implementations

Communicating materials are materials intrinsically able to measure, process, store and exchange information. These have the ability to quantify their environment and their own internal states through the measurement of various physical parameters. This concept was firstly introduced in [538] and previous implementations were attempted. Thus, [539] presents an attempt of making communicating wood by using nuclear quadrupole resonance to mass marking it, and thus, to identify it even if cut, thanks to its frequency response obtained by a reader. In [540], a communicating textile is designed by embedding micro radiofrequency identification (μ-RFID) tags in which data are disseminate at each step of its lifecycle, since its manufacture to its recycling through its transformation and use, and this data is conserved even if the textile is cut. Finally, the communicating materials paradigm was theoretically applied to the civil engineering industry in [541] and [542] where a reinforced concrete embedding radiofrequency identification (RFID) tags is imagined and more especially where the strategy of data dissemination is detailed. Thus, to date, no implementation of communicating materials, whether wood, textile or reinforced concrete, have satisfied all the requirements of the paradigm: the intrinsically ability to measure, process, store and communicate, during all the lifespan of the communicating materials.

2. Communicating concretes and alternatives

None of the propositions presented above satisfy the communicating materials paradigm in the case of reinforced concretes: the self-sensing concretes required external equipment to be used; the wireless sensor networks dedicated to the structural health monitoring are added to existing concrete structure for a determine period; the solutions based on radiofrequency identification (RFID) tags are limited to the storage of data wirelessly provided by a local reader during a short range wireless communication; and finally, the solutions using ambient energy harvesting and wireless power transfer increase the lifetime of the wireless sensor network but are application dependent, not embedded into the concretes and concern only one step of the lifecycle of the concretes.

Other proposals partially respond to the implementation of a communicating reinforced concrete.

Some uses of radiofrequency identification (RFID) tags embedded into concretes are presented in [121, 122, 543-550] and cover different steps in the lifecycle of an element made of concrete. In [121, 122, 543-546], the logistic aspects of concrete elements, such as materials management, tracking and traceability as well as data management, from the manufacture to the recycling through the construction of a structure, are covered by the used of embedded radiofrequency identification (RFID) tags. More, [546] introduces the integration of radiofrequency identification (RFID) tags with other technologies as cameras, global positioning systems (GPS) and microcontroller for other applications as the localisation and the monitoring. In [547-549], the monitoring of internal properties of concretes are covered by the used of radiofrequency identification (RFID) tags embedded into concrete. In [547] and [548], semi-active radiofrequency identification (RFID) tags are designed in order to become corrosion sensors, able to measure temperature, humidity and corrosion rate, from

the manufacture to the exploitation phases. In [549], a radiofrequency identification (RFID) tag is designed in order to become strain and crack sensor, during the exploitation.

In [550], a resistivity sensor is designed to be embedded into concrete and monitor the corrosion during its exploitation phase, even if it has not yet been achieved, this sensor is intended to be used with a semi-active radiofrequency identification (RFID) tag, both for the power supply and the short-range communication.

In [551] and [552], passive resonant sensors are introduced. In [551], a LC resonator, whose the frequency response is function of the rate of corrosion, can be interrogate by a reader coil through the coupled magnetic induction, whilst in [552], a nested split-ring resonator, whose the frequency response is function of the displacement or strain, can be interrogated by a reader antenna connected to a vector network analyser (VNA).

In [553-558], wireless sensor nodes designed to be embedded into concretes are reported. In [553], an "early-age" impedance-based wireless sensor using a piezoelectric transducer and a "micro" personal computer (PC) for signal processing is presented. This is powered by a battery but was imagined to use an ambient vibrations energy harvester based on piezoelectric effect to recharge the battery and increase its lifetime, and can be used during the exploitation phase. A wireless ZigBee sensor node powered by a battery and measuring temperature and humidity inside concretes during their curing and exploitation phases is provided in [554]. In [555], a temperature, humidity and strain wireless sensor node is presented. This is powered by a battery but was imagined to harvest ambient mechanical energy to increase its lifetime, and can be used during the curing and exploitation phases. In [556] and [557], a wireless M-BUS stress and temperature sensor node embedded into reinforce concretes, powered by a battery which can be recharges through a short-range resonant inductive wireless power transfer system and dedicated to the structural health monitoring during the exploitation phase is reported. Finally, [558] provides a wireless LoRa temperature sensor node dedicated to the structural health monitoring of buildings which is powered by a radiative wireless power transfer system and an electrochemical capacitor, and which is not designed to be embedded into concretes. In [559] and [560], two wireless temperature and humidity sensor nodes powered by batteries are introduced. These respectively communicate with an unspecified IEEE 802.15.4 protocol and with ZigBee and are designed so that the sensor is in the concretes and the rest of the node outside. Thus, in [547, 548, 550, 554, 555, 559, 560] the packaging to protect the electronics from the concretes which are highly corrosive while in the time allowing a reliable measurement of the physical properties of the concretes are discussed.

3. Conclusion

In this section, the communicating materials paradigm has been introduced, as well as some partial implementations. Then, some works which can be related to the communicating concretes have been presented. Nevertheless, to date, there are no satisfying and full implementation for communicating concretes.

The main objective of the McBIM project is to provide a full implementation of a communicating concrete, thus intrinsically able to measure, process, store and exchange information from their environment and their own properties, with other communicating

materials and with virtual models, during all their lifetime. To meet all the requirements, a reinforced concrete equipped with a network of buried wireless sensors will be designed and implemented. This one could employ various relevant sensors (e.g. temperature, humidity, resistivity, strain, etc.) to monitor the reinforced concrete during all the steps of its lifecycle and wireless sensor communication technologies adapted to the needs. Finally, to be independent of the application and of the ambient energy sources, energy autonomous and battery-free, a radiative electromagnetic wireless power transfer system will be used.

F. Conclusion

All along this state of the art, several and diverse domains have been introduced: the concretes and their various forms, whose some are qualified of smarts and others are improved by embedding sensing or transducing systems; the relevant parameters for the structural health monitoring of the reinforced concretes during all their lifetime and their destructive and non-destructive measurement methods, as well as the use of wireless sensor networks in this same purpose; the wireless machine-to-machine communication technologies with their different performances and their uses again in the case of structural health monitoring of the reinforced concretes, sometimes embedded; then the techniques allowing the energy autonomy of wireless sensor networks, thanks to several ambient or dedicated energy sources respectively by energy harvesting and wireless power transfer and energy storage devices, as well as some software and hardware optimisation aspects, and their applications for the structural health monitoring of concretes; and lastly, the communication material paradigm and its partial implementations, especially in the case of communicating reinforced concretes.

Thus, this doctoral thesis, which is part of the ANR McBIM project, is at the crossroads of all these domains, and also concerns a system sizing, in order to design an energy autonomous wireless sensor network embedded in reinforced concrete, to make this reinforced concrete communicating during its whole lifetime. This last also must be intrinsically able to measure, process, store and exchange information from its environment and its own properties, with other communicating materials and with virtual models, to monitor itself during all its lifetime. According to each introduced field, this communicating reinforced concrete can be qualified of intrinsic self-sensing and self-communicating reinforced concrete; will use non-destructive methods to monitor its internal states during each step of its lifecycle: from the manufacture to the recycling, through the curing, the construction and the exploitation, by measuring relevant physical parameters as temperature, humidity, resistivity (closely related to the corrosion risk) or strain; could employ various far-field wireless electromagnetic communications in function of the targeted application, which could require medium to long range communications, with low to moderate data-rates, but always with low power consumptions; must properly work during all the lifetime of the concrete, thus for decades, and so must be energy autonomous, independent of the application and of the ambient energy sources, and battery-free, so, the radiative electromagnetic wireless power transfer approach has been privileged.

Even if this state of the art is already quite dense, some aspects have been silenced or just overviewed. This is the case for the wireless sensor node location techniques, the wake-up radio techniques, the biochemical cells and other recent energy storage techniques, etc., as well as the radiofrequency identification (RFID) technologies and the design of rectennas, antennas, rectifiers and impedance matching networks, of power management units, etc.

In the next chapter, a more detailed contextualisation of the ANR McBIM project will be provided and the contributions of the project partners will be introduced. Then, the technology choices and the wireless sensor network architecture will be explained.

III. The McBIM research project and its network architecture

In this chapter and in order to contextualize the works presented below (Chapters III. to VIII.), more details about the McBIM research project will be provided, and then, the chosen network architecture will be explained.

A. The McBIM research project

1. Introduction

From decades, the use of electronic systems, in particular the embedded ones, continues to grow and to diversify, providing news technologies and paradigms. This is notably the case with the huge increase of the Internet of Things (IoT), commonly based on the wireless Machine-to-Machine (M2M) communications and the Wireless Sensor Networks (WSN), both always more efficient, diversified and deployed. In parallel, the computer systems, especially with the use of the Internet, are being used more and more widely, in particular for data computing, sharing and storage aspects, but even for modelling. By merging these physical and digital worlds, it becomes possible to implement Cyber-Physical Systems (CPS) to monitor and/or control some physical objects from digital models, especially by using Digital Twins which are precise and evolving digital models of physical elements. For instance, the Building Information Modelling (BIM) is an implementation of this digital twin in the construction field, which is not today directly and automatically fed with data from the physical building, but provides new tools to efficiently plan, design, construct and manage buildings and civil infrastructures during the different stages of their lifecycle. Nevertheless, today, the ownership and accessibility of the Building Information Modelling (BIM) is not necessarily made available for next owners, users or other stakeholders. Thus, the data is, in the worst case, lost or "better" only never reused or accessible. More, the cyber-physical systems can be employed in a wide variety of applications, such as Structural Health Monitoring (SHM) of civil or transportation infrastructures, for instance in the framework of the Smart City. The communicating materials paradigm is another way to implement cyber-physical systems by making materials intrinsically self-sensing and communicating with its digital twin(s).

In this context, the McBIM research project (Material communicating with the Building Information Modelling (BIM)) -funded by the French National Research Agency (ANR)- tends to propose an implementation of the concept of communicating materials in the civil engineering industry by developing a communicating reinforced concrete [561-564]. This one must be intrinsically able to generate, store -locally and remotely-, process and exchange data -from its own health and/or its environment- locally with other communicating components, and with dedicated and associated digital twins -especially to directly and automatically fed a BIM- through the Internet. More, it must meet some constraints.

First of all, it must be usable and useful during the entire life of the structure (e.g. building, bridge, tunnel, etc.) made of communicating reinforced concrete elements, but even during all the lifetime of the communicating reinforced concrete itself, and for each step of its lifecycle:

from its manufacture and eventual storage and transportation, to its recycling, through the construction of a complete structure based on a combination of communicating reinforced concrete elements, as well as the exploitation of this structure for, between others, structural health monitoring. Thus, its lifespan can be estimated in terms of decades.

Then, the targeted communicating reinforced concrete must be scalable in terms of format and recipes (e.g. fluid screeds, precast elements for a wall, a bridge deck, etc.), workable regardless its environment (e.g. office building, factory, traffic bridge, storage tunnel, etc.), and reconfigurable over time, particularly with regard to the type and quantity of collected data, as well as the periodicity of measurement and wireless communication. Indeed, the needs in data are function of the step in the lifecycle. As introduced above (Section II.B.1.), during the manufacturing process, the curing process can be monitored on an hourly basis through the evolution of the temperature and humidity, and can help in the decision to proceed or not the works (e.g. to unmould a precast element, to tile a floor, etc.). During the storage, the eventual shipping (e.g. for the precast elements), the construction of a complete structure and the recycling, this is the logistic data that matter on demand, such as identifier, current owner, location, delivery address, associated project, elements in the neighbourhood, etc., to assure traceability. During the exploitation phase, structural health monitoring applications are relevant and diverse: the hourly or daily monitoring of temperature and humidity could give information about maturity, the hourly monitoring during few days of the temperature at each side of a wall could be used to quantify its real thermal resistance and certify standards, the daily cracks detection, or the daily or weekly estimation of the corrosion rate could allow the application of preventive treatments to avoid irreversible damages and collapses, etc.

Whatever the step in the lifecycle, the Building Information Modelling, or other digital twin, must be regularly updated and must maintain a history, for continuously sharing information between all the stakeholders during all the lifetime of the communicating reinforced concrete.

Thus, with a unique solution, different communicating reinforced concretes can be manufactured regarding the use and different applications can be processed during their entire lifespan by using specific sensor nodes at specific periodicities.

Finally, to design communicating reinforced concretes, several scientific obstacles must be overcome. First, a wireless machine-to-machine communication technology must be designed or chosen to be robust, reliable and resilient in strongly constrained electromagnetic propagation media, which are reinforced concretes. Then, an innovative way to power the wireless sensor nodes, which are inaccessible because embedded into reinforced concretes, during all the lifetime of the reinforced concretes must be designed independently of the targeted environment, structure and/or application. Next, the data management strategy, for local and remote data exchange and storage (or dissemination) as well as routing in wireless sensor networks constantly evolving, must be defined. Ultimately, the interoperability between the physical and digital worlds, especially with the Building Information Modelling, must be achieved by being compatible with the Industry Foundation Classes (IFC) standards. Thus, the McBIM research project is multi-disciplinary and is expected to provide innovative solutions in different domains. Moreover, it must have future impacts on various non-scientific aspects: economically, it could help to reduce costs and time by improving the

traceability and supervision thanks to the ability to continuously, automatically and in "real-time" monitor structures (including those difficult to access or hazardous), up to allow predictive maintenances; environmentally, it could help to reduce energy consumption in the construction domain by optimizing time and transport, help to optimize concretes recycling process, and its implementations are hoped to be eco-responsible by using low power electronic components for long term applications, by avoiding the most polluting batteries and by promoting energy harvesting technologies; socially, it could improve the security and safety of civil infrastructures, more, social acceptability was considered during the design; etc.

2. The McBIM consortium

To meet the requirements of a communicating reinforced concrete linked to a BIM as introduced above (Section II.F.), a consortium of three French laboratories and one company was set up in the framework of the McBIM research project, where each one has its own role and objectives.

i. LAAS-CNRS

We, the LAAS-CNRS (Laboratory for Analysis and Architecture of Systems of the French National Centre for Scientific Research) located in Toulouse, FRANCE, have to address the first two scientific objectives of the McBIM research project (as a reminder: designing or choosing a robust, reliable and resilient wireless machine-to-machine communication technology usable by an evolving wireless sensor network embedded in reinforced concretes; and designing a system to power wireless sensor nodes once embedded into reinforced concretes during all their lifetime) [565]. Thus, we must implement the hardware part of the communicating reinforced concretes by developing a wireless sensor network able to sense various physical parameters, process and store these collected data and then, exchange these especially with a Building Information Modelling through the Internet. The publications from the LAAS-CNRS for the McBIM research project can be found in [563, 564, 566-575].

ii. CRAN

The CRAN (Research Centre for Automatic Control) located in Nancy, FRANCE, has to address the third scientific objective of the McBIM research project (as a reminder: designing the data management strategy) [576]. Thus, it works on the data collection, dissemination and/or storage and retrieval protocols in the network of communicating reinforced concrete components, with the purpose to expend as much as possible their lifetime by minimizing their energy consumption and their needs of maintenance, while ensuring their resilience and assuring their scalability. The publications from the CRAN for the McBIM research project can be found in [563, 564, 577-581].

iii. LIB

The LIB (Computer Science Laboratory of Burgundy) located in Dijon, FRANCE, has to address the last scientific objective of the McBIM research project (as a reminder: achieving the interoperability between the wireless sensor network and the Building Information Modelling by respecting the Industry Foundation Classes (IFC) standards) [582]. Thus, it trades with the data exchanges and integration within a BIM platform according to the current standards. The publications from the LIB for the McBIM research project can be found in [563, 564].

iv. FINAO SAS/360SmartConnect

FINAO SAS/360SmartConnect located in Trans-en-Provence, FRANCE, has to provide an industrial perspective on the McBIM research project by prospecting building and civil engineering companies to obtain real-life use cases and expressions of interest, but also by providing reinforced concrete elements for the experiments pursued by the academic partners [121].

v. Consortium prototypes

One of the aims of the McBIM research project is to provide a complete prototype of a communicating reinforced concrete as a proof-of-concept, which will integrate all specifically designed software and hardware components. To achieve this purpose, intermediate prototypes for each individual task as well as for each interface will be developed.

3. Objectives of this doctoral thesis work and implementation constraints

In the framework of this doctoral thesis work, the two objectives devoted to the LAAS-CNRS have been considered and prototypes of wireless sensor network intended to be buried into reinforced concrete in order to make this communicating have been designed and implemented. Regarding the final goal of the McBIM research project some main constraints have been imposed whilst others have been released.

Regarding the reinforced concrete, the final goal is to consider the wireless sensor nodes as aggregates that are part of the concrete recipes. Thus, these will be randomly located and oriented into the concrete during its manufacture and must be relatively compact (that says having a volume similar to that of the conventional aggregates). Thus, by using randomly placed wireless instead of precisely placed wire sensor nodes, the costs and time issues concerning installation and maintenance are highly reduced.

For our experimentations, a 135 cm x 35 cm x 35 cm (for nearly 356 kg) reinforced concrete beam has been provided by FINAO SAS/360SmartConnect, as defined by the Figure III.1 and Figure III.2. This one includes three equidistant 15 cm x 15 cm x 15 cm cavities enclosable thanks to specific covers. Thus, the tested prototypes of wireless sensor nodes are only located in these cavities and their orientation can be controlled. More their size is in this case only limited by the one of the cavities. Also, the presence of air around the wireless sensor nodes allows to release the constraints in terms of antenna design (by providing the air dielectric parameters, and not those of concretes constantly varying) but is not equivalent to the full burial. In the same way, by using a cured reinforced concrete and cavities, the wireless sensor nodes are not subject to the harsh conditions imposed by the wet concrete and so, the packaging to protect from the corrosive and conductive medium is not considered.

Because of the geometry of the reinforcement in the test reinforced concrete beam was unknow, as well as its recipe, its characterisation based on the use of a Ground Penetrating Radar (GPR) loaned by the LMDC (Laboratory for Materials and Sustainability in Construction) located in Toulouse, FRANCE, was achieved. The Figure III.3 presents the interpretation of the results issued from the characterisation. In blue are the long screws used for the manipulation and transportation, and in red is the reinforcement on the studied side. This characterisation has made it possible to interpret some unexpected electromagnetics behaviours.

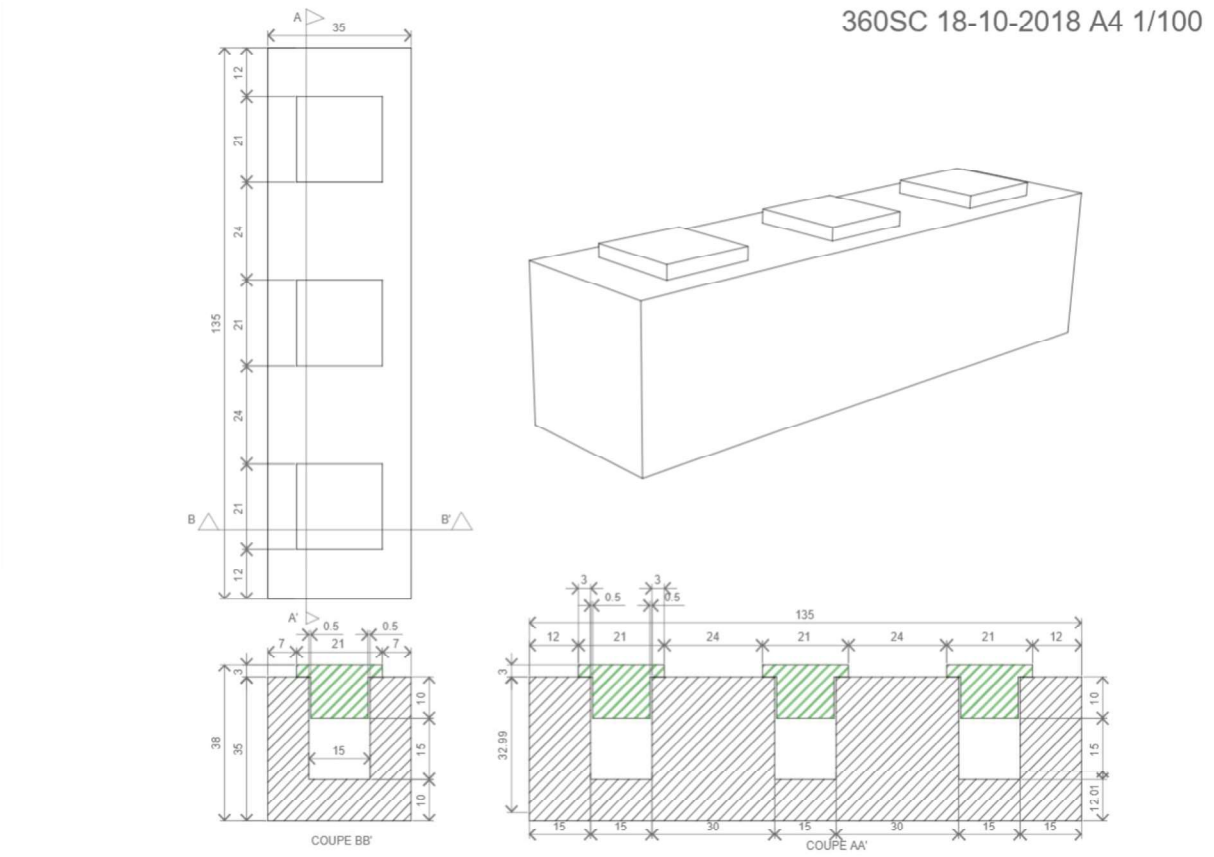

Figure III.1: Reinforced concrete beam designed and manufactured to perform experiments for the McBIM research project (dimensions in centimetres).

Figure III.2: Photographs of the reinforced concrete beam used to perform experiments for the McBIM research project.

With regards on the wireless machine-to-machine communications, these must work through the reinforced concrete, from and/or to buried wireless sensor node(s), without the need of a human intervention and without needing to know the precise location of the wireless sensor node. There can be at least two interfaces on each wireless sensor node: one dedicated to the communications within the wireless sensor network; and one, optional, for the connection with the Building Information Modelling through the Internet. The proposed network architecture will be explained in the next subsection.

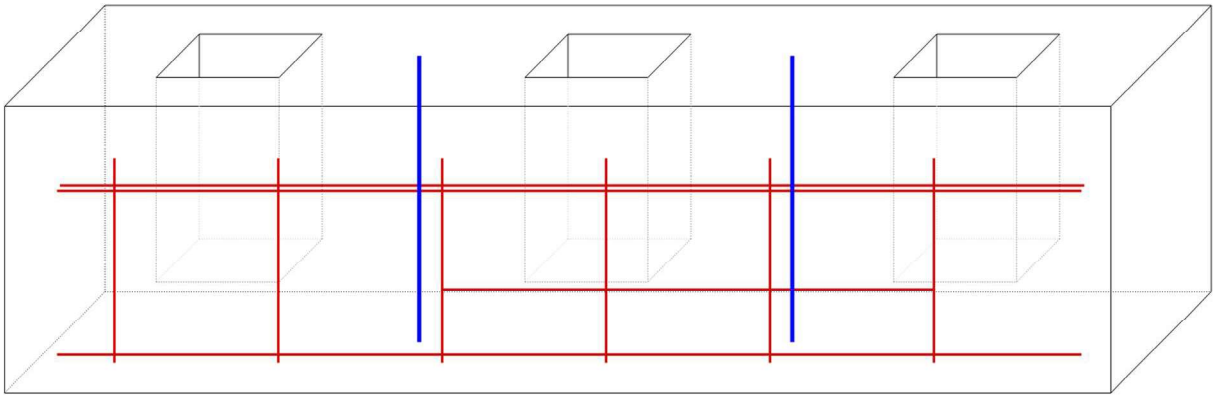

Figure III.3: Diagram of the reinforcement in the reinforced concrete beam achieved after the interpretation of the results issued from the characterisation with a Ground Penetrating Radar (GPR).

For the communications within the wireless sensor network, the useful range must be at least a ten of metres up to few hundreds of metres, in fact function of the structure in which it is deployed and the density of wireless sensor nodes. More, the data-rate as well as the frequency of exchanges are low (for instance, few bytes or kilobytes, hourly, daily or weekly) and the lowest possible power consumption is desired.

For the communications with the Internet, the range is function of available infrastructures around the deployment area which will define possible solutions. More, the data-rate as well as the frequency of exchanges are more important than for those within the wireless sensor network. Again, the lowest possible power consumption is required.

Because of higher scientific interest and their high connection with the problematic of power management, these are the wireless machine-to-machine communications within the wireless sensor network embedded into the reinforced concrete which are privileged in this work.

Concerning the power management of the wireless sensor nodes inaccessible once embedded into the reinforced concrete and for their entire lifetime, the targeted solution must be independent of the targeted environment, structure and/or application.

Thus, wireless power transfer is preferred to the ambient energy harvesting. Because of the very long-term operation, battery-free architectures are required. In order to have several meters (ideally ten(s) of meters) of range of use, the radiative electromagnetic wireless power transfer is selected, unlike inductive techniques which are very low ranges.

Ideally, wireless communication and wireless power transfer must have the same order of magnitude in terms of range of use, be independent and non-interfering.

Because of too restrictive power consumption conditions for the entire wireless sensor network, it was admitted that for a first approximation a unique wireless sensor node per subnetwork is accessible, has an unlimited power source (e.g. connected to the mains power, using a battery periodically recharged and/or changed, etc.), and so, is chosen to interconnect the Internet, to be a wireless local human access point/interface, and to wirelessly power the other wireless sensor nodes.

Finally, about the targeted applications which are function of the step in the lifecycle, the focus has been made on the structural health monitoring during the exploitation phase of the structures. Indeed, the logistical aspects have already been treated by then CRAN and FINAO SAS/360SmartConnect by using radio-frequency identification (RFID) tags. To upgrade a wireless sensor network to meet the requirements for the logistic, adding an interface to transmit at least an identifier is sufficient. Regarding the curing process, the solutions provided for the exploitation phase can be scaled by considering a liquid environment, which will induce a specific package to protect the system and an adaptation of this system to the new electromagnetic constraints. The structural health monitoring seems the more interesting because using a wide range of methods and usable in a wide range of applications.

Even if the project deals with the design and implementation of a communicating reinforced concrete, which creates number of constraints, the developed proposals presented below can be transposed to other applications with different use cases and other constraints.

Now that all the theoretical aspects as well as the main constraints imposed in the McBIM research project have been introduced, the rest of the manuscript will deal with the work carried out during the doctoral thesis.

B. Architecture of the wireless sensor network

1. Global architecture

In order to implement the hardware part of the communicating reinforced concrete, such as presented in Figure III.4, a wireless sensor network composed of two kinds of node organised on two levels is proposed. There are the communicating nodes (CN) and the sensing nodes (SN). Each element made of communicating reinforced concrete embeds at least one communicating node and several sensing nodes. Indeed, the number of communicating and sensing nodes in each element will vary in function of the size of the element and the needs in terms of measurement required by the stakeholders and the targeted application(s).

The communicating nodes form an *ad-hoc* meshed network within a structure or a set of adjacent structures, with the aim of aggregating, sharing and storing the data provided by the sensing nodes and/or by the building information modelling through an Internet interface. Thus, bi-directional medium to long range wireless communications are required and the electromagnetic propagation medium is composed of air and/or reinforced concrete. More, at least one communicating node per meshed network must provide a reliable bi-directional connection to the Internet and become an access point (or a gateway) to the digital world. Around each communicating node, which also becomes a central hub, a star network of sensing nodes is implemented. The sensing nodes are dedicated to the measurement of physical parameters from the reinforced concrete and/or its environment and to the transmission of the collected data to the associated communicating node(s). The communicating nodes must recover the transmitted data from the sensing nodes, but even must wirelessly power the sensing nodes located in its neighbourhood thanks to a radiative wireless power transfer system. By tuning their radiative wireless power source, the communicating nodes can set up the periodicity of measurement and communication of the sensing nodes. Here, directional medium range wireless communications are required and the electromagnetic propagation medium is essentially composed of reinforced concrete.

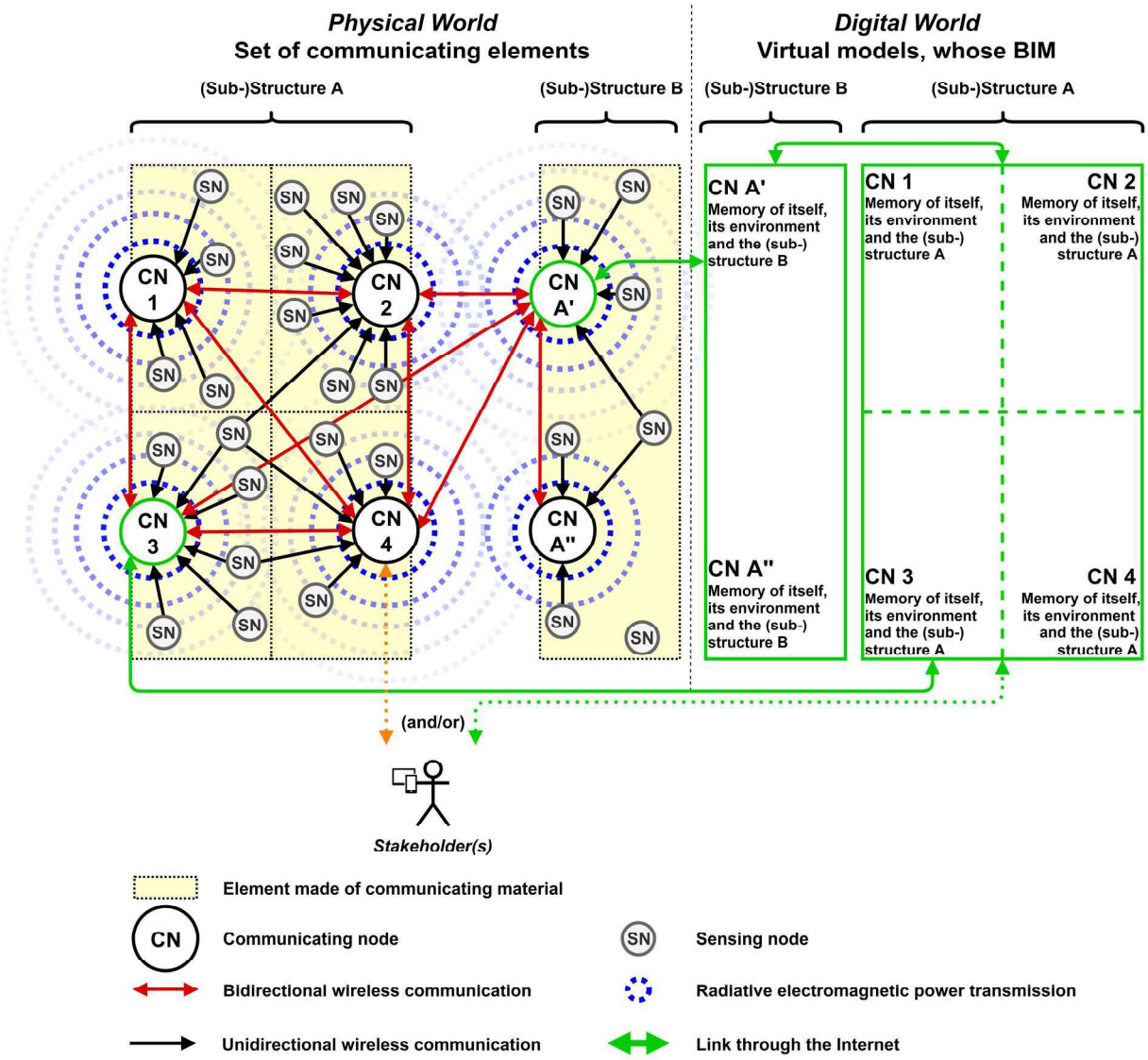

Figure III.4: Bloc diagram of the architecture of the cyber-physical system composing the communicating reinforced concrete.

2. Architecture of the communicating node

The architecture of the communicating node is presented in Figure III.5. This one must achieve several functions: collect the data sent by the sensing node; aggregate, process, store and share the data provided by the sensing nodes and by the building information modelling within the meshed network of communicating nodes and through the Internet; and wirelessly power the sensing nodes in its neighbourhood thanks to a radiative wireless power transfer system. Thus, it is composed of three distinct subsystems which interact: the first is a radiative electromagnetic power source; the second is the data management system (especially used to assure the collect, process, exchange and storage of the data) which controls the previous; and the third and last is the power management system which powers the two others. More, the communicating node, or each of its three subsystems, can be defined by its, or their, interfaces with its, or their, external environment, as well as their components.

The radiative electromagnetic power source includes a unique output through an antenna, which is dedicated to wirelessly power the sensing nodes in its neighbourhood. By tuning the waveform, the power and/or the periodicity of the wireless power transfer, the communicating node can remotely configure the periodicity of measurement and data emission of the sensing nodes. This subsystem requires at least a signal generator, a radiofrequency amplifier and an antenna, and must be controllable.

The data management subsystem includes at least three interfaces, which can mutualize some resources and require antenna(s): one is dedicated to the collection of the data sent by the sensing node; another is required for the communication between communicating nodes; the next is optionally active but allows to connect the Internet. An extra one can be implemented to locally interface the devices of the various stakeholders. As each interface needs particular specifications (in terms of directionality, of periodicity of use, of range of use, etc.), different wireless communication technologies can be employed for one or several of these interfaces. This subsystem requires at least a microcontroller unit (MCU), memory and transceiver(s) with antenna.

The power management system includes at least a power input. This one can be composed of a power management unit (PMU) and/or converter(s) and/or energy storage device(s).

As explained above (Section III.A.3.) and in order to release constraints, the communicating node is left accessible and has an unlimited power source. More, the connexions with the sensing nodes, through the data reception and the wireless power transfer, are privileged over the other interfaces. Next, the routing and data dissemination and exchange within the meshed network of communicating nodes is a task allocated to the CRAN.

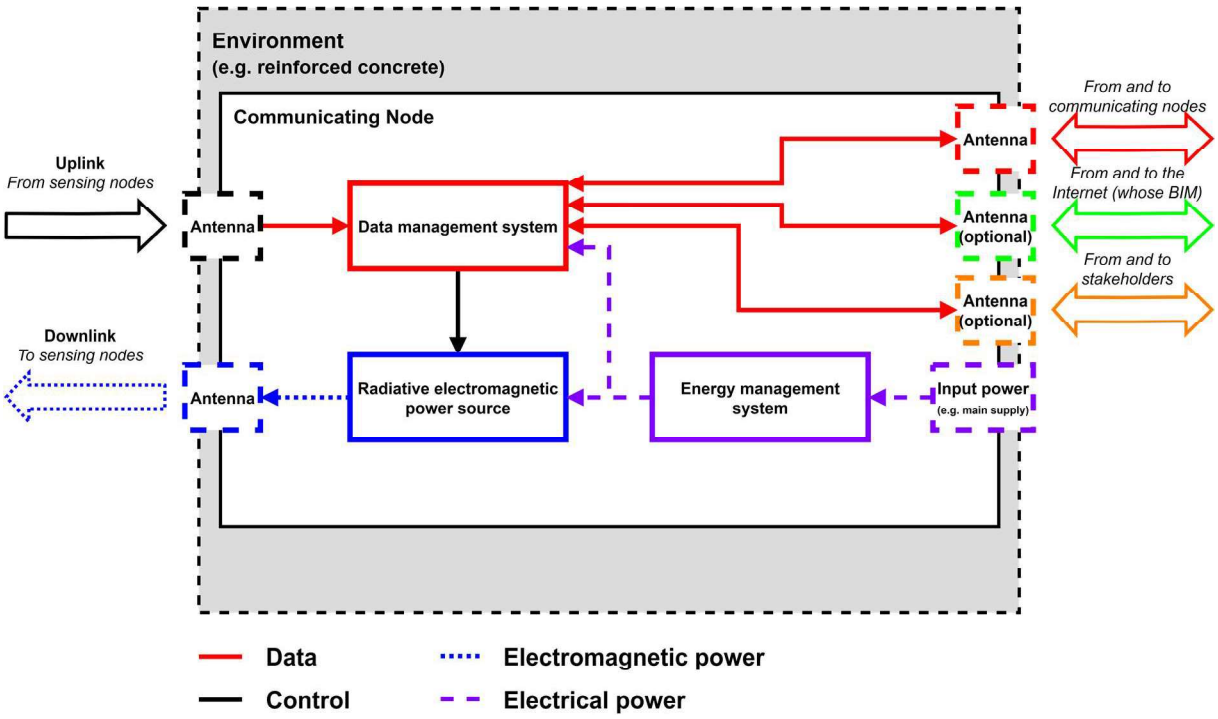

Figure III.5: Bloc diagram of the architecture of the communicating node.

3. Architecture of the sensing node

The architecture of the sensing node is presented in Figure III.6. This one must sense some physical parameters to quantify the internal states of the reinforced concrete and/or its environment, and wirelessly transmit the collected, and eventually pre-processed, data to the communicating node(s). Because it becomes inaccessible once deployed and embedded into the reinforced concrete, it must be usable, reliable, resilient, battery-free and energy autonomous for the lifespan of the reinforced concrete, that says decades. Thus, it is designed as simple as possible and is composed of two distinct subsystems which interact, one dedicated to the power management and the other to the collect and transmission of data.

The power management subsystem is composed of a rectenna used to harvested the radiative electromagnetic power generated and transmitted by the communicating node(s) and to convert it into direct-current electrical power, and of a power management unit (PMU) which efficiently recovers the power provided by the rectenna to store it in energy storage device and to power the other subsystem once enough energy is available.

The data management subsystem is composed of a microcontroller unit (MCU) which drive sensor(s) and a wireless transceiver with an antenna, in order to sense physical parameter(s), pre-process data and wirelessly send these to the communicating node(s).

It is this sensing node which is the core of this doctoral thesis work, because the more challenging to design and implement by overcoming the associated constraints.

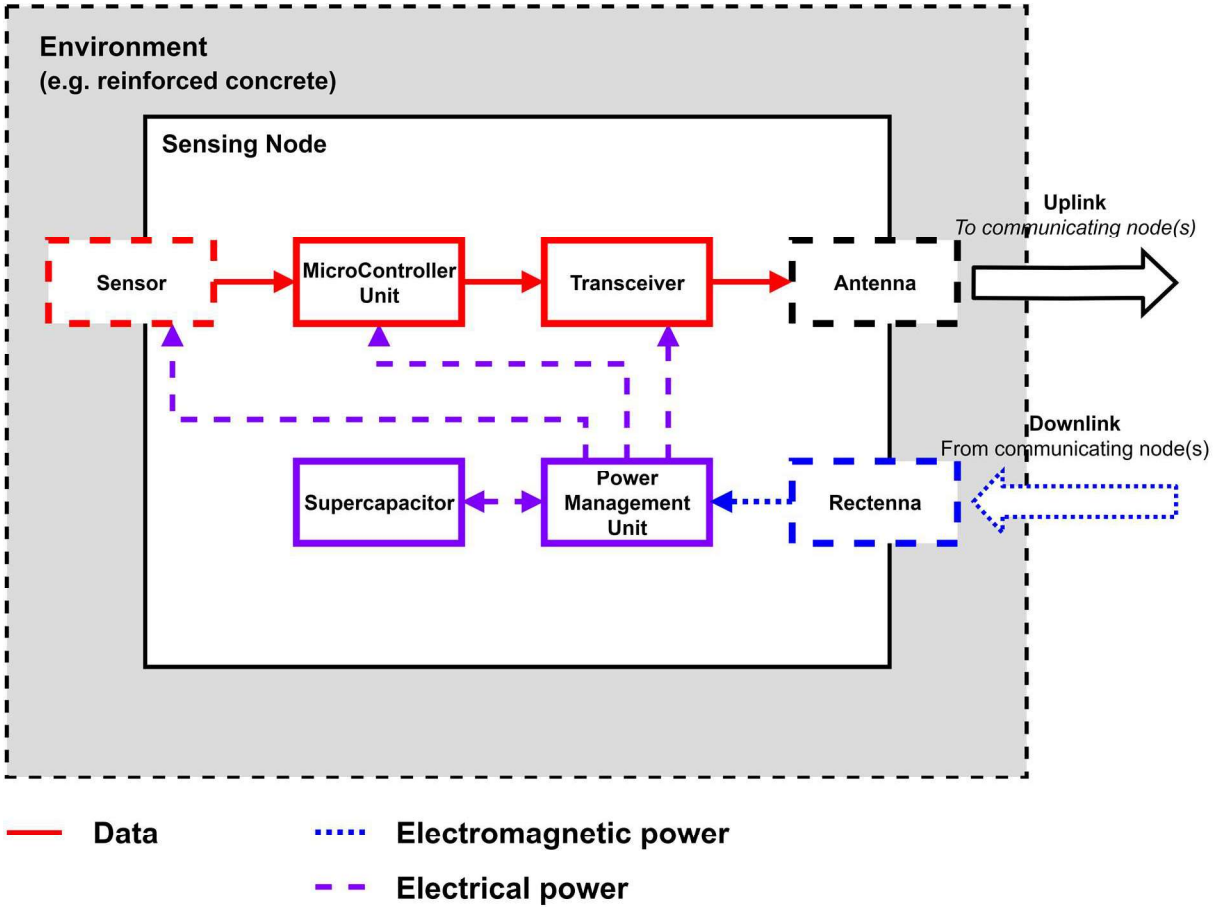

Figure III.6: Bloc diagram of the architecture of the sensing node.

C. Conclusion

Along this chapter, the McBIM research project, in which this doctoral thesis work takes place, has been introduced as well as the partners and the division of tasks within the consortium. More, the main scientific challenges have been made explicit, especially in regard of this doctoral thesis work. Then, the main constraints and the simplifications carried out have been detailed. Finally, the architecture of the wireless sensor network proposed to be embedded into the reinforced concrete in order to implement a communicating reinforced concrete has been presented, as well as each of its components, namely the communicating nodes and the sensing nodes.

The fact that the proposed solution to implement the wireless sensor network which will be embedded inside the reinforced concrete to make it communicating, as well as the context of the McBIM research project, have been well established, the next chapters will deal with the implementations of this solution and their tests.

IV. Implementation of communicating nodes based on the LoRaWAN technology

In agreement with the Figure III.4 and the Figure III.5, two communicating nodes based on the LoRaWAN technology have been implemented and tested. Even though our efforts have been focused on the designed and implementation of the sensing nodes, the communicating nodes are required to certify the good functioning of the sensing nodes, both by wirelessly powering these through a radiative electromagnetic power transmission system, and connecting these to the meshed network of communicating nodes and to the digital world *via* the Internet, by collecting, processing, storing and sharing the transmitted data. As presented above (Section III.B.3.), the three main subsystems that make up the communicating nodes will be detailed here. As a reminder and with the aim to release constraints, the communicating nodes are considered accessible, have an unlimited power source and the interfaces with the sensing nodes are preferred to others. Finally, the CRAN deals with the routing and data dissemination and exchange within the meshed network of communicating nodes, thus, these aspects will not be described in this manuscript.

A. Radiative electromagnetic power source

In order to wirelessly power the sensing nodes located in their neighbourhood, the communicating nodes are composed of a radiative electromagnetic power transmission system. This one is the unique downlink from the communicating nodes to the sensing nodes and also, musts be used to remotely set up the behaviour of the sensing nodes.

1. Technology choice

As shortly described above (Section II.D.5.), the choice has been made to employed a radiative electromagnetic wireless power transfer system to power the sensing nodes by the communicating nodes. The objective is to provide a generic solution usable in all possible cases and for long term, that says for decades. Thus, the chosen solution must be independent of the targeted environment, structure and/or application. More, the sensing nodes become inaccessible once deployed and are randomly located.

First, wired solutions are not desired. Indeed, these require an external power source (e.g. mains power, engine-generator, etc.) which are not necessary present or usable in all cases (e.g. isolated site, during the transportation of precast elements, etc.). More, these demand a manual installation, are expensive and heavy, and are difficult to deploy on a large scale. So, the wireless solutions are preferred.

Next, the batteries and fuel cells do not achieve the targeted lifetimes estimated in decades and because of the inaccessibility cannot be changed. For the rechargeable ones, a recharge system must be used. However, and today, only wired or short-range wireless solutions are available. Both require the knowledge of the location and the accessibility. The change and the recharge processes are human performed, time consuming and costly. So, "unlimited" wireless energy sources are privileged.

Then, the ambient energy harvesting solutions are not all possible and are hardly dependent of the environment structure and/or application. The reinforced concretes do not allow the light transmission and do not provide high temperature changes or gradients. The mechanical vibration, as well as the electromagnetic waves, depend of the environment. The first could be exploited on circulation bridges but not in office buildings, whilst it is the opposite for the second. So, dedicated energy sources are chosen to avoid the dependence on the environment.

Finally, regarding the wireless power transfer systems, those based on the light cannot be used because the reinforced concretes do not allow the light transmission and those based on the mechanical waves are out of the scope of our competences and are generally large in size. Thus, the electromagnetic waves seem the more appropriated propagation media for the wireless power transfer in our case (even if light is an electromagnetic wave, the optic solutions are excluded of the "electromagnetic solutions" appellation). In order to obtain ranges of use large enough, especially to power sensing nodes without the knowledge of their location, the far-field radiative power is more appreciated than the near-field inductive and/or capacitive. Thus, the radiative electromagnetic wireless power transfer system is chosen. Nevertheless, its settings will affect its performances, and also, must be well considered.

2. Design and implementation

The implemented radiative electromagnetic power sources have been designed to work in the 868 MHz or in the 915 MHz industrial, scientific and medical (ISM) frequency bands, respectively defined for the International Telecommunication Union (ITU) region 1 (whose Europe) and region 2 (whose Americas) [583]. The choice of these frequency bands is imposed by the design of the sensing nodes and will be justified below (Section V.C.1.).

The choice has been made of generating a continuous wave because of its ease of hardware implementation and even if it is considered as the one of the less efficient in the literature [277, 345, 400, 402, 442, 446, 447]. Nevertheless, optimization of the waveform to make the system as efficient as possible is expected. Moreover, by designing a functional system in the worst-case scenarios, this one can only be improved and will present the minimum necessary features.

Finally, according to the regulations and recommendations, these radiative electromagnetic power sources can generate an effective isotropic radiated power (EIRP) of up to 2 W (or +33 dBm) [411 - 414]. For comparison purposes, the maximal effective isotropic radiated power (EIRP) in the 2.45 GHz industrial, scientific and medical (ISM) frequency band is limited at 500 mW (or +27 dBm).

To meet all these requirements (a +33 dBm (or 2W) continuous wave radiative electromagnetic power source in the 868 MHz (or 915 MHz) industrial, scientific and medical (ISM) frequency band), a hardware solution has been implemented. The schematics, the board and a photograph of the implemented power source are presented in Figure IV.1, Figure IV.2 and Figure IV.3.

This one uses off-the-shelf Mini-Circuits components [584], respectively a ROS-950-219+ voltage control oscillator (VCO) to generate a +6.2 dBm (or +6.4 dBm) radiofrequency continuous wave signal at 868 MHz (or 915 MHz) [585]; a VACC-09+ voltage variable

attenuator (VVA) to control the output power by adding an attenuation down to -20 dBm (or -25 dBm) [586]; a PGA-105+ low power monolithic amplifier to amplify the radiofrequency signal by +15.1 dBm and up to +20.5 dBm [587], which is biased by a TCBT-14+ bias tee [588]; a PHA-202+ high power monolithic amplifier to amplify again the radiofrequency signal by +17 dBm (or +17.9 dBm) and up to +30.2 dBm (or +30.4 dBm) [589]; and a SMA (subminiature version A) radiofrequency connector to connect an antenna. In our case, as a +30 dBm output is measured, a RF Solutions ANT-8WHIP3H half-length whip antenna is used to obtain a +33 dBm (or 2 W) radiofrequency output [590]. This commercial antenna is an almost omnidirectional antenna with a vertical polarization, a centre frequency of 868 MHz and a theoretical gain of +3 dBi at 868 MHz. Thus, the combination of all these components allows to obtain a +33 dBm (or 2W) continuous wave radiative electromagnetic power source in the 868 MHz (or in the 915 MHz) industrial, scientific and medical (ISM) frequency band.

This one is powered by a conventional 12 V transformer connected to the mains supply. Then a power supply shaft is designed on the 10 cm x 5 cm printed circuit board (PCB) to provide a 11 V voltage through a Rohm Semiconductor BD00D0AWHFP low drop-out regulator [591], a 5.5 V voltage through a ABLIC S-812C55AMC-C3JT2U voltage regulator [592], a 5 V voltage through a ON Semiconductor NCV4264-2ST50T3G linear regulator [593], a 7 to 8 V (or 3 to 4 V) voltage through a STMicroelectronics STLQ50C-R low drop linear regulator tuned by a Bourns Trimpot 3296 [594, 595] and a 0 to 5 V voltage through a Linear Technology LT3082EST#TRPBF low drop linear regulator tuned by a Bourns Trimpot 3299 [596, 597], all required for the power supply or the tuning of the radiofrequency components.

The power consumption of this +33 dBm (or 2 W) continuous wave radiative electromagnetic power source has been measured at about 4.5 W for a 12 V supply voltage. More, this one is heating and a thermal study should be conducted to optimize the heat dissipation, especially in an enclosed environment (e.g. in a box, etc.). Finally, each source costs less than 75 € for 10 pieces, without the 12 V transformer and an enclosure package.

3. Remote control of the periodicity of measurement and communication of the sensing nodes

By tuning the output power and the activation cycle of the radiative electromagnetic power source, it is possible to remotely control of the periodicity of measurement and communication of the sensing nodes. Indeed, these latter will make a measurement and will transmit the collected data whenever these have harvested enough energy, with the scavenged power which is mainly, if not entirely, due to the radiative electromagnetic power source. More details will be presented below (Section V.D.3.).

In the current implementation, the control of radiative electromagnetic power source by the data management system is not yet implemented.

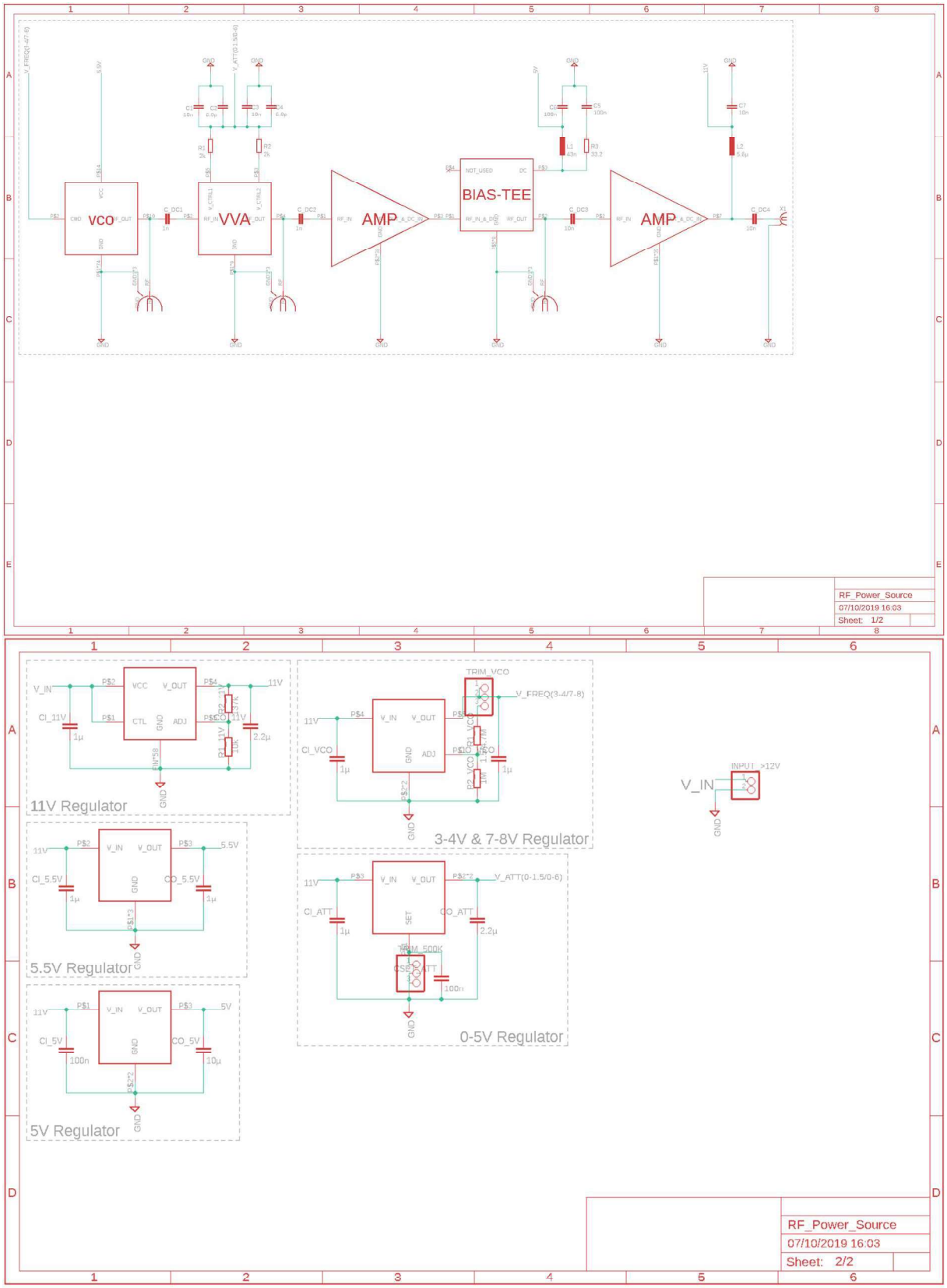

Figure IV.1: Schematics of the designed and implemented +33 dBm continuous wave radiative electromagnetic power source in the 868 MHz industrial, scientific and medical (ISM) frequency band.

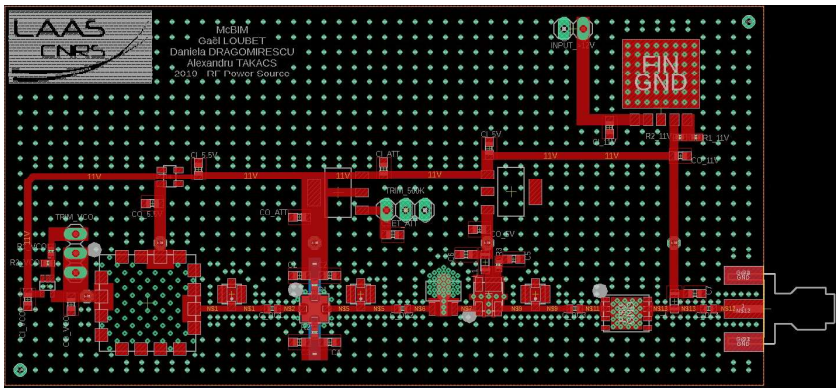

Figure IV.2: Board (10 cm x 5 cm) of the designed and implemented +33 dBm continuous wave radiative electromagnetic power source in the 868 MHz industrial, scientific and medical (ISM) frequency band.

Figure IV.3: Photograph of the designed and implemented +33 dBm continuous wave radiative electromagnetic power source in the 868 MHz industrial, scientific and medical (ISM) frequency band.

4. Work in progress

At the time of writing, some experimentations are still in progress regarding the impact of the waveform on the efficiency of the wireless power transfer, related to [277, 345, 400, 402, 442, 446, 447]. To perform these, an Ettus Research B210 universal software radio peripheral (USRP) is directly connected to the first amplification stage of the designed and implemented radiative electromagnetic power source [598]. Thus, by using GNURadio software, the universal software radio peripheral can be easily programmed to generate various radiofrequency signals [599]. In our case, tests are conducted in the 868 MHz industrial, scientific and medical (ISM) frequency band, for various output powers up to +33 dBm (or 2 W), and for various signals, whose continuous wave, amplitude modulated, frequency modulated, chirps, pulsed and orthogonal frequency-division multiplexed ones. Nevertheless, no definitive results are yet available.

5. Alternatives and perspectives

Before designing and implementing the radiative electromagnetic power source, an Anritsu MG3694A or MG3694B radiofrequency or microwave signal generator has been used [600, 601]. These last can be easily tuned in terms of frequency and power, but are limited in its basic configuration, that says without adding options, to the continuous waves. More, the output power is limited at less than +17 dBm (or 50 mW) at 868 MHz.

In parallel, there are few available commercial radiative electromagnetic power sources. The Powercast TX91501 is an enclosed 17 cm x 16 cm x 4 cm radiative electromagnetic power source which transmits a +30 dBm (or 1 W) or a +34.8 dBm (or 3 W) direct-sequence spread spectrum (DSSS) signal in the 915 MHz industrial, scientific and medical (ISM) frequency band [602]. It uses an embedded linearly polarized antenna. Its power consumption is less than 5 W and it is powered by an external 5 V transformer connected to the mains supply. The +30 dBm version costs nearly 170 € per piece for 10 pieces, whilst the +34.8 dBm version costs 220 €. The Powercast TX91503 is an enclosed 19 cm x 5 cm x 5 cm radiative electromagnetic power source which transmits a +34.8 dBm (or 3 W) direct-sequence spread spectrum (DSSS) signal in the 915 MHz industrial, scientific and medical (ISM) frequency band [603]. It uses an embedded linearly polarized antenna. Its power consumption is less than 5 W and it is powered by an external 5 V transformer connected to the mains supply. It costs nearly 80 € per piece for 10 pieces. The GREENWAKE PWT-04 is an enclosed 16 cm x 13 cm x 4 cm radiative electromagnetic power source which transmits a +27 to +36 dBm (or 500 mW to 4 W) continuous wave signal in the 2.45 GHz industrial, scientific and medical (ISM) frequency band [604]. It uses an external antenna through a SMA connector. Its power consumption is 13 W and it is powered by an external 12 V transformer connected to the mains supply. No availability or prices have been found. Comparatively, our solution is more compact (without package and without considering the heat dissipation), its power consumption and its cost are among the lowest, it allows to use of any antenna with an SMA connector, like the others an external transformer is required, and it is the only one which generates a continuous wave signal up to +33 dBm (or 2 W) in the 868 MHz industrial, scientific and medical (ISM) frequency band.

In its current version, the radiative electromagnetic power source is manually controlled: its functioning is function of the activation or deactivation of its power supply, and its central

frequency and its output power are tuned through potentiometers. In future works, it could be relevant to have a low-cost software defined radio (SDR) (e.g. an Adalm-Pluto [605], a HackRF One [606], an RTL-SDR [607], etc., or even a homemade one) as signal generator, controlled by the data management system. In this way, the signal can be tuned in a software and dynamic way in terms of frequency, waveform and power, according to the needs. In the case where a well-defined signal is needed, a specifically designed hardware signal generator controlled by the data management system could be implemented in order to limit the complexity and power consumption. More, the amplification stages, still required to obtain a +33 dBm (or 2 W) output power, could be optimised and modified in order to have a lowest voltage supply, if possible, the same that for the data management system (e.g. 5 V in our case).

A major improvement in the radiative electromagnetic power source could be to implement a beamforming system able to target specific sensing nodes in order to increase to global efficiency [277, 389, 390, 397, 399, 400, 402, 410, 431, 434-436, 438, 439, 445, 448, 449, 451, 455, 458, 459, 469]. In this case, as well as the current one, a learning period could be relevant to know the sensing nodes in the neighbourhood of the communicating node (at least in terms of identifier, but also in terms of location in the case of beamforming), as well as their needs in terms of power and duration of wireless power transfer.

B. Data management system

In order to collect, process, store and share the data transmitted by the sensing nodes within the meshed network of communicating nodes and with the digital world, whose the building information modelling, through the Internet, the communicating nodes are composed of a data management system. This one manages various interfaces, whose the one used as the uplink from the sensing nodes to the communicating nodes and also, those to the Internet, with the other communicating nodes and with the stakeholders.

1. Design process

In a general way, the communicating nodes have been designed to be an embedded system allowing the functional test of both the star network of sensing nodes around a communicating node (main objective) and the meshed network of communicating nodes linked to the Internet (additional objective). Thus, the main efforts concern the main objective and the additional one has been only performed to have a full proof-of-concept. Even if it is a main constraint, the energy consumption has not been considered in a first time. More, the routing and dissemination and exchange of the data within the meshed network of communicating nodes has not been treated as these aspects are the responsibility of CRAN. So, only functional and usable interfaces have been provided to allow the implementation of the solutions proposed by the CRAN.

Concerning the acquisition of the data sent by the sensing nodes, the technology choice has been imposed by the design of the sensing nodes, which will be detailed below (Section IV.A.1.).

Concerning the process, the storage and the exchange of the data within the meshed network of communicating nodes and through the Internet, the technology choices have been derived from the resources available in the proposed solution to meet the first objective. Thus, the proposals made are not optimal.

2. Design and implementation

As explained above (Section III.B.2.), the main objective in the design of the data management system as a part of the communicating node is to collect all the data sent by the sensing nodes. Then, the others interfaces and functions have been treated to get a full but non-optimal proof-of-concept. The designed and implemented LoRaWAN gateways as the data management system are presented in Figure IV.4.

i. Interfaces for the wireless communications

a. Collection of the data sent by the sensing nodes

As the sensing nodes transmit their measured data *via* the LoRaWAN technology, the communicating nodes must be able to collect the LoRaWAN frames to recover the data sent. The choice of the LoRaWAN wireless communication technology is imposed by the design of the sensing nodes and will be justified below (Section IV.A.1.). In few words, its main advantages are its long range (several tens of kilometres in the air), its low but sufficient data-

Figure IV.4: Photographs of the designed and implemented LoRaWAN gateways.

rate and transmission frequency, its low noise sensibility, the availability of off-the-shelf components, the possibility of deploying and managing its own network, etc., whilst its main drawback is its power consumption considered as low but not really in comparison with other wireless communication technologies.

Thus, the data management system is in fact a LoRaWAN gateway composed of off-the-shelf components, especially an IMST iC880A LoRaWAN concentrator working in the 868 MHz industrial, scientific and medical (ISM) frequency band [608] based on a Semtech SX1301 transceiver [609] with a RF Solutions ANT-8WHIP3H half-length whip antenna [590], driven and powered through wired jumpers by a Raspberry Pi 3 model B+ micro-computer [610] embedding the Raspberry Pi OS Lite operating system (OS) [611] and powered by an external 5 V transformer. By using the Semtech UDP (user datagram protocol) packet-forwarder [612], it is possible to continuously listen the 868 MHz industrial, scientific and medical (ISM) frequency band to collected and demodulated all the LoRaWAN frames, which are then transmitted to a local or remote application server through a gateway bridge and a local or remote network server to be finally processed and stored.

b. Sharing of the collected data within the meshed network of communicating nodes

Two solutions have been implemented and successfully tested, only as a proof-of-concept, to share the data between the communicating nodes. These are based on the Wi-Fi wireless communication technology, which is natively available on the Raspberry Pi 3 model B+

micro-computer and which is obviously not the most suitable for the needs of the project (e.g. high-power consumption, short to medium range, high data-rate, etc.).

The first solution consists to use a pre-existing Wi-Fi network on which each communicating node is connected. In this way, the communicating nodes can exchange their data by sending the received LoRaWAN frames to a unique application server, on which all the communicating nodes are connected and thus, receive all the data. Nevertheless, this solution requires a pre-existing Wi-Fi network, the permission to connect several communicating nodes on it and to connect or deploy a network server as well as an application server on it, and could be unsecure. Furthermore, without static addresses, communicating nodes can hardly communicate directly with each other.

The second solution consists to use the Raspberry Pi 3 model B+ micro-computer as both a Wi-Fi access point and as a Wi-Fi client. This native ability presents some limitations as the use of a unique channel for all the Wi-Fi interfaces. Nevertheless, each communicating node can connect to each of the Wi-Fi networks provided by other communicating nodes in its neighbourhood and provided a Wi-Fi network to which the other communicating nodes can connect. In this way, a dynamic and *ad-hoc* meshed network of communicating nodes can be obtained, without being dependent of a pre-existing Wi-Fi network and with the possibility to adopt its own network strategy for instance by using specific static address for each communicating node in all deployed Wi-Fi networks.

c. Sharing of the collected data across the Internet

To exchange the collected and shared data in the meshed network of communicating nodes across the Internet, several solutions have been implemented and tested. These are function of the solutions used for the implementation of the meshed network of communicating nodes.

For the first solution presented in the previous subsection, the choice has been made to allow each communicating node connected to the pre-existing Wi-Fi to directly access the Internet *via* this last. For this, the pre-existing Wi-Fi network must have an Internet connection and must allow each communicating nodes to send and receive data through it and on various ports. Once again, without being the owner of this Wi-Fi network, the good functioning of this solution is dependant of the goodwill of its owner.

For the second solution presented in the previous subsection, two alternatives have been implemented and tested. This first consists to use a pre-existing Wi-Fi network with an Internet connection on which is connected a unique communicating node from the meshed network. This is relatively close to the previous one with the main difference in the number of connections to the host Wi-Fi network. The second one consists to use a connection to the cellular network linked to the Internet (in our case thanks to a smartphone connected to a 4G network and wired to the Raspberry Pi 3 model B+ micro-computer) for a unique communicating node from the meshed network. This solution, more secure, allows to be independent to local deployment of a Wi-Fi network, but required a cellular network coverage as well as an additional transceiver with a subscription and a relatively high-power consumption.

With all these solutions, it is possible to send the collected data to remote network and application servers only accessible through the Internet, as well as to receive data from these servers.

d. Local and remote accesses to the communicating nodes by the stakeholders' devices

By installing a secure shell (SSH) server on the Raspberry Pi 3 model B+ micro-computer, it becomes possible for the stakeholders to access to the communicating nodes with their devices (e.g. laptop, tablet, smartphone, etc.). This access can be locally done *via* the pre-existing Wi-Fi network if each or a unique communicating node is connected to it, or directly *via* a Wi-Fi network deployed by a communicating node. Regardless of the access point to the meshed network of communicating nodes, once connected to this it is possible to access all the communicating nodes knowing their network identifier or their address and having an account on it.

In order to connect remotely the meshed network through the Internet, this one must at least get a public address and allowing remote connections. This last solution has been indirectly implemented: a virtual private network (VPN) connection is achieved to the pre-existing Wi-Fi network in which at least a communicating node is connected, and through this tunnel it is possible to connect the meshed network of communicating nodes wherever the stakeholder is. For the local connection, both the Wi-Fi and Ethernet interfaces can be used, if accessible. No solution has been currently provided for a remote connection to the meshed network of communicating nodes connected to the Internet by a cellular network.

Moreover, by managing accounts and their permissions on the operating system of the communicating nodes, it is easily possible to limit the access rights of each stakeholder to some or all of the embedded data and/or software.

ii. Processing and storage of the collected data

Once received and demodulated by the Semtech UDP (user datagram protocol) packet-forwarder, the LoRaWAN frames are made available to the ChirpStack open-source LoRaWAN tools [613].

First, the ChirpStack LoRaWAN gateway bridge, deployed on each communicating nodes, converts the demodulated LoRaWAN frames transmitted by the Semtech UDP packet-forwarder into JSON (JavaScript object notation) data format as presented in Code IV.1. These JSON data frames are published *via* a Mosquitto MQTT (message queuing telemetry transport) broker [614].

A ChirpStack LoRaWAN network server -subscribing to the gateway bridge MQTT stream and managing the LoRaWAN network- collects, de-duplicates, and stores in a PostgreSQL database [615] these JSON data frames, before forwarding these *via* a Mosquitto MQTT broker, to a ChirpStack LoRaWAN application server.

This last -subscribing to the network server MQTT stream- allows to manage the users, gateways, applications, devices, etc. of the network through a web interface, and decodes thanks to the Code IV.2, then stores in a PostgreSQL database the JSON data frames as presented in Code IV.3, before publishing these to the subscribing stakeholders through a Mosquitto MQTT broker and through APIs (application programming interface).

All these ChirpStack components can be configured (through .toml file) to meet the requirements defined by the targeted application.

The databases, the network server and the application server can be deployed on each gateway (Figure IV.5), on a unique gateway in the meshed network of communicating nodes (Figure IV.7) or on a remote server as well as in the Cloud (Figure IV.6). All the three implementations have been tested. The first solution (the deployment on each communicating node) can be relevant in the case of an isolated communicating node, but does not allow the easy sharing of the received data in the case of a meshed network of communicating nodes. The second solution (the deployment on a unique communicating node within the meshed network) is achieved by connecting each gateway bridge to the same network server, itself connected to a unique application server and the two using a single database, and all embedded on a unique communicating node; and by subscribing each communicating node to the MQQT stream of the network and application servers. By this way, the data is shared by all the communicating nodes and stored by each of these. The third solution (the deployment on a remote server) has been tested by deploying the network and application servers as well as the databases on an online server provided by FINAO SAS/360SmartConnect. This solution is similar to the previous but requires a reliable Internet connection to avoid the loss of data and allows to easily share the collected and decoded data to the stakeholders through the Internet, as well as to easily deploy other tools.

In order to make the decoded LoRaWAN frames more human readable, a script designed in TCL (tool command language) programming language has been developed and allows to get a text file with the format presented in Code IV.4. More, this one and others TCL scripts have been designed in order to store daily logs and reboot logs (thanks to the cron or crontab (chrono table) tool) in text files containing all the received LoRaWAN frames (the demodulated ones and the decoded ones). These tools are only used for development purposes and to facilitate the monitoring of the network.

As tasks linked to the routing and dissemination and exchange of the data within the meshed network of communicating nodes have been allocated to the CRAN, no additional works and tests have been achieved in this domain.

iii. Power consumption

The implemented data management system consumes between 4.0 and 4.8 W to work properly with a 5 V supply voltage. This power consumption is function of the mode of operation of the LoRaWAN concentrator (listening, receiving, etc.) and of the micro-computer (idle, standby, processing, communicating, etc.), but even to the active interfaces (none, Wi-Fi, Ethernet, etc.).

3. Alternatives and perspectives

As the wireless communication technology used by the sensing nodes is imposed by their design, the alternatives to the LoRaWAN technology will be discussed below (Section V.A.1.).

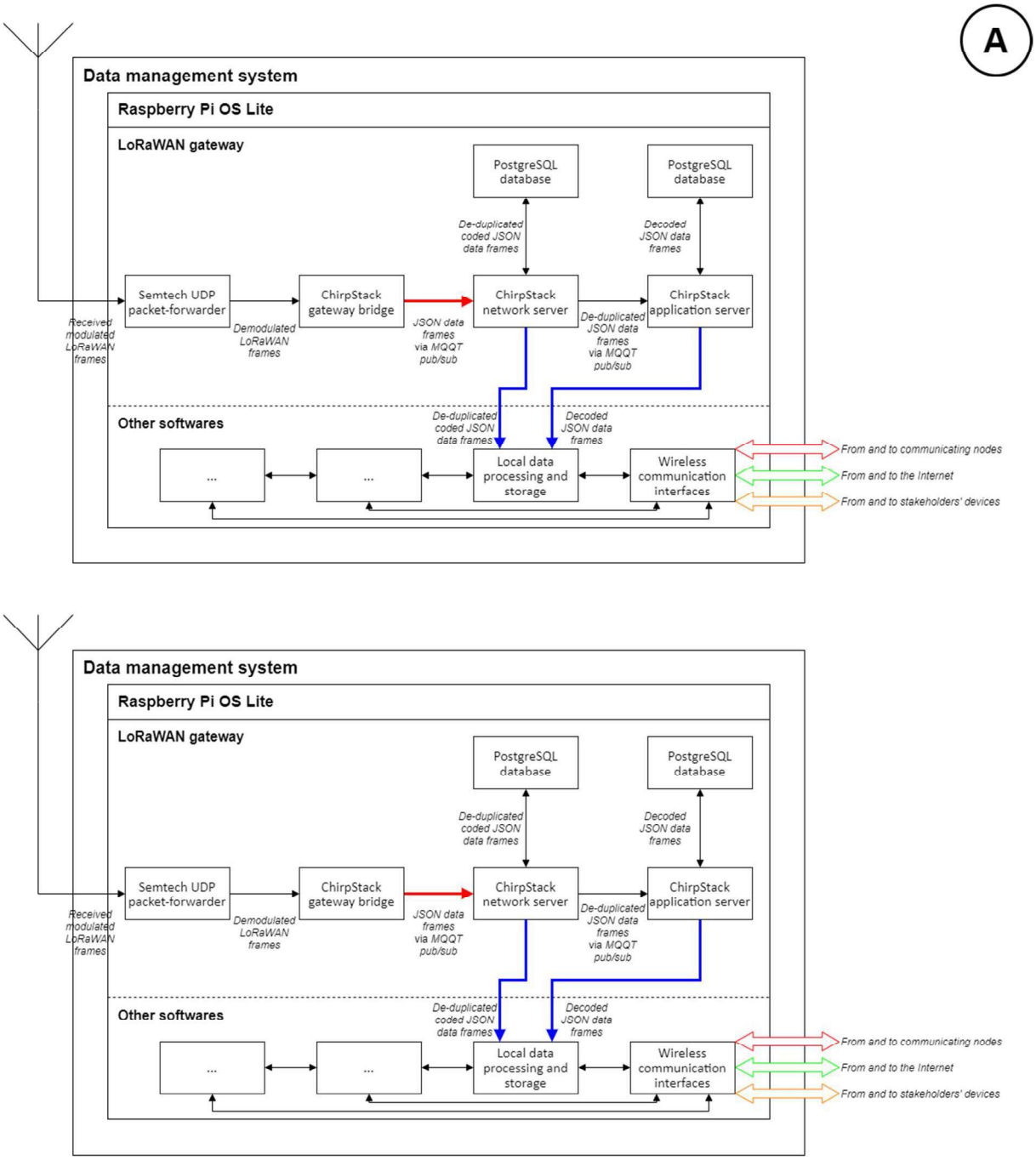

Figure IV.5: Bloc diagrams of the different implementations of the software (ChirpStack servers and PostgreSQL databases) required by the LoRaWAN gateway: Part A. *(to be continued)*

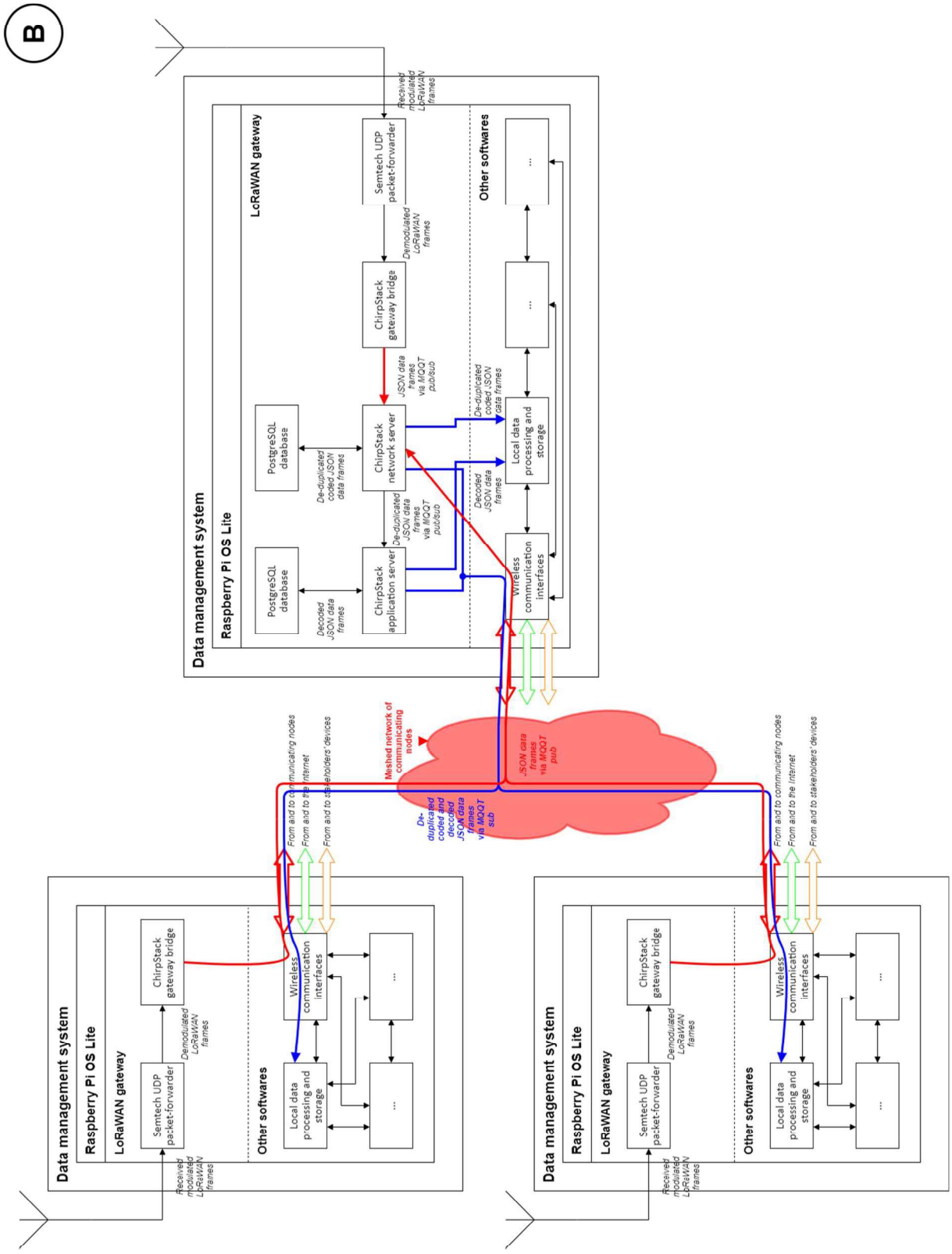

Figure IV.6: Bloc diagrams of the different implementations of the software (ChirpStack servers and PostgreSQL databases) required by the LoRaWAN gateway: Part B. *(continuation)*

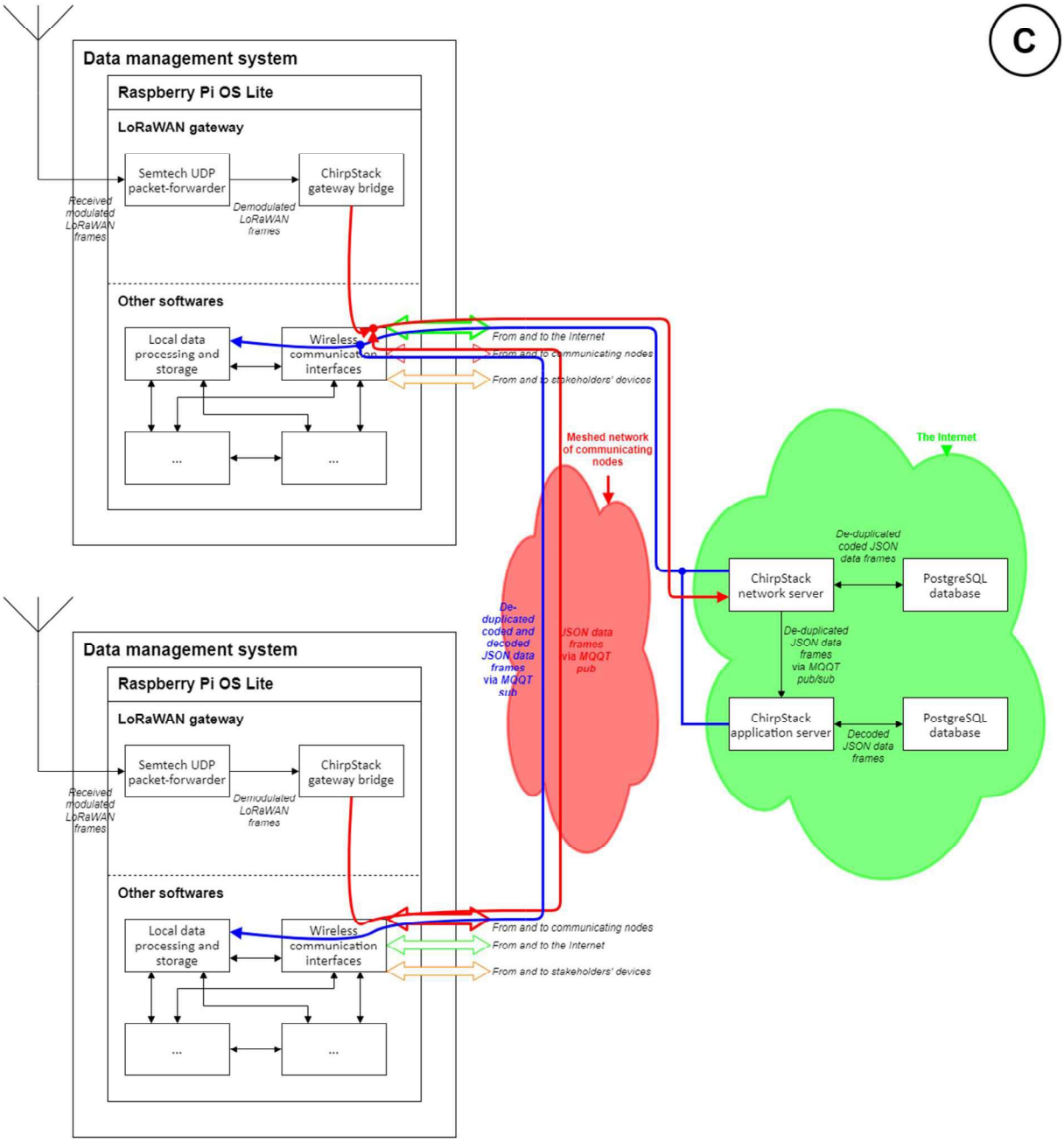

Figure IV.7: Bloc diagrams of the different implementations of the software (ChirpStack servers and PostgreSQL databases) required by the LoRaWAN gateway: Part C. *(end)*

Code IV.1: Example of a LoRaWAN frame converted into JSON format by the ChirpStack LoRaWAN gateway bridge.

```
{"phyPayload":"QOs24PmAAQABnPTZL9/ZaBE=","txInfo":{"frequency":868100000,"modulati
on":"LORA","loRaModulationInfo":{"bandwidth":125,"spreadingFactor":12,"codeRate":"
4/5","polarizationInversion":false}},"rxInfo":{"gatewayID":"EhJXBZuf1fw=","time":"
2021-05-18T13:32:35Z","timeSinceGPSEpoch":null,"rssi":-
54,"loRaSNR":9,"channel":0,"rfChain":1,"board":0,"antenna":0,"location":null,"fine
TimestampType":"NONE","context":"iGYNbA==","uplinkID":"fW6jnWrfTKan9h0qzCjK4g==","
crcStatus":"CRC_OK"}}
```

Code IV.2: Decode function used by the application server.

```
// Decode decodes an array of bytes into an object.
//  - fPort contains the LoRaWAN fPort number
//  - bytes is an array of bytes, e.g. [225, 230, 255, 0]
//  - variables contains the device variables e.g. {"calibration": "3.5"} (both
the key / value are of type string)
// The function must return an object, e.g. {"temperature": 22.5}

function Decode(fPort, bytes, variables) {
  var decoded = {};
  //LoRa communication test
  if (((bytes[0] << 8) | bytes[1]) === 0xC0DE) {
    decoded.LoRa_Communication = "OK";
  }
  //Internal temperature sensor
  else if (((bytes[2] << 8) + (bytes[3])) === 0xDEAD) {
    decoded.Temperature = ((bytes[0] << 8) + bytes[1]) / 10;
  }
  //Error (HDC2010)
  else if (((bytes[0] << 8) + (bytes[1])) === 0xDEAD) {
    decoded.Error_Index = ((bytes[2] << 8) + bytes[3]);
  } else {
  //Temperature and humidity sensors (DHT22 and HDC2010)
    decoded.Temperature = ((bytes[0] << 8) + bytes[1]) / 10;
    decoded.Humidity = ((bytes[2] << 8) + bytes[3]) / 10;
  //Temperature sensor (Thermodiodes)
    //decoded.Temperature_Bulk_Substrate = (((bytes[0] << 8) + bytes[1]) - 5000) /
100;
    //decoded.Temperature_Membrane_Substrate = (((bytes[2] << 8) + bytes[3]) -
5000) / 100;
  //Resitivity sensor (Wenner probe)
    //decoded.Voltage = ((bytes[0] << 8) + bytes[1]) / 1000;
    //decoded.Resistivity = ((bytes[2] << 8) + bytes[3]);
  //Strain gauge
    //decoded.Voltage = ((bytes[0] << 8) + bytes[1]) / 1000;
    //decoded.Strain = ( ((bytes[2] << 8) + bytes[3]) - 10000) / 1000000;
  }
  return decoded;
}
```

Code IV.3: Example of a LoRaWAN frame decoded by the ChirpStack LoRaWAN application server.


```
{"applicationID":"1","applicationName":"McBIM","deviceName":"McBIM_-
_Modular_2","devEUI":"ACKPHlld4Ts=","rxInfo":[{"gatewayID":"EhJXBZuf1fw=","time":"
2021-05-18T13:32:35Z","timeSinceGPSEpoch":null,"rssi":-
54,"loRaSNR":9,"channel":0,"rfChain":1,"board":0,"antenna":0,"location":{"latitude
":43.56243084940792,"longitude":1.4775055646896362,"altitude":0,"source":"UNKNOWN"
,"accuracy":0},"fineTimestampType":"NONE","context":"iGYNbA==","uplinkID":"fW6jnWr
fTKan9h0qzCjK4g==","crcStatus":"CRC_OK"}],"txInfo":{"frequency":868100000,"modulat
ion":"LORA","loRaModulationInfo":{"bandwidth":125,"spreadingFactor":12,"codeRate":
"4/5","polarizationInversion":false}},"adr":true,"dr":0,"fCnt":1,"fPort":1,"data":
"AN0B2g==","objectJSON":"{\"Humidity\":47.4,\"Temperature\":22.1}","tags":{},"conf
irmedUplink":false,"devAddr":"+eA26w=="}
```

Code IV.4: Format of the daily log.

```
========================================
====== GATEWAY =========================
========================================
ID(HEX)         EhJXBZuf1fw=
========================================

========================================
====== APPLICATION =====================
========================================
Name            McBIM
ID              1
========================================

========================================
====== SENSING NODE ====================
========================================
= Modular_1 =
========================================
Name            McBIM_-_Modular_1
devEUI          ACKPsxBjb6s=
devAddr(HEX)    +eA8aw==
========================================
Measurement     n°0
======
ID(HEX)         LerjuJMSSn6tK83/s/p7lQ==
Status          CRC_OK
Time            2021-05-15T23:54:38Z
RSSI            -52dB
SNR             11dB
======
phyPayload(HEX) QGs84PmAAQABiLJ+3Za2/fc=
data(HEX)       ABUANA==
context(HEX)    34A51A==
======
Resistivity:    52
Voltage:        0.021
========================================


Measurement     n°1
======
ID(HEX)         M63cD1Q/TQ264mQEoRbNoA==
Status          CRC_OK
Time            2021-05-16T03:43:54Z
RSSI            -52dB
SNR             9.2dB
======
phyPayload(HEX) QGs84PmAAQABiLJ+3Za2/fc=
data(HEX)       ABUANA==
context(HEX)    E2VmtA==
======
Resistivity:    52
Voltage:        0.021
========================================
…
========================================
```

```
Measurement     n°5
======
ID(HEX)         i8HZH/byRxWRlMzBmGxukw==
Status          CRC_OK
Time            2021-05-16T18:53:12Z
RSSI            -53dB
SNR             10.5dB
======
phyPayload(HEX) QGs84PmAAQABiLN+25Y6vtk=
data(HEX)       ABQAMg==
context(HEX)    x0tRHA==
======
Resistivity:    50
Voltage:        0.02
========================================

========================================
====== SENSING NODE ====================
========================================
= Modular_2 =
========================================
Name            McBIM_-_Modular_2
devEUI          ACKPHlld4Ts=
devAddr(HEX)    +eA26w==
========================================
Measurement     n°0
======
ID(HEX)         X2xcI5/gQVu7vvKfj3OTyw==
Status          CRC_OK
Time            2021-05-15T22:03:35Z
RSSI            -52dB
SNR             8dB
======
phyPayload(HEX) QOs24PmAAQABnPPauVuCKD4=
data(HEX)       ANoCTA==
context(HEX)    UlXeJA==
======
Humidity:       58.8
Temperature:    21.8
========================================
…
========================================
Measurement     n°38
======
ID(HEX)         SnayDo18RgiqhHLRT+rFGA==
Status          CRC_OK
Time            2021-05-16T21:48:22Z
RSSI            -53dB
SNR             10dB
======
phyPayload(HEX) QOs24PmAAQABnPHaoAJ4HlU=
data(HEX)       ANgCVQ==
context(HEX)    Ob4NdA==
======
Humidity:       59.7
Temperature:    21.6
========================================

========================================
```

```
====== SENSING NODE ======================
==========================================
= Modular_Mini =
==========================================
Name             McBIM_-_Modular_Mini
devEUI           ACKP6sCAjX0=
devAddr(HEX)     +eAnIQ==
==========================================
Measurement      n°0
======
ID(HEX)          AJQu33+MT5OtYx1bDNb2sQ==
Status           CRC_OK
Time             2021-05-16T09:36:01Z
RSSI             -75dB
SNR              -3.5dB
======
phyPayload(HEX) QCEn4PmAAQABgi1tgBAHsCw=
data(HEX)        HegfXQ==
context(HEX)     /qXk7A==
======
Temperature_Membrane_Substrate:   30.29
Temperature_Bulk_Substrate:       26.56
==========================================
```

For the LoRaWAN gateway, which costs less than 250 € per piece, its design has been chosen because based on a full, available, documented and recommended LoRa concentrator, which is compatible with free and open source software (ChirpStack tools, Mosquitto broker, PostgreSQL database, Raspberry Pi OS) and open and flexible hardware (Rapsberry Pi). Nevertheless, other solutions, both software and hardware, are available and no comprehensive and objective comparison has been achieved. More, private LoRaWAN networks requiring subscription are available, but in order to be independent to an access provider and to assure that the network will maintain during decades to ensure the proper functioning of the communicating reinforced concrete throughout its life, the choice of deployed and used its own LoRaWAN network seems the more relevant.

Regarding wireless communication technology used for the sharing of the collected data within the meshed network of communicating nodes and the local access to the communicating nodes by the stakeholders' devices, the choice made has been the simplest to implement but probably not the most efficient. These wireless links must be more defined to make the more relevant and adapted choice to the constraints. With the current hardware implementation, the native Bluetooth device embedded into the Raspberry Pi could be an option to follow to reduce the power consumption without strongly altering the range of use and by staying a common technology generally available on laptops, tablets and smartphones. By being accessible the data management part of the communicating node can be reconfigured, updated and modified according to new constraints or needs. Thus, the interfaces used for sharing the collected data across the Internet and remotely accessing to the communicating nodes by the stakeholders' devices could be evolving and for instance based on the most recent and/or the most deployed cellular technology. Finally, all the interfaces can employ various wireless communication technologies regarding the users and application constraints. The proposed implementation is just one among others, all with their advantages and drawbacks.

It is similar regarding the processing and the storage of the collected data, whose the possible solutions are numerous and varied, and these are again the constraints imposed by the users and applications which will allow to define a good trade-off.

A middle-term perspective could be the design and implementation of a one-part and compact version of the data management system, based on off-the-shelf components such as LoRaWAN transceiver and microcontroller instead of the LoRaWAN concentrator and the micro-computer. This will allow gains in terms of compactness, energy consumption and efficiency, at the cost of a more complex and less user-friendly system.

C. Energy management system

In order to power the radiative electromagnetic power source and the data management system, the third part composing the communicating node is an energy management system.

1. Technology choice

As explained above (Section II.A.3.) and in order to release the constraints in the design of the communicating reinforced concrete, the communicating nodes are considered as having an unlimited power source. In practice, this means that these can be connected to the mains supply. Thanks to this hypothesis, the design of the communicating node has been facilitated.

2. Design and implementation

Thus, two transformers, one with a 12 V voltage supply and the other with a 5 V voltage supply, have been used, respectively for the radiative electromagnetic power source and the data management system *via* the Raspberry Pi 3 model B+ micro-computer which powers the LoRaWAN concentrator. For the radiative electromagnetic power source, the power supply shaft designed to power each component has been presented above (Section IV.A.2.). As a reminder, the radiative electromagnetic power source has a power consumption measured at nearly 4.5 W, whilst the data management system has a power consumption measured 4.0 and 4.8 W. That says the communicating node requires 9.3 W in the worst case to work properly.

3. Alternatives and perspectives

By considering a battery, and without considering its limitation in terms of overvoltage and undervoltage constraints, its losses and its self-discharge as well as the required power management circuit and its own power consumption, a 1 Ah battery could allow to continuously power a full communicating node for nearly 45 minutes in the worst case, whilst a battery of nearly 32 Ah would be needed for 24 hours (or 1 day). Thus, in its current implementation, the use of a battery as power source for the communicating nodes is not feasible.

By regarding the ambient energy harvesting or the wireless power transfer, only the photovoltaic cells have been investigated in particular use cases and in high luminosity locations, both to intermittently power a LoRaWAN gateway as presented in [291, 292] and to power a low power radiative electromagnetic power source as presented [426, 427]. Nevertheless, with the current implementation of the communicating nodes, none of these solutions seems suitable, but are still ways to explore.

A short-term perspective could be the design of a unique power supply shaft, which would power each component of the radiative electromagnetic power source and of the data management system, and which would have a unique transformer connected to the mains power.

D. Reconfigurability of the communicating nodes

The communicating nodes could be reconfigured and upgraded during all their lifetime thanks to their physical accessibility (these are considered as located on the surface of the reinforced concrete element) and the various available bidirectional communication interfaces.

Thus, their operating system and their software are stored on a microSD (secure digital) non-volatile memory card of at least 8 GB, which can easily be removed to be changed or reprogrammed. Moreover, the wire Ethernet interface, as well as the wireless interfaces for a local (by the other communicating nodes or the stakeholders) or a remote (by the remote servers through the Internet or the stakeholders) accesses can be used to remotely update both the operating system and the software. It is also possible to remotely change the configuration of the communicating nodes during their entire lifetime. These software modifications could affect different aspects of the network: the periodicity of the measurement and transmission of the sensing nodes through the control of the radiative electromagnetic power sources; the kind of measurements in the case of different fleets of sensing nodes independently controllable; the pre-processing of the collected data; some other on-board processing; the managing of the data storage in the memory; the routing protocol in the meshed network of communicating nodes; the affectation between the different communicating nodes of the Internet gateway role; etc. These modifications could be provided by a specific stakeholder or come from the digital world and be made by a decisions-maker.

For the hardware, it is conceivable to change or add parts (e.g. change the complete communicating node, a battery, or the microcontroller unit; add memory or a new wireless communication interface; upgrade a wireless communication interface, especially in the case of cellular networks; repair a radiative electromagnetic power source; etc.). Nevertheless, the wireless communication interface with the sensing nodes must be maintained in order to assume their functioning during all their lifespan. Thus, and in order to certify a long-term use, the use of a personal and self-administered network is privileged to a third-party network, which could be upgraded or stopped and become incompatible with the initial needs, without the possibility to the users to intervene.

To go further and to upgrade the power efficiency and the security in the network, a learning period could be useful in order to characterize the environment of each communicating node, *id est* to discover the legal sensing nodes and communicating nodes located in its neighbourhood; to eventually know the location of the sensing nodes and communicating nodes by implementing beamforming solutions both for the wireless power transfer and the wireless communications; to know the needs of the sensing nodes in terms of power to transmit for fully charging these in function of the waveform, the transmitted power and the activation periodicity of the radiative electromagnetic power source; and to define the rights for each stakeholder (e.g. the bidirectional communication interfaces they can use, the kind of modifications they can make, etc.); as well as backup solutions. Anyhow, energy efficiency and security aspects must be considered before deploying a network of communicating materials.

E. Complete implementation and tests of the communicating nodes

In the current version of the communicating nodes, as presented in Figure IV.8, each subsystem has been individually tested and thus, works properly and meets its own requirements: the energy management subsystem powers the two other subsystems efficiently by being connected to the mains power; the reconfigurable and evolving data management subsystem collects, processes and stores (locally and/or remotely) the LoRaWAN data frames sent by the sensing nodes which contain the measurement data, wirelessly shares the collected data within a meshed network of communicating nodes, links the digital world through the Internet and is locally and remotely accessible by the stakeholders from their devices, all this with several possible implementations depending on the needs (communicating node isolated, in a meshed network with or without an Internet connection); and the radiative electromagnetic power source powers wirelessly all the sensing nodes located in its neighbourhood (over several meters in all directions).

Even if this current implementation is composed of two distinct hardware parts: the LoRaWAN gateway and the radiative electromagnetic power source; with various useful distances, respectively tens of kilometres and meters; these two components can be located at the same place without communication losses. However, the alternative consisting of using these two components separately and independently, maybe in different quantities, can be relevant in many cases, especially when a single radiative electromagnetic power source does not cover the whole element made of reinforced concrete to monitor.

In any case, it must be noted that this system answers the simultaneous wireless information and power transmission (SWIPT) paradigm by using at the same time the same frequency band for the both functions. In the case of the use of two antennas (one for the reception of the LoRaWAN frames and one for the wireless power transfer), the two function could be more discriminated by using orthogonal polarisations. To go further, qualitative preliminary tests of the use of a radiofrequency circulator between a unique antenna, the LoRaWAN gateway input and the radiative electromagnetic power source output have been successfully performed. Nevertheless, this works better when the channels used for the LoRaWAN communications are "far" from the frequency used for the wireless power transfer and when the output power of the radiative electromagnetic power source is reduced. At the time of writing, no quantitative tests have been performed in this configuration.

Some tests have been performed to validate the various complete implementations proposed: for a communicating node in a single location and for the spatial separation of its two main functions; for isolated communicating nodes and for a network of two communicating nodes; for various number of sensing nodes (from 1 to 4) at various distances; for local or remote management of the process and storage functions; etc. Even if the network of communicating nodes is limited to two entities, due to the lack of more equipment, the performed tests are a proof-of-concept of the possibility to use the current implementation in larger networks by providing means to exchange data between communicating nodes.

For the future, it would be nice to design and implement a one-piece and integrated communicating node which includes and interfaces its three subsystems.

Considering the energy management system, the design of a unique power supply shaft, the use of a unique transformer connected to the mains power and the investigation of alternative power sources could be relevant.

Considering the data management system, the hardware and software optimization, especially in order to reduce the power consumption, seems to be a relevant line of work, as well as the use of other wireless communication technologies for the various wireless interfaces and according to well-defined constraints and needs.

Considering the radiative electromagnetic power source, the design and implementation of a solution dynamically adjustable with software by the data management system as well as the hardware optimization of the amplification stages seem to be away of improvement. More, the deployment of a beamforming system will allow a gain in efficiency.

It could also be planned to add the possibility of carrying out measurements directly from the communicating nodes. To go even further, it could be investigated the possibility of performing frequency analysis on the LoRaWAN data frames sent by the sensing nodes to deduce some physical properties of the propagation medium, in the manner of indirect and non-destructive test methods.

Figure IV.8: Photographs of a communicating node in various configuration: using two independent subsystems located at the same place; and using a radiofrequency circulator and a unique antenna.

F. Conclusion

In this chapter, the implementation of the communicating nodes based on the LoRaWAN wireless communication technology has been proposed. These are composed of three subsystems, whose the design, the implementation, the improvements and the alternatives have been discussed. There are: a radiative electromagnetic power source generating a +33 dBm (or 2 W) continuous wave at 868 MHz and dedicated to the wireless and remote powering of the sensing nodes; a data management system which deals with the reception of the LoRaWAN frames sent by the sensing nodes, the exchange, the processing and the local and/or remote storage of the collected data within a meshed network of communicating nodes, and the connection with the digital world through the Internet and with the stakeholders; and an energy management system used to power the two other subsystems. Finally, a complete view as well as some perspectives have been introduced.

The next chapter will detail the design and implementation of the sensing nodes based on the LoRaWAN technology and will provide some justifications and additional information allowing to fill the gaps of this chapter.

V. Implementation of sensing nodes based on the LoRaWAN technology

In agreement with the Figure III.4 and Figure III.6, several sensing nodes based on the LoRaWAN technology have been implemented and tested. These, considered as inaccessible once deployed because embedded into the reinforced concrete, measure some physical parameters (e.g. temperature, humidity, resistivity, strain, etc.) to quantify the internal states of the reinforced concrete and/or its environment; transmit wirelessly the collected and eventually pre-processed data to the communicating nodes; and harvest the radiative electromagnetic power provided by the communicating nodes to power themselves. To be useful during all the lifespan of the communicating reinforced concrete, that says decades, these must be reliable and resilient. As introduced above (Section III.B.3.), the different components that make up the sensing nodes will be detailed.

A. Data collection, pre-processing and wireless transmission

In order to wirelessly transmit the measured data to the communicating nodes, the sensing nodes use the LoRaWAN wireless communication technology. For reasons of hardware security and power consumption, only the data uplink from the sensing nodes to the communicating nodes is available. Thus, the sensing nodes could not receive data, especially through LoRaWAN frames, from the communicating nodes or other devices. Nevertheless, these are partially reconfigurable: indeed, their periodicity of measurement and wireless communication can be tuned by the communicating nodes through the use of their radiative electromagnetic power source.

1. Technology choice

This is the wireless communication technology which has been firstly defined, and thus, which imposes some constraints to the design of the entire sensing nodes. As mentioned above (Section II.C.5.), there are several solutions which can be employed for the wireless transmissions, each one with its own advantages and drawbacks. In our case, the objective is to transmit the measured data from the sensing nodes to the communicating nodes. Also, the conceivable solutions must meet some requirements, such as -and at a minimum- be usable in a unidirectional configuration (from the sensing nodes to the communicating nodes, without connection or acknowledgement), low power consumption (to be wirelessly powered), medium range (at least ten of metres), low data-rate (a few bytes a few times an hour/day/week), be available (in terms of off-the-shelf components and/or network infrastructures), be well standardized and documented, have a good reputation, and, above all, be able to communicate through reinforced concrete.

Thus, the wireless communication technologies based on the light can be quickly discarded because the light cannot propagate through the reinforced concrete. Because there are no available commercial solutions and that it is out of our field of competence, the mechanical solutions can be discarded too. That leaves all the electromagnetic wireless communications technologies which are diversified. As previously, a distinction is made between light and

electromagnetic waves (essentially the radiofrequency ones), even if the light can itself be considered as an electromagnetic wave.

First, the near-field communication (NFC) technology does not provided sufficient range of use. Then, the radio-frequency identification (RFID) technologies have been put aside because initially, and always, standardized only for identification purposes and not for data measurement and/or storage, and their more common implementations are short-range (rarely beyond few meters). More, the opportunistic backscattering technologies are not yet available and required specific environments (with exploitable electromagnetic waves, that says sufficiently energetic). On another aspect, the Wi-Fi, the cellular and the satellite networks are not energy efficient enough. Even if, it provides very attractive characteristics especially with its ability theoretical ability to be minimally impacted by the reinforced concrete, the RuBee technology cannot be implemented because not available. Nevertheless, in the future, it could be the most relevant trend of investigations. Among the remaining solutions, two main technology families emerge: the wireless personal area networks (e.g. Bluetooth, ultra-wide band, ZigBee, etc.) and the low power wide area networks (e.g. LoRaWAN, DASH7, SigFox, etc.).

Concerning the wireless personal area networks, the fully proprietary technologies have been rejected because the medium-term uncertainty of their availability and support. Thanks to its extensive and common use, especially in almost all the general public devices with wireless communication abilities (e.g. laptops, tablets, smartphones, etc.), the Bluetooth technology, and its Low Energy implementation, seems the most promising, ahead of the ZigBee. Because based on another approach, the ultra-wide band technology could be studied too. Nevertheless, this technology is essentially used for accurate real-time location applications. As an exception, Decawave provides commercial implementations of ultra-wide band transceivers, dedicated for the location but with the ability of performing high data-rate wireless communication [616]. This last aspect is too few exploited, studied and documented, and the global power consumption of the available transceivers remains relatively high.

Concerning the low power wide area networks, the proprietary technologies or those requiring subscription to an access provider, such as SigFox, have been dismissed in favour of those that can be fully deployed by the users. Among the two last alternatives: DASH7 and LoRaWAN; the last has been privileged, in particular for the reasons exposed right after.

Thus, three wireless communication technologies: Bluetooth Low Energy, DASH7 and LoRaWAN; have been pre-selected, whilst two others: RuBee and ultra-wide band; are kept under surveillance until an eventually commercial availability. Among these five wireless communication technologies, three: Bluetooth Low Energy, ultra-wide band and LoRaWAN; have been tested for indoors wireless communications, in order to compare their ability to pass through walls and ceilings/floors, especially those made of reinforced concrete. According to these tests performed before the begin of the McBIM project, the ultra-wide band technology has the shortest range (few meters) and was not able to pass through reinforced concrete elements; the Bluetooth Low Energy technology has a range of ten of metres and was able to pass through a few reinforced concrete elements; whilst the LoRaWAN technology has a range larger than a hundred of metres and the was able to pass through a lot of reinforced concrete elements. In fact, a unique LoRaWAN gateway was sufficient to cover more than all the LAAS buildings, which is distributed over 4 levels, with

distances of few hundreds of meters. Thus, it seems that a wideband signal obtained through chirp spread spectrum (CSS) technique, is less sensitive to the reinforced concrete. Regarding only these preliminary tests, the best candidate to implement wireless communication through reinforced concrete seems to be LoRaWAN, even if its range is largely beyond what is needed and even if its power consumption, which is considered as low, stays comparatively relatively high. More, as the INSA (National Institute for Applied Sciences) of Toulouse -neighbour and close collaborator of the LAAS- has been the first French campus connected by its own LoRaWAN network, this technology is well known here and was privileged to the less known DASH7. To go further, as LoRaWAN can be considered as the "worst" case in terms of power consumption, the success of its implementation with its power supply by wireless power transfer will provide the "worst" characteristics, which can only be improved with the use of technologies requiring less energy.

Thus, the first wireless communication technology to be tested has been LoRaWAN. Nevertheless, some experimentations with Bluetooth Low Energy were performed thereafter and will be presented below (Chapter VI. and Chapter VII.).

2. Design and implementation

To implement the part of the sensing nodes dedicated to the data collection, pre-processing and wireless transmission, an all-in-one Murata CMWX1ZZABZ-091 LoRaWAN module has been used [617]. This one is the first known solution that is compact (12.5 mm x 11.6 mm x 1.7 mm with a metal-shielded package), inexpensive and complete for the design of LoRaWAN devices. Based on a Semtech SX1276 transceiver (allowing the use of either the LoRa modulation, or the frequency-shift keying (FSK) modulation) [618] and a STMicroelectronics STM32L072CZ microcontroller itself based on an ARM Cortex M0+ microprocessor, which can embed a LoRaWAN stack, and which owns 192 kB of flash memory [619, 620], the user must only add an antenna, a power source and eventually one or some sensors, as well as program the microcontroller with its own firmware, to get a complete LoRaWAN device. Its current implementation is presented in Figure V.1. This module requires a 3.3 V voltage supply.

In order to keep its power consumption as low as possible, to ensure long-term reliability and resilience, the part of the sensing nodes dedicated to the data collection, pre-processing and transmission is designed as simple as possible, both in terms of hardware and software.

The developed firmware, coded in C language and using a LoRaWAN stack, allows the microcontroller to initialise itself and all the desired peripherals -whose the transceiver- and required interfaces as soon as it is powered; then to drive the chosen sensor to get measurements; to pre-process the data from the sensor especially to format these; to send into a LoRaWAN frame the formatted data to the communicating node(s); and finally to go into a deep-sleep mode until its power supply is stopped by the power management part. Nearly 1.6 seconds are required from the power-up to the end of the transmission, of which about 1.3 seconds is for this transmission alone. Each step in this process is observable in the use by the sensing nodes of the available energy as presented in Figure V.2. Thus, the process is reduced to a one-shot measurement and LoRaWAN transmission, whose periodicity is not controlled by the software (e.g. with events or timer interruptions) but by the power supply *via* the hardware.

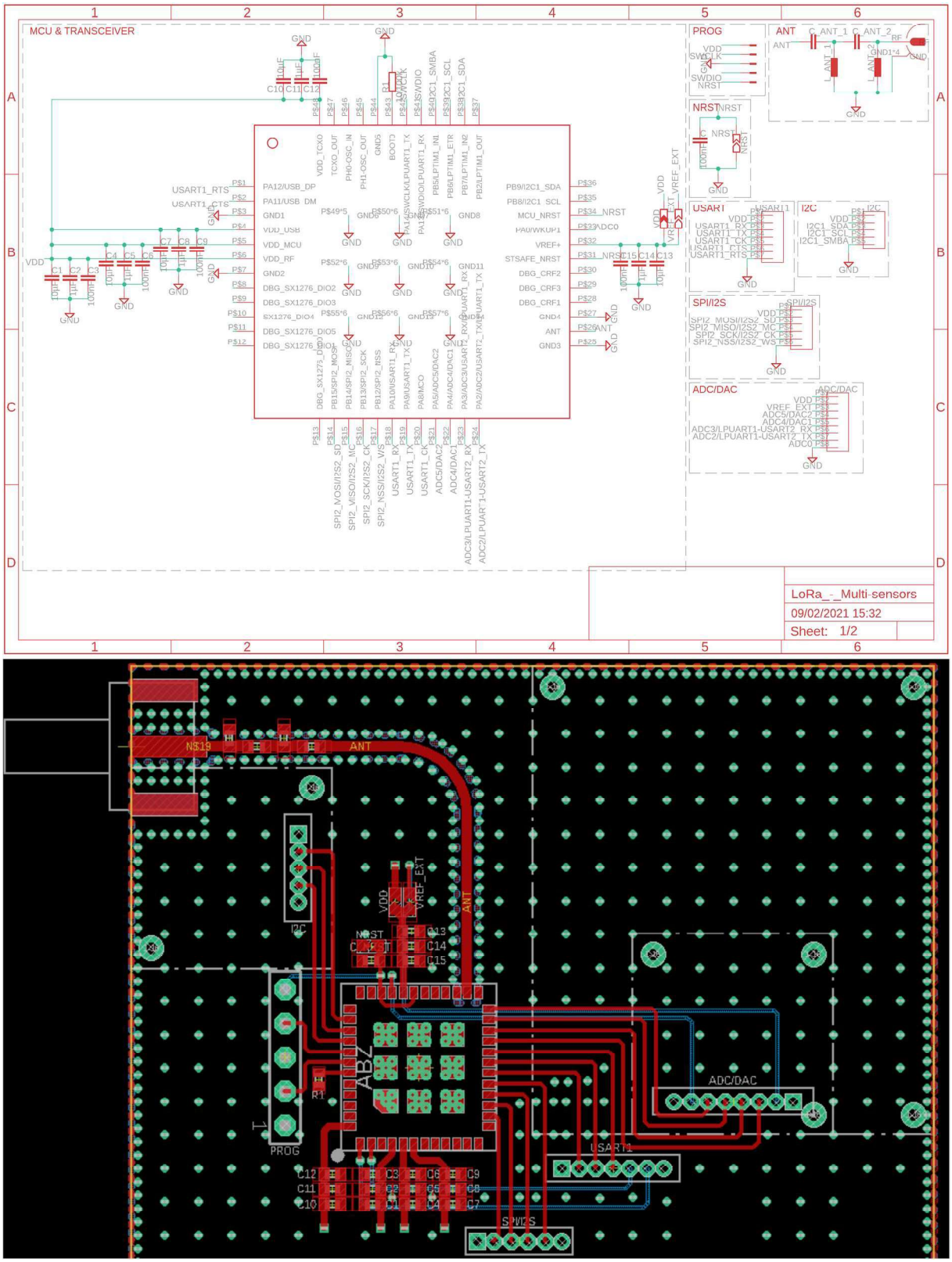

Figure V.1: Schematics and board of the implementation of the Murata CMWX1ZZABZ-091 LoRaWAN module.

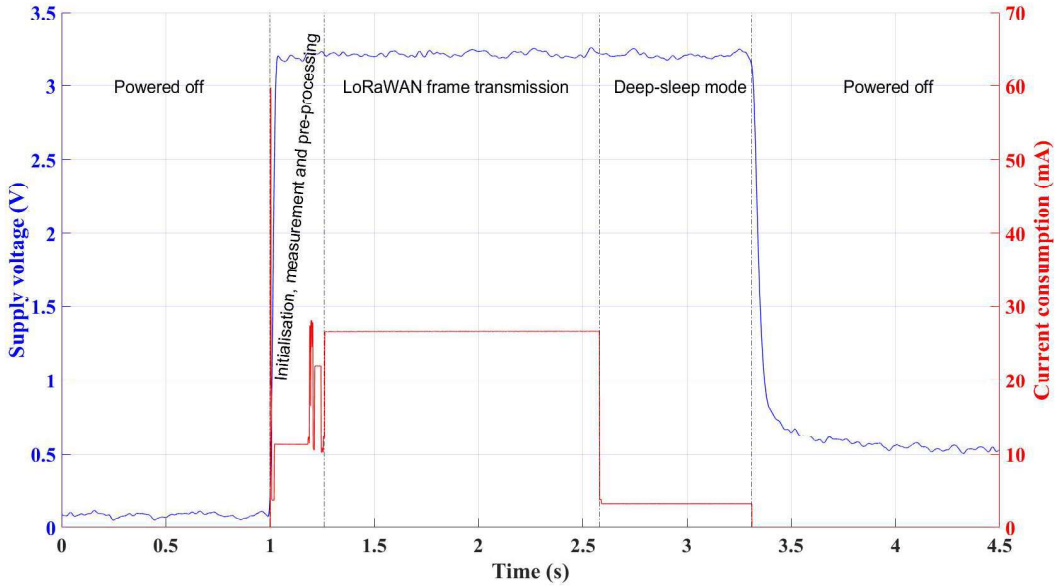

Figure V.2: Energy consumption of the sensing nodes according to the phase of operation.

Concerning the LoRaWAN medium access control (MAC) frames, these are 17 bytes long, whose 13 bytes dedicated to the LoRaWAN protocol and 4 bytes dedicated to the data payload (generally two measurements, each encoded on 2 bytes), as presented in Figure V.3. The LoRaWAN communications are class-A without the reception windows required for the downlink. Thus, the downlink is deliberately made unavailable: the power consumption is reduced by deleting the time dedicated to the listening of the medium for receiving eventual "acknowledgement", data or firmware update; and the security is increased by imposing a fixed firmware and by blocking all accesses required to alter or update it. Without downlink, the sensing nodes cannot use the over-the-air activation (OTTA) method and so, need to be connected to the network by activation by personalisation (ABP) method, which is more secure, and with their own unique security keys. The transmissions follow the 1.0.3 version of the LoRaWAN MAC (medium access control) protocol, with the parameters dedicated to the region A (whose Europe), with 3 channels in the 868 MHz industrial, scientific and medical (ISM) frequency band (868.1 MHz, 868.3 MHz and 868.5 MHz), a bandwidth of 125 kHz, a spreading factor of 12, a code rate of 4/5 and a power between +4 dBm and +14 dBm. A data-rate (generally noted DR_0) of 250 bps is obtained, which is the slowest but allows the best reception rates and the largest range of use. Finally, the frame counter is currently disable for development purposes, because the application deployed on the ChirpStack application server must be updated each time a sensing node is programmed with a new firmware. Moreover, its implementation requires the use of non-volatile memory in the sensing node to conserve its value when the sensing node is not powered, that says for most of the time.

The developed hardware is essentially a printed circuit board (PCB) dedicated to solder the Murata CMWX1ZZABZ-091 LoRaWAN module with its decoupling capacitors; its communication interfaces to be programmed and to drive various sensors; and its radiofrequency line to excite an antenna; as presented in Figure V.1.

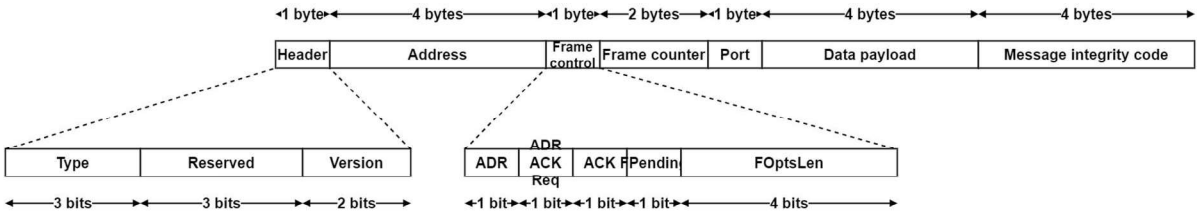

Figure V.3: Format of the LoRaWAN MAC frames used.

A SWD (serial wire debug) JTAG (joint test action group) interface is used to program the microcontroller with the developed firmware, whilst other GPIO (general purpose input/output) pins are used to interface external peripherals according to several wire communication standards, such as UART (universal asynchronous receiver transmitter), SPI (serial peripheral interface), I²S (inter-IC sound), I²C (inter-integrate circuit), as well as with ADC (analogue-to-digital converter) inputs and DAC (digital-to-analogue converter) outputs. The objective is to provide a generic platform, where the measurement capabilities are achieved by connecting to the available interfaces some daughter boards designed around sensors.

For the antenna, a 50 Ω radiofrequency line at 868 MHz is used to connect a SMA (subminiature version A) connector or directly a printed antenna. A LPSR ANT-SS900 compressed (quart-wavelength) whip antenna was used for the wireless communication part of the first prototypes of the sensing nodes [621]. This is an almost omnidirectional antenna with a linear polarization, usable at 868 MHz and 915 MHz and with a theoretical gain of +2 dBi at 868 MHz, which was interfaced through the SMA connector. Then, a printed on 1.6 mm FR4 (flame resistant 4) substrate quart-wavelength meandered monopole antenna, whose the design is provided by Texas Instruments, was used for the wireless communication part of the first integrated prototypes of the sensing nodes [622]. This is an almost omnidirectional antenna with a linear polarization, usable at 868 MHz and 915 MHz and with a theoretical gain of +5.05 dBi at 868 MHz, which was directly interfaced to the radiofrequency line. Its main advantages are that this has a higher gain and is directly integrated on the printed circuit board, and thus, allows a more compact implementation in two dimensions. For the next prototypes of the sensing nodes, a unique antenna was used both for the wireless communication part and the radiative electromagnetic power harvesting part. The used antenna will be presented in the part dedicated to the radiative electromagnetic power harvesting.

In order to design the power management part of the sensing nodes, it is necessary to know the energy these need to work properly. Thus, the power consumed by the part of the sensing nodes dedicated to the data collection, pre-processing and wireless transmission has been measured for four prototypes (SN1, SN2, SN3 and SN4) from three different generations (SN1 and SN2 are from the last generation, SN3 is from a more compact implementation of the last generation, and SN4 is from the first generation of complete prototypes). All these prototypes are based on the same schematics, presented in Figure V.1, and their routing is similar for this part. The only differences concern the size of the PCB and some minor routing variations throughout the PCB. The measurements have been achieved thanks to a Keysight N6705B DC Power Analyser providing a 3.3 V voltage supply [623]. In Figure V.4, the power consumption in function of the transmission power for each of the tested prototypes are

presented, whilst in Figure V.5 the power consumption of each of the tested prototypes for transmission power of +4 dBm and +14 dBm are plotted. It can be observed that higher is the transmission power, higher is the power consumption, and that there is a high variability of power consumption between prototypes for the highest transmission powers. Thus, 171.8±31.2 mJ are required for the transmission of a LoRaWAN frame, as presented in Figure V.3, at +14 dBm, and 91.9±4.4 mJ at +4 dBm, with respectively maximum measured values of 205.8 mJ and 98.5 mJ. Only, 11.275±0.4 mJ are needed for the initialisation of the full module. The observed high variability could be justified by several causes. Firstly, the Murata CMWX1ZZABZ-091 LoRaWAN modules used for the prototypes SN1 and SN2 have been stripped from "old" prototypes to be soldered again on the "new" prototypes. This unrecommended process can easily cause damage to the components and was imposed by the worldwide stockout of these modules during the COVID-19 crisis and the need to manufacture and test the new prototypes. Secondly, in addition to the difference in the PCB size, there are some minor variations in the routing, and it is not excluded that there are some routing mistakes that still exist despite the investigations carried out. Finally, it could exist a variability in the components themselves, which present different characteristics, which are only expressed as typical values in the datasheet. In any case, the power consumption will be lightly increased by the use of a sensor, as explained below (Section V.B.).

Whatever the used transmission power, all the frames sent by the sensing nodes were successfully received by the communicating nodes during the tests. The sensing nodes were placed in a 15 cm x 15 cm x 15 cm cavity of a reinforced concrete beam and the communicating node located at several metres in the same room or in another room separated by few reinforced concrete walls.

3. Alternatives and perspectives

The considered alternatives to the use of the LoRaWAN technology have been introduces above (Section V.A.1.) and the performed experimentations with Bluetooth Low Energy will be presented below (Chapter VI. and Chapter VII.).

Regarding the design and implementation of the part of the sensing nodes dedicated to the data collection, pre-processing and wireless transmission, both the hardware and the software can still be optimized. For the hardware, the study of alternatives to the Murata CMWX1ZZABZ-091 LoRaWAN module could be achieved with the aim of reducing both the size and the power consumption. Solutions based of independent microcontroller and LoRa transceiver could allow a wider design flexibility at the price of a more complex system. For the software, the optimization of the LoRaWAN stack focused solely on the needs of the sensing nodes could be relevant, as well as the test of other LoRaWAN parameters. For instance, the use of a bandwidth of 125 kHz with a spreading factor of 7 could allow a data-rate of 5.47 kbps (generally noted DR_5) for a transmission duration estimated at 51.5 milliseconds. First qualitative tests in this configuration made it possible to communicate over several tens of metres indoors (through reinforced concrete walls and ceilings), as well as over several metres from the reinforced concrete beam (larger ranges have not been tested but seem quite feasible). At the time of writing, no power consumption measurements have been performed but have been planned. In this way, a large gain in energy consumption could be achieved at the price of less sensitive system, as presented in [624]. For

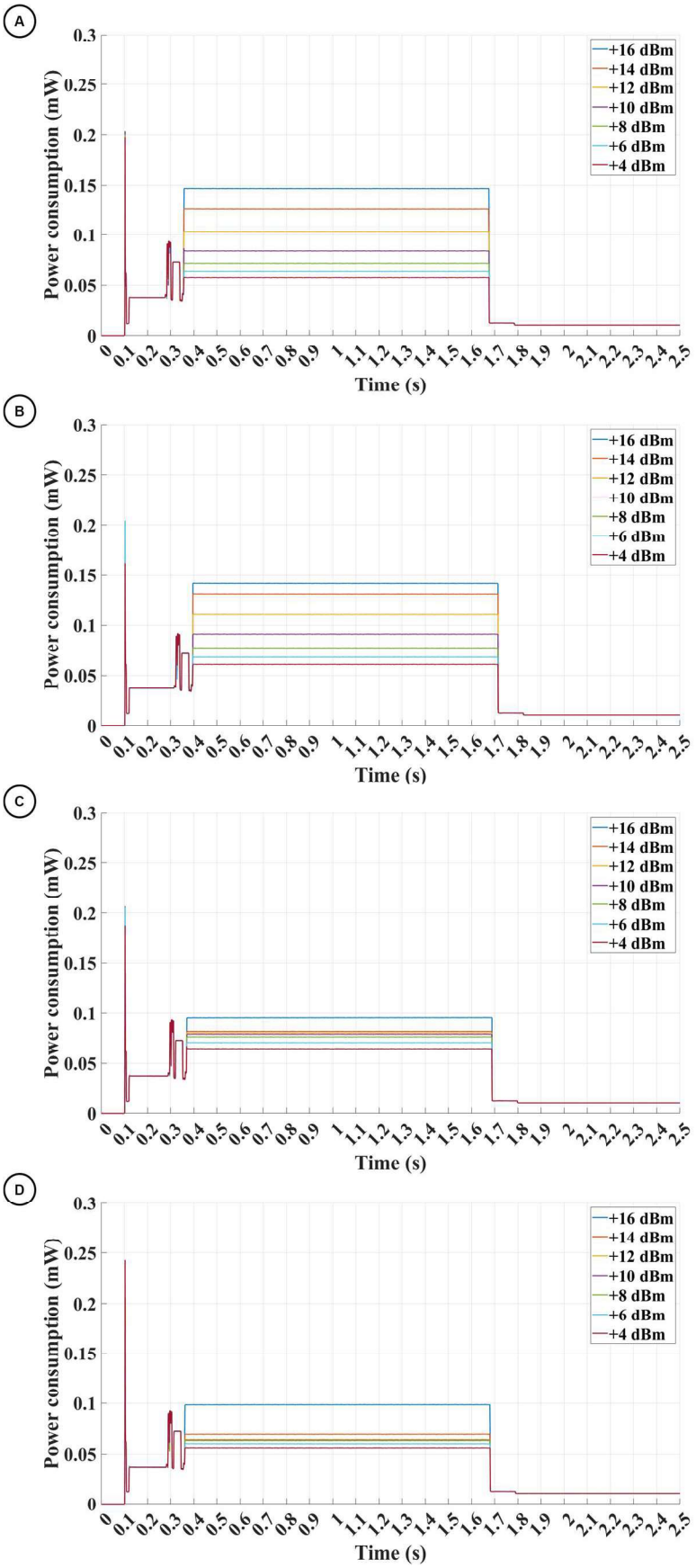

Figure V.4: Power consumption in function of the transmission power for the tested prototypes: (A) SN1, (B) SN2, (C) SN3 and (D) SN4.

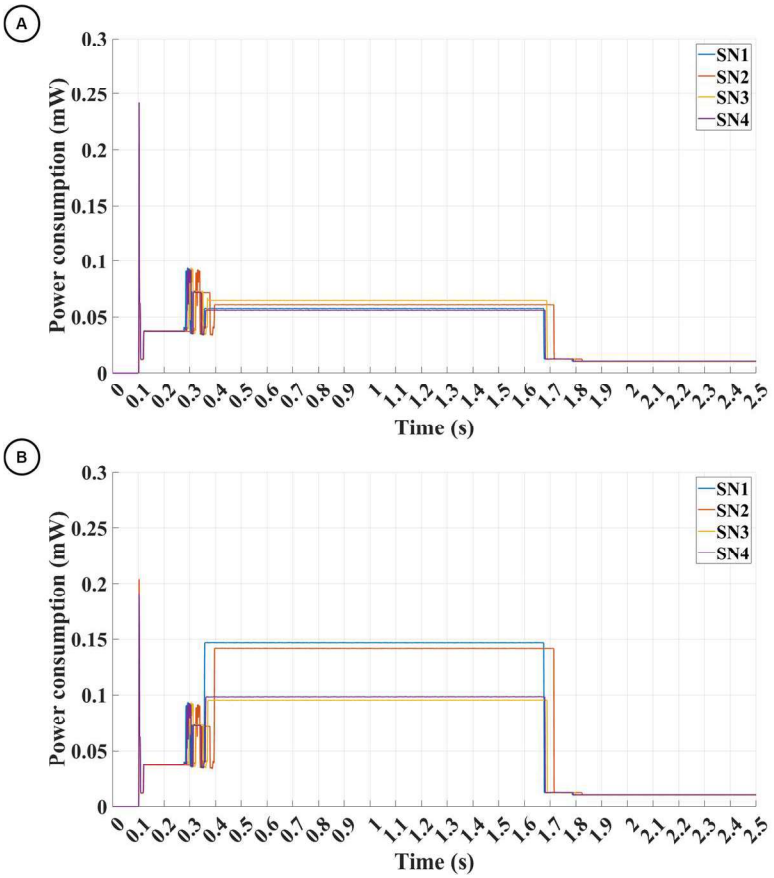

Figure V.5: Power consumption of the tested prototypes for transmission power of (A) +4 dBm and (B) +14 dBm.

instance, the use of a bandwidth of 250 kHz with a spreading factor of 7 allowing a data-rate of 11 kbps (generally noted DR_6) for a transmission duration estimated at 25.7 milliseconds, which reduces higher the power consumption, did not allow any frame to be received, even at few metres in air. Finally, the payload of the LoRaWAN frames could be adapted to the sensor(s) used in order to send as few bytes as possible to reduce the energy required by the transmission of the LoRaWAN frames, or on the contrary a larger payload (e.g. by using several sensor) could be used to reduce the energy required per data byte at the cost of a higher energy required by the complete transmission of the LoRaWAN frames.

In Section VIII.D. some security aspects of the LoRaWAN communications will be treated.

B. Measurements of the properties of the reinforced concrete

Now that the choice of the wireless communication technology has been made and that both hardware and software implementations have been proposed, it is time to deal with the measurement part. As explained above (Section II.B.1.), several parameters can be measured to assure the monitoring of the reinforced concrete during all its lifetime. The main objective is to warranty a safe use of the material and the structure, particularly by checking for their proper aging, and by detecting, locating and quantifying the damages, or even predicting these. This allows to perform maintenance, or even predictive maintenance, when requiring and before the damages become irreparable.

1. Design process

For each step in its lifecycle, the reinforced concrete can be monitored by focusing on several properties and/or damages. These properties can be mechanical (e.g. strain, stress, strength, displacement, etc.), physical (e.g. temperature, humidity, etc.) or chemical (e.g. pH, corrosion, etc.), whilst the damages can be shocks, cracks, delamination, etc. As summarized in [108], the more relevant parameters to monitor into reinforced concretes during all the step of their lifecycle are the temperature, the humidity, the pH, the corrosion, and the strain or stress, whilst the detection and location of the damages are also targeted.

In order to meet these needs, several daughter boards designed around a specific sensor have been developed to be connected to the Murata CMWX1ZZABZ-091 LoRaWAN module thanks to the available routed interfaces. Used in a non-destructive testing approach, these sensors must be low power consumption to satisfy the expectations of the project. That is why only the sensors performing direct measurements are targeted. This means that the measurements requiring signal processing are excluded, especially those based on the study of the frequency of the mechanical waves, as these require a lot of resources in terms of processing, memory and energy.

Regarding the targeted parameters, first have been the physical ones with the temperature (the most commonly measured physical parameter, for which there is a wide variety of available sensors) and the humidity (often associated to the temperature in various applications). Taken together, these can be used in various applications during all the life of the reinforced concrete, especially for the curing phase and the exploitation one, but even much more. Then, the corrosion (a chemical parameter) has been targeted, through the use of a resistivity sensor. This one allows to estimate the corrosion rate by the study of the evolution of the measurements over time. This sensor can be conjointly used with a temperature and humidity sensor, and the measurements can be correlated. Finally, the mechanical parameters have been targeted *via* the case of the strain. This have been estimated thanks to the use of a strain gauge.

2. Design and implementation

To implement the measurement part of the sensing nodes, several sensors have been interfaced with the data collection, pre-processing and wireless transmission part.

i. Temperature sensors, and temperature and relative humidity sensors

First implemented sensors have been those dedicated to the measurements of the temperature, and to the simultaneous measurements of the temperature and relative humidity.

a. Sensors choice

Two temperature sensors and two temperature and relative humidity sensors have been tested. First tests have been carried out with the temperature sensor embedded inside the STMicroelectronics STM32L072CZ microcontroller, in order to easily verify the good operation of the part related to the data collection, pre-processing and wireless transmission, by transmitting measured data of a dynamic physical parameter. Then, an Adafruit DHT22 temperature and relative humidity sensor has been implemented [625]. This one has been chosen only for its immediate availability. For the next, a comparison of various commercial humidity and temperature sensors, presented in Table V.1, has been achieved with the objective to choose a compact one with the lowest power consumption and the highest accuracy. This study is obviously not exhaustive but covers the most usual sensors. Thus, this is the Texas Instruments HDC2010 which has been chosen [627]. To finish, very low power and high accuracy thermodiodes designed and provided by the University of Cambridge, UNITED-KINGDOM, have been integrated as temperature sensors [631].

b. Design and implementation

The targeted temperature range is -40 °C to +125 °C which is the conventional one for electronic components. Actually, this range is imposed by the lowest operating temperature range of the used components. Here, the Semtech SX1276 transceiver has an operating temperature range of -40 °C to +85 °C.

The full scale, from 0 % to 100 %, is targeted in the case of the relative humidity range.

* STMicroelectronics STM32L072CZ microcontroller internal temperature sensor

To use the STMicroelectronics STM32L072CZ microcontroller internal temperature sensor, it has been sufficient to follow and adapt the instructions provided in [620]. The ADC must be initialized and enabled in order to measure on 12 bits both the reference voltage and the voltage provided by the temperature sensor. Once achieved these two measurements, the temperature could be computed in Celsius degrees, then formatted on two bytes by being rounded to the first decimal, in order to be sent in a LoRaWAN frame. In fact, only 11 bits could be sufficient to store the temperature to the tenth of a Celsius degree for a range from -40 °C to +125 °C.

Table V.1: A comparison of various commercial humidity and temperature sensors from information available on datasheets. Average power consumption is defined as continuous operation with one measurement per second. Measurement time is the time to start-up and record an initial measurement.

Reference		Adafruit DHT22 [625]	Texas Instruments HDC2080 [626]	Texas Instruments HDC2010 [627]	Bosch BME280 [628]	Sensirion SHTW2 [629]	Sensirion SHTC3 [630]
Functionality	Temperature	Yes	Yes	Yes	Yes	Yes	Yes
	Humidity	Yes	Yes	Yes	Yes	Yes	Yes
	Measure in isolation	No	Yes	Yes	Yes	No	No
Humidity characteristics	Average accuracy (± %RH)	3	2	2	3	3	2
	Specified range (%RH)	0 to 100	0 to 100	0 to 100	0 to 100	0 to 100	0 to 100
Temperature characteristics	Average accuracy (± °C)	0.5	0.2	0.2	0.5	0.3	0.2
	Specified range (°C)	-40 to +80	-40 to +125	-40 to +125	-40 to +85	-30 to +100	-40 to +125
General characteristics	Response time (s)	2	8	8	1	<5 to 30	<5 to 30
	Average power consumption (µW)	2800	1	1	3.3	8.6	16
	Sleep current (µA)	N/A	0.05	0.05	0.1	0.7	0.3
	Measurement time (ms)	800	N/A	N/A	2	1	1
	Supply voltage (V)	3 to 5	1.62 to 3.6	1.62 to 3.6	1.71 to 3.6	1.62 to 2.98	1.62 to 3.6

* Adafruit DHT22 temperature and relative humidity sensor

To use the Adafruit DHT22 temperature and relative humidity sensor, a daughter board have been developed in order to interface the Murata CMWX1ZZABZ-091 LoRaWAN module through a GPIO. This daughter board is presented in Figure V.6 and Figure V.7. The GPIO is used to implement the non-standardized one wire half-duplex communication protocol required by the sensor and presented in [625]. This software implementation is based on the use of a GPIO (used alternatively as output and input) and timers. After the stabilisation of its 3.3 V power supply (estimated at about 1 second), the sensor can be queried to provide a temperature measurement and a relative humidity measurement. These measurements are then formatted on two bytes by being rounded to the first decimal, in order to be sent in a LoRaWAN frame. Once again, only 11 bits could be sufficient to store the temperature to the tenth of a Celsius degree for a range from -40 °C to +125 °C and only 10 bits could be sufficient to store the relative humidity to the tenth of a percent for a range from 0% to 100 %. Thus, the payload could be reduced to three bytes.

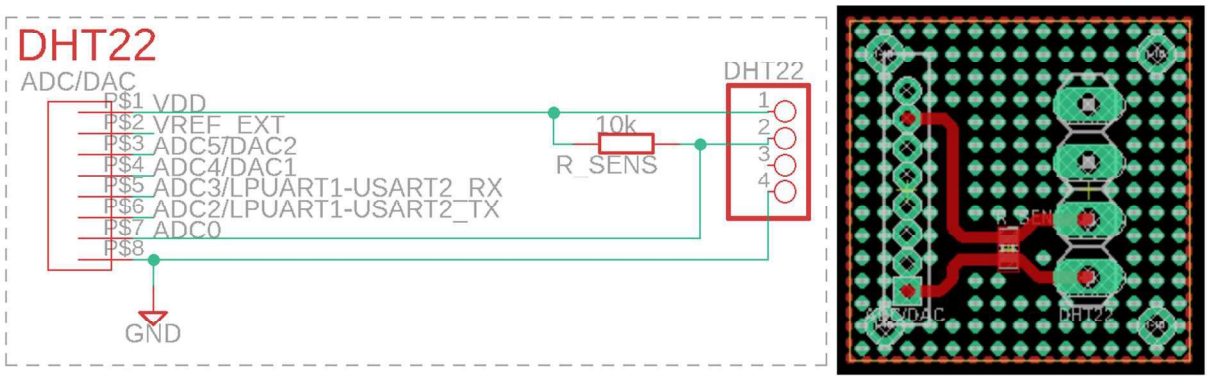

Figure V.6: Schematics and board (1.5 cm x 1.5 cm) of the designed and implemented daughter board interfacing the Adafruit DHT22 temperature and relative humidity sensor.

Figure V.7: Photograph of the designed and implemented daughter board interfacing the Adafruit DHT22 temperature and relative humidity sensor.

* Texas Instruments HDC2010 temperature and relative humidity sensor

To use the Texas Instruments HDC2010 temperature and relative humidity sensor, a daughter board have been developed in order to interface the Murata CMWX1ZZABZ-091 LoRaWAN module through a SPI interface. This daughter board is presented in Figure V.8 and Figure V.9. The SPI must be initialized and enabled, and after the quick stabilisation of its 3.3 V power supply, the sensor can be queried and configured to provide a temperature measurement and a relative humidity measurement as explained in [627]. These measurements are then formatted on two bytes by being rounded to the first decimal, in order to be sent in a LoRaWAN frame. Once again, only 11 bits could be sufficient to store the temperature to the tenth of a Celsius degree for a range from -40 °C to +125 °C and only 10 bits could be sufficient to store the relative humidity to the tenth of a percent for a range from 0% to 100 %. Thus, the payload could be reduced to three bytes.

* Thermodiodes from the University of Cambridge as temperature transducers

The thermodiodes from the University of Cambridge are manufactured with the complementary metal-oxide-semiconductor (CMOS) fabrication technology compatible with microelectromechanical systems (MEMS), and dedicated to the accurate (±0.1 °C maximum

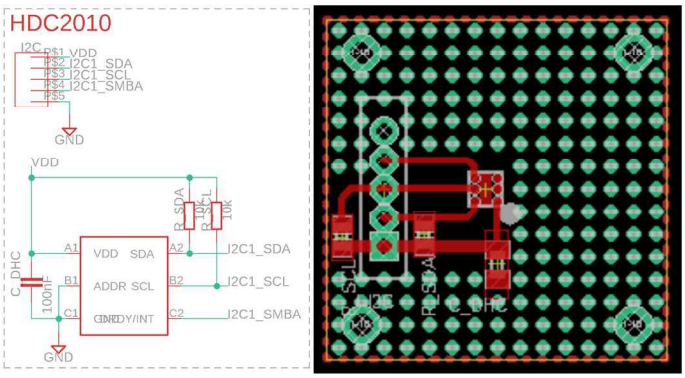

Figure V.8: Schematics and board (1.5 cm x 1.5 cm) of the designed and implemented daughter board interfacing the Texas Instruments HDC2010 temperature and relative humidity sensor.

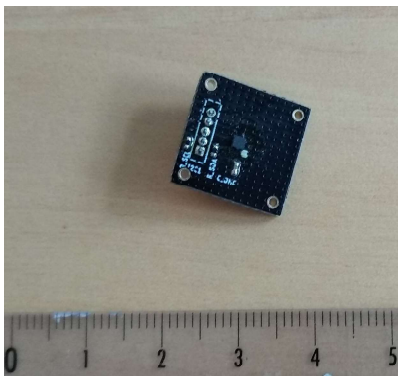

Figure V.9: Photograph of the designed and implemented daughter board interfacing the Texas Instruments HDC2010 temperature and relative humidity sensor.

non-linearity) and low power measurement of temperature on a wide range (estimated from -193 °C to +777 °C). These very small Silicon-on-insulator (SOI) thermodiodes are manufactured both on the Silicon bulk substrate (as a reference design) and on a Silicon dioxide (SiO2) membrane substrate. To use these thermodiodes from the University of Cambridge as temperature sensors, a daughter board have been developed in order to make these usable for embedded systems and to interface the Murata CMWX1ZZABZ-091 LoRaWAN module through two ADC. This daughter board is presented in Figure V.10 and Figure V.11.

On the software side, two ADC channels must be initialized and enabled in order to measure on 12 bits the voltages of the thermodiodes located on the bulk substrate and on the membrane substrate. The ADC have been configured in order to oversample, and then average 256 measurements. Once achieved these two measurements, each temperature could be computed in Celsius degrees, then formatted on two bytes by being rounded to the first decimal, in order to be sent in a LoRaWAN frame. Again, only 11 bits could be sufficient to store the temperature to the tenth of a Celsius degree for a range from -40 °C to +125 °C. Thus, the payload could be reduced to three bytes. It must be noted that the measurement precision is due to the limitations of the ADC more than these of the transducers.

On the hardware side, unlike the previous off-the-shelf sensors, the thermodiodes from the University of Cambridge are not commercially available or even packaged. Thus, the only provided data were their characterisation as temperature transducer obtained directly on the Silicon wafer with table equipment (both for the power supply and the measurement) as presented in Figure V.12. Thus, a first step was to package the thermodiodes in 8 pins ceramic dual inline package (CDIP) by using wire bonding technique. Then, these must be powered by a 1µA, 10 µA or 100 µA direct current source. But on the prototypes of the sensing nodes, only a 3.3 V voltage source is available. Thus, a 100 µA direct current source powered by a 3.3 V supply voltage has been designed to power the thermodiodes. This one is based on a STMicroelectronics LM234 current sources [632], whose the temperature dependant drift is compensated as explained in [633] by using a ON Semiconductor Schottky barrier diode RB751540T1G [634]. This configuration induces in the worst case a maximum drop voltage of 1.2 V, that says that the output voltage of the thermodiodes can go up to 2.1 V. By using the equations provided by the voltage output against temperature characterisation of the thermodiodes, available in Figure V.12 (respectively for the thermodiode on the bulk substrate and on the membrane substrate, $T(°C) = -704.20 \cdot V(V) + 590.63$ and $T(°C) = -779{,}76 \cdot V(V) + 663{,}46$), the voltage range for a temperature range of -40 °C to +125 °C is about 0.91 V to 0.65 V, which induces a measurement step of around 0.6 °C with the 12 bits ADC. In order to better exploit to voltage range measurable by the used ADC (for 0 V to supply voltage) and in order to be usable with a supply voltage down to 2.2 V, a voltage subtractor circuit with gain, based on a Microchip MCP6V61 rail-to-rail zero-bias operational amplifier [635] and an Analog Devices ADR130 0.5 V voltage reference [636], has been designed and implemented to exploit a measurement range from 0 V to 1 V. In this configuration, the theoretical linear model of the temperature against the output voltage is $T(°C) = -182.57 \cdot V(V) + 134.20$ for the thermodiode on bulk substrate and $T(°C) = -202.16 \cdot V(V) + 158.06$ for the thermodiode on membrane substrate. This induces respectively a theoretical temperature range of -34 °C to +135 °C with a measurement step of 0.15 °C, and of -44 °C to +158 °C with a 0.16 °C step, both with the 12 bits ADC. As each thermodiode (the one on the bulk substrate and the one on the membrane substrate) are independent, all these electronic circuits must be deployed for each one.

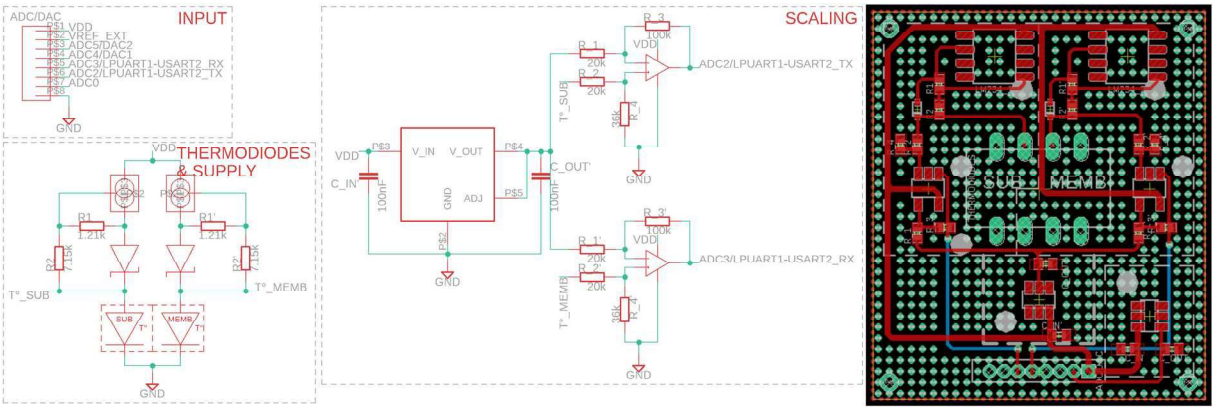

Figure V.10: Schematics and board (3 cm x 3.5 cm) of the designed and implemented daughter board interfacing the thermodiodes from the University of Cambridge as temperature sensors.

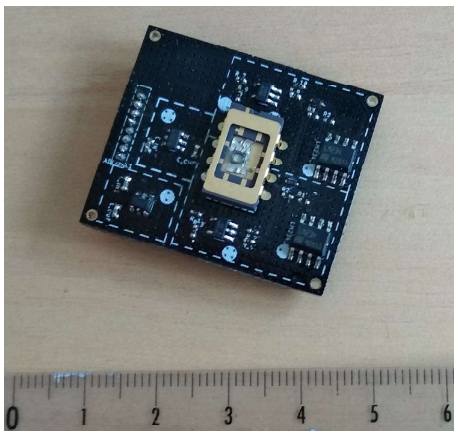

Figure V.11: Photograph of the designed and implemented daughter board interfacing the thermodiodes from the University of Cambridge as temperature sensors.

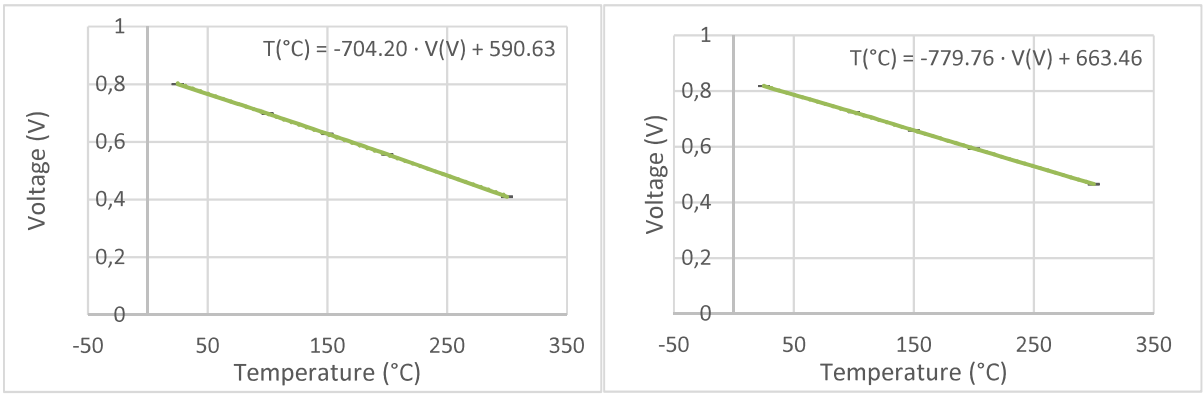

Figure V.12: Voltage output against temperature characterisation of the thermodiodes, respectively on bulk substrate and on membrane substrate, from the University of Cambridge as temperature transducers.

c. Tests and characteristics

Once designed and implemented, the daughter boards embedding the various temperature sensors and temperature and relative humidity sensors have been successfully tested and characterized.

* STMicroelectronics STM32L072CZ microcontroller internal temperature sensor

The use of the STMicroelectronics STM32L072CZ microcontroller internal temperature sensor located in the Murata CMWX1ZZABZ-091 LoRaWAN module allows to test a full data chain: from the measurement of the temperature, to its transmission in a LoRaWAN frame to the communicating node(s), through its pre-processing and its formatting. In this case, even if the payload is fixed to 4 bytes, only two are used to transmit the useful data.

This sensor allows to measure by using a 12 bits ADC the internal temperature of the STMicroelectronics STM32L072CZ microcontroller in a range from -40 °C to +125 °C with a linearity accuracy of ±2 °C and a measurement step of around 0.04 °C. The measured data is also rounded to the first decimal before its transmission. Even if easy to use, this sensor has a major drawback which is that it measures the temperature in the microcontroller. And, this one tends to heat up during its use. Thus, the use of this sensor is non-recommended for the measurement of the ambient temperature. As presented in Figure V.13, the use of the STMicroelectronics STM32L072CZ microcontroller internal temperature sensor increases the energy required for a full process of around +0.425 mJ and +0.275 mJ in average, respectively for a +14 dBm and a +4 dBm transmission powers.

* Adafruit DHT22 temperature and relative humidity sensor

The simultaneous use of the daughter board embedding the Adafruit DHT22 temperature and relative humidity sensor and of the Murata CMWX1ZZABZ-091 LoRaWAN module allows to test a full data chain: from the measurements of the temperature and the relative humidity, to their transmission in a LoRaWAN frame to the communicating node(s), through their pre-processing and their formatting. In this case, all the 4 bytes of the payload are used to transmit the useful data.

This sensor allows to collected the temperature and relative humidity measurements by using a non-standardized one-wire half-duplex communication protocol. The temperature can be measured in a range from -40 °C to +80 °C with a linearity accuracy of ±0.5 °C, whilst the relative humidity can be measured in a range from 0 % to 100 % with a linearity accuracy of ±3 %. The measured data are rounded to the first decimal before their transmission. As presented in Figure V.14, the use of the Adafruit DHT22 temperature and relative humidity sensor increases the energy required for a full process of around +24.65 mJ and +23.50 mJ in average, respectively for a +14 dBm and a +4 dBm transmission powers. More, this sensor consumes 4.7 mW to be powered in standby mode at 3.3 V, without considering the additional power required to the measurements and the communication with the Murata CMWX1ZZABZ-091 LoRaWAN module.

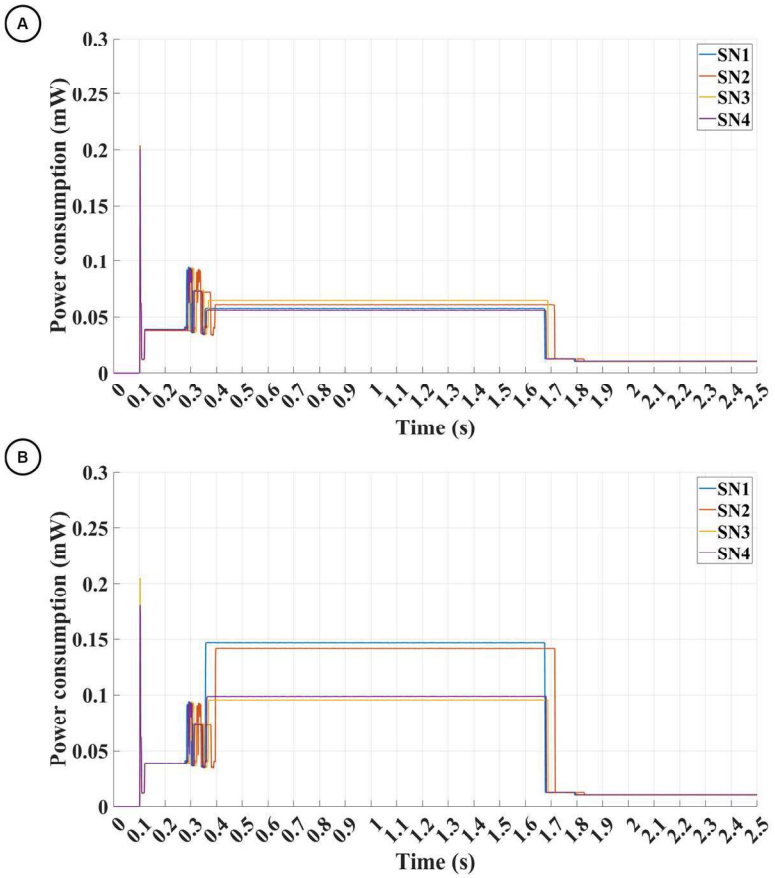

Figure V.13: Power consumption of the tested prototypes using the STMicroelectronics STM32L072CZ microcontroller internal temperature sensor and for transmission power of respectively (A) +4 dBm and (B) +14 dBm.

* Texas Instruments HDC2010 temperature and relative humidity sensor

The simultaneous use of the daughter board embedding the Texas Instruments HDC2010 temperature and relative humidity sensor and of the Murata CMWX1ZZABZ-091 LoRaWAN module allows to test a full data chain: from the measurements of the temperature and the relative humidity, to their transmission in a LoRaWAN frame to the communicating node(s), through their pre-processing and their formatting. In this case, all the 4 bytes of the payload are used to transmit the useful data.

This sensor allows to collected the temperature and relative humidity measurements by using a SPI communication protocol. The temperature can be measured in a range from -40 °C to +125 °C with a linearity accuracy of ±0.2 °C, whilst the relative humidity can be measured in a range from 0 % to 100 % with a linearity accuracy of ±2 %. The measured data are rounded to the first decimal before their transmission. As presented in Figure V.15, the use of the Texas Instruments HDC2010 temperature and relative humidity sensor increases the energy required for a full process of around +0.75 mJ and +0.60 mJ in average, respectively for a +14 dBm and a +4 dBm transmission powers. More, this sensor consumes 200 nW to be powered in standby mode at 3.3 V, without considering the additional power required to the measurements and the communication with the Murata CMWX1ZZABZ-091 LoRaWAN module.

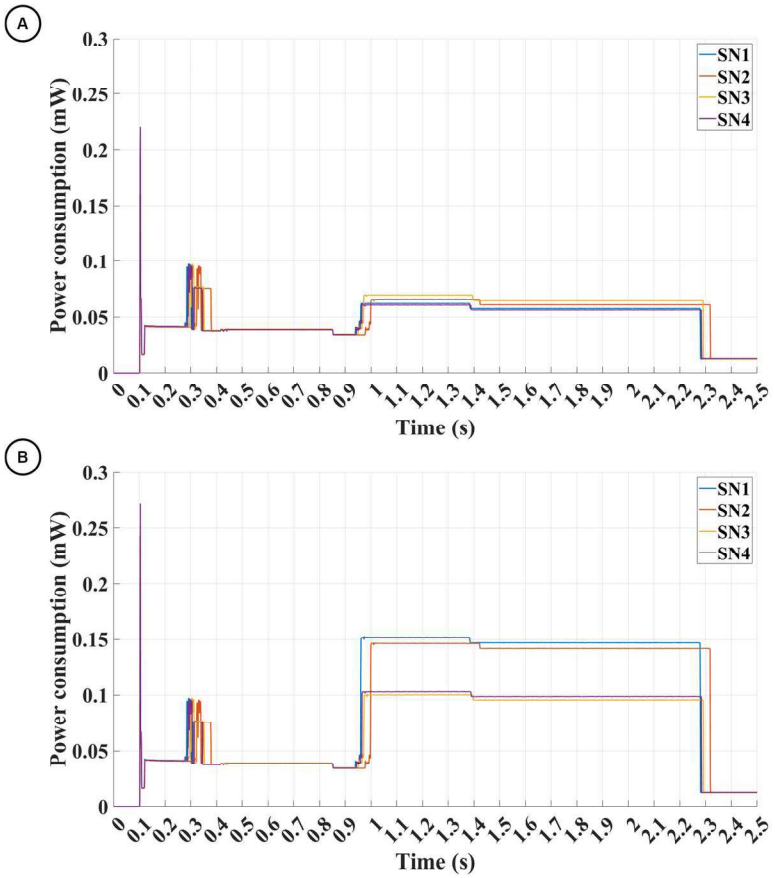

Figure V.14: Power consumption of the tested prototypes using the Adafruit DHT22 temperature and relative humidity sensor and for transmission power of respectively (A) +4 dBm and (B) +14 dBm.

* Thermodiodes from the University of Cambridge as temperature transducers

The simultaneous use of the daughter board embedding the thermodiodes from the University of Cambridge as temperature transducers and of the Murata CMWX1ZZABZ-091 LoRaWAN module allows to test a full data chain: from the measurements of the temperatures on the bulk substrate and on the membrane substrate, to their transmission in a LoRaWAN frame to the communicating node(s), through their pre-processing and their formatting. In this case, all the 4 bytes of the payload are used to transmit the useful data.

This sensor allows to collected the temperature on the bulk substrate and on the membrane substrate by using a 12 bits ADC. The temperature on the bulk substrate can be measured in a range from -34 °C to +135 °C with a step of ±0.15 °C, whilst the temperature on the membrane substrate can be measured in a range from -44 °C to +158 °C with a step of ±0.16 °C. The measured data are rounded to the first decimal before their transmission. As presented in Figure V.16, the use of the thermodiodes from the University of Cambridge as temperature transducers increases the energy required for a full process of around +7.50 mJ and +7.17 mJ in average, respectively for a +14 dBm and a +4 dBm transmission powers. More, this sensor consumes around 600 µW to be powered in standby mode at 3.3 V and for a temperature of 25 °C, without considering the additional power required to the voltage measurements by Murata CMWX1ZZABZ-091 LoRaWAN module through the ADC.

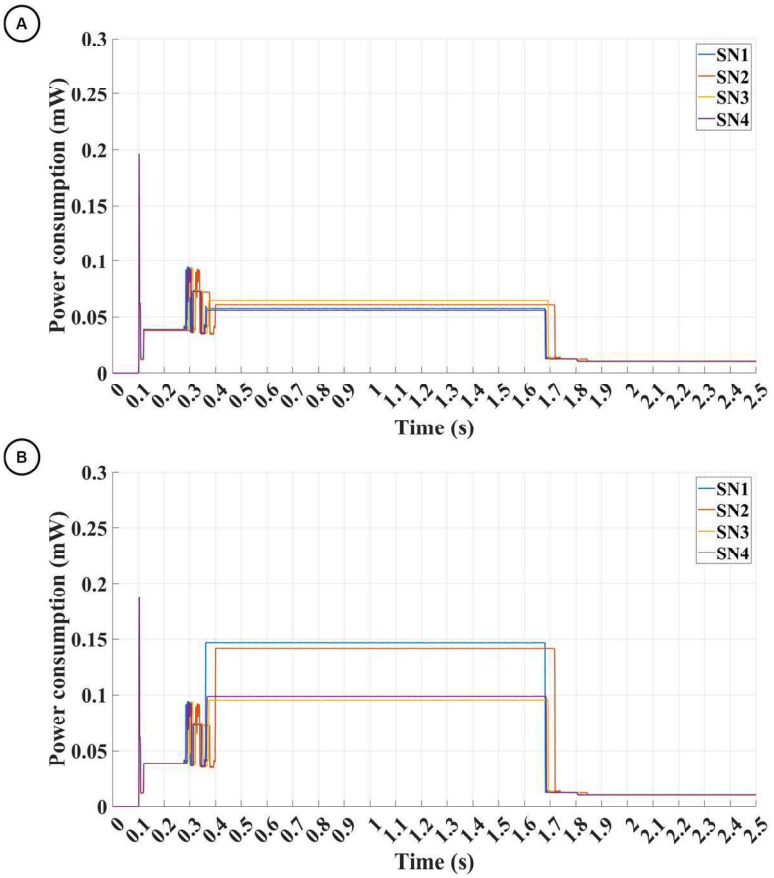

Figure V.15: Power consumption of the tested prototypes using the Texas Instruments HDC2010 temperature and relative humidity sensor and for transmission power of respectively (A) +4 dBm and (B) +14 dBm.

Unlike to the previous off-the-shelf sensors, the circuits developed to be able to use the thermodiodes from the University of Cambridge as temperature sensors have been characterised in temperature to certify their good functioning. The voltage output against temperature characterisation, as well as the power consumption against temperature characterisation have been carried out for two sensors between -40°C and +135°C and for a supply voltage of 3.3V and are respectively presented in Figure V.17 and Figure V.18. To achieve these characterizations, a Binder MKF 56 dynamic climate chamber [637], a Keithley 2612B sourcemeter [638] and 4 Keithley 2000 multimeters [639] have been used, as well as a thermometer with a K probe to check the temperature.

The theoretical linear models of the temperature against the output voltage at the direct output of the packaged thermodiodes are:

* T(°C) = -711,54 · V(V) + 589,53 for the first sample and T(°C) = -715,00 · V(V) + 592,45 for the second sample, close to the one provided without the package T(°C) = -704.20 · V(V) + 590.63 for the thermodiode on bulk substrate

* T(°C) = -721,76 · V(V) + 603,16 for the first sample and T(°C) = -721,50 · V(V) + 603,06 for the second sample, close to the one provided without the package T(°C) = -779,76 · V(V) + 663,46 for the thermodiode on membrane substrate,

which respectively allow theoretical temperature ranges of:

* -122 °C to 589 °C for the first sample and -123 °C to 592 °C for the second sample, for the thermodiode on bulk substrate

* -118°C to 603 °C for the first sample and -118°C to 603 °C for the second sample, for the thermodiode on membrane substrate.

The theoretical linear models of the temperature against the output voltage at the output of the scaling stage circuit dedicated to the thermodiodes are:

* T(°C) = -182,20 · V(V) + 126,45 for the first sample and T(°C) = -182,79 · V(V) + 128,85 for the second sample, close to the theoretically computed one T(°C) = -182.57 · V(V) + 134.20 for the thermodiode on bulk substrate,

* T(°C) = -184,54 · V(V) + 133,82 for the first sample and T(°C) = -185,08 · V(V) + 135,23 for the second sample, closed to the theoretically computed one T(°C) = -202.16 · V(V) + 158.06 for the thermodiode on membrane substrate

which respectively allow theoretical temperature ranges of:

* -56 °C à 126 °C for the first sample and -54 °C to 128 °C for the second sample, consistent with the theoretical computed one -34 °C to +135 °C for the thermodiode on bulk substrate

* -51 °C à 133 °C for the first sample and -50 °C to 135 °C for the second sample, consistent with the theoretical computed one -44 °C to +158 °C for the thermodiode on membrane substrate.

Moreover, the maximum deviations at the direct output of the packaged thermodiodes are 3.5 mV or 2.5 °C for the bulk thermodiodes and 2.3 mV or 1.6 °C for the membrane thermodiodes, whilst the maximum deviations at the output of the scaling stage circuit dedicated to the thermodiodes are 10.7 mV or 2.0 °C for the bulk thermodiodes and 7.0 mV or 1.3 °C for the membrane thermodiodes.

Also, the standard error at the direct output of the packaged thermodiodes are 0.9 mV or 0.6 °C for the bulk thermodiodes and 1.2 mV or 0.9 °C for the membrane thermodiodes, whilst the standard error at the output of the scaling stage circuit dedicated to the thermodiodes are 8.2 mV or 1.5 °C for the bulk thermodiodes and 6.4 mV or 1.2 °C for the membrane thermodiodes.

Thus, for voltages at the direct output of the packaged thermodiodes, there is little variation (less than 2 mV), so manufacturing induces little or no variability. And, for the voltages at the output of the scaling stage circuit dedicated to the thermodiodes, there is a little more variation, which can be seen in offset and/or poorer linearity. At the offset, this variation is less than 5 mV. All these variations can be justified by the tolerance on the components and potentially by the current source which is not fully temperature independent. However, this scaling stage circuit allows for easier measurement in the range of interest from -40 °C to +125 °C by increasing the voltage range from less than 300 mV to 1 V.

To finish, the power consumption of the complete daughter board dedicated to the thermodiodes increases with the temperature but never exceeds the 2 mW. The difference observed between the two samples is essentially induced by the use of a 1 V reference voltage circuit in the first sample and not in the second. This one was dedicated to be a reference voltage for the ADC, but this was not usable because this reference voltage must be at least

1.8 V for the used microcontroller. Finally, the power consumption of the board is overestimated in these measurements. Indeed, both the nearly 1 metre shielded cables used to drive the signals from the dynamic climate chamber to the measurement equipment, as well as this measurement equipment, generates non-negligible power losses. Another measurement with a board powered and characterised with a Keithley 2612B sourcemeter provides a power consumption of around 600 µW in standby mode (thus, without consider the power required for the measurement by the ADC) at 3.3 V and for a temperature of 25 °C.

Nevertheless, the designed and implemented circuit was successfully tested.

d. Alternatives and perspectives

The Table V.2 summarizes the characteristics of the temperature sensors and temperature and relative humidity sensors implemented and tested.

As presented in Table V.1, the choice of the Texas Instruments HDC2010 temperature and relative humidity sensor has been based on the study of the commercially available sensors, and with the objective to have a compact, reliable and low power solution.

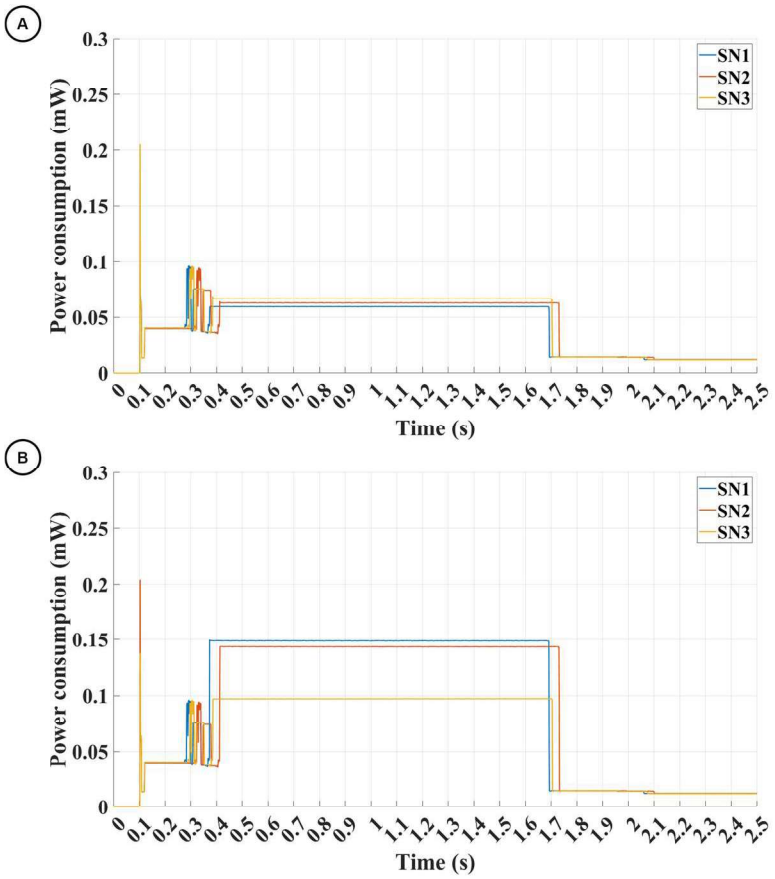

Figure V.16: Power consumption of the tested prototypes using the thermodiodes from the University of Cambridge as temperature sensors and for transmission power of respectively (A) +4 dBm and (B) +14 dBm.

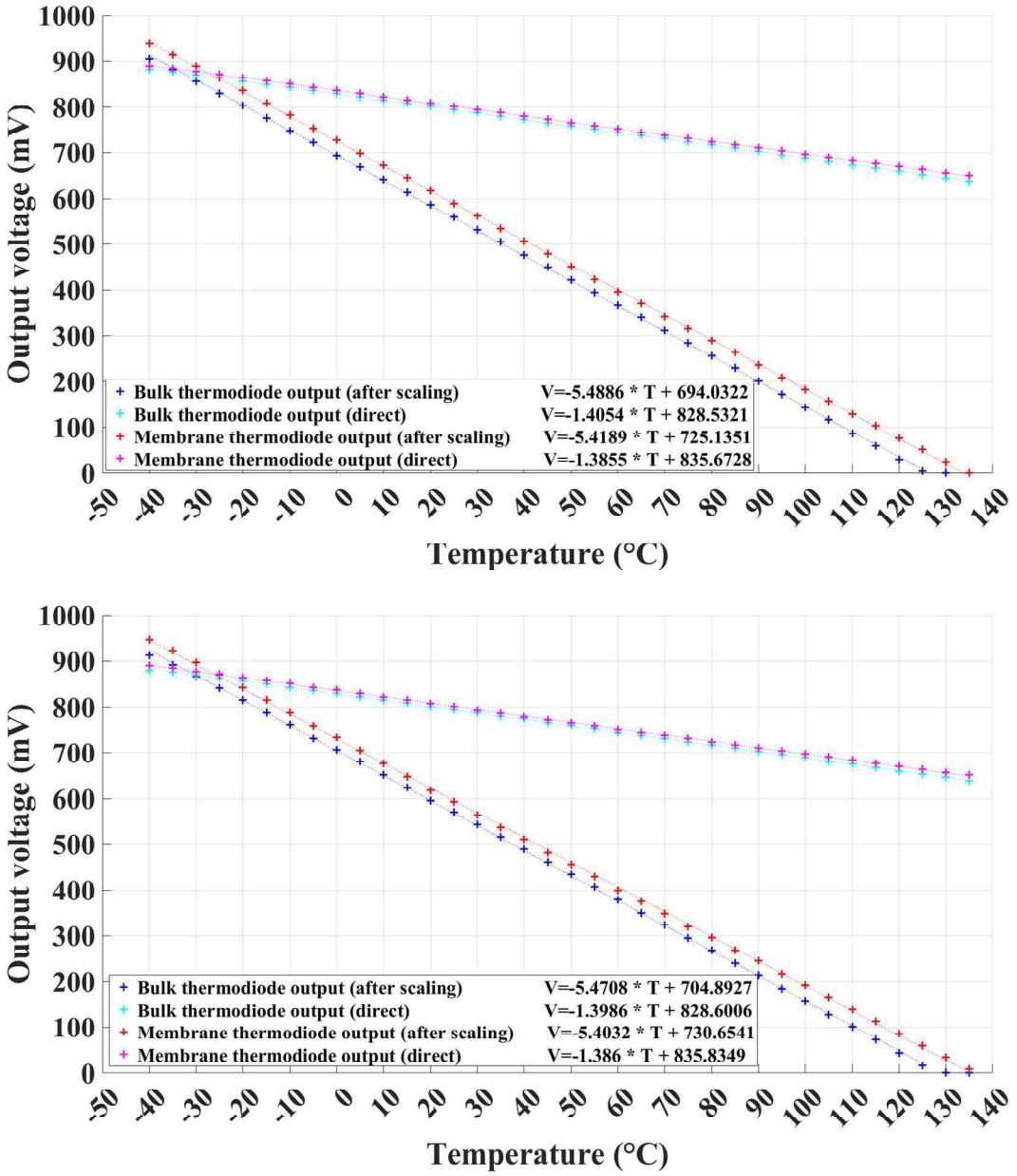

Figure V.17: Voltage output against temperature characterisation of the thermodiodes from the University of Cambridge, both on bulk substrate and on membrane substrate and used as full temperature sensors, before and after the scaling stage for two samples (A) and (B).

Concerning the thermodiodes from the University of Cambridge, it could be relevant to integrate the 100 µA current source (or even a 1 µA or 10 µA current source, for lower power consumption) and a well-tuned scaling stage directly on the substrate. In this way, a very compact, easy to use and very low power solution could be provided. This approach could be extremely relevant in the case of the development of an ASIC (application specific integrated circuit) manging all the tasks of the sensing nodes: the measurement, the pre-processing and the wireless transmission of the data, but even the energy harvesting, management and storage.

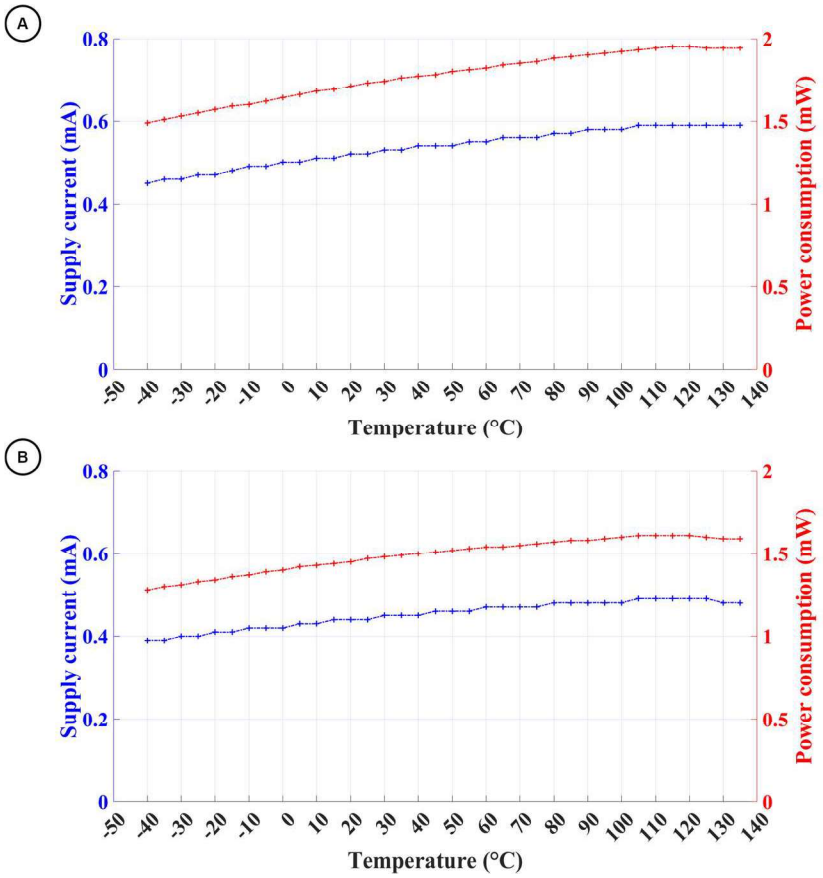

Figure V.18: Power consumption against temperature characterisation of the circuit developed to use of both on bulk substrate and on membrane substrate thermodiodes from the University of Cambridge as full temperature sensors for two samples (A) and (B).

ii. Resistivity sensor provided by the LMDC (Laboratory for Materials and Sustainability in Construction) of Toulouse

Once the temperature sensors, and temperature and relative humidity sensors implemented, the objective has been to interface other kinds of sensors, especially to be able to estimate the corrosion rate of the concrete.

a. Sensor choice

As no low-power commercial solution for sensors buried in reinforced concretes to measure and/or estimate their corrosion rate has been found, a solution provided by the LMDC (Laboratory for Materials and Durability of Constructions) of Toulouse has been used. This one consists in four metallic probes fully buried in a concrete sample according to a specific geometry, and which are commonly used with a resistimeter to quantify the resistivity of the concrete. The objective was to interface these buried probes to the sensing nodes in order to be able to measure the resistivity of the concrete in a low power way and to wirelessly transmit the collected data over medium to long ranges.

Table V.2: Summary of the temperature sensors and temperature and relative humidity sensors implemented and tested.

Reference	STMicroelectronics STM32L072CZ internal sensor	Adafruit DHT22	Texas Instruments HDC2010	University of Cambridge CMOS-MEMS thermodiode on bulk substrate	University of Cambridge CMOS-MEMS Thermodiode on membrane substrate
Temperature measurement	Yes	Yes	Yes	Yes	Yes
Temperature average accuracy (±°C)	2	0.5	0.2	0.15	0.16
Temperature range (°C)	-40 to +125	-40 to +80	-40 to +125	-34 to +135	-44 to +158
Humidity measurement	No	Yes	Yes	No	No
Humidity average accuracy (±%)	N/A	3	2	N/A	N/A
Humidity range (%)	N/A	0 to 100	0 to 100	N/A	N/A
Measure in isolation	N/A	No	Yes	N/A	N/A
Communication type	Voltage (12 bits ADC)	Non-standardized one-wire protocol	I²C	Voltage (12 bits ADC)	Voltage (12 bits ADC)
Supply	3.3 V	3.3 V	3.3 V	3.3 V	3.3 V
Measured power consumption in standby mode (µW)	N/A	4700	0.2	601	
Additional energy required (mJ)	+0.275 at +4 dBm +0.425 at +14 dBm	+ 24.65 at +4 dBm + 23.5 at +14 dBm	+ 0.60 at +4 dBm + 0.75 at +14 dBm	+ 7.17 at +4 dBm + 7.5 at +14 dBm	

b. Design and implementation

The four probes are buried in concrete at 4 cm intervals (distance noted d) and are used in a Wenner probe configuration, as presented in Figure V.19. In this configuration, the external probes are connected to a current source to generate a current in the concrete between the external probes (noted I_{14}), whilst a potentials difference measurement is performed between the two internal probes (noted U_{23}). It is then possible to estimate by computation the electric resistance between the internal probes (noted R_{23}) thanks to Ohm's law. By considering the sample of concrete as quasi-infinite and the current flow homogeneous between the probes,

the relation presented in Equation V.1 can be applied to estimate the resistivity (noted ρ) of the concrete. By monitoring its variation over time, it is possible to estimate the corrosion rate.

$$\rho = 2 \cdot \pi \cdot d \cdot R_{23} = 2 \cdot \pi \cdot d \cdot \frac{U_{23}}{I_{14}} \ (\Omega \cdot m) \qquad \text{(Equation V.1)}$$

To implement a first proof-of-concept of the use of a resistivity sensor with the sensing nodes in an embedded way, the daughter board designed for the thermodiodes has been adapted to the new needs, and again, this one interfaces the Murata CMWX1ZZABZ-091 LoRaWAN module through a 12 bits ADC, as presented in Figure V.20 and Figure V.21.

On the hardware side, the direct current source with its temperature drift compensation and powered by a 3.3 V supply voltage has been reused to generate a 100 µA direct current between the two external probes. Then, the potential difference measurement is achieved by measuring, with the 12 bits ADC of the Murata CMWX1ZZABZ-091 LoRaWAN module, the output voltage of a differential circuit (a voltage subtractor circuit with a unit gain) based on the rail-to-rail zero-bias operational amplifier.

On the software side, an ADC channel must be initialized and enabled in order to measure on 12 bits the output voltage. The ADC has been configured in order to oversample, and then average 256 measurements. Once achieved the voltage measurement, the estimated resistivity is computed, then formatted on two bytes, in order to be sent in a LoRaWAN frame. Its computation step is of 2 Ω·m and its range is from 0 Ω·m to more than 5 kΩ·m. For development purpose, the voltage measurement is also formatted on two bytes and rounded at the millivolt, to be sent in the LoRaWAN frame.

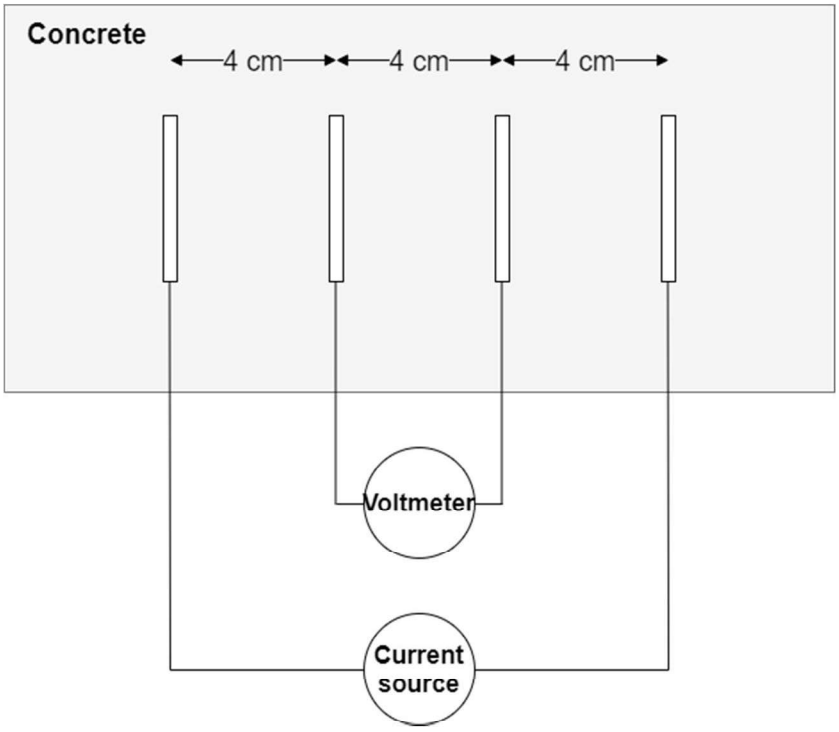

Figure V.19: Diagram of the geometry of the used buried probes into concrete, and their connection in a Wenner probe configuration.

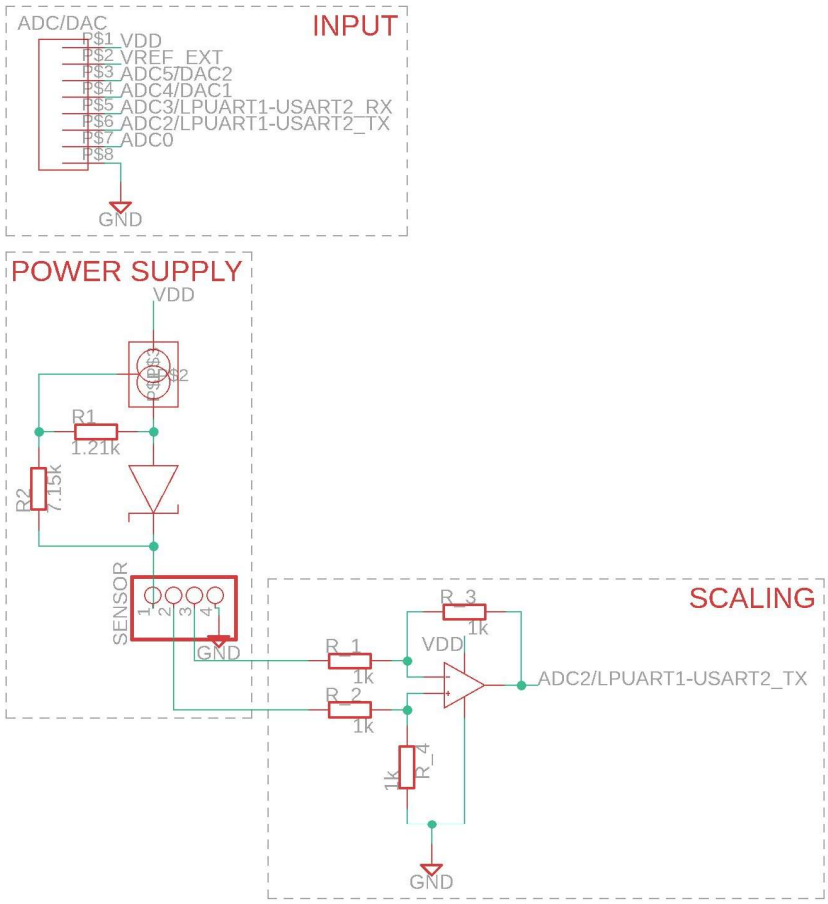

Figure V.20: Schematics of the adapted daughter board to implement the resistivity sensor.

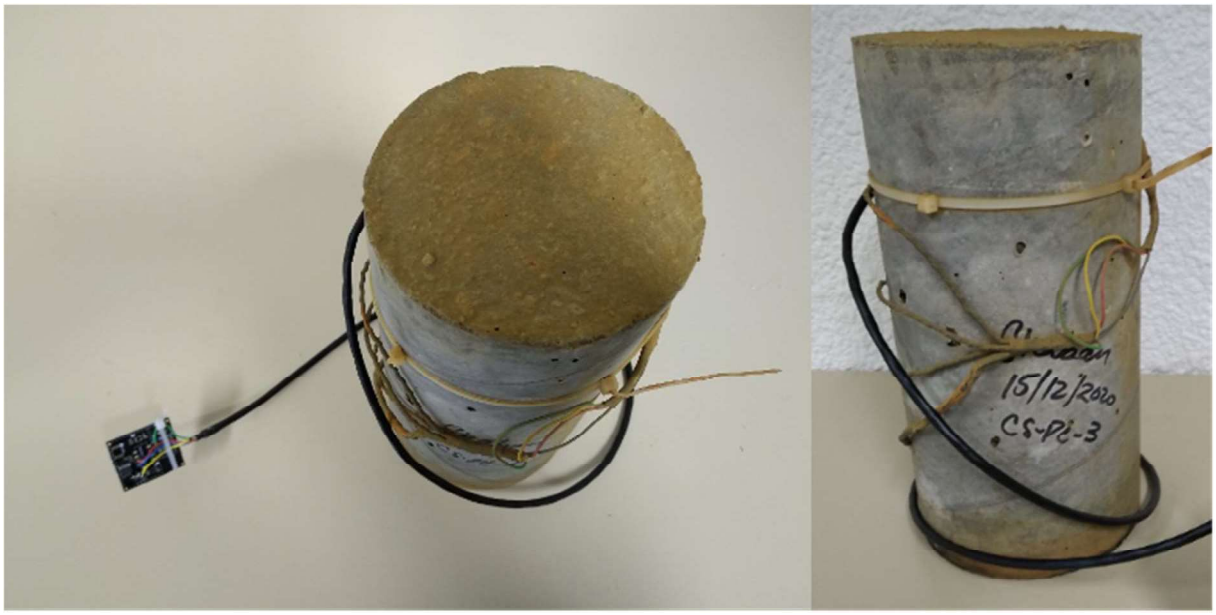

Figure V.21: Photograph of the adapted daughter board to implement the resistivity sensor and its connection to the concrete sample.

c. Tests and characteristics

The simultaneous use of the daughter board embedding the resistivity sensor and of the Murata CMWX1ZZABZ-091 LoRaWAN module allows to test a full data chain: from the measurements of the resistivity to estimate the corrosion rate, to its transmission in a LoRaWAN frame to the communicating node(s), through its pre-processing and its formatting. In this case, all the 4 bytes of the payload are used to transmit twice the same data, since the resistivity is computed from the measured voltage.

This sensor allows to compute the resistivity of the concrete by using a 12 bits ADC voltage measurement. The voltage can be measured in a range from 0 V to 2.1 V, that induces that the resistivity can be computer in a range from 0 Ω·m to more than 5 kΩ·m. Before the transmission, the measured voltage is rounded to the millivolt, that induces a step in the resistivity of 2 Ω·m. As presented in Figure V.22, the use of the resistivity sensor increases the energy required for a full process of around +4.13 mJ and +4.03 mJ in average, respectively for a +14 dBm and a +4 dBm transmission powers. More, this sensor consumes around 580 µW to be powered in standby mode at 3.3 V, without considering the additional power required to the voltage measurements by Murata CMWX1ZZABZ-091 LoRaWAN module through the ADC. This is so a low power consumption sensor.

To certify its good design and implementation, punctual measurements have been performed with a Keithley 2612B sourcemeter to power the daughter board in a 3.3 V voltage on a channel and measure the output voltage on another, and then with a sensing node. These measurements have been achieved in a similar configuration: with a water saturated concrete sample (taken out of the water where it was stored for periods of few days) and during its first hours of drying. Thus, the measurement reproducibility has been checked.

To validate its long-term reliability, a long duration experimentation has been carried out, as presented in Figure V.23. This one allows to check the coherent evolution of the computed resistivity during the drying phase of the concrete and to correlated the resistivity values with the temperature and relative humidity measurements obtained in the same place. Before the begin of the experimentation the sample of concrete, where have been buried the probes, has been stored in the water for a long time. Once taken out of the water, it has been embedded on a full sensing node powered by a nearly -8 dBm (or 158.5 µW) radiofrequency signal, whilst another sensing node embedding a Texas Instruments HDC2010 sensor and powered by a nearly -6 dBm (or 251.2 µW) radiofrequency signal has been located in the same place. For this experimentation, the sensing nodes are powered by radiofrequency signals which are conducted and not radiated, to have a constant input power. Nevertheless, it would similarly work with radiative signals with a higher variability imposed by the environment variations.

Nevertheless, the designed and implemented circuit was successfully tested.

d. Alternatives and perspectives

As no low-power, wireless and/or embeddable, commercial sensors buried in concretes to measure and/or estimate their corrosion rate has been found, the alternatives to the resistivity sensor are always under investigations.

Obviously, a new daughter board specifically designed for the resistivity sensor could be developed.

Concerning the resistivity sensor itself, when it is powered for "long" times (from few seconds) with a direct current, the concrete starts to become electrically polarised. This phenomenon has been observed during the punctual experimentations. As the relaxation time is high, this effect is not negligible for frequent measurements (e.g. under a period of one hour). To avoid this affect, an alternative current source could be used and implemented in a daughter board dedicated to the resistivity sensor.

More, there are other configurations than the Wenner probe to exploit the 4 four buried probes. In fact, all the combinations allowing a power supply between two probes and a measurement between two probes, not necessarily exclusive, are possible. This concept can be scaled to a larger number of probes as presented in [640]. In this way, the resistivity can be estimated through several different measurements and for various zones, more or less extended. Nevertheless, the use of this kind of system is more complex and required reconfigurability abilities which can be energy consuming. In the case of an extended area to monitor, it could be more energy efficient to deploy several wirelessly powered sensing nodes, each with a resistivity sensor based on few probes and which achieves few measurements in a short time, than to deploy a unique wirelessly powered sensing node with a

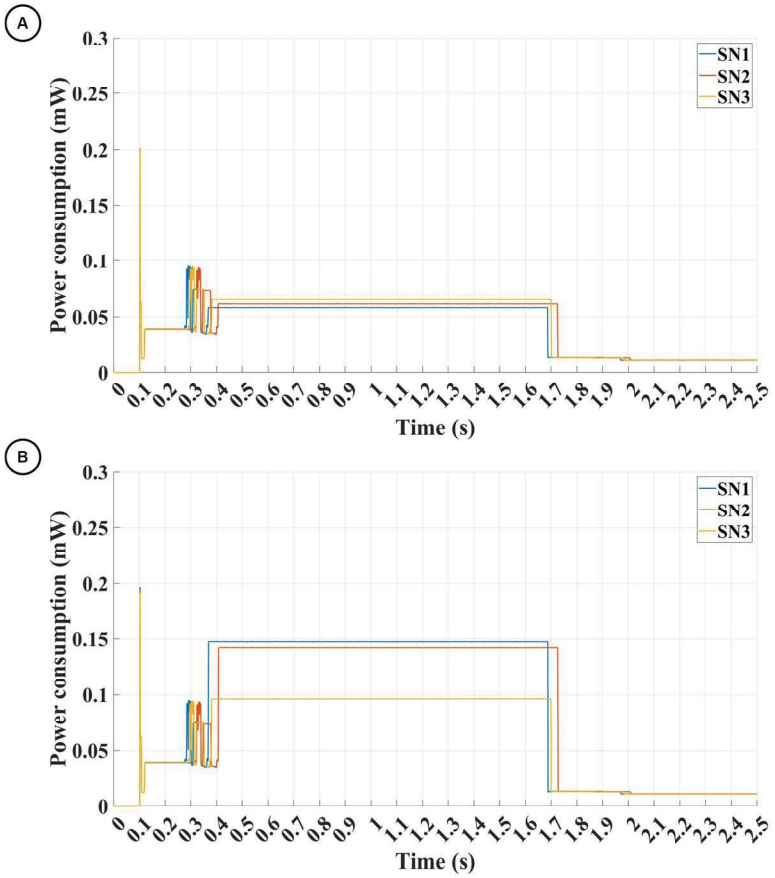

Figure V.22: Power consumption of the tested prototypes using the resistivity sensor and for transmission power of respectively (A) +4 dBm and (B) +14 dBm.

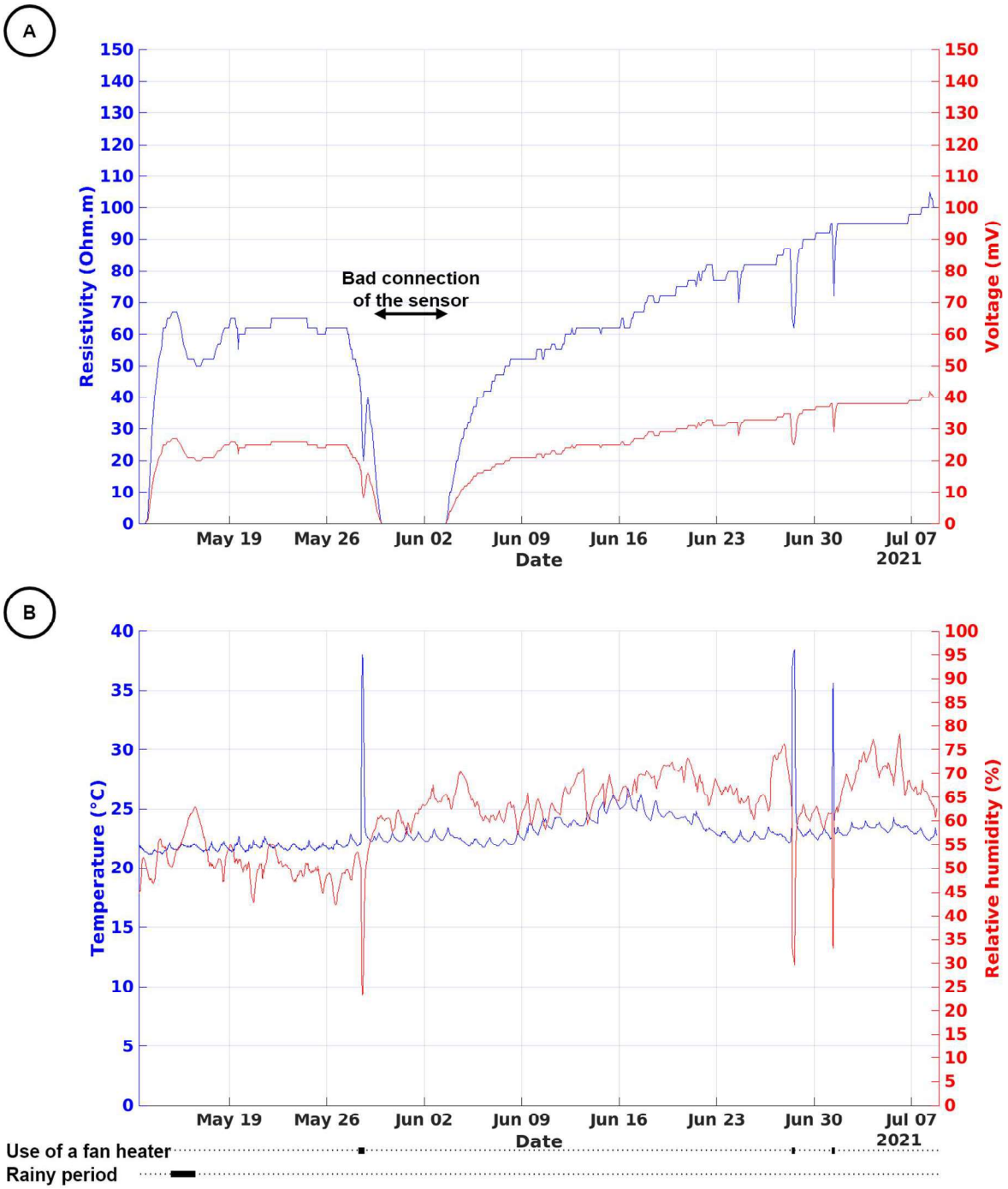

Figure V.23: Evolutions (A) of the computed resistivity and of the measured output voltage of the resistive sensor, and (B) of the temperature and relative humidity, for several days of drying of the concrete.

resistivity sensor using several probes which needs a long time to achieved all the desired measurements, and thus, a lot of energy both for the measurements and the reconfigurations. In any case, the implementation of a reconfigurable solution could be considered for the design of a daughter board dedicated to the resistivity sensor.

iii. Strain Gauges

Once the temperature sensors, the temperature and relative humidity sensors and a resistivity sensor dedicated to the monitoring of the corrosion rate implemented, the objective has been to interface a new family of sensors as proof-of-concept: this is the mechanical sensors, with the particular case of the strain gauges which can be used to monitor the mechanical deformation.

a. Sensor choice

In order to implement a proof-of-concept, a simple and low-cost wire lead strain gauge was sought. The linear RS Pro wire lead strain gauge of 8 mm x 4 mm, with a resistance of 120 Ω (noted R) and a gauge factor of 2 (noted GF) has been chosen for its cost, its "large" geometry and its availability [641]. By this way, it has been possible to implement a dedicated solution with the aim to be low power consumption.

b. Design and implementation

The wire lead strain gauge, which could be buried into concretes, is used in a quarter Wheatstone bridge configuration, that says only one resistance of the bridge is variable and this one is the strain gauge. More, the Wheatstone bridge is powered with a direct current source (with a current noted I_{IN}), which allows to increase the linearity and to limit the power consumption, in comparison to a Wheatstone bridge powered by a voltage source. A potentials difference measurement (noted V_{OUT}) is performed between the middle points of each of the two branches of the Wheatstone bridge. From this measurement, it becomes possible to estimate the mechanical deformation (noted ε) by using the Equation V.2.

$$\varepsilon = \frac{1}{GF} \cdot \frac{4 \cdot V_{OUT}}{R \cdot I_{IN} - V_{OUT}} \qquad \text{(Equation V.2)}$$

As in the case of a quarter Wheatstone bridge powered by a 100 µA direct current source and a strain gauge with a maximum resistance change of around 1 %, the measurable voltage extremes are ±30 µV, which are not directly usable with the 12 bits ADC of the Murata CMWX1ZZABZ-091 LoRaWAN module; an amplifier stage with a gain of 1,000 and an offset (to measure the positive and negative variations with only a positive supply voltage) is used in order to increase the useful voltage range.

To implement a first proof-of-concept of the use of a strain gauge with the sensing nodes in an embedded way, the daughter board designed for the thermodiodes has been once again adapted to the new needs, and once more, this one interfaces the Murata CMWX1ZZABZ-091 LoRaWAN module through a 12 bits ADC, as presented in Figure V.24 and Figure V.25.

On the hardware side, the direct current source with its temperature drift compensation and powered by a 3.3 V supply voltage has been reused to generate a 100 µA direct current in the Wheatstone bridge. Then, the potential difference measurement is achieved by measuring, with the 12 bits ADC of the Murata CMWX1ZZABZ-091 LoRaWAN module, the output voltage of a differential circuit with a gain of 1,000 (a voltage subtractor circuit) based on the rail-to-rail zero-bias operational amplifier. The partial rejection of the common mode by the differential circuit has been exploited (and manually tuned by changing some resistors) to generate the offset required both for the positive and the negative variation measurements.

Nevertheless, this manual tuning is not recommended, required a calibration phase and cannot present a usable solution.

On the software side, an ADC channel must be initialized and enabled in order to measure on 12 bits the output voltage. The ADC has been configured in order to oversample, and then average 256 measurements. Once achieved the voltage measurement, the estimated mechanical deformation is computed, then formatted on two bytes, in order to be sent in a LoRaWAN frame. For development purpose, the voltage measurement is also formatted on two bytes and rounded at the millivolt, to be sent in the LoRaWAN frame.

c. Tests and characteristics

The simultaneous use of the daughter board embedding the strain gauge and of the Murata CMWX1ZZABZ-091 LoRaWAN module allows to test a full data chain: from the measurements of the mechanical deformation, to its transmission in a LoRaWAN frame to the communicating node(s), through its pre-processing and its formatting. In this case, all the 4 bytes of the payload are used to transmit twice the same data, since the mechanical deformation is computed from the measured voltage.

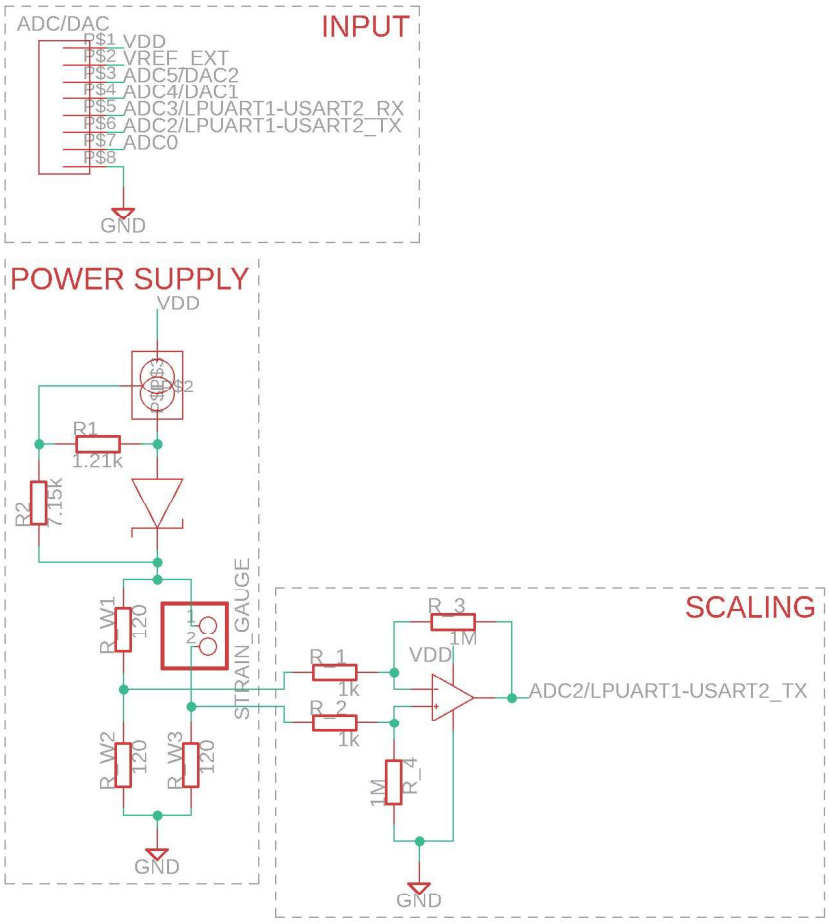

Figure V.24: Schematics of the adapted daughter board to implement the strain gauge.

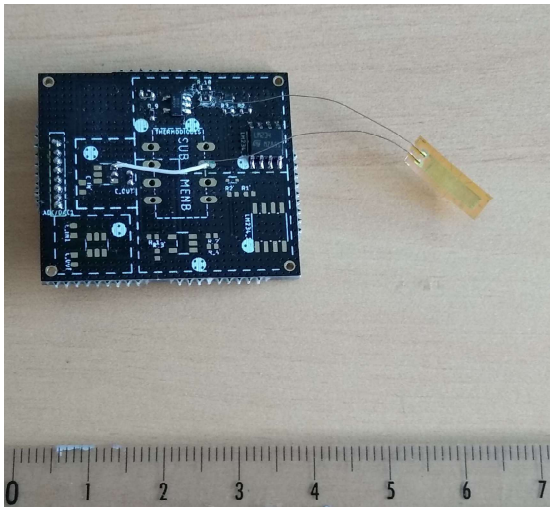

Figure V.25: Photograph of the adapted daughter board to implement the strain gauge.

This sensor allows to compute the mechanical deformation by using a 12 bits ADC voltage measurement. The voltage can be measured in a range from 0 V to 2.1 V. Before the transmission, the measured voltage is rounded to the millivolt. As presented in Figure V.26, the use of the strain gauge increases the energy required for a full process of around +4.03 mJ and +4.13 mJ in average, respectively for a +14 dBm and a +4 dBm transmission powers. More, this sensor consumes around 1.46 mW to be powered in standby mode at 3.3 V, without considering the additional power required to the voltage measurements by Murata CMWX1ZZABZ-091 LoRaWAN module through the ADC. This is so a low power consumption sensor.

To certify its good design and implementation, measurements have been performed with a Keithley 2612B sourcemeter to power the daughter board in a 3.3 V voltage on a channel and measure the output voltage on another, and then with a sensing node. Because of the mismatch of the resistor pairs and the use of a low-quality differential circuit, the measurements are of poor quality, but sufficient to observe a major change in the geometry of the strain gauge caused by a mechanical deformation.

Nevertheless, and one more, the designed and implemented circuit was successfully tested.

d. Alternatives and perspectives

First of all, a new daughter board specifically designed for the strain gauge could be developed.

For this proof-of-concept, a unique "naked" linear strain gauge has been used. However, there are more complex geometries for strain gauges, especially to measure the mechanical deformation in several directions (e.g. with a rosette geometry, etc.). Nevertheless, each direction requires its own circuit, based on a current source, a Wheatstone bridge and a differential amplifier.

In order to get more accurate and with a larger output voltage range, the use of a half or even a full Wheatstone bridge could be relevant. Each Wheatstone bridge requires its own power circuit and can be exploited with a unique measurement.

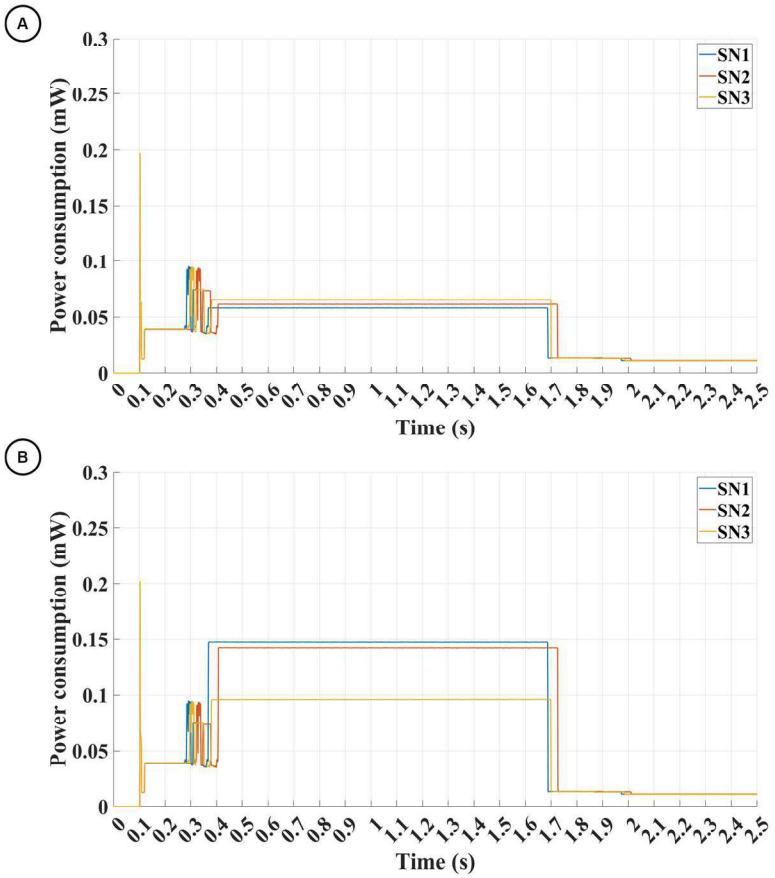

Figure V.26: Power consumption of the tested prototypes using the strain gauge and for transmission power of respectively (A) +4 dBm and (B) +14 dBm.

More, the strain gauge(s) can be mounted a specifically designed mechanical specimen in order to implement a load cell. In this way, the measurement will be more accurate and reliable. The mechanical deformation of the strain gauge is then the image of the mechanical deformation of the larger specimen.

Concerning the components, and in order to get more accurate measurements, well paired resistors and/or strain gauges must be used in the Wheatstone bridge. As well, a more adapted differential amplifier, such as an instrumentation amplifier, must be used, in a configuration where an offset can be imposed, and with well paired resistors.

Nevertheless, whatever the chosen topology, a particular attention must be paid to the power consumption, which can quickly increase with the use of multiple circuits (for instance, to monitor the mechanical deformation in several directions) or less energy efficient components (for instance, the instrumentation amplifier) in each sensing node. Also here, in order to monitor mechanical deformation in several directions and/or in an extended area, it could be more energy efficient to deploy several wirelessly powered sensing nodes, each with a strain gauge for a unique direction and which achieves a measurement in a short time, than to deploy a unique wirelessly powered sensing node with several strain gauges which needs a long time to achieved all the desired measurements, and thus, a lot of energy.

C. Energy harvesting and management

Once the part of the sensing nodes dedicated to the data management fully designed: from the measurement to the wireless communication, through the pre-processing and formatting of the data; and its energy needs characterized, it is time to implement the power management part. This one must allow the energy autonomous of the sensing nodes by harvesting the radiative electromagnetic power generated by the communicating nodes through a wireless power transfer system; and efficiently store and use the energy to power the active components of the sensing nodes. This is the most challenging part of the sensing nodes design.

1. Design process and technology choices

The energy harvesting and management part of the sensing nodes is composed of three main components: a hardware power management unit (PMU), an energy storage device, and a rectenna.

The power management unit (PMU) is the central element of this part. Indeed, its role is to efficiently scavenge the direct current power provided by the rectenna, to efficiently store it in the energy storage device, and to efficiently use the stored energy, once enough is available, to power the active components of the sensing nodes. It must properly work with the lowest possible input powers.

The role of the energy storage device is to efficiently store enough energy to meet the needs of the active components. Its use must be compatible with the power management unit functionalities and it must have the lowest possible energy losses and a long lifetime without large alterations of its properties over time. Thus, the energy consumption of the active part of the sensing nodes must be known before conjointly designing this component with the power management unit.

Finally, the role of the rectenna is to efficiently harvest the radiative electromagnetic power generated by the communicating nodes to provide a direct current power to the power management unit. Thus, the rectenna must be well designed to be in adequation with the properties of the transmitted power (e.g. power level, central frequency, frequency band, polarisation, etc.) and to convert as much of the radiative electromagnetic power as possible into direct current electrical power.

Even if the technology choice made to wirelessly power and assure the energy autonomy for long term (that says decades) of the sensing nodes has been justified above (Section IV.A.1.), the choice of the 868 MHz industrial, scientific and medical (ISM) frequency band for the radiative electromagnetic wireless power transfer has not been yet. And, the choice of the frequency is crucial for the implementation of the sensing nodes.

Regarding the radiative electromagnetic wireless power transfer solution, its used frequency is closely related to its range of use. First, the free space path losses are function of the frequency: the higher the frequency, the greater the free space losses, and the shorter the useful range of use; secondly, the maximal usable effective isotropic radiated power (EIRP) is function of the frequency and of the geographical area. For scientific projects, the industrial,

scientific and medical (ISM) radiofrequency bands are privileged. The free space path losses and the range for a defined effective isotropic radiated power can be computed thanks to the Equation V.3 and the Equation V.4, respectively in function of the distance (noted d), the frequency (noted f) and the celerity of light (noted c); and in function of the wavelength (noted λ), the maximal equivalent isotropic radiated power (noted P_{EIRP}) and the minimal permitted input power (noted P_{IN}).

$$free\_space\_path\_losses = 20 \cdot log\left(\frac{4 \cdot \pi \cdot d \cdot f}{c}\right) (dB) \qquad \text{(Equation V.3)}$$

$$range = \sqrt{\frac{\lambda^2}{4 \cdot \pi} \cdot \frac{P_{EIRP}}{3600 \cdot \pi \cdot P_{IN}}} (m) \qquad \text{(Equation V.4)}$$

Regarding the overall size of the sensing nodes, this one will be for a large part constrained by the size of the antenna(s), and the size of an antenna is closely related to its wavelength (generally in a ratio of one half or one quarter), or in other words its frequency: the higher the frequency, the smallest the antenna; and its bandwidth: the widest the bandwidth, the largest the antenna.

The Table V.3 summarizes some information to compare the different industrial, scientific and medical (ISM) frequency bands and leading up to a decision in the design of the radiative electromagnetic wireless power transfer system. Thus, the most acceptable trade-off between the range of use of the radiative electromagnetic wireless power transfer system and the size of the sensing node *via* the size of its antenna(s) seems to be for the 868 MHz industrial, scientific and medical (ISM) frequency band. Indeed, a range of several meters can be obtained, whilst the antenna is relatively small (several centimetres). It has to be noted that ambient radiative electromagnetic energy is not considered into the different bands because of its very low power level.

2. Design and implementation

To implement the part of the sensing nodes dedicated to the energy harvesting and management, both the design of the radiative electromagnetic power source of the communicating nodes and the design of the full part of the sensing nodes dedicated to the measurement, the data collection, pre-processing and wireless transmission, must be considered. Indeed, the first gives an idea of the available power, whilst the second gives an idea of the needed energy. The main objective was to implemented a solution which allows a medium range wireless power transfer in the reinforced concrete. This can be translated as a system which works with the lowest possible input power. More, as said above (Section II.D.5.), the "store then use" strategy is privileged for the use of the collected energy.

i. The power management unit

As introduced, the goal of the power management unit is to efficiently recover the direct current power provided by the rectenna, to efficiently store it in an energy storage device, and to power the active components of the sensing nodes once enough energy is available. This is then the core of the energy harvesting and management part.

Table V.3: Comparison of the main industrial, scientific and medical (ISM) frequency band for the design of the radiative electromagnetic wireless power transfer system used to power the sensing nodes.

Central frequency (MHz)	13.56	433	868	2,450	5,800
Wavelength in the air (cm)	2.210	69.2	34.4	12.2	5.2
Bandwidth (MHz)	0.014	1.74	5	100	150
Maximal EIRP (mW / dBm)	/	10 / +10	2,000 / + 33	100 / +20	200 / +23 or 1,000 / +30
Free space losses at 1 m (dBm)	/	25.17	31.21	40.23	47.71
Free space losses at 5 m (dBm)	/	39.15	45.19	54.20	61.69
Theoretical range for P_{IN}=+0 dBm (cm)	/	17	123	9	6 / 13
Theoretical range for P_{IN}=-10 dBm (cm)	/	55	388	30	18 / 41
Theoretical range for P_{IN}=-14 dBm (cm)	/	87	615	48	29 / 65

a. Component choice

As the direct current power required to supply the active components of the sensing nodes is far greater than that available (the radiative electromagnetic power), the "store then use" strategy was adopted. In that way, the active components of the sensing nodes are powered only when enough energy is available, which ensures that the entire treatment will be carried out correctly. More, as the charge level of the energy storage device is never known and as this one can be empty, a cold-start system is required.

At the beginning of this work, there has been no power management unit dedicated to the harvesting of radiative electromagnetic energy, such as now proposed by E-PEAS [488] or Powercast [489]. Thus, the choice has been made on the existing solutions that could be

adapted to meet these new requirements. The Texas Instruments BQ25504 [481] and BQ25505 [482], and more recently BQ25570 [483], and the Linear Technology, now Analog Devices, LTC3105 and LTC3108 [484] devices have been in particular studied and have been tested.

Although it provides the lowest minimum start-up voltage and it has been successfully but only partially tested at the very beginning, because of its limited maximum input voltage, its comparatively higher quiescent currents, its comparatively higher measured minimal input power, its poor configurability, and its output current insufficient to power the Murata CMWX1ZZABZ-091 LoRaWAN module, the Linear Technology LTC3108 power management unit has been discarded. Even if it provides higher start-up voltages, because of lowest quiescent currents, and mainly because of greater configuration abilities and lowest minimal input powers, the Texas Instruments BQ255xx family has been preferred to the Linear Technology LTC3105 power management unit. More, even with the use of the development board [642], this last has never been able to achieve satisfactory operation in a "store then use" strategy. Regarding the Texas Instruments BQ255xx family, all the power management units are relatively similar. The differences are in the minimal input powers, the input voltage and current ranges, in the minimal output voltages, the available configurations, etc. but the main ones are the management of two storage element devices (whose a primary battery) in the BQ25505 and the presence of a partially regulated output in the BQ25570 (as long as the voltage in the energy storage device is 200 mV higher than the configured output voltage, then the output voltage follows the discharge of the energy storage device). Otherwise, the three devices use the same MPPT (maximum power point tracking) and cold-start circuits. The hardware maximum power point tracking (MPPT) system attempts to optimise the energy transfer from the input to the load or to the energy storage device; whilst the cold-start circuit allows to operate even with an empty energy storage device. Because of its greater ease of implementation, its availability and a choice made before the last revision of the datasheet (which indicated the lowest minimal input voltage for the family, despite a higher minimum input power required), the BQ25504 has been initially chosen, and the design will be detailed with it. Nevertheless, the BQ25505 has been also tested in some version of the prototypes of the sensing nodes and the BQ25570 has been used in the implementation of the sensing nodes based on the Bluetooth Low Energy wireless communication technology.

It must be noted that these power management units are designed for a "simultaneous use and store" strategy with higher power harvesters (especially solar cells) and with larger energy storage devices (especially secondary batteries). Thus, in the general case, the load, often put in a sleep mode, is continuously powered by the harvester, and only the spared energy is stored in order to compensate the variations of the input power over time. To use these in "store then use" strategy, the conventional implementation must be modified.

b. Design and implementation

The Texas Instruments BQ25504 power management unit is used to efficiently store in an energy storage device its input power, and to efficiently use the stored energy to power the active components of the sensing nodes once a sufficient amount is available. Its current implementation is presented in Figure V.27.

As presented in Figure V.28, if the energy storage device is empty, the Texas Instruments BQ25504 power management unit will use its cold-start ability to start storing its available input power in this last. When a sufficient voltage is reached, the hardware maximal power point tracking (MPPT) system is powered-up and will allow to optimize the power transfer from the input to the energy storage device. In fact, this circuit will sample the open-circuit input voltage each 16 seconds to impose on the input a ratio of it. This ratio is configurable with a resistor divider, and is currently set to 40 % of the open-circuit input voltage. Then, when the voltage in the energy storage device will reach the activation threshold, the power good indicator will be raised and will activate the power supply of the active components of the sensing nodes. The energy storage device will start its discharge. When the voltage in the energy storage device will reach the deactivation threshold, the power good indicator will be turned down and will deactivate the power supply of the active components of the sensing nodes. Thus, the activation and deactivation thresholds, configurable with resistor dividers, allow to control the charge and discharge levels of the energy storage device. And this process will be periodically done as long as a sufficient power is available at the input. It must be note that undervoltage (to prevent the deep discharge), overvoltage (to prevent the over charge) and overheating protection mechanisms are available and configurable with resistors.

By tuning the capacitance of the energy storage device (noted C), as well as the activation and deactivation thresholds of the Texas Instruments BQ25504 power management unit (respectively noted V_{max} and V_{min}), the amount of stored energy (noted E) can be adjusted. This one must be quantified to meet the needs of all the active components composing the part of the sensing nodes dedicated to the measurement, the data collection, pre-processing and wireless transmission. The Equation V.5 allows to computed an estimation of the energy stored in the energy storage device.

$$E = \frac{C}{2} \cdot \left({V_{max}}^2 - {V_{min}}^2 \right) \qquad \text{(Equation V.5)}$$

As the supply voltage provided by the Texas Instruments BQ25504 power management unit to the load continuously follows the energy storage device voltage between the undervoltage and overvoltage thresholds, a Texas Instruments TPS63031 DC-to-DC buck/boost converter enabled by the power good indicator is used between the Texas Instruments BQ25504 power management unit and the load, as presented in Figure V.27 [643]. In that way, a constant 3.3 V supply voltage is provided to the load only when enough energy is available, as presented in Figure V.29 and Figure V.2. Prior to the use of this component, a transistor was used to enable and disable the power supply to the load according to the power good indicator. As the supply voltage was not constant over time, the power provided to the load varied, resulting in a loss of power at the end of the LoRaWAN frame transmission, which was no longer received systematically.

c. Tests and characteristics

The use of the Texas Instruments BQ25504 power management unit and Texas Instruments TPS63031 DC-to-DC buck/boost converter allows to efficiently store the input energy in an energy storage device, before using the stored energy, only when enough is available, to power the active components of the sensing nodes. The direct current input power can be provided by a conventional source in particular during

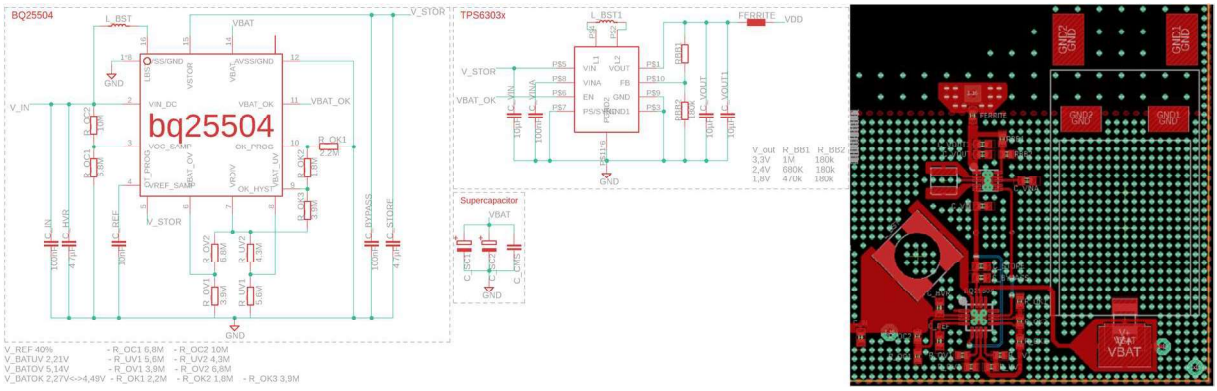

Figure V.27: Schematics and board of the implementation of the power management and storage part of the sensing nodes based on the use of the Texas Instruments BQ25504 power management unit.

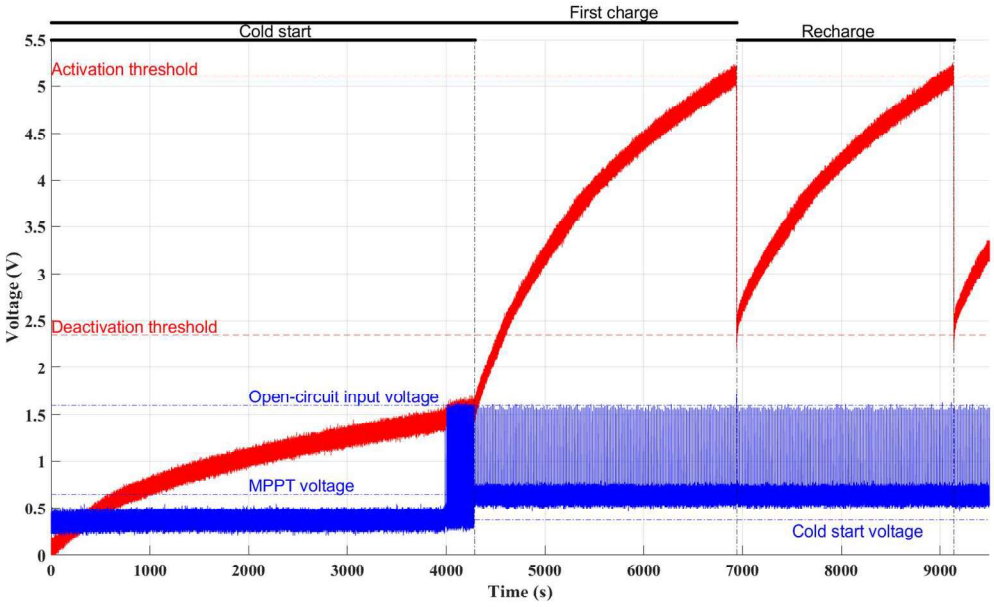

Figure V.28: Voltages, during a cold-start, a complete first recharge and then a recharge, at the input of the Texas Instruments BQ25504 power management unit (blue) and in the energy storage device (red).

tests, or by a rectifier, especially in a rectenna, in order to be used in a radiative electromagnetic wireless power transfer configuration. The proper design of the energy storage device and of the activation and deactivation thresholds ensures that enough energy is stored to correctly power (with a 3.3 V supply voltage and a sufficient current) the active components of the sensing nodes dedicated to the measurement, the data collection, pre-processing and wireless transmission.

To work properly, the power management and storage part of the sensing nodes needs a minimum input power. This one depends of all the components used. In this case, mainly the Texas Instruments BQ25504 power management unit and Texas Instruments TPS63031 DC-to-DC buck/boost converter, as well as the energy storage device (considered below (Section

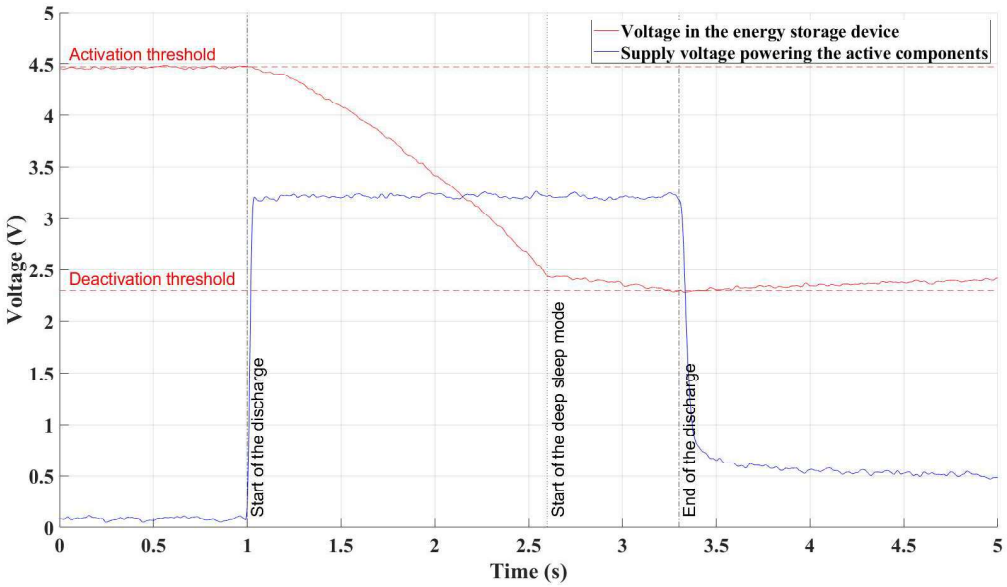

Figure V.29: Voltages, during a discharge, in the energy storage device (red) and at the input of the powered active components (blue).

V.C.2.ii.)) will impose a minimal input power. Thus, the Texas Instruments BQ25504 power management unit requires typically a 15 µW input power during the cold-start and at least 10 µW during the normal charging, whilst the Texas Instruments TPS63031 DC-to-DC buck/boost converter has maximum losses of 4.725 µW in the worst case (disable and with an input power of 5.25 V) and 1.62 µW at the end of the cold-start (with a voltage of 1.8 V). Thus, at least around 14.725 µW are needed at the input of this part to be almost certain that this one will alwayswork properly during the normal charging, and 16.62 µW during the cold-start.

d. Alternatives and perspectives

In the Texas Instruments BQ255xx family, both the BQ25505 and the BQ25570 power management units could be alternatively used with the same behaviour and with similar performances. Nevertheless, at least 15 µW would be needed at the input to be almost certain to obtain a properly work during the cold-start and at least around 5 µW during the normal charging. This gain must be considered for further developments. That says, at least around 9.725 µW are needed at the input of this part to be almost certain that this one will always work properly during the normal charging, and 16.62 µW during the cold-start.

More, the hardware maximal power point tracking (MPPT) system could be characterized with the associated rectenna in order to find the most appropriate input ratio (in other word, the most appropriate input impedance) to optimise as much as possible the efficiency of the direct current power transfer.

For the e-peas AEM30940 power management unit, at least 3 µW would be needed at the input to be almost certain to obtain a properly work during the cold-start and at least -19 dBm (or 12.5 µW) during the normal charging at the input of their rectifier [644]. This power management unit offers a consequent variety of configurations and options. This one seems to

be the most relevant for the project and, at the time of writing, some implementation and characterisation works are already planned or in progress.

For the Powercast power management units, these embed a radiofrequency rectifier and are only designed to be used in a "simultaneous use and store" strategy, and thus, are not configurable. Also, at least -5 dBm (or 316 µW) and -12 dBm (or 63 µW) would be needed at the input to be almost certain to obtain a properly work during the normal use respectively for the P1110B [645] and the P2110B [646] power management unit.

The ultimate way to get the most adapted power management unit (with the lowest minimal input powers both for the cold-start and the normal charging, with fixed and well-defined threshold voltages and protections, with a constant output voltage controlled by internal threshold voltages, etc.) would be the development of a specifically designed ASIC (application specific integrated circuit). Nevertheless, for development purposes, the reconfigurability of the devices is very important, and this solution will only be relevant once the system would be definitively fixed.

ii. The energy storage device

Conjointly designed with the power management unit, the energy device storage must be able to store enough energy, harvested by the rectenna and managed by power management unit, to power all the active components of the sensing nodes during all the time required for their full process: from the measurement to the wireless data transmission.

a. Component choice

As the sensing nodes must have a lifespan of the several decades and require several tens of milli-joules of energy to properly work each time these are powered, the choice fell on the supercapacitors, against the batteries and the capacitors, as introduced above (Section II.D.3.ii.).

In order to implement a battery-free solution, the batteries, even the rechargeable ones, have obviously been discarded. More, the batteries have too large capacitances according to the needs and too limited lifetimes. In the opposite, the capacitor, whose the ceramic ones, have too small capacitances according to the needs. More, the banks of capacitors which could meet the capacitance needs have to important self-discharge currents. Finally, the supercapacitors meet all the requirement with wide range of medium capacitances and theoretical unlimited lifetime. Even considering a number of cycles of 1,000,000, this corresponds to one daily discharge (thus, a full process of the sensing nodes from the measurement to the wireless data transmission) for almost 2,739 years, or an hourly discharge for almost 114 years.

Regarding the technology, the supercapacitors that store the energy in an electrostatic way, such as electric double layer capacitors (EDLC), have been favoured over those that store the energy in an electro-chemical way, such as polarized aluminium electrolytic supercapacitors, in order to have a better ratio between energy density and power density, a longer lifetime, a lower self-discharge current and a lower sensitivity to the environment.

Two families of electric double layer supercapacitors have been studied: the AVX Corporation BestCap family [647] and the KEMET FM0H family [648]. All present a maximal voltage of at least 5.5 V and up to 15 V, which is higher or equal to the maximum one which can be provided by the Texas Instruments power management units, and a wide range of capacitance (whose 10 mF, 22 mF, 47 mF or 50 mF and 100 mF). However, the AVX Corporation BestCap supercapacitors propose generally the lowest self-discharge currents in the interest range, in comparison with KEMET FM0H supercapacitors. To compensate these losses in the worst case (for a voltage of 5.25 V according to the design of the power management unit) an input power of 289 µW, 26 µW, 26 µW and 53 µW respectively for a capacitance of 10 mF, 22 mF, 50 mF and 100 mF must be applied for the AVX Corporation devices, against an input power of 79 µW, 173 µW, 373 µW and 788 µW respectively for a capacitance of 10 mF, 22 mF, 47 mF and 100 mF for the KEMET devices. For the voltage at the end of the cold-start and for a 22 mF AVX Corporation BestCap supercapacitors, this input power is 9 µW.

Thus, for all the capacitances excepted the 10 mF, the AVX Corporation BestCap supercapacitors are chosen.

b. Design and implementation

The choice of the supercapacitor is made in regards of the energy required by the active components of the sensing nodes to achieve a full process (whose the maximum measured values are 208 mJ and 106 mJ, respectively for a +14 dBm and a +4 dBm LoRaWAN frame transmission of the data measured with the thermodiodes) plus a margin to compensate the variability between components and the alterations over time (around 20 %, *i.e.* almost 127 mJ and 250 mJ); and of the design of the power management unit (whose the available range of the activation and deactivation threshold voltages is from 2.2 V to 5.25 V). The achieved implementation is presented in Figure V.27.

By using the Equation V.5, and considering a 10 mF supercapacitor and the extremum activation and deactivation threshold voltages, 114 mJ can be stored; whilst considering a 22 mF supercapacitor in the same configuration, 250 mJ can be stored. Thus, a 10 mF supercapacitor cannot store enough energy for the full process of the sensing node, whilst a 22 mF supercapacitor can, whatever the transmission power. A supercapacitor with a higher capacitance could be used, but regarding the energy stored and unavailable (all the one under the deactivation threshold voltage), respectively of 24 mJ, 53 mJ and 121 mJ, for a 10 mF, a 22 mF and a 50 mF supercapacitor, this is not relevant and even less energy efficient.

Finally, to be more energy efficient, the activation threshold voltage can be tuned and decreased in order to limit the energy uselessly stored. For instance, in the case where 127 mJ are required, the activation threshold voltage can be decreased down to 4.05 V. Even if it is possible, it is less energy efficient to increase the deactivation threshold voltage to limit the energy uselessly stored because this increases the energy stored and unavailable (all the one under the deactivation threshold voltage). More, lowest the maximum voltage in the supercapacitor, lowest the self-discharge currents.

c. Tests and characteristics

The simultaneous use of the supercapacitor with both the energy and data management parts has been successfully tested, as presented in Figure V.28 and Figure V.29. Thus, the supercapacitor driven by the power management unit allows to store enough energy to efficiently power the active components of the sensing nodes for a full process.

According to the energy needs of each sensing node, various configurations of the activation and deactivation thresholds voltages have been implemented, but always with 22 mF supercapacitor. Nevertheless, to work properly over time and for all the configurations, the sensing nodes can require in the worst case up to 250 mJ of energy, which must be stored by the supercapacitor.

In all cases, the power management unit and the supercapacitor must be conjointly designed by considering the needs of the active components of the sensing nodes. In the actual configuration and in the worst case, at least 25.62 µW of input energy would be needed to be almost certain to obtain a properly work of the energy management and storage parts of the sensing nodes during the cold-start, and at least 40.725 µW during the normal charging.

d. Alternatives and perspectives

At the writing time, no off-the-shelf supercapacitor more suitable than the AVX Corporation ones, especially with lower self-discharge current, has been found.

By using the Texas Instruments BQ25505 and BQ25570 power management units, the minimal input power required for the energy management and storage parts of the sensing node could be reduced to 35.725 µW during the normal charging and in the worst case, whilst it stays at 25.62 µW for the cold-start.

iii. The rectenna

The rectenna is used to harvest the radiative electromagnetic power generated and transmitted by the communicating nodes and convert it into direct-current electrical power to power the input of the power management unit. The rectenna is composed of an antenna and of a rectifier circuit, and must provide enough energy to "power" the energy management and storage parts of the sensing nodes (in other words, must compensate the power losses of these parts and provide additional energy to be stored). The useful range of the wireless power transfer system depends on its performances, in particular its efficiency and gain.

a. Design process

As there are no off-the-shelf rectennas, the rectennas used are all designed and implemented by the research team. The presented rectennas are developed as a unique device, that says the rectifier and the antenna are designed together, for the same application. Nevertheless, each element can be used separately, according to the needs of the user.

Here, the rectenna must harvest as much radiative electromagnetic power as possible, in order to allow the energy management and storage part of the sensing nodes to efficiently and sufficiently store this energy to then use it to power the active components composing the data management part. To do this, in the worst case, the rectenna must at least provide 40.725 µW to the power management unit in the normal charging case and 25.62 µW in the cold-start

case. More, this one must be designed and then tuned to work in the targeted frequency band. Thus, the best trade-off between compactness and high RF-to-DC efficiency for low incident power density levels is sought.

Regarding the rectifier, this one must be as efficient as possible to convert as much power collected by the antenna as possible especially for the lowest input power, and provide a sufficient voltage to power management unit to allow it to function both in the cold-start and in the normal charging with the hardware maximum power point tracking system. More, it must be impedance matched with the associated antenna in the targeted frequency band and must be followed by a low pass filter in order to provide a voltage without high-frequency variations, by filtering the fundamental and harmonics.

Regarding the antenna, this one must be chosen to offer the best trade-off between its volume, its gain, its radiation pattern and its polarization. Indeed, to have a low impact in the mechanical properties of the reinforced concrete, the sensing nodes, whose the size depends strongly on the size of the antenna, must be as compact as possible; to have the largest possible range of use in the radiative electromagnetic wireless power transfer, the gain of the antenna must be as high as possible; and to be as independent as possible from the location and orientation of the radiative electromagnetic power source, the radiation pattern must be as isotropic/omnidirectional as possible and the polarisation is preferred circular.

b. Design and implementation

* Software

The Keysight Technologies ADS (Advanced Design System) software has been used to design and simulate the rectifiers, whilst the Ansys Electronics HFFS (High-Frequency Structure Simulator) software has been used to design and simulate the antennas.

* Rectifiers

The first rectifier used (noted Rect3) has been a half-wave rectifier designed for the Rogers Corporation RT/Duroid 5870 substrate (thickness: 0.787 mm; relative permittivity: 2.3; and loss tangent: 0.0012) and optimized to be sufficiently efficient for an input power of -15 dBm (or 31.6 µW) in the industrial scientific and medical 868 MHz frequency band and for a 5 kΩ resistive load. This is based on the use of an Avago Technologies (now Broadcom) HSMS2850 surface mount zero bias Schottky diode, which is mounted in series configuration. A shunt surface mount capacitor is used at its output as a low-pass filter, whilst an impedance matching circuit is used at its input. The matching network is composed of a short-circuited folded stub and a lumped surface mount inductor in order to get a 50 Ω impedance at the input of the full rectifier. It should ensure the maximal power transfer from the antenna to the rectifier. The obtained design and implementation are presented in Figure V.30, and more details can be found in [456, 566-568, 570, 649-652].

Before designing other rectifiers, a theoretical study based on ADS simulations has been achieved in order to compare the Avago Technologies HSMS2850 surface mount Schottky diode [655] and the Skyworks SMS7630 surface mount Schottky diode [656], in various rectifier topologies (series, shunt, doubler), with various impedance matching network

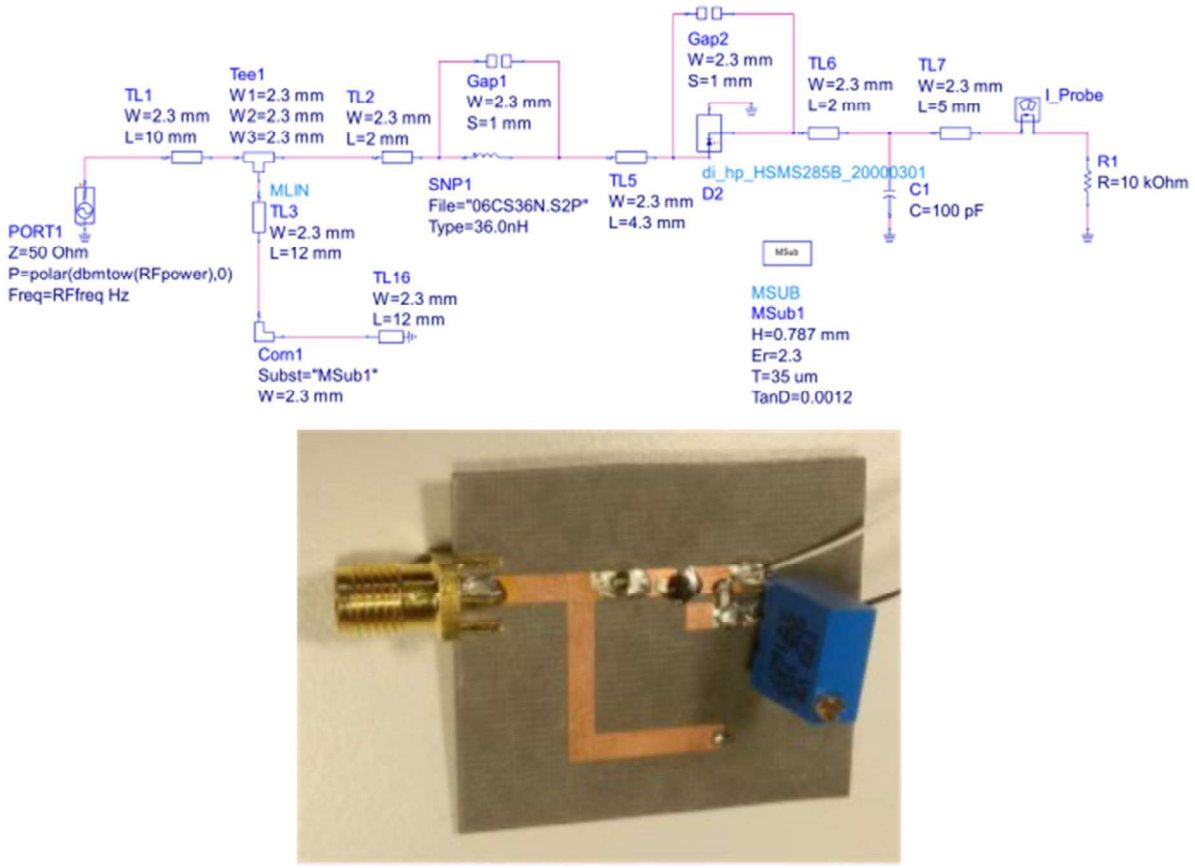

Figure V.30: Schematics and photograph of the designed and implemented half-wave rectifier on Rogers Corporation RT/duroid 5870 substrate.

topologies (lumped, distributed and mixed, in 'L', 'T' and 'π' networks) for the targeted conditions (input power of -15 dBm (or 31.6 µW) in the industrial scientific and medical 868 MHz frequency band). As in all the tested configurations, the Skyworks SMS7630 Schottky diode have been more performant than the Avago Technologies HSMS2850 Schottky diode, this first has been used for the next designs. More, the impedance matching network based on lumped surface mount components have been seen as more performant because easier to tune.

Then, a compact (1 cm x 2 cm) half-wave rectifier (noted Rect2) designed for a FR4 substrate (thickness: 1.6 mm; relative permittivity: 4.4; and loss tangent: 0.02) and optimized to be sufficiently efficient for an input power of -15 dBm (or 31.6 µW) in the industrial scientific and medical 868 MHz frequency band and for a 10 kΩ resistive load, has been designed and implemented. This is based on the use of a Skyworks SMS7630 surface mount Schottky diode (on the SMS7630- 040LF implementation) [656], which is mounted in series configuration. A shunt surface mount capacitor is used at its output as a low-pass filter, whilst an 'L'-topology impedance matching network is used at its input. This last circuit is used in order to ensure the maximal power transfer from the antenna to the diode, and is composed of two lumped surface mount inductors in order to get a 50 Ω impedance at the input of the full rectifier. The obtained design and implementation are presented in Figure V.31, are shortly presented in [571].

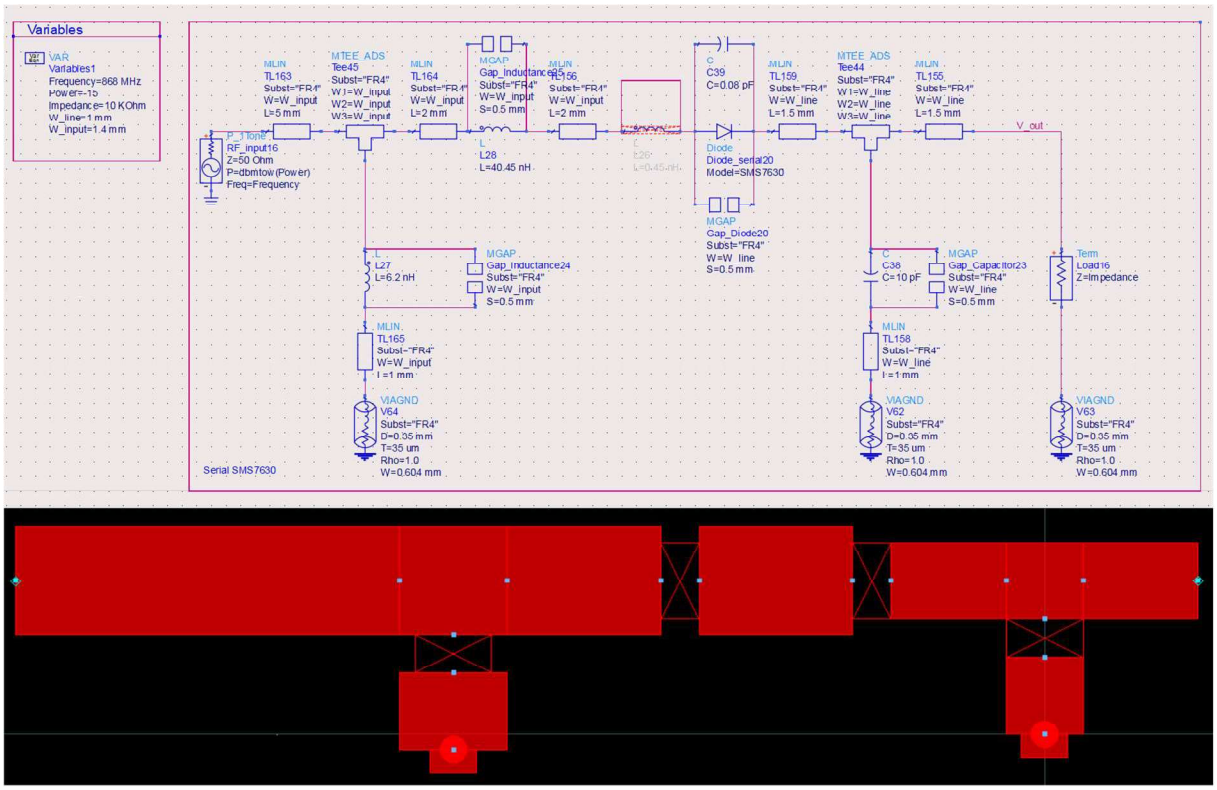

Figure V.31: Schematics and layout of the designed and implemented half-wave rectifier on FR4 substrate.

Finally, a full-wave rectifier (noted Rect1) designed for a FR4 substrate (thickness: 0.8 mm; relative permittivity: 4.4; and loss tangent: 0.01) and optimized to be sufficiently efficient for an input power of -15 dBm (or 31.6 µW) in the industrial scientific and medical 868 MHz frequency band and for a 10 kΩ resistive load, has been designed and implemented. This is based on a microstrip coupled transmission line allowing differential feeding, and on the use of two Skyworks SMS7630 surface mount Schottky diodes (on the SMS7630-005LF implementation) [656], which are mounted in doubler configuration. A shunt surface mount capacitor is used at its output as a low-pass filter, whilst an 'L'-topology impedance matching network is used at its input. This last circuit is used in order to ensure the maximal power transfer from the antenna to the diodes, and is composed of a surface mount inductor and a surface mount capacitor, both lumped, in order to get a 50 Ω impedance at the input of the full rectifier. The obtained design and implementation are presented in Figure V.32, are shortly presented in [573-575, 653].

This last rectifier has finally been adapted to be implemented on a higher FR4 substrate (thickness: 1.6 mm; relative permittivity: 4.4; and loss tangent: 0.02).

* Antennas

Two main families of antennas have been used for the harvesting of the radiative electromagnetic power, both designed to work in the industrial, scientific and medical 868 MHz frequency band (and if possible, in the 915 MHz band too), to provide a 50 Ω input impedance and to offer a good trade-off between volume, gain, radiation pattern and polarization.

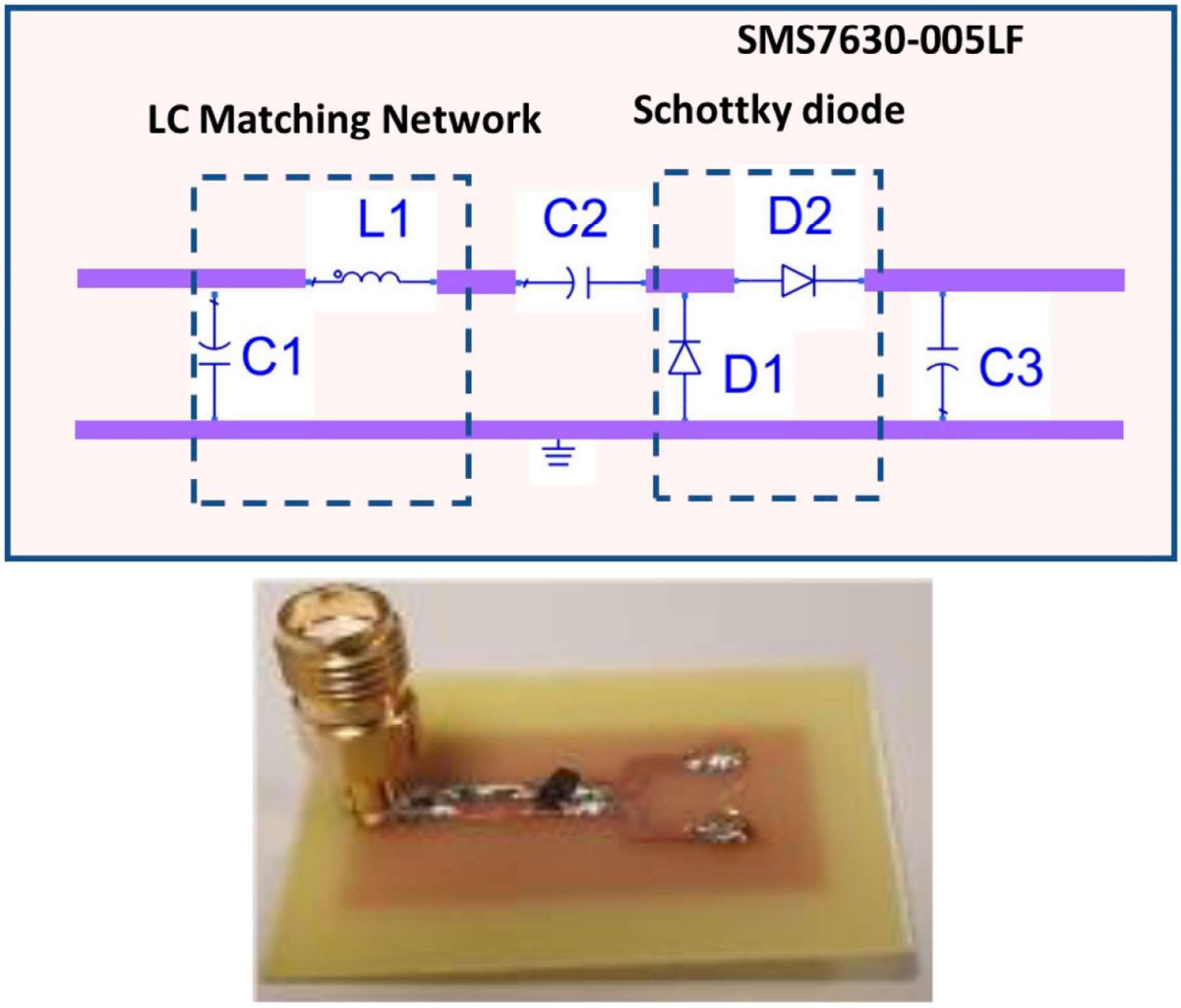

Figure V.32: Schematics and photograph of the designed and implemented full-wave rectifier on 0.8 mm thick FR4 substrate.

The first is a printed rounded quarter-wavelength dipole antenna with resonant rectangular ring. This one has been designed on a FR4 substrate (thickness: 1.6 mm; relative permittivity: 4.4; and loss tangent: 0.01) and measures 11 cm x 6 cm. A quarter-wavelength dipole antenna, whose each monopole have a quasi-circular shape, is used as a base, which allows broadband and almost isotropic behaviour. A rectangular full-wavelength loop encloses the dipole antenna, which induces electromagnetic coupling between the two components and allows the reduction of the size of the antenna at the targeted frequency. The design and optimization processes are more detailed in [456, 566-568, 570, 649-652].

The second is a printed folded quart-wavelength dipole antenna with capacitive arms. This one has been designed on a FR4 substrate (thickness: 0.8 mm; relative permittivity: 4.4; and loss tangent: 0.02) and measures 5.6 cm x 3.2 cm x 1.0 cm. A folded quarter-wavelength dipole antenna with a short-circuited loop, to make a T-match structure, is used as a base, which allows an input impedance matching to 50 Ω, and a narrow-band and almost isotropic behaviour. Metallic arms, orthogonal to the plane of the folded quarter-wavelength dipole antenna, are connected to each monopole which induces a capacitive coupling allowing to reduce the size of the antenna at the targeted frequency. The design and optimization processes are more detailed in [572-575, 653].

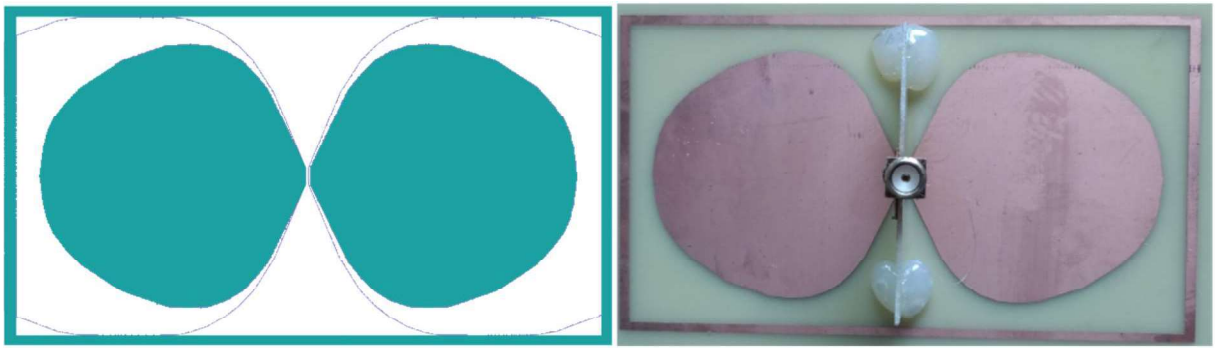

Figure V.33: Diagram and photograph of the designed and implemented printed rounded quart-wavelength dipole antenna with resonant rectangular ring at 868 MHz.

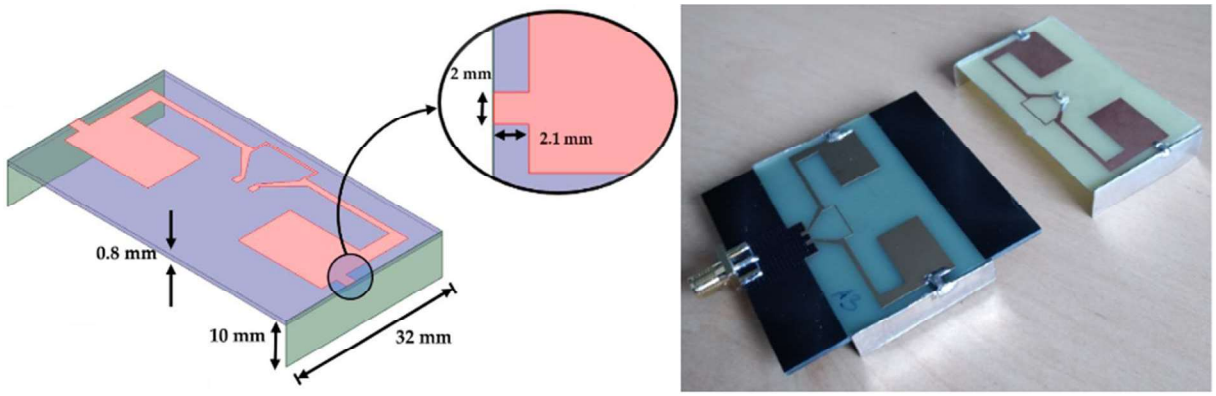

Figure V.34: Diagram and photograph of the designed and implemented printed folded quart-wavelength dipole antenna with capacitive arms at 868 MHz, on a 1.6 mm (black) and 0.8 mm (yellow) FR4 substrate.

This last antenna has finally been adapted to be implemented on a higher FR4 substrate (thickness: 1.6 mm; relative permittivity: 4.4; and loss tangent: 0.01).

For the two antennas, the use of metallic reflector has been studied. By this way, the gain can be increased up to be almost double, at the cost of the modification of the radiation pattern whose a half is deleted (and thus, the directivity is increased) (the "bottom" side of the radiation pattern is translated and added to the "front" side) and at the cost of the rise of the volume. Thus, a 14 cm x 9 cm metallic reflector plane, located at 6 cm, has been added to the two antennas for additional tests, as well as an 8 cm x 6 cm one, located at 5 cm, for the last antenna.

* Rectenna

From the three presented rectifiers and the two presented antennas, two combinations have been chosen to implement different types of rectennas. Thus, there are two main types of rectennas which have been used for the prototypes of the sensing nodes. The first is well detailed in [456, 566-568, 570, 649-652], whilst the second in [571-575, 653].

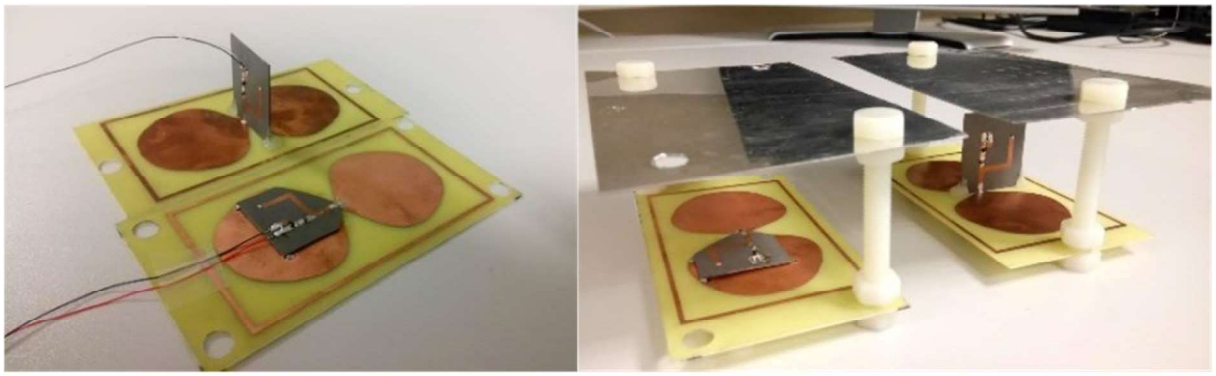

Figure V.35: Photograph of the printed rounded quarter-wavelength dipole rectenna with resonant rectangular ring at 868 MHz, in the three-dimensional and coplanar implementation, with and without the use of a metallic reflector plane.

The first is composed of the printed rounded quarter-wavelength dipole antenna with resonant rectangular ring and of the half-wave rectifier designed for the Rogers Corporation RT/Duroid 5870 substrate. The implementations of this rectenna have been achieved in a three-dimensional way [566, 650]: the rectifier is orthogonally connected to the antenna; and in a planar way [567, 652]: the rectifier is overlap connected to the antenna. Once again, the use of a 14 cm x 9 cm metallic reflector plane, located at 6 cm, has been studied [567, 568, 570].

The second is composed of the printed folded quart-wavelength dipole antenna with capacitive arms and of the full-wave rectifier designed for a FR4 substrate. The implementations of this rectenna have been achieved by adding on the same substrate the antenna and the rectifier. Here too, the use of a 14 cm x 9 cm metallic reflector plane, located at 6 cm, and another of 8 cm x 6 cm, located at 5 cm, has been studied [571, 574, 575, 652], as well as the use of a 15 cm x 15 cm x 15 cm metallic cavity with a unique open face [572, 573].

c. Tests and characteristics

* Rectifier

The designed and implemented rectifiers have been characterized in the industrial, scientific and medical 868 MHz frequency band and especially at 868 MHz, which is within not necessarily the frequency of their optimum use, and for an input power of -15 dBm (or 31.6 µW). Some of their characteristics are summarized in Table V.4.

The rectifier Rect3, optimized for a 5 kΩ resistive load, has a reflection coefficient (noted S11) of -12 dB at the input port, a nearly 330 mV output voltage, an almost 35 % efficiency (noted ηrectifier, defined as the ratio between the output power on the input power), that says an output power of nearly 11 µW for a -15 dBm (or 31.6 µW) input, and has a 30 MHz bandwidth.

The rectifier Rect2, optimized for a 10 kΩ resistive load, has a reflection coefficient (noted S11) of -28.1 dB at the input port, a nearly 353 mV output voltage, an almost 39 % efficiency (noted ηrectifier, defined as the ratio between the output power on the input power), that says an output power of nearly 12.5 µW for a -15 dBm (or 31.6 µW) input, and has a 36 MHz bandwidth.

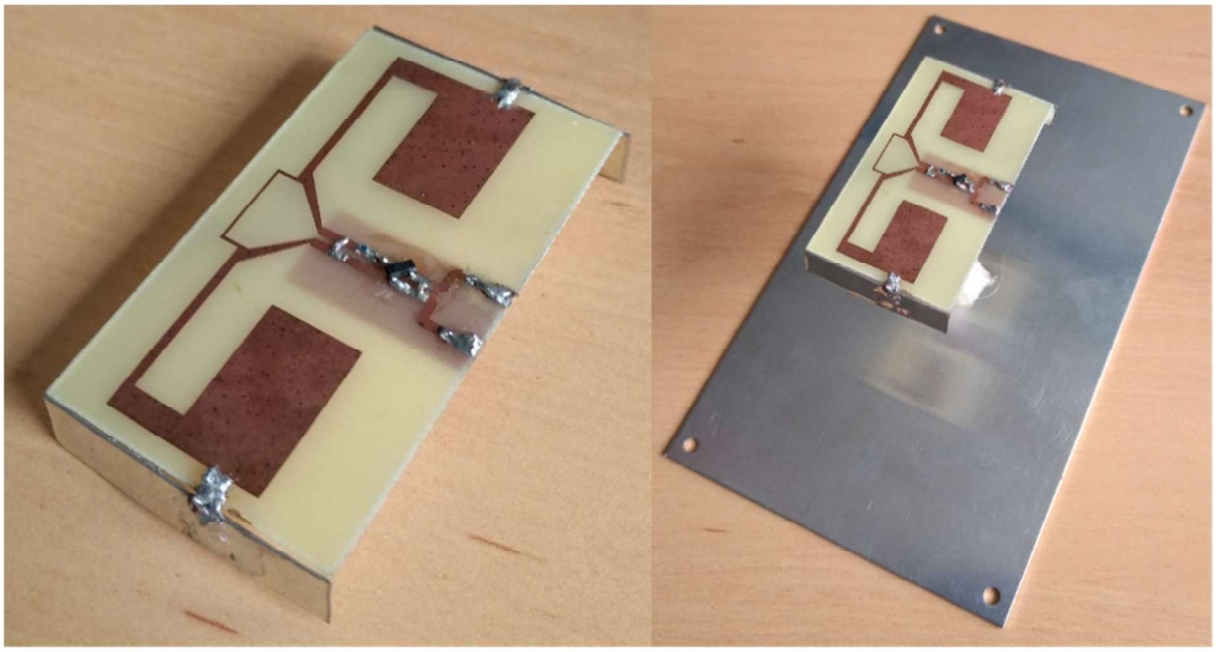

Figure V.36: Photograph of the folded quart-wavelength dipole rectenna with capacitive arms at 868 MHz, with and without the use of a metallic reflector plane.

The rectifier Rect1, optimized for a 10 kΩ resistive load, has a reflection coefficient (noted S_{11}) of -19 dB at the input port, a nearly 330 mV output voltage, an almost 35 % efficiency (noted $\eta_{rectifier}$, defined as the ratio between the output power on the input power), that says an output power of nearly 11 µW for a -15 dBm (or 31.6 µW) input, and has a 60 MHz bandwidth.

Even if the rectifiers Rect3 and Rect1 have similar characteristics at 868 MHz and with an input power of -15 dBm (or 31.6 µW), these have not been designed for the same load. Thus, by using a more complex load (e.g. a power management unit) these characteristics will no more be relevant and differences may occur.

Table V.4: Summary of the measured characteristics of the rectifiers used.

Rectifier	Rect1	Rect2	Rect3
Frequency used during the characterization (MHz)	868	868	868
Measured bandwidth * (MHz)	60	36	30
Typical RF input power (dBm)	-15	-15	-15
Charge used (kΩ)	10	10	5
Measured reflection coefficient * (dB)	-19	-28.1	-12
Measured output voltage for the defined input power and charge * (mV)	330	353	330
Computed efficiency for the defined input power and charge * (%)	35	39	35

* Experimental results obtained for the typical RF input power (-15 dBm) and the specified load.

* Antenna

Some characteristics of the designed and used antennas are summarized in Table V.5.

The printed rounded quarter-wavelength dipole antenna with resonant rectangular ring is an almost omnidirectional antenna with a linear polarization, usable between 850 MHz and 910 MHz, with a measured gain of +2.64 dBi at 868 MHz and with a measured -3 dB beamwidth of 80 ° in the E-plane and of 120 ° in the H-plane. By adding a 14 cm x 9 cm reflector plane at 6 cm from it, the measured gain is increased up to +6.80 dBi at the cost of the increase of the directionality and the rise of the volume.

The printed folded quart-wavelength dipole antenna with capacitive arms is an almost omnidirectional antenna with a linear polarization, usable between 848 MHz and 886 MHz, with a measured gain of +1.54 dBi at 868 MHz and with a measured -3 dB beamwidth of 110 ° in the E-plane. By adding an 8 cm x 6 cm reflector plane at 5 cm from it, the measured gain is increased up to +5.00 dBi at the cost of the increase of the directionality and the rise of the volume. The measured -3 dB beamwidth is then 70 ° in the E-plane.

* Rectenna

All the rectenna have been characterized with a 10 kΩ resistive load at 868 MHz. Their efficiency (noted $\eta_{rectenna}$) is computed thanks to the Equation V.6, with the measured output DC power of the rectenna (noted P_{DC}) and the estimated input radiative electromagnetic (or radiofrequency) power of the rectenna (noted P_{RF}), which can be expressed as the product of the incident electromagnetic power density (noted S) by the effective area of the antenna (noted A_{eff}).

$$\eta_{rectenna} = \frac{P_{DC}}{P_{RF}} = \frac{P_{DC}}{S \cdot A_{eff}} \qquad \text{(Equation V.6)}$$

The incident electromagnetic power density (noted S) can be estimated thanks to the Equation V.8, in function of the effective electric field (noted E), itself estimated by the Equation V.7 and function of the power generated by the radiative electromagnetic source (noted P_{TX}), the gain of the antenna used by the radiative electromagnetic source (noted G_{TX}), and the distance between the radiative electromagnetic source and the rectenna (noted d).

$$E = \frac{\sqrt{30 \cdot P_{TX} \cdot G_{TX}}}{d} \ (V \cdot m^{-1}) \qquad \text{(Equation V.7)}$$

$$S = \frac{E^2}{120 \cdot \pi} = \frac{30 \cdot P_{TX} \cdot G_{TX}}{120 \cdot \pi \cdot d^2} = \frac{P_{TX} \cdot G_{TX}}{4 \cdot \pi \cdot d^2} (W \cdot m^{-2}) \qquad \text{(Equation V.8)}$$

The effective area of the antenna (noted A_{eff}) can be estimated thanks to the Equation V.9, in function of the gain of the antenna used by the rectenna (noted G_{RX}) and the wavelength (noted λ).

$$A_{eff} = G_{RX} \cdot \frac{\lambda^2}{4 \cdot \pi} (m^2) \qquad \text{(Equation V.9)}$$

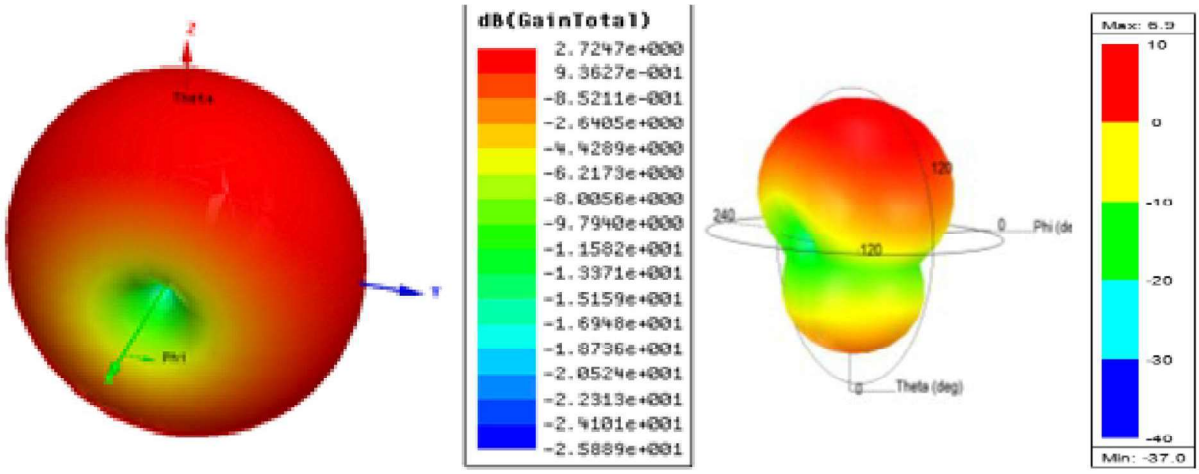

Figure V.37: Simulated (HFSS) radiation patterns of the printed rounded quarter-wavelength dipole antenna with resonant rectangular ring at 868 MHz, with and without the use of a metallic reflector plane.

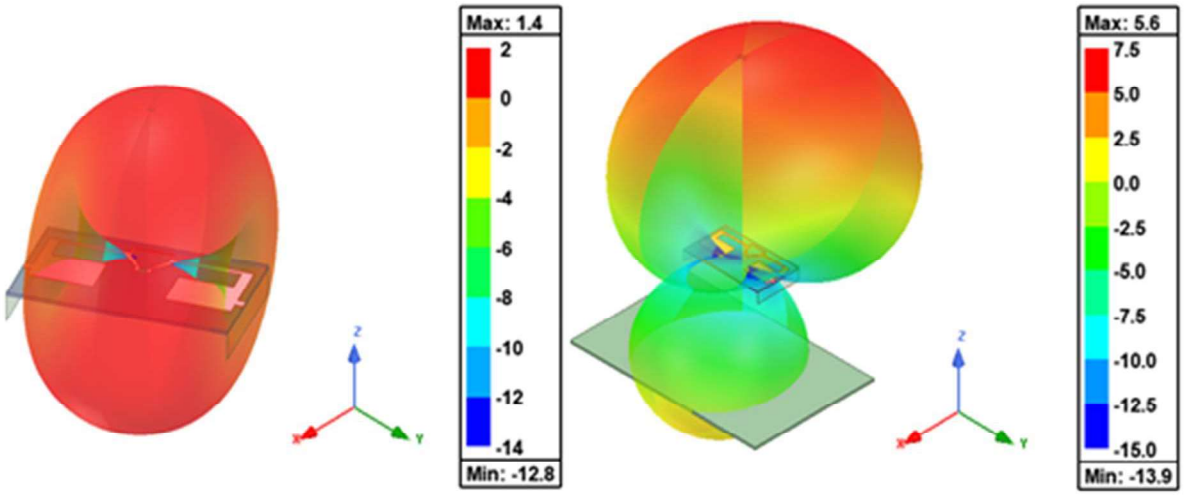

Figure V.38: Simulated (HFSS) radiation patterns of the printed folded quart-wavelength dipole antenna with capacitive arms at 868 MHz, with and without the use of a metallic reflector plane.

Thus, the input radiative electromagnetic (or radiofrequency) power of the rectenna (noted P_{RF}) can be estimated through the Equation V.10.

$$P_{RF} = S \cdot A_{eff} = \frac{P_{TX} \cdot G_{TX} \cdot G_{RX} \cdot \lambda^2}{4 \cdot \pi \cdot d^2 \cdot 4 \cdot \pi} = \frac{P_{TX} \cdot G_{TX} \cdot G_{RX} \cdot \lambda^2}{16 \cdot \pi^2 \cdot d^2} \ (W) \qquad \text{(Equation V.10)}$$

From these equations, the efficiency can be finally computed thanks to the Equation V.11.

$$\eta_{rectenna} = \frac{P_{DC}}{P_{RF}} = \frac{P_{DC}}{S \cdot A_{eff}} = \frac{16 \cdot \pi^2 \cdot d^2}{P_{TX} \cdot G_{TX} \cdot G_{RX} \cdot \lambda^2} \cdot P_{DC} \qquad \text{(Equation V.11)}$$

Table V.5: Summary of the simulated characteristics of the antennas designed.

Antenna	Printed rounded quarter-wavelength dipole antenna with resonant rectangular ring	Printed rounded quarter-wavelength dipole antenna with resonant rectangular ring with reflector plane	Printed folded quart-wavelength dipole antenna with capacitive arms	Printed folded quart-wavelength dipole antenna with capacitive arms and reflector plane
Main frequency band * (MHz)	850 to 910	850 to 910	848 to 886	848 to 886
Maximum gain at 868 MHz (dBi)	+2.64	+ 6.8	+1.54	+5
Volume (cm^3) / Size (mm x mm x mm)	≈ 198 / 110 x 60 x 30	≈ 756 / 140 x 90 x 60	≈ 17.92 / 56 x 32 x 10	≈ 240 / 80 x 60 x 50
Input impedance (Ω)	50	50	50	50
Radiation pattern	Almost omni-directional	Almost semi-omni-directional	Almost omni-directional	Almost semi-omni-directional
Polarization	Linear	Linear	Linear	Linear

* Defined for a reflection coefficient of -10 dB.

First, the different implementations of the printed rounded quarter-wavelength dipole rectenna with resonant rectangular ring, based on a half-wave rectifier, have been compared, especially in [456, 570, 568, 649, 651]. This comparison concerns both the coplanar and the orthogonal implementations, and these two with and without a reflector plane, as presented in Figure V.39 and Figure V.40.

According to the Figure V.39, the two tested topologies (coplanar and orthogonal) provide a sufficient voltage to the load (higher than the minimal required by the power management unit, even if the two loads are not similar) in an interesting bandwidth around 868 MHz (even if it is not the frequency allowing the highest voltage), both for low and medium power densities. By using the reflector plane, the voltages are still increased. According to the Figure V.40 and at 868 MHz, the orthogonal topology seems more efficient than the coplanar one without the reflector but it is the opposite with the reflector plane. This is coherent with the Figure V.39, where the orthogonal topology provides higher voltages than the coplanar one without the reflector plane, but the opposite with the reflector plan, at 868 MHz. Thus, the orthogonal topology seems to be more performant than the coplanar one for a bandwidth around 868 MHz, with and without using the reflector plane, but not precisely for the 868 MHz frequency with the reflector plane. Finally, even if the reflector plane allows to harvest more power, the efficiency of the rectenna is lower with it.

Second, the printed folded quart-wavelength dipole rectenna with capacitive arms, based on a full-wave rectifier, with and without using a reflector plane, has been characterized as presented in Figure V.41 and Figure V.42.

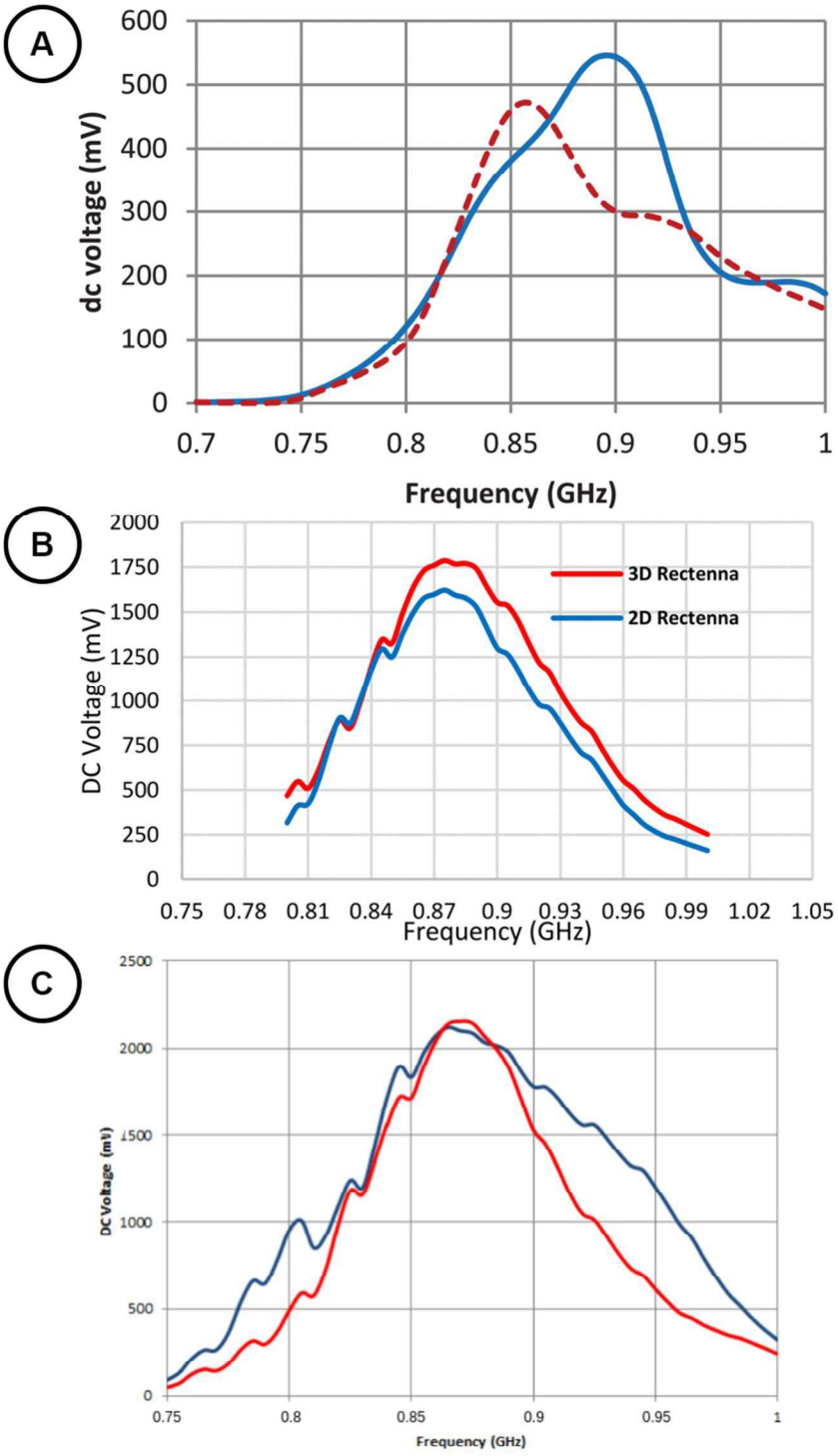

Figure V.39: Measured output DC voltage against frequency for the printed rounded quarter-wavelength dipole rectenna with resonant rectangular ring (A) without the use of a reflector plane for low power densities (between 0.46 $\mu W \cdot cm^{-2}$ and 0.54 $\mu W \cdot cm^{-2}$ according the frequency) for the orthogonal implementation (blue) and for the coplanar implementation (red); (B) without the use of a reflector plane for medium power densities (between 2.8 $\mu W \cdot cm^{-2}$ and 4.46 $\mu W \cdot cm^{-2}$ according to the frequency) for the orthogonal implementation (red) and for the coplanar implementation (blue); and (C) with the use of a reflector plane for an input power of +0 dBm (or 1 mW) both for the orthogonal implementation (blue) and for the coplanar implementation (red), for a 10 kΩ resistive load.

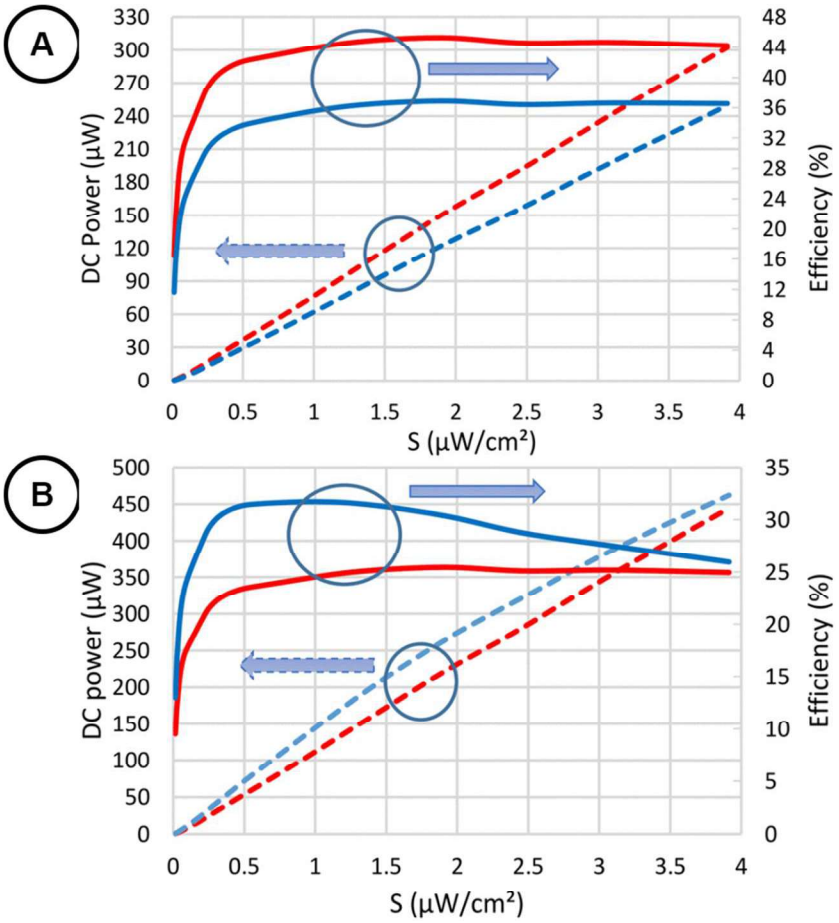

Figure V.40: Measured output DC power and computed efficiency against power densities for the printed rounded quarter-wavelength dipole rectenna with resonant rectangular ring in the coplanar (blue) and orthogonal (red) configuration (A) without and (B) with the use of a reflector p lane, at 868 MHz and for a 10 kΩ resistive load.

According to the Figure V.41, the tested rectenna provides a sufficient voltage to the load (higher than the minimal required by the power management unit, even if the two loads are not similar) in an interesting bandwidth around 868 MHz (even if it is not the frequency allowing the highest voltage), for medium power densities. By using the reflector plane, the voltages are still increased without a significant frequency shift. According to the Figure V.42 and at 868 MHz, the rectenna with reflector is more efficient than without for power densities below 2 $\mu W \cdot cm^{-2}$, but is less efficient above. More, a sufficient voltage can be provided to the load (higher than the minimal required by the power management unit, even if the two loads are not similar) for power densities from around 0.1 $\mu W \cdot cm^{-2}$.

Some characteristics of the designed and used rectennas are summarized in Table V.6.

To compare the two rectennas, the printed folded quart-wavelength dipole rectenna with capacitive arms provides higher voltages for the frequency band around 868 MHz, with and without using the reflector plane, than the printed rounded quarter-wavelength dipole rectenna with resonant rectangular ring, with and without using the reflector plane. Regarding the efficiency at 868 MHz with a 10 kΩ resistive load, the printed folded quart-wavelength dipole

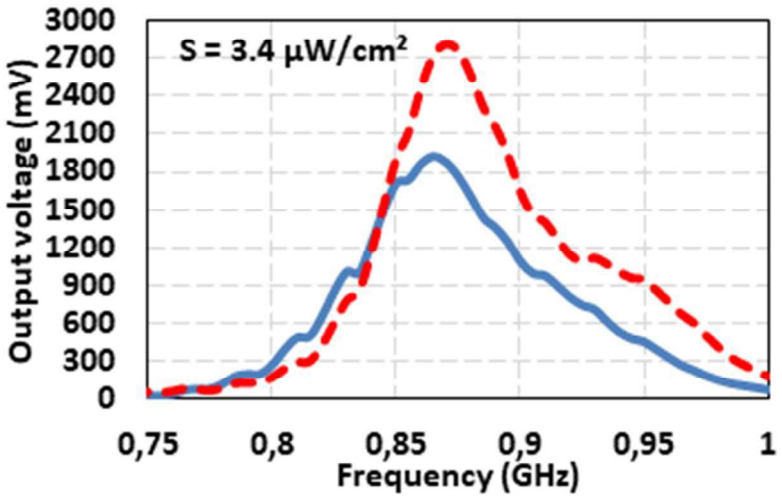

Figure V.41: Measured output DC voltage against frequency for the printed folded quart-wavelength dipole rectenna with capacitive arms without (blue) and with (red) the use of a reflector plane for power densities of 3.4 µW·cm^{-2} (at 868 MHz, but varying around), for a 10 kΩ resistive load.

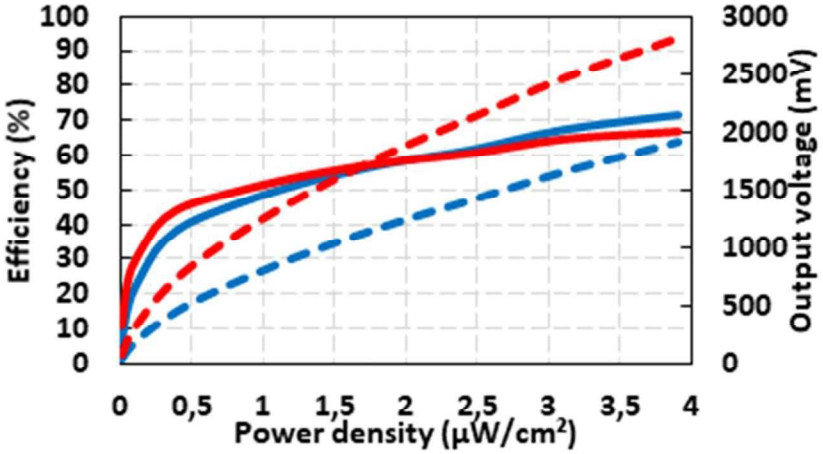

Figure V.42: Computed efficiency (full lines) and measured output DC voltage (dashed lines) against power densities for the printed folded quart-wavelength dipole rectenna with capacitive arms without (blue) and with (red) the use of a reflector plane, at 868 MHz and for a 10 kΩ resistive load.

rectenna with capacitive arms provides higher efficiency for all the power densities, with and without using the reflector plane, than the printed rounded quarter-wavelength dipole rectenna with resonant rectangular ring, with and without using the reflector plane. Thus, despite a lower gain, the printed folded quart-wavelength dipole rectenna with capacitive arms has been privileged to the printed rounded quarter-wavelength dipole rectenna with resonant rectangular ring thanks to its smaller volume, its ability to provide higher voltages and its higher efficiency.

Table V.6: Summary of the measured characteristics of the rectennas used at 868 MHz with a 10 kΩ resistive load.

Rectenna	1	2	3	4	5	6
Antenna	Printed rounded quarter-wavelength dipole antenna with resonant rectangular ring	Printed rounded quarter-wavelength dipole antenna with resonant rectangular ring	Printed rounded quarter-wavelength dipole antenna with resonant rectangular ring with reflector plane	Printed rounded quarter-wavelength dipole antenna with resonant rectangular ring with reflector plane	Printed folded quart-wavelength dipole antenna with capacitive arms	Printed folded quart-wavelength dipole antenna with capacitive arms and reflector plane
Rectifier	Rect3	Rect3	Rect3	Rect3	Rect1	Rect1
Topology	Coplanar	Orthogonal	Coplanar	Orthogonal	Coplanar	Coplanar
Maximum output voltage (mV)	1581 for a 3.9 µW·cm^{-2} power density	1746 for a 3.9 µW·cm^{-2} power density	2145 for a 3.9 µW·cm^{-2} power density	2110 for a 3.9 µW·cm^{-2} power density	1918 for a 3.9 µW·cm^{-2} power density	3799 for a 3.9 µW·cm^{-2} power density
Maximum efficiency (%)	37.0 for a 2 µW·cm^{-2} power density	45.0 for a power density between 0.5 and 1.5 µW·cm^{-2}	32.0 for a 2.0 µW·cm^{-2} power density	25.5 for a 2.0 µW·cm^{-2} power density	71.7 for a 3.9 µW·cm^{-2} power density	66.6 for a 3.9 µW·cm^{-2} power density
Estimated output voltage for a 0.1 µW·cm^{-2} power density (mV)	264	272	474	387	194	292
Efficiency for a 0.1 µW·cm^{-2} power density (mV)	25.5	32.5	25.0	18.0	21.1	28.9
Output voltage for a 3.9 µW·cm^{-2} power density (mV)	1581	1746	2145	2110	1918	3799
Efficiency for a 3.9 µW·cm^{-2} power density (mV)	36.5	44.0	26.0	25.0	71.7	66.6

By using a model of the rectenna efficiency against power densities (noted $\eta_{rectenna}(S)$, based on the measured results presented in Figure V.42, and approximated by a logarithmic function for the low power densities (best correlation)), it has been possible to compute an estimation of the minimal power density required to "power" the energy management and storage part of the sensing nodes in the worst use case; both for the normal charging and the cold-start (respectively requiring 40.725 µW and 25.62 µW, noted P_{DC_min}); by considering the printed folded quart-wavelength dipole rectenna with capacitive arms, with and without

using the reflector plane (respectively with G_{RX} = +1.54 dBi and G_{RX} = +5.00 dBi); and for a +33 dBm (or 2W) radiative electromagnetic power source at 868 MHz ($P_{TX} \cdot G_{TX}$ = +33 dBm); by solving the problem modelled by the Equation V.12.

$$S \cdot \eta_{rectenna}(S) = \frac{P_{DC\_min}}{A_{eff}} = \frac{P_{DC\_min} \cdot 4 \cdot \pi}{G_{RX} \cdot \lambda^2} \quad \text{(Equation V.12)}$$

From this value (noted $S_{computed}$), it has been possible to estimate the maximum range of use of the wireless power transfer system, in the air, in the same configuration and always for the worst case, by using the Equation V.13.

$$d = \sqrt{\frac{\eta_{rectenna}(S_{computed}) \cdot P_{TX} \cdot G_{TX} \cdot G_{RX} \cdot \lambda^2}{16 \cdot \pi^2 \cdot P_{DC\_min}}} \quad \text{(Equation V.13)}$$

Thus, the rectenna without the reflector plane could work from a power density of 0.462 $\mu W \cdot cm^{-2}$ (for -12.04 dBm or 62.6 µW harvested) for the cold-start and from 0.667 $\mu W \cdot cm^{-2}$ (for -10.45 dBm or 90.2 µW harvested) for the normal charging, whilst the rectenna with the reflector plane could work from a power density of 0.228 $\mu W \cdot cm^{-2}$ (for -11.64 dBm or 68.5 µW harvested) for the cold-start and from 0.331 $\mu W \cdot cm^{-2}$ (for -10.03 dBm or 99.2 µW harvested) for the normal charging. This corresponds for a maximum range between a communicating node and a sensing node of respectively 5.86 m, 4.88 m, 8.34 m and 6.93 m. These are obviously only very simplified theoretical estimations considering only the unique path through the direct line of sight (no multipath propagation, nor interferences), and for a 10 kΩ resistive load. In the case of the targeted load (the energy management and storage part of the sensing nodes), because of a variation of its input impedance and more generally of its properties (function of the input and the outputs, such as the voltage in the energy storage device), it is not feasible to obtain in a simple way the efficiency against power densities measurement for the rectennas.

d. Alternatives and perspectives

* Rectifier

As shortly introduced above (Section II.D.2.V.), there are a lot of rectifiers recorded in the academic literature, and very few commercial solutions (PowerCast is the only company found which proposes two industrial complete radiofrequency rectifiers [423]). Nevertheless, each rectifier is designed with very specific targeted performances: central frequency, bandwidth, input impedance (related to the targeted antenna), input impedance (related to the targeted load), size, minimum and typical range input powers, etc. and more generally the targeted application (energy harvesting against wireless power transfer, "store then use" strategy against "simultaneous use and store" strategy, etc.).

At the same time, the rectifying element (e.g. diode, Schottky diode, tunnel diode, metal-insulator-metal diode, spin-diode, complementary metal oxide semi-conductor (CMOS) transistor, etc.), the topology of the rectifier (e.g. shunt, in series, doubler, Dickson charge pump, etc.) and its associated components (e.g. low pass filter, etc.), and the impedance matching network (e.g. the topology ('L', 'T', 'π', etc.), the components (e.g. lumped, distributed, etc.), the size, etc.) can be optimized for meet the targeted performances.

The design and implementation of new rectifiers dedicated to the targeted application are always under investigations. These must be designed to work in the industrial, scientific and medical 868 MHz frequency band and in particular at 868 MHz, to provide a sufficient high output voltage to a power management unit, and to be as efficient as possible for a range of input power from below -15 dBm (or 31.6 µW) to above +0 dBm (or 1 mW), as well as to be compact and to have a 50 Ω input impedance.

* Antenna

As also introduced above (Section II.D.2.V.), there are a lot of antennas provided both by academics and companies. Nevertheless, each antenna is designed with very specific targeted performances: type (e.g. patch, dipole, etc. and array), frequency bands (e.g. single band, dual-band or multiband), central frequency(ies), bandwidth(s) (e.g. narrow-band or wideband), gain(s), radiation pattern(s), polarization (e.g. linear, circular, elliptic, etc.), input impedance (related to the targeted load), size, etc.

The Table V.7 summarizes all the antenna used in the framework of the McBIM project. In order to get the best trade-off between compactness and performances in terms of gain and diagram pattern, the printed folded quart-wavelength dipole antenna with capacitive arms has been privileged to the printed rounded quarter-wavelength dipole rectenna with resonant rectangular ring. The used reflector plan has also been reduced. Even if the printed meandered monopole seems to have equivalent or even better characteristics than the printed folded quart-wavelength dipole antenna with capacitive arms, these have been obtained in optimal conditions, especially with a very large ground plan, and thus, it seems unrealistic to get a same behaviour by integrating it in the sensing nodes.

In order to minimize the volume of the sensing nodes, the use of a unique antenna both for the wireless power transfer and the wireless communication has been investigated through the use of a radiofrequency circulator. More, the printed circuit board developed for the electronic has been used as a reflector plan in a coplanar way in order to increase the gain of the antenna dedicated to the wireless power transfer. These two aspects are detailed below (Section V.D.1.).

Moreover, first designs of printed folded quart-wavelength dipole antenna with capacitive arms on a flexible substrate (Kapton) have been carried out, and even if some manufacturing problems have been highlighted, the preliminary results are encouraging.

The design and implementation of new antennas dedicated to the targeted application are always under investigations. These must be designed to work in the industrial, scientific and medical 868 MHz frequency band and in particular at 868 MHz, to be compact, to have an almost isotropic radiation pattern, to have a high gain, to have a 50 Ω input impedance, and if possible to have a circular polarization.

Finally, the used antennas have been successfully tested into a reinforced concrete beam, both for the wireless power transfer and the wireless communication. Nevertheless, the current sensing nodes are not in a direct contact with the reinforced concrete (there is an air gap in the cavity). And, it is very probable that an impedance mismatch occurs when the antenna will be directly buried into the reinforced concrete. Thus, new designs could be provided by considering the reinforced concrete as the main propagation medium and in a direct contact with the antenna.

Table V.7: Comparison of the antennas used in the McBIM project both for the wireless communication and the wireless power transfer.

Antenna	RF Solutions ANT8WHIP3H whip antenna [590]	LPSR ANTSS900 compressed whip antenna [621]	Printed meandered monopole [622]	Printed rounded quarter-wavelength dipole antenna with resonant rectangular ring	Printed rounded quarter-wavelength dipole antenna with resonant rectangular ring with reflector plane	Printed folded quart-wavelength dipole antenna with capacitive arms	Printed folded quart-wavelength dipole antenna with capacitive arms and reflector plane
Initial use	Wireless communication	Wireless communication	Wireless communication	Wireless power transfer	Wireless power transfer	Wireless power transfer	Wireless power transfer
Main frequency band	868 MHz	868 MHz - 915 MHz	825 to 913 MHz	850 to 910 MHz	850 to 910 MHz	848 to 886 MHz	848 to 886 MHz
Gain at 868 MHz	+3 dBi	+2 dBi	+ 5.05 dBi	+2.64 dBi	+ 6.8 dBi	+1.54 dBi	+5 dBi
Volume / Size	≈ 31.87 cm^3 / ⌀ 14 mm x 207 mm	≈ 2.56 cm^3 / ⌀ 8 mm x 51 mm	≈ 1.52 cm^3 / 38 mm x 25 mm x 1.6 mm	≈ 198 cm^3 / 110 mm x 60 mm x 30 mm	≈ 756 cm^3 / 140 mm x 90 mm x 60 mm	≈ 17.92 cm^3 / 56 mm x 32 mm x 10 mm	≈ 240 cm^3 / 80 mm x 60 mm x 50 mm
Input impedance	50 Ω	50 Ω	50 Ω	50 Ω	50 Ω	50 Ω	50 Ω
Radiation pattern	Almost omni-directional	Almost omni-directional	Almost omni-directional	Almost omni-directional	Almost semi-omni-directional	Almost omni-directional	Almost semi-omni-directional
Polarization	Linear	Linear	Linear	Linear	Linear	Linear	Linear

* Rectenna

There are a lot of rectennas presented in the academic literature, and no commercially available. Each is designed for a specific application and is not necessary reusable for another. As it is a combination of a rectifier and an antenna, all the relevant characteristics of each must be considered: antenna type, frequency band(s) covered by the two components with their central frequencies and bandwidths, radiation pattern with gain and polarization, input impedance, size, minimum and typical range input powers, etc., always according to the targeted application. The rectenna can be designed as a pure combination of two elements or as a unique component. In the two cases, the impedance matching must be achieved.

In spite of a lower gain, the printed folded quart-wavelength dipole rectenna with capacitive arms has been privileged to the printed rounded quarter-wavelength dipole rectenna with resonant rectangular ring thanks to its smaller volume, its ability to provide higher voltages and its higher efficiency, especially for low power densities.

Finally, the design and implementation of new rectennas, with rectifiers and antennas conjointly designed, dedicated to the targeted application are always under investigations. These must be designed to work in the industrial, scientific and medical 868 MHz frequency

band and in particular at 868 MHz, to provide a sufficient high output voltage to a power management unit, and to be as efficient as possible for a range of input power from below -15 dBm (or 31.6 µW) to above +0 dBm (or 1 mW), as well as to be compact, to have a high gain and an almost isotropic radiation pattern and if possible a circular polarization.

3. Alternatives and perspectives

As explained all along this subsection, each element of the energy harvesting and management part of the sensing nodes could be optimized, but these optimizations must consider all the other components of the sensing nodes: the active components to power and the components which allow the energy harvesting and management.

An easy way, with few configuration changes, to provide a more efficiency energy harvesting and management system, is to use the Texas Instruments BQ25505 or BQ25570 power management units. In this way 5 µW are saved in the worst case for a normal charging. By using the e-peas AEM30940 power management unit, a non-negligible gain could be achieved in the required input energy to do work properly the system. More, e-peas provides under non-disclosure agreement signature the designs of a matching network and a rectifier to their customers. Their test and a comparison with state-of-the-art solutions could be relevant.

Regarding the supercapacitor itself, the study of new off-the-shelf alternatives is pursued.

For the rectenna, only the design of new components could allow the gain in terms of targeted performances.

In fact, this is the reduction of the energy required by the active components which could have the highest impact on the performances of the energy harvesting and management part. By reducing the required energy, the capacitance of the supercapacitor could be reduced and the use of a bank of capacitors could be considered, and/or the activation threshold of the power management unit could be decreased, this reduces the maximum losses of the supercapacitor. These could allow a reduction of the required energy in the worst case, which could induce a use with lower power densities, and thus, on a wider range. Moreover, lower the required energy, faster the charging time, and for equivalent power losses, lower the energy losses.

To reduce the energy consumption of the active components of the sensing nodes, these must be chosen with attention. And, their hardware and software implementations must be optimized. Finally, it could be relevant to implement a power shaft which could allow to power the active component only when required: currently the sensor, the microcontroller unit and maybe the LoRaWAN transceiver are powered during all the time of the process, but once the measurement performed the sensor could be powered off, as well as the microcontroller once the LoRaWAN frame transmitted to the transceiver. In addition to reducing the energy consumption, this could allow to avoid the polarisation of the concrete in the case of the resistivity sensor, to avoid the heating of the microcontroller, of the strain gauge, of the thermodiodes, etc.

D. Complete implementation and tests of the sensing nodes

Now, the design and the implementation of each element well introduced, it is time to present the complete implementations of the sensing nodes, as well as their performances and characteristics.

1. Prototypes

Several generations of prototypes of the sensing nodes have been implemented.

First has been an exploded version based on: a specifically designed two-layer 1.6 mm FR4 printed circuit board for the power management and storage part (composed of the Texas Instruments BQ25504 power management unit and the 22 mF AVX Corporation BZ01CA223ZSB supercapacitor) -presented in Figure V.43-; the STMicroelectronics B-L072Z-LRWAN1 development board [657] (composed of a Murata CMWX1ZZABZ-091 LoRaWAN module and a RF Solutions ANT8WHIP3H whip antenna) for the data pre-processing and their wireless transmission; a temperature and humidity sensor (the Adafruit DHT22) for the data measurements; and the various configurations of the printed rounded quarter-wavelength dipole rectenna with resonant rectangular ring, with and without the reflector plane, for the power harvesting part; as presented in Figure V.44.

Then, 14 cm x 9 cm x 6 cm complete integrated prototypes of the sensing nodes have been implemented, as presented in Figure V.45. These are based on: a specifically designed two-layer 1.6 mm FR4 14 cm x 9 cm printed circuit board -presented in Figure V.46- on which are the Texas Instruments BQ25504 power management unit, the 22 mF AVX Corporation BZ01CA223ZSB supercapacitor, the Texas Instruments TPS63031 DC-to-DC buck/boost converter (introduced at this time), the Murata CMWX1ZZABZ-091 LoRaWAN module with printed meandered monopole (or a SMA connector), and the Texas Instruments HDC2010 and the Adafruit DHT22 temperature and humidity sensors; and whose the ground plane is used as a metallic reflector plane for the various configurations of the printed rounded quarter-wavelength dipole rectenna with resonant rectangular ring, or the printed folded quart-wavelength dipole antenna with capacitive arms. This is the version that has been the most studied and characterised, and that corresponds to the prototype noted SN4. The first tests of the use of the radiofrequency circulator have been also done with these.

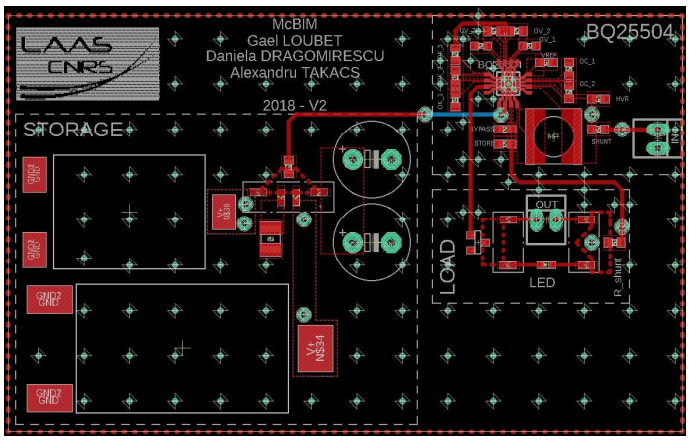

Figure V.43: Board used for the first version of the prototypes of the sensing nodes.

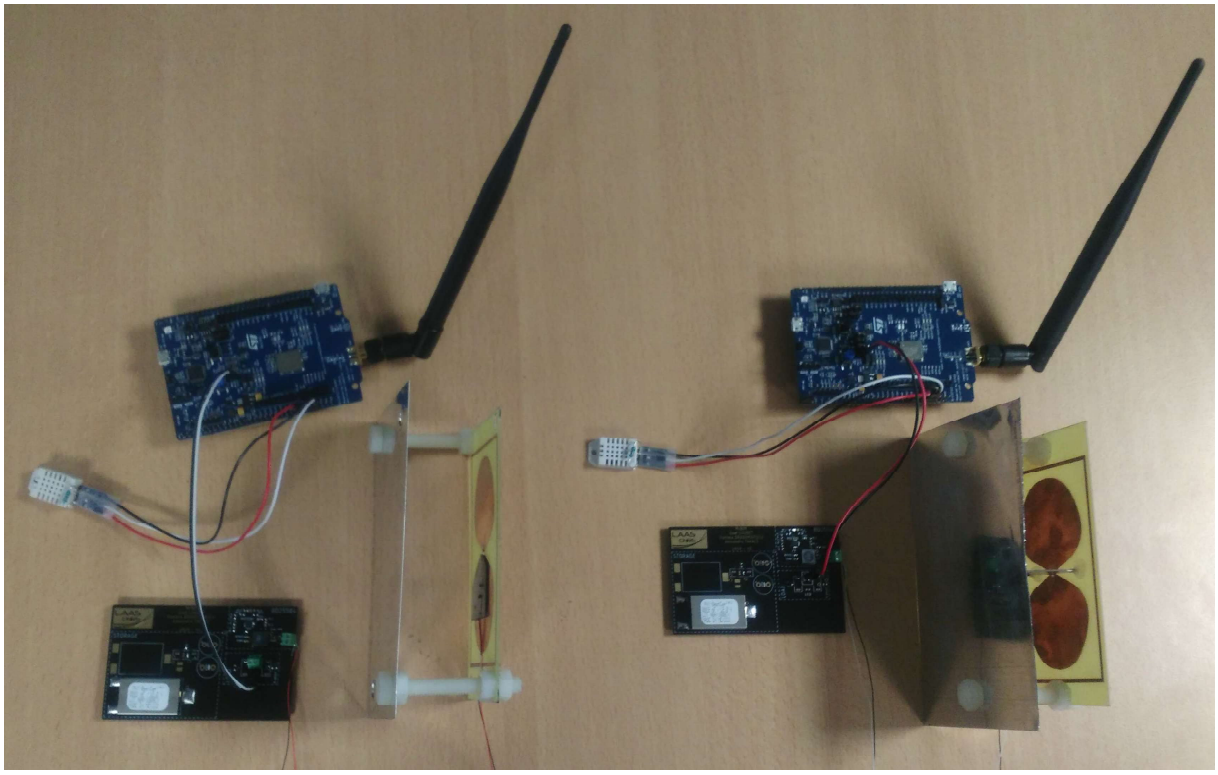

Figure V.44: Photographs of the first version of the prototypes of the sensing nodes.

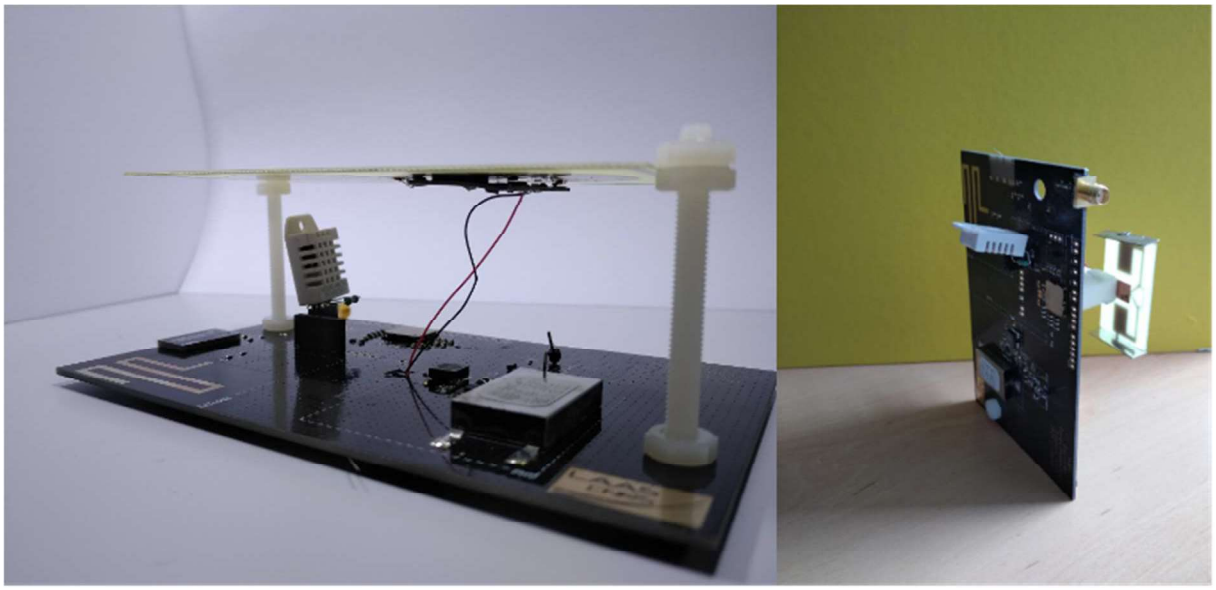

Figure V.45: Photographs of the first full integrated version of the prototypes of the sensing nodes with two different rectennas (for the first photograph, the rectenna is placed on the wrong side only for presentation purpose).

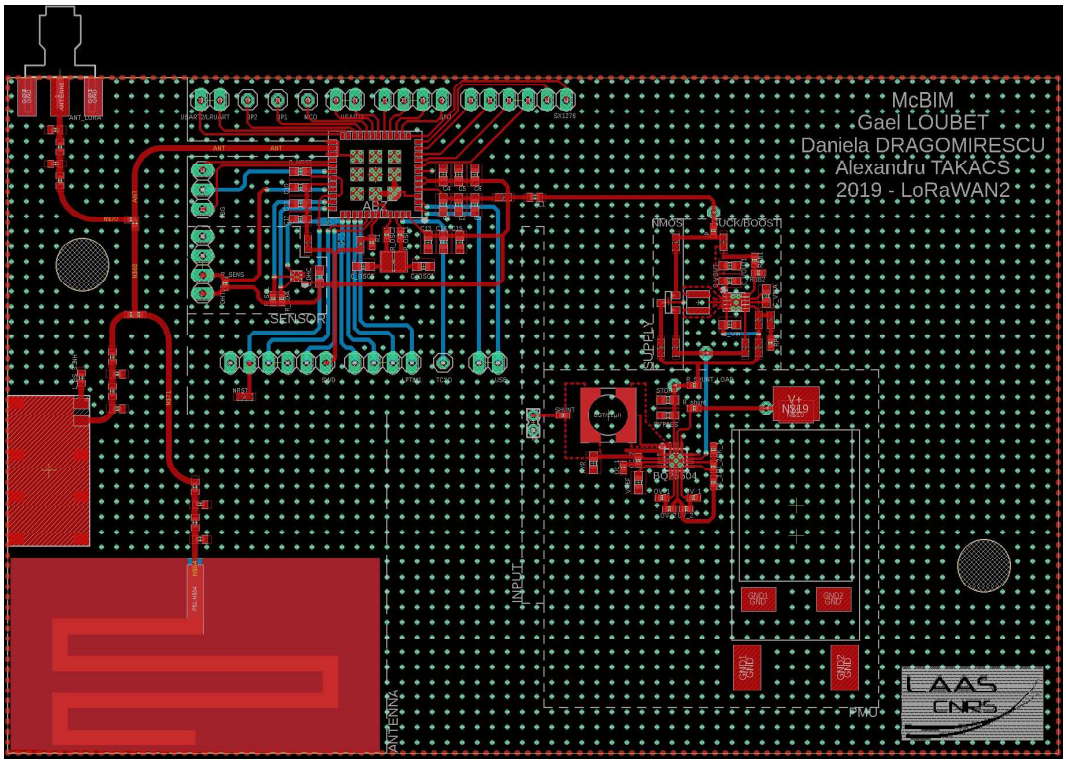

Figure V.46: Board of the first complete integrated prototypes of the sensing nodes.

By using a radiofrequency circulator, it has been possible to use a unique antenna both for the wireless communication and the wireless power transfer, which both use the same industrial, scientific and medical 868 MHz frequency band. This is possible because the wireless power transfer is the only downlink channel and the wireless communication is the only uplink channel. By implementing the full LoRaWAN class A specifications (thus, with receiving times for LoRaWAN downlink) this become no more possible. From then, this is the printed folded quart-wavelength dipole antenna with capacitive arms which has been used as the unique antenna.

The use of a radiofrequency circulator has allowed to improve the trade-off between the compactness and the performances of the sensing nodes. Indeed, by using the Aerotek C11-1FFF/OPT.N radiofrequency circulator [658], one antenna has been removed at the expense of a low insertion loss between the antenna and the rectifier, and between the LoRa transceiver and the antenna. In fact, to integrate the radiofrequency circulator, the architecture of the sensing nodes has been changed from the one presented in Figure III.6 to the one presented in Figure V.47. Thus, the rectenna has been split in its two components: the antenna and the rectifier. Thanks to their design, the rectifiers and the antennas, both with a 50 Ω input impedance, could be directly connected to the radiofrequency circulator for testing. So, the unique antenna is connected to the port 1 of the radiofrequency circulator, whilst the rectifier is on the port 2, and the LoRa transceiver on the port 3. In this way, thanks to a maximum measured 0.2 dB insertion loss (with a maximum theoretical value of 0.5 dB) and a minimum measured 25 dB isolation (with a minimum theoretical value of 20 dB), almost all the radiative electromagnetic power harvested by the antenna is transmitted to the rectifier, for the wireless power transfer part; almost all the radiofrequency power generated by the LoRa transceiver for the LoRaWAN frame transmission is transmitted to the antenna, for the

wireless communication; and there are almost no power transmission between the rectifier and the Lora transceiver. Thus, despite the use of the radiofrequency circulator and a unique antenna, the discrimination between the wireless power transfer (which must harvest as much radiative electromagnetic power as possible) and the wireless communication (which must reliably transmit data to the communicating nodes) is always effective, without interference problem. The paradigm of simultaneous wireless power and information transmission is also always met with this architecture: simultaneously, the sensing nodes can be wirelessly powered by the communicating nodes and the communicating nodes can successfully receive all the data sent by the sensing nodes.

If the frequency bands used for the wireless power transfer and the wireless communication are different, the use of a unique antenna with a radiofrequency circulator is always possible only if the antenna and the radiofrequency circulator cover the both frequency bands (e.g. by being broadband or bi-band antennas). Anyhow, these kinds of antennas and radiofrequency circulators are more complex to design and their characteristics in each frequency band will differ.

From this new architecture based on the use of a radiofrequency circulator, two versions of a three-dimensional 8 cm x 6 cm x 5 cm complete integrated and modular prototypes of the sensing nodes have been implemented, as presented in Figure V.48. The two versions are based on the same components: the Texas Instruments BQ25504 power management unit; the 22 mF AVX Corporation BZ01CA223ZSB supercapacitor; the Texas Instruments TPS63031 DC-to-DC buck/boost converter; the Murata CMWX1ZZABZ-091 LoRaWAN module with a SMA connector and a connector for each available communication protocol and dedicated to the interfacing of all the sensors presented above (Section V.B.) (the Texas Instruments HDC2010 and the Adafruit DHT22 temperature and humidity sensors; the thermodiodes, such as temperature sensors; the resistivity sensor; the strain gauge); and a printed folded quart-

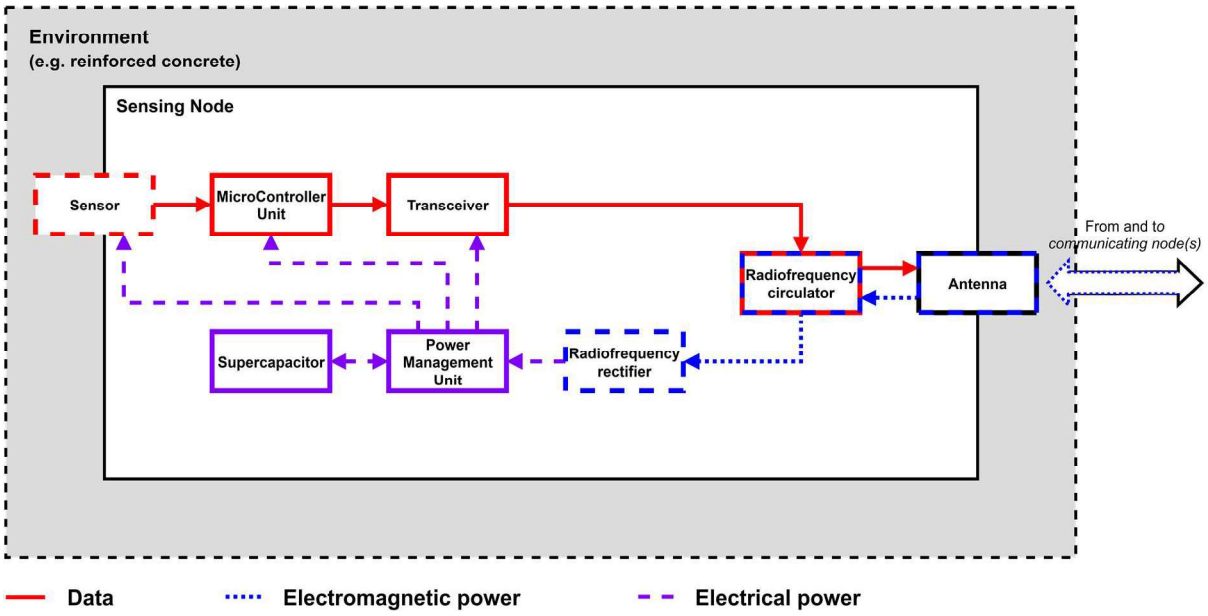

Figure V.47: Bloc diagram of the architecture of the sensing node with a radiofrequency circulator.

wavelength dipole antenna with capacitive arms. For these two versions, the ground plane of a 1.6 mm FR4 8 cm x 6 cm printed circuit board is used as a metallic reflector plane for the unique antenna. Nevertheless, these versions differ in the modular aspect and in the choices of the radiofrequency circulator and the rectifier.

The first, whose each element is presented in the first part of the Figure V.49, is the most modular. This is based on a main 1.6 mm FR4 8 cm x 6 cm two-layer printed circuit board only dedicated to the LoRaWAN module (presented at the bottom left corner of the first part of Figure V.49), whose the ground plane is used as the reflector plane for the antenna, and on which several secondary 1.6 mm FR4 two-layer printed circuit boards are interfaced. Two kinds of daughter boards are interfaced on the routed side of the main board in a coplanar manner. There are: the three daughter boards dedicated to the various sensors and presented above (Section V.B.) (presented on the second line on the right of the first part of Figure V.49); and three 1.6 mm FR4 printed circuit boards dedicated to three different power management units and their associated DC-to-DC buck/boost converter and supercapacitor, respectively the Texas Instruments BQ25504, Texas Instruments BQ25505 and the e-peas AEM30940 (respectively presented in the first line and on the third on the right, of the first part of Figure V.49). Due to their unavailability during the test period, the e-peas AEM30940 have not still not be mounted and tested. However, now that these are available, tests are already planned. Another daughter board (presented at the bottom right corner of the first part of Figure V.49) is interfaced on the un-routed (*i.e.* ground plane) side of the main board in an orthogonal manner, through two SMA connectors: one connected to the output of the LoRa transceiver (located on the main board), and the other to the input of the power management unit (located on a daughter board, thus, through the main board). This daughter board is dedicated to the Aerotek FC23-S-S drop-in flange mounted radiofrequency circulator [659] (the unpackaged version of the previous one) and the specifically design compact half-wave series rectifier Rect2 (Section V.C.). More, this one allows to connect on the last port of the radiofrequency circulator the unique printed on 1.6 mm FR4 antenna (presented on the second line on the left of the first part of Figure V.49) through a SMA connector, which is then centred and located at 5 cm in a coplanar plane of the main board used as a reflector plane.

This version of the sensing nodes has been successfully functionally tested, but has presented poor performances due to some conception defaults and questionable choices. The integration of the Aerotek FC23-S-S drop-in flange mounted radiofrequency circulator has been wrong, and thus, has induced high insertion losses and low isolations. The used rectifier has provided inequal performances due to the variability of the components and the difficulty to tune it properly. The boards dedicated to the Texas Instruments BQ25504 and BQ25505 power management units have presented lower performances than for the previous version, especially because of a worst inductor choice for their input. Because of these defaults, another version has been quickly implemented.

This second version, whose the main element is presented in the second part of the Figure V.49, is less modular. This is based on the daughter boards dedicated to the sensors and the antenna of the previous one, but changes the main board and substitutes the one dedicated to the radiofrequency circulator and rectifier. For this version, the main 1.6 mm FR4 8 cm x 6 cm four-layer printed circuit board, whose the ground plane is still used as the reflector plane for the antenna, is composed of the LoRaWAN module, the Texas Instruments BQ25504 power management unit and its associated DC-to-DC buck/boost converter and

supercapacitor, and the full-wave doubler rectifier Rect1 (Section V.B.). The daughter boards dedicated to the various sensors are still interfaceable through connectors on the routed side of the main board and in a coplanar manner. The mechanic aspect required to hold the antenna centred at 5 cm of the un-routed ground plane of the main board (always, used as a reflector plane) in a coplanar plane, is achieved by the Aerotek C11-1FFF/OPT.N radiofrequency circulator which replaces the previous board.

This version of the sensing nodes has been successfully functionally tested, and presented satisfactory performances. Nevertheless, its full characterisation is still in progress. And the slight drop observed in the performances could be justified by slight decrease in efficiency of the full-wave doubler rectifier initially deigned for a 0.8 mm FR4 substrate and adapted here for 1.6 mm FR4 one; by the variability in the components, especially for the power management units (from various production runs); by the hand assembly process; and by the punctual modifications of the routing. This is the version that corresponds to the SN1 and SN2 prototypes, for which the power consumption is higher than for SN4 for high output transmission powers, which is still not fully explained, as discussed above (Section V.A.2.).

Finally, a more compact version of the prototypes of the sensing nodes has been implemented, as presented in Figure V.50. This one compacts the main board of the previous generation in a 1.6 mm FR4 8 cm x 2.5 cm four-layer printed circuit board, presented in Figure V.51, while retaining all its modularity. The main change is to stop using a reflector plane for the antenna. This is the version that corresponds to the SN3 prototype.

Whatever the considered generation of the prototypes of the LoRaWAN sensing nodes, this is wireless power transfer which is limiting in terms of range of use and not the wireless communication. And this limitation is imposed by the minimum input power required by the energy harvesting and management part of the sensing nodes, and its global efficiency, highly linked to the efficiency of each components (especially the rectifier (or more generally the rectenna), the power management unit and the energy storage device). Moreover, the less energy the active components of the sensing nodes required, the faster is the charging time.

Now that, the complete implementation of the prototypes of the sensing nodes have been reported, it is time to discuss their performances.

2. Power consumption of the sensing nodes

As presented above (Section V.A.2. and Section V.B.2.c.), the power consumption of the active components of the sensing nodes constraints the design of the power harvesting and management part of these latter. This power consumption depends essentially of the properties of the transmission of the LoRaWAN frames (in particular the transmission power and the duration of the transmission (related to the data-rate -defined by the frequency bandwidth and the spreading factor- and to the size of the data payload); and of the used sensor. The Table V.8 summarizes the power consumption of the tested prototypes against the transmission power and the used sensor, whilst the Figures V.52, V.53, V.54 and V.55 -respectively for SN1, SN2, SN3 and SN4- presented the power consumption of the tested prototypes against the used sensor for a transmission power of (A) +4 dBm and (B) +14 dBm.

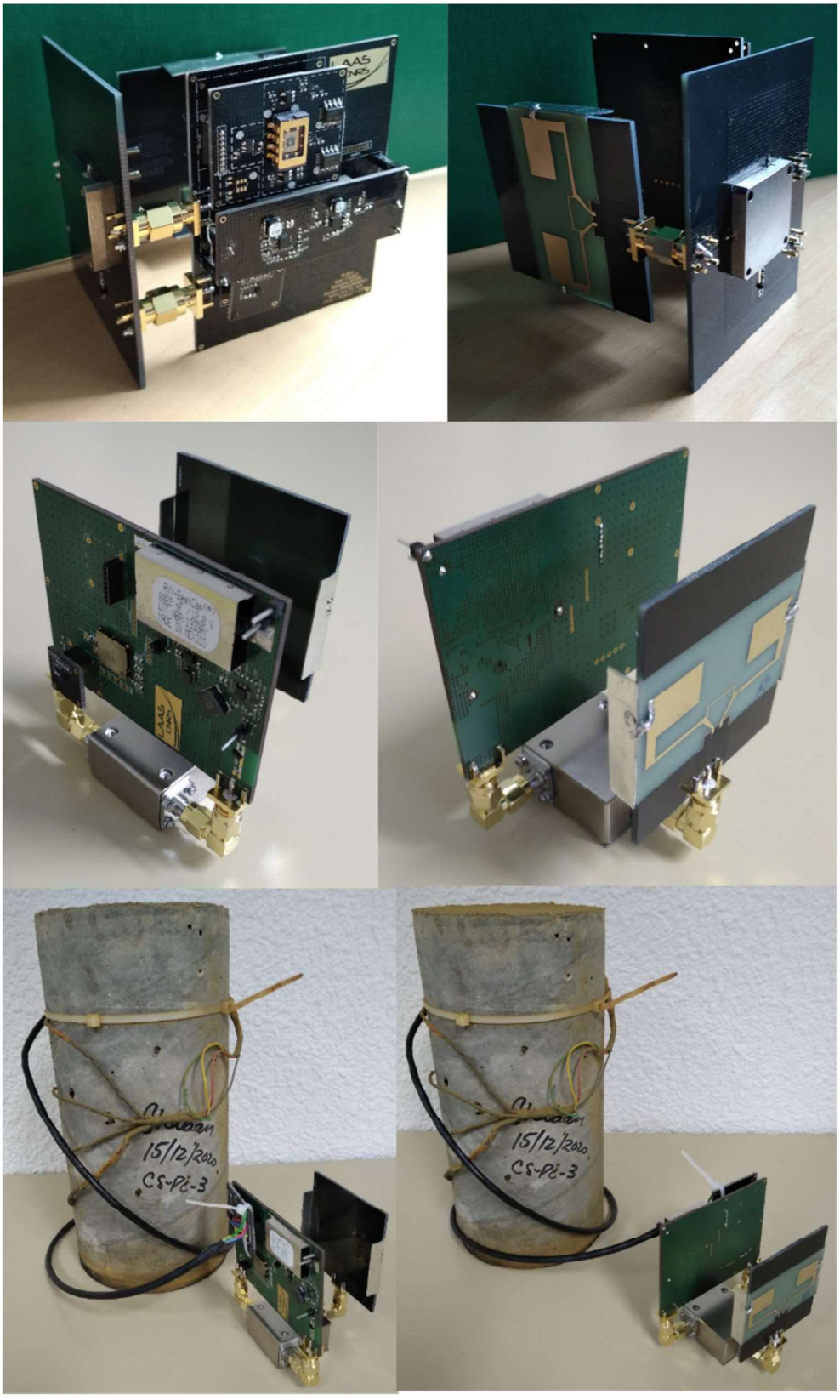

Figure V.48: Photographs of the two modular versions of the sensing nodes using a unique antenna thanks to a radiofrequency circulator: the first line corresponds to the most modular version with the Texas Instruments BQ25504, and the thermodiodes; the second and third lines to the less modular version with respectively the Texas Instruments HDC2010 and the resistivity sensor.

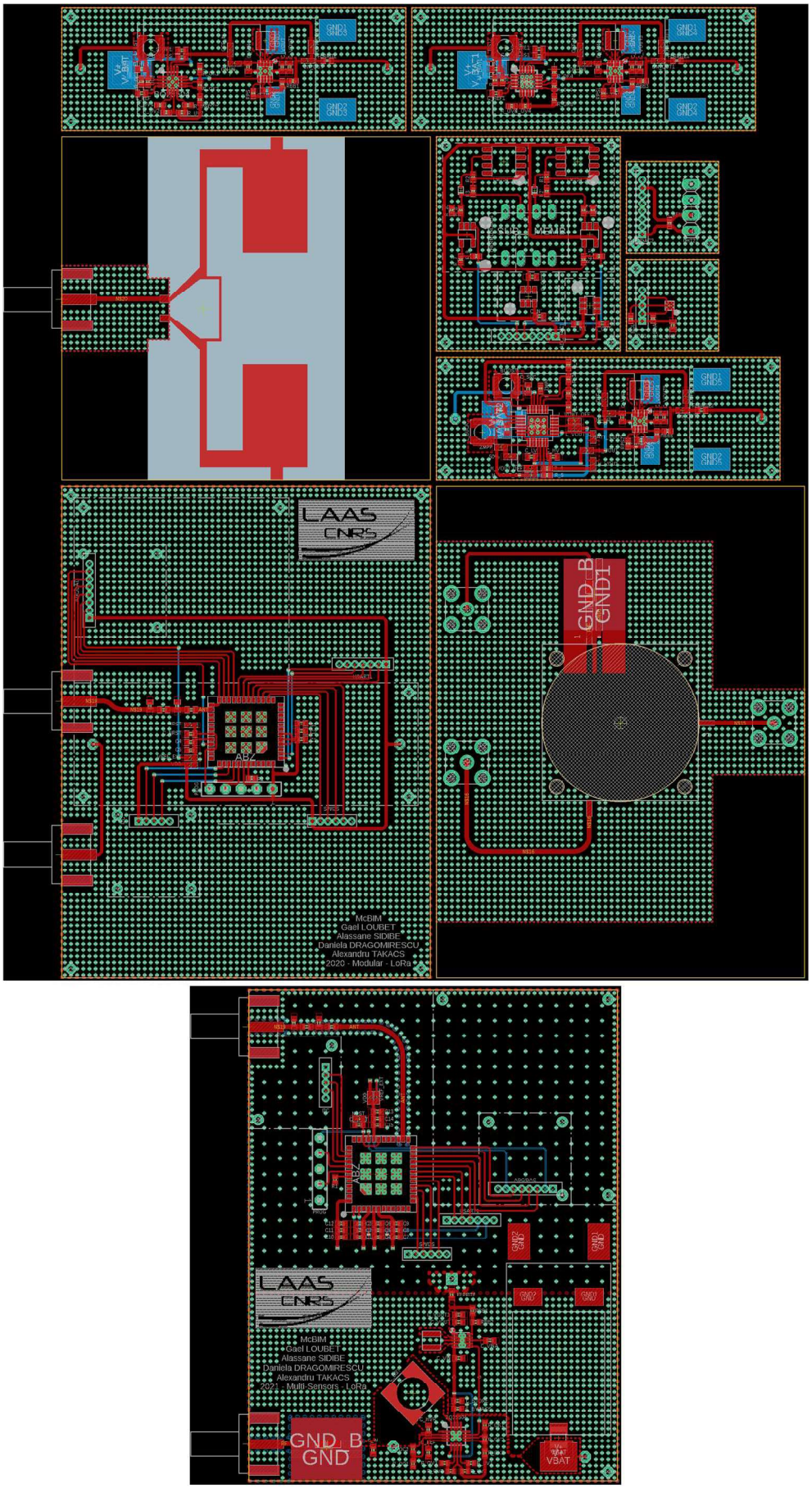

Figure V.49: Boards of the modular versions of the prototypes of the sensing nodes.

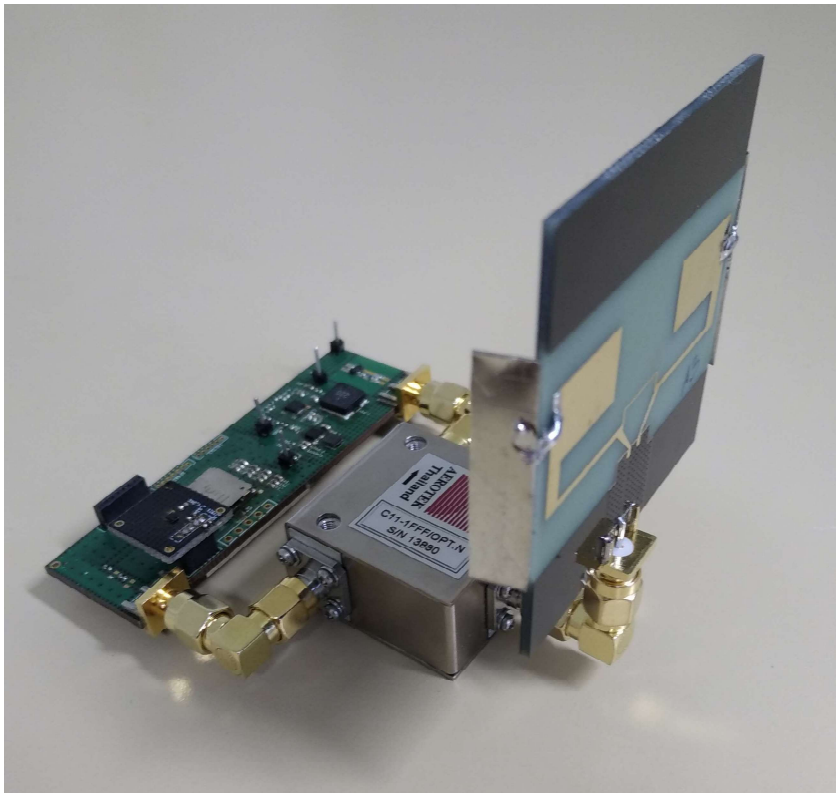

Figure V.50: Photograph of the most compact version of the prototypes of the sensing nodes using a unique antenna thanks to a radiofrequency circulator and with the Texas Instruments HDC2010.

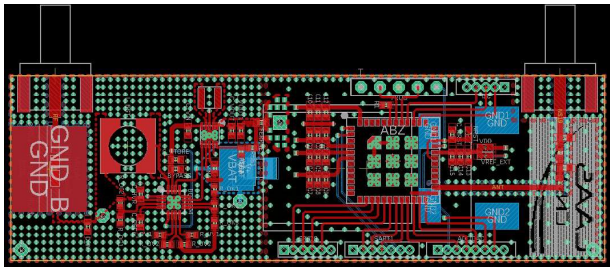

Figure V.51: Board of the most compact version of the prototypes of the sensing nodes.

Thus, for all the tested prototypes, the energy required for the initialisation is quite similar (around 11.3 ± 0.4 mJ, that says nearly 12 % of the energy required for a full process with a transmission power of +4 dBm). Moreover, for each prototype, higher is the transmission power for the LoRaWAN frame, higher is the energy needed. However, there is a high variability of energy needed between the SN1 and SN2 prototypes and the SN3 and SN4 prototypes for the highest transmission powers, especially at +14 dBm; which is not the case for the lowest transmission powers, especially at +4 dBm, where around 91.9 ± 4.4 mJ are required for the initialisation and a LoRaWAN frame transmission. Some elements of justification of the high variability of the energy required for the highest transmission powers are proposed above (Section V.A.2). Nevertheless, whatever the prototype and the transmission power used, the additional energy required for each sensor is similar and limited: almost 0.4 mJ for the internal temperature sensor; almost 0.7 mJ for the Texas Instruments HDC2010 temperature and humidity sensor; almost 7.5 mJ for the thermodiodes such as temperature sensors; almost 4.1 mJ for the strain gauge; and almost 4.1 mJ for the resistivity sensor, or

respectively an additional energy of: less than 1 %, less than 1 %, about 8 %, about 5 %, and about 5 %; of the energy required for a full process without measurement and with a transmission power of +4 dBm. The exception is for the Adafruit DHT22 temperature and humidity sensor which requires an additional energy of almost 24.9 mJ (27 % of the energy required for a full process without measurement and with a transmission power of +4 dBm).

As discussed above (Section V.A.3., Section V.B.3. and Section V.C.3.), there are several trends of improvements in order to minimize the energy required. For the LoRaWAN module, this could be achieved by the hardware and software optimisation, mainly by the use of lower power components and the reduction of the duration of the LoRaWAN frame transmission (by changing the LoRaWAN parameters and reducing the data payload). For the sensors, this could be achieved by the hardware optimisation, mainly by the use of lower power components. For the complete sensing nodes, this could be achieved by the hardware optimisation of the power supply shaft of the active components.

Table V.8: Power consumption of the tested prototypes of the sensing nodes.

Prototypes		SN1		SN2		SN3		SN4		Average	
Energy required for the initialisation (mJ)	Without sensor	10.8		12.0		11.3		11.0		11.3	
	With internal temperature sensor	11.1 (+0.3)		N/A		N/A		N/A		N/A	
	With the Adafruit DHT22 temperature and humidity sensor	40.4 (+29.6)		N/A		N/A		N/A		N/A	
	With the Texas Instruments HDC2010 temperature and humidity sensor	11.2 (+0.4)		N/A		N/A		N/A		N/A	
	With the thermodiodes such as temperature sensors	12.1 (+1.3)		N/A		N/A		N/A		N/A	
	With the strain gauge	11.6 (+0.8)		N/A		N/A		N/A		N/A	
	With the resistivity sensor	11.6 (+0.8)		N/A		N/A		N/A		N/A	
Transmission power (dBm)		+4	+14	+4	+14	+4	+14	+4	+14	+4	+14
Energy required for the full process (mJ)	Without sensor	88.3	205.8	94.1	200.2	98.5	138.7	86.6	142.4	91.9	171.8
	With internal temperature sensor	88.6 (+0.3)	206.0 (+0.2)	94.3 (+0.2)	200.7 (+0.5)	98.8 (+0.3)	139.0 (+0.3)	86.9 (+0.3)	143.1 (+0.7)	92.2 (+0.3)	172.2 (+0.4)
	With the Adafruit DHT22 temperature and humidity sensor	113.3 (+25.0)	230.7 (+24.9)	118.8 (+24.7)	224.9 (+24.7)	123.4 (+23.9)	163.6 (+24.9)	111.6 (+25.0)	166.9 (+19.5)	116.8 (+24.9)	196.5 (+24.7)
	With the Texas Instruments HDC2010 temperature and humidity sensor	89.0 (+0.7)	206.4 (+0.6)	94.6 (+0.5)	200.8 (+0.6)	99.2 (+0.7)	139.5 (+0.8)	87.1 (+0.5)	143.4 (+1.0)	92.5 (+0.6)	172.5 (+0.7)
	With the thermodiodes such as temperature sensors	96.0 (+7.7)	213.3 (+7.5)	100.4 (+6.3)	207.7 (+7.5)	106.0 (+7.5)	146.2 (+7.5)	N/A	N/A	100.8 (+7.3)	189 (+7.5)
	With the strain gauge	92.5 (+4.2)	209.8 (+4.0)	98.3 (+4.2)	204.3 (+4.1)	102.5 (+4.0)	142.7 (+4.0)	N/A	N/A	97.8 (+4.0)	185.6 (+4.1)
	With the resistivity sensor	92.3 (+4.0)	209.8 (+4.0)	98.2 (+4.1)	204.3 (+4.1)	102.5 (+4.0)	142.9 (+4.2)	N/A	N/A	97.7 (+4.1)	185.7 (+4.0)

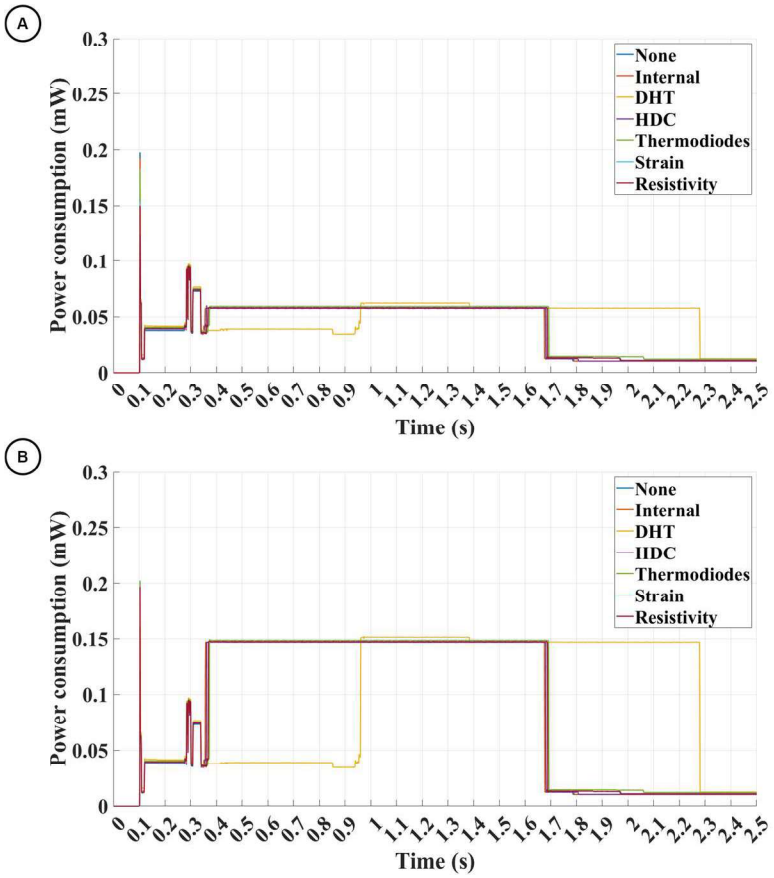

Figure V.52: Power consumption of the prototype SN1 against the sensor used and for transmission power of respectively (A) +4 dBm and (B) +14 dBm.

3. Remote control of the periodicity of measurement and wireless communication of the sensing nodes by the communicating nodes and energy efficiency

i. Reconfigurability of the sensing nodes

The sensing nodes become inaccessible once buried into the reinforced concrete. This inaccessibility is both hardware and software: there is no mean to have a physical access (excepted by the destruction of the reinforced concrete); and no mean to have a wireless digital access due to the absence of the LoRaWAN downlink (especially in order to limit as far as possible the energy required and to close all the back doors for preventing malicious attacks). Neither the hardware nor the software can be updated or replaced, and also, these must work for the entire lifespan of the reinforced concrete element in which these are embedded. It must also be added that the chosen wireless communication technology must be supported during all the lifetime of the sensing nodes. Thus, the configuration of each sensing node must be performed during its manufacturing by choosing the appropriate hardware parts (including the power management unit, the energy storage device, the antenna(s) with or without the radiofrequency circulator, the rectifier, the sensor(s), the transceiver and the microcontroller unit, or their future alternatives; through the various available daughter boards in the case of the modular prototypes); by tuning the quantity of energy to store especially through the activation and deactivation voltage thresholds of the power management unit (determining how much energy must be stored in the energy storage device in order to power

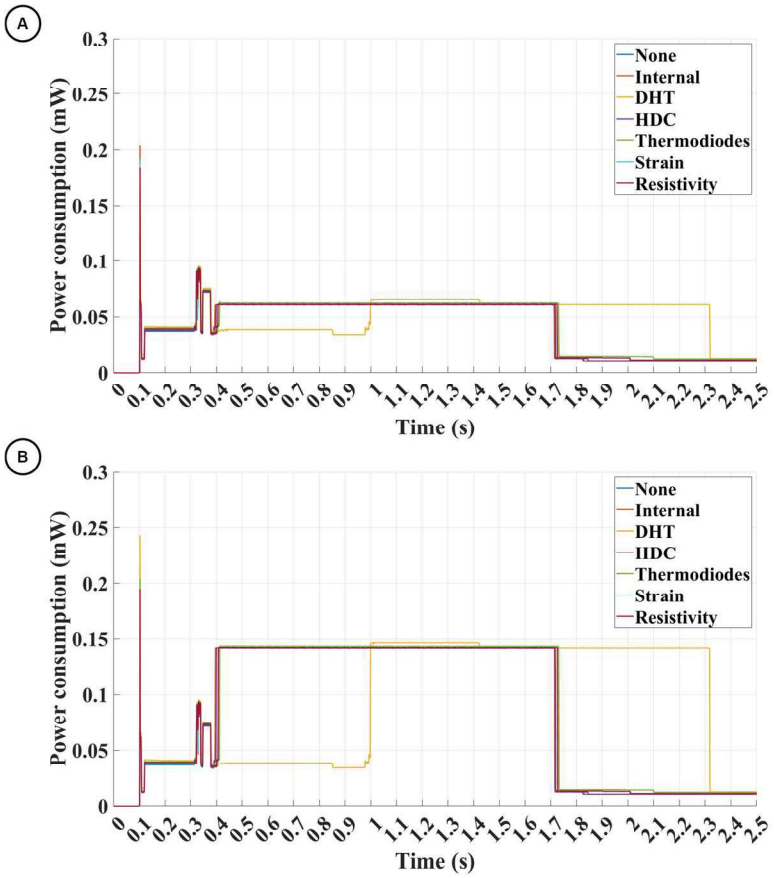

Figure V.53: Power consumption of the prototype SN2 against the sensor used and for transmission power of respectively (A) +4 dBm and (B) +14 dBm.

all the active components of the sensing nodes to achieve at least a measurement and a wireless transmission of the collected -and eventually pre-processed- data); and by programming the microcontroller unit with the appropriate firmware (including the unique identifier(s), the security key(s), the software to drive the sensor(s), the software to drive the transceiver, etc.). Because of these conception choices, there is no real reconfigurability of the sensing nodes and no conventional way to communicate with these (especially for remote software updated).

However, the sensing nodes are equipped with an unusual downlink, namely their power harvesting system, and have a functioning based on the "store then use" strategy. Thus, the communicating nodes which generate the radiative electromagnetic power harvested by the sensing nodes in their neighbourhood can remotely and wirelessly control the behaviour of the sensing nodes. Indeed, by controlling the generated radiative electromagnetic power, these can impose a periodicity of measurement and wireless communication for the sensing nodes. The control of the generated radiative electromagnetic power can be achieved by tuning the radiative electromagnetic power source in terms of waveforms, transmission power and duty-cycle, and must be based on the knowledge by the communicating nodes of the energy needs of each sensing node in their neighbourhood, both in terms of power to transmit and duration of the wireless power transfer. For instance, by considering that a communicating node requires H hours to wirelessly power all the sensing nodes in its neighbourhood, and if a

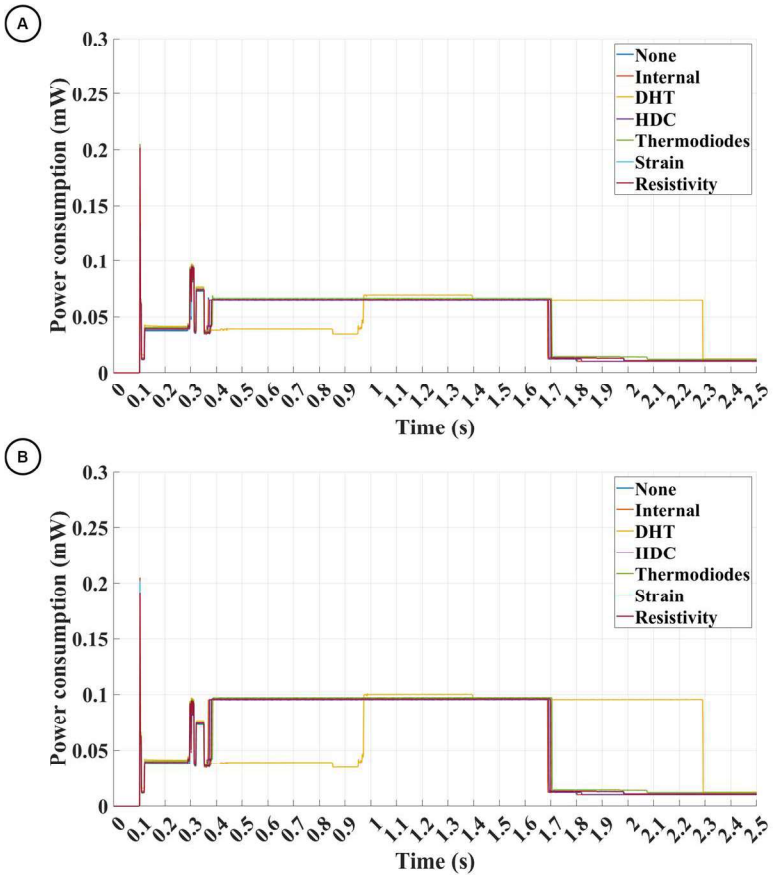

Figure V.54: Power consumption of the prototype SN3 against the sensor used and for transmission power of respectively (A) +4 dBm and (B) +14 dBm.

measurement is required each H (or less) hours, the communicating node can activate continuously its radiative electromagnetic power source; but if a measurement is required each D days, it can activate its radiative electromagnetic power source only H hours each D days, or reduce the transmission power in condition that all the sensing nodes can be harvested enough energy and for a duration higher than H hours.

To go further in terms of reconfigurability of the sensing nodes, it can be considered the case of several fleets of sensing nodes, where each fleet are dedicated to the measurement of a specific parameters and whose the frequency band dedicated to the wireless power transfer does not overlap the bands of the other fleets. Thus, each fleet can be discriminated by its configuration of its wireless power transfer interface, and can be powered independently. Thus, by tuning both the central frequency and the bandwidth of the generated radiative electromagnetic power by the communicating nodes, it become possible power only one or several fleets of sensing nodes, or to provide different periodicity of measurement and wireless communication for each fleet of sensing nodes.

As introduced above (Section IV.A.5. and Section IV.D.), each sensing node could be independently and individually powered by using a beamforming solution in the radiative electromagnetic power source of the communicating nodes, at the condition that these perform before a learning process.

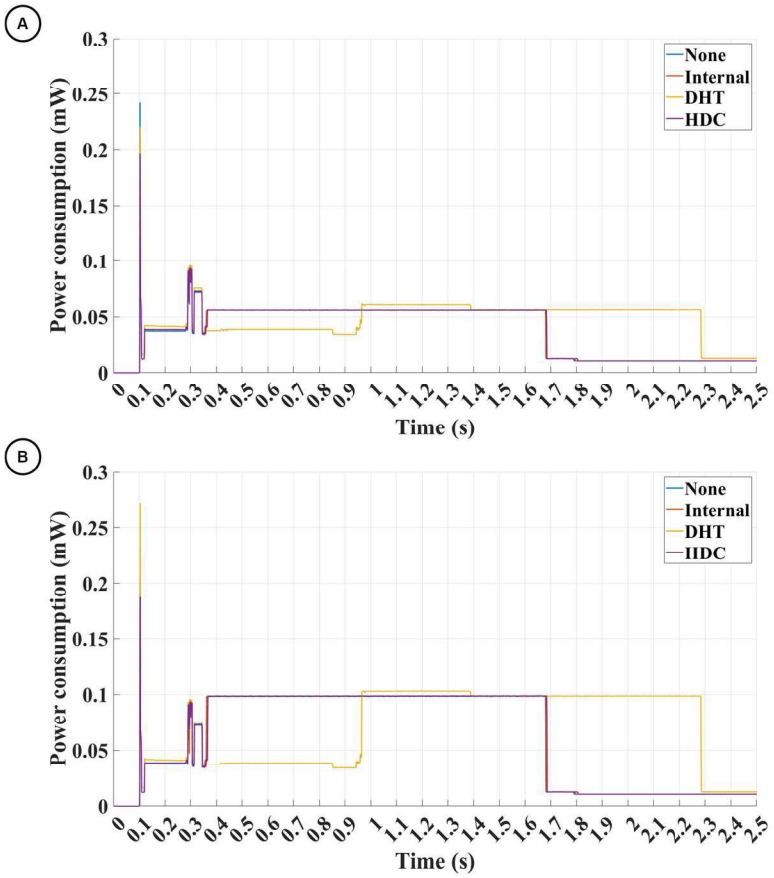

Figure V.55: Power consumption of the prototype SN4 against the sensor used and for transmission power of respectively (A) +4 dBm and (B) +14 dBm.

From there, it seems relevant to characterize the times needed for the first charge and the recharges of the sensing nodes against the available input power and the employed rectifier.

ii. Characterisation of the required time for a first charge and recharges of the sensing nodes.

The three rectifiers presented above: Rect1, Rect2 and Rect3 (Section V.C.2.iii.) have been used in order to characterize for the sensing nodes the required time for a first charge (from an empty energy storage device, to the first measurement and LoRaWAN frame transmission) and for the next recharges (minimum duration required between two consecutive measurements and LoRaWAN frame transmissions), as presented in Figure V.56. To perform this characterisation, a conducted electromagnetic power is applied at the input of the rectifier under test whose the output is connected to the input of the power management unit of the sensing node, and the times are estimated by using the time stamps provided by the communicating node for each received LoRaWAN frame transmitted by the sensing node under test, or through the direct observation of the charge and discharge curves on a LeCroy WaveRunner 6100A oscilloscope [660]. It must be noted that the observation with the LeCroy WaveRunner 6100A oscilloscope, whose the input impedance is about 1 MΩ, induces non-negligible current losses. Therefore, for a measured voltage of 5.25 V (the maximum voltage in the energy storage device in some studied cases), 27.6 µW of power are consumed for the observation, whilst 5.3 µW at 2.30 V (the minimum voltage in the energy storage device after a discharge). The characterization has been performed with sensing nodes of the same

generation than SN4 and at 868 MHz, which is not necessarily the frequency to get the optimum use of the rectifier, but which is within a few MHz of this optimum value. The choice of the rectifier made above (Section V.C.2.iii.d.) is based on these characterizations.

Much of the first charge takes place in the cold-start state during which an input voltage of about 330 mV is imposed by the power management unit, as presented in Figure V.28. Because of that, Rect1 (the full-wave rectifier) is slower than Rect3 (a half-wave rectifier) for the highest input powers; and the two rectifiers have similar performances for lowest input powers. In a general way, the full-wave rectifier is more efficient than the half-wave rectifier for sufficient input powers and when the imposed voltage is sufficiently "high". That why, once the cold-start achieved, Rect1 is faster than Rect3 for all the tested input powers, and provide higher voltages. It must be noted that output voltage of Rect1 saturates for input powers higher than +6 dBm (or 3.98 mW). Because of much weaker performances (longer durations both for the first charge and recharges, and lower voltages), Rect2 has not been considered as a relevant solution. This one has been designed with the compactness as main constraint, and despite of very good simulated characteristics, the ones obtained after the implementation have been weaker and difficult to improve because of the difficult tuning induces by a narrow bandwidth.

Regardless of the chosen rectifier, the sensing nodes have a periodicity of measurement and wireless communication which variates between several tens of seconds to several hours in function of the available input power, which has been tested here from -12 dBm (or 63.1 µW) to +15 dBm (or 31.6 mW). As a reminder, the minimum input power required to operate properly the sensing nodes in the worst case has been estimated above (Section V.C.2.iii.) around -10 dBm (or 100 µW). This worst case has apparently never been met during the various tests and characterization carried out.

Finally, by controlling the generated radiative electromagnetic power, the communicating nodes can impose a periodicity of measurement and wireless communication for the sensing nodes, without altering neither their software or their hardware.

iii. Reproducibility analysis

In order to find out whether it is possible to generalise the data measured over some iterations, a quick statistical analysis was carried out. Because of the very long measurement time required, this one has been limited to the study of two sensing nodes powered with a +15 dBm (or 31.6 mW) and a +0 dBm (or 1 mW) input conducted electromagnetic powers. A first sensing node has been used as a reference, whilst the second has produced several sets of data at different times and under different environmental conditions.

Regarding the time required for a recharge with a +15 dBm (or 31.6 mW) input conducted electromagnetic power, as summarized in Table V.9, there is a small variability between the two studied sensing nodes, mainly due to the variability in the components. However, the average duration of a recharge is closely similar (33 seconds against 34 seconds), the maximum deviation is similar (4 seconds) and the standard deviation is limited to few percent (or 1 second, the measurement step). This remains true for each set of measurements considered independently. The deviations can be in a major part explained the measurement precision (at the second) and by the functioning of the maximum power point tracking system.

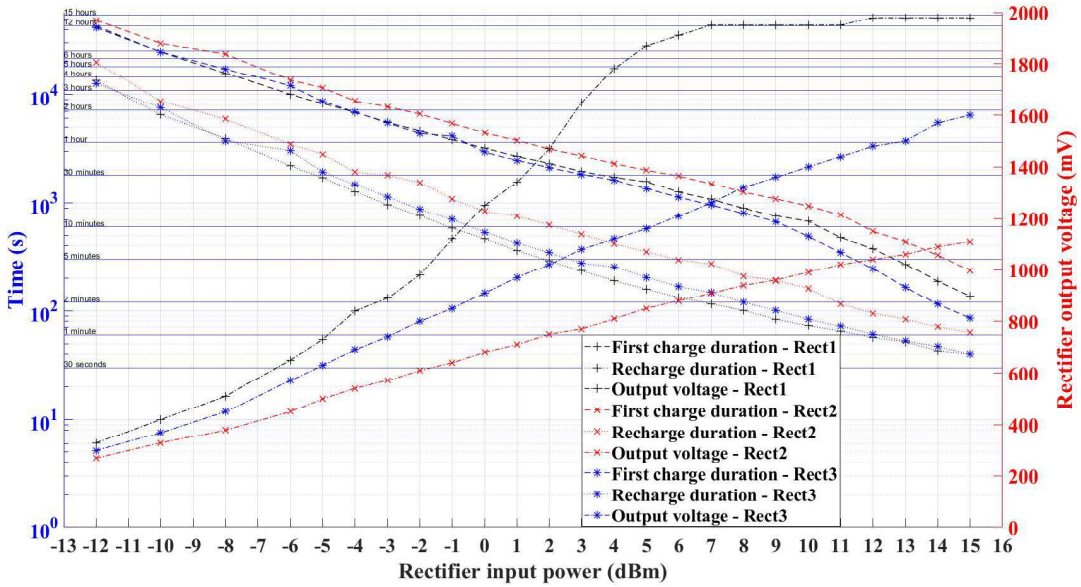

Figure V.56: Durations of the first charge (dashed lines, left) and recharges (dotted lines, left), and rectifier output voltages in open-circuit during the recharges (dotted and dashed lines, right) against the conducted electromagnetic input power applied at the input of the rectifier of the sensing nodes, for a frequency of 868 MHz and against the rectifier under test (Rect1: black '+'; Rect2: red 'x'; and Rect3: blue '*').

Indeed, this one achieves a sampling of the input open-circuit voltage each 16 s for nearly 256 ms, and adapts its impedance in function of the sampled voltage and the voltage available in the energy storage device. Thus, there is 2 (eventually 3) sampling during each recharge, depending on when these are carried out (e.g. just after the discharge, just before the discharge, etc.), the input impedance will be different and the efficiency of the rectifier will vary, which induces non-negligible variation for the short recharge times.

Regarding the time required for a first charge with a +15 dBm (or 31.6 mW) input conducted electromagnetic power, its average duration is of 1 minute 09 seconds, with a standard deviation of 1 second (or 0.88 %), for both the two tested sensing nodes and for a reduced set of 11 measurements.

Table V.9: Statistical analysis of the recharge time for two sensing nodes powered by a +15 dBm (or 31.6 mW) input conducted electromagnetic powers.

Set	Reference	N°1	N°2	N°3	N°4	N°5	N°6	N°7	N°8	N°9	N°10	N°11	Total
Sensing node	1	2	2	2	2	2	2	2	2	2	2	2	2
Number of measurements	5	10	10	10	10	10	10	10	10	10	10	50	150
Average	34 s	33 s	34 s	33 s	33 s	33 s	33 s	33 s	33 s	34 s	33 s	33 s	33 s
Minimum	31 s	31 s	33 s	32 s	31 s	31 s	31 s	31 s	32 s	33 s	31 s	31 s	31 s
Maximum	37 s	36 s	36 s	36 s	36 s	37 s	36 s	36 s	35 s	36 s	36 s	36 s	37 s
Median	32 s	33 s	34 s	33 s	33 s	33 s	33 s	33 s	33 s	34 s	32 s	33 s	33 s
Standard deviation	3 s (8.04 %)	2 s (5.08 %)	1 s (3.10 %)	1 s (3.32 %)	1 s (3.97 %)	2 s (4.95 %)	2 s (5.35 %)	1 s (4.38 %)	1 s (3.78 %)	1 s (2.93 %)	1 s (4.50 %)	1 s (3.38 %)	1 s (3.94 %)
Variance	7 s	3 s	1 s	1 s	2 s	3 s	3 s	2 s	2 s	1 s	2 s	1 s	2 s

Regarding the time required for a recharge with a +0 dBm (or 1 mW) input conducted electromagnetic power, as summarized in Table V.10, there is a variability between the two studied sensing nodes, mainly due to the variability in the components. However, the average is constant for each sensing nodes and the standard deviation is limited to few seconds, or around 1%. This remains true for each set of measurements considered independently.

Regarding the time required for a first charge with a +0 dBm (or 1 mW) input conducted electromagnetic power, its average duration is of 42 minute 25 seconds, with an average deviation of 1 minute 05 second (or 2,56 %) between the two tested sensing nodes, based for a very reduced set of measurements.

From these observations, it has been decided to consider the average value for at least 10 measurements for high input power (higher than +0 dBm (or 1 mW)), at least 5 measurements for medium input power (between -6 dBm (or 251.2 µW) and +0 dBm (or 1 mW)), and at least 3 for very low input power (lower -6 dBm (or 251.2 µW)), for the characterisation of the sensing nodes, in order to get a relevant order of magnitude.

iv. Power supply of the sensing nodes through the radiative electromagnetic power transmission

To validate the proper functioning of the wireless power transfer to wirelessly power the sensing nodes, several characterizations of the sensing nodes in terms of required times both for a first charge and for recharges have been performed. To carry out these characterisations, a radiative electromagnetic power is generated by a communicating node through its wireless power source, and the full sensing node is located under the generated electromagnetic field. By using the Equation V.10, the power harvested by the antenna and provided at the input of the rectifier is estimated in function of the distance. Thus, if LoRaWAN frames are received by the communicating node, this means that the sensing node work properly by being wirelessly powered. The required times both for a first charge and for recharges can be estimated from the time stamps provided by the communicating node for each well received LoRaWAN frame transmitted by the sensing node under test, or through the direct observation of the charge and discharge curves on a LeCroy WaveRunner 6100A oscilloscope.

As presented in Figure V.57, the characterization of a wirelessly powered sensing node in terms of required time for recharges and of output open-circuit voltage can be compared to the same characterization of an equivalent sensing node powered by a conducted electromagnetic input power. Here, the characterization is performed with a sensing node of the same

Table V.10: Statistical analysis of the recharge time for two sensing nodes powered by a +0 dBm (or 1 mW) input conducted electromagnetic powers.

Set	Reference	N°1	N°2	Total
Sensing node	1	2	2	2
Number of measurements	5	126	12	138
Average	7 min 25 s	7 min 8 s	7 min 12 s	7 min 9 s
Minimum	7 min 22 s	6 min 58 s	7 min 02 s	6 min 58 s
Maximum	7 min 29 s	7 min 15 s	7 min 20 s	7 min 20 s
Median	7 min 25 s	7 min 10 s	7 min 12 s	7 min 10 s
Standard deviation	3 s (0.56 %)	5 s (1.12 %)	5 s (1.24 %)	5 s (1.15 %)
Variance	6 s	23 s	29 s	24 s

generation than SN4 and at 868 MHz. For the measurements, the sensing node has been located in the air at a range between 60 cm and 300 cm to the communicating node (and more precisely from its wireless power source) and have been achieved with a 20 cm step. The major part of the sensing nodes is used for the two characterisations, the only difference is that the rectenna used in the case of the radiated input power is replaced by a rectifier equivalent to the one used in the rectenna is the case of the conducted input power.

As presented in Figure V.57, there are relatively good correlations for the time required for the recharges and for the output open-circuit voltage of the rectifier, between the sensing node powered with radiated power and the one powered with a conducted power, in the cases of input powers higher than +2 dBm (or 1.58 mW). For lower powers, the differences are more important. The variations can be explained by several elements, whose: the handling errors and approximations; the variations between components, especially for the rectifier, and the eventual impedance mismatch between the rectifier and the antenna, which can induce a lower efficiency; the theoretical model used to estimate the energy harvested by the antenna, which between others, does not consider the environment effect, such as the multipath effect.

v. Energy efficiency of the sensing nodes

One of the most interesting features of the sensing nodes is their energy efficiency. Here, this is defined as the ratio of the energy available at the input of the sensing node (i.e. the power available at the input of the sensing node (the one harvested by the antenna) integrated over the period of interest) to the energy required for a measurement and a wireless transmission of the collected -and eventually pre-processed- data. This criterium must be considered in order to provide a sustainable system.

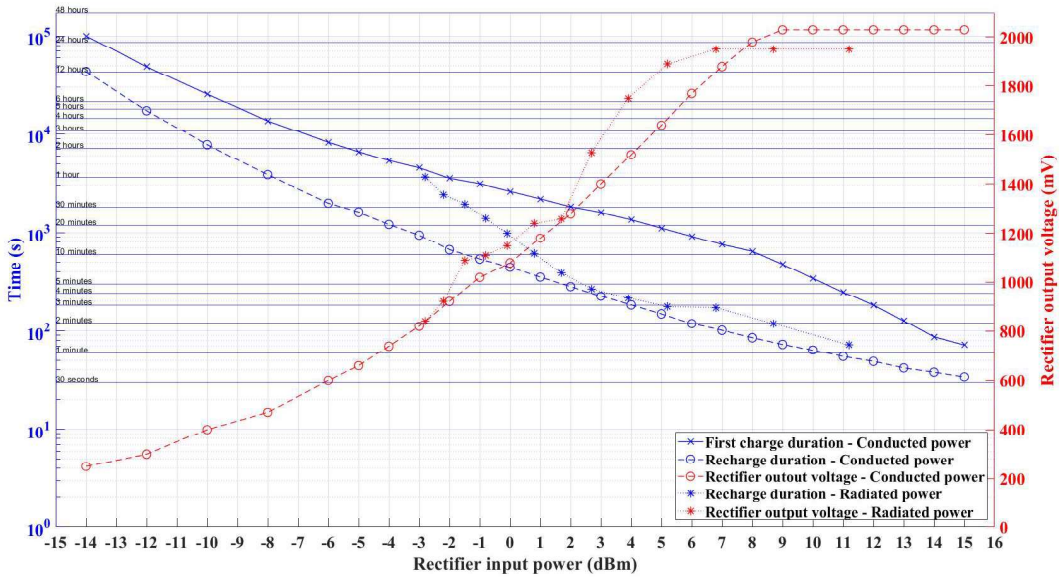

Figure V.57: Durations of the first charge and recharges (blue, left), and rectifier output voltages in open-circuit during the recharges (red, right) against the measured conducted (dashed line and 'o') and estimated radiated (dotted line and '*') electromagnetic input power applied at the input of the rectifier of the sensing nodes, for a frequency of 868 MHz.

According to the Figure V.58, this one is rather low for the first charge: between 3.4 % and 9.2 % for Rect1 (the full-wave rectifier) and between 4.7 % and 9.2 % for Rect3 (the half-wave rectifier); and according to the Figure V.58, this one is increased for the recharges: between 13.1 % and 36.4 % for Rect1 and between 13.1 % and 31.0 % for Rect3. The interpretations done above (Section V.D.3.ii.) can be made again: during the first charge, Rect1 is less efficient than Rect3 for the highest input powers; and the two rectifiers have similar performances for lowest input powers; during the recharge, Rect1 is more efficient than Rect3 for all the tested input powers; and Rect2 it falls short of the other two. More, whatever the rectifier, the lowest efficiencies during the first charges are for input powers higher than +4 dBm (or 2.51 mW). Only the serial rectifier sees its efficiency re-increasing for input powers higher than +12 dBm (or 15.85 mW); whilst the lowest efficiencies during the recharges are for the lowest and the highest input powers.

To improve the energy efficiency of the sensing node, according to the energy required for a measurement and a wireless transmission of the collected -and eventually pre-processed- data, the time required for the first charge and for the recharges must be reduced (e.g. by optimizing the efficiency of each components which will allow to reduce the minimum required input power linked to the power needs and losses of the various components, etc.). As explained all along this chapter, this can be achieved by optimizing the hardware of the sensing nodes.

Another efficiency which could be relevant to express is the one defined as the ratio of the energy transmitted by a communicating node to wirelessly power all the sensing nodes in its neighbourhood to the sum of the energies consumed by each sensing node for measurements and wireless transmissions of the collected -and eventually pre-processed- data. In this, the more sensing nodes there are, the higher the overall efficiency; and the higher the efficiency of each sensing node, the higher the overall efficiency.

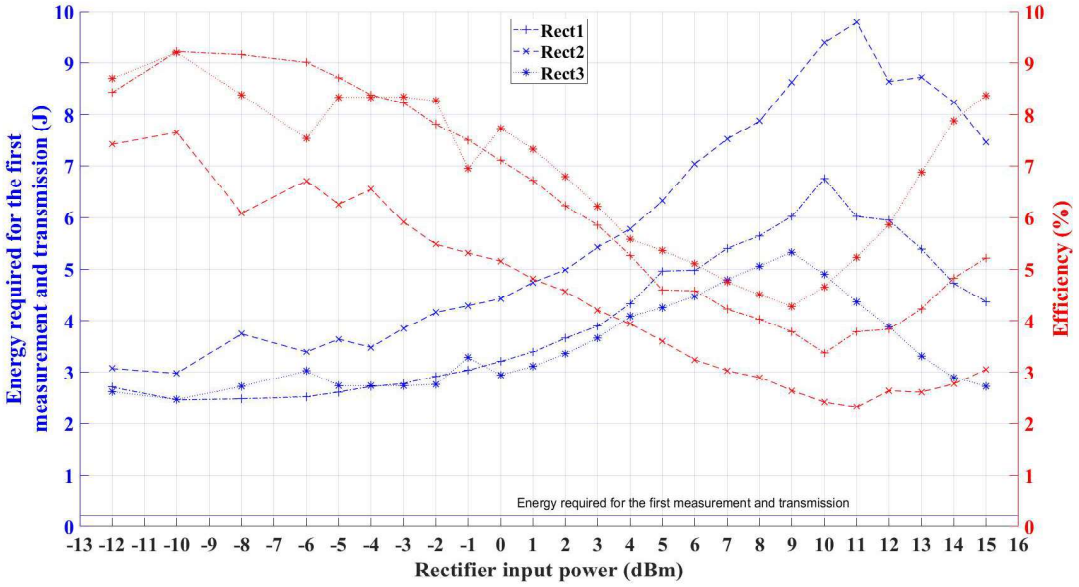

Figure V.58: Energy required for the first charge (blue, left) and the energy efficiency of the sensing nodes during this first charge (red, right) against the conducted electromagnetic input power applied at the input of the rectifier of the sensing nodes, for a frequency of 868 MHz and against the rectifier under test (Rect1: dashed lines and '+'; Rect2: dotted and dashed lines and 'x'; and Rect3: dotted lines and '*').

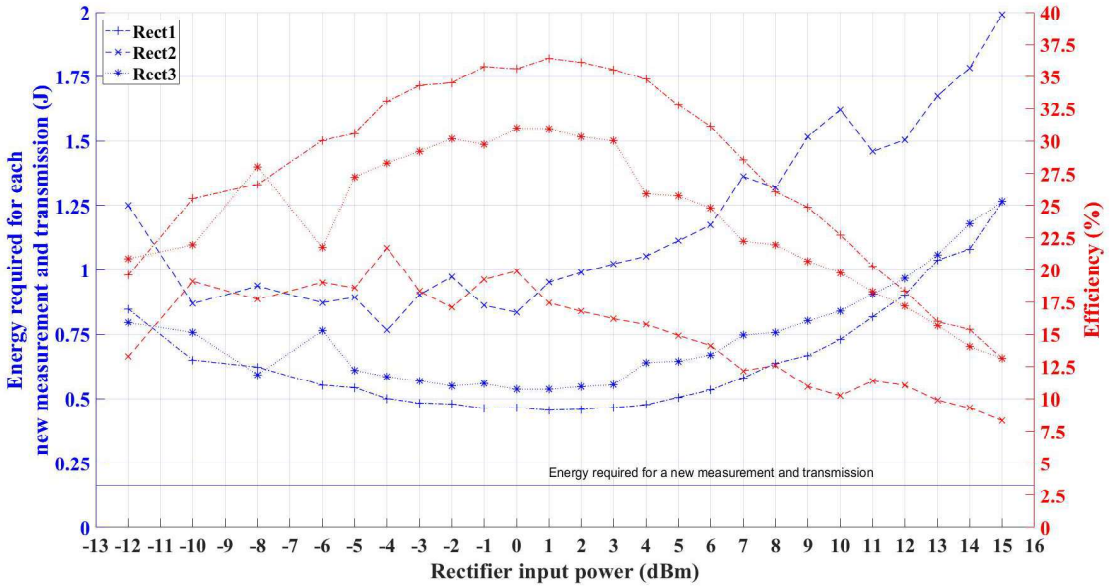

Figure V.59: Energy required for the recharges (blue, left) and the energy efficiency of the sensing nodes during these recharges (red, right) against the conducted electromagnetic input power applied at the input of the rectifier of the sensing nodes, for a frequency of 868 MHz and against the rectifier under test (Rect1: dashed lines and '+'; Rect2: dotted and dashed lines and 'x'; and Rect3: dotted lines and '*').

vi. Use of a unique antenna in the sensing nodes, both for the radiative electromagnetic power harvesting and the wireless communication

In order to use a unique antenna in the sensing nodes, both for the radiative electromagnetic power harvesting and the wireless communication, a radiofrequency circulator can be used as introduced above (Section V.D.1.). Nevertheless, this one induces insertion losses, which could impact the functioning of the sensing nodes. To quantify the impact of the use of the radiofrequency circulator, several sensing nodes have been characterized in terms of required times for a first charge and for the recharges, with and without the use of the radiofrequency circulator, as presented in Figure V.60.

To perform this characterisation, a conducted electromagnetic power is applied at port 1 of the radiofrequency circulator (to emulate the energy harvested by the antenna), whilst the port 2 is connected to the input of the rectifier of the sensing node and the port 3 to a 50 Ω load (to emulate the LoRaWAN transceiver (which is connected to another antenna during the characterization) and to avoid to inject power in the power source). The times are estimated by using the time stamps provided by the communicating node for each received LoRaWAN frame transmitted by the sensing node under test. The characterization has been performed with sensing nodes of the same generation than SN4 and at 868 MHz, and for input power range from -14 dBm (or 39.8 µW) -well below the estimated minimum input power required to operate properly the sensing nodes in the worst case (Section V.C.2.iii.)- to + 15 dBm (or 31.6 mW).

As presented in Figure V.60, the use of the circulator induces a low loss, which is constant regardless the input power. This analysis is confirmed by the analysis of the efficiency which

is weakly impacted by the use of the radiofrequency circulator, as presented in Figure V.61 and Figure V.62.

Regarding the characterizations presented respectively in the Figure V.56, Figure V.58 and Figure V.59, and in the Figure V.60, Figure V.61 and Figure V.62, the second set of data provides higher performances but maintaining the same trends (in terms of durations and efficiencies of the sensing nodes during the first charge and the recharges): from between 3.4 % and 9.2 %, to between 4.8 % and 10.8 % with the radiofrequency circulator, and between 5.85 % and 11.5 % without the radiofrequency circulator, concerning the energy efficiency of the first charge; and from between 13.1 % and 36.4 %, to between 8.2 % and 40.4 % with the radiofrequency circulator, and between 9.9 % and 40.6 % without the radiofrequency circulator, concerning the energy efficiency of the recharges. The differences can mainly be explained by the fact that the energy stored have been minimized (from 245 mJ to 159 mJ) by reducing the activation and deactivation threshold voltages (respectively from 5.25 V to 4.45 V, and from 2.35 V to 2.30 V), which has been possible thanks to the only use of the Texas Instruments HDC2010 temperature and relative humidity sensor and no longer the Adafruit DHT22.

To conclude, by controlling the generated radiative electromagnetic power, the communicating nodes can impose a periodicity of measurement and wireless communication for the sensing nodes, without altering neither their software or their hardware. This is the only possibility of reconfigurability for the sensing nodes in the way these have been designed, without downlink excepted through the radiative electromagnetic power harvesting. By characterizing the sensing nodes in terms of durations for a first charge and recharges and of energy efficiency, the minimum time required to wirelessly power all the sensing nodes in

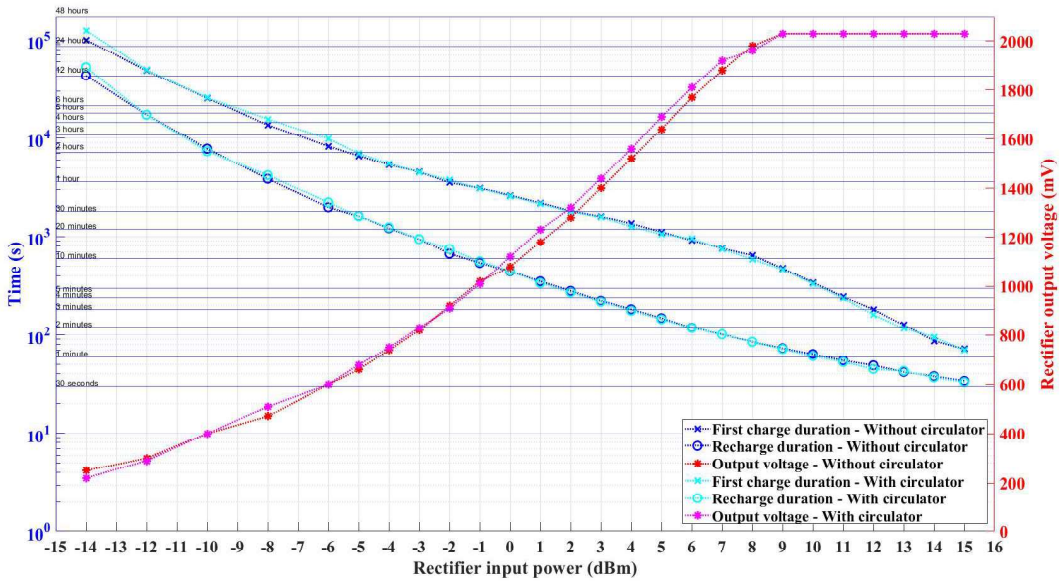

Figure V.60: Durations of the first charge and recharges (left), and rectifier output voltages in open-circuit during the recharges (right) against the conducted electromagnetic input power applied at the input of the sensing nodes, for a frequency of 868 MHz, and with and without the use of the radiofrequency circulator.

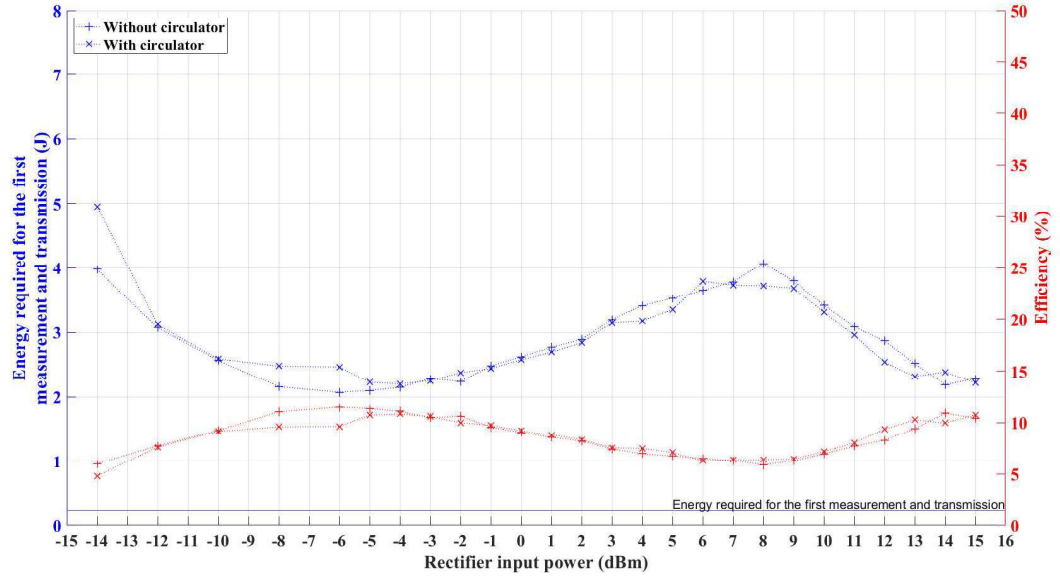

Figure V.61: Energy required for the first charge (blue, left) and the energy efficiency of the sensing nodes during this first charge (red, right) against the conducted electromagnetic input power applied at the input of the sensing nodes, for a frequency of 868 MHz, and with and without the use of the radiofrequency circulator.

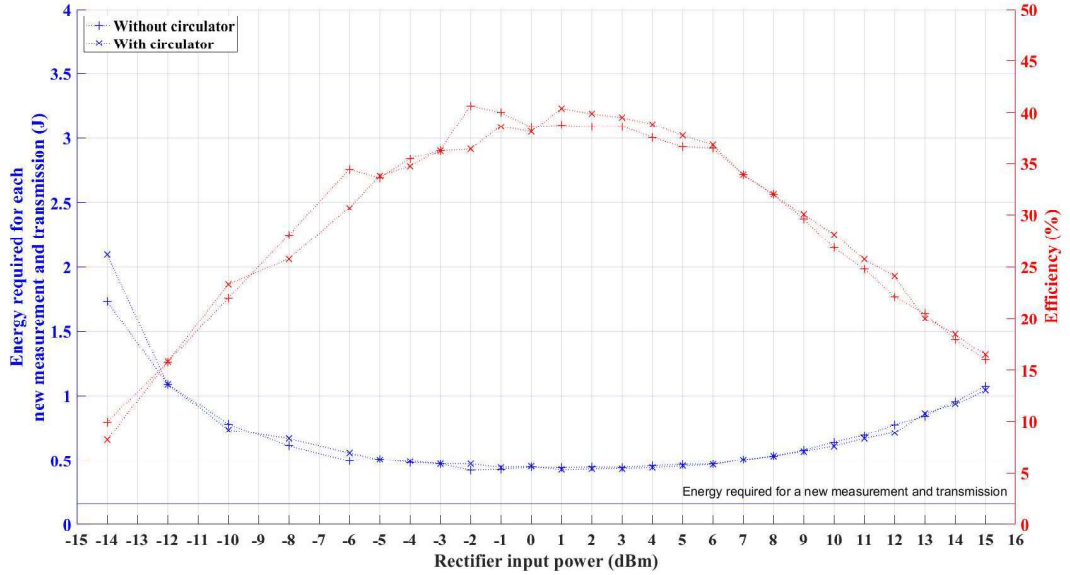

Figure V.62: Energy required for the recharges (blue, left) and the energy efficiency of the sensing nodes during the recharges (red, right) against the conducted electromagnetic input power applied at the input of the sensing nodes, for a frequency of 868 MHz, and with and without the use of the radiofrequency circulator.

its neighbourhood of the communicating node can be deducted and allows to this last to implement its own strategy of wireless power transfer. This energy efficiency could be increased and must be considered in the purpose of deploying large scale complete wireless

sensor networks. Moreover, the use of a radiofrequency circulator allows the use of a unique antenna, both for the radiative electromagnetic power harvesting and the wireless communication, and the reduction of the size of the sensing nodes, at the price of a low degradation of the performances.

4. Qualitative tests and results

To certify the proper functioning of the sensing nodes, and more generally of the wireless sensor network, several qualitative tests have been achieved, in addition to the quantitative ones. Several configurations were tested, between others: a unique communicating node with a unique sensing node, indoors (as presented in Figure V.63), outdoors, in an anechoic chamber and in a reinforced concrete beam, for range between 50 centimetres up to 7 meters (in the air; during the experimentation shown in Figure V.64); a unique communicating node with several sensing nodes (up to 4, *i.e.* all those available at the time), indoors, outdoors, in an anechoic chamber and in a reinforced concrete beam (up to three inside and one outside as presented in Figure V.65); several communicating nodes (up to 2, *i.e.* all those available at the time) and with several sensing nodes (up to 4, *i.e.* all those available at the time), indoors and in a reinforced concrete beam (up to three inside and one outside); a radiative electromagnetic power source located in one of the cavities of the reinforced concrete beam (central and lateral), two sensing nodes in the other cavities, and other sensing nodes and the LoRaWAN gateway in the same room; etc.

Several results can be drawn from these qualitative experimentations. First, but essential, the sensing nodes can be wirelessly powered by the communicating nodes through the radiative electromagnetic power transmission, and all the transmitted data (in the air or from the reinforced concrete beam) have been well received, thanks to the LoRaWAN technology, and processed by the same communicating node. A unique communicating node can easily manage several sensing nodes (both for the wireless power transfer and the wireless communication) over several metres in an almost omnidirectional way: in the air, the maximum distance tested between the communicatings node and the sensing nodes has been 7 meters; and for the sensing nodes embedded in the reinforced concrete beam, 2 metres, distributed in 15 cm of reinforced concrete and 185 cm of air. In the two cases, it seems possible to achieve higher distances (the periodicity of measurement and wireless data transmission were of several hours). By controlling the radiative electromagnetic power generated by the communicating node (tested here by changing the output power), the periodicity of measurement and wireless communication of the sensing nodes can be controlled. Then, the use of a network of two communicating nodes is also effective and allows a larger volume to be covered. In spite of the theoretical minimum input power required by the sensing node to operate properly in the worst case has been estimated above (Section V.C.2.iii.) at -10 dBm or 100 µW), the current implementations of the sensing nodes have been successfully tested for an input power down to -14 dBm (39.8 µW), that says a theoretical maximum range in the air of 10.94 metres.

Nevertheless, the solution implemented currently is a first proof-of-concept of a battery-free wireless sensing node, which is energy autonomous (by being wirelessly powered by a radiative electromagnetic wireless power transfer system), and dedicated to the structural health monitoring of the reinforced concretes (as demonstrated by the types of sensors usable and tested (e.g. temperature and relative humidity sensor, resistivity sensor, strain gauge,

etc.)). The wireless sensor network provided is mainly constrained by the wireless power transfer, which has a useful range of few meters, and not by the wireless communication, achieved thanks to the LoRaWAN technology, which can transmit data over kilometres in the air, and at least a hundred of meters in indoors, even in non-optimal configurations.

5. Work in progress and perspectives

Even if encouraging results have already been achieved, several works on several aspects are still in progress, are planned or seem relevant.

Figure V.63: Photographs of an experimentation in indoors (room) of an integrated sensing node of the same generation than SN4, wirelessly powered by a communicating node.

Figure V.64: Photographs of an experimentation in indoors (subbasement of the laboratory) of an integrated sensing node of the same generation than SN4, wirelessly powered by a communicating node.

Figure V.65: Photographs of an experimentation of three integrated sensing nodes of the same generation than SN4 embedded into the reinforced concrete beam, wirelessly powered by a communicating node.

As explained throughout this chapter, each subpart of the sensing nodes can be improved. For the data collection, pre-processing and wireless transmission both the hardware and the software can still be optimized with as main objective to reduce the required energy. That is why, the characterization of the power consumption according to the data-rate, or indirectly the duration of the LoRaWAN transmission, is planned and first qualitative tests have been achieved in this sense. For the part dedicated to the measurements of the properties of the reinforced concrete, the integration of new sensors is hoped, as well as the improvement in terms of precision and power consumption of those already used. For the energy harvesting and management part, the test of the e-peas AEM30940 power management unit is already planned and the design of new rectenna (both the rectifier and the antenna) are continuously under investigations, whilst the use of flexible substrates for the current solutions are still in progress (the first antennas on Kapton are always under test and the process is being finalised).

Regarding to the complete sensing nodes, the tests and characterizations of the last versions are still in progress. The reasons for the low decline in performances are still investigated, especially the higher power consumption of the LoRaWAN modules and the slightly less good overall energy efficiency. Additional qualitative experimentations are planned, especially by embedding the sensing nodes in the reinforced concrete beam but in smaller cavities (by using additional concrete box around). Moreover, the test of different waveforms to excite the rectenna (e.g. frequency modulation, chirps, pulse, etc.) is currently underway.

With a broader point of view, a package will be necessary for burying the sensing nodes into the damp reinforced concrete without altering the electronics. However, this package must allow to interface the transducers with the reinforced concrete in order to perform measurements of its properties.

Also, the estimation of the energy efficiency of the entire wireless power transfer system could be relevant to estimate, according to the number of sensing nodes. This one can be defined as the ratio of the energy transmitted by a communicating node to wirelessly power all the sensing nodes in its neighbourhood to the sum of the energies consumed by each sensing node for measurements and wireless transmissions of the collected -and eventually pre-processed- data.

Finally, new approaches to reduce the size of the sensing nodes are under investigations, as well as alternative ways to deploy the sensing nodes in the reinforced concrete regarding the elements and needs defined by the LMDC. The two discussed alternatives are the next: deploying only the sensor in the core of the concrete and the rest of the sensing node near or on the surface, so, the measurements are performed in the places defined as the most relevant and the sensing nodes are accessible, thus replaceable and updatable; deploying the sensing nodes in the core of the concrete and the antenna near or on the surface, so, the measurements are performed in the places defined as the most relevant and the sensing nodes are inaccessible but the constraints of the electromagnetic propagation through the reinforced concrete are released. In the two cases, the use of wires between the different parts can create weaknesses in the reinforced concrete and an access on the surface is also an access point for the pollutants and other contaminants, such as the air and the water which can induce a faster corrosion.

E. Conclusion

In this chapter, the implementations of the sensing nodes based on LoRaWAN technology have been proposed. These are composed of three subsystems, whose the design, the implementation, the characterisation, the improvements and the alternatives have been discussed. There are: the part dedicated to the data collection, pre-processing and wireless transmission, allowing to drive the sensors, to pre-process the collected data before to wirelessly sent these through a LoRaWAN frame; the part dedicated to the measurements of the properties of the reinforced concrete based on the use of various sensors, such as temperature and relative humidity sensors, resistivity sensor and strain gauge; and the part dedicated to the energy harvesting and management, allowing to power the two other parts by harvesting the radiative electromagnetic power provided by the communicating nodes and storing it until enough energy is available. Finally, the complete implementations of the sensing nodes and of the wireless sensor network, as well as some perspectives, have been introduced.

It is also time for a short conclusion on the current implementation of the targeted wireless sensor network based on the LoRaWAN technology. This one is composed of a "meshed" network of two exploded communicating nodes and of four integrated and relatively compact sensing nodes. The communicating nodes are able to collect the LoRaWAN data frames sent by the sensing nodes; aggregate, process, store and share the data provided by the sensing nodes within the meshed network of communicating nodes, the stakeholders and through the Internet; and wirelessly power over several meters the sensing nodes in their neighbourhood (both in the air and in a reinforced concrete beam), and remotely control the periodicity of measurement and wireless communication of the sensing nodes through the tuning of the radiative electromagnetic wireless power transfer system. The sensing nodes can sense some physical parameters (e.g. the temperature and the relative humidity, the electrical resistivity, the mechanical deformation, etc.) to quantify the internal states of the reinforced concrete and/or its environment, and wirelessly transmit over tens or hundreds of meters the collected and eventually pre-processed data to the communicating nodes through LoRaWAN frames. Because the sensing nodes become inaccessible once deployed and embedded into the reinforced concrete, these are battery-free and energy autonomous, with a targeted lifespan of decades, as for the reinforced concrete itself. Finally, the sensing nodes use a unique antenna both for the wireless power transfer and the wireless communication, thanks to the use of a radiofrequency circulator and the use of the same frequency band for the two functions. The current implementation is a complete cyber-physical system which meets the requirements of the simultaneous wireless information and power transmission paradigm.

The two next chapters will detail the first works made in order to design and implement the targeted wireless sensor network with the use of the Bluetooth Low Energy technology.

VI. First works on the implementation of communicating nodes based on the Bluetooth Low Energy technology

In agreement with the Figure III.4 and the Figure III.5, and on the base of the communicating nodes based on the LoRaWAN technology presented above (Chapter IV.), a unique communicating node based on the Bluetooth Low Energy (BLE) technology has been partially implemented. This one has for main purpose the certification of the good functioning of the sensing nodes based on the Bluetooth Low Energy (BLE) technology, especially by collecting, processing and storing the data sent *via* Bluetooth Low Energy frames. This has the same constraints than the previous, *i.e.* is considered accessible, has an unlimited power source and the design of the interfaces with the sensing nodes are preferred to others.

In contrast to the detailed presentation made of the communicating nodes based on the LoRaWAN technology (Chapter IV.), only the differences with these previous implementations will be presented here.

A. Radiative electromagnetic power source

The radiative electromagnetic power source used by the unique communicating node, for wirelessly powering the sensing nodes located in its neighbourhood, is exactly the same than the one introduced above (Section VI.A.). Again, the wireless power transfer system is the unique downlink from the communicating nodes to the sensing nodes and can be used to remotely set up the behaviour of the sensing nodes as explained above (Section V.D.3.).

B. Data management system

The main differences with the previous implementations concern the data management subsystem. This one must collect, process, store and share the data transmitted by the sensing nodes within the meshed network of communicating nodes and with the digital world through the Internet. Priority has been given to the uplink interface with the sensing nodes.

1. Interfaces for the wireless communications

i. Collection of the data sent by the sensing nodes

As the sensing nodes transmit their measured data *via* the Bluetooth Low Energy technology, as a broadcaster generic access profile (GAP) and through advertising data frames, the communicating nodes must be able to collect the Bluetooth Low Energy advertising frames to recover the data sent, as an observer generic access profile (GAP). The choices of the Bluetooth Low Energy wireless communication technology and of the topology based on broadcasters and observers are imposed by the design of the sensing nodes and will be justified below (Section VII.A.1. and Section VII.A.2.). In few words, the use of the Bluetooth Low Energy technology instead of the LoRaWAN one allows to get theoretically the same order of magnitude for the ranges of use of both the wireless power transfer and the wireless communication (over several metres); but above all it, to significantly reduce the energy required to power the sensing nodes. Moreover, the Bluetooth, and thus its Low Energy version, are common and widely used technologies, especially in almost all the general public devices with wireless communication abilities (e.g. laptops, tablets, smartphones, etc.).

Thus, the system dedicated to the reception of the Bluetooth Low Energy frames sent by the sensing nodes is based on an off-the-shelf NXP QN9080 DK development board [661]. This one embedded an NXP QN9080 module, which is a full system-on-chip (SoC) based on a 32-bit ARM Cortex-M4F based microcontroller unit (MCU), on-chip memory and a Bluetooth Low Energy compatible transceiver working in the 2.45 GHz industrial, scientific and medical (ISM) frequency band [662]. The microcontroller embeds the full Bluetooth Low Energy stack (from the driver of the radio transceiver, to the GATT (generic attribute) profiles, through the link controller, the host layers and the GAP (generic access profile)). This implementation allows the good reception of the Bluetooth Low Energy frames sent by the sensing nodes.

ii. Sharing of the collected data within the meshed network of communicating nodes

To date, no solution has been implemented to share the data between the communicating nodes. By conserving the current hardware implementation, it could be possible for the Bluetooth Low Energy module to manage both: the reception of the advertising data frames sent by the sensing node by using an observer generic access profile; and the bidirectional communication with other communicating nodes in order to share the data in a connected way (for higher safety and higher data-rate) by using a central (or master) or peripheral (or slave) generic access profile. However, these two modes (unconnected (broadcaster/observer) and connected (central/peripheral)) are exclusive and cannot be used simultaneous, and thus, the time repartition between these must be managed. More, during the connected communications

between communicating nodes, the advertising data frames sent by the sensing nodes could be lost. To manage the time repartition, the next architecture could be tested: the communicating nodes are by default configured as observers; for each advertising frame these check if it is a data frame from a sensing node or if it is a connection request from an already known communicating node; in the second case, the communicating nodes stop their radiative electromagnetic power source (to minimize the probability of the reception of a new advertising data frame from a sensing node), connect the other communicating node and share data; once finished, these come back in their default configuration. These could also initiate the communication with other communicating nodes, for instance, once enough new data are received and stored.

Only very few tests of the connected Bluetooth Low Energy wireless communications between the communicating nodes and without considering the sensing nodes have been achieved.

iii. Sharing of the collected data across the Internet and remote access to the communicating nodes by the stakeholders' devices

To date, no solution has been implemented to share the data collected and stored in the communicating nodes across the Internet, as well as for the remote access to the communicating nodes by the stakeholders' devices. With the current hardware implementation, this seems unfeasible. Thus, a more complex architecture, with additional transceiver(s), must be designed in this purpose.

iv. Local access to the communicating nodes by the stakeholders' devices

In the current hardware implementation, the collect by the user(s) of the data stored by the communicating nodes is done thanks to a wire USB (universal serial bus) connection and by the use of a serial COM port (communication port). As no authentication process is possible, everyone with a physical access to the communicating nodes can collect the stored data or modify the firmware through its JTAG programming interface.

2. Processing and storage of the collected data

Once received, demodulated and decoded, the Bluetooth Low Energy advertising data frames can be processed and stored in the available 512 kB of flash memory. As only a small microcontroller is used, the processing possibilities are limited.

3. Alternatives and perspectives

The proposed design is very limited and is at its early age. Indeed, the main objective has only been to provide a tool to check the good transmission of the Bluetooth Low Energy advertising data frames by the sensing nodes, and nothing more.

For a real implementation of the data management part of the communicating nodes based on the Bluetooth Low Energy wireless communication technology, a more complex system with higher performances must be implemented, whilst staying accessible to be reconfigured, updated and modified according to new constraints or needs. Indeed, it seems impossible for the current microcontroller and its 512 kB of flash memory to manage all the software

required by the different interfaces and processes (especially for the routing of the meshed network of the communicating nodes and the data dissemination within, as well as the connection with the digital world through the Internet). More, the interfaces, excepted the one dedicated to wireless communication with sensing nodes, must be more defined to make the most relevant and adapted choices of the wireless communication technology(ies) to employ in regards of the users and application constraints. It is similar regarding the processing and the storage of the collected data, whose the possible solutions are numerous and varied, and these are again the constraints imposed by the users and applications which will allow to define the best trade-offs.

Regarding the reception of the Bluetooth Low Energy advertising data frames, other hardware solutions are available and no comprehensive and objective comparison has been achieved. Nevertheless, the use of the employed low power all-in-one module allows an easy development and a compact implementation.

A perspective could be the design and implementation of a full data management system with higher performances and features, whose the wireless communication interfaces with the other communicating nodes and locally with the stakeholders, larger processing and storage abilities, etc. This one could be based on the use of a Raspberry Pi microcomputer, as for the LoRaWAN version, or a microcontroller on which a light operating system (OS) could be implemented.

C. Energy management system

In order to power the radiative electromagnetic power source and the data management system, the third part composing the communicating nodes is the energy management system. As explained above (Section II.A.3.) and in order to release the constraints, the communicating nodes are considered as accessible and with an unlimited power source. In practice, this means that these can be connected to the mains supply or their batteries can be recharged or changed.

Thus, the same solution than for the LoRaWAN implementation is used to power the radiative electromagnetic power source (Section IV.C.), whilst the data management system can be powered with 5 V supply voltage through the USB interface, or thanks to a coin cell battery.

D. Complete implementation and tests of the communicating node

The current and incomplete version of the communicating nodes based on the Bluetooth Low Energy wireless communication technology works properly, but only partially. Thus, the energy management subsystem powers the two other subsystems; the data management subsystem collects, processes and locally stores the Bluetooth Low Energy advertising data frames sent by the sensing nodes which contain the measurement data, and is locally accessible by everyone through an USB connection; and the radiative electromagnetic power source powers wirelessly all the sensing nodes located in its neighbourhood (over several meters in all directions). These are the lower priority wireless communication interfaces which are not yet implemented, including those dedicated to: deploying the meshed network of communicating nodes; connecting to the digital world through the Internet; and providing only for the stakeholders (from their devices) a local and/or remote access to the communicating nodes and their network.

In this implementation, the communicating nodes are composed of two distinct hardware parts: the Bluetooth Low Energy observer and the radiative electromagnetic power source. These two have similar ranges of use, with an order of magnitude of several meters, and up to few tens of meters for the wireless communications. As these use different and non-overlapped industrial, scientific and medical (ISM) frequency bands, respectively the 868 MHz one and the 2.45 GHz one, these two components can be located at the same place without interferences. Also here, the provided system meets the requirements of the simultaneous wireless information and power transmission (SWIPT) paradigm but through frequency multiplexing. It could be possible to use a unique bi-band antenna both for the wireless communication and the wireless power transfer, only if a bi-band or broadband radiofrequency circulator is used or if the antenna has two feeding ports.

Some preliminary tests have been performed to validate the proposed implementation: for a communicating node in a single location and for the spatial separation of its two main functions, and for various number of sensing nodes (from 1 to 3), at various distances, in the air and in a reinforced concrete beam.

For the future, it would be nice to design and implement a one-piece and integrated communicating node which includes and interfaces its three subsystems, once these are fully designed and tested.

E. Conclusion

In this short chapter, the current and partial implementation of a communicating node based on the Bluetooth Low Energy technology has been proposed. This is composed of three subsystems, whose only the differences with their version designed and implemented for the communicating nodes based on the LoRaWAN technology have been discussed. There are: a radiative electromagnetic power source generating a +33 dBm (or 2 W) continuous wave at 868 MHz and dedicated to the wireless and remote powering of the sensing nodes; a data management system which only deals with the reception, the processing and the local storage of the data wirelessly sent by the sensing nodes thanks to Bluetooth Low Energy advertising data frames in the industrial, scientific and medical (ISM) 2.45 GHz frequency band; and an energy management system used to power the two other subsystems.

The next chapter will detail the differences between the design and implementation of the sensing nodes based on the Bluetooth Low Energy technology, and those based on the LoRaWAN technology.

VII. First implementation of sensing nodes based on the Bluetooth Low Energy technology

In agreement with the Figure III.4 and Figure III.6, and on the base of the sensing nodes based on the LoRaWAN technology presented above (Chapter V.), first sensing nodes based on the Bluetooth Low Energy technology have been implemented and tested. As previous ones, these are considered as inaccessible once deployed because embedded into the reinforced concrete, and must measure some physical parameters to quantify the internal states of the reinforced concrete and/or its environment; transmit wirelessly the collected and eventually pre-processed data to the communicating nodes; and harvest the radiative electromagnetic power generated by the communicating nodes to power themselves. To be useful during all the lifespan of the communicating reinforced concrete, that says decades, these must be reliable and resilient.

In contrast to the detailed presentation made of the sensing nodes based on the LoRaWAN technology (Chapter V.), only the differences with these previous implementations will be presented here.

A. Data collection, pre-processing and wireless transmission

In order to wirelessly transmit the measured data to the communicating nodes, these new sensing nodes use the Bluetooth Low Energy wireless communication technology. Again, and for reasons of hardware security and power consumption, only the data uplink from the sensing nodes to the communicating nodes is available. Thus, the sensing nodes could not receive data, especially through Bluetooth Low Energy frames from the communicating nodes or other devices. Indeed, their design does not allow themselves neither to take part of a connected Bluetooth Low Energy communication, or to be configured as an observer. Nevertheless, these are partially reconfigurable: indeed, their measurement and wireless communication periodicity can be tuned by the communicating nodes through the use of their radiative electromagnetic power source.

1. Technology choice

As explained above (Section V.A.1.), the targeted specifications for the wireless communications from the sensing nodes to the communicating nodes are, and as a minimum: the possibility of a unidirectional configuration (only from the sensing nodes to the communicating nodes, without connection or acknowledgement), a low power consumption (to be wirelessly powered), a medium range (at least a ten of metres), a low data-rate (a few bytes a few times an hour/day/week), the availability (in terms of off-the-shelf components and/or network infrastructures), the standardization and the documentation, a good reputation, and, above all, the ability to communicate through reinforced concrete.

As always introduced above (Section V.A.1.), the implementation of sensing nodes based on a wireless communication technology dedicated to the low power wide area networks (LPWAN), and in particular based on LoRaWAN, can be considered as the "worst" solution in terms of power consumption. Thus, its successful implementation with its power supply by

wireless power transfer has provided the supposed "worst" characteristics, which can be considered as only improvable with the use technologies requiring less energy. It seems that the wireless communication technologies dedicated to the wireless personal area networks (WPAN), in particular the Bluetooth Low Energy, are the most suitable alternatives to test in order to minimize the energy required for the wireless communication and to get a range of use in the same order of magnitude than the one of the wireless power transfer (that says several meters). Indeed, the Bluetooth Low Energy has a theoretical range of few tens of metres and, during preliminary indoor tests, has been able to pass through few reinforced concrete elements, such as walls. Moreover, the Bluetooth, and thus its Low Energy version, are standardized, well documented, usual and widely used technologies, especially in almost all the general public devices with wireless communication abilities (e.g. laptops, tablets, smartphones, etc.).

Finally, first quantitative tests of the Bluetooth Low Energy communications in the topology based on broadcasters and observers have been performed into the reinforced concrete beam by using NXP QN9080 DK development boards [661]. These have shown that ranges of more than 20 meters are achievable with less than 5% of packet error rate (PER), whilst almost no communication have failed before 11 meters, for a broadcaster embedded in the reinforced concrete beam and an observer outside, in an outdoors environment. More, lossless communications have been achieved between two boards embedded in the reinforced concrete beam at a distance of around 90 cm. Nevertheless, there is no evidence to support that communications took place only in the reinforced concrete, maybe another path (through reinforced concrete and air, with a reflection on the ground) has been followed.

2. Design and implementation

To implement the part of the sensing nodes dedicated to the data collection, pre-processing and wireless transmission, an all-in-one NXP QN9080 Bluetooth Low Energy module has been used [662]. This one is a full system-on-chip (SoC) based on a 32-bit ARM Cortex-M4F based microcontroller unit (MCU), on-chip memory and a Bluetooth Low Energy compatible (in its fifth version) transceiver working in the 2.45 GHz industrial, scientific and medical (ISM) frequency band. The user must only add an antenna, a power source and eventually one or some sensors, as well as program the microcontroller with its own firmware embedding the full Bluetooth Low Energy stack (from the driver of the radio transceiver, to the GATT (generic attribute) profiles, through the link controller, the host layers and the GAP (generic access profile)), to get a complete Bluetooth Low Energy device. Its current implementation is presented in Figure VII.1. This module requires a voltage supply between 1.62 V and 3.6 V, thanks to the use of an integrated DC-to-DC buck converter.

In order to keep its power consumption as low as possible, to ensure long-term reliability and resilience, the part of the sensing nodes dedicated to the data collection, pre-processing and transmission is designed as simple as possible, both in terms of hardware and software.

The developed firmware, coded in C language and using a Bluetooth Low Energy stack, allows the microcontroller to initialise itself and all the desired peripherals -whose the transceiver- and required interfaces as soon as it is powered; then to drive the chosen sensor to get measurements; to pre-process the data from the sensor especially to format these; to

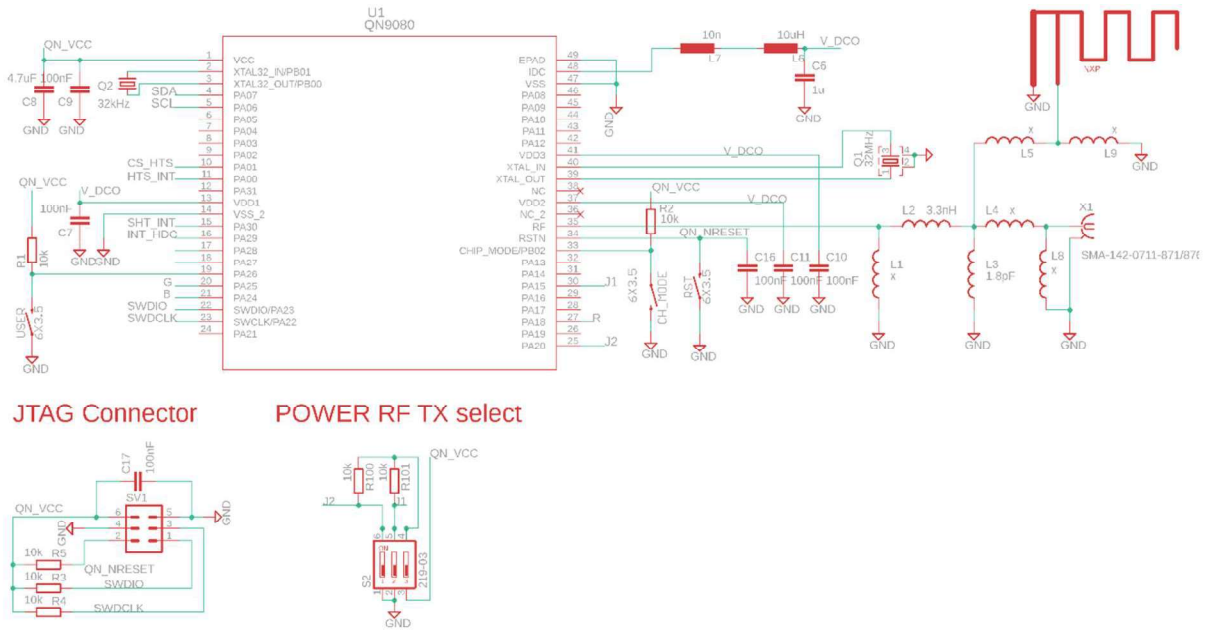

Figure VII.1: Schematics of the implementation of the NXP QN9080 Bluetooth Low Energy module.

send into four Bluetooth Low Energy advertising data frames the formatted data to the communicating nodes; and finally to go into a deep-sleep mode in order to consumed all the spared energy until its power supply is stopped by power management part. The sensing nodes are configured according to the broadcaster generic access profile (GAP) without the ability to receive frames because of its configuration in the notification mode for the advertising transmissions. This one does not require acknowledgement contrary to the indication mode. Thus, these can only send advertising frames, in which are embedded the data. This design is chosen because the downlink is not desired at this point. Indeed, the power consumption is reduced by deleting the time dedicated to the listening of the medium for receiving acknowledgement, data or firmware update; and the security is increased by imposing a fixed firmware and by blocking all accesses required to alter or update it. More, and according to the first measurements of the power consumption of the NXP QN9080 Bluetooth Low Energy module embedded on the NXP QN9080 DK development board [661], the process of the transmission of 2 bytes of data consumes over 18 times more in a connected communication than for a broadcast transmission in the three dedicated advertising channels. Moreover, to maintain a connected communication an advertising frame must be exchanged at least each 65 seconds. For minimizing the power consumption of the sensing nodes, the topology based on broadcasters and observers is highly privileged. In this way, nearly 1 second is required from the power-up to the end of the transmissions, of which about 750 milliseconds are used for the four transmissions which are separated by times of deep-sleep. Each step in the employed process is observable in the use by the sensing nodes of the available energy as presented in Figure VII.2. Thus, the process is reduced to the power-up, the initialization and a one-shot measurement (between 0 s to 210 ms) and four transmissions of the same Bluetooth Low Energy advertising data frame (from 210 ms to the end, each 250 ms). The periodicity of this process is not controlled by the software (e.g. with events or timer interruptions) but by the power supply *via* the hardware.

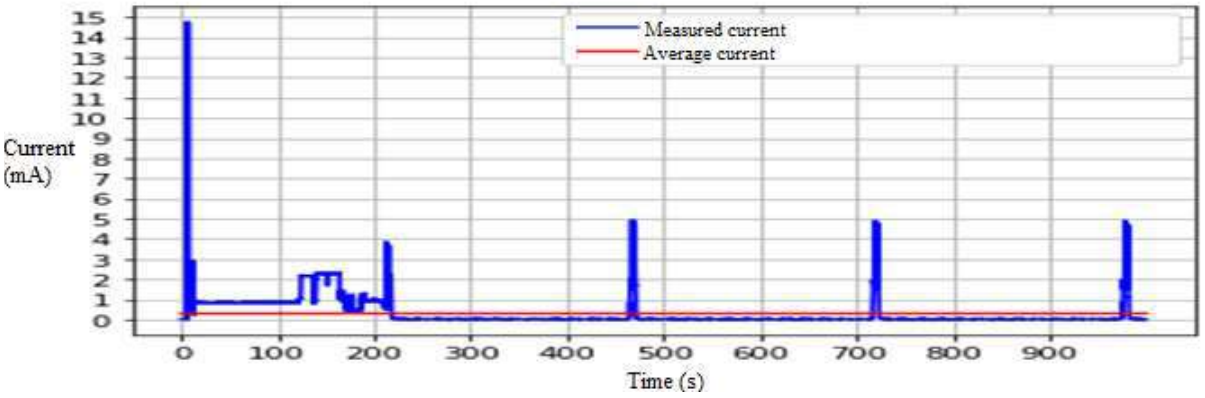

Figure VII.2: Power consumption of the sensing nodes powered by a 3 V supply voltage.

Concerning the Bluetooth Low Energy advertising frames, these are 19 bytes long, whose 16 bytes dedicated to the Bluetooth Low Energy protocol and 3 bytes dedicated to the data payload (two measurements formatted on 3 bytes), as presented in Figure VII.3. In a usual use, each advertising frame is sent three times in the three 2 MHz advertising channels of the 2.45 GHz industrial, scientific and medical (ISM) frequency band (channel 37 around 2.402 GHz, channel 38 around 2.426 GHZ and channel 39 around 2.800 GHz). Nevertheless, since the fifth version and the advertising extensions, all the 40 advertising and data channels can be employed for advertising purpose. In order to increase the probability of a good reception without increasing too much the power consumption, each advertising frame is sent four times in this implementation, only in the three advertising channels, with an advertising interval of 250 ms and with a power of +0 dBm.

The developed hardware is essentially a printed circuit board (PCB) dedicated to solder the NXP QN9080 Bluetooth Low Energy module with its decoupling capacitors; its communication interfaces to be programmed and to drive various sensors; the components required to its hardware configuration; and its radiofrequency line to excite an antenna; as presented in Figure VII.1.

A JTAG (joint test action group) interface is used to program the microcontroller with the developed firmware, whilst some GPIO (general purpose input/output) pins are used to interface the sensors through the SPI (serial peripheral interface) wire communication standard.

For the antenna, a 50 Ω radiofrequency line at 2.45 GHz is used to connect a SMA (subminiature version A) connector or directly a printed antenna. This is a printed on 1.0 mm FR4 substrate meandered inverted-f antenna (MIFA) provided on the NXP QN9080 DK development board which has been implemented and used for the wireless communication part of the first prototype of the sensing nodes [663]. This is an almost omnidirectional

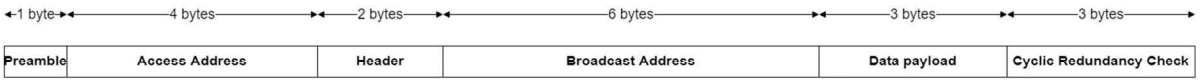

Figure VII.3: Format of the Bluetooth Low Energy frames used.

antenna with a linear polarization, usable at 2.45 GHz and with a theoretical gain of +1.7 dBi at 2.45 GHz, which has been directly interfaced to the radiofrequency line. Its main advantage is its direct integration on the printed circuit board, which allows a compact implementation. Nevertheless, the first qualitative tests achieved with NXP QN9080 DK development board have shown that this antenna is highly impact by the close presence of the reinforced concrete (less than few centimetres) and thus required an air gap. More, its directivity makes certain relative positions between the broadcaster and the observer ineffective.

In order to design the power management part of the new sensing nodes, it is necessary to know the energy these need to work properly. Thus, the power consumed by the part of the sensing nodes dedicated to the data collection, pre-processing and wireless transmission has been measured for two prototypes. The measurements have been achieved thanks to the tools provided by the MCUXpresso Integrated Development Environment (IDE) [664], in particular the one allowing the monitoring of the power consumption, and a Keithley 2000 multimeter [665], to get more precise values of the current consumed in the deep-sleep mode. Thus, around 920 µJ are required for a complete process, as presented in Figure VII.2, with a power transmission of +0 dBm.

3. Conclusion

Regarding the design and implementation of the part of the sensing nodes dedicated to the data collection, pre-processing and wireless transmission, both the hardware and the software can still be optimized. For the hardware, the study of alternatives to the NXP QN9080 Bluetooth Low Energy module could be achieved with the aim of reduce the power consumption. For the software, the optimization of the Bluetooth Low Energy stack focused solely on the needs of the sensing nodes could be relevant, as well as the test of other Bluetooth Low Energy advertising parameters. For instance, the power consumption in function of the radiofrequency output power could be characterized; the impact on the transmission of the time intervals between advertising frame transmission could be investigated, with the aim to decrease it to obtain a quicker process; the use of the 40 channels instead of only the three dedicated only to the advertising could be studied in order to increase the probability of good reception; etc. In fact, the best trade-off between power consumption and transmission reliability must be sought. It must be noted that a de-duplication process, and eventually a correction process of the received frames by merging all the reception on the different channels, could be implemented in the communicating nodes.

In Section VIII.D. some security aspects of the Bluetooth Low Energy communications will be treated.

B. Measurements of the properties of the reinforced concrete

To date, for the part of the new sensing nodes dedicated to the measurements of the properties of the reinforced concrete, only a temperature and relative humidity sensor has been implemented on the same printed circuit board (PCB) than for the NXP QN9080 Bluetooth Low Energy module. This is the Texas Instrument HDC2080 which is accessible *via* a SPI interface [626]. This one is identical in terms of characteristics to the Texas Instrument HDC2010 [627] implemented in the sensing nodes based on the LoRaWAN technology. The only differences are the package and the side of the package where is located the transducer: the bottom side for HDC2010 (more protected) and the top side for the HDC2080 (more ventilated).

To use the Texas Instruments HDC2080 temperature and relative humidity sensor, the SPI interface must be initialized and enabled by the NXP QN9080 Bluetooth Low Energy module, and after the quick stabilisation of its power supply (here 2.96 V), the sensor can be queried and configured to provide a temperature measurement and a relative humidity measurement as explained in [626]. These measurements are then formatted respectively on 9 bits by being rounded to the quarter of Celsius degrees, and on 7 bits by being rounded to percent, in order to be sent in Bluetooth Low Energy advertising data frames. The temperature is in the range of -40 °C to +125 °C and the relative humidity in the range from 0% to 100 %. Thus, the payload is reduced to three bytes, which limits the size of the frame, and thus, reduce the energy required for its four transmissions. Finally, the simultaneous use of the Texas Instruments HDC2080 temperature and relative humidity sensor and of the NXP QN9080 Bluetooth Low Energy module allows to test a full data chain: from the measurements of the temperature and the relative humidity, to their transmission in Bluetooth Low Energy advertising data frames to the communicating node(s), through their pre-processing and their formatting. The power consumption and the energy required to use this sensor in these new sensing nodes have not yet been measured.

A short-term objective would be to implement at least the same sensors usable in the monitoring of the reinforced concretes than those presented above (Section V.B.).

C. Energy harvesting and management

As previously, once the part of the sensing nodes dedicated to the data management fully designed: from the measurement to the wireless communication, through the pre-processing and formatting of the data; and its energy needs characterized, the power management part can be designed. This one must allow the energy autonomous of the sensing nodes by harvesting with a rectenna the radiative electromagnetic power generated at 868 MHz by the communicating nodes through a wireless power transfer system; and by efficiently storing the harvested energy in a well-designed energy storage device, and then by managing the stored energy thanks to the use of a power management unit. The same architecture than the one detailed above (Section V.C.) has been used.

1. The power management unit

This is the Texas Instruments BQ25570 which has been chosen for this new implementation of the sensing nodes. Its functioning is closely similar as the one of the Texas Instruments BQ25504 presented above (Section V.C.2.i.). This power management unit is used to efficiently store in an energy storage device its input power, and to efficiently use the stored energy to power the active components of the sensing nodes once a sufficient amount is available. Its current implementation is presented in Figure VII.4. Its hardware maximal power point tracking (MPPT) is currently set to 40 % of the open-circuit input voltage. More, its internal DC-to-DC buck converter is set-up to provide an output power of 2.96 V, when the power good indicator is activated, that says when enough energy is stored. By using this device, which has an efficiency of 93 %, as well as the internal DC-to-DC buck converter of the NXP QN9080 Bluetooth Low Energy module, the use of an external DC-to-DC buck/boost converter, such as the Texas Instruments TPS63031, is no more required.

To work properly, the power management and storage part of the sensing nodes needs a minimum input power. This one depends of all the components used. In this case, mainly the Texas Instruments BQ25570 power management unit and the energy storage device (considered below (Section VII.C.2.)) will impose this one. Thus, the Texas Instruments BQ25570 power management unit requires typically a 15 µW input power during the cold-start and at least 5 µW during the normal charging.

2. The energy storage device

Conjointly designed with the power management unit, as more detailed above (Section V.C.2.ii.), the energy device storage must be able to store enough energy, harvested by the rectenna and managed by power management unit, to power all the active components of the sensing nodes during all the time required for their full process: from the measurement to the wireless data transmission. As the sensing nodes must have a lifespan of the several decades and require around one milli-joule of energy to properly work each time these are powered, the choice fell on the capacitors which provide the more adequate capacitances.

The choice of the capacitor is made in regards of the energy required by the active components of the sensing nodes to achieve a full process (around 920 µJ for four +0 dBm Bluetooth Low Energy advertising data frames transmission of the data measured with the

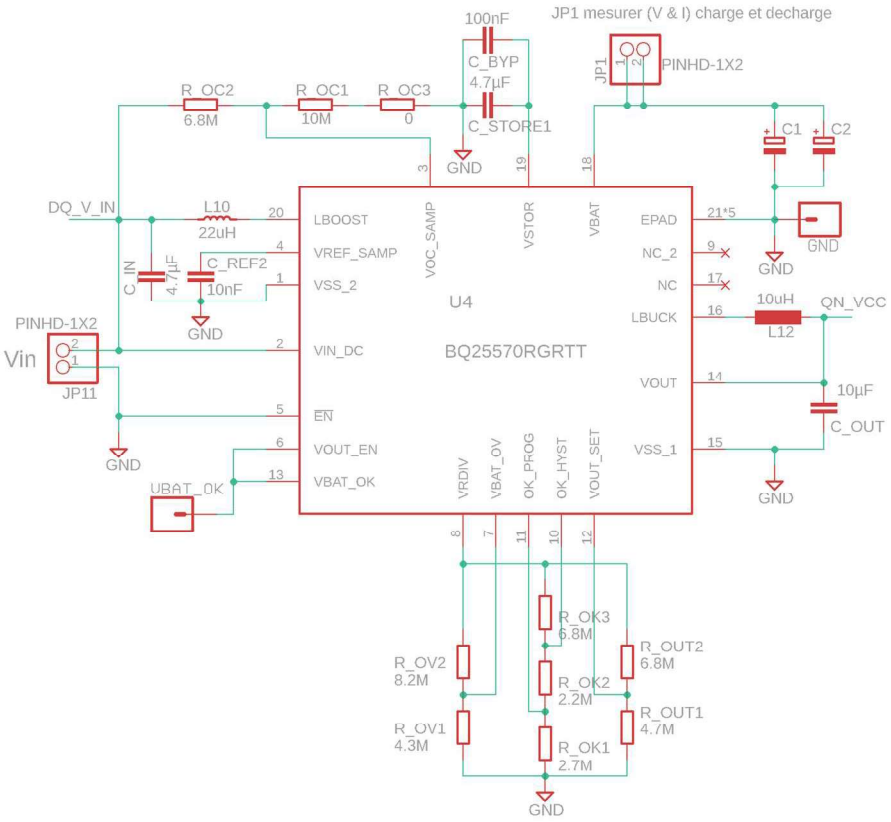

Figure VII.4: Schematics of the implementation of the power management and storage part of the sensing nodes based on the use of the Texas Instruments BQ25570 power management unit.

temperature and relative humidity sensor) plus a margin to compensate the variability between components and the alterations over time (around 20 %, *i.e.* almost 1.10 mJ) and of to design of the power management unit (whose the available range of the activation and deactivation threshold voltages is from 2.2 V to 5.5 V). The achieved implementation is presented in Figure VII.4.

By using the Equation 5.5, and considering an 82 µF and a 100 µF capacitors (values in the E12 series) and the extremum activation and deactivation threshold voltages, respectively 1.04 mJ and 1.27 mJ can be stored. A capacitor with a higher capacitance could be used, but regarding the energy stored and unavailable (all the one under the deactivation threshold voltage) which is 240 µJ for a 100 µF capacitor, this is not relevant and even less energy efficient.

Moreover, to be more energy efficient, the activation threshold voltage can be tuned and decreased in order to limit the energy uselessly stored. For instance, in the case where 1.16 mJ are required, the activation threshold voltage can be decreased down to 5.3 V. Even if it is possible, it is less energy efficient to increase the deactivation threshold voltage to limit the energy uselessly stored because this increases the energy stored and unavailable (all the one under the deactivation threshold voltage). More, lowest the maximum voltage in the supercapacitor, lowest the self-discharge currents.

Finally, this is a Panasonic EEEFK0J101P 100 µF aluminium electrolytic capacitor which has been chosen [666]. This one has maximum voltage of 6.3 V, higher than the 5.5 V maximum voltage provided by the Texas Instruments BQ25570. Its self-discharge currents are in the worst case around 5.5 µA at 5.5 V and 3 µA at 1.7 V (respectively the maximum voltage provided by the Texas Instruments BQ25570 and the voltage at the end of the cold-start). To compensate these losses in the worst case, and respectively for a 5.5 V and 1.7 V voltages, input powers of 30 µW and 5.1 µW must be applied.

The simultaneous use of the capacitor with both the energy and data management parts has been successfully tested. Thus, the capacitor driven by the power management unit allows to store enough energy to efficiently power the active components of the sensing nodes for a full process.

In all cases, the power management unit and the capacitor must be conjointly designed by considering the needs of the active components of the sensing nodes. In the actual configuration and in the worst case, at least 20.1 µW of input energy would be needed to be almost certain to obtain a properly work of the energy management and storage parts of the sensing node during the cold-start, and at least 35.0 µW during the normal charging.

The study of alternatives to the Panasonic EEEFK0J101P 100 µF aluminium electrolytic capacitor could be achieved with the aim of reducing the power consumption by limiting the current losses by self-discharge.

3. The rectenna

The rectenna is used to harvest the radiative electromagnetic power generated and transmitted by the communicating nodes and convert it into direct-current electrical power to power the input of the power management unit. The rectenna is composed of an antenna and of a rectifier and must provide enough energy to "power" the energy management and storage parts of the sensing nodes (in other words, must compensate the power losses of these parts and provide additional energy to store). The useful range of the wireless power transfer system depends on its performances, in particular its efficiency and gain.

This is the same rectenna printed on a 0.8 mm FR4 substrate and composed of the folded quart-wavelength dipole antenna with capacitive arms and its 14 cm x 9 cm metallic reflector plane located at 6 cm, and of the full-wave rectifier based on the use of two Skyworks SMS7630 surface mount Schottky diodes, presented above (Section V.C.2.iii.), which has been chosen for this new implementation of the sensing nodes.

By using a model of the rectenna efficiency against power densities, it has been possible to compute an estimation of the minimal power density required to "power" the energy management and storage part of the sensing nodes: in the worst use case; both for the normal charging and the cold-start (respectively requiring 35.0 µW and 20.1 µW, noted P_{DC_min}); by considering the printed folded quart-wavelength dipole rectenna with capacitive arms, with the reflector plane (G_{RX} = +5.00 dBi); and for a +33 dBm (or 2W) radiative electromagnetic power source at 868 MHz ($P_{TX} \cdot G_{TX}$ = +33 dBm); by solving the problem modelled by the Equation 5.12. From this value (noted $S_{computed}$), it has been possible to estimate the maximum range of use of the wireless power transfer system, in the air, in the same configuration and

always for the worst case, by using the Equation 5.13. Thus, the rectenna with the reflector plane could work from a power density of 0.210 $\mu W \cdot cm^{-2}$ (for -12.00 dBm or 63.1 µW harvested) for the cold-start and from 0.319 $\mu W \cdot cm^{-2}$ (for -10.19 dBm or 95.6 µW harvested) for the normal charging. This corresponds for distances between the communicating nodes and the sensing nodes of respectively 8.69 m and 7.06 m. These are obviously only very simplified theoretical estimations in the worst case, in the air, in the case of a unique path through the direct line of sight, and for a 10 kΩ resistive load, but which are in the targeted order of magnitude. In the case of the targeted load (the energy management and storage part of the sensing nodes), because of a variation of its input impedance and more generally of its properties (function of the input and the outputs, such as the voltage in the energy storage device), it is not feasible to obtain in a simple way the efficiency against power densities measurement for the rectennas.

4. Conclusion

By minimizing the energy required by the active components of the sensing nodes to achieve a full process, the energy stored have been drastically reduced: from 250 mJ to 1.17 mJ. Besides, the estimated maximum range of use of the wireless power transfer system is always in the same order of magnitude. This is due to the fact that the power required by the power management unit, the power lost by the energy storage element and the efficiency and gain of the rectenna are always in the same order of magnitude. Thus, this is on these aspects that the improvements must be achieved in order to obtain larger ranges of use. Nevertheless, this diminution of the required energy will allow faster charging times as presented next right.

The same alternatives and perspectives as the ones proposed above can be done (Section V.C.3.).

D. Complete implementation and tests of the sensing nodes

The first implemented prototypes are based on a semi-integrated solution based on two separated components, presented in Figure VII.5. First is a specifically designed four-layer 1.0 mm FR4 printed circuit board on which are the Texas Instruments BQ25570 power management unit, the Panasonic EEEFK0J101P 100 µF aluminium electrolytic capacitor, the NXP QN9080 Bluetooth Low Energy module with printed meandered inverted-F antenna (MIFA) and a SMA connector, and the Texas Instruments HDC2080 temperature and humidity sensor. Second is the rectenna printed on a 0.8 mm FR4 substrate and composed of the folded quart-wavelength dipole antenna with capacitive arms and its 14 cm x 9 cm metallic reflector plane located at 6 cm, and of the full-wave rectifier.

This first implementation of the prototypes of the sensing nodes based on the Bluetooth Low Energy technology have been tested successfully, but is still under characterization. Its functioning is similar to the one of the LoRaWAN sensing nodes.

To certify its proper functioning, several qualitative tests have been achieved. Several configurations were tested, between others: a unique communicating node with a unique sensing node, indoors, in an anechoic chamber and in a reinforced concrete beam, for range of 2 meters; a unique communicating node with several sensing nodes (up to 3, *i.e.* all those available at the time), indoors, and in a reinforced concrete beam (up to three inside); etc. Several results can be drawn from these qualitative experimentations. First, but essential, the new sensing nodes can be wirelessly powered by the communicating nodes through the radiative electromagnetic power transmission, and a major part of the transmitted data (in the air or from the reinforced concrete beam) have been well received and managed by the same communicating node. A unique communicating node can easily manage several sensing nodes (both for the wireless power transfer and the wireless communication) over several metres in an almost omnidirectional way. Higher distances than those tested can be reached. By controlling the radiative electromagnetic power generated by the communicating node (tested here by changing the output power), the periodicity of measurement and wireless communication of the sensing nodes can be controlled.

The Table VII.1 summarizes the durations of the first charge and recharges of a sensing node placed in the air and in the reinforced concrete beam and at a distance of 2 metres of the communicating node according to the radiative electromagnetic power transmitted at 868

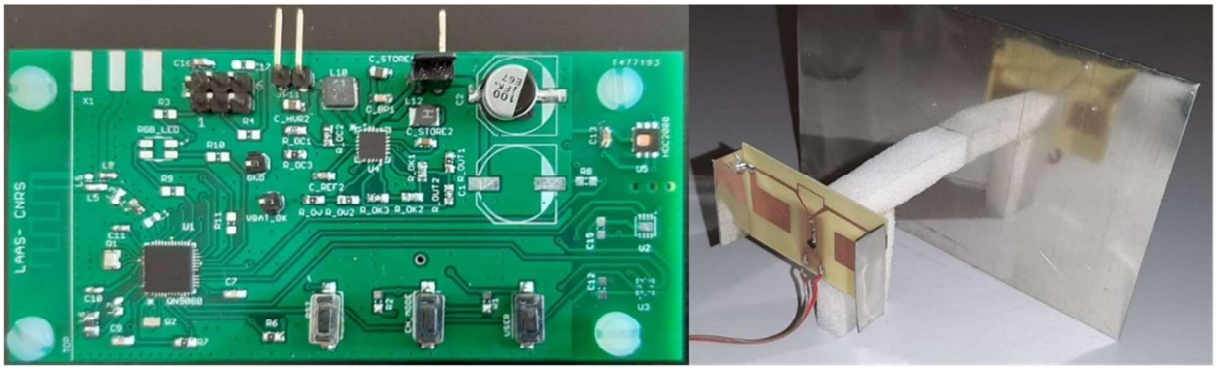

Figure VII.5: Photographs of the printed circuit board and the rectenna dedicated to the first implementation of the prototypes of the sensing nodes based on the Bluetooth Low Energy technology.

MHz, as well as the estimation of the efficiency (as defined in Section V.D.3.v.) in the case of a wireless power transfer in the air (from the estimated power at the input of the rectenna based on the Equation 5.10). The energy required for a first charge and for a recharge are estimated thanks to the Equation 5.5, to respectively 1.40 mJ and 1.16 mJ. For the sensing nodes embedded in the reinforced concrete beam, the 2 metres are distributed in 15 cm of reinforced concrete and 185 cm of air. From these measurements, the impact of the reinforced concrete is highly visible: for an equivalent distance and an equivalent generated power, the first charge duration goes from 17 seconds to 1 minute 52 seconds, and from 45 seconds to 5 minutes 33 seconds and the recharge from 4 seconds to 33 seconds and from 11 seconds to 1 minutes 58 seconds, for respectively a +33 dBm and a +29 dBm generated power. To compare with the LoRaWAN implementation, for a nearly -7.2 dBm input power this implementation provided a first charge duration of 1 minute 11 seconds and a recharge of 22 seconds against a first charge duration of around 3 hours and a recharge of around 45 minutes for the LoRaWAN implementation, whilst for a nearly +0.8 dBm input power this implementation provided a first charge duration of 17 seconds and a recharge of 4 seconds against a first charge duration of around 35 minutes and a recharge of around 6 minutes for the LoRaWAN implementation. The estimated efficiencies of the sensing nodes wirelessly powered both for the first charge and the recharge are low, respectively from 3.7 % to 6.9 % and from 9.6 % to 24.4 %, and decrease with the input power drop. As explained above (Section V.D.3.v.), to improve the energy efficiency of the sensing nodes, according to the energy required for a measurement and a wireless transmission of the collected -and eventually pre-processed- data, the time required for the first charge and for the recharges must be reduced. This can only be achieved by optimizing the hardware, especially by optimizing the efficiency of each component which will allow to reduce the minimum required input power linked to the power needs, and by reducing the losses of the various components.

Nevertheless, the current implementation is a first proof-of-concept of a battery-free wireless sensing node based on the Bluetooth Low Energy wireless communication technology, which is energy autonomous (by being wirelessly powered by a radiative electromagnetic wireless power transfer system), and dedicated to the structural health monitoring of the reinforced concretes. The wireless sensor network provided has a similar range of use of several metres both for the wireless power transfer and the wireless communication, and these two functions can be improved.

Table VII.1: Durations of the first charge and recharges of a sensing node placed in the air and in the reinforced concrete beam and at a distance of 2 metres of the communicating node according to the radiative electromagnetic power transmitted at 868 MHz.

Sensing node location	In the air						In the reinforced concrete beam	
Transmitted power (dBm)	Estimated rectenna input power (dBm)	Estimated rectenna input power (µW)	First charge duration (s)	Recharges duration (s)	Estimated efficiency of the first charge (%)	Estimated efficiency of the recharge (%)	First charge duration (s)	Recharges duration (s)
+33	+0.8	1191.6	17	4	6.9	24.4	112	33
+32	-0.2	946.5	N/A	N/A	N/A	N/A	110	35
+31	-1.2	751.8	N/A	N/A	N/A	N/A	154	52
+30	-2.2	597.2	38	8	6.2	24.3	236	81
+29	-3.2	474.4	45	11	6.6	22.3	333	118
+28	-4.2	376.8	N/A	N/A	N/A	N/A	503	190
+27	-5.2	299.3	71	22	6.6	17.7	N/A	N/A
+26	-6.2	237.7	97	32	6.1	15.3	N/A	N/A
+25	-7.2	188.9	137	40	5.4	15.4	N/A	N/A
+24	-8.2	150.0	150	54	6.2	14.4	N/A	N/A
+23	-9.2	119.2	213	80	5.5	12.2	N/A	N/A
+22	-10.2	94.7	398	128	3.7	9.6	N/A	N/A

E. Work in progress and perspectives

Even if encouraging results have been achieved for these news sensing nodes, several works on several aspects are still in progress, are planned or seem relevant.

Once again, each subpart of the sensing nodes can be improved. For the data collection, pre-processing and wireless transmission mainly the software can still be optimized with as main objective to further reduce the required energy, while ensuring reliable communications. That is why, the characterizations of: the power consumption according to the radiofrequency output power; the impact on the reliability of the wireless communication of the time intervals between advertising frames transmission, of the number of frames sent, of the use of the 40 channels instead of only the three only dedicated to the advertising; etc. are planned or seems relevant to study. For the part dedicated to the measurements of the properties of the reinforced concrete, the integration of all the sensors used in the LoRaWAN sensing nodes are planned, with the same targeted improvements (e.g. integration of new sensors, increase of the measurement precision, decrease of the power consumption, etc.). For the energy harvesting and management part, the reduction of the minimum required input energy is targeted, by the search of capacitors with less losses, by the test of the e-peas AEM30940 power management unit, and by the design of new and more efficient rectennas (both the rectifier and the antenna). This will allow both the increase of the efficiency and the increase of the maximum range of use.

Regarding to the current prototypes of the sensing nodes, their tests and characterizations are still in progress. These must be characterized in terms of power consumption and energy required, of the time required for a first charge and for recharges, and in efficiency. Additional qualitative experimentations are planned, especially by embedding the sensing nodes in the reinforced concrete beam but in smaller cavities (by using additional concrete box around).

A short-term perspective is to design a one-piece fully integrated prototype on which allows the interfacing of all the targeted sensors.

Finally, the investigation of the use of a unique antenna in the sensing nodes, both for the radiative electromagnetic power harvesting and the wireless communication could be investigated. This one could be a bi-band or broadband antenna, used with a bi-band or broadband radiofrequency circulator or through two feeding ports.

F. Conclusion

In this chapter, the implementation of the sensing nodes based on Bluetooth Low Energy technology has been proposed. These have the same architecture than the ones based on the LoRaWAN technology. Thus, the differences for each of their three subsystems has been discussed in terms of design, implementation, and tests. Have been introduced: the part dedicated to the data collection, pre-processing and wireless transmission, allowing to drive the sensor, to pre-process the collected data before to wirelessly sent these through four Bluetooth Low Energy advertising data frames; the part dedicated to the measurements of the properties of the reinforced concrete currently based on the use of a temperature and relative humidity sensor; and the part dedicated to the energy harvesting and management, allowing to power the two other parts by harvesting the radiative electromagnetic power provided by the communicating nodes and storing it until enough energy is available. Finally, the first complete implementation of the sensing nodes and its tests, have been introduced.

Now, it is time for a short conclusion on the current implementation of the targeted wireless sensor network based on the Bluetooth Low Energy technology. This one is composed of a unique and exploded communicating node and of three semi-integrated sensing nodes. The communicating node is able to collect the Bluetooth Low Energy data frames sent by the sensing nodes; locally process and store the data provided by the sensing nodes and make them available to users through a USB connection; wirelessly power over several meters the sensing nodes in their neighbourhood (both in the air and in a reinforced concrete beam); and remotely control the periodicity of measurement and wireless communication of the sensing nodes through the tuning of the radiative electromagnetic wireless power transfer system. The sensing nodes can sense the temperature and the relative humidity to quantify their environment in the cavity of the reinforced concrete beam, and wirelessly transmit over several metres the collected, and pre-processed, data to the communicating node through four Bluetooth Low Energy advertising data frames. Because these become inaccessible once deployed and embedded into the reinforced concrete, these are battery-free and energy autonomous, with a targeted lifespan of decades, as for the reinforced concrete itself. The current implementation meets the requirements of the simultaneous wireless information and power transmission paradigm, by being based on the frequency multiplexing.

The next chapter will detail the main differences between the proposed solutions respectively based on the LoRaWAN and the Bluetooth Low Energy wireless communication technologies, and will compare these with the state-ot-the-art projects available in the literature. As well, some low-level security aspects of the proposed architecture for a wireless sensor network embedded into reinforced concretes to make these communicating will be introduced.

VIII. Positioning and low-level security aspects

In this chapter, the implementations of the two kinds of sensing nodes respectively based on the LoRaWAN and the Bluetooth Low Energy wireless communication technologies will be compared. Then, the contributions of this doctoral thesis work in the McBIM project and in order to implement a communicating reinforced concrete will be highlighted and compared with the state-of-the-art solutions available both commercially and in the academic literature. To go further, an analysis of the low-level security aspects of the proposed wireless sensor network will be provided.

A. Comparison between the solutions based on the LoRaWAN and the Bluetooth Low Energy wireless communication technologies

The two implementations of the sensing nodes are based on the same architecture, presented in Figure III.6, and use two different technologies for the wireless communications: LoRaWAN and Bluetooth Low Energy. Whatever the implementation, the sensing nodes are able to achieve a measurement, to pre-process the collected data, and to transmit wirelessly these data to the communicating nodes. More, these are battery-free and wirelessly powered by the communicating nodes through a radiative electromagnetic power transmission system. Thus, these two implementations meet the requirements of the simultaneous wireless information and power transmission paradigm, by using a unique frequency band in the case of the LoRaWAN implementation, and two independent frequency bands in the case of the Bluetooth Low Energy implementation, both without temporal multiplexing and power splitting (because the unavailability of the data downlink), and without spatial multiplexing thanks to the use of a unique antenna for the LoRaWAN implementation, and with for the Bluetooth Low Energy implementation.

In order to reduce as much as possible the power consumption, the downlink of the wireless communications has been disabled: for LoRaWAN that says to not open the receiving windows planned by the class A; and for Bluetooth Low Energy that says to configure only broadcasters using the notification mode; and the "store then use" strategy has been implemented: because the available input power is much lower than the required output power, the sensing nodes are powered only when enough harvested energy is available, otherwise these are fully shut-down (not in a deep-sleep mode). Thanks to the cold start ability and the use of energy storage devices which are insensitive to the deep discharges and which can be completely empty, the sensing nodes can be "forgotten" for long times without becoming unusable. More, as the sensing nodes are inaccessible once deployed in the reinforced concrete, neither software nor hardware change, replacement or update are possible. Thus, the only possibility to modify their behaviour is made through the tuning of the radiative electromagnetic power generated by the communicating nodes: by managing the duty-cycle and the output power of the power source, the periodicity of measurement and wireless transmission can be chosen. Thus, this is the lifetime of the electronics which will become the critical element and major cause of failure.

The main characteristics of these two implementations of the sensing nodes are summarized in Table VIII.1.

Regarding the implementation of the systems dedicated to the wireless communications, the two implementations provide different performances. The LoRaWAN implementation allows reliable (at least) medium range wireless communications: over kilometres in the air, at least hundred metres indoors and at least tens of metres from a reinforced concrete beam, without any data loss and an unquantified impact of the reinforced concrete; whilst the Bluetooth Low Energy implementation allows only short range wireless communications, highly impacted by the propagation path: up to tens of metres in the air, at least ten metres indoors and at least ten metres from a reinforced concrete beam, with data losses and a non-negligible impact of the reinforced concrete. Nevertheless, the Bluetooth Low Energy implementation requires very little energy to operate, and therefore, very little energy needs to be stored: only 1.16 mJ; whilst 117 mJ (up to 250 mJ) are required for the LoRaWAN implementation. And, the lower the stored energy, the faster the time to a first charge or a recharge. The Bluetooth Low Energy implementation is more efficient than the LoRaWAN one in terms of energy per transmitted byte and of energy per byte of data transmitted. The LoRaWAN frame requires 6.2 mJ at +4 dBm and 12.2 mJ at +14 dBm per byte, and the Bluetooth Low Energy frame 48 µJ at +0 dBm; whilst 26.5 mJ at +4 dBm and 52.0 mJ at +14 dBm are required per byte of data transmitted with the LoRaWAN frame and 304 µJ with the Bluetooth Low Energy frame. Thus, a trade-off between the reliability of the wireless communications and the energy consumption must be sought. Nevertheless, and in the two implementations, some improvements can be performed for this purpose. For the LoRaWAN implementation, by changing the transmission parameters, especially the data-rate (through the spreading factor and the bandwidth), and limiting the data payload, the duration of the transmissions (or time in air) can be reduced. This will induce a decrease of the energy required, at the cost of a probable reduction of the range of use because the transmissions will become more sensitive to the propagation path and their reception more difficult. For the Bluetooth Low Energy implementation, by increasing the redundancy through the transmission of more frames on more channels, by tuning the duration between advertising frames and maybe by reducing the data-rate, the probability of a good reception could be increased (if a de-duplication process, and eventually a correction process of the received frames could be implemented in the communicating nodes) at the cost of an increase of the required energy.

Regarding the implementation of the energy harvesting and management systems, the two implementations are quite similar, because based on same or similar components: the rectennas are the same (both the antennas and the rectifiers), the power management units are from the same family and have similar behaviours and characteristics (Texas Instruments BQ25504 and BQ25570); and the energy storage devices have similar losses despite capacitances in very different orders of magnitude (22 mF supercapacitor and 100 µF capacitor). These allow a range of use of several metres. In order to increase it, two aspects must be improved: the minimum required input power, which must be minimized and which is due to the minimum input power of the power management unit and the losses of the energy storage device; and the global efficiency, which must be increase and which is here mainly due to the rectenna efficiency. This last can be improved both on the antenna and the rectifier side. For the antenna, an omnidirectional radiation pattern, a circular polarisation and a high gain are targeted, whilst for the rectifier, high efficiencies for low input powers are desired.

Regarding the implementation of the measurement systems, these are more ahead for the LoRaWAN implementation for which several sensors have been interfaced: temperature and relative humidity sensors, temperature sensors, electric resistivity sensor (for corrosion estimation), and mechanical deformation sensor (strain gauge), whilst only a temperature and relative humidity sensor has been interfaced in the Bluetooth Low Energy implementation. However, the upgrade of the Bluetooth Low Energy implementation is planned, as well as the integration of other kinds of sensors for the two implementations. The precision and power consumption of each sensor must be improved, which will allow to reduce the energy required by the sensing nodes.

Regarding the global implementations, compact, integrated and optimized solutions are targeted. These ones must be well tested and characterized, especially in terms of efficiency for the wider range of input powers possible, and of ranges of use both for the wireless power transfer and the wireless communication.

Finally, all these aspects concern only the sensing nodes and its wireless communications with the communicating nodes. These lasts have not the same level of maturity for the two implementations. The two are based on the same continuous wave radiative electromagnetic power source working in the ISM 868 MHz frequency band for the wireless power transfer. But for the Bluetooth Low Energy implementation, only the reception and local storage of the data sent by the sensing nodes are implemented, whilst for the LoRaWAN implementation, the communicating nodes can receive, process, -locally and/or remotely- store and exchange the data sent by the sensing nodes in a meshed network of communicating nodes, with the digital world through the Internet and -locally and/or remotely- with the various stakeholders.

Table VIII.1: Summary of the characteristics of the implemented sensing nodes based on the LoRaWAN and on the Bluetooth Low Energy wireless communication technologies.

					LoRaWAN sensing node	Bluetooth Low Energy sensing node	Objective
Data measurement, collection, pre-processing and wireless transmission	Sensor	Measured parameter(s)			Temperature and relative humidity	Temperature and relative humidity	At least: temperature and relative humidity; temperature; electric resistivity (for corrosion estimation); and mechanical deformation; and even more if possible.
		Reference			Texas Instruments HDC2010	Texas Instruments HDC2080	
		Type			Temperature	N/A	
		Reference			Thermodiodes	N/A	
		Type			Electric resistivity (for corrosion estimation)	N/A	
		Reference			LMDC	N/A	
		Type			Mechanical deformation	N/A	
		Reference			Strain gauge	N/A	
	Wireless communication technology	Name			LoRaWAN	Bluetooth Low Energy	
		Standard			LoRaWAN	IEEE 802.15.1	
		Implemented version			1.0.3	5.0	
		Components		Module	Murata CMWX1ZZABZ-091 LoRaWAN module	NXP QN9080 Bluetooth Low Energy module	
				Antenna	Printed folded quart-wavelength dipole antenna with capacitive arms and metallic reflector plane	Printed folded quart-wavelength dipole antenna with capacitive arms and metallic reflector plane	
				Supply voltage (V)	3.3	2.96	
				Energy required for a temperature and relative humidity measurement and its transmission (mJ)	106 (+4 dBm) 208 (+14 dBm)	0.920 (+0 dBm)	As low as possible
				Energy per transmitted byte (mJ)	6.2 (+4 dBm) 12.2 (+14 dBm)	0.048 (+0 dBm)	As low as possible
				Energy per byte of data transmitted (mJ)	26.5 (+4 dBm) 52.0 (+14 dBm)	0.307 (+0 dBm)	As low as possible
		Characteristics		Network topology	Star based on the class A devices	Star based on broadcasters and observers	Star
				Directionality	Only uplink	Only uplink	Only uplink
				ISM frequency band (HZ)	868 M	2.45 G	
				Theoretical range of use	Kilometres	Tens of metres	
				Maximum distance tested for communication from inside the reinforced beam (m)	Few tens	2	Tens of meters
				Used packet length (bytes)	17 (4 for the data payload)	19 (3 for the data payload)	
				Used data-rate (bps)	250	1 M	
				Transmission power (dBm)	+4	+0	As low as possible with high reliability
Energy harvesting and management	Power management unit	Reference(s)			Texas Instruments BQ25504 and TPS63031	Texas Instruments BQ25570	
		Activation threshold (V)			4.05 (+4 dBm) 5.25 (+14 dBm)	5.3	
		Deactivation threshold (V)			2.3	2.2	
		Minimum input power (µW)		Cold start	16.62	15	As low as possible
				Normal Charging	14.725	5	As low as possible

	Energy storage device	Type			Supercapacitor	Capacitor	
		Reference			AVX Corporation BZ01CA223ZSB	Panasonic EEEFK0J101P	
		Capacitance (mF)			22	0.1	As low as possible
		Energy stored (mJ)			117 (+4dBm) 250 (+14 dBm)	1.16	As low as possible
		Maximum power losses (µW)	Cold start		9	5.1	As low as possible
			Normal Charging		26	30	
	Rectenna	Antenna	Type		Printed folded quart-wavelength dipole antenna with capacitive arms and metallic reflector plane	Printed folded quart-wavelength dipole antenna with capacitive arms and metallic reflector plane	
			Maximum gain (dBi)		+5.00	+5.00	As high as possible
			Radiation pattern		Almost semi-omni-directional	Almost semi-omni-directional	Omni-directional
			Central frequency (HZ)		868 M	868 M	
			Polarisation		Linear	Linear	Circular
		Rectifier	Type		Full-wave doubler rectifier based on Skyworks SMS7630 Schottky diodes	Full-wave doubler rectifier based on Skyworks SMS7630 Schottky diodes	
			Efficiency at 868 MHz, -15 dBm, with a 10 kΩ resistive load (%)		35 %	35 %	As high as possible
			Central frequency (HZ)		868 M	868 M	
		Rectenna	Central frequency (HZ)		868 M	868 M	
			Minimum input power (µW)	Cold-start	25.62	20.1	As low as possible
				Normal Charging	40.725	35.0	
			Minimum estimated power density ($\mu W \cdot cm^{-2}$)	Cold-start	0.331	0.210	
				Normal Charging	0.228	0.319	
			Maximum estimated range of use (m)	Cold-start	8.34	8.69	As high as possible
				Normal Charging	6.93	7.06	
Complete prototype	Type				Integrated	Partially integrated	Integrated
	Unique antenna				Radiofrequency circulator Aerotek C11-1FFF/OPT.N	None	
	Size (cm x cm x cm)				8 x 6 x 5	More than 8 x 6 x 5	As small as possible
	Reconfigurability				Control of the periodicity of measurement and wireless communication of the sensing nodes through the radiative electromagnetic power generated by the communicating node	Control of the periodicity of measurement and wireless communication of the sensing nodes through the radiative electromagnetic power generated by the communicating node	Without software and hardware change due to the inaccessibility
	Tested input power range (dBm)				-14 to +15	Approximatively from -10.2 to +0.8	As wide as possible
	First charge time				From more than 1 minute (+15 dBm) to more than one day (-14 dBm)	From 17 seconds (+0.8 dBm) to more than 6 minutes (-10.2 dBm)	As short as possible
	Recharge time				From more than 30 seconds (+15 dBm) to more than 12 hours (-14 dBm)	From 4 seconds (+0.8 dBm) to more than 2 minutes (-10.2 dBm)	
	Efficiency range (%)	First charge			4.8 to 10.8	3.7 to 6.9	As high as possible
		Recharge			13.1 to 36.4	9.6 to 24.4	

B. Comparison with the current solutions for the monitoring of reinforced concretes

The McBIM project aims to design and implement a communicating reinforced concrete. This one will be a non-intrinsic self-sensing and data storing reinforced concrete based on the use of an embedded wireless sensor network dedicated to the monitoring of the reinforced concrete during its entire lifespan. This monitoring concerns the curing process and the exploitation phase of both the reinforced concrete element and the structure of which it is a part, but must also deal with the traceability during the transportation, the construction, the exploitation, the demolition and the recycling. The wireless sensor network will be based on two kinds of nodes. The sensing nodes, which will be buried in the reinforced concrete and be a generic platform, are battery-free, wirelessly powered and able to perform measurements of various relevant parameters and wirelessly transmit the collected data to a meshed network of communicating nodes. And the communicating nodes, which will be embedded on the reinforced concrete (on its surface in a first approximation), collect, process, store (locally and remotely) and share the data sent by the sensing nodes in a meshed network of communicating nodes, with the digital world and especially with a building information modelling (BIM) through the Internet, and locally and/or remotely with the stakeholders. These also power wirelessly the sensing nodes in their neighbourhood and store data in the material in order to conserve a detailed historic of its health locally accessible. The measurements are based on non-destructive testing methods (e.g. the maturity method during the curing process, etc.). And in order to limit the needs of energy and of computing capacity, only direct and temporally punctual measurements (e.g. on a daily, weekly or monthly base) are considered. This allows between others to get measurements of physical parameters (e.g. temperature, relative humidity, etc.), of mechanical parameters (e.g. deformation, etc.), or of chemical parameters (e.g. corrosion rate through the evolution of the electric resistivity, etc.). Thus, methods requiring signal processing and/or energy-consuming equipment (as optic, acoustic and ultrasonic, thermographic, electromagnetic (based on waves propagation), radiographic, sclerometric, etc.) are currently discarded. The range of use of both the wireless power transfer and the wireless communication of this wireless sensor network must allow to cover the volume of a reinforced concrete element and of an assembly of reinforced concrete elements (e.g. a building, a bridge, etc.), that says from several metres to tens of metres, and for all its lifetime, that says for decades. Finally, its use is automated and does not required the human interventions.

Regarding the current intrinsic [37-44] and non-intrinsic [37-38, 95-107] self-sensing concretes, these are subjects of laboratory studies, which are not able to collect, store or transmit data without the use of external equipment, generally complex and power consuming, driven by an operator. These are able to sense various parameters (e.g. strain, stress, strength, displacement, moisture (or humidity), hydration process, temperature, pH, corrosion, etc.), and even detect and localize damages (e.g. impacts (or shocks), cracks, delamination, etc.). Nevertheless, some of these are based on indirect measurements requiring signal processing, whilst others could be investigated to become transducers for the proposed wireless sensor network.

Regarding the wireless passive solutions, these can be used for traceability [121, 122, 543-546] or monitoring purposes [547-552]. These are able to sense various parameters (strain, displacement, humidity, temperature, corrosion, electric resistivity), and even detect and

localize damages (cracks, delamination). The major part of these are based on radiofrequency identification (RFID) tags embedded into concretes [121, 122, 543-550] and few on passive resonators [551, 552]. These are not able to collect and then transmit the data without the use of a wireless external "reader" usually driven by an operator who must know their location because of the short range of the employed wireless communication technologies based on backscattering. More, the solutions proposed in the case of the traceability cannot store a significant amount of data.

Regarding the wireless sensor networks dedicated to the monitoring of the reinforced concretes by their instrumentation, most of them are based on the use of a wireless datalogger or a wireless transmitter located on the surface of the reinforced concrete [109-115, 117-120, 281, 288, 322, 558-560]. The wireless dataloggers can be compared to communicating nodes working without sensing nodes, and able to measure and wirelessly transmit the collected data directly or through a local gateway to the user(s) (local or remotely through the Internet); whilst the wireless transmitters can be compared to sensing nodes located on the surface of the reinforced concrete which transmit the collected data to a gateway. The transmitted data are measured thanks to one or several wired and sacrificed sensors connected to the datalogger or the transmitter and are buried in the reinforced concrete or placed on its surface. The use of wires connected to the outside of the reinforced concrete can create weaknesses in it and an access point for the pollutants and other contaminants, such as the air and the water which can for instance induce a faster corrosion. These are able to sense various parameters (e.g., temperature, relative humidity, strength, resistivity, elastic and inelastic deformations, inclination, load or pressure, displacement, etc.), and even detect and localize damages (e.g. shocks, cracks, defects, etc.). Both the wired sensors and the wireless dataloggers or wireless transmitters must be manually placed to specific locations respectively in and on the concrete elements, that is expensive and time consuming. More, a part of these solutions is only dedicated to the curing process or to the exploitation phase. Nevertheless, [114, 116, 554-557] provide temperature, relative humidity and strength wireless sensors, used for the curing process or during the exploitation phase, which are fully embedded into concrete but with a maximum depth of 15 cm and a range of use up to hundreds of metres in the air. All these solutions are powered by a battery, and thus, those of the accessible solutions must periodically recharge or change, and for the inaccessible solutions the lifetime is limited to few months or few years. Nevertheless, an inductive wireless power transfer system to recharge the battery located in the concrete is proposed in [556, 557]; and in [558] no use a battery is done but the sensor is only power by a radiative wireless power transfer system outside the concrete. Finally, few solutions of wireless sensors dedicated to structural health monitoring applications discuss the use of energy harvesting solutions to recharge the battery and extend their lifetime. This is the case of [281] and [288] where the batteries are recharged by the solar energy harvesting; and of [322] where the wireless sensor is supplied by the mechanical vibrations energy harvesting. Nevertheless, none of these systems is designed to be embedded in concrete and these are highly dependent of the environment of the deployment and its ambient energy sources and of the targeted application.

Thus, the proposed solution allows to overcome some limitations of the current solutions: no external equipment or human intervention is required because the system is automated, wireless and connected to the digital world through the Internet; the traceability, the data storage and the structural health monitoring are simultaneous ensured during each step of the lifecycle thanks to the proposed architecture; the proposed implementation is independent of

services providers for the wireless communication unlike most of the available commercial solutions; the deployment is also independent of the environment and of the targeted application because does not required specific ambient energy sources; and its lifespan is expected similar to the one of the reinforced concretes because based on inaccessible battery-free sensing nodes wirelessly powered (whose the more probable cause of global failure could be the electronics failure) and accessible and updatable communicating nodes.

Thus, and to the best of our knowledge, the proposed solution is the first based on sensing nodes, which are battery-free, wirelessly powered by radiative electromagnetic wireless power transfer system, and designed to be fully buried into the reinforced concrete to ensure its structural health monitoring during its entire lifespan.

C. Comparison with the current solutions of wireless sensor networks wirelessly powered

Today are few commercially available solutions to recharge the batteries of devices through radiative electromagnetic wireless power transfer [423, 424]. Moreover, these ones are limited in terms of distance and of efficiency: it is more a question of increasing the discharge time of a device than really recharging it during its use. For instance, and according to the data collected on [423], the recommended distance is between 10 cm and 25 cm to efficiently fully recharge a controller not in use; and the "sold" maximum distance to harvest some power is up to ten of meters with high gain antennas.

Nevertheless, some academic researches or few start-up companies deal with complete battery-free sensor nodes wirelessly powered through radiative electromagnetic wireless power transfer and using low power wide area network (LPWAN) or wireless personal area network (WPAN) wireless communication technologies [416, 418-422, 425]. More, these meet the requirements of the simultaneous wireless information and power transmission (SWIPT) paradigm, thanks to frequency and/or spatial multiplexing. Between these, few are dedicated to the structural health monitoring of civil infrastructures but are always deployed on the surface of existing structures and could require the use of a vehicle (respectively a car and an unmanned aerial vehicle (UAV) (presented as not necessary, only used to increase the range of use)) [422, 425]. Comparison elements of all these works (plus [415] and [417]) are summarized in Table VIII.2.

Finally, some works theoretically and experimentally the radiative electromagnetic wireless power transfers into concretes, and especially the impact of the reinforcements [533-537]. However, these systems are incomplete and no load such as wireless sensor node is used during experimentations.

Thus, the proposed solutions, only based on off-the-shelf components (excepted for the rectenna, for which no commercial solution is available), introduce some new features, such as: the use of a unique antenna both for the wireless communication and the wireless power transfer, which take place in the same frequency band, thanks to the use of a radiofrequency circulator; the implementation and test of a full cyber-physical system composed of a wireless sensor network based on two layers, and thus, on several communicating nodes and sensing nodes; and based on sensing nodes embedded (because not yet buried) in the reinforced concrete, a harsh medium of propagation for the electromagnetic waves. Regarding the range of use, this is mainly constrained by the wireless power transfer and not by the wireless communication, but covers several meters, that say more than a major part of the presented solution. Only [419] and [425] provide higher ranges of use, respectively 16.8 metres and up to few tens of metres, but the first uses a commercially unavailable power management unit and for the second only commercial data are available. Nevertheless, by optimizing the proposed solutions (especially by using a power management unit requiring lower input power and an energy storage device with lower self-discharge, as well as a rectenna more efficient), these ranges of use seem to be reachable. Finally, both the "simultaneous store and use" and the "store then use" strategies are used with various periodicity of the measurements and transmissions. In a general way, lower the energy required, faster the recharge. Because long periodicities are targeted (on a daily, weekly or monthly base) the "store then use" strategy with a cold start ability seems the most appropriate configuration for the targeted

application. More, as long lifespans are wanted, the design provides as few components and complexity as possible in order to limit as much as possible the points of failure. Thus, the complex systems, as the one introduced in [419], to optimize the power management is not desired, even if relevant on the point of view of the energy efficiency.

Table VIII.2: Summary of the characteristics of the current solutions of wireless sensor networks wirelessly powered by radiative electromagnetic power transmission.

Reference		[422]	[415]	[416]	[421]	[417]	[418]	[419]	[420]	[425]	This work	
Date		2009	2015	2017	2019	2018	2021	2017	2018	2021	Since 2018	
Wireless communication technology	Name	ZigBee	N/A	Bluetooth Low Energy		LoRaWAN	LoRa	DASH7	Bluetooth Low Energy	N/A	LoRaWAN	Bluetooth Low Energy
	Standard	IEEE 802.15.4	N/A	IEEE 802.15.1		LoRaWAN	LoRa	DASH7	IEEE 802.15.1	N/A	LoRaWAN	IEEE 802.15.1
	Frequency (Hz)	2.45 G	868 M	2.45 G		868 M	2.45 G	433 M	2.45 G	868 M	868 M	2.45 G
Measurement technology	Sensor	Impedance (piezoelectric)	N/A	Temperature and relative humidity; acceleration		N/A	Acceleration	Temperature and relative humidity	Temperature; pressure; acceleration	Various interfaces (SPI, I²C, DAC, ADC); Temperature; relative humidity; pressure; acceleration; inclination; magnetic field; luminosity; mechanical deformation (strain gauge)	Temperature and relative humidity; corrosion (electric resistivity); mechanical deformation (strain gauge)	Temperature and relative humidity
	Application	Bridge SHM	N/A	Rotating machine SHM		N/A	Automobile engine SHM	Indoors SHM	N/A	SHM	Communicating reinforced concrete	

Wireless power transfer and energy management systems													
	Frequency (Hz)		2.45 G	868 M	868 M		868 M	2.45 G	868 M	868 M	2.45 G	868 M	
	Transmitted power (dBm)		+30	+34.8	+23 to +35	+34.6	+32.4	2 x +27	+27 or +33	+27	+27 to +36	+33	
	Maximum tested range of use (m)		1	1 to 10 (non-tested)	0.5 to 1	1.5	1 to 3.2 (non-tested)	0.54	Up to 8.4 or 16.8	2	Several meters to few tens of metres (FAQ)	7 (more expected)	
	Range of input power (dBm)		N/A	-14 to -10	-10 to +5	-10 to +5	-20 to +2	N/A	From -17	From -10.5	-9 to +15	-14 to +15	
	Periodicity (s)	Normal charging	27	8.7 (at -10 dBm)	0.5		2.4 (at 3.2m of a +26.4 dBm power source)	8 to 259	Controlled by the MCU according to the input power 21 s to 2 h 20 min	5 to 18	N/A	30 to more than 12 hours	4 to more than 2 min10
		First charge	N/A	N/A	N/A		N/A	300	30 min to 5 h 30 min	30 to 90	N/A	1 min to more than one day	17 to more than 6 min
	Antenna	Type	Array of patches	Patch	Patch		Log periodic	Patch	PIFA	N/A	SMA	Printed folded quart-wavelength dipole antenna with capacitive arms and metallic reflector plane	
		Gain (dBi)	+5.08	+6.1	+6.7	+7.5	+6.0	+1.8	+1.4	+1.0	N/A	+5.0	
	Rectifier	Topology	N/A	Doubler	Two-stage Dickson charge pump		Doubler	Doubler	Dickson rectifier	N/A	N/A	Doubler	
		Shottky diodes reference	N/A	Avago HSMS-2852	Avago HSMS 285C		Avago HSMS-285C	Skyworks SMS7630-079	Skyworks SMS7630-079	N/A	N/A	Skyworks SMS7630	

Strategy	Size	Energy storage device		Power management unit
		Capacitance (F)	Type	
Simultaneous store and use	Not- fully implemented	100 µ	Capacitor	N/A
Simultaneous store and use (sleep mode)	Not- fully implemented	1 m	Capacitor	Texas Instruments BQ25570
Simultaneous store and use	Not integrated	N/A	Capacitor	(Texas Instruments BQ255??)
Simultaneous store and use	Not- fully implemented	N/A	N/A	PowerCast P2110B
Store then use	3 x 3 x 0.5	2 x 470 µ	Capacitors	Texas Instruments BQ25570 and Analog Devices LTC3106 controlled by a MCU
Simultaneous store and use or store then use, according to the input power	Non-integrated	8 m	Capacitor	STMicroelectronics manufactured non-commercially available integrated circuit
Store then use	Non-integrated	1 m	Capacitor	STMicroelectronics manufactured non-commercially available integrated circuit
N/A	7 x 5.2 x 0.9 (without antenna)	200 µ (tunable)	Capacitor (tunable)	N/A
Store then use	8 x 6 x 5	22 m	Super-scapacitor	Texas Instruments BQ25504
	Non-integrated	100 µ	Capacitor	Texas Instruments BD25570

D. Low-level security aspects of the wireless communications protocols used

For the next, both the LoRaWAN and Bluetooth Low Energy wireless communication technologies will be analysed regarding the low-level security aspects. The implemented security features and the most usual vulnerabilities will be introduced for each one, then a security analysis regarding the McBIM project will be achieved.

1. LoRaWAN

For the LoRaWAN wireless communication technology, the current implementation will be considered. This one is based on the 1.0.3 version of the LoRaWAN specification and use class A devices, without acknowledgment. Its low-level security aspects are research topics [213, 214, 667-673].

i. LoRaWAN security features

A LoRaWAN device has a unique 64 bits identifier (DevEUI) and a unique 32 bits address (DevAddr), and must be authenticated in order to transmit data to a network. This authentication can be achieved by over-the-air activation (OTAA) or by activation by personalisation (APB). In the both cases, the device get two unique AES-128 symmetric session keys named AppSKey and NwkSKey assigned before data communication for a unique communication session. NwkSKey is shared with the network server and is used to calculate and verify the MIC (message integrity code) of all data frames to ensure data integrity; and to encrypt and decrypt the payload field of a MAC data frames. Whilst, AppSKey is shared with the application server and is used to encrypt, by a XOR operation, and decrypt the payload field of application-specific data frames. The OTAA procedure ensures unicity for keys by generating these from a unique key named AppKey, this at each reset or re-join request; whilst this is the responsibility of the developer in the ABP procedure to ensure the unicity for the static keys assigned and stored directly in the device. This unicity allows to reduce the probability of compromising the whole network while a node is compromising. In order to prevent replay attacks and packet losses, two frame counters can be used to keep uplink and downlink messages synchronized. If the difference between these is greater than a limitation value, the frames are dropped. In the current implementation, the frame counter is disable for development purposes, because the application deployed on the application server must be updated each time a sensing node is programmed with a new firmware. An acknowledgement frame can be sent in response of an accepted uplink frame. If not received, the uplink frame can be retransmitted. After several attempts, the frame can be considered as lost or rejected. In the current implementation, the acknowledgement is disable in order to limit the energy consumption by not considering the downlink, whatever its form. Thus, the LoRaWAN specification provides an authentication procedure to join a network; the encryption of the payload based on an advanced encryption standard (AES) algorithm and the use of the NwkSKey or the AppSKey; and an integrity check of each data frame sent. More, some additional procedures are available to ensure some security functions.

ii. Common LoRaWAN vulnerabilities

a. Physical access to devices

By having a physical access to devices, it becomes possible to extract the device and network security keys (e.g. through reverse engineering by deriving key from public information, etc.), especially AppSKey and NwkSKey which are necessary to decrypt the communications; and thus, to compromise both the device and the network. The consequences are that: the communications could be decrypted; an attacker could create a mock device with the same credentials to impersonate a legitimate device; the data payload can be manipulated; etc. It is also possible to use hardware, especially a radio module, near the targeted device to intercept its communications. To prevent compromises, the critical data should not be shared.

b. Lack of association between frames

One of the most important vulnerability is the lack of association between data frames and their acknowledgements, especially during the OTAA procedure, which promotes replay attacks and acknowledgement spoofing. Two solutions have been implemented: the frame counter is included in the calculation of the message integrity code; and an acknowledgement flag is added.

c. Re-use of nonce values

Nonce values are values pseudo-randomly generated and used only once to derive the security keys during the OTAA procedure. Because not tracked in some versions, there is a risk of generating a value already used, making the network vulnerable to replay attack or eavesdropping. A solution has been implemented: the nonce values is turn into counters; and the last used values are stored and tracked.

d. Frame counter management

When a device is rebooted or when its frame counters overflow, these latter are set to 0. By being able to reset a device, the frames obtained before by sniffing the communications could be replayed back during a replay attack. For the ABP procedure, a solution could be to store the counter values in the server during the reboot of a device, and rejecting all the messages while the new counter does not reach the stored value. This would decrease the availability of the device. For the OTAA procedure, a solution has been implemented: new security keys are generated at each reconnection.

e. Lack of end-to-end integrity protection

The integrity of the application data is not protected during its transmission between the network and application servers. The specifications acknowledge this vulnerability but left to the developer of the application to implement its own security features.

f. Packet and payload vulnerabilities

The frames are not time-stamped to validate the time of the transmission, which makes it vulnerable to replay attacks. More, its payload length is the same before and after the encryption. Therefore, an attacker could overflow counters to restore the key stream from the encrypted messages.

iii. Common LoRaWAN attacks and security analysis

a. Radio jamming

The radio jamming consists for a malicious entity in transmitting a powerful radio signal near devices and/or gateways, to disrupt the radio transmissions. Because of CSS modulation coexistence issues, malicious LoRa transmissions on the same frequency and with the same spreading factor used by the legal LoRa transmissions is sufficient to interfere with these. Almost all the transmissions can be affected and wiped out at the frequency used. This attack can be detected by observing a sudden drop out from the network. Once detected, it is recommended to change the frequency band.

b. Replay attack

During a replay attack, the attacker captures a valid data transmission to repeat or delay it to fool the network (both device and gateway can be targeted). The attack requires the knowledge of the frequencies and channels used during the communications. These can be prevented with the use of the tracking frame counters, join procedure *via* OTAA, or physical protection; and could lead to denial of service (DOS) which intends to disrupt services.

c. Acknowledgement spoofing

This attack results from the lack of association between a frame and its acknowledgment. The attacker prevents the reception (e.g. *via* jamming) and captures the downlink acknowledgement in order to acknowledge another uplink frame from the same device. The purpose of this attack is mainly: to take control of the gateways; to damage the network; or to provoke DOS. This is also possible on uplink frames if the attacker can prevent their reception by gateways.

d. Bit flipping

The lack of end-to-end integrity protection of application data enables bit flipping. If the transport layer security between the network and application servers does not exist or is compromised, and if the attacker is able to act on this channel, then the application data can be altered and the confidentiality of the application compromised.

e. Eavesdropping

Eavesdropping can be passive (e.g. sniffing) or active (e.g. relay attack, man-in-the middle). During sniffing attack, the most common passive eavesdropping method, the attacker captures the frames transmitted over a network between the devices and the gateways. From the gathered information, the attacker can launch further to compromise the operation of the network at several levels.

f. Other attacks

Relay attack occurs when a malicious entity creates a relay between the devices and the network server, and initiates a communication to relay the frames to another malicious entity.

Other attacks exist but are not considered in this short study.

2. Bluetooth Low Energy

For the Bluetooth Low Energy wireless communication technology, the current implementation will be considered. This one is based on the fifth version of the Bluetooth specification and use the topology based on broadcasters and observers. Its low-level security aspects are research topics [181, 674-683].

i. Bluetooth Low Energy security features

Several security mechanisms are already implemented by default in Bluetooth Low Energy technology, such as the frequency hopping which avoids interferences with other devices using the same frequency band. More, the implementation of some security processes is recommended in [181] and [684]. First, two security modes with several levels of security are defined to encrypt and sign data. The mode 1 is dedicated to the data encryption. Its level 1 provides no security; its level 2 the unauthenticated pairing with encryption; its level 3 the authenticated pairing with encryption; and its level 4 the authenticated secure connection pairing with encryption. The mode 2 is dedicated to the connection-based data signing. Its level 1 and level 2 provide respectively the unauthenticated and the authenticated pairing with data signing. Second, a security manager is used for the pairing process during which devices exchange information to establish secure connection (Mode 1, level 4) which avoids temporary key brute-force attack. The pairing process has three main phases: the exchange (with no encryption) of pairing features (based on the abilities) between the devices in order to select the most suitable method to generated short-term (or temporary) key (four methods are available, namely "just works", "passkey", "out-of-bands" and "numeric comparison"); the generation and the exchange of the short-term key used to encrypt the frames dedicated to the pairing and the authentication, and which protect against man-in-the-middle attacks; finally, the generation and the exchange of the long term key used to encrypt all the next communications. An optional phase consists in the exchange of transport keys parameters which can be used to store the security keys and the information exchanged during the pairing process, which will allow later re-connections without needing to repeat the entire process. Then, the Bluetooth Low Energy communications are encrypted using an AES-128 cipher block chaining-message authentication code algorithm based on 128 bits key length generated with the elliptic curve Diffie-Hellman method. The communications using encryption and authentication use a message integrity code (MIC) appended to the payload, and a cyclic redundancy check (CRC) mechanism to protect it all. The communications using authentication but not encryption use a 12-byte signature computed with a 128-bit AES algorithm placed after the data payload, as well as an input counter to prevent the replay attacks. Moreover, a privacy feature is provided to limit the tracking of the identity of a device: its address is private and changes frequently, *via* the encryption of its public address. Finally, trust modes are defined to characterize the communications. A communication with a device "trusted" allows a fixed connection and unrestricted access to all its services, while a communication with an "untrusted" device restricts its access to a set of services.

ii. Common Bluetooth Low Energy vulnerabilities

a. Pairing process

Although the short-term key is not transmitted through packet, its 16 bytes input value is predictable. For the "just works" method, its value is predefined to 0x00 and this method is vulnerable to man-in-the-middle attacks because the authenticity of the connection cannot be

verified. For the "passkey" method the generation parameters are transmitted through packets. Thus, an attacker could calculate its value and decrypt data.

b. Discoverability

Bluetooth Low Energy has a discoverability mode used before the pairing process. A discoverable device is vulnerable because it allows all the devices located in its neighbourhood to access information, such as its name, its class and its services. Turning off the discoverability mode prevents devices to scanning attacks.

iii. Common Bluetooth Low Energy attacks and security analysis

Bluetooth Low Energy technology, and more generally Bluetooth technology, is vulnerable to many attacks, whose: the PIN (personal identification number) theft (by cracking or off-line recovery etc.); the eavesdropping (sniffing, man-in-the-middle, relay etc.); the cloning (MAC address spoofing, forced re-pairing, brute-force, chopping, etc.); the treacherous (backdoor, bumping, etc.); the denial of service (DOS) (radio jamming, MAC address duplication, synchronous connection-oriented, enhanced synchronous connection-oriented, battery exhaustion, big negative-acknowledgement, guaranteed service, smacking, etc.); the surveillance (printing, stumbling, tracking, etc.); and the miscellaneous others (snarfing, bugging, jacking, free calling, whisperer, etc.); etc. Nevertheless, the eavesdropping and denial of service attacks are the more usual.

a. Eavesdropping: sniffing

Sniffing is the most common passive approach for eavesdropping. This attack can take place during different stages of the Bluetooth Low Energy communication, such as a new connection, an active connection, or an negotiation phase. However, in the case of the Bluetooth Low Energy, sniffing is complex and expensive as 40 channels are used with a fast frequency hopping spread spectrum technique. During the establishment of a new connection, the connection request packet can be captured. This one contains several parameters to set the frequency hopping algorithm and the cyclic redundancy check (CRC) calculation. Knowing these parameters, the attacker can used these to set up its algorithm to listen from at least one of the three advertising channels, if it is too expensive to sniff all of these at once. During an active connection, the attacker can deduce the connection parameters through an exhaustive approach which assumes that all channels are systematically used, and which is not effective on short communications because a lot of time is required. During the negotiation phase, the attacker can get the encryption keys to decrypt next communications.

b. Eavesdropping: man-in-the-middle

Man-in-the-middle attacks occur when an attacker intercepts the communications between two devices and modifies it. Some attacks consist in cloning the GATT (generic attribute) server to simulate an identical device to which the master device will be connected. It allows the fake device to connect to the legitimate device to capture the traffic, impersonate a device, inject data, modify or redirect packets, provoke denial of service, etc. These attacks are easy to implement as only requiring a communication between two devices and as the attacker can negotiate the encryption parameters.

c. Radio jamming

Using a strong radio signal near a Bluetooth Low Energy device can cause interferences and jam communications. The attacker can jam the connected communications and the advertising transmissions by saturating the radio spectrum, until interrupting connected communications or hijacking connected communications by forcing the master to disconnect. Preventing radio jamming is difficult as it requires physical protection from interferences.

d. Other attacks

Bluetooth Low Energy is also vulnerable to replay attacks, relay attacks and spoofing attacks.

Other attacks exist but are not considered in this short study.

e. Audit tools

Several audit tools, such as [685], exist to test the resistance to attacks of the devices under test.

3. Low-level security aspects in the framework of the McBIM project

Both the LoRaWAN and Bluetooth Low Energy wireless communication technologies will be studied regarding their current implementation in the framework of the McBIM project. The wireless communications between inaccessible sensing nodes buried in the reinforced concrete and accessible communicating nodes located on the surface of the reinforced concrete will be mainly considered. These are currently only unidirectional from the sensing nodes to the communicating nodes and carry non-critical measurement data. More, the sensing nodes are not able to receive downlink frames but can be controlled by the communicating nodes through the wireless power transfer system. Then, the bidirectional communications within the meshed network of communicating nodes and with the Internet will be only skimmed through. In any case, all the wireless communications: from the sensing nodes to the communicating nodes; between the communicating nodes; and between a communicating node and the Internet; raise low-level security issues, whose the importance depends on the data transmitted: their type, their criticality, their reliability, etc.

i. Malicious objectives

Three main types of malicious objectives have been identified: the invasion of privacy; the alteration of service; and the interruption of service. Because of a low computing resources, the hijacking of the network for others activities seems improbable.

a. Invasion of privacy

Invasion of privacy consists in gathering information on the activities in the instrumented infrastructure, for instance through sniffing or other eavesdropping techniques. This could be realized by the infrastructure owner to acknowledge, for instance, the movements or activities of the users (such as employees, etc.) in the infrastructure. An outsider of the structure could also gather information on activities in order to identify the best moment to trespass in the infrastructure (such as for robbing or degrading, etc.) or to collect classified information (such as the use of the infrastructure, the available equipment, etc.).

b. Alteration of service

The services delivered by the communicating reinforced concrete can be altered by the falsification of the measurement, for instance through man-in-the-middle attacks, relay attacks or replay attacks; or by modifying the transmitted frames. As an example, an attacker could emulate a failure (such as a significant crack, a fire, etc.) to make people believe in the possible collapse of the infrastructure or at least its unsafety.

c. Interruption of service

The services delivered by the communicating reinforced concrete can be interrupted by stopping the communications, for instance through denial of service (DOS) attacks, radio jamming attacks, or battery exhaustion attacks (such as by avoiding the wireless power transfer from the communicating nodes to the sensing nodes, etc.).

ii. Threat model

The proposed threat model is based on two-range attacks: the short-range and the long-range.

a. Short-range attack

The short-range attacks provide a physical access to the attacker which can be either inside the infrastructure or outside it but near enough to place malicious objects (such as malicious sensing nodes, malicious communicating nodes, etc.).

b. Long-range attack

The maximum range of the attacks depends on the wireless communication technology, the transmission power and the type of communication. In this case, the attacker is able to communicate with legitimate nodes or to emit an enough powerful radio signal to jam the wireless communications.

iii. Risks

The risk scales, both for the probability and the impact of an attack, are based on personal estimation related to the scientific literature. The impact of an attack depends on the potential harm this can inflict both to the material and the humans, due to failure of its detection

a. Invasion of privacy

The invasion of privacy implies several risks such as the surveillance, the insertion of a malicious node into the network, the insertion of fake data, and the compromise of node(s). Their analysis in proposed in Table VIII.3.

b. Alteration of service

The alteration of service implies several risks such as the deduction of the infrastructure activities or the alteration of data; and is time consuming and expensive to detect and correct. Their analysis in proposed in Table VIII.4.

Table VIII.3: Analysis of the risks implied by an invasion of privacy.

Risk	Probability	Impact
Surveillance	Likely	Insignificant to critical according to the activities
Insertion of a malicious node into the network	Sensing node embedded in the reinforced concrete: **unlikely** Sensing node non-embedded in the reinforced concrete: **likely** Communicating node: **even**	Sensing node embedded in the reinforced concrete: **minor** Sensing node non-embedded in the reinforced concrete: **minor** Communicating node: **major to critical** (especially if a gateway to Internet is targeted)
Insertion of fake data	**Likely**	**Moderate to critical**
Compromise of node(s)	Sensing node: **unlikely** Communicating node: **likely**	Sensing node: **minor** Communicating node: **major to critical** (especially if a gateway to Internet is targeted)

Table VIII.4: Analysis of the risks implied by an alteration of service.

Risk	Probability	Impact
Deduction of the infrastructure activities	**Likely,** depends on the implemented security mechanisms	**Minor to critical**, depends on the activities (e.g. critical in a nuclear plant, etc.)
Alteration of data	**Even**, depends on the implemented security mechanisms	**Moderate to critical** (e.g. emulation of a failure, a collapse, a fire, etc.)

c. Interruption of service

The interruption of service implies several risks such as the radio jamming, the battery exhaustion, the creation of relays, the creation of cycles, the damage of the rectenna, the data recovery from nodes, and the alteration of the full infrastructure; and is time consuming and expensive during the time of unavailability. Their analysis in proposed in Table VIII.5.

iv. Technical solutions

Three main technical solutions can be employed separately or conjointly to prevent the attacks: the cryptography; the secure element (SE); and the intrusion detection system (IDS).

a. Cryptography

The wireless communications can be secured by employing the cryptography features offered both by the LoRaWAN and the Bluetooth Low Energy protocols, especially through the encryption of the data, respectively thanks to an AES-128 counter algorithm and an AES-128 cipher block chaining-message authentication code algorithm. Nevertheless, additional level(s) of cryptography can be employed. The use of cryptography is a flexible solution easy to implement, but which is computationally expensive and which requires secrets to be stored in a safe and non-volatile manner. Moreover, it is power consuming and generating of latency, thus poorly suited to low energy devices.

Table VIII.5: Analysis of the risks implied by an interruption of service.

Risk	Probability	Impact
Radio jamming	Between the sensing nodes and the communicating nodes: **likely** Between the communicating nodes: **likely** Between a communicating node and the Internet: **likely**	Between the sensing nodes and the communicating nodes: **insignificant to critical**, depends of the number of affected nodes Between the communicating nodes: **moderate to major** Between a communicating node and the Internet: **critical**
Battery exhaustion	Alteration of the wireless power transfer: **improbable** Destruction of the sensing nodes components: **unlikely** (e.g. mechanical break, etc.) Destruction of the communicating nodes: **even**	Sensing nodes: **insignificant to critical**, depends of the number of affected nodes Communicating nodes: **major to critical**, depends of the number of affected nodes
Creation of relays	Sensing node embedded in the reinforced concrete: **unlikely** Sensing node non-embedded in the reinforced concrete: **likely** Communicating node: **likely**	Sensing node embedded in the reinforced concrete: **minor** Sensing node non-embedded in the reinforced concrete: **major** Communicating node: **major to critical** (e.g. a malicious device takes the place of a failed node)
Creation of cycles	**Likely**	**Minor to critical**, depends on the type of activities and of data
Damage of the rectenna	**Unlikely** (e.g. very energetic electromagnetic wave, etc.)	**Critical**
Data recovery from nodes	**Even**	**Minor to critical**, depends on the type of data
Alteration of the full infrastructure	**Unlikely**	**Critical**

b. Secure elements (SE)

The use of secure elements can be an alternative way to secure the wireless sensor network. This one is tamper-resistant hardware embedded chip used to secure the storage of confidential and cryptographic data, to host securely applications, and to implement end-to-end security. Resistive random-access memory physical unclonable functions can be implemented to manage the authentication, the key generation and the storage. The secure elements are relatively cheap and consume less energy than using cryptography. However, it requires the integration of its driver software and the adaptation of the existing firmware. Finally, the wire connection to the microcontroller unit must be protected.

c. Intrusion detection system (IDS)

An intrusion detection system (IDS) can be another alternative way to secure the wireless sensor network. This one is based on two detection methods: the signature-based and the

anomaly-based methods. The first is not yet adapted for the low power wireless sensor networks, whilst the second uses learning systems to identify the legitimate behaviours and detect the suspicious behaviours. In the McBIM project, two learning phases can be imagined: one during the manufacture of an element made of communicating reinforced concrete, during which the communicating node(s) detect the legitimate sensing nodes in its neighbourhood; and the other during the construction of a complete structure made of several elements, during which each communicating node detects the legitimate communicating nodes in its neighbourhood. The intrusion detection systems provide a visibility on the network and adds a layer of defence, but requires maintenance and can be sensitive to false positives and negatives.

v. LoRaWAN and Bluetooth Low Energy implementable features

The Table VIII.6 and Table VIII.7 gather some optional security features respectively provided by the LoRaWAN and the Bluetooth Low Energy protocols, with the attacks this prevents and its drawbacks. Just because some attacks are avoided does not mean that there are no more risks.

Table VIII.6: LoRaWAN security issues and protection mechanisms

Security mechanisms	Attacks prevented	Consequences of a successful attack	Drawbacks
Over-the-air activation procedure	Replay attack	Connection of a malicious device to the network server Injection of (fake) data Etc.	Risk of replay attacks reduced but still possible if the reset and overflow of the frame counter are not well considered Increases latency Increases power consumption Requires downlink
Frame counter	Replay attack	(Re)Use of a valid message to connect a malicious device to the network server (Re)Injection of (fake) data Etc.	Could decrease the availability of a device Reset and overflow must be well considered
Message acknowledgement	Replay attack Acknowledgement spoofing	(Re)Use of a valid message to connect a malicious device to the network server (Re)Injection of (fake) data Etc.	Increases latency Increases power consumption Requires downlink

Table VIII.7: Bluetooth Low Energy security issues and protection mechanisms

Security mechanisms		Attacks prevented	Consequences of a successful attack	Drawbacks
Security Mode 1: Encryption	Level 1	None	Decryption of data Traffic observation Traffic injection Denial of service	N/A
	Level 2	Limited eavesdropping protection		Requires encrypted link Requires downlink
	Level 3	Eavesdropping Replay attack		Requires encrypted link Requires downlink
	Level 4	Eavesdropping Replay attack Man-in-the-middle		Requires encrypted link Requires secure communication Requires downlink
Security Mode 2: Data signing	Level 1	None	Traffic observation Traffic injection	Cannot be combined with security Mode 1 Connection based data signing Requires signing Requires downlink
	Level 2	Eavesdropping Replay attack		Cannot be combined with security Mode 1 Connection based data signing Requires signing Requires downlink
Pairing process: Temporary key generation	"Just work"	Passive attacks	Impersonate devices Decryption of data Traffic observation Traffic injection Denial of services	Requires downlink
	"Passkey"	Passive attacks Man-in-the-middle		Input or output ability Requires downlink
	"Out-of-band"	Passive attacks Man-in-the-middle		Requires another interface Requires downlink
	"Numeric comparison"	Passive attacks Man-in-the-middle		Requires binary input Requires downlink
Discoverable mode disabled		Prevents from accessing information such as names, class, services, etc.	Steal of sensitive data	No data transmission allowed
Trust mode		Limits automatic access to all services	Only a trusted device just compromised enables the access to all the services to an attacker	Removes pairing information
Privacy feature		Identity tracking	Steal of sensitive data	Available only with connected mode Only a trusted device can be connected

IX. Conclusion

During this doctoral thesis, several works has been carried out in order to provide a hardware solution to the implementation of a communicating reinforced concrete. The proposed solution is based on a two-layer wireless sensor network intended to be embedded in the reinforced concrete. This network is composed of two kinds of nodes: the communicating nodes and the sensing nodes.

The communicating nodes, which are considered as accessible and powered by an available and not restricted source of energy, are dedicated to the recovery, the processing and the storage of the data received from the sensing nodes, as well as the sharing of these data within a meshed network of communicating nodes, the digital world through the Internet, and locally and/or remotely with the different stakeholders. Moreover, the communicating nodes must be able (by using a dedicated radiative electromagnetic power source) to wirelessly power the sensing nodes located in a three-dimensional area with a radius of several metres.

Two implementations of the communicating nodes have been provided, with different wireless communication technologies used between the sensing nodes and the communicating nodes: LoRaWAN and Bluetooth Low Energy. In their most advanced implementation, the communicating nodes are able to receive all the data sent by the sensing nodes, to process these locally, to store these locally and remotely, and to share these: in a reduced network of communicating nodes; with the digital world through the Internet; and locally and remotely with the stakeholders. Moreover, thanks to the use of a radiative electromagnetic power source, the communicating nodes can wirelessly power all the sensing nodes located at several meters around, although located in a reinforced concrete beam or positioned on the surface of a reinforced concrete wall.

The sensing nodes, which are considered as inaccessible once deployed because fully buried in the reinforced concrete, are dedicated to the measurement of the properties of the reinforced concrete and/or of its environment. These must be battery-free and energy autonomous during all the lifetime of the reinforced concrete, that says for decades.

Two implementations of the sensing nodes have been provided, with different wireless communication technologies used to transmit the collected data to the communicating nodes: LoRaWAN and Bluetooth Low Energy. In the two implementations, the sensing nodes are able to measure several parameters of the internal state of the reinforced concrete: such as the temperature, the relative humidity, the electric resistivity, or the mechanical deformation; useful to estimate its structural health, especially by the estimation of the corrosion rate. The collected data are then pre-processed and wirelessly transmitted to the communicating nodes. Moreover, the sensing nodes are battery-free, cold start-up compatible and able to harvest the radiative electromagnetic power generated by the communicating nodes over several metres although embedded in a reinforced concrete beam, until having enough to achieve a full process and even from a completely empty energy storage device. In order to reduce the power consumption of sensing node, only the uplink communication (*i.e.* from the sensing nodes to the communicating nodes) is implemented. The downlink way (from the communicating nodes to the sensing nodes) is only used for the wireless power transfer. Also, by controlling the radiative electromagnetic power source, the communicating nodes can remotely roughly control the periodicity of process of the sensing nodes. Because essentially powered-off, battery-free, wirelessly powered and designed as simple as possible, the sensing

nodes should reliably operate in the long-term. The age-related failure of an electronic component seems to be the more probable cause of a failure of the sensing nodes. Finally, the sensing nodes have been designed to be sufficiently compact to be buried in the reinforced concrete without altering its mechanical properties. As long as possible, the sensing nodes use a unique antenna both for the wireless communication and the wireless power harvesting.

The tests of the different implementations have allowed the deployment of a proof-of-concept wireless sensor network. This is composed of two communicating nodes and four sensing nodes located in a reinforced concrete beam or in a large room, measuring some parameters (e.g. temperature, relative humidity, electric resistivity, mechanical deformation) in or around the reinforced concrete, and transmit these to the communicating nodes. The communicating nodes collect, process, store and share together, with the remote servers (through the Internet) and/or with users, the data sent by the sensing nodes. The wireless communications are achieved over several metres, but can be extended to tens or hundreds of metres thanks to the LoRaWAN technology, whilst the wireless power transfer is currently limited to several metres. The maximum successfully tested range for the wireless power transfer is 7 metres in the air, but higher ranges are expected.

Although some encouraging results have been achieved, several lines of progression have been defined all along this manuscript. Thus, and between others, the range of use and the energy efficiency must be increase by using components requiring less power and rectenna more efficient; the time required to charge or recharge the sensing nodes must be reduce by limiting the global energy need; both the sensing and the communicating nodes must be improved to be more compact, to consume less energy, and to provide all the features required by the targeted application; etc.

Concerning the monitoring of the reinforced concrete, an innovative low-cost solution was proposed, which is wireless, fully integrated and buried, deployed for long-term, wirelessly powered, and based mainly on the use of appropriate sensors for the targeted application. To the best of our knowledge, this is the first battery-free and wirelessly powered by radiative electromagnetic waves (that says in far-field) sensing nodes designed to be buried into the (reinforced) concrete in order to monitor its structural health throughout its life.

Regarding the wireless power transfer, the proposed solution is in the state-of-the-art in terms of performance, whose the range of use; makes available a new wireless communication technology; provides the implementation of a full cyber-physical system based on a two-layer wireless sensor network; and met the requirement of the simultaneous wireless information and power transmission paradigm.

Finally, the proposed solutions can be adapted to other applications and use cases, with various sensors and/or actuators, and in different fields.

To go further, several innovative and on the state-of-the-art technologies could be employed to improve the current solution, such as: the use of beamforming techniques both for the wireless communication and the wireless power transfer; the use of flexible substrate and/or three-dimensional printing and/or additive techniques to the manufacture of the sensing and communicating nodes; or even, the design of a performing application specific integrated circuit (ASIC) dedicated to the wireless communication, the wireless power transfer and the measurement systems, and if possible with compatible on-chip sensors.

Bibliography

[1] Neville A.M., "Properties of concrete," 5th Ed., London: Longman, 1995.

[2] Mindess S., Young F.J., and Darwin D., "Concrete," 2nd Ed., Technical Documents, 2003.

[3] Mehta P.K., and Monteiro P.J., "Concrete: microstructure, properties, and materials," 4th Ed., McGraw-Hill Education, 2014.

[4] Darwin D., Dolan C.W., and Nilson A.H., "Design of concrete structures," 15th Ed., New York, NY, USA, McGraw-Hill Education, 2016.

[5] Kosmatka S.H., Kerkhoff B., and Panarese W.C., "Design and control of concrete mixtures," 16. Ed., vol. 5420, pp. 60077-1083, Skokie, IL: Portland Cement Association, 2016.

[6] "American Concrete Institute, Standards," Available online: https://www.concrete.org/publications/technicaldocuments.aspx.aspx (accessed on 3 March 2021).

[7] "Japan Society of Civil Engineers, Standard Specifications and Guidelines," Available online: https://www.jsce-int.org/about/guideline (accessed on 3 March 2021).

[8] "European Committee for Standardization, CEN/TC 104 - Concrete and related products," Available online: https://standards.cen.eu/dyn/www/f?p=204:7:0::::FSP_LANG_ID,FSP_ORG_ID:25,6087&cs=1876910561260458176C499F18EC12B1D#1 (accessed on 3 March 2021).

[9] "Norme NF EN 206/CN Béton - Partie 1 : Spécification, performances, production et conformité," Available online: https://www.boutique.afnor.org/norme/nf-en-206a1/beton-specification-performances-production-et-conformite/article/918602/fa188531 (accessed on 3 March 2021).

[10] Miller S.A., Horvath A., and Monteiro P.J., "Readily implementable techniques can cut annual CO2 emissions from the production of concrete by over 20%," Environmental Research Letters, vol. 11, no. 7, p. 074029, 2016.

[11] Liew K.M., Sojobi A.O., and Zhang, L.W., "Green concrete: Prospects and challenges," Construction and building materials, vol. 156, pp. 1063-1095, 2017.

[12] Monteiro P.J., Miller S.A., and Horvath A., "Towards sustainable concrete," Nature materials, vol. 16, no. 7, pp. 698-699, 2017.

[13] Miller S.A., and Moore F.C., "Climate and health damages from global concrete production," Nature Climate Change, pp. 1-5, 2020.

[14] Adesina A., Awoyera P.O., and Kumar K.R., "Green concrete: A review of recent developments," Materials Today: Proceedings, vol. 27, pp. 54-58, 2020.

[15] Skocek J., Zajac M., and Haha M.B., "Carbon capture and utilization by mineralization of cement pastes derived from recycled concrete," Scientific reports, vol. 10, no. 1, pp. 1-12, 2020.

[16] De Brito J., and Kurda R., "The past and future of sustainable concrete: A critical review and new strategies on cement-based materials," Journal of Cleaner Production, p. 123558, 2020.

[17] Calvi G.M., Moratti M., O'Reilly G.J., Scattarreggia, N. Monteiro, R. Malomo D., Calvi P.M., and Pinho R., "Once upon a time in Italy: The tale of the Morandi Bridge," Structural Engineering International, vol. 29, no. 2, pp. 198-217, 2019.

[18] Al-Qadi I.L., Hazim O.A., Su W., and Riad S.M., "Dielectric properties of Portland cement concrete at low radio frequencies," Journal of materials in Civil Engineering, vol. 7, no. 3, pp. 192-198, 1995.

[19] Buyukozturk O., "Electromagnetic properties of concrete and their significance in nondestructive testing," Transportation research record, vol. 1574, no. 1, pp.10-17, 1997.

[20] Stone W.C., "Electromagnetic signal attenuation in construction materials," 1997.

[21] Haddad R.H., and Al-Qadi I.L., "Characterization of portland cement concrete using electromagnetic waves over the microwave frequencies," Cement and concrete research, vol. 28, no. 10, pp. 1379-1391, 1998.

[22] Robert A., "Dielectric permittivity of concrete between 50 MHz and 1 GHz and GPR measurements for building materials evaluation," Journal of applied geophysics, vol. 40, no. 1-3, pp. 89-94, 1998.

[23] Pokkuluri K.S., "Effect of admixtures, chlorides, and moisture on dielectric properties of Portland cement concrete in the low microwave frequency range," Master dissertation, Virginia Tech, Virginia Polytechnic Institute and State University, 1998.

[24] Dalke R.A., Holloway C.L., McKenna P., Johansson M., and Ali A.S., "Effects of reinforced concrete structures on RF communications," IEEE Transactions on electromagnetic compatibility, vol. 42, no. 4, pp. 486-496, 2000.

[25] Richalot E., Bonilla M., Wong M.F., Fouad-Hanna V., Baudrand H., and Wiart J., "Electromagnetic propagation into reinforced-concrete walls," IEEE Transactions on Microwave Theory and Techniques, vol. 48, no. 3, pp. 357-366, 2000.

[26] Soutsos M.N., Bungey J.H., Millard S.G., Shaw M.R., and Patterson A., "Dielectric properties of concrete and their influence on radar testing," NDT & e International, vol. 34, no. 6, pp. 419-425, 2001.

[27] Pena D., Feick R., Hristov H.D., and Grote W., "Measurement and modeling of propagation losses in brick and concrete walls for the 900-MHz band," IEEE Transactions on Antennas and Propagation, vol. 51, no. 1, pp. 31-39, 2003.

[28] Sagnard F., and Zein, G.E., "In situ characterization of building materials for propagation modeling: Frequency and time responses," IEEE Transactions on antennas and propagation, vol. 53, no. 10, pp. 3166-3173, 2005.

[29] Adous M., "Caractérisation électromagnétique des métariaux traités de génie civil dans la bande de fréquence 50 MHz-13 GHz," Doctoral dissertation, Université de Nantes, 2006.

[30] Sandrolini L., Reggiani U., and Ogunsola A., "Modelling the electrical properties of concrete for shielding effectiveness prediction," Journal of Physics D: Applied Physics, vol. 40, no. 17, p. 5366, 2007.

[31] Filali B., Boone F., Rhazi J., and Ballivy G., "Design and calibration of a large open-ended coaxial probe for the measurement of the dielectric properties of concrete," IEEE Transactions on Microwave Theory and Techniques, vol. 56, no. 10, pp. 2322-2328, 2008.

[32] Pinhasi Y., Yahalom A., and Petnev S., "Propagation of ultra wide-band signals in lossy dispersive media," in 2008 IEEE International Conference on Microwaves, Communications, Antennas and Electronic Systems, IEEE, pp. 1-10, 2008 May.

[33] Jamil M., Hassan M.K., Al-Mattarneh H.M.A., and Zain M.F.M., "Concrete dielectric properties investigation using microwave nondestructive techniques," Materials and structures, vol. 46, no. 1, pp. 77-87, 2013.

[34] Chinh Mai T., "Evaluation non destructive des matériaux de construction par technique électromagnétique aux fréquences radar: modélisation et expérimentation en laboratoire," Doctoral dissertation, Université de Bordeaux, 2015.

[35] Zhekov S.S., Franek O., and Pedersen G.F., "Dielectric properties of common building materials for ultrawideband propagation studies [Measurements Corner]," IEEE Antennas and Propagation Magazine, vol. 62, no. 1, pp. 72-81, 2020.

[36] Kamila S., "Introduction, classification and applications of smart materials: an overview," American Journal of Applied Sciences, vol. 10, no. 8, p. 876, 2013.

[37] Han B., Wang Y., Dong S., Zhang L., Ding S., Yu X., and Ou J., "Smart concretes and structures: A review," Journal of intelligent material systems and structures, vol. 26, no. 11, pp. 1303-1345, 2015.

[38] Han B., Zhang L., and Ou J., "Smart and multifunctional concrete toward sustainable infrastructures," Singapore, Springer, p. 409, 2017.

[39] Makul N., "Advanced smart concrete-A review of current progress, benefits and challenges," Journal of Cleaner Production, p. 122899, 2020.

[40] Han B., Ding S., and Yu X., "Intrinsic self-sensing concrete and structures: A review," Measurement, vol. 59, pp. 110-128, 2015.

[41] Tian Z., Li Y., Zheng J., and Wang S., "A state-of-the-art on self-sensing concrete: Materials, fabrication and properties," Composites Part B: Engineering, vol. 177, p. 107437, 2019.

[42] Chen P.W., and Chung D.D.L., "Carbon fiber reinforced concrete as an intrinsically smart concrete for damage assessment during dynamic loading," MRS Online Proceedings Library Archive, vol. 360, 1994.

[43] Sun M., Li Z., Liu Q., Tang Z., and Shen D., "A study on thermal self-diagnostic and self-adaptive smart concrete structures," Cement and Concrete Research, vol. 30, no. 8, pp. 1251-1253, 2000.

[44] Demircilioglu E., Teomete E., and Ozbulut O.E., "Strain sensitivity of steel-fiber-reinforced industrial smart concrete," Journal of Intelligent Material Systems and Structures, vol. 31, no. 1, pp. 127-136, 2020.

[45] De Belie N., Gruyaert E., Al-Tabbaa A., Antonaci P., Baera C., Bajare D., Darquennes A., Davies R., Ferrara L., Jefferson T., and Litina C., "A review of self-healing concrete for damage management of structures," Advanced Materials Interfaces, vol. 5, no. 17, p. 1800074, 2018.

[46] Yang Y., Lepech M.D. Yang E.H., and Li V.C., "Autogenous healing of engineered cementitious composites under wet–dry cycles," Cement and Concrete Research, vol. 39, no. 5, pp. 382-390, 2009.

[47] Wu M., Johannesson B., and Geiker M., "A review: Self-healing in cementitious materials and engineered cementitious composite as a self-healing material," Construction and Building Materials, vol. 28, no. 1, pp. 571-583, 2012.

[48] Vijay K., Murmu M., and Deo S.V., "Bacteria based self healing concrete–A review," Construction and Building Materials, vol. 152, pp. 1008-1014, 2017.

[49] Mo J., Zeng L., Liu Y., Ma L., Liu C., Xiang S., and Cheng G., "Mechanical properties and damping capacity of polypropylene fiber reinforced concrete modified by rubber powder," Construction And Building Materials, vol. 242, p. 118111, 2020.

[50] Chen J., Zhang W., Shi X., Yao C., and Kuai C., "Use of PEG/SiO2 phase change composite to control porous asphalt concrete temperature," Construction and Building Materials, vol. 245, p. 118459, 2020.

[51] Liang J., Zhang X., and Ji J., "Hygroscopic phase change composite material - A review," Journal of Energy Storage, vol. 36, p. 102395, 2021.

[52] Liu J.C., Tan K.H., and Yao Y., "A new perspective on nature of fire-induced spalling in concrete," Construction and Building Materials, vol. 184, pp. 581-590, 2018.

[53] Li V.C., "On engineered cementitious composites (ECC) a review of the material and its applications," Journal of advanced concrete technology, vol. 1, no. 3, pp. 215-230, 2003.

[54] Su Y.F., Kotian R.R., and Lu N., "Energy harvesting potential of bendable concrete using polymer based piezoelectric generator," Composites Part B: Engineering, vol. 153, pp. 124-129, 2018.

[55] Singh M., Saini B., and Chalak H.D., "Performance and composition analysis of engineered cementitious composite (ECC)–A review," Journal of Building Engineering, vol. 26, p. 100851, 2019.

[56] Doyle K., Reese L., Radlińska A., and Qiu T., "Material properties of crushable concrete for use in vehicle antiram barriers," Journal of materials in civil engineering, vol. 29, no. 4, p. 04016253, 2017.

[57] Sassani A., Ceylan H., Kim S., Gopalakrishnan K., Arabzadeh A., and Taylor P.C., "Influence of mix design variables on engineering properties of carbon fiber-modified electrically conductive concrete," Construction and Building Materials, vol. 152, pp. 168-181, 2017.

[58] El-Dieb A.S., El-Ghareeb M.A., Abdel-Rahman M.A., and El Sayed A.N., "Multifunctional electrically conductive concrete using different fillers," Journal of Building Engineering, vol. 15, pp. 61-69, 2018.

[59] Chang C., Ho M., Song G., Mo Y.L., and Li H., "A feasibility study of self-heating concrete utilizing carbon nanofiber heating elements," Smart Materials and Structures, vol. 18, no. 12, p. 127001, 2009.

[60] Jang S.H., and Park Y.L., "Carbon nanotube-reinforced smart composites for sensing freezing temperature and deicing by self-heating," Nanomaterials and Nanotechnology, vol. 8, p. 1847980418776473, 2018.

[61] Armoosh S.R., and Oltulu M., "Self-heating of electrically conductive metal-cementitious composites," Journal of Intelligent Material Systems and Structures, vol. 30, no. 15, pp. 2234-2240, 2019.

[62] Faneca Llesera G., Ikumi Montserrat T., Torrents Dolz J.M., Aguado de Cea A., and Segura Pérez I., "Conductive concrete made from recycled carbon fibres for self-heating and de-icing applications in urban furniture," Materiales de construcción (Madrid), vol. 70, no. 339, pp. e223-1, 2020.

[63] Nguyen L., Krause A., Tuan C., Blasey J.D., Zemotel J.P., McNerney H., and Metzger F.J., "Shielding effectiveness performance of conductive concrete structures;" in 2017 IEEE International Symposium on Electromagnetic Compatibility & Signal/Power Integrity (EMCSI), IEEE, pp. 360-363, 2017 August.

[64] Lu L., He Y., Ping B., Wang F., and Hu S., "TiO2 containing electromagnetic wave absorbing aggregate and its application in concrete," Construction and Building Materials, vol. 134, pp. 602-609, 2017.

[65] Xie S., Ji Z., Zhu L., Zhang J., Cao Y., Chen J., Liu R., and Wang J., "Recent progress in electromagnetic wave absorption building materials," Journal of Building Engineering, vol. 27, p. 100963, 2020.

[66] Alwaeli, M., "Investigation of gamma radiation shielding and compressive strength properties of concrete containing scale and granulated lead-zinc slag wastes," Journal of Cleaner Production, vol. 166, pp. 157-162, 2017.

[67] Azreen N.M., Rashid R.S., Haniza M., Voo Y.L., and Amran Y.M., "Radiation shielding of ultra-high-performance concrete with silica sand, amang and lead glass," Construction and Building Materials, vol. 172, pp. 370-377, 2018.

[68] Azeez M.O., Ahmad S., Al-Dulaijan S.U., Maslehuddin M., and Naqvi A.A., "Radiation shielding performance of heavy-weight concrete mixtures," Construction and Building Materials, vol. 224, pp. 284-291, 2019.

[69] Lotfi-Omran O., Sadrmomtazi A., and Nikbin I.M., "A comprehensive study on the effect of water to cement ratio on the mechanical and radiation shielding properties of heavyweight concrete," Construction and Building Materials, vol. 229, p. 116905, 2019.

[70] Said S.H., "State-of-the-art developments in light transmitting concrete," Materials Today: Proceedings, vol. 33, pp. 1967-1973, 2020.

[71] Kousis I., Fabiani C., Gobbi L., and Pisello A.L., "Phosphorescent-based pavements for counteracting urban overheating-A proof of concept," Solar Energy, vol. 202, pp. 540-552, 2020.

[72] Hüsken G., Hunger M., and Brouwers H.J.H., "Experimental study of photocatalytic concrete products for air purification," Building and environment, vol. 44, no. 12, pp. 2463-2474, 2009.

[73] Boonen E., Beeldens A., Dirkx I., and Bams V., "Durability of cementitious photocatalytic building materials," Catalysis Today, vol. 287, pp. 196-202, 2017.

[74] Xu Y., Chen W., Jin R., Shen J., Smallbone K., Yan C., and Hu L., "Experimental investigation of photocatalytic effects of concrete in air purification adopting entire concrete waste reuse model," Journal of hazardous materials, vol. 353, pp. 421-430, 2018.

[75] Mahy J.G., Paez C.A., Hollevoet J., Courard L., Boonen E., and Lambert S.D., "Durable photocatalytic thin coatings for road applications," Construction and Building Materials, vol. 215, pp. 422-434, 2019.

[76] Witkowski H., Jackiewicz-Rek W., Chilmon K., Jarosławski J., Tryfon-Bojarska A., and Gąsiński A., "Air purification performance of photocatalytic concrete paving blocks after seven years of service," Applied Sciences, vol. 9, no. 9, p. 1735, 2019.

[77] Souto-Martinez A., Arehart J.H., and Srubar III W.V., "Cradle-to-gate CO2e emissions vs. in situ CO2 sequestration of structural concrete elements," Energy and Buildings, vol. 167, pp. 301-311, 2018.

[78] Liang C., Pan B., Ma Z., He Z., and Duan Z., "Utilization of CO2 curing to enhance the properties of recycled aggregate and prepared concrete: A review," Cement and concrete composites, vol. 105, p. 103446, 2020.

[79] Tam V.W., Butera A., Le K.N., and Li W., "Utilising CO2 technologies for recycled aggregate concrete: A critical review," Construction and Building Materials, vol. 250, p. 118903, 2020.

[80] Al-Kheetan M.J., Rahman M.M., and Chamberlain D.A., "Development of hydrophobic concrete by adding dual-crystalline admixture at mixing stage," Structural Concrete, vol. 19, no. 5, pp. 1504-1511, 2018.

[81] Feng Z., Wang F., Xie T., Ou J., Xue M., and Li W., "Integral hydrophobic concrete without using silane," Construction and Building Materials, vol. 227, p. 116678, 2019.

[82] Song J., Zhao D., Han Z., Xu W., Lu Y., Liu X., Liu B., Carmalt C.J., Deng X., and Parkin I.P., "Super-robust superhydrophobic concrete," Journal of Materials Chemistry A, vol. 5, no. 28, pp. 14542-14550, 2017.

[83] Song J., Li Y., Xu W., Liu H., and Lu Y., "Inexpensive and non-fluorinated superhydrophobic concrete coating for anti-icing and anti-corrosion," Journal of colloid and interface science, vol. 541, pp. 86-92, 2019.

[84] Zailan S.N., Mahmed N., Abdullah M.M.A.B. Sandu A.V., and Shahedan N.F., "Review on characterization and mechanical performance of self-cleaning concrete," in MATEC Web of Conferences, EDP Sciences, Vol. 97, p. 01022, 2017.

[85] Xie N., Akin M., and Shi X., "Permeable concrete pavements: A review of environmental benefits and durability," Journal of cleaner production, vol. 210, pp. 1605-1621, 2019.

[86] Santos S., Da Silva P.R., and De Brito J., "Self-compacting concrete with recycled aggregates-a literature review," Journal of Building Engineering, vol. 22, pp. 349-371, 2019.

[87] Revilla-Cuesta V., Skaf M., Faleschini F., Manso J.M., and Ortega-López V., "Self-compacting concrete manufactured with recycled concrete aggregate: An overview," Journal of Cleaner Production, vol. 262, p. 121362, 2020.

[88] Nguyen T.B.T., Chatchawan R., Saengsoy W., Tangtermsirikul S. and, Sugiyama T., "Influences of different types of fly ash and confinement on performances of expansive mortars and concretes," Construction and Building Materials, vol. 209, pp. 176-186, 2019.

[89] Lokeshwari M., Bandakli B.P., Tarun S.R., Sachin P., and Kumar V., "A review on self-curing concrete," Materials Today: Proceedings, 2021.

[90] Paul S.C., van Zijl G.P., Tan M.J., and Gibson I., "A review of 3D concrete printing systems and materials properties: Current status and future research prospects," Rapid Prototyping Journal, 2018.

[91] Roussel N., "Rheological requirements for printable concretes," Cement and Concrete Research, vol. 112, pp. 76-85, 2018.

[92] Rahul A.V., Santhanam M., Meena H., and Ghani Z., "3D printable concrete: Mixture design and test methods," Cement and Concrete Composites, vol. 97, pp. 13-23, 2019.

[93] Ahmad S., Abdul Mujeebu M., and Farooqi M.A., "Energy harvesting from pavements and roadways: A comprehensive review of technologies, materials, and challenges," International Journal of Energy Research, vol. 43, no. 6, pp. 1974-2015, 2019.

[94] Gholikhani M., Roshani H., Dessouky S., and Papagiannakis A.T., "A critical review of roadway energy harvesting technologies," Applied Energy, vol. 261, p. 114388, 2020.

[95] Bazán A.M., Gálvez J.C., Reyes E., and Galé-Lamuela D., "Study of the rust penetration and circumferential stresses in reinforced concrete at early stages of an accelerated corrosion test by means of combined SEM, EDS and strain gauges," Construction and Building Materials, vol. 184, pp. 655-667, 2018.

[96] Grattan S.K., Taylor S.E., Sun T., Basheer P.A.M., and Grattan K.T., "Monitoring of corrosion in structural reinforcing bars: performance comparison using in situ fiber-optic and electric wire strain gauge systems," IEEE Sensors Journal, vol. 9, no. 11, pp. 1494-1502, 2009.

[97] Kaklauskas G., Sokolov A., Ramanauskas R., and Jakubovskis R., "Reinforcement strains in reinforced concrete tensile members recorded by strain gauges and FBG sensors: experimental and numerical analysis," Sensors, vol. 19, no. 1, p. 200, 2019.

[98] Li H.N., Li D.S., and Song G.B., "Recent applications of fiber optic sensors to health monitoring in civil engineering," Engineering structures, vol. 26, no. 11, pp. 1647-1657, 2004.

[99] Majumder M., Gangopadhyay T.K., Chakraborty A.K., Dasgupta K., and Bhattacharya D.K., "Fibre Bragg gratings in structural health monitoring-Present status and applications," Sensors and Actuators A: Physical, vol. 147, no. 1, pp. 150-164, 2008.

[100] Nguyen T.H., Venugopala T., Chen S., Sun T., Grattan K.T., Taylor S.E., Basheer P.M., and Long A.E., "Fluorescence based fibre optic pH sensor for the pH 10–13 range suitable for corrosion monitoring in concrete structures," Sensors and Actuators B: Chemical, vol. 191, pp. 498-507, 2014.

[101] Gu H., Song G., Dhonde H., Mo Y.L., and Yan S., "Concrete early-age strength monitoring using embedded piezoelectric transducers," Smart materials and structures, vol. 15, no. 6, p. 1837, 2006.

[102] Song G., Gu H., and Mo Y.L., "Smart aggregates: multi-functional sensors for concrete structures-a tutorial and a review," Smart materials and structures, vol. 17; no. 3, p. 033001, 2008.

[103] Deraemaeker A., and Dumoulin C., "Embedding ultrasonic transducers in concrete: A lifelong monitoring technology," Construction and Building Materials, vol. 194, pp. 42-50, 2019.

[104] Song G., Mo Y.L., Otero K., and Gu H., "Health monitoring and rehabilitation of a concrete structure using intelligent materials," Smart materials and structures, vol. 15, no. 2, p. 309, 2006.

[105] Muto N., Arai Y., Shin S.G., Matsubara H., Yanagida H., Sugita M., and Nakatsuji T., "Hybrid composites with self-diagnosing function for preventing fatal fracture," Composites Science and Technology, vol. 61, no. 6, pp. 875-883, 2001.

[106] Downey A., D'Alessandro A., Baquera M., García-Macías E., Rolfes D., Ubertini F., Laflamme S., and Castro-Triguero R., "Damage detection, localization and quantification in conductive smart concrete structures using a resistor mesh model," Engineering Structures, vol. 148, pp. 924-935, 2017.

[107] Downey A., D'Alessandro A., Ubertini F., and Laflamme S., "Automated crack detection in conductive smart-concrete structures using a resistor mesh model," Measurement Science and Technology, vol. 29, no. 3, p. 035107, 2018.

[108] Taheri S., "A review on five key sensors for monitoring of concrete structures," Construction and Building Materials, vol. 204, pp. 492-509, 2019.

[109] "CAPTAE et le monitoring des structures," Available online: https://lerm.fr/instruments/captae/captae/ (accessed on 3 March 2021).

[110] "TELEMAC - Leading Supplier of Geotechnical & Structural Instrumentation," Available online: https://telemac.fr/en/ (accessed on 3 March 2021).

[111] "CEMENTYS - Surveille vos infrastructures," Available online: https://cementys.com/fr/ (accessed on 3 March 2021).

[112] "itmsol instrumentation & monitoring," Available online: https://www.itmsol.fr/ (accessed on 3 March 2021).

[113] "WAKE - powerful wireless concrete temperature monitoring and reporting" Available online: https://www.wakeinc.com/ (accessed on 3 March 2021).

[114] "GIATEC - Revolutionizing Concrete Testing" Available online: https://www.giatecscientific.com/ (accessed on 3 March 2021).

[115] "LumiCON - Concrete sensors" Available online: https://lumicon.io/concrete-sensors/ (accessed on 3 March 2021).

[116] "HILTI - Concrete sensors" Available online: https://www.hilti.com/content/hilti/W1/US/en/services/tool-services/internet-of-things/concrete-sensors.html (accessed on 3 March 2021).

[117] "Sensohive - Wireless sensors and IoT solutions" Available online: https://sensohive.com/ (accessed on 3 March 2021).

[118] "Maturix" Available online: https://maturix.com/ (accessed on 3 March 2021).

[119] "Doka" Available online: https://www.doka.com/ (accessed on 3 March 2021).

[120] "Concrefy" Available online: https://www.concrefy.com/ (accessed on 3 March 2021).

[121] "360 SmartConnect" Available online: https://www.360sc.io/?lang=en (accessed on 3 March 2021).

[122] "idencia - connected concrete" Available online: http://www.idencia.com/connected-concrete (accessed on 3 March 2021).

[123] Juez J.M., Artoni R., and Cazacliu B., "Monitoring of concrete mixing evolution using image analysis," Powder technology, vol. 305, pp. 477-487, 2017.

[124] Jang W.S., and Skibniewski M.J., "A wireless network system for automated tracking of construction materials on project sites," Journal of civil engineering and management, vol. 14, no. 1, pp. 11-19, 2008.

[125] Sherafat B., Ahn C.R., Akhavian R., Behzadan A.H., Golparvar-Fard M., Kim H., Lee Y.C., Rashidi A., and Azar E.R., "Automated methods for activity recognition of construction workers and equipment: state-of-the-art review," Journal of Construction Engineering and Management, vol. 146, no. 6, p. 03120002, 2020.

[126] Tawie R., and Lee H.K., "Monitoring the strength development in concrete by EMI sensing technique," Construction and Building Materials, vol. 24, no. 9, pp. 1746-1753, 2010.

[127] Lim Y.Y., Smith S.T., and Soh C.K., "Wave propagation based monitoring of concrete curing using piezoelectric materials: Review and path forward," NDT & E International, vol. 99, pp. 50-63, 2018.

[128] Butler L.J., Gibbons N., He P., Middleton C., and Elshafie M.Z., "Evaluating the early-age behaviour of full-scale prestressed concrete beams using distributed and discrete fibre optic sensors," Construction and Building Materials, vol. 126, pp. 894-912, 2016.

[129] Norris A., Saafi M., and Romine P., "Temperature and moisture monitoring in concrete structures using embedded nanotechnology/microelectromechanical systems (MEMS) sensors," Construction and building Materials, vol. 22, no. 2, pp. 111-120, 2008.

[130] Ergen E., Akinci B., and Sacks R., "Tracking and locating components in a precast storage yard utilizing radio frequency identification technology and GPS," Automation in construction, vol. 16, no. 3, pp. 354-367, 2007.

[131] Kim M.K., Wang Q., Park J.W., Cheng J.C., Sohn H., and Chang C.C., "Automated dimensional quality assurance of full-scale precast concrete elements using laser scanning and BIM," Automation in Construction, vol. 72, pp. 102-114, 2016.

[132] Bungey J.H., and Grantham M.G., "Testing of concrete in structures," 4th Ed., Crc Press, 2006.

[133] Malešev M., Radonjanin V., and Marinković S., "Recycled concrete as aggregate for structural concrete production," Sustainability, vol. 2, no. 5, pp. 1204-1225, 2010.

[134] Rangel C.S., Toledo Filho R.D., Amario M., Pepe M., de Castro Polisseni G., and de Andrade G.P., "Generalized quality control parameter for heterogenous recycled concrete aggregates: A pilot scale case study," Journal of Cleaner Production, vol. 208, pp. 589-601, 2019.

[135] Hoła J., Bień J., and Schabowicz K., "Non-destructive and semi-destructive diagnostics of concrete structures in assessment of their durability," Bulletin of the Polish Academy of Sciences, Technical Sciences, vol. 63, no. 1, pp. 87-96, 2015.

[136] No T.C.S., "Guidebook on non-destructive testing of concrete structures," Training Course Series, 2003.

[137] Malhotra V.M., and Carino N.J., "Handbook on nondestructive testing of concrete," 2nd Ed., CRC press, London, 2003.

[138] Verma S.K., Bhadauria S.S., and Akhtar S., "Review of nondestructive testing methods for condition monitoring of concrete structures," Journal of construction engineering, vol. 2013, no. 2008, pp. 1-11, 2013.

[139] Kim H., Lee J., Ahn E., Cho S., Shin M., and Sim S.H., "Concrete crack identification using a UAV incorporating hybrid image processing," Sensors, vol. 17, no. 9, p. 2052, 2017.

[140] Khaloo A., Lattanzi D., Jachimowicz A., and Devaney C., "Utilizing UAV and 3D computer vision for visual inspection of a large gravity dam," Frontiers in Built Environment, vol. 4, p. 31, 20018.

[141] Garnier V., Piwakowski B., Abraham O., Villain G., Payan C., and Chaix J.F., "Acoustic techniques for concrete evaluation: Improvements, comparisons and consistency," Construction and Building Materials, vol. 43, pp. 598-613, 213.

[142] Miller G., Gaydecki P., Quek S., Fernandes B.T., and Zaid M.A., "Detection and imaging of surface corrosion on steel reinforcing bars using a phase-sensitive inductive sensor intended for use with concrete," NDT & E International, vol. 36; no. 1, pp. 19-26, 2003.

[143] Maierhofer C., "Nondestructive evaluation of concrete infrastructure with ground penetrating radar," Journal of materials in civil engineering, vol. 15, no. 3, pp. 287-297, 2003.

[144] Azarsa P., and Gupta R., "Electrical resistivity of concrete for durability evaluation: a review," Advances in Materials Science and Engineering, 2017.

[145] Balázs G.L., Lublóy É., and Földes T., "Evaluation of concrete elements with X-ray computed tomography" Journal of Materials in Civil Engineering, vol. 30, no. 9, p. 06018010, 2018.

[146] Zhang P., Wittmann F.H., Lura P., Müller H.S., Han S., and Zhao T., "Application of neutron imaging to investigate fundamental aspects of durability of cement-based materials: A review," Cement and Concrete Research, vol. 108, pp. 152-166, 2018.

[147] Mizoguchi T., Koda Y., Iwaki I., Wakabayashi H., Kobayashi Y., Shirai K., Hara Y., and Lee H.S., "Quantitative scaling evaluation of concrete structures based on terrestrial laser scanning," Automation in construction, vol. 35, pp. 263-274, 2013.

[148] Mukupa W., Roberts G.W., Hancock C.M., and Al-Manasir K., "A review of the use of terrestrial laser scanning application for change detection and deformation monitoring of structures," Survey review, vol. 49, no. 353, pp. 99-116, 2016.

[149] Titman D.J., "Applications of thermography in non-destructive testing of structures," NDT & e International, vol. 34, no. 2, pp. 149-154, 2001.

[150] Carino N.J., "The maturity method: theory and application. Cement, concrete and aggregates," vol. 6, no. 2, pp. 61-73, 1984.

[151] Lantsoght E.O., van der Veen C., de Boer A., and Hordijk D.A., "State-of-the-art on load testing of concrete bridges," Engineering Structures, vol. 150, pp. 231-241, 2017.

[152] Zhang J., Tian G.Y., Marindra A.M., Sunny A.I., and Zhao A.B., "A review of passive RFID tag antenna-based sensors and systems for structural health monitoring applications," Sensors, vol. 17, no. 2, p. 265, 2017.

[153] López-Higuera J.M., Cobo L.R., Incera A.Q., and Cobo A., "Fiber optic sensors in structural health monitoring," Journal of lightwave technology, vol. 29, no. 4, pp. 587-608, 2011.

[154] Lynch J.P., and Loh K.J., "A summary review of wireless sensors and sensor networks for structural health monitoring," Shock and Vibration Digest, vol. 38, no. 2, pp. 91-130, 2006.

[155] Quinn W., Angove P., Buckley J., Barrett J., and Kelly G., "Design and performance analysis of an embedded wireless sensor for monitoring concrete curing and structural health," Journal of Civil Structural Health Monitoring, vol. 1, no. 1, pp. 47-59, 2011.

[156] Ceriotti M., Mottola L., Picco G.P., Murphy A.L., Guna S., Corra M., Pozzi M., Zonta D., and Zanon P., "Monitoring heritage buildings with wireless sensor networks: The Torre Aquila deployment," in 2009 International Conference on Information Processing in Sensor Networks, IEEE, pp. 277-288, 2009 April.

[157] Noel A.B., Abdaoui A., Elfouly T., Ahmed M.H., Badawy A., and Shehata M.S., "Structural health monitoring using wireless sensor networks: A comprehensive survey," IEEE Communications Surveys & Tutorials, vol. 19, no. 3, pp. 1403-1423, 2017.

[158] Bhuiyan M.Z.A., Wu J., Wang G., Cao J., Jiang W., and Atiquzzaman M., "Towards cyber-physical systems design for structural health monitoring: Hurdles and opportunities," ACM Transactions on Cyber-Physical Systems, vol. 1, no. 4, pp. 1-26, 2017.

[159] Abdulkarem M., Samsudin K., Rokhani F.Z., and A Rasid M.F., "Wireless sensor network for structural health monitoring: A contemporary review of technologies, challenges, and future direction," Structural Health Monitoring, vol. 19, no. 3, pp. 693-735, 2020.

[160] Sethi P., and Sarangi S.R., "Internet of things: architectures, protocols, and applications," Journal of Electrical and Computer Engineering, vol. 2017, 2017.

[161] Al-Sarawi S., Anbar M., Alieyan K., and Alzubaidi M., "Internet of Things (IoT) communication protocols," in 2017 8th International conference on information technology (ICIT), IEEE, pp. 685-690, 2017 May.

[162] Montori F., Bedogni L., Di Felice M., and Bononi L., "Machine-to-machine wireless communication technologies for the Internet of Things: Taxonomy, comparison and open issues," Pervasive and Mobile Computing, vol. 50, pp. 56-81, 2018.

[163] NFC Forum, "NFC Data Exchange Format (NDEF)," Technical specification, 2006.

[164] Coskun V., Ozdenizci B., and Ok K., "A survey on near field communication (NFC) technology," Wireless personal communications, vol. 71, no. 3, pp. 2259-2294, 2012.

[165] International Organization for Standardization/International Electrotechnical Commission, "Identification cards - Contactless integrated circuit cards - Proximity cards," ISO/IEC 14443, 2018.

[166] International Organization for Standardization/International Electrotechnical Commission / European Computer Manufacturers Association, "Information technology - Telecommunications and information exchange between systems - Near Field Communication - Interface and Protocol-1 (NFCIP-1)," ISO/IEC 18092 / ECMA 340, 2011.

[167] International Organization for Standardization/International Electrotechnical Commission / European Computer Manufacturers Association, "Information technology - Telecommunications and information exchange between systems - Near Field Communication - Interface and Protocol-2 (NFCIP-2)," ISO/IEC 21481 / ECMA 352, 2011.

[168] International Organization for Standardization/International Electrotechnical Commission, "Information technology - Radio frequency identification for item management," ISO/IEC 18000, 2015.

[169] "RuBee – Visible Assets, Inc.," Available online: https://www.ru-bee.com/ (accessed on 3 March 2021).

[170] Wyld D.C., "RuBee: applying low-frequency technology for retail and medical uses," Management Research News, 2008.

[171] Dantas S., Barreto A.N., Aguayo L., Braga A.J., Silva L.S., and Garcia L.G.U., "Simulation of IEEE 1902.1 (RuBee) protocol for communication with buried assets," in 2017 IEEE 28th Annual International Symposium on Personal, Indoor, and Mobile Radio Communications (PIMRC), IEEE, pp. 1-6, 2017 October.

[172] IEEE 1902.1 Working Group, "IEEE Standard for long wavelength wireless network protocol", IEEE Standard 1902.1, 2009.

[173] Finkenzeller K., "RFID handbook: fundamentals and applications in contactless smart cards, radio frequency identification and near-field communication," 3rd Ed., John wiley & sons, 2010.

[174] Lee J.S., Su Y.W., and Shen C.C., "A comparative study of wireless protocols: Bluetooth, UWB, ZigBee, and Wi-Fi," in IECON 2007-33rd Annual Conference of the IEEE Industrial Electronics Society, IEEE, pp. 46-51, 2007 November.

[175] Ghasempour Y., da Silva C.R., Cordeiro C., and Knightly E.W., "IEEE 802.11 ay: Next-generation 60 GHz communication for 100 Gb/s Wi-Fi," IEEE Communications Magazine, vol. 55, no. 12, pp. 186-192, 2017.

[176] Khorov E., Kiryanov A., Lyakhov A., and Bianchi G., "A tutorial on IEEE 802.11 ax high efficiency WLANs," IEEE Communications Surveys & Tutorials, vol. 21, no. 1, pp. 197-216, 2018.

[177] IEEE 802.11 Working Group, "IEEE Standard for information technology - Telecommunications and information exchange between systems - Local and metropolitan area networks - Specific requirements - Part 11: Wireless LAN Medium Access Control (MAC) and Physical layer (PHY) specifications", IEEE Standard 802.11, 2007.

[178] Bisdikian C., "An overview of the Bluetooth wireless technology," IEEE Communications magazine, vol. 39, no. 12, pp. 86-94, 2001.

[179] Gomez C., Oller J., and Paradells J., "Overview and evaluation of bluetooth low energy: An emerging low-power wireless technology," Sensors, vol. 12, no. 9, pp. 11734-11753, 2012.

[180] Darroudi S.M., and Gomez C., "Bluetooth low energy mesh networks: A survey," Sensors, vol. 17, no. 7, p. 1467, 2017.

[181] IEEE 802.15.1 Working Group, "IEEE Standard for information technology - Telecommunications and information exchange between systems - Local and metropolitan area networks - Specific requirements - Part 15.1: Wireless Medium Access Control (MAC) and Physical layer (PHY) specifications for Wireless Personal Area Networks (WPANs)", IEEE Standard 802.15.1, 2005.

[182] Oppermann I., Hämäläinen M., and Iinatti J., "UWB: theory and applications," John Wiley & Sons, 2005.

[183] Win M.Z., Dardari D., Molisch A.F., Wiesbeck W., and Jinyun Zhang W., "History and applications of UWB," Proceedings of the IEEE, vol. 97, no. 2, pp. 198-204, 2009.

[184] IEEE 802.15.3 Working Group, "IEEE Standard for information technology - Telecommunications and information exchange between systems - Local and metropolitan area networks - Specific requirements - Part 15.3: Wireless Medium Access Control (MAC) and Physical layer (PHY) specifications for high rate Wireless Personal Area Networks (WPAN)", IEEE Standard 802.15.3, 2003.

[185] IEEE 802.15.3 Working Group, "IEEE Standard for high data-rate wireless multi-media networks", IEEE Standard 802.15.3, 2016.

[186] Baronti P., Pillai P., Chook V.W., Chessa S., Gotta A., and Hu Y.F., "Wireless sensor networks: A survey on the state of the art and the 802.15. 4 and ZigBee standards," Computer communications, vol. 30, no. 7, pp. 1655-1695, 2007.

[187] Salman N., Rasool I., and Kemp A.H., "Overview of the IEEE 802.15. 4 standards family for low rate wireless personal area networks," in 2010 7th International Symposium on Wireless Communication Systems, IEEE, pp. 701-705), 2010 September.

[188] IEEE 802.15.4 Working Group, "IEEE Standard for information technology - Telecommunications and information exchange between systems - Local and metropolitan area networks - Specific requirements - Part 15.4: Wireless Medium Access Control (MAC) and Physical layer (PHY) specifications for low-rate Wireless Personal Area Networks (WPANs)", IEEE Standard 802.15.4, 2006.

[189] IEEE 802.15.4 Working Group, "IEEE Standard for local and metropolitan area networks - Part 15.4: Low-rate Wireless Personal Area Networks (LR-WPANs)", IEEE Standard 802.15.4, 2011.

[190] Kwak K.S., Ullah S., and Ullah N., "An overview of IEEE 802.15.6 standard," in 2010 3rd International Symposium on Applied Sciences in Biomedical and Communication Technologies (ISABEL 2010), IEEE, pp. 1-6, 2010 November.

[191] Arefin M.T., Ali M.H., and Haque A.F., "Wireless body area network: An overview and various applications," Journal of Computer and Communications, vol. 5, no. 7, pp. 53-64, 2017.

[192] IEEE 802.15.6 Working Group, "IEEE Standard for information technology - Telecommunications and information exchange between systems - Local and metropolitan area networks - Specific requirements - Part 15-6: Wireless body area network", IEEE Standard 802.15.6, 2017.

[193] IEEE 802.15.6 Working Group, "IEEE Standard for local and metropolitan area networks - Part 15.6: Wireless Body Area Networks", IEEE Standard 802.15.6, 2012.

[194] Ghosh A., Wolter D.R., Andrews J.G., and Chen R., "Broadband wireless access with WiMax/802.16: current performance benchmarks and future potential," IEEE communications magazine, vol. 43, no. 2, pp. 129-136, 2005.

[195] Ahson S.A., and Ilyas M., "WiMAX: Standards and security," CRC press, 2018.

[196] IEEE 802.16 Working Group, "IEEE Standard for local and metropolitan area networks - Part 16: Air interface for broadband wireless access systems", IEEE Standard 802.16, 2009.

[197] IEEE 802.16 Working Group, "IEEE Standard for air interface for broadband wireless access systems", IEEE Standard 802.16, 2017.

[198] Bolton W., Xiao Y., and Guizani M., "IEEE 802.20: mobile broadband wireless access," IEEE Wireless Communications, vol. 14, no. 1, pp. 84-95, 2007.

[199] Greenspan A., Klerer M., Tomcik J., Canchi R., and Wilson J., "IEEE 802.20: Mobile broadband wireless access for the twenty-first century," IEEE Communications Magazine, vol. 46, no. 7, pp. 56-63, 2008.

[200] IEEE 802.20 Working Group, "IEEE Standard for local and metropolitan area networks - Part 20: Air interface for mobile broadband wireless access systems supporting vehicular mobility - Physical and Media Access Control layer specification", IEEE Standard 802.20, 2009.

[201] Stevenson C.R., Chouinard G., Lei Z., Hu W., Shellhammer S.J., and Caldwell W., "IEEE 802.22: The first cognitive radio wireless regional area network standard," IEEE communications magazine, vol. 47, no. 1, pp. 130-138, 2009.

[202] IEEE 802.22 Working Group, "IEEE Standard for information technology - Telecommunications and information exchange between systems Wireless Regional Area Networks (WRAN) - Specific requirements - Part 22: Cognitive wireless RAN Medium Access Control (MAC) and Physical layer (PHY) specifications: policies and procedures for operation in the TV bands", IEEE Standard 802.22, 20011.

[203] Raza U., Kulkarni P., and Sooriyabandara M., "Low power wide area networks: An overview," IEEE Communications Surveys & Tutorials, vol. 19, no. 2, pp. 855-873, 2017.

[204] Ayoub W., Samhat A.E., Nouvel F., Mroue M., and Prévotet J.C., "Internet of mobile things: Overview of lorawan, dash7, and nb-iot in lpwans standards and supported mobility," IEEE Communications Surveys & Tutorials, vol. 21, no. 2, pp. 1561-1581, 2018.

[205] Ikpehai A., Adebisi B., Rabie K.M., Anoh K., Ande R.E., Hammoudeh M., Gacanin H., and Mbanaso U.M., "Low-power wide area network technologies for internet-of-things: A comparative review," IEEE Internet of Things Journal, vol. 6, no. 2, pp. 2225-2240, 2018.

[206] Mekki K., Bajic E., Chaxel F., and Meyer F., "A comparative study of LPWAN technologies for large-scale IoT deployment," ICT express, vol. 5, no. 1, pp. 1-7, 2019.

[207] Weyn M., Ergeerts G., Berkvens R., Wojciechowski B., and Tabakov Y., "DASH7 alliance protocol 1.0: Low-power, mid-range sensor and actuator communication," in 2015 IEEE Conference on Standards for Communications and Networking (CSCN), IEEE, pp. 54-59, 2015 October.

[208] Wixted A.J., Kinnaird P., Larijani H., Tait A., Ahmadinia A., and Strachan N., "Evaluation of LoRa and LoRaWAN for wireless sensor networks," in 2016 IEEE SENSORS, IEEE, pp. 1-3, 2016 October.

[209] Adelantado F., Vilajosana X., Tuset-Peiro P., Martinez B., Melia-Segui J., and Watteyne T., "Understanding the limits of LoRaWAN," IEEE Communications magazine, vol. 55, no. 9, pp. 34-40, 2017.

[210] De Carvalho Silva J., Rodrigues J.J., Alberti A.M., Solic P., and Aquino A.L., "LoRaWAN—A low power WAN protocol for Internet of Things: A review and opportunities," in 2017 2nd International Multidisciplinary Conference on Computer and Energy Science (SpliTech), IEEE, pp. 1-6, 2017 July.

[211] Lavric A., and Popa V., "Internet of things and LoRa™ low-power wide-area networks: a survey," in 2017 International Symposium on Signals, Circuits and Systems (ISSCS), IEEE, pp. 1-5, 2017 July.

[212] Haxhibeqiri J., De Poorter E., Moerman I., and Hoebeke J., "A survey of LoRaWAN for IoT: From technology to application," Sensors, vol. 18, no. 11, p. 3995, 2018.

[213] LoRa Alliance Technical Committee, "LoRaWAN 1.0.3 specification", 2018.

[214] LoRa Alliance Technical Committee Regional Parameters Workgroup, "LoRaWAN 1.0.3 regional parameters", 2018.

[215] Lavric A., Petrariu A.I., and Popa V., "Long range sigfox communication protocol scalability analysis under large-scale, high-density conditions," IEEE Access, vol. 7, pp. 35816-35825, 2019.

[216] "SigFox," Available online: https://www.sigfox.com/en/ (accessed on 3 March 2021).

[217] Agiwal M., Roy A., and Saxena N., "Next generation 5G wireless networks: A comprehensive survey," IEEE Communications Surveys & Tutorials, vol. 18, no. 3, pp. 1617-1655, 2016.

[218] Shafi M., Molisch A.F., Smith P.J., Haustein T., Zhu P., De Silva P., Tufvesson F., Benjebbour A., and Wunder G., "5G: A tutorial overview of standards, trials, challenges, deployment, and practice," IEEE journal on selected areas in communications, vol. 35, no. 6, pp. 1201-1221, 2017.

[219] Gandotra P., Jha R.K., and Jain S., "Green communication in next generation cellular networks: A survey," IEEE Access, vol. 5, pp. 11727-11758, 2017.

[220] Liberg O., Sundberg M., Wang E., Bergman J., and Sachs J., "Cellular Internet of things: technologies, standards, and performance," Academic Press, 2017.

[221] Chettri L., and Bera R., "A comprehensive survey on Internet of Things (IoT) toward 5G wireless systems," IEEE Internet of Things Journal, vol. 7, no. 1, pp. 16-32, 2019.

[222] Guo F., Yu F.R., Zhang H., Li X., Ji H., and Leung V.C.M, "Enabling Massive IoT Toward 6G: A Comprehensive Survey," IEEE Internet of Things Journal, 2021.

[223] Evans J.V., "Satellite systems for personal communications," Proceedings of the IEEE, vol. 86, no. 7, pp. 1325-1341, 1998.

[224] De Sanctis M., Cianca E., Araniti G., Bisio I., and Prasad R., "Satellite communications supporting internet of remote things," IEEE Internet of Things Journal, vol. 3, no. 1, pp. 113-123, 2015.

[225] Qu Z., Zhang G., Cao H., and Xie J., "LEO satellite constellation for Internet of Things," IEEE Access, vol. 5, pp. 18391-18401, 2017.

[226] Sohraby K., Minoli D., Occhiogrosso B., and Wang W., "A review of wireless and satellite-based m2m/iot services in support of smart grids," Mobile Networks and Applications, vol. 23, no. 4, pp. 881-895, 2018.

[227] Ferrer T., Céspedes S., and Becerra A., "Review and evaluation of MAC protocols for satellite IoT systems using nanosatellites," Sensors, vol. 19, no. 8, p. 1947, 2019.

[228] Liu V., Parks A., Talla V., Gollakota S., Wetherall D., and Smith J.R., "Ambient backscatter: Wireless communication out of thin air," ACM SIGCOMM Computer Communication Review, vol. 43, no. 4, pp. 39-50, 2013.

[229] Parks A.N., Liu A., Gollakota S., and Smith J.R., "Turbocharging ambient backscatter communication," ACM SIGCOMM Computer Communication Review, vol. 44, no. 4, pp. 619-630, 2014.

[230] Talla V., Hessar M., Kellogg B., Najafi A., Smith J.R., and Gollakota S., "Lora backscatter: Enabling the vision of ubiquitous connectivity," Proceedings of the ACM on Interactive, Mobile, Wearable and Ubiquitous Technologies, vol. 1, no. 3, pp. 1-24, 2017.

[231] Peng Y., Shangguan L., Hu Y., Qian Y., Lin X., Chen X., Fang D., and Jamieson K., "PLoRa: A passive long-range data network from ambient LoRa transmissions," in Proceedings of the 2018 Conference of the ACM Special Interest Group on Data Communication, pp. 147-160, 2018 August.

[232] Van Huynh N., Hoang D.T., Lu X., Niyato D., Wang P., and Kim D.I., "Ambient backscatter communications: A contemporary survey," IEEE Communications Surveys & Tutorials, vol. 20, no. 4, pp. 2889-2922, 2018.

[233] Xu C., Yang L., and Zhang P., "Practical backscatter communication systems for battery-free Internet of Things: A tutorial and survey of recent research," IEEE Signal Processing Magazine, vol. 35, no. 5, pp. 16-27, 2018.

[234] Rajagopal S., Roberts R.D., and Lim S.K., "IEEE 802.15. 7 visible light communication: modulation schemes and dimming support," IEEE Communications Magazine, vol. 50, no. 3, pp. 72-82, 2012.

[235] Sarbazi E., and Uysal M., "PHY layer performance evaluation of the IEEE 802.15.7 visible light communication standard," in 2013 2nd International workshop on optical wireless communications (IWOW), IEEE, pp. 35-39, 2013 October.

[236] IEEE 802.15.7 Working Group, "IEEE Standard for information technology - Telecommunications and information exchange between systems - Local and metropolitan area networks - Specific requirements - Part 15.7: Short-range wireless optical communication using visible light ", IEEE Standard 802.15.7, 2011.

[237] Pathak P.H., Feng X., Hu P., and Mohapatra P., "Visible light communication, networking, and sensing: A survey, potential and challenges," IEEE communications surveys & tutorials, vol. 17, no. 4, pp. 2047-2077, 2015.

[238] Kahn J.M., and Barry J.R., "Wireless infrared communications," Proceedings of the IEEE, vol. 85, no. 2, pp. 265-298, 1997.

[239] Majumdar A.K., and Ricklin J.C. "Free-space laser communications: principles and advances," Vol. 2, Springer Science & Business Media, 2010.

[240] Hemmati H., "Near-earth laser communications," Vol. 1, 2nd Ed., CRC press, 2020.

[241] Kailaswar S., Zheng R., Kovitz J., Phung Q., Wang H., Ding Z., and Song G., "ConcreteCom: A new communication paradigm for building structural health monitoring," in Proceedings of the Fourth ACM Workshop on Embedded Sensing Systems for Energy-Efficiency in Buildings, pp. 131-137, 2012 November.

[242] Siu S., Ji Q., Wu W., Song G., and Ding Z., "Stress wave communication in concrete: I. Characterization of a smart aggregate based concrete channel," Smart materials and structures, vol. 23, no. 12, p. 125030, 2014.

[243] Siu S., Qing J., Wang K., Song G., and Ding Z., "Stress wave communication in concrete: II. Evaluation of low voltage concrete stress wave communications utilizing spectrally efficient modulation schemes with PZT transducers," Smart materials and structures, vol. 23, no. 12, p. 125031, 2014.

[244] Wu A., He S., Ren Y., Wang N., Ho S.C.M., and Song G., "Design of a new stress wave-based pulse position modulation (PPM) communication system with piezoceramic transducers," Sensors, vol. 19, no. 3, p. 558, 2019.

[245] Welle R.P., "Ultrasonic data communication system," U.S. Patent No. 5,982,297. 9 November 1999.

[246] Welle R.P., "Ultrasonic power communication system," U.S. Patent No. 6,037,704. 14 March 2000.

[247] Welle R.P., "Ultrasonic power sensory system," U.S. Patent No. 6,127,942. 3 October 2000.

[248] Saulnier G., Scarton H., Shoudy D., Das P., and Gavens A., "Ultrasonic Through-Wall Communication (UTWC) System," U.S. Patent Application No. 12/443,878, 2010.

[249] Shams K.M., Ali M., and Miah A.M., "Characteristics of an embedded microstrip patch antenna for wireless infrastructure health monitoring," in 2006 IEEE Antennas and Propagation Society International Symposium, IEEE, pp. 3643-3646, 2006 July.

[250] Rad M.F., and Shafai L., "Embedded microstrip patch antenna for structural health monitoring applications," in 2008 IEEE Antennas and Propagation Society International Symposium, IEEE, pp. 1-4, 2008 July.

[251] Jin X., and Ali M., "Reflection and transmission properties of embedded dipoles and PIFAs inside concrete at 915 MHz," in 2009 IEEE Antennas and Propagation Society International Symposium, IEEE, pp. 1-4, 2009 June.

[252] Jin X., and Ali M., "Embedded antennas in dry and saturated concrete for application in wireless sensors," Progress in electromagnetics research, vol. 102, pp. 197-211, 2010.

[253] Jeong S.H., and Son H.W., "UHF RFID tag antenna for embedded use in a concrete floor," IEEE Antennas and Wireless Propagation Letters, vol. 10, pp. 1158-1161, 2011.

[254] Salama R., and Kharkovsky S., "An embeddable microwave patch antenna module for civil engineering applications," in 2013 IEEE International Instrumentation and Measurement Technology Conference (I2MTC), IEEE, pp. 27-30, 2013 May.

[255] Castorina G., Di Donato L., Morabito A.F., Isernia T., and Sorbello G., "Analysis and design of a concrete embedded antenna for wireless monitoring applications [antenna applications corner]," IEEE Antennas and Propagation Magazine, vol. 58, no. 6, pp. 76-93, 2016.

[256] Rault T., Bouabdallah A., and Challal Y., "Energy efficiency in wireless sensor networks: A top-down survey," Computer Networks, vol. 67, pp. 104-122, 2014.

[257] Park G., Rosing T., Todd M.D., Farrar C.R., and Hodgkiss W., "Energy harvesting for structural health monitoring sensor networks," Journal of Infrastructure Systems, vol. 14, no. 1, pp. 64-79, 2008.

[258] Seah W.K., Eu Z.A., and Tan H.P., "Wireless sensor networks powered by ambient energy harvesting (WSN-HEAP)-Survey and challenges," in 2009 1st International Conference on Wireless Communication, Vehicular Technology, Information Theory and Aerospace & Electronic Systems Technology, IEEE, pp. 1-5, 2009 May.

[259] Priya S., and Inman D.J., "Energy harvesting technologies," New York: Springer, 2009.

[260] Sudevalayam S., and Kulkarni P., "Energy harvesting sensor nodes: Survey and implications," IEEE Communications Surveys & Tutorials, vol. 13, no. 3, pp. 443-461, 2010.

[261] Kausar A.Z., Reza A.W., Saleh M.U., and Ramiah H., "Energizing wireless sensor networks by energy harvesting systems: Scopes, challenges and approaches," Renewable and Sustainable Energy Reviews, vol. 38, pp. 973-989, 2014.

[262] Akhtar F., and Rehmani M.H., "Energy replenishment using renewable and traditional energy resources for sustainable wireless sensor networks: A review," Renewable and Sustainable Energy Reviews, vol. 45, pp. 769-784, 2015.

[263] Shaikh F.K., and Zeadally S., "Energy harvesting in wireless sensor networks: A comprehensive review," Renewable and Sustainable Energy Reviews, vol. 55, pp. 1041-1054, 2016.

[264] Adu-Manu K.S., Adam N., Tapparello C., Ayatollahi H., and Heinzelman W., "Energy-Harvesting Wireless Sensor Networks (EH-WSNs) A Review," ACM Transactions on Sensor Networks (TOSN), vol. 14, no. 2, pp .1-50, 2018.

[265] Prauzek M., Konecny J., Borova M., Janosova K., Hlavica J., and Musilek P., "Energy harvesting sources, storage devices and system topologies for environmental wireless sensor networks: A review," Sensors, vol. 18, no. 8, p. 2446, 2018.

[266] Huang J., Zhou Y., Ning Z., and Gharavi H., "Wireless power transfer and energy harvesting: Current status and future prospects," IEEE wireless communications, vol. 26, no. 4, pp. 163-169, 2019.

[267] Peruzzi G., and Pozzebon A., "A review of energy harvesting techniques for Low Power Wide Area Networks (LPWANs)," Energies, vol. 13, no. 13, p. 3433, 2020.

[268] Chalasani S., and Conrad J.M., "A survey of energy harvesting sources for embedded systems," in IEEE SoutheastCon 2008, IEEE, pp. 442-447, 2008 April.

[269] Gilbert J.M., and Balouchi F., "Comparison of energy harvesting systems for wireless sensor networks," International Journal of automation and computing, vol. 5, no. 4, pp. 334-347, 2008.

[270] Yildiz F., "Potential Ambient Energy-Harvesting Sources and Techniques," Journal of technology Studies, vol. 35, no. 1, pp. 40-48, 2009.

[271] Moghe R., Yang Y., Lambert F., and Divan D., "A scoping study of electric and magnetic field energy harvesting for wireless sensor networks in power system applications," in 2009 IEEE Energy Conversion Congress and Exposition, IEEE, pp. 3550-3557, 2009 September.

[272] Vullers R.J., Van Schaijk R., Visser H.J., Penders J., and Van Hoof C., "Energy harvesting for autonomous wireless sensor networks," IEEE Solid-State Circuits Magazine, vol. 2, no. 2, pp. 29-38, 2010.

[273] Matiko J.W., Grabham N.J., Beeby S.P., and Tudor M.J., "Review of the application of energy harvesting in buildings," Measurement Science and Technology, vol. 25, no. 1, p. 012002, 2013.

[274] Zhou G., Huang L., Li W., and Zhu Z., "Harvesting ambient environmental energy for wireless sensor networks: a survey," Journal of Sensors, vol. 2014, 2014.

[275] Cao S., and Li J., "A survey on ambient energy sources and harvesting methods for structural health monitoring applications," Advances in Mechanical Engineering, vol. 9, no. 4, p. 1687814017696210, 2017.

[276] Singh J., Kaur R., and Singh D., "Energy harvesting in wireless sensor networks: A taxonomic survey," International Journal of Energy Research, vol. 45, no. 1, pp. 118-140, 2021.

[277] Georgiadis A., Collado A., and Tentzeris M.M., "Energy Harvesting: Technologies, Systems, and Challenges," Cambridge University Press, 2021.

[278] Sampaio P.G.V., and González M.O.A., "Photovoltaic solar energy: Conceptual framework," Renewable and Sustainable Energy Reviews, vol. 74, pp. 590-601, 2017.

[279] Nayak P.K., Mahesh S., Snaith H.J., and Cahen D., "Photovoltaic solar cell technologies: analysing the state of the art," Nature Reviews Materials, vol. 4, no. 4, pp. 269-285, 2019.

[280] "Best research cell efficiencies, National Renewable Energy Laboratory (NREL), United States Department of Energy," Available online: https://www.nrel.gov/pv/assets/pdfs/best-research-cell-efficiencies.20190802.pdf (accessed on 3 March 2021).

[281] Polonelli T., Brunelli D., Guermandi M., and Benini, L, "An accurate low-cost Crackmeter with LoRaWAN communication and energy harvesting capability," in 2018 IEEE 23rd International Conference on Emerging Technologies and Factory Automation (ETFA), IEEE, vol. 1, pp. 671-676, 2018 September.

[282] Kobayashi M., Matsumoto T., and Beering J., "Development of Water Temperature Measuring Application Based on LoRa/LoRWAN," in 2019 4th International Conference on Information Technology (InCIT), IEEE, pp. 254-258, 2019 October.

[283] Rossi M., and Tosato P., "Energy neutral design of an IoT system for pollution monitoring," in 2017 IEEE Workshop on Environmental, Energy, and Structural Monitoring Systems (EESMS), IEEE, pp. 1-6, 2017 July.

[284] Mabon M., Gautier M., Vrigneau B., Le Gentil M., and Berder O., "The smaller the better: Designing solar energy harvesting sensor nodes for long-range monitoring," Wireless Communications and Mobile Computing, vol. 2019, 2019.

[285] Wu F., Redouté J.M., and Yuce M.R., "We-safe: A self-powered wearable iot sensor network for safety applications based on lora," IEEE Access, vol. 6, pp. 40846-40853, 2018.

[286] Nikolov D.N., Ganev B.T., and Rusev R.P., "Energy harvesting power supply for an autonomous environmental sensor node," in 2019 IEEE XXVIII International Scientific Conference Electronics (ET), IEEE, pp. 1-4, 2019 September.

[287] Petrariu A.I., Lavric A., and Coca E., "Renewable energy powered LoRa-based IoT multi sensor node," in 2019 IEEE 25th International Symposium for Design and Technology in Electronic Packaging (SIITME), IEEE, pp. 94-97, 2019 October.

[288] Boccadoro P., Montaruli B., and Grieco L.A., "Quakesense, a LoRa-compliant earthquake monitoring open system," in 2019 IEEE/ACM 23rd International Symposium on Distributed Simulation and Real Time Applications (DS-RT), IEEE, pp. 1-8, 2019 October.

[289] Matthews V.O., Ajala A.O., Atayero A.A., and Popoola S.I., "Solar photovoltaic automobile recognition system for smart-green access control using RFID and LoRa LPWAN technologies," Journal of Engineering and Applied Sciences, vol. 12, no. 4, pp. 913-919, 2017.

[290] Meli M., Brütsch M., Stajic S., Böbel M., Lorenz D., Hegetschweiler L., Karanassos D., and Kouzinopoulos C., "Low Light Energy Autonomous LoRaWAN Node," in 2020 IEEE 5th International Symposium on Smart and Wireless Systems within the Conferences on Intelligent Data Acquisition and Advanced Computing Systems (IDAACS-SWS), IEEE, pp. 1-6, 2020 September.

[291] Sherazi H.H.R., Piro G., Grieco L.A., and Boggia G., "When renewable energy meets LoRa: A feasibility analysis on cable-less deployments," IEEE Internet of Things Journal, vol. 5, no. 6, pp. 5097-5108, 2018.

[292] Lin H., Chen Z., and Wang, L., "Offloading for edge computing in low power wide area networks with energy harvesting," IEEE Access, vol. 7, pp. 78919-78929, 2019.

[293] Di Gennaro P., Lofú D., Vitanio D., Tedeschi P., and Boccadoro P., "WaterS: A Sigfox-compliant prototype for water monitoring," Internet Technology Letters, vol. 2, no. 1, p. e74, 2019.

[294] Joris L., Dupont F., Laurent P., Bellier P., Stoukatch S., and Redouté J.M., "An autonomous sigfox wireless sensor node for environmental monitoring," IEEE Sensors Letters, vol. 3, no. 7, pp. 01-04, 2019.

[295] Meli M., Stajic S., and Wick S., "Powering Sigfox nodes with harvested energy," in Embedded World Conference 2020, WEKA, 2020 Februar.

[296] Haridas A., Rao V.S., Prasad R.V., and Sarkar C., "Opportunities and challenges in using energy-harvesting for NB-IoT," ACM Sigbed Review, vol. 15, no. 5, pp. 7-13, 2018.

[297] D'Elia A., Perilli L., Viola F., Roffia L., Antoniazzi F., Canegallo R., and Cinotti T.S., "A self-powered WSAN for energy efficient heat distribution," in 2016 IEEE Sensors Applications Symposium (SAS), IEEE, pp. 1-6, 2016 April.

[298] Fraternali F., Balaji B., Agarwal Y., Benini L., and Gupta R., "Pible: battery-free mote for perpetual indoor BLE applications," in Proceedings of the 5th Conference on Systems for Built Environments, pp. 168-171, 2018 November.

[299] Jeon K.E., She J., Soonsawad P., and Ng P.C., "Ble beacons for internet of things applications: Survey, challenges, and opportunities," IEEE Internet of Things Journal, vol. 5, no. 2, pp. 811-828, 2018.

[300] Sharma H., Haque A., and Jaffery Z.A., "Solar energy harvesting wireless sensor network nodes: A survey," Journal of Renewable and Sustainable Energy, vol. 10, no. 2, p. 023704, 2018.

[301] Kazmierski T.J., and Beeby S., "Energy harvesting systems," New York: Springer, p. 2011, 2014.

[302] Khaligh A., Zeng P., and Zheng C., "Kinetic energy harvesting using piezoelectric and electromagnetic technologies - state of the art," IEEE transactions on industrial electronics, vol. 57, no. 3, pp. 850-860, 2009.

[303] Wei C., and Jing X., "A comprehensive review on vibration energy harvesting: Modelling and realization," Renewable and Sustainable Energy Reviews, vol. 74, pp. 1-18, 2017.

[304] Khan F.U., and Qadir M.U., "State-of-the-art in vibration-based electrostatic energy harvesting," Journal of Micromechanics and Microengineering, vol. 26, no. 10, p. 103001, 2016.

[305] Liu Z., Li H., Shi B., Fan Y., Wang Z.L., and Li Z., "Wearable and implantable triboelectric nanogenerators," Advanced Functional Materials, vol. 29, no. 20, p. 1808820, 2019.

[306] Beeby S.P., Torah R.N., Tudor M.J., Glynne-Jones P., O'donnell T., Saha C.R., and Roy S., "A micro electromagnetic generator for vibration energy harvesting," Journal of Micromechanics and microengineering, vol. 17, no. 7, p. 1257, 2007.

[307] Liu H., Hou C., Lin J., Li Y., Shi Q., Chen T., Sun L., and Lee C., "A non-resonant rotational electromagnetic energy harvester for low-frequency and irregular human motion," Applied Physics Letters, vol. 113, no. 20, p. 203901, 2018.

[308] Erturk A., and Inman D.J., "Piezoelectric energy harvesting," John Wiley & Sons, 2011.

[309] Elvin N.G., Lajnef N., and Elvin A.A., "Feasibility of structural monitoring with vibration powered sensors," Smart materials and structures, vol. 15, no. 4, p. 977, 2006.

[310] Liu H., Zhong J., Lee C., Lee S.W., and Lin L., "A comprehensive review on piezoelectric energy harvesting technology: Materials, mechanisms, and applications," Applied Physics Reviews, vol. 5, no. 4, p. 041306, 2018.

[311] Safaei M., Sodano H.A., and Anton S.R., "A review of energy harvesting using piezoelectric materials: state-of-the-art a decade later (2008–2018)," Smart Materials and Structures, vol. 28, no. 11, p. 113001, 2019.

[312] Seol M.L., Jeon S.B., Han J.W., and Choi Y.K., "Ferrofluid-based triboelectric-electromagnetic hybrid generator for sensitive and sustainable vibration energy harvesting," Nano Energy, vol. 31, pp. 233-238, 2017.

[313] Wang P., Pan L., Wang J., Xu M., Dai G., Zou H., Dong K., and Wang Z.L., "An ultra-low-friction triboelectric–electromagnetic hybrid nanogenerator for rotation energy harvesting and self-powered wind speed sensor," ACS nano, vol. 12, no. 9, pp. 9433-9440, 2018.

[314] Yang H., Wang M., Deng M., Guo H., Zhang W., Yang H., Xi Y., Li X., Hu C., and Wang Z., "A full-packaged rolling triboelectric-electromagnetic hybrid nanogenerator for energy harvesting and building up self-powered wireless systems," Nano Energy, vol. 56, pp. 300-306, 2019.

[315] Jung W.S., Kang M.G., Moon H.G., Baek S.H., Yoon S.J., Wang Z.L., Kim S.W., and Kang C.Y., "High output piezo/triboelectric hybrid generator," Scientific reports, vol. 5, no. 1, pp. 1-6, 2015.

[316] Li Z., Saadatnia Z., Yang Z., and Naguib H., "A hybrid piezoelectric-triboelectric generator for low-frequency and broad-bandwidth energy harvesting," Energy conversion and management, vol. 174, pp. 188-197, 2018.

[317] Challa V.R., Prasad M.G., and Fisher F.T., "A coupled piezoelectric–electromagnetic energy harvesting technique for achieving increased power output through damping matching," Smart materials and Structures, vol. 18, no. 9, p. 095029, 2009.

[318] Tadesse Y., Zhang S., and Priya S., "Multimodal energy harvesting system: piezoelectric and electromagnetic," Journal of Intelligent Material Systems and Structures, vol. 20, no. 5, pp. 625-632, 2009.

[319] Yu H., Zhou J., Yi X., Wu H., and Wang W., "A hybrid micro vibration energy harvester with power management circuit," Microelectronic Engineering, vol. 131, pp., 36-42, 2015.

[320] Toyabur R.M., Salauddin M., Cho H., and Park J.Y., "A multimodal hybrid energy harvester based on piezoelectric-electromagnetic mechanisms for low-frequency ambient vibrations," Energy conversion and management, vol. 168, pp. 454-466, 2018.

[321] He J., Wen T., Qian S., Zhang Z., Tian Z., Zhu J., Mu J., Hou X., Geng W., Cho J., and Han J., "Triboelectric-piezoelectric-electromagnetic hybrid nanogenerator for high-efficient vibration energy harvesting and self-powered wireless monitoring system," Nano Energy, vol. 43, pp. 326-339, 2018.

[322] Orfei F., Mezzetti C.B., and Cottone F., "Vibrations powered LoRa sensor: An electromechanical energy harvester working on a real bridge," in 2016 IEEE SENSORS, IEEE, pp. 1-3, 2016 October.

[323] Rodriguez J.C., Nico V., and Punch J., "A vibration energy harvester and power management solution for battery-free operation of wireless sensor nodes," Sensors, vol. 19, no. 17, p. 3776, 2019.

[324] Carandell M., Toma D.M., Carbonell M., Gasulla M., and del Río J., "Design and development of a kinetic energy harvester device for oceanic drifter applications," in 2019 IEEE International Instrumentation and Measurement Technology Conference (I2MTC), IEEE, pp. 1-6, 2019 May.

[325] Sebald G., Guyomar D., and Agbossou A., "On thermoelectric and pyroelectric energy harvesting," Smart Materials and Structures, vol. 18, no. 12, p. 125006, 2009.

[326] Kishore R.A., and Priya S., "A review on low-grade thermal energy harvesting: materials, methods and devices," Materials, vol. 11, no. 8, p. 1433, 2018.

[327] Yang Y., Wang S., Zhang Y., and Wang Z.L., "Pyroelectric nanogenerators for driving wireless sensors," Nano letters, vol. 12, no. 12, pp., 6408-6413, 2012.

[328] Bowen C.R., Taylor J., LeBoulbar E., Zabek D., Chauhan A., and Vaish R., "Pyroelectric materials and devices for energy harvesting applications," Energy & Environmental Science, vol. 7, no. 12, pp. 3836-3856, 2014.

[329] Thakre A., Kumar A., Song H.C., Jeong D.Y., and Ryu J., "Pyroelectric energy conversion and its applications-flexible energy harvesters and sensors," Sensors, vol. 19, no. 9, p. 2170, 2019.

[330] Champier D., "Thermoelectric generators: A review of applications," Energy Conversion and Management, vol. 140, pp. 167-181, 2017.

[331] Petsagkourakis I., Tybrandt K., Crispin X., Ohkubo I., Satoh N., and Mori T., "Thermoelectric materials and applications for energy harvesting power generation," Science and technology of advanced materials, vol. 19, no. 1, pp. 836-862, 2018.

[332] Jaziri N., Boughamoura A., Müller J., Mezghani B., Tounsi F., and Ismail M., "A comprehensive review of Thermoelectric Generators: Technologies and common applications," Energy Reports, vol. 6, pp. 264-287, 2019.

[333] Kim Y.J., Gu H.M., Kim C.S., Choi H., Lee G., Kim S., Kevin K.Y., Lee S.G., and Cho B.J., "High-performance self-powered wireless sensor node driven by a flexible thermoelectric generator," Energy, vol. 162, pp. 526-533, 2018.

[334] Meli M., and Hegetschweiler L., "Harvesting energy from trees in order to power LPWAN IoT nodes," in Wireless Congress 2018, WEKA, 2018 March.

[335] Alegret R.N., Aragones R., Oliver J., and Ferrer C., "Exploring IIoT and Energy Harvesting Boundaries," in IECON 2019-45th Annual Conference of the IEEE Industrial Electronics Society, IEEE, vol. 1, pp. 6732-6736, 2019 October.

[336] Rösch A.G., Gall A., Aslan S., Hecht M., Franke L., Mallick M.M., Penth L., Bahro D., Friderich D., and Lemmer U., "Fully printed origami thermoelectric generators for energy-harvesting,". npj Flexible Electronics, vol. 5, no. 1, pp .1-8, 2021.

[337] Magno M., Sigrist L., Gomez A., Cavigelli L., Libri A., Popovici E., and Benini L., "SmarTEG: An autonomous wireless sensor node for high accuracy accelerometer-based monitoring," Sensors, vol. 19, no. 12, p. 2747, 2019.

[338] Yang F., Du L., Yu H., and Huang P., "Magnetic and Electric Energy Harvesting Technologies in Power Grids: A Review," Sensors, vol. 20, no. 5, p. 1496, 2020.

[339] Cetinkaya O., and Akan O.B., "Electric-field energy harvesting in wireless networks," IEEE Wireless Communications, vol. 24, no. 2, pp. 34-41, 2017.

[340] Wright S.W., Kiziroglou M.E., Spasic S., Radosevic N., and Yeatman E.M., "Inductive energy harvesting from current-carrying structures," IEEE Sensors Letters, vol. 3, no. 6, pp. 1-4, ,2019.

[341] Gulati M., Parizi F.S., Whitmire E., Gupta S., Ram S.S., Singh A., and Patel S.N., "CapHarvester: A stick-on capacitive energy harvester using stray electric field from AC power lines," Proceedings of the ACM on Interactive, Mobile, Wearable and Ubiquitous Technologies, vol. 2, no. 3, pp. 1-20, 2018.

[342] Dalpiaz G., Longo A., Nardello M., Passerone R., and Brunello D., "A battery-free non-intrusive power meter for low-cost energy monitoring," in 2018 IEEE Industrial Cyber-Physical Systems (ICPS), IEEE, pp. 653-658, 2018 May.

[343] Maharjan P., Salauddin M., Cho H., and Park J.Y., "An indoor power line based magnetic field energy harvester for self-powered wireless sensors in smart home applications," Applied energy, vol. 232, pp. 398-408, 2018.

[344] Kim S., Vyas R., Bito J., Niotaki K., Collado A., Georgiadis A., and Tentzeris M.M., "Ambient RF energy-harvesting technologies for self-sustainable standalone wireless sensor platforms," Proceedings of the IEEE, vol. 102, no. 11, pp. 1649-1666, 2014.

[345] Soyata T., Copeland L., and Heinzelman W., "RF energy harvesting for embedded systems: A survey of tradeoffs and methodology," IEEE Circuits and Systems Magazine, vol. 16, no. 1, pp. 22-57, 2016.

[346] Kawahara Y., Bian X., Shigeta R., Vyas R., Tentzeris M.M., and Asami T., "Power harvesting from microwave oven electromagnetic leakage," in Proceedings of the 2013 ACM international joint conference on Pervasive and ubiquitous computing, pp. 373-382, 2013 September.

[347] Vyas R., Nishimoto H., Tentzeris M., Kawahara Y., and Asami T., "A battery-less, energy harvesting device for long range scavenging of wireless power from terrestrial TV broadcasts," in 2012 IEEE/MTT-S International Microwave Symposium Digest, IEEE, pp. 1-3, 2012 June.

[348] Vyas R.J., Cook B.B., Kawahara Y., and Tentzeris M.M., "E-WEHP: A batteryless embedded sensor-platform wirelessly powered from ambient digital-TV signals," IEEE Transactions on microwave theory and techniques, vol. 61, no. 6, pp. 2491-2505, 2013.

[349] Nishimoto H., Kawahara Y., and Asami T., "Prototype implementation of ambient RF energy harvesting wireless sensor networks," in SENSORS, 2010 IEEE, IEEE, pp. 1282-1287, 2010 November.

[350] Parks A.N., Sample A.P., Zhao Y., and Smith J.R., "A wireless sensing platform utilizing ambient RF energy," in 2013 IEEE Topical Conference on Biomedical Wireless Technologies, Networks, and Sensing Systems, IEEE, pp. 154-156, 2013 January.

[351] Jung E.M., Cui Y., Lin T.H., He X., Eid A., Hester J.G., Abowd G.D., Starner T.E., Lee W.S., and Tentzeris M.M., "A wideband, quasi-isotropic, kilometer-range fm energy harvester for perpetual IoT," IEEE Microwave and Wireless Components Letters, vol. 30, no. 2, pp. 201-204, 2019.

[352] Finnegan J., Niotaki K., and Brown S., "Exploring the Boundaries of Ambient RF Energy Harvesting with LoRaWAN," IEEE Internet of Things Journal, 2020.

[353] Weddell A.S., Magno M., Merrett G.V., Brunelli D., Al-Hashimi B.M., and Benini L., "A survey of multi-source energy harvesting systems," in 2013 Design, Automation & Test in Europe Conference & Exhibition, IEEE, pp. 905-908, 2013 March.

[354] Yu H., Yue Q., Zhou J., and Wang W., "A hybrid indoor ambient light and vibration energy harvester for wireless sensor nodes," Sensors, vol. 14, no. 5, pp. 8740-8755, 2014.

[355] Zhang B., Li M., Zhong S., He Z., and Zhang Y., "Design of a hybrid power system based on solar cell and vibration energy harvester," in Journal of Physics: Conference Series, IOP Publishing, vol. 986, no. 1, p. 012025, 2018 March.

[356] Rahman M.S., and Chakravarty U.K., "Design and Analysis of a Hybrid Solar and Vibration Energy Harvester," Energy Harvesting and Systems, vol. 1, 2019.

[357] Wang J., Nabawy M.R., Cioncolini A., and Revell A., "Solar Panels as Tip masses in low frequency vibration harvesters," Energies, vol. 12, no. 20, p. 3815, 2019.

[358] Lemey S., Declercq F., and Rogier H., "Textile antennas as hybrid energy-harvesting platforms," Proceedings of the IEEE, vol. 102, no. 11, pp. 1833-1857, 2014.

[359] Magno M., Aoudia F.A., Gautier M., Berder O., and Benini L., "WULoRa: An energy efficient IoT end-node for energy harvesting and heterogeneous communication," in Design, Automation & Test in Europe Conference & Exhibition (DATE), IEEE, pp. 1528-1533, 2017 March.

[360] Lee W.K., Schubert M.J., Ooi B.Y., and Ho S.J.Q., "Multi-source energy harvesting and storage for floating wireless sensor network nodes with long range communication capability," IEEE Transactions on Industry Applications, vol. 54, no. 3, pp. 2606-2615, 2018.

[361] Singh G., Mumtaz F., Bohara V.A., and Srivastava A., "Experimental Observations on Hybrid RF-Solar Energy Harvesting Circuit for Low Power Applications," in 2018 IEEE International Conference on Advanced Networks and Telecommunications Systems (ANTS), IEEE, pp. 1-3, 2018 December.

[362] Niotaki K., Collado A., Georgiadis A., Kim S., and Tentzeris M.M., "Solar/electromagnetic energy harvesting and wireless power transfer," Proceedings of the IEEE, vol. 102, no. 11, pp. 1712-1722, 2014.

[363] Georgiadis A., Collado A., Via S., and Meneses C., "Flexible hybrid solar/EM energy harvester for autonomous sensors," in 2011 IEEE MTT-S International Microwave Symposium, IEEE, pp. 1-4, 2011 June.

[364] Collado A., and Georgiadis A., "Conformal hybrid solar and electromagnetic (EM) energy harvesting rectenna," IEEE Transactions on Circuits and Systems I: Regular Papers, vol. 60, no. 8, pp. 2225-2234, 2013.

[365] Niotaki K., Giuppi F., Georgiadis A., and Collado A., "Solar/EM energy harvester for autonomous operation of a monitoring sensor platform," Wireless Power Transfer, vol. 1, no. 1, p. 44, 2014.

[366] Jadhav S.B., and Lambor S.M., "Hybrid solar and radio frequency (RF) energy harvesting," in 2017 IEEE International Conference on Power, Control, Signals and Instrumentation Engineering (ICPCSI), IEEE, pp. 1975-1980, 2017 November.

[367] Bito J., Hester J.G., and Tentzeris M.M., "A fully autonomous ultra-low power hybrid RF/photovoltaic energy harvesting system with− 25 dBm sensitivity," in 2017 IEEE Wireless Power Transfer Conference (WPTC), IEEE, pp. 1-4, 2017 May.

[368] Bito J., Bahr R., Hester J.G., Nauroze S.A., Georgiadis A., and Tentzeris M.M., "A novel solar and electromagnetic energy harvesting system with a 3-D printed package for energy efficient Internet-of-Things wireless sensors," IEEE Transactions on Microwave Theory and Techniques, vol. 65, no. 5, pp. 1831-1842, 2017.

[369] Abdelnour A., Hallet A., Dkhil S.B., Pierron P., Kaddour D., and Tedjini S., "Energy Harvesting Based On Printed Organic Photovoltaic Cells for RFID Applications," in 2019 IEEE International Conference on RFID Technology and Applications (RFID-TA), IEEE, pp. 110-112, 2019 September.

[370] Sample A.P., Braun J., Parks A., and Smith J.R., "Photovoltaic enhanced UHF RFID tag antennas for dual purpose energy harvesting," in 2011 IEEE International Conference on RFID, IEEE, pp. 146-153, 2011 April.

[371] Shih W.C., Chou P.H., and Chen W.T., "A batteryless beacon based on dual ISM-band RF harvesting with solar-biasing current," in Proceedings of the 4th International Workshop on Energy Harvesting and Energy-Neutral Sensing Systems, pp. 7-12, 2016 November.

[372] Wang Y., Huang Y., and Song C., "A new smart sensing system using LoRaWAN for environmental monitoring," in 2019 Computing, Communications and IoT Applications (ComComAp), IEEE, pp. 347-351, 2019 October.

[373] Oh Y., Kwon D.S., Eun Y., Kim W., Kim M.O., Ko H.J., Kang S.G., and Kim J., "Flexible energy harvester with piezoelectric and thermoelectric hybrid mechanisms for sustainable harvesting," International Journal of Precision Engineering and Manufacturing-Green Technology, vol. 6, no. 4, pp. 691-698, 2019.

[374] Gu X., Hemour S., and Wu K., "Integrated cooperative radiofrequency (RF) and kinetic energy harvester," in 2017 IEEE Wireless Power Transfer Conference (WPTC), IEEE, pp. 1-3), 2017 May.

[375] Nguyen S., and Amirtharajah R., "A hybrid RF and vibration energy harvester for wearable devices," in 2018 IEEE Applied Power Electronics Conference and Exposition (APEC), IEEE, pp. 1060-1064, 2018 March.

[376] Virili M., Georgiadis A., Niotaki K., Collado A., Alimenti F., Mezzanotte P., Roselli L., and Carvalho N.B., "Design and optimization of an antenna with Thermo-Electric Generator (TEG) for autonomous wireless nodes," In 2014 IEEE RFID Technology and Applications Conference (RFID-TA), IEEE, pp. 21-25, 2014 September.

[377] Virili M., Georgiadis A., Collado A., Niotaki K., Mezzanotte P., Roselli L., Alimenti F., and Carvalho N.B., "Performance improvement of rectifiers for WPT exploiting thermal energy harvesting," Wireless Power Transfer, vol. 2, no. 1, p. 22, 2015.

[378] Guo L., Gu X., Chu P., Hemour S., and Wu K., "Collaboratively harvesting ambient radiofrequency and thermal energy," IEEE Transactions on Industrial Electronics, vol. 67, no. 5, pp. 3736-3746, 2019.

[379] Bandyopadhyay S., and Chandrakasan A.P., "Platform architecture for solar, thermal, and vibration energy combining with MPPT and single inductor," IEEE Journal of Solid-State Circuits, vol. 47, no. 9, pp. 2199-2215, 2012.

[380] Ferrero F., and Le-Quoc H., "Multi-harvesting solution for autonomous sensing node based on LoRa technology," in 2017 International Conference on Advanced Technologies for Communications (ATC), IEEE, pp. 250-253, 2017 October.

[381] Ambrosio R., Torrealba R., Guerrero-C J.F., González V., Limon A., and Moreno M., "Energy harvesting combining three different sources for low power applications," in 2015 12th International Conference on Electrical Engineering, Computing Science and Automatic Control (CCE), IEEE, pp. 1-6, 2015 October.

[382] Virili M., Georgiadis A., Collado A., Mezzanotte P., and Roselli L., "EM characterization of a patch antenna with thermo-electric generator and Solar Cell for hybrid Energy Harvesting," in 2015 IEEE Radio and Wireless Symposium (RWS), IEEE, pp. 44-46, 2015 January.

[383] Khan A.A., Mahmud A., and Ban D., "Evolution from single to hybrid nanogenerator: a contemporary review on multimode energy harvesting for self-powered electronics," IEEE Transactions on Nanotechnology, vol. 18, pp. 21-36, 2018.

[384] Wang S., Wang Z.L., and Yang Y.A., "A one-structure-based hybridized nanogenerator for scavenging mechanical and thermal energies by triboelectric-piezoelectric-pyroelectric effects," Advanced Materials, vol. 28, no. 15, pp. 2881-2887, 2016.

[385] Ghosh S.K., Xie M., Bowen C.R., Davies P.R., Morgan D.J., and Mandal D., "A hybrid strain and thermal energy harvester based on an infra-red sensitive Er 3+ modified poly (vinylidene fluoride) ferroelectret structure," Scientific reports, vol. 7, no. 1, pp. 1-13, 2017.

[386] Zhang K., Wang S., and Yang Y., "A one-structure-based piezo-tribo-pyro-photoelectric effects coupled nanogenerator for simultaneously scavenging mechanical, thermal, and solar energies," Advanced Energy Materials, vol. 7, no. 6, p. 1601852, 2017.

[387] Georgiadis A., and Collado A., "Improving range of passive RFID tags utilizing energy harvesting and high efficiency class-E oscillators," in 2012 6th European Conference on Antennas and Propagation (EUCAP), IEEE, pp. 3455-3458, 2012 March.

[388] Gu X., Grauwin L., Dousset D., Hemour S., and Wu K., "Dynamic Ambient RF Energy Density Measurements of Montreal for Battery-Free IoT Sensor Network Planning," IEEE Internet of Things Journal, 2021.

[389] Zeng Y., Clerckx B., and Zhang R., "Communications and signals design for wireless power transfer," IEEE Transactions on Communications, vol. 65, no. 5, pp. 2264-2290, 2017.

[390] Jin K., and Zhou W., "Wireless laser power transmission: a review of recent progress," IEEE transactions on power electronics, vol. 34, no. 4, pp. 3842-3859, 2018.

[391] Summerer L., and Purcell O., "Concepts for wireless energy transmission via laser," Europeans Space Agency (ESA)-Advanced Concepts Team, 2009.

[392] Kang S., Park K., Shin S., Chang K., and Kim H., "Zero standby power remote control system using light power transmission," IEEE transactions on Consumer Electronics, vol. 57, no. 4, pp. 1622-1627, 2011.

[393] Sahai A., and Graham D., "Optical wireless power transfer at long wavelengths," in 2011 International Conference on Space Optical Systems and Applications (ICSOS), IEEE, pp. 164-170, 2011 May.

[394] Roes M.G., Duarte J.L., Hendrix M.A., and Lomonova E.A., "Acoustic energy transfer: A review," IEEE Transactions on Industrial Electronics, vol. 60, no. 1, pp. 242-248, 2012.

[395] Zaid T., Saat S., Yusop Y., and Jamal N., "Contactless energy transfer using acoustic approach-A review," in 2014 International conference on computer, communications, and control technology (I4CT), IEEE, pp. 376-381, 2014 September.

[396] Awal M.R., Jusoh M., Sabapathy T., Kamarudin M.R., and Rahim R.A., "State-of-the-art developments of acoustic energy transfer," International Journal of Antennas and Propagation, 2016.

[397] Shahab S., Gray M., and Erturk A., "Ultrasonic power transfer from a spherical acoustic wave source to a free-free piezoelectric receiver: Modeling and experiment," Journal of Applied Physics, vol. 117, no. 10, p. 104903, 2015.

[398] Shinohara N., "Power without wires," IEEE Microwave magazine, vol. 12, no. 7, pp. S64-S73, 2011.

[399] Lu X., Wang P., Niyato D., Kim D.I., and Han Z., "Wireless charging technologies: Fundamentals, standards, and network applications," IEEE Communications Surveys & Tutorials, vol. 18, no. 2, pp. 1413-1452, 2015.

[400] Team C.A.I., "Europe and the future for WPT: European contributions to wireless power transfer technology," IEEE Microwave Magazine, vol. 18, 4, pp. 56-87, 2017.

[401] Zhang Z., Pang H., Georgiadis A., and Cecati C., "Wireless power transfer - An overview," IEEE Transactions on Industrial Electronics, vol. 66, no. 2, pp. 1044-1058, 2018.

[402] Carvalho N.B., and Georgiadis A. "Wireless power transfer for Sustainable Electronics: COST WiPE-IC1301," John Wiley & Sons, 2020.

[403] Lu F., Zhang H., and Mi C., "A review on the recent development of capacitive wireless power transfer technology," Energies, vol. 10, no. 11, p. 1752, 2017.

[404] Sample A.P., Meyer D.T., and Smith J.R., "Analysis, experimental results, and range adaptation of magnetically coupled resonators for wireless power transfer," IEEE Transactions on industrial electronics, vol. 58, no. 2, pp. 544-554, 2010.

[405] "Wireless Power Consortium - The Wireless Power Standards," Available online: https://www.wirelesspowerconsortium.com/ (accessed on 3 March 2021).

[406] "AirFuel Alliance - AirFuel is cutting the cord," Available online: https://airfuel.org/ (accessed on 3 March 2021).

[407] Molefi M., Markus E.D., and Abu-Mahfouz A., "Wireless power transfer for LoRa low-power wide-area networks (LPWANs)," in 2019 Southern African Universities Power Engineering Conference/Robotics and Mechatronics/Pattern Recognition Association of South Africa (SAUPEC/RobMech/PRASA), IEEE, pp. 105-110, 2019 January.

[408] Brown W.C., "The history of power transmission by radio waves," IEEE Transactions on microwave theory and techniques, vol. 32, no. 9, pp. 1230-1242, 1984.

[409] Valenta C.R., and Durgin G.D., "Harvesting wireless power: Survey of energy-harvester conversion efficiency in far-field, wireless power transfer systems," IEEE Microwave Magazine, vol. 15, no. 4, pp. 108-120, 2014.

[410] Shinohara N., "Wireless power transfer via radiowaves," ISTE-Wiley, 2014.

[411] European Union, "COMMISSION IMPLEMENTING DECISION (EU) 2017/1483 of 8 August 2017 amending Decision 2006/771/EC on harmonisation of the radio spectrum for use by short-range devices and repealing Decision 2006/804/EC," Official Journal of the European Union, Decision C(2017) 5464, 2017.

[412] Electronic Communication Committed (ECC) / European Radiocommunications Committee (ERC), " Relating to the use of Short Range Devices (SRD)," ERC Recommendation 70-03, ERC/CEPT-ECC, 2015.

[413] ETSI, "Electromagnetic compatibility and radio spectrum matters (ERM); short range devices (SRD) intended for operation in the bands 865 MHz to 868 MHz and 915 MHz to 921 MHz; guidelines for the installation and commissioning of radio frequency identification (RFID) equipment at UHF," ETSI TR 102 436, V2.1.1, ETSI: Sophia Antipolis FRANCE, 2014.

[414] Autorité de régulation des communications électroniques, des postes et de la distribution de la presse, "Décision n° 06-0841 de l'Autorité de régulation des communications électroniques et des postes en date du 25 juillet 2006 fixant les conditions d'utilisation des fréquences radioélectriques pour les applications d'identification par radiofréquences dans la bande 865 - 868 MHz," ARCEP 06-0841, 2006.

[415] Pflug H.W., Visser H.J., and Keyrouz S., "Practical applications of radiative wireless power transfer," in 2015 IEEE Wireless Power Transfer Conference (WPTC), IEEE, pp. 1-4, 2015 May.

[416] Janhunen J., Mikhaylov K., and Petäjäjärvi J., "Experimental RF-signal based wireless energy transmission," in 2017 European Conference on Networks and Communications (EuCNC), IEEE, pp. 1-6, 2017 June.

[417] Tjukovs S., Eidaks J., and Pikulins D., "Experimental verification of wireless power transfer ability to sustain the operation of LoRaWAN based wireless sensor node," in 2018 Advances in Wireless and Optical Communications (RTUWO), IEEE, pp. 83-88, 2018 November.

[418] Paolini G., Masotti D., Guermandi M., Shanawani M., Benini L., and Costanzo A., "An Ambient-Insensitive Battery-Less Wireless Node for Simultaneous Powering and Communication," in 2020 50th European Microwave Conference (EuMC), IEEE, pp. 522-525, 2021 January.

[419] Pizzotti M., Perilli L., Del Prete M., Fabbri D., Canegallo R., Dini M., Masotti D., Costanzo A., Franchi Scarselli E., and Romani A., "A long-distance RF-powered sensor node with adaptive power management for IoT applications," Sensors, vol. 17, no. 8, p. 1732, 2017.

[420] La Rosa R., Trigona C., Zoppi G., Di Carlo C.A., Di Donato L., and Sorbello G., "RF energy scavenger for battery-free Wireless Sensor Nodes," in 2018 IEEE International Instrumentation and Measurement Technology Conference (I2MTC), IEEE, pp. 1-5, 2018 May.

[421] Janhunen J., Mikhaylov K., Petäjäjärvi J., and Sonkki M., "Wireless energy transfer powered wireless sensor node for green IoT: Design, implementation and evaluation," Sensors, vol. 19, no. 1, p. 90, 2019.

[422] Farinholt K.M., Park G., and Farrar C.R., "RF energy transmission for a low-power wireless impedance sensor node," IEEE Sensors Journal, vol. 9, no. 7, pp. 793-800, 2009.

[423] "Powercast - Wireless power for a wireless world," Available online: https://www.powercastco.com/ (accessed on 3 March 2021).

[424] "Ossia," Available online: https://www.ossia.com/ (accessed on 3 March 2021).

[425] "GreenWake Technologies - Remote powering of sensors - no wires, no batteries, no worries," Available online: http://gnw-tech.com/home.htm (accessed on 3 March 2021).

[426] Georgiadis A., Kim S., Lee H., and Tentzeris M.M., "UHF solar powered active oscillator antenna on low cost flexible substrate for wireless identification applications," in 2012 IEEE/MTT-S International Microwave Symposium Digest, IEEE, pp. 1-3, 2012 June.

[427] Georgiadis A., and Collado A., "Solar powered class-E active antenna oscillator for wireless power transfer," in 2013 IEEE Radio and Wireless Symposium, IEEE, pp. 40-42, 2013 January.

[428] Chen Y., Cheng Y., Jie Y., Cao X., Wang N., and Wang Z.L., "Energy harvesting and wireless power transfer by a hybridized electromagnetic–triboelectric nanogenerator," Energy & Environmental Science, vol. 12, no. 9, pp. 2678-2684, 2019.

[429] Varshney L.R., "Transporting information and energy simultaneously," in 2008 IEEE international symposium on information theory, IEEE, pp. 1612-1616, 2008 July.

[430] Grover P., and Sahai A., "Shannon meets Tesla: Wireless information and power transfer," in 2010 IEEE international symposium on information theory, IEEE, pp. 2363-2367, 2010 June.

[431] Zhang R., and Ho C.K., "MIMO broadcasting for simultaneous wireless information and power transfer," IEEE Transactions on Wireless Communications, vol. 12, no. 5, pp. 1989-2001, 2013.

[432] Zhou X., Zhang R., and Ho C.K., "Wireless information and power transfer: Architecture design and rate-energy tradeoff," IEEE Transactions on communications, vol. 61, no. 11, pp. 4754-4767, 2013.

[433] Krikidis I., Timotheou S., Nikolaou S., Zheng G., Ng D.W.K., and Schober, R., "Simultaneous wireless information and power transfer in modern communication systems," IEEE Communications Magazine, vol. 52, no. 11, pp. 104-110, 2014.

[434] Bi S., Zeng Y., and Zhang R., "Wireless powered communication networks: An overview," IEEE Wireless Communications, vol. 23, no. 2, pp. 10-18, 2016.

[435] Perera T.D.P., Jayakody D.N.K., Sharma S.K., Chatzinotas S., and Li J., "Simultaneous wireless information and power transfer (SWIPT): Recent advances and future challenges," IEEE Communications Surveys & Tutorials, vol. 20, no. 1, pp. 264-302, 2017.

[436] Clerckx B., Zhang R., Schober R., Ng D.W.K., Kim D.I., and Poor H.V., "Fundamentals of wireless information and power transfer: From RF energy harvester models to signal and system designs," IEEE Journal on Selected Areas in Communications, vol. 37, no. 1, pp. 4-33, 2018.

[437] Hossain M.A., Noor R.M., Yau K.L.A., Ahmedy I., and Anjum S.S., "A survey on simultaneous wireless information and power transfer with cooperative relay and future challenges," IEEE access, vol. 7, pp. 19166-19198, 2019.

[438] Costanzo A., and Masotti D., "Energizing 5G: Near- and far-field wireless energy and data transfer as an enabling technology for the 5G IoT," IEEE Microwave Magazine, vol. 18, no. 3, pp. 125-136, 2017.

[439] Clerckx B., Costanzo A., Georgiadis A., and Carvalho N.B., "Toward 1G mobile power networks: RF, signal, and system designs to make smart objects autonomous," IEEE Microwave Magazine, vol. 19, no. 6, pp. 69-82, 2018.

[440] Masotti D., Shanawani M., Murtaza G., Paolini G., and Costanzo A., "RF systems design for simultaneous wireless information and power transfer (SWIPT) in automation and transportation," IEEE Journal of Microwaves, vol. 1, no. 1, pp. 164-175, 2021.

[441] Pereira F., Correia R., Jordão M., and Carvalho N.B., "A Hybrid System combining SWIPT and Backscatter Techniques," in 2020 IEEE Wireless Power Transfer Conference (WPTC), IEEE, pp. 323-326, 2020 November.

[442] Boaventura A., Collado A., Carvalho N.B., and Georgiadis A., "Optimum behavior: Wireless power transfer system design through behavioral models and efficient synthesis techniques," IEEE Microwave Magazine, vol. 14, no. 2, pp. 26-35, 2013.

[443] Visser H.J., and Vullers R.J., "RF energy harvesting and transport for wireless sensor network applications: Principles and requirements," Proceedings of the IEEE, vol. 101, no. 6, pp. 1410-1423, 2013.

[444] Costanzo A., Dionigi M., Masotti D., Mongiardo M., Monti G., Tarricone L., and Sorrentino R., "Electromagnetic energy harvesting and wireless power transfer: A unified approach," Proceedings of the IEEE, vol. 102, no. 11, pp. 1692-1711, 2014.

[445] Lu X., Wang P., Niyato D., Kim D.I., and Han Z., "Wireless networks with RF energy harvesting: A contemporary survey," IEEE Communications Surveys & Tutorials, vol. 17, no. 2, pp. 757-789, 2014.

[446] Carvalho N.B., Georgiadis A., Costanzo A., Rogier H., Collado A., García J.A., Lucyszyn S., Mezzanotte P., Kracek J., Masotti D., and Boaventura A.J.S., "Wireless power transfer: R&D activities within Europe," IEEE Transactions on Microwave Theory and Techniques, vol. 62, no. 4, pp. 1031-1045, 2014.

[447] Boaventura A., Belo D., Fernandes R., Collado A., Georgiadis A., and Carvalho N.B., "Boosting the efficiency: Unconventional waveform design for efficient wireless power transfer," IEEE Microwave Magazine, vol. 16, no. 3, pp. 87-96, 2015.

[448] Masotti D., Costanzo A., Del Prete M., and Rizzoli V., "Time-modulation of linear arrays for real-time reconfigurable wireless power transfer," IEEE Transactions on Microwave Theory and Techniques, vol. 64, no. 2, pp. 331-342, 2016.

[449] Belo D., Ribeiro D.C., Pinho P., and Carvalho N.B., "A selective, tracking, and power adaptive far-field wireless power transfer system," IEEE Transactions on Microwave Theory and Techniques, vol. 67, no. 9, pp. 3856-3866, 2019.

[450] Nguyen D.K., Jayakody D.N.K., Chatzinotas S., Thompson J.S., and Li J., "Wireless energy harvesting assisted two-way cognitive relay networks: Protocol design and performance analysis," IEEE Access, vol. 5, pp. 21447-21460, 2017.

[451] Massa A., Oliveri G., Viani F., and Rocca P., "Array designs for long-distance wireless power transfer: State-of-the-art and innovative solutions," Proceedings of the IEEE, vol. 101, no. 6, pp. 1464-1481, 2013.

[452] Piñuela M., Mitcheson P.D., and Lucyszyn S., "Ambient RF energy harvesting in urban and semi-urban environments," IEEE Transactions on microwave theory and techniques, vol. 61, no. 7, pp. 2715-2726, 2013.

[453] Palazzi V., Hester J., Bito J., Alimenti F., Kalialakis C., Collado A., Mezzanotte P., Georgiadis A., Roselli L., and Tentzeris M.M., "A novel ultra-lightweight multiband rectenna on paper for RF energy harvesting in the next generation LTE bands," IEEE Transactions on Microwave Theory and Techniques, vol. 66, no. 1, pp. 366-379, 2017.

[454] Fantuzzi M., Del Prete M., Masotti D., and Costanzo A., "Quasi-isotropic RF energy harvester for autonomous long distance IoT operations," in 2017 IEEE MTT-S International Microwave Symposium (IMS), IEEE, pp. 1345-1348, 2017 June.

[455] Vandelle E., Vuong T.P., Ardila G., Wu K., and Hemour S., "Harvesting ambient RF energy efficiently with optimal angular coverage," IEEE Transactions on Antennas and Propagation, vol. 67, no. 3, pp. 1862-1873, 2018.

[456] Okba A., Takacs A., and Aubert H., "Compact rectennas for ultra-low-power wireless transmission applications," IEEE Transactions on Microwave Theory and Techniques, vol. 67, no. 5, pp. 1697-1707, 2019.

[457] Adeyeye A., Eid A., Hester J., Nauroze S.A., Tehrani B., Cui Y., and Tentzeris M.M., "Inkjet-/3D-/4D-Printed Wireless Ultrabroadband Modules for IoT, Smartag and Smart City Applications,". in Nanotechnology For Electronics, Photonics, Biosensors, And Emerging Technologies, pp. 41-49, 2019.

[458] Eid A., Hester J.G., and Tentzeris M.M., "5G as a wireless power grid," Scientific Reports, vol. 11, no. 1, pp. 1-9, 2021.

[459] Balanis C.A., "Antenna theory: analysis and design," John wiley & sons, 2016.

[460] Adams J.J., Slimmer S.C., Malkowski T.F., Duoss E.B., Lewis J.A., and Bernhard J.T., "Comparison of spherical antennas fabricated via conformal printing: helix, meanderline, and hybrid designs," IEEE Antennas and Wireless Propagation Letters, vol. 10, pp. 1425-1428, 2011.

[461] Adams J.J., Duoss E.B., Malkowski T.F., Motala M.J., Ahn B.Y., Nuzzo R.G., Bernhard J.T., and Lewis J.A., "Conformal printing of electrically small antennas on three-dimensional surfaces," Advanced Materials, vol. 23, no. 11, pp. 1335-1340, 2011.

[462] Adams J.J., Slimmer S.C., Lewis J.A., and Bernhard J.T., "3D-printed spherical dipole antenna integrated on small RF node," Electronics Letters, vol. 51, no. 9, pp. 661-662, 2015.

[463] Eid A., Hester J., Fang Y., Tehrani B., Nauroze S.A., Bahr R., and Tentzeris M.M., "Nanotechnology-empowered flexible printed wireless electronics: A review of various applications of printed materials," IEEE Nanotechnology Magazine, vol. 13, no. 1, pp. 18-29, 2018.

[464] Masotti D., Costanzo A., and Adami S., "Design and realization of a wearable multi-frequency RF energy harvesting system," in Proceedings of the 5th European Conference on Antennas and Propagation (EUCAP), IEEE, pp. 517-520, 2011 April.

[465] Herth E., Seok S., Rolland N., and Lasri T., "Wafer level packaging compatible with millimeter-wave antenna," Sensors and Actuators A: Physical, vol. 173, no. 1, pp. 238-243, 2012.

[466] Vena A., Perret E., Tedjini S., Tourtollet G.E.P., Delattre A., Garet F., and Boutant Y., "Design of chipless RFID tags printed on paper by flexography," IEEE Transactions on Antennas and Propagation, vol. 61, no. 12, pp. 5868-5877, 2013.

[467] Vandelle E., Vuong T.P., Ardila G., Hemour S., and Wu K., "Miniaturized Antenna on a Paper Substrate," in 2019 49th European Microwave Conference (EuMC), IEEE, pp. 73-76, 2019 October.

[468] Kimionis J., Isakov M., Koh B.S., Georgiadis A., and Tentzeris M.M., "3D-printed origami packaging with inkjet-printed antennas for RF harvesting sensors," IEEE Transactions on Microwave Theory and Techniques, vol. 63, no. 12, pp. 4521-4532, 2015.

[469] Pires D., Belo D., Jordão M., Pinho P., and Carvalho N.B., "3D Antenna Array for SWIPT Sensing with WPT Capabilities," in 2020 14th European Conference on Antennas and Propagation (EuCAP), IEEE, pp. 1-4, 2020 March.

[470] He X., Fang Y., Bahr R.A., and Tentzeris M.M., "RF systems on antenna (SoA): A novel integration approach enabled by additive manufacturing," in 2020 IEEE/MTT-S International Microwave Symposium (IMS), IEEE, pp. 1157-1160, 2020 August.

[471] Guerchouche K., Herth E., Calvet L.E., Roland N., and Loyez, C. "Conductive polymer based antenna for wireless green sensors applications," Microelectronic Engineering, vol. 182, pp. 46-52, 2017.

[472] Hemour S., and Wu K., "Radio-frequency rectifier for electromagnetic energy harvesting: Development path and future outlook," Proceedings of the IEEE, vol. 102, no. 11, pp. 1667-1691, 2014.

[473] Hemour S., Zhao Y., Lorenz C.H.P., Houssameddine D., Gui Y., Hu C.M., and Wu K., "Towards low-power high-efficiency RF and microwave energy harvesting," IEEE transactions on microwave theory and techniques, vol. 62, no. 4, pp. 965-976, 2014.

[474] Guler U., and Ghovanloo M., "Power management in wireless power-sipping devices: A survey," IEEE circuits and systems magazine, vol. 17, no. 4, pp. 64-82, 2017.

[475] Daskalakis S.N., Georgiadis A., Goussetis G., and Tentzeris M.M., "A rectifier circuit insensitive to the angle of incidence of incoming waves based on a Wilkinson power combiner," IEEE Transactions on Microwave Theory and Techniques, vol. 67, no. 7, pp. 3210-3218, 2019.

[476] Han Y., Leitermann O., Jackson D.A., Rivas J.M., and Perreault D.J., "Resistance compression networks for radio-frequency power conversion," IEEE Transactions on Power Electronics, vol. 22, no. 1, pp. 41-53, 2007.

[477] Eid A., Hester J.G., Costantine J., Tawk Y., Ramadan A.H., and Tentzeris M.M., "A compact source–load agnostic flexible rectenna topology for IoT devices," IEEE Transactions on Antennas and Propagation, vol. 68, no. 4, pp. 2621-2629, 2019.

[478] Allane D., Vera G.A., Duroc Y., Touhami R., and Tedjini S., "Harmonic power harvesting system for passive RFID sensor tags," IEEE Transactions on microwave theory and techniques, vol. 64, no. 7, pp. 2347-2356, 2016.

[479] Ju H., and Zhang R., "Throughput maximization in wireless powered communication networks," IEEE Transactions on Wireless Communications, vol. 13, no. 1, pp.4 18-428, 2013.

[480] "Texas Instruments - BQ24210," Available online: https://www.ti.com/product/BQ24210 (accessed on 3 March 2021).

[481] "Texas Instruments - BQ25504," Available online: https://www.ti.com/product/BQ5504 (accessed on 3 March 2021).

[482] "Texas Instruments - BQ25505," Available online: https://www.ti.com/product/BQ25505 (accessed on 3 March 2021).

[483] "Texas Instruments - BQ225570," Available online: https://www.ti.com/product/BQ25570 (accessed on 3 March 2021).

[484] "Analog Devices - Ahead of what possible - Energy harvesting," Available online: https://www.analog.com/en/parametricsearch/11503#/ (accessed on 3 March 2021).

[485] "ST - life.augmented - Energy Harvesting and Solar Charging ICs," Available online: https://www.st.com/en/power-management/energy-harvesting-and-solar-charging-ics.html (accessed on 3 March 2021).

[486] "Maxim integrated - MAX17710," Available online: https://www.maximintegrated.com/en/products/power/battery-management/MAX17710.html (accessed on 3 March 2021).

[487] "Maxim integrated - MAX20361," Available online: https://www.maximintegrated.com/en/products/power/battery-management/MAX20361.html (accessed on 3 March 2021).

[488] "e-peas semiconductors - Energy harvesting - ambient energy managers (AEM family)," Available online: https://e-peas.com/types/energy-harvesting/ (accessed on 3 March 2021).

[489] "Powercast - wireless power for a wireless world - Powerharvester receiver chips & modules," Available online: https://www.powercastco.com/products/powerharvester-receivers/ (accessed on 3 March 2021).

[490] "NOWI - NH2D0245," Available online: https://www.nowi-energy.com/products-nh2/ (accessed on 3 March 2021).

[491] "Trameto - enabling battery-free IoT," Available online: https://trameto.com/technology/ (accessed on 3 March 2021).

[492] Popović Z., Falkenstein E.A., Costinett D., and Zane R., "Low-power far-field wireless powering for wireless sensors," Proceedings of the IEEE, vol. 101, no. 6, pp. 1397-1409, 2013.

[493] Dolgov A., Zane R., and Popovic Z., "Power management system for online low power RF energy harvesting optimization," IEEE Transactions on Circuits and Systems I: Regular Papers, vol. 57, no. 7, pp. 1802-1811, 2010.

[494] Costanzo A., Romani A., Masotti D., Arbizzani N., and Rizzoli V., "RF/baseband co-design of switching receivers for multiband microwave energy harvesting," Sensors and Actuators A: Physical, vol. 179, pp. 158-168, 2012.

[495] Masotti D., Costanzo A., Francia P., Filippi M., and Romani A., "A load-modulated rectifier for RF micropower harvesting with start-up strategies," IEEE Transactions on Microwave Theory and Techniques, vol. 62, no. 4, pp. 994-1004, 2014.

[496] Syed Y., Hegde B.G., Prabhakar T.V., Manjunath M., and Vinoy K.J., "RF energy harvesting chip powered sensor node," in 2016 IEEE International Conference on Electronics, Circuits and Systems (ICECS), IEEE, pp. 748-751, 2016 December.

[497] La Rosa R., Livreri P., Trigona C., Di Donato L., and Sorbello G., "Strategies and techniques for powering wireless sensor nodes through energy harvesting and wireless power transfer," Sensors, vol. 19, no. 12, p. 2660, 2019.

[498] La Rosa R., Dehollain C., Pellitteri F., Miceli R., and Livreri P., "An RF Wireless Power Transfer system to power battery-free devices for asset tracking," in 2019 26th IEEE International Conference on Electronics, Circuits and Systems (ICECS), IEEE, pp. 534-537, 2019 November.

[499] La Rosa R., Costanza M., and Livreri P., "Advanced Techniques for Powering Wireless Sensor Nodes through Energy Harvesting and Wireless Power Transfer," in 2020 AEIT International Conference of Electrical and Electronic Technologies for Automotive (AEIT AUTOMOTIVE), IEEE, pp. 1-6, 2020 November.

[500] Sample A., and Smith J.R., "Experimental results with two wireless power transfer systems," in 2009 IEEE Radio and Wireless Symposium, IEEE, pp. 16-18, 2009 January.

[501] Gleonec P.D., Ardouin J., Gautier M., and Berder O., "Architecture exploration of multi-source energy harvester for IoT nodes," in 2016 IEEE Online Conference on Green Communications (OnlineGreenComm), IEEE, pp. 27-32, 2016 November.

[502] Assimonis S.D., Daskalakis S.N., and Bletsas A., "Sensitive and efficient RF harvesting supply for batteryless backscatter sensor networks," IEEE Transactions on Microwave Theory and Techniques, vol. 64, no. 4, pp. 1327-1338, 2016.

[503] Shi Y., Xie L., Hou Y.T., and Sherali H.D., "On renewable sensor networks with wireless energy transfer. In 2011 Proceedings IEEE INFOCOM, IEEE, pp. 1350-1358, 2011 April.

[504] "Atmosic - Products," Available online: https://atmosic.com/products/ (accessed on 3 March 2021).

[505] Dyer C.K., "Fuel cells for portable applications," Journal of Power Sources, vol. 106, no. 1-2, pp. 31-34, 2002.

[506] Ong B.C., Kamarudin S.K., and Basri S., "Direct liquid fuel cells: A review," International journal of hydrogen energy, vol. 42, no. 15, pp. 10142-10157, 2017.

[507] Wang Y., Diaz D.F.R., Chen K.S., Wang Z., and Adroher X.C., "Materials, technological status, and fundamentals of PEM fuel cells–a review," Materials today, vol. 32, pp. 178-203, 2020.

[508] Santoro C., Arbizzani C., Erable B., and Ieropoulos I., "Microbial fuel cells: From fundamentals to applications. A review," Journal of power sources, vol. 356, pp. 225-244, 2017.

[509] Slate A.J., Whitehead K.A., Brownson D.A., and Banks C.E., "Microbial fuel cells: An overview of current technology," Renewable and sustainable energy reviews, vol. 101, pp. 60-81, 2019.

[510] Xiao X., Xia H.Q., Wu R., Bai L., Yan L., Magner E., Cosnier S., Lojou E., Zhu Z., and Liu A., "Tackling the challenges of enzymatic (bio) fuel cells," Chemical reviews, vol. 119, no. 16, pp. 9509-9558, 2019.

[511] Simon P., and Gogotsi Y., "Materials for electrochemical capacitors," Nanoscience and technology: a collection of reviews from Nature journals, pp. 320-329, 2010.

[512] Wang Y., Song Y., and Xia Y., "Electrochemical capacitors: mechanism, materials, systems, characterization and applications," Chemical Society Reviews, vol. 45, no. 21, pp. 5925-5950, 2016.

[513] Pan M.J., and Randall C.A., "A brief introduction to ceramic capacitors," IEEE electrical insulation magazine, vol. 26, no. 3, pp. 44-50, 2010.

[514] Pech D., Brunet M., Taberna P.L., Simon P., Fabre N., Mesnilgrente F., Conédéra V., and Durou H., "Elaboration of a microstructured inkjet-printed carbon electrochemical capacitor," Journal of Power Sources, vol. 195, no. 4, pp. 1266-1269, 2010.

[515] Scrosati B., Hassoun J., and Sun Y.K., "Lithium-ion batteries. A look into the future," Energy & Environmental Science, vol. 4, no. 9, pp. 3287-3295, 2011.

[516] Kim T., Song W., Son D.Y., Ono L.K., and Qi Y., "Lithium-ion batteries: outlook on present, future, and hybridized technologies," Journal of materials chemistry A, vol. 7, no. 7, pp. 2942-2964, 2019.

[517] Xie J., and Lu Y.C., "A retrospective on lithium-ion batteries," Nature Communications, vol. 11, no. 1, pp. 1-4, 2020.

[518] Yabuuchi N., Kubota K., Dahbi M., and Komaba S., "Research development on sodium-ion batteries," Chemical reviews, vol. 114, no. 23, pp. 11636-11682, 2014.

[519] Liang Y., Zhao C.Z., Yuan H., Chen Y., Zhang W., Huang J.Q., Yu D., Liu Y., Titirici M.M., Chueh Y.L., and Yu H., "A review of rechargeable batteries for portable electronic devices," InfoMat, vol. 1, no. 1, pp. 6-32, 2019.

[520] Lethien C., Zegaoui M., Roussel P., Tilmant P., Rolland N., and Rolland P.A., "Micro-patterning of LiPON and lithium iron phosphate material deposited onto silicon nanopillars array for lithium ion solid state 3D micro-battery," Microelectronic engineering, vol. 88, no. 10, pp. 3172-3177, 2011.

[521] Eustache E., Tilmant P., Morgenroth L., Roussel P., Patriarche G., Troadec D., Rolland N., Brousse T., and Lethien C., "Silicon-Microtube Scaffold Decorated with Anatase TiO2 as a Negative Electrode for a 3D Litium-Ion Microbattery," Advanced Energy Materials, vol. 4, no. 8, p. 1301612., 2014

[522] Raza W., Ali F., Raza N., Luo Y., Kim K.H., Yang J., Kumar S., Mehmood A., and Kwon E.E., "Recent advancements in supercapacitor technology," Nano Energy, vol. 52, pp. 441-473, 2018.

[523] Sharma K., Arora A., and Tripathi S.K., "Review of supercapacitors: Materials and devices," Journal of Energy Storage, vol. 21, pp. 801-825, 2019.

[524] Pech D., Brunet M., Durou H., Huang P., Mochalin V., Gogotsi Y., Taberna P.L., and Simon P., "Ultrahigh-power micrometre-sized supercapacitors based on onion-like carbon," Nature nanotechnology, vol. 5, no. 9, pp. 651-654, 2010.

[525] Kyerematen N.A., Brousse T., and Pech D., "Microsupercapacitors as miniaturized energy-storage components for on-chip electronics," Nature nanotechnology, vol. 12, no. 1, pp. 7-15, 2016.

[526] Ferris A., Bourrier D., Garbarino S., Guay D., and Pech D., "3D interdigitated microsupercapacitors with record areal cell capacitance," Small, vol. 15, no. 27, p. 1901224, 2019.

[527] Zuo W., Li R., Zhou C., Li Y., Xia J., and Liu J., "Battery-supercapacitor hybrid devices: recent progress and future prospects," Advanced science, vol. 4, no. 7, p. 1600539, 2017.

[528] Ding J., Hu W., Paek E., and Mitlin D., "Review of hybrid ion capacitors: from aqueous to lithium to sodium," Chemical reviews, vol. 118, no. 14, pp. 6457-6498, 2018.

[529] Jonah O. and Georgakopoulos S.V., "Wireless power transfer to sensors embedded in concrete via magnetic resonance," in WAMICON 2011 Conference Proceedings, IEEE, pp. 1-6, 2011 April.

[530] Jonah O., and Georgakopoulos S.V., "Efficient wireless powering of sensors embedded in concrete via magnetic resonance," in 2011 IEEE International Symposium on Antennas and Propagation (APSURSI), IEEE, pp. 1425-1428, 2011 July.

[531] Jonah O., and Georgakopoulos S.V., "Wireless power transfer in concrete via strongly coupled magnetic resonance," IEEE Transactions on Antennas and Propagation, vol. 61, no. 3, pp. 1378-1384, 2012.

[532] Jang Y., Han J.K., Baek J.I., Moon G.W., Kim J.M., and Sohn H., "Novel multi-coil resonator design for wireless power transfer through reinforced concrete structure with rebar array," in 2017 IEEE 3rd International Future Energy Electronics Conference and ECCE Asia (IFEEC 2017-ECCE Asia), IEEE, pp. 2238-2243, 2017 June.

[533] Shams K.M., and Ali M., "Wireless power transfer to a buried sensor in concrete," IEEE Sensors Journal, vol. 7, no. 12, pp. 1573-1577, 2007.

[534] Jiang S., and Georgakopoulos S.V., "Optimum wireless power transfer through reinforced concrete structure," in 2011 IEEE International Conference on RFID, IEEE, pp. 50-56, 2011 April.

[535] Jiang S., and Georgakopoulos S.V., "Optimum wireless powering of sensors embedded in concrete," IEEE transactions on antennas and propagation, vol. 60, no. 2, pp. 1106-1113, 2011.

[536] Jiang S., Georgakopoulos S.V., and Jin H., "Effects of periodic reinforced-concrete structures on power transmission," in 2012 IEEE International Conference on RFID (RFID), IEEE, pp. 16-23, 2012 April.

[537] Jiang S., Georgakopoulos S.V., and Jonah O., "Power transmission for sensors embedded in reinforced concrete structures," in Proceedings of the 2012 IEEE International Symposium on Antennas and Propagation, IEEE, pp. 1-2, 2012 July.

[538] Kubler S., Derigent W., Thomas A., and Rondeau E., "Problem definition methodology for the "Communicating Material" paradigm," IFAC Proceedings Volumes, vol. 43, no. 4, pp. 198-203, 2010.

[539] Jover J., Thomas A., Leban J.M., and Canet D., "Interest of new communicating material paradigm: An attempt in wood industry," in Journal of physics: conference series, IOP Publishing, vol. 416, no. 1, p. 012031, 2013.

[540] Kubler S., Derigent W., Främling K., Thomas A., and Rondeau E., "Enhanced product lifecycle information management using "communicating materials"," Computer-Aided Design, vol. 59, pp. 192-200, 2015.

[541] Mekki K., Zouinkhi A., Derigent W., Rondeau E., Thomas A., and Abdelkrim M.N., "Usee: A uniform data dissemination and energy efficient protocol for communicating materials," Future Generation Computer Systems, vol. 56, pp. 651-663, 2016.

[542] Mekki K., Derigent W., Rondeau E., and Thomas A., "Data lifecycle management in smart building using wireless sensors networks," IFAC-PapersOnLine, vol. 50, no. 1, pp. 12944-12949, 2017.

[543] Build E.R.A., "Review of current state of radio frequency identification (RFID) technology, its use and potential future use in construction," 2006.

[544] Li N., and Becerik-Gerber B., "Life-cycle approach for implementing RFID technology in construction: Learning from academic and industry use cases," Journal of Construction Engineering and Management, vol. 137, no. 12, pp. 1089-1098, 2011.

[545] Ikonen J., Knutas A., Hämäläinen H., Ihonen M., Porras J., and Kallonen T., "Use of embedded RFID tags in concrete element supply chains," Journal of Information Technology in Construction (ITcon), vol. 18, no. 7, pp. 119-147, 2013.

[546] Valero E., and Adán A., "Integration of RFID with other technologies in construction," Measurement, vol. 94, pp. 614-620, 2016.

[547] Johann S., Strangfeld C., Müller M., Mieller B., and Bartholmai M., "RFID sensor systems embedded in concrete–requirements for long–term operation," Materials Today: Proceedings, vol. 4, no. 5, pp. 5827-5832, 2017.

[548] Murthy S.G.N., "Batteryless Wireless RFID based embedded sensors for long term monitoring of reinforced concrete structures," in Proceedings of the International Symposium Non-Destructive Testing in Civil Engineering (NDT-CE), pp. 15-17, 2015 September.

[549] Yi X., Cho C., Cooper J., Wang Y., Tentzeris M.M., and Leon R.T., "Passive wireless antenna sensor for strain and crack sensing - Electromagnetic modeling, simulation, and testing," Smart Materials and Structures, vol. 2, 2013.

[550] Corva D.M., Hosseini S.S., Collins F., Adams S.D., Gates W.P., and Kouzani A.Z., "Miniature resistance measurement device for structural health monitoring of reinforced concrete infrastructure," Sensors, vol. 20, no. 15, p. 4313, 2020.

[551] Andringa M.M., Neikirk D.P., Dickerson N.P., and Wood S.L., "Unpowered wireless corrosion sensor for steel reinforced concrete," in SENSORS 2005, IEEE, p. 4, 2005 November.

[552] Ozbey B., Erturk V.B., Demir H.V., Altintas A., and Kurc O., "A wireless passive sensing system for displacement/strain measurement in reinforced concrete members," Sensors, vol. 16, no. 4, p. 496, 2016.

[553] Grisso B.L., Martin L.A., and Inman D.J., "A wireless active sensing system for impedance-based structural health monitoring," in Proceedings of 23rd International Modal Analysis Conference (IMAC XXIII), 2005 January.

[554] Chang C.Y., and Hung S.S., "Implementing RFIC and sensor technology to measure temperature and humidity inside concrete structures," Construction and Building Materials, vol. 26, no. 1, pp. 628-637, 2012.

[555] Abbadi A., "Développement des réseaux de capteurs sans fil noyés dans le béton pour la surveillance des ouvrages de génie civil," Doctoral dissertation, Université Lille 1, 2015.

[556] Gallucci L., Menna C., Angrisani L., Asprone D., Moriello R.S.L., Bonavolontà F., and Fabbrocino F., "An embedded wireless sensor network with wireless power transfer capability for the structural health monitoring of reinforced concrete structures," Sensors, vol. 17, no. 11, p. 2566, 2017.

[557] Angrisani L., Moriello R.S.L. Bonavolontà F., Gallucci L., Menna C., Asprone D., and Fabbrocino F., "An innovative embedded wireless sensor network system for the structural health monitoring of RC structures," in 2017 IEEE 3rd International Forum on Research and Technologies for Society and Industry (RTSI), IEEE, pp. 1-4, 2017 September.

[558] Bosma D., and Lindeman P., "Autonomous battery less sensor for IoT applications in Smart Buildings: Low-power Energy Conversion and Storage for RF Energy Harvesting," Bachelor dissertation, Delft University of Technology, 2018.

[559] Barroca N., Borges L.M., Velez F.J., Monteiro F., Gorski M., and Castro-Gomes J., "Wireless sensor networks for temperature and humidity monitoring within concrete structures," Construction and Building Materials, vol. 40, pp. 1156-1166, 2013.

[560] Fraile-Garcia E., Ferreiro-Cabello J., de Pison Ascacibar E.M., Ceniceros J.F., and Espinoza A.V.P., "Implementing a technically and economically viable system for recording data inside concrete," Construction and Building Materials, vol. 157, pp. 860-872, 2017.

[561] "McBIM Research Project," Available online: https://anr.fr/Project-ANR-17-CE10-0014 (accessed on 3 March 2021).

[562] "Mc BIM," Available online: https://mcbim.cran.univ-lorraine.fr/ (accessed on 3 March 2021).

[563] Derigent W., David M., Wan H., Dragomirescu D., Takacs A., Loubet G., Roxin A., Melet R., and Montegut L., "Materials communicating with the BIM: aims and first results of the McBIM project," 12th International Workshop on Structural Health Monitoring (IWSHM), 2019.

[564] Roxin A., Abdou W., Ginhac D., Derigent W., Dragomirescu D., and Montegut L., "Digital building twins-Contributions of the ANR McBIM project," in 2019 15th International Conference on Signal-Image Technology & Internet-Based Systems (SITIS), IEEE, pp. 404-410, 2019 November.

[565] "LAAS CNRS - Laboratory for Analysis and Architecture of Systems," Available online: https://www.laas.fr/public/en (accessed on 3 March 2021).

[566] Loubet G., Takacs A., and Dragomirescu D., "Towards the Design of Wireless Communicating Reinforced Concrete," IEEE Access, vol. 6, pp. 75002-75014, 2018.

[567] Loubet G., Takacs A., and Dragomirescu D., "Implementation of a Battery-Free Wireless Sensor for Cyber-Physical Systems dedicated to Structural Health Monitoring Applications," IEEE Access, vol. 7, pp. 24679-24690, 2019.

[568] Loubet G., Takacs A., Gardner E., De Luca A., Udrea F., and Dragomirescu D., "LoRaWAN Battery-Free Wireless Sensors Network Designed for Structural Health Monitoring in the Construction Domain," Sensors, vol. 19, no. 7, p. 1510, 2019.

[569] Loubet G., Takacs A., Gardner E., De Luca A., Udrea F., and Dragomirescu D., "Wirelessly Powered and Battery-Free LoRaWAN Wireless Sensing Nodes Designed for Communicating Reinforced Concrete," 12th International Workshop on Structural Health Monitoring (IWSHM), 2019.

[570] Sidibe A., Takacs A., Okba A., and Loubet G., "An Improved Rectenna Design for Battery-free Wireless Sensors and Structural Health Monitoring," in 2019 IEEE Wireless Power Transfer Conference (WPTC), IEEE, pp. 440-445, 2019.

[571] Loubet G., Takacs A., and Dragomirescu D., "Implementation of a Wireless Sensor Network Designed to be Embedded in Reinforced Concrete," 46th Annual Conference of the IEEE Industrial Electronics Society, IECON 2020, pp. 2195-2200, 2020.

[572] Sidibe A., Loubet G., Takacs A., and Dragomirescu D., "Design and Characterization of Compact Antennas for Wireless Sensing Applications," in 2020 International Workshop on Antenna Technology (iWAT), IEEE, pp. 1-4, 2020.

[573] Sidibe A., Loubet G., Takacs A., and Dragomirescu D., "Ultra-Compact and High-Efficiency Rectenna for Wireless Sensing Applications in Concrete Structure," in 2020 IEEE/MTT-S International Microwave Symposium (IMS), IEEE, pp. 988-991, 2020.

[574] Sidibe A., Loubet G., Takacs A., and Dragomirescu D., "Energy Harvesting for Battery-Free Wireless Sensors Network Embedded in a Reinforced Concrete Beam," in 2020 50th European Microwave Conference (EuMC), IEEE, pp. 702-705, 2021.

[575] Sidibe A., Takacs A., Loubet G., and Dragomirescu D., "Compact Antenna in 3D Configuration for Rectenna Wireless power transfer Applications," Sensors, vol. 21, no. 9, p. 3193, 2021.

[576] "CRAN - Interdisciplinary Research Laboratory in Lorraine," Available online: http://www.cran.univ-lorraine.fr/index.php?codelangue=EN (accessed on 3 March 2021).

[577] Hang W., Michael D., and Derigent W., "Defining the communication architecture for data aggregation in Wireless Sensor Networks: application to communicating concrete design," in 2019 7th International Conference on Future Internet of Things and Cloud (FiCloud), IEEE, pp. 102-108, 2019 August.

[578] Wan H., David M., and Derigent W., "A holonic manufacturing approach applied to communicate concrete: Concept and first development," in International Workshop on Service Orientation in Holonic and Multi-Agent Manufacturing, Springer, Cham, pp. 414-425, 2019 October.

[579] Wan H., David M., and Derigent W., "Design of a multi-agent system for exploiting the communicating concrete in a SHM/BIM context," IFAC-PapersOnLine, vol. 53, no. 3, pp. 372-379, 2020.

[580] Wan H., David M., and Derigent W., "Energy-efficient chain-based data gathering applied to communicating concrete," International Journal of Distributed Sensor Networks, vol. 16, no. 8, p. 1550147720939028, 2020.

[581] Wan H., David M., and Derigent W., "Is communicating material an intelligent product instantiation? Application to the McBIM project," in 10th Workshop on Service Oriented, Holonic and Multi-Agent Manufacturing Systems for Industry of the Future, SOHOMA 2020, 2020 October.

[582] "LIB: Computer Science Laboratory of Burgundy," Available online: https://lib.u-bourgogne.fr/en/home-page (accessed on 3 March 2021).

[583] "International Telecommunication Union - ITU: Committed to connecting the world," Available online: https://www.itu.int/ (accessed on 3 March 2021).

[584] "Mini-Circuits," Available online: https://www.minicircuits.com/homepage/homepage.html (accessed on 3 March 2021).

[585] "Mini-Circuits - ROS-950-219+," Available online: https://www.minicircuits.com/pdfs/ROS-950-219+.pdf (accessed on 3 March 2021).

[586] "Mini-Circuits - VACC-09+," Available online: https://www.minicircuits.com/pdfs/VACC-09+.pdf (accessed on 3 March 2021).

[587] "Mini-Circuits - PGA-105+," Available online: https://www.minicircuits.com/pdfs/PGA-105+.pdf (accessed on 3 March 2021).

[588] "Mini-Circuits - TCBT-14+," Available online: https://www.minicircuits.com/pdfs/TCBT-14+.pdf (accessed on 3 March 2021).

[589] "Mini-Circuits - PHA-202+," Available online: https://www.minicircuits.com/pdfs/PHA-202+.pdf (accessed on 3 March 2021).

[590] "RF Solutions - 868MHz Antenna - +3dBm Whip," Available online: https://www.rfsolutions.co.uk/downloads/1456239963ANT-8WHIP3H.pdf (accessed on 3 March 2021).

[591] "Rohm Semiconductor - BD00D0AWHFP," Available online: https://fscdn.rohm.com/en/products/databook/datasheet/ic/power/linear_regulator/bd00d0awhfp-e.pdf (accessed on 3 March 2021).

[592] "ABLIC - S-812C Series," Available online: https://www.ablic.com/en/doc/datasheet/voltage_regulator/S812C_E.pdf (accessed on 3 March 2021).

[593] "ON Semiconductor - NCV4264-2," Available online: https://www.onsemi.com/pdf/datasheet/ncv4264-2-d.pdf (accessed on 3 March 2021).

[594] "STMicroelectronics - STLQ50," Available online: https://www.st.com/content/ccc/resource/technical/document/datasheet/0d/ba/9a/6e/e5/7e/4b/68/CD00151464.pdf/files/CD00151464.pdf/jcr:content/translations/en.CD00151464.pdf (accessed on 3 March 2021).

[595] "Bourns - 3296," Available online: https://www.bourns.com/docs/Product-Datasheets/3296.pdf (accessed on 3 March 2021).

[596] "Linear Technology - LT3082," Available online: https://www.analog.com/media/en/technical-documentation/data-sheets/3082f.pdf (accessed on 3 March 2021).

[597] "Bourns - 3299," Available online: https://www.bourns.com/docs/Product-Datasheets/3299.pdf (accessed on 3 March 2021).

[598] "Ettus Research - USRP B200/210," Available online: ettus.com/wp-content/uploads/2019/01/b200-b210_spec_sheet.pdf (accessed on 3 March 2021).

[599] "GNURadio - the free & open woftware radio ecosystem," Available online: https://www.gnuradio.org/ (accessed on 3 March 2021).

[600] "Anritsu - MG3690A RF/Microwave Signal Generators," Available online: https://dl.cdn-anritsu.com/en-us/test-measurement/files/Brochures-Datasheets-Catalogs/datasheet/11410-00327E.pdf (accessed on 3 March 2021).

[601] " Anritsu - MG3690B RF/Microwave Signal Generators," Available online: https://dl.cdn-anritsu.com/en-us/test-measurement/files/Brochures-Datasheets-Catalogs/datasheet/11410-00344K.pdf (accessed on 3 March 2021).

[602] "Powercast - TX91501B," Available online: https://www.powercastco.com/wp-content/uploads/2019/10/User-Manual-TX-915-01B-Rev-A-1.pdf (accessed on 3 March 2021).

[603] "Powercast - TX91503," Available online: https://www.powercastco.com/wp-content/uploads/2020/08/TX91503-UserManual_Final_July-2020.pdf (accessed on 3 March 2021).

[604] "GreenWake technologies - PWT-04," Available online: http://gnw-tech.com/GnW_PWT-04_datasheet_EN_2.pdf (accessed on 3 March 2021).

[605] "Analog Devices - Adalm-Pluto," Available online: https://www.analog.com/media/en/news-marketing-collateral/product-highlight/ADALM-PLUTO-Product-Highlight.pdf (accessed on 3 March 2021).

[606] "Great Scott Gadgets - HackRF One," Available online https://greatscottgadgets.com/hackrf/one/ (accessed on 3 March 2021).

[607] "RTL-SDR Blog V3," Available online: https://www.rtl-sdr.com/wp-content/uploads/2018/02/RTL-SDR-Blog-V3-Datasheet.pdf (accessed on 3 March 2021).

[608] "IMST GmbH - WiMOD iC880A," Available online: https://lora-alliance.org/wp-content/uploads/2019/09/iC880A_Datasheet_V1_1.pdf (accessed on 3 March 2021).

[609] "Semtech - SX1301," Available online: https://semtech.my.salesforce.com/sfc/p/#E0000000JelG/a/44000000MDnR/Et1KWLCuNDI6MDagfSPAvqqp.Y869Flgs1LleWyfjDY (accessed on 3 March 2021).

[610] "Raspberry Pi Foundation - Raspberry Pi 3 model B+," Available online: https://static.raspberrypi.org/files/product-briefs/200206+Raspberry+Pi+3+Model+B+plus+Product+Brief+PRINT&DIGITAL.pdf (accessed on 3 March 2021).

[611] " Raspberry Pi Foundation - Operating system images," Available online: https://www.raspberrypi.org/software/operating-systems/ (accessed on 3 March 2021).

[612] "Semtech - Semtech UDP packet-forwarder," Available online: https://github.com/lora-net/packet_forwarder (accessed on 3 March 2021).

[613] "ChirpStack - ChirpStack open-source LoRaWAN Network Server," Available online: https://www.chirpstack.io/ (accessed on 3 March 2021).

[614] " Eclipse Mosquitto - An open source MQTT broker," Available online: http://mosquitto.org/ (accessed on 3 March 2021).

[615] "PostgreSQL - PostgreSQL: The World's Most Advanced Open Source Relational Database," Available online: https://www.postgresql.org/ (accessed on 3 March 2021).

[616] "Decawave," Available online: https://www.decawave.com/ (accessed on 3 March 2021).

[617] "Murata - Sub-G Module Data Sheet," Available online: https://wireless.murata.com/pub/RFM/data/type_abz.pdf (accessed on 3 March 2021).

[618] "Semtech - SX1276/77/78/79," Available online: https://semtech.my.salesforce.com/sfc/p/#E0000000JelG/a/2R0000001Rbr/6EfVZUorrpoKFfvaF_Fkpgp5kzjiNyiAbqcpqh9qSjE (accessed on 3 March 2021).

[619] "STMicroelectronics - STM32L072x8 STM32L072xB STM32L072xZ," Available online: https://www.st.com/resource/en/datasheet/stm32l072v8.pdf (accessed on 3 March 2021).

[620] "STMicroelectronics - RM0376 Reference manual," Available online: https://www.st.com/resource/en/reference_manual/dm00108281-ultra-low-power-stm32l0x2-advanced-arm-based-32-bit-mcus-stmicroelectronics.pdf (accessed on 3 March 2021).

[621] "LPRS - ANT-SS900 - 868-915MHz Compressed Whip / Stubby Antenna," Available online: http://www.lprs.co.uk/assets/files/LPRS_ANT-SS900.pdf (accessed on 3 March 2021).

[622] "Texas Instruments - Design Note DN024 - Monopole PCB Antenna with Single or Dual Band Option," Available online: https://www.ti.com/lit/an/swra227e/swra227e.pdf (accessed on 3 March 2021).

[623] "Keysight Technologies - N6700 Modular Power System Family," Available online: https://www.keysight.com/us/en/assets/7018-01522/data-sheets/5989-6319.pdf (accessed on 3 March 2021).

[624] Bouguera T., Diouris J.F., Chaillout J.J., Jaouadi R., and Andrieux G., "Energy consumption model for sensor nodes based on LoRa and LoRaWAN," Sensors, vol. 18, no. 7, p. 2104, 2018.

[625] "Aosong Electronics Co., Ltd - DHT22," Available online: https://www.sparkfun.com/datasheets/Sensors/Temperature/DHT22.pdf (accessed on 3 March 2021).

[626] "Texas Instruments - HDC2080 Low-Power Humidity and Temperature Digital Sensor," Available online: https://www.ti.com/lit/ds/symlink/hdc2080.pdf?ts=1621819843107&ref_url=https%253A%252F%252Fwww.ti.com%252Fproduct%252FHDC2080 (accessed on 3 March 2021).

[627] "Texas Instruments - HDC2010 Low-Power Humidity and Temperature Digital Sensors," Available online: https://www.ti.com/lit/ds/symlink/hdc2010.pdf (accessed on 3 March 2021).

[628] "Bosch - BME280," Available online: https://www.bosch-sensortec.com/media/boschsensortec/downloads/datasheets/bst-bme280-ds002.pdf (accessed on 3 March 2021).

[629] "Sensirion - Data Sheet SHTW2," Available online: https://www.sensirion.com/fileadmin/user_upload/customers/sensirion/Dokumente/2_Humidity_Sensors/Datasheets/Sensirion_Humidity_Sensors_SHTW2_Datasheet.pdf (accessed on 3 March 2021).

[630] "Sensirion - Datasheet SHTC3," Available online: https://www.sensirion.com/fileadmin/user_upload/customers/sensirion/Dokumente/2_Humidity_Sensors/Datasheets/Sensirion_Humidity_Sensors_SHTC3_Datasheet.pdf (accessed on 3 March 2021).

[631] De Luca A., Pathirana V., Ali S.Z., Dragomirescu D., and Udrea F., "Experimental, analytical and numerical investigation of non-linearity of SOI diode temperature sensors at extreme temperatures," Sensors and Actuators A: Physical, vol. 222, pp. 31-38, 2015.

[632] "STMicroelectronics - LM134-LM234-LM334," Available online: https://www.st.com/resource/en/datasheet/lm234.pdf (accessed on 3 March 2021).

[633] "Texas Instruments - LM134/LM234/LM334 3-Terminal Adjustable Current Sources," Available online: https://www.ti.com/lit/ds/symlink/lm134.pdf?ts=1588770978246 (accessed on 3 March 2021).

[634] "ON Semiconductor - RB751S40 Schottky Barrier Diode," Available online: https://www.onsemi.cn/pdf/datasheet/rb751s40t1-d.pdf (accessed on 3 March 2021).

[635] "Microchip - MCP6V61/1U/2/4," Available online: http://ww1.microchip.com/downloads/en/DeviceDoc/20005367B.pdf (accessed on 3 March 2021).

[636] "Analog Devices - Precision Series Sub-Band Gap Voltage Reference ADR130," Available online: https://www.analog.com/media/en/technical-documentation/data-sheets/ADR130.pdf (accessed on 3 March 2021).

[637] "Binder - Data Sheet Model MKF 56," Available online: https://www.binder-world.com/en/content/download/124780/5607510/file/Data%20Sheet%20Model%20MKF%20056%20en.pdf (accessed on 3 March 2021).

[638] "Keithley - Models 2611B, 2612B, and 2614B System SourceMeter Instruments Quick Start Guide," Available online: https://download.tek.com/manual/2612B_903-01D_QSG_Jan_2019_web.pdf (accessed on 3 March 2021).

[639] "Keithley - Model 2000 6½-Digit Multimeter Datasheet," Available online: https://download.tek.com/datasheet/2000-DMM-Data-Sheet-1KW612970.pdf (accessed on 3 March 2021).

[640] Badr J., "Conception et validation d'un capteur noyé de résistivité électrique en vue du suivi des profils de teneur en eau dans les bétons," Doctoral dissertation, Université Paul Sabatier-Toulouse III, 2019.

[641] "RS Pro - Datasheet RS Pro Wire Lead Strain Gauge 4mm, 120Ω," Available online: https://docs.rs-online.com/1c95/0900766b815882e1.pdf (accessed on 3 March 2021).

[642] "Linear Technology - DEMO MANUAL DC2042A," Available online: https://www.analog.com/media/en/technical-documentation/user-guides/DC2042AF.PDF (accessed on 3 March 2021).

[643] "Texas Instruments - TPS6303x High Efficiency Single Inductor Buck-Boost Converter," Available online: https://www.ti.com/lit/ds/symlink/tps63030.pdf (accessed on 3 March 2021).

[644] "e-peas semiconductors - AEM30940," Available online: https://e-peas.com/wp-content/uploads/2021/03/e-peas-AEM30940-datasheet-RF-Vibration-energy-harvesting.pdf (accessed on 3 March 2021).

[645] "Powercast - P1110B," Available online: https://www.powercastco.com/documentation/p1110b-module-datasheet/ (accessed on 3 March 2021).

[646] "Powercast - P2110B," Available online: https://www.powercastco.com/documentation/p2110b-module-datasheet/ (accessed on 3 March 2021).

[647] "AVX - BestCap," Available online: https://catalogs.avx.com/BestCap.pdf (accessed on 3 March 2021).

[648] "KEMET - Supercapacitors FM series," Available online: https://content.kemet.com/datasheets/KEM_S6012_FM.pdf (accessed on 3 March 2021).

[649] Okba A., Takacs A., and Aubert H., "Compact flat dipole rectenna for IoT applications," Progress in Electromagnetics Research, vol. 87, pp. 39-49, 2018.

[650] Okba A., Takacs A., and Aubert H., "900 MHz miniaturized rectenna," in 2018 IEEE Wireless Power Transfer Conference (WPTC), IEEE, pp. 1-4, 2018 June.

[651] Takacs A., Okba A., and Aubert H., "Compact Planar Integrated Rectenna for Batteryless IoT Applications," in 2018 48th European Microwave Conference (EuMC), IEEE, pp. 777-780, 2018 September.

[652] Sidibe A., Takacs A., Okba A., and Aubert H., "Design and Characterization of a Compact Rectenna for Structural Health Monitoring Applications," in 2019 IEEE International Symposium on Antennas and Propagation and USNC-URSI Radio Science Meeting, IEEE, pp. 1803-1804, 2019 July.

[653] Sidibe A., and Takacs A., "A Miniature and High-Efficiency Rectenna in ISM 868 MHz Frequency Band," in 2020 IEEE International Symposium on Antennas and Propagation and North American Radio Science Meeting, IEEE, pp. 1509-1510, 2020 July.

[654] "Rogers Corporation - RT/duroid 5870/5880," Available online: https://rogerscorp.com/-/media/project/rogerscorp/documents/advanced-connectivity-solutions/english/data-sheets/rt-duroid-5870---5880-data-sheet.pdf (accessed on 3 March 2021).

[655] "Avago Technologies - HSMS-285x Series," Available online: https://docs.broadcom.com/doc/AV02-1377EN (accessed on 3 March 2021).

[656] "Skyworks - Surface-mount mixer and detector Schottky diodes," Available online: https://www.skyworksinc.com/-/media/SkyWorks/Documents/Products/201-300/Surface_Mount_Schottky_Diodes_200041AG.pdf (accessed on 3 March 2021).

[657] "STMicroelectronics - UM2115 User manual," Available online: https://www.st.com/content/ccc/resource/technical/document/user_manual/group0/ac/62/15/c7/60/ac/4e/9c/DM00329995/files/DM00329995.pdf/jcr:content/translations/en.DM00329995.pdf (accessed on 3 March 2021).

[658] "Aerotek Co., LTD. - Coaxial circulators/isolators," Available online: http://www.aerotek.co.th/classic/coaxstd.php (accessed on 3 March 2021).

[659] "Aerotek Co., LTD. - Flange mount circulators/isolators," Available online: http://www.aerotek.co.th/classic/flange.php (accessed on 3 March 2021).

[660] "Teledyne LeCroy - WaveRunner 6000A Series," Available online: http://cdn.teledynelecroy.com/files/pdf/lecroy_waverunner_6000a_datasheet.pdf (accessed on 3 March 2021).

[661] "NXP - QN908x DK User Guide," Available online: https://www.nxp.com/webapp/Download?colCode=QN908x-DK (accessed on 3 March 2021).

[662] "NXP - QN908x Ultra low power Bluetooth 5 system-on-chip solution," Available online: https://www.nxp.com/docs/en/nxp/data-sheets/QN908x.pdf (accessed on 3 March 2021).

[663] "NXP - AN11994 QN908x BLE Antenna Design Guide," Available online: https://www.nxp.com/docs/en/nxp/application-notes/AN11994.pdf (accessed on 3 March 2021).

[664] "NXP - MCUXpresso Integrated Development Environment (IDE)," Available online: https://www.nxp.com/design/software/development-software/mcuxpresso-software-and-tools-/mcuxpresso-integrated-development-environment-ide:MCUXpresso-IDE (accessed on 3 March 2021).

[665] "Keithley - Model 2000 6½-Digit Multimeter," Available online: https://download.tek.com/datasheet/2000-DMM-Data-Sheet-1KW612970.pdf (accessed on 3 March 2021).

[666] "Panasonic - Aluminum electrolytic capacitors surface mount type FK series," Available online: https://industrial.panasonic.com/cdbs/www-data/pdf/RDE0000/ABA0000C1181.pdf (accessed on 3 March 2021).

[667] Yang X., "LoRaWAN: Vulnerability analysis and practical exploitation," Delft University of Technology, Master of Science, 2017.

[668] Aras E., Ramachandran G.S., Lawrence P., and Hughes D., "Exploring the security vulnerabilities of LoRa," in 2017 3rd IEEE International Conference on Cybernetics (CYBCONF), IEEE, pp. 1-6, 2017 June.

[669] Dönmez T.C., and Nigussie E., "Security of lorawan v1. 1 in backward compatibility scenarios," Procedia computer science, vol. 134, pp. 51-58, 2018.

[670] Butun I., Pereira N., and Gidlund M., "Analysis of LoRaWAN v1. 1 security," in Proceedings of the 4th ACM MobiHoc Workshop on Experiences with the Design and Implementation of Smart Objects, pp. 1-6, 2018 June.

[671] Eldefrawy M., Butun I., Pereira N., and Gidlund M., "Formal security analysis of LoRaWAN," Computer Networks, vol. 148, pp. 328-339, 2019.

[672] Noura H., Hatoum T., Salman O., Yaacoub J.P., and Cheha, A., "LoRaWAN Security Survey: Issues, Threats and Possible Mitigation Techniques," Internet of Things, p. 100303, 2020.

[673] Tsai K.L., Leu F.Y., Hung L.L., and Ko C.Y., "Secure Session Key Generation Method for LoRaWAN Servers," IEEE Access, vol. 8, pp. 54631-54640, 2020.

[674] Dunning J., "Taming the blue beast: A survey of bluetooth based threats," IEEE Security & Privacy, vol. 8, no. 2, pp. 20-27, 2010.

[675] Sandhya S., and Devi K.S., "Analysis of Bluetooth threats and v4. 0 security features," in 2012 International Conference on Computing, Communication and Applications, IEEE, pp. 1-4, 2012 February.

[676] Ryan M., "Bluetooth: With low energy comes low security," in 7th {USENIX} Workshop on Offensive Technologies ({WOOT} 13), 2013 August.

[677] Bräuer S., Zubow A., Zehl S., Roshandel M., and Mashhadi-Sohi S., "On practical selective jamming of Bluetooth Low Energy advertising," in 2016 IEEE Conference on Standards for Communications and Networking (CSCN), IEEE, pp. 1-6, 2016 October.

[678] Kwon G., Kim J., Noh J., and Cho S., "Bluetooth low energy security vulnerability and improvement method," in 2016 IEEE International Conference on Consumer Electronics-Asia (ICCE-Asia), IEEE, pp. 1-4, 2016 October.

[679] Cope P., Campbell J., and Hayajneh T., "An investigation of Bluetooth security vulnerabilities," in 2017 IEEE 7th Annual Computing and Communication Workshop and Conference (CCWC), IEEE, pp. 1-7, 2017 January.

[680] Lonzetta A.M., Cope P., Campbell J., Mohd B.J., and Hayajneh T., "Security vulnerabilities in Bluetooth technology as used in IoT," Journal of Sensor and Actuator Networks, vol. 7, no. 3, p. 28, 2018.

[681] Hassan S.S., Bibon S.D., Hossain M.S., and Atiquzzaman M., "Security threats in Bluetooth technology," Computers & Security, vol. 74, pp. 308-322, 2018.

[682] Zhang Y., Weng J., Dey R., and Fu X., "Bluetooth Low Energy (BLE) Security and Privacy," Encyclopedia of Wireless Networks, Springer, Cham, pp. 1-12, 2019.

[683] Pallavi S., and Narayanan V.A., "An overview of practical attacks on BLE based IoT devices and their security," in 2019 5th International Conference on Advanced Computing & Communication Systems (ICACCS), IEEE, pp. 694-698, 2019 March.

[684] National Institute of Standards and Technology, "NIST Special Publication 800-121 - Revision 2 - Guide to Bluetooth Security," Available online: https://nvlpubs.nist.gov/nistpubs/SpecialPublications/NIST.SP.800-121r2.pdf (accessed on 3 March 2021).

[685] Cayre R., Nicomette V., Auriol G., Alata E., Kaaniche M., and Marconato G., "Mirage: towards a Metasploit-like framework for IoT," in 2019 IEEE 30th International Symposium on Software Reliability Engineering (ISSRE), IEEE, pp. 261-270, 2019 October.

Publications

International journals

[1] Sidibe A., Takacs A., Loubet G., and Dragomirescu D., "Compact Antenna in 3D Configuration for Rectenna Wireless power transfer Applications," Sensors, vol. 21, no. 9, p. 3193, 2021.

[2] Sidibe A., Loubet G., Takacs A., Ferré G., and Ghiotto A., "Miniature drone antenna design for the detection of airliners," International Journal of Microwave and Wireless Technologies, vol. 13, no.1, pp. 21-27, 2020.

[3] Loubet G., Takacs A., Gardner E., De Luca A., Udrea F., and Dragomirescu D., "LoRaWAN Battery-Free Wireless Sensors Network Designed for Structural Health Monitoring in the Construction Domain," Sensors, vol. 19, no. 7, p. 1510, 2019.

[4] Loubet G., Takacs A., and Dragomirescu D., "Implementation of a Battery-Free Wireless Sensor for Cyber-Physical Systems dedicated to Structural Health Monitoring Applications," IEEE Access, vol. 7, pp. 24679-24690, 2019.

[5] Loubet G., Takacs A., and Dragomirescu D., "Towards the Design of Wireless Communicating Reinforced Concrete," IEEE Access, vol. 6, pp. 75002-75014, 2018.

International conferences

[6] Sidibe A., Loubet G., Takacs A., and Dragomirescu D., "Energy Harvesting for Battery-Free Wireless Sensors Network Embedded in a Reinforced Concrete Beam," in 2020 50th European Microwave Conference (EuMC), IEEE, pp. 702-705, 2021.

[7] Loubet G., Takacs A., and Dragomirescu D., "Implementation of a Wireless Sensor Network Designed to be Embedded in Reinforced Concrete," 46th Annual Conference of the IEEE Industrial Electronics Society, IECON 2020, pp. 2195-2200, 2020.

[8] Sidibe A., Loubet G., Takacs A., and Dragomirescu D., "Ultra-Compact and High-Efficiency Rectenna for Wireless Sensing Applications in Concrete Structure," in 2020 IEEE/MTT-S International Microwave Symposium (IMS), IEEE, pp. 988-991, 2020.

[9] Sidibe A., Loubet G., Takacs A., and Dragomirescu D., "Design and Characterization of Compact Antennas for Wireless Sensing Applications," in 2020 International Workshop on Antenna Technology (iWAT), IEEE, pp. 1-4, 2020.

[10] Loubet G., Takacs A., Gardner E., De Luca A., Udrea F., and Dragomirescu D., "Wirelessly Powered and Battery-Free LoRaWAN Wireless Sensing Nodes Designed for Communicating Reinforced Concrete," 12th International Workshop on Structural Health Monitoring (IWSHM), 2019.

[11] Derigent W., David M., Wan H., Dragomirescu D., Takacs A., Loubet G., Roxin A., Melet R., and Montegut L., "Materials communicating with the BIM: aims and first results of the McBIM project," 12th International Workshop on Structural Health Monitoring (IWSHM), 2019.

[12] Sidibe A., Takacs A., Okba A., and Loubet G., "An Improved Rectenna Design for Battery-free Wireless Sensors and Structural Health Monitoring," in 2019 IEEE Wireless Power Transfer Conference (WPTC), IEEE, pp. 440-445, 2019.

National conference

[13] Loubet G., Takacs A., Rumeau A., and Dragomirescu D., "*Nœuds de mesure sans-fil et sans batterie communiquant en LoRa et commandés par leur interface d'alimentation par transfert d'énergie radiofréquence en champ lointain*," *21ème Journées Nationales Microondes* (*JNM*), 2019.